CEREBRAL AUTOREGULATION AND NEUROVASCULAR COUPLING IN BRAIN DISORDERS

EDITED BY: Xiuyun Liu, Marek Czosnyka, Dong Ming and Chiara Robba
PUBLISHED IN: Frontiers in Neurology

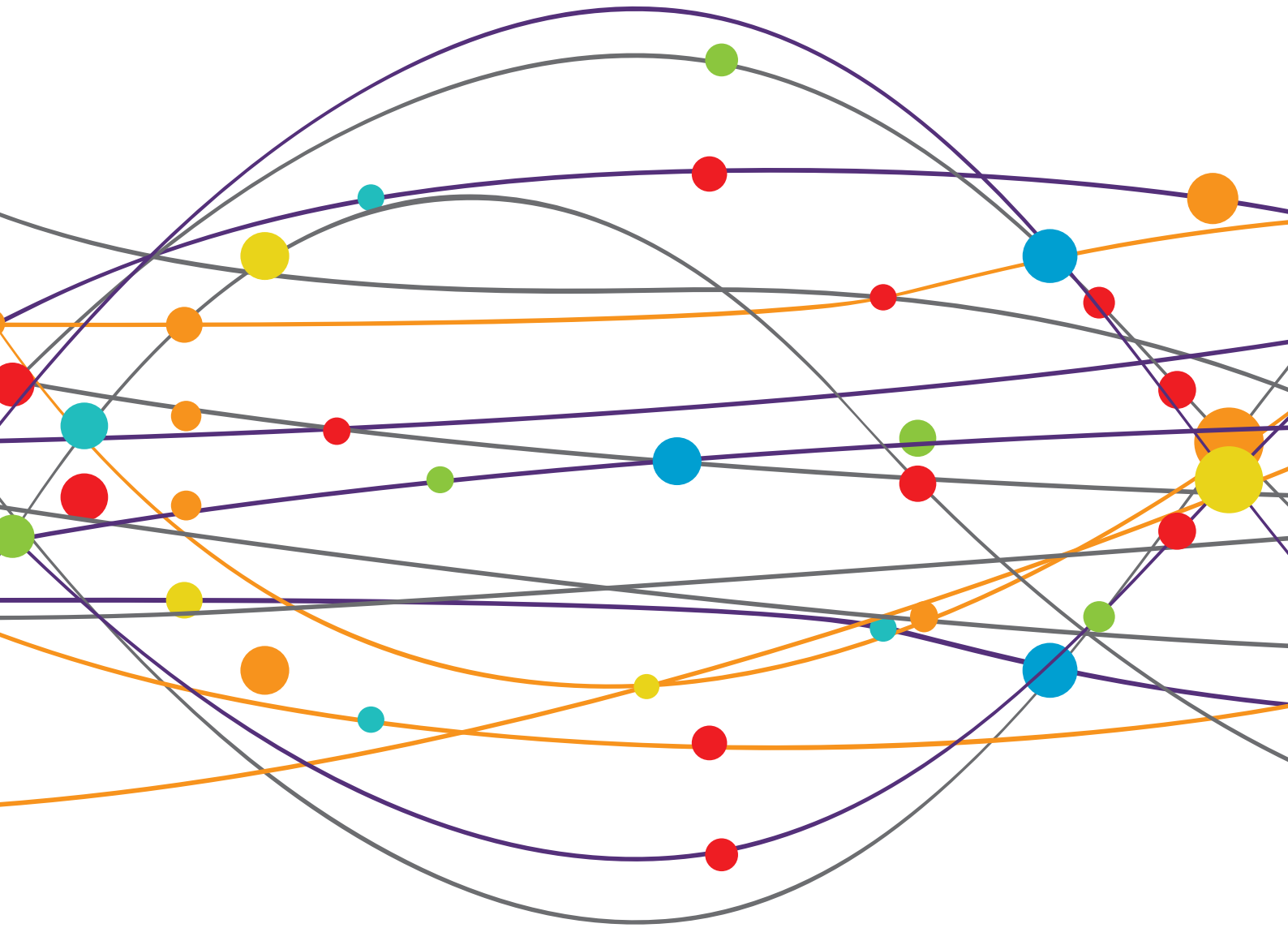

frontiers Research Topics

frontiers

ISSN 1664-8714
ISBN 978-2-88976-594-2
DOI 10.3389/978-2-88976-594-2

About Frontiers

Frontiers is more than just an open-access publisher of scholarly articles: it is a pioneering approach to the world of academia, radically improving the way scholarly research is managed. The grand vision of Frontiers is a world where all people have an equal opportunity to seek, share and generate knowledge. Frontiers provides immediate and permanent online open access to all its publications, but this alone is not enough to realize our grand goals.

Frontiers Journal Series

The Frontiers Journal Series is a multi-tier and interdisciplinary set of open-access, online journals, promising a paradigm shift from the current review, selection and dissemination processes in academic publishing. All Frontiers journals are driven by researchers for researchers; therefore, they constitute a service to the scholarly community. At the same time, the Frontiers Journal Series operates on a revolutionary invention, the tiered publishing system, initially addressing specific communities of scholars, and gradually climbing up to broader public understanding, thus serving the interests of the lay society, too.

Dedication to Quality

Each Frontiers article is a landmark of the highest quality, thanks to genuinely collaborative interactions between authors and review editors, who include some of the world's best academicians. Research must be certified by peers before entering a stream of knowledge that may eventually reach the public - and shape society; therefore, Frontiers only applies the most rigorous and unbiased reviews.
Frontiers revolutionizes research publishing by freely delivering the most outstanding research, evaluated with no bias from both the academic and social point of view. By applying the most advanced information technologies, Frontiers is catapulting scholarly publishing into a new generation.

What are Frontiers Research Topics?

Frontiers Research Topics are very popular trademarks of the Frontiers Journals Series: they are collections of at least ten articles, all centered on a particular subject. With their unique mix of varied contributions from Original Research to Review Articles, Frontiers Research Topics unify the most influential researchers, the latest key findings and historical advances in a hot research area! Find out more on how to host your own Frontiers Research Topic or contribute to one as an author by contacting the Frontiers Editorial Office: frontiersin.org/about/contact

CEREBRAL AUTOREGULATION AND NEUROVASCULAR COUPLING IN BRAIN DISORDERS

Topic Editors:
Xiuyun Liu, Johns Hopkins University, United States
Marek Czosnyka, University of Cambridge, United Kingdom
Dong Ming, Tianjin University, China
Chiara Robba, University of Genoa, Italy

Citation: Liu, X., Czosnyka, M., Ming, D., Robba, C., eds. (2022). Cerebral Autoregulation and Neurovascular Coupling in Brain Disorders. Lausanne: Frontiers Media SA. doi: 10.3389/978-2-88976-594-2

Table of Contents

frontiers | Frontiers in Neurology

TYPE Editorial
PUBLISHED 09 September 2022
DOI 10.3389/fneur.2022.1001342

OPEN ACCESS

EDITED AND REVIEWED BY
Michael J. Schneck,
Loyola University Chicago,
United States

*CORRESPONDENCE
Dong Ming
richardming@tju.edu.cn

SPECIALTY SECTION
This article was submitted to Neurocritical and Neurohospitalist Care,
a section of the journal Frontiers in Neurology

RECEIVED 23 July 2022
ACCEPTED 17 August 2022
PUBLISHED 09 September 2022

CITATION
Liu X, Czosnyka M, Robba C and Ming D (2022) Editorial: Cerebral autoregulation and neurovascular coupling in brain disorders.
Front. Neurol. 13:1001342.
doi: 10.3389/fneur.2022.1001342

Editorial: Cerebral autoregulation and neurovascular coupling in brain disorders

Xiuyun Liu[1,2], Marek Czosnyka[3,4], Chiara Robba[5,6] and Dong Ming[1,2]*

[1]Academy of Medical Engineering and Translational Medicine, Tianjin University, Tianjin, China, [2]Department of Biomedical Engineering, College of Precision Instruments and Optoelectronics Engineering, Tianjin University, Tianjin, China, [3]Department of Clinical Neurosciences, University of Cambridge, Cambridge, United Kingdom, [4]Institute of Electronic Systems, Warsaw University of Technology, Warsaw, Poland, [5]Department of Surgical Sciences and Integrated Diagnostics (DISC), University of Genoa, Genoa, Italy, [6]San Martino Policlinico Hospital, Istituto di Ricovero e Cura a Carattere Scientifico for Oncology and Neuroscience, Genoa, Italy

KEYWORDS

cerebral autoregulation, neurovascular coupling, multi-modality monitoring, neuro intensive care unit, brain disorders

Editorial on the Research Topic
Cerebral autoregulation and neurovascular coupling in brain disorders

Introduction

Although the brain represents only 2% of our body weight, it consumes 20–25% of the total oxygen and nutrition of the body (1). Keeping adequate and constant blood supply to the brain is extremely important. This ensures the stable delivery of oxygen and other substances and the removal of the waste products of brain metabolism, especially in patients with brain disorders. Two important mechanisms involved in cerebral hemodynamic management are cerebral autoregulation (CA) and neurovascular coupling (NVC). Cerebral autoregulation refers to the ability of the brain to keep stable cerebral blood flow despite changes in cerebral perfusion pressure or arterial blood pressure (2), while NVC adapts cerebral blood flow in accordance with local neuronal activities [Liu et al.; (3)]. These two functions may be disturbed in patients with brain disorders in neuro intensive care units (NICU). The brain disorders could include stroke, hypoxia, traumatic brain injury (TBI), or subarachnoid hemorrhage (SAH). The damaged cerebral arterioles and capillaries in these patients would result in a lack of blood supply to the brain which may further aggravate cell death *via* blood-brain-barrier damage, inflammatory response, and endothelial cell and receptor dysfunction.

The early detection of the functional impairment of CA and NVC would enable early-stage decisions and prevent brain deterioration such as secondary brain injury, vasospasm, delayed cerebral infarction (DCI) after SAH, and sudden and severe headaches due to vessel constriction in reversible cerebral vasoconstriction syndrome (RCVS). Therefore, effective and prompt monitoring of brain blood perfusion and oxygenation with the quantitative metrics of CA or NVC assessment is in urgent need. Moreover, the mechanisms of impaired CA and NVC in brain disorders, the influence of clinical interventions on these two functions, and the effect of personalized treatment based on CA or NVC still need further investigation.

This Research Topic aims to provide the most recent update on the basic science of, and advanced techniques for, CA and NVC. The issue currently includes 24 papers on the dynamic mechanism of CA, new techniques for CA and NVC monitoring, the cellular mechanism of NVC, and reviews or commentaries on the current progress in this field. The papers cover several fields, including physics, biomedical engineering, clinical engineering, critical care medicine, pathology, and translational studies.

Novel techniques for CA monitoring

This thematic section introduces various novel and updated techniques for quantitative CA assessment, including transcranial doppler (TCD), near-infrared spectroscopy (NIRS), electroencephalograph (EEG), retina vessel diameter, and magnetic resonance imaging (MRI), aiming to find a non-invasive, efficient, and appropriate method for CA assessment applied at a patient's bedside.

Warner et al. provide a detailed temporal analysis of impaired cerebral vascular reactivity to hypercapnia after SAH in rats. They highlight the promising role of retinal vessel diameter as a non-invasive screening tool after SAH. Eleveld et al. investigate a newly developed NIRS-based CA index, i.e., oxygenated–deoxygenated hemoglobin phase differences in the (very) low frequency (VLF/LF) in an endotoxemia study population. The results show a reversible decrease in NIRS-derived CA phase difference after endotoxin infusion, suggesting that endotoxin administration in healthy participants reversibly impairs CA, accompanied by sustained microvascular vasodilation. Pham et al. applies a hemodynamic model of coherent hemodynamics spectroscopy (CHS) to assess CA in five healthy subjects and 3 NCCU patients. They demonstrate the feasibility of measuring coherent de-oxygenated hemoglobin concentrations and blood pressure oscillations to assess autoregulation in NICU patients. However, in a study by Robba, Cardim et al., they report that changes in arterial-oxyhemoglobin components detected by NIRS had the highest accuracy to assess CBF changes. Nonetheless, these studies propose the use of indexes derived from the different components of rSO_2 for the bedside evaluation of cerebral hemodynamics.

CA in different brain disorders with clinical interventions

In this section, the authors investigate the changes in CA in patients with different brain disorders, such as acute ischemic stroke, aneurysmal subarachnoid hemorrhage (aSAH), steno-occlusive disease, and even COVID-19. They aim to investigate the influences of brain disorders on cerebral vasculature and cerebral perfusion to better understand the pathogenesis.

Uryga et al. investigate the influence of aSAH on the relationship between baroreflex sensitivity (BRS) and CA, which normally shows a compensatory interaction in healthy volunteers. However, this inverse relationship was lost in patients who developed cerebral vasospasm after aSAH, both before and during vasospasm.

Wu et al. report reduced network degree, local and global efficiency, and enhanced modularity in the contralateral normal hemispheres of steno-occlusive disease patients, compared with healthy volunteers using resting-state blood oxygen level-dependent (BOLD) imaging.

COVID-19 became a pandemic in 2020 and studies have shown the long-term impact of COVID-19 on the lungs, heart, and cognition. In this special collection, Robba, Messina et al. test the effects of the passive leg-raising test, fluid challenge, and norepinephrine on CA and oxygenation in critically ill COVID-19 patients. The study showed that the PLA test introduced adverse effects in CA in COVID-19 patients on a ventilator.

Concerning the influences of other treatments on CA, Wellard et al. investigate the changes of volume pressure compensation indices, cerebrovascular pressure reactivity indices, and heart rate variability indices after hyperosmolar admission in 30 children. They conclude that bolus therapy of hyperosmolar without preceding intracranial hypertension may alter cerebral dynamics by increasing intracranial pressure and decreasing pressure-volume compensation.

Yao et al. report a negative relationship between successive blood pressure variations and 3-month neurological outcome in acute ischemic stroke patients with intracranial artery stenosis or occlusion (SIASO) treated with intravenous thrombolysis. However, this relationship does not exist in patients without SIASO.

Novel techniques for NVC monitoring

This thematic section focuses on the new techniques for NVC assessment *via* either animal models or human studies. Albanna et al. introduce a new method to non-invasively assess

NVC *via* retinal vessel analysis in patients after aSAH. They report that aSAH results in sustained impairments of NVC in the retina and characteristic changes in the kinetics of retinal arterial responses may be associated with delayed cerebral ischemia. Meanwhile, based on similar techniques, the same research group (Neumaier et al.) compare the response of retinal vessels during flicker stimulation between Cav2.3-deficient mice and control mice. They propose that Cav2.3 channels could be involved in NVC and may contribute to the impairment of vasomotor responses under pathophysiological conditions.

Seker et al. present a fast, reliable, and unbiased data processing tool for the analysis of NVC. This was assessed by laser speckle contrast imaging and two-photon microscopy. Using the new analysis tool, they find that NVC is differently affected during the aging process in mice, with maximal NVC reached in 1-year-old mice compared with mice aged 6–8 weeks and 2 years old.

Review articles in CA and NVC

This special collection also includes several review articles on the most up-to-date information about CA and NVC.

Longhitano et al. systematically review CA in three groups of non-brain injured patients: sepsis and septic shock, during surgery, and in pediatric population. They summarize that impaired CA may result in cognitive dysfunction, neurological damage, worse outcomes, and increased mortality. The authors conclude that monitoring CA might be a useful tool for the optimization of bedside treatment and the individualization of the clinical management of this group of patients.

Spilka et al. present a perspective on CA monitoring in neonatal cardiac surgery requiring cardiopulmonary bypass. They review the technical considerations for CA monitoring in the operating room and point out two requirements for cardiac surgery: that it should be hands-free and non-invasive, which reflects the advantage of using NIRS for CA monitoring.

Szczygielski et al. review the role of the Aquaporin-4 as a gatekeeper, regulating the water exchange between intracellular space, glymphatic system, and intravascular compartment. They point out that AQP4 as the key component of cerebral fluid homeostasis, acting not only as a passive channel for water and small molecular substances but playing a key role in the proper functioning of the blood-brain barrier and perivascular unit. As such, adapting the glymphatic flow to the phases of neuronal activity with increased blood flow demand is shown to be important.

Conclusion

In conclusion, this special collection provides the most recent findings about CA and NVC, focusing on new assessment techniques, basic mechanisms of CA and NVC functions, comparisons of CA or NVC between patients with brain diseases and healthy controls, and the change in CA and NVC during neuroprotective interventions. The collection highlights the importance of CA and NVC monitoring in NICU, which could potentially enable early treatment and improve patient outcomes. Nevertheless, great challenges in this field exist and the following are needed: (1) a standardized method for CA and NVC assessment at the patient's bedside; (2) multi-disciplinary knowledge to better understand the pathologies and course of cerebral vasculature changes over time in different brain diseases; (3) clinical trial validation for these novel techniques for patient-personalized treatment to improve patients' clinical outcomes.

Author contributions

All authors listed have made a substantial, direct, and intellectual contribution to the work and approved it for publication.

Funding

This study was supported by the National Science and Technology Major Project of the Ministry of Science and Technology of China (No. 2021YFF1200600) and the Tianjin University Foundation (No. 0903069003 and No. 0903069004).

Acknowledgments

We deeply thank all the authors and reviewers who have participated in this Research Topic.

Conflict of interest

The authors declare that the research was conducted in the absence of any commercial or financial relationships that could be construed as a potential conflict of interest.

Publisher's note

References

1. Raichle ME, Gusnard DA. Appraising the brain's energy budget. *Proc Natl Acad Sci USA*. (2002) 99:10237–9. doi: 10.1073/pnas.172399499

2. Paulson OB, Strandgaard S, Edvinsson L. Cerebral autoregulation. *Cerebrovasc Brain Metab Rev*. (1990) 2:161–92.

3. Hosford PS, Wells JA, Nizari S, Christie IN, Theparambil SM, Castro PA, et al. CO_2 signaling mediates neurovascular coupling in the cerebral cortex. *Nat Commun*. (2022) 13:1. doi: 10.1038/s41467-022-29622-9

frontiers in Neurology

BRIEF RESEARCH REPORT
published: 23 March 2021
doi: 10.3389/fneur.2021.653167

Differentiating Dynamic Cerebral Autoregulation Across Vascular Territories

*Navpreet Reehal[1], Stephanie Cummings[1], Michael T. Mullen[1], Wesley B. Baker[2], David Kung[3], William Tackett[1] and Christopher G. Favilla[1]**

[1] Department of Neurology, University of Pennsylvania, Philadelphia, PA, United States, [2] Department of Neurology, Children's Hospital of Philadelphia, Philadelphia, PA, United States, [3] Department of Neurosurgery, University of Pennsylvania, Philadelphia, PA, United States

Objective: Transcranial Doppler is commonly used to calculate cerebral autoregulation, but measurements are typically restricted to a single cerebral artery. In exploring topographic heterogeneity, this study reports the first thorough comparison of autoregulation in all major cerebral vessels.

Methods: In forty healthy adults, flow velocity was monitored in the anterior, middle, and posterior cerebral arteries, and synchronized with arterial blood pressure. A transfer function analysis provided characteristics of autoregulation by quantifying the relationship between blood pressure and cerebral blood flow velocity.

Results: Phase, which quantifies the time course of autoregulation, was similar in all vessels. Gain, which quantifies the magnitude of hemodynamic regulation, was lower in posterior cerebral artery, indicative of tighter regulation. However, after adjusting for baseline flow differences in each vascular territory, *normalized* gain was similar in all vessels.

Conclusions: Discriminating dynamic cerebral autoregulation between cerebrovascular territories is feasible with a transcranial doppler based approach. In the posterior cerebral artery of healthy volunteers, *absolute* flow is more tightly regulated, but *relative* flow regulation is consistent across cerebrovascular territories.

Significance: The methodology can be applied to focal disease states such as stroke or posterior reversible encephalopathy syndrome, in which the topographic distribution of autoregulation may be particularly critical.

Keywords: cerebral autoregulation, cerebral blood flow, cerebral hemodynamics, transcranial Doppler, transfer function analysis

OPEN ACCESS

Edited by:
Xiuyun Liu,
Johns Hopkins University, United States

Reviewed by:
Danilo Cardim,
University of Texas Southwestern Medical Center, United States
Stephen John Payne,
University of Oxford, United Kingdom
Jia Liu,
Chinese Academy of Sciences (CAS), China

****Correspondence:***
Christopher G. Favilla
christopher.favilla@pennmedicine.upenn.edu

Specialty section:
This article was submitted to Applied Neuroimaging, a section of the journal Frontiers in Neurology

Received: *13 January 2021*
Accepted: *25 February 2021*
Published: *23 March 2021*

Citation:
Reehal N, Cummings S, Mullen MT, Baker WB, Kung D, Tackett W and Favilla CG (2021) Differentiating Dynamic Cerebral Autoregulation Across Vascular Territories. Front. Neurol. 12:653167. doi: 10.3389/fneur.2021.653167

INTRODUCTION

Cerebral autoregulation (CA) describes the ability to maintain stable cerebral blood flow (CBF) despite fluctuations in blood pressure (BP), thus protecting the brain from hypoperfusion and hyperperfusion (1, 2). In acute stroke, subarachnoid hemorrhage, or traumatic brain injury, impaired CA contributes to secondary brain injury (3–5). CA impairment is also associated with cerebral small vessel disease and dementia (6, 7). In patients with carotid stenosis, CA impairment

predicts stroke risk and cognitive decline (8, 9). A reliable approach to CA quantification is critical to understanding the pathophysiology of multiple disease states, and holds the potential to personalize care.

CA is typically assessed in a single cerebral vessel, neglecting potential topographic heterogeneity. There are many differences between the anterior and posterior circulation, including absolute CBF (10), vascular tone (11), autonomic innervation (12), and metabolism (13). Thus, CA may vary across vascular territories, both in healthy individuals and in various disease states (14–16). Quantifying CA in different territories could improve our understanding of the pathophysiology underlying cerebrovascular disease. In focal diseases, such as stroke or posterior reversible encephalopathy syndrome (PRES), the topographic distribution of CA may be particularly critical.

Dynamic CA (dCA) is a well-studied method for quantifying and reporting autoregulatory function. By synchronizing waveforms from transcranial Doppler ultrasonography (TCD) and arterial BP, a transfer function analysis (TFA) uses a Fourier decomposition of the two waveforms to quantify the effect of spontaneous BP fluctuations on CBF (17, 18). This approach negates the need to induce a BP change with a maneuver or medication and quantifies both the dampening effect and speed of CA. Typically, TCD assessments of dCA rely on middle cerebral artery (MCA) measurements (19); however, TCD reliably differentiates intracranial vessels, thus facilitating dCA measurements in other vessels. Still, a thorough comparison of the anterior (ACA), middle (MCA), and posterior (PCA) cerebral arteries is lacking.

Thus, the current study aimed to calculate dCA parameters in the ACA, MCA, and PCA in healthy volunteers, to test the hypothesis that there are differences in dCA between the anterior circulation (ACA and MCA) and posterior circulation (PCA).

MATERIALS AND METHODS

Subjects

Forty healthy adult volunteers were enrolled in this study at the Hospital of the University of Pennsylvania between 6/21/19 and 8/8/19. Individuals were eligible if they were at least 18 years but excluded if they had a history of stroke, structural brain lesion, cervico-cerebral vascular abnormality, skull defect, or prior cranial surgery that would interfere with TCD monitoring. The protocol was approved by the University of Pennsylvania Institutional Review Board (protocol #833083). The study was conducted according to the principles expressed in the Declaration of Helsinki. Written informed consent was signed by each study participant prior to enrollment.

Hemodynamic Monitoring

Subjects were positioned in the supine position, with head-of-bed elevated to 30°. Bed position may impact cerebral hemodynamics, so the bed position was held constant for all measurements and all subjects. The room was quiet and temperature controlled (22°C). The same room and bed were used for all subjects. Cerebral blood flow velocity (CBFv) was assessed using a Spencer Technologies ST3 TCD. A 2 MHz ultrasound probe was positioned over the subject's temporal bone window and adjusted to identify the ACA, MCA, and PCA. Each vessel was confirmed using standard velocity ranges, depth, and probe positioning (20). The ultrasound probe was secured to the subjects head using a Spencer Technologies Marc 600 transducer fixation headframe. Each vessel was sequentially monitored for 5 minutes. Symmetry was assumed in this healthy population (21), so data were collected from the right hemisphere to consolidate the protocol.

A finger plethysmograph system (Finometer® Pro, Finapres Medical Systems) was secured to the wrist and third digit was used to provide a continuous non-invasive measurement of the arterial blood pressure waveform. An inflatable brachial cuff was placed on the same arm and used to calibrate the Finometer® Pro prior to data collection. Re-calibration was performed before TCD data collection for each cerebral vessel. CBFv and BP waveforms were digitized and time synchronized.

Dynamic Cerebral Autoregulation Calculation

To calculate dCA, TFA quantifies the relationship between the input signal, the arterial BP waveform, and the output signal, the CBFv waveform. Exemplar BP and CBFv waveform data from the ACA, MCA, and PCA vessels is shown in **Figure 1**. TFA was performed using a Matlab script and algorithm provided by the International Cerebral Autoregulation Research Network (CARNet: www.car-net.org), to calculate gain, normalized gain, phase, and coherence for each vessel across three frequency bands (very low frequency (VLF): 0.02 – 0.07 Hz; low frequency (LF): 0.07 – 0.2 Hz; high frequency (HF): 0.2–0.5 Hz) (18). Gain ($cm.s^{-1}.mmHg^{-1}$) quantifies the damping effect of autoregulation (lower gain indicates more effective CA). Normalized gain ($\%.mmHg^{-1}$) accounts for mean CBFv differences between ACA, MCA, and PCA by using relative changes in CBFv rather than absolute. Phase, calculated in degrees, quantifies the time delay of cerebrovascular adaptation (larger phase shift indicates more effective CA). The coherence function assesses the validity of phase and gain estimates at each frequency band.

TCD and BP data were sampled at 200Hz. During data collection, care was taken to ensure the TCD signal was strong and largely free of artifact. If the vessel insonation was interrupted, the monitoring was extended to ensure 5 minutes of artifact-free monitoring. Data are synchronized during collection, so re-alignment was not performed during post-processing. After collection, raw waveform data were manually inspected to ensure they were free of excessive noise and artifact. Data from one subject was discarded due to excessive noise and low quality TCD data. For all other subjects, because of the lack of substantial artifacts, the waveform data were analyzed and used for the TFA, rather than beat-to-beat data. Low or high-pass filtering was not performed. A 100-second window length with 50% overlap was applied during TFA. The coherence threshold is inversely proportional to the duration of data collection. Based on 5 minutes of data collection for each vessel, a coherence threshold of 0.29 was applied, which represents the

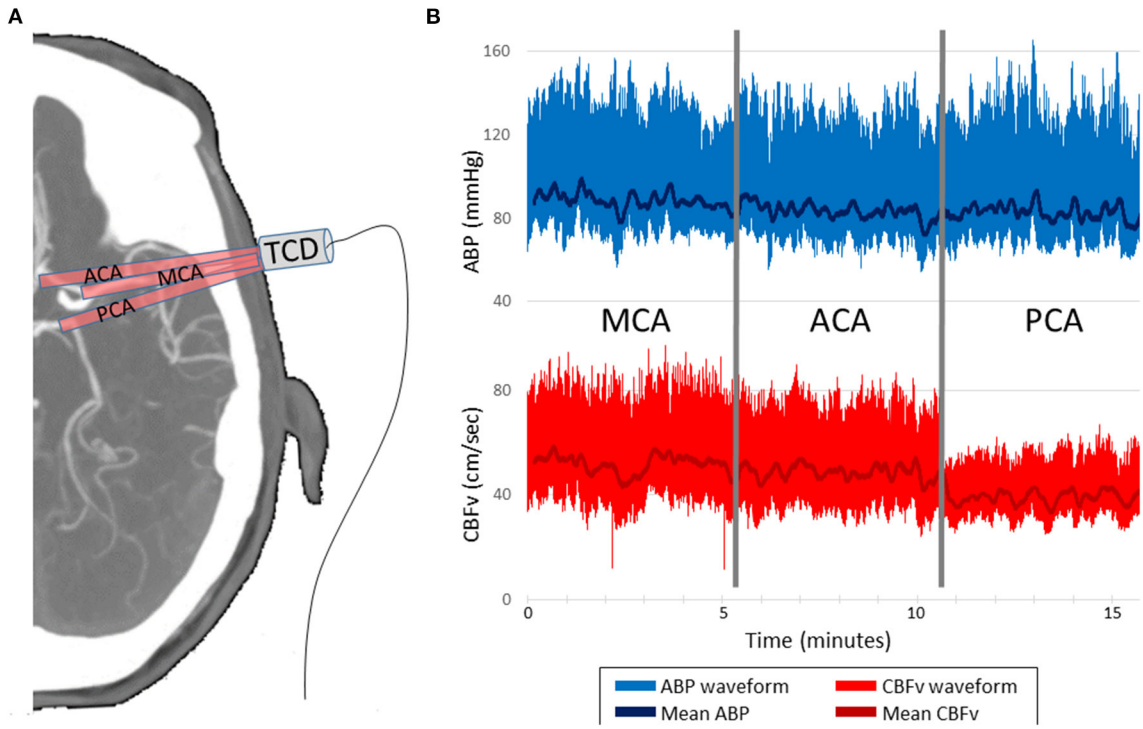

FIGURE 1 | Representative data acquisition and time-series. **(A)** TCD probe is mounted over the temporal window in order to insonate the ACA, MCA and PCA, 5 min per vessel. **(B)** CBFv is synchronized with ABP, which serves as the input for the transfer function analysis. CBFv and ABP waveforms and mean values are depicted. TCD indicates transcranial Doppler. ABP indicates finometer measured arterial blood pressure. CBFv indicates TCD measured cerebral blood flow velocity. ACA indicates anterior cerebral artery. MCA indicates middle cerebral artery. PCA indicates posterior cerebral artery.

95% confidence limit based on Monte Carlo simulation (18). If a coherence value was below the standard threshold, phase and gain values were discarded, as per the CARNet algorithm. As a result, the final analyzable sample size varied across frequency bands and vessels (**Table 1**).

Finally, for a secondary analysis, the CARNet algorithm was used to compute the spectral powers of CBFv and BP across frequency bands and vessels for the analyzable sample size. Low frequency power in hemodynamic signals have been proposed as biomarkers of neuronal activity (22, 23).

Statistical Analyses

Summary statistics are presented using means and standard deviations. For all statistical tests, a p-value of <0.05 was deemed to represent statistical significance. Phase, gain, and normalized gain values were tested for normality using Shapiro-Wilk normality test. The primary goal was to assess whether dCA varied by vascular territory. To this end, we compared phase, gain, and normalized gain between the ACA, MCA, and PCA vessels with repeated measures ANOVA, and if significance was found, a paired t-test between each group was used (i.e., ACA vs MCA, ACA vs PCA, MCA vs PCA). Analyses were repeated for each frequency band. In a secondary analysis, the same procedure was used to compare low frequency spectral powers of CBFv and BP between the ACA, MCA, and PCA vessels. All statistical analyses were performed in STATA/SE version 15.1 (StataCorp LLC, College Station, TX).

RESULTS

Forty consecutive healthy volunteers completed the study protocol. The median age was 21 years (IQR: 20–29) and 68% were female. Subject reported race was 60% Caucasian, 18% Asian, 12% African American, and 10% Other. Vascular risk factors were very uncommon: 8% of subjects had well controlled hypertension, and no subjects had a history of stroke, diabetes, hyperlipidemia, coronary artery disease, or heart failure. The monitoring protocol was well tolerated. Three subjects (8%) reported transient discomfort due to the TCD headframe, which resolved at the completion of the protocol and removal of headframe. No subjects elected to interrupt or terminate the protocol prior to completion. Data from the PCA in one subject was technically limited (waveform poorly captured) and was thus discarded. Data from all other vessels was analyzed.

CBFv and BP summary data, along with TFA results are summarized in **Table 1**. As expected, there were differences in mean CBFv between vessels. BP was stable between measurements performed on each vessel, and $<10\%$ of gain and phase values were discarded due to inadequate coherence. The resulting samples for each vessel and frequency band are

TABLE 1 | Hemodynamic data and TFA results.

	ACA	MCA	PCA	*P*-value
Mean flow velocity, cm.sec^{-1}	39.8 (16.0)	50.6 (15.4)	27.5 (13.3)	<0.0001
Mean arterial pressure, mmHg	83.5 (14.7)	85.6 (10.7)	84.2 (16.4)	0.80
VLF	*n = 34*	*n = 33*	*n = 32*	
Gain	0.41 (0.15)	0.52 (0.26)	0.31 (0.11)	0.0001
Normalized gain	0.77 (0.28)	0.81 (0.33)	0.83 (0.27)	0.69
Phase	53.4° (32.0°)	57.9° (31.4°)	55.1° (28.0°)	0.84
Coherence	0.40 (0.16)	0.37 (0.15)	0.38 (0.18)	0.77
CBFv spectral power	10.8 (6.4)	10.1 (7.1)	12.3 (7.3)	0.30
BP spectral power	8.8 (6.3)	8.8 (5.2)	9.9 (5.5)	0.67
LF	*n = 39*	*n = 39*	*n = 36*	
Gain	0.52 (0.26)	0.59 (0.24)	0.37 (0.13)	0.001
Normalized gain	0.99 (0.37)	0.93 (0.37)	1.02 (0.38)	0.56
Phase	33.1 (24.3°)	34.2 (17.7 °)	30.9 (17.8°)	0.78
Coherence	0.47 (0.20)	0.48 (0.21)	0.48 (0.21)	0.90
CBFv spectral power	9.4 (5.3)	8.3 (4.8)	8.7 (4.1)	0.66
BP spectral power	7.2 (5.1)	6.4 (3.8)	7.4 (5.3)	0.97
HF	*n = 38*	*n = 39*	*n = 35*	
Gain	0.57 (0.33)	0.61 (0.32)	0.44 (0.19)	0.03
Normalized gain	1.1 (0.53)	0.94 (0.44)	1.16 (0.55)	0.17
Phase	−2.7 (17. 3°)	3.0 (21.7°)	−8.6 (23.5°)	0.06
Coherence	0.34 (0.16)	0.40 (0.23)	0.31 (0.17)	0.15
CBFv spectral power	3.9 (2.4)	3.8 (3.2)	4.2 (2.1)	0.16
BP spectral power	2.2 (1.7)	2.7 (2.3)	2.0 (1.6)	0.53

Gain is presented as cm.s^{-1}.mmHg^{-1}.
Normalized Gain is presented as %.mmHg^{-1}.
Phase is presented as °.
BP and CBFv spectral power are presented as (mmHg)^2 and (cm/s)^2, respectively.
P-values were calculated by repeated measures one-way ANOVA.
CBFv indicates cerebral blood flow velocity.
BP indicates blood pressure.
Sample sizes vary because data were discarded if there was a failure to meet the standard coherence threshold for each frequency band in each vessel.

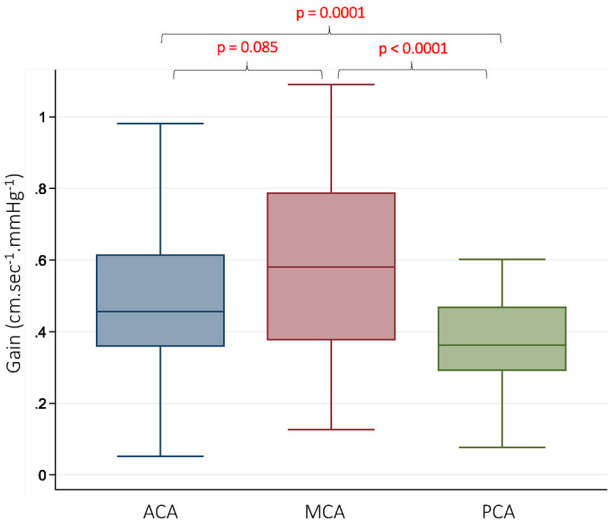

FIGURE 2 | Absolute Gain in Different Vascular Territories. Gain is presented from the low frequency band (0.07–0.2 Hz). ACA indicates anterior cerebral artery. MCA indicates middle cerebral artery. PCA indicates posterior cerebral artery. Reported *p*-values were calculated by paired *t*-tests.

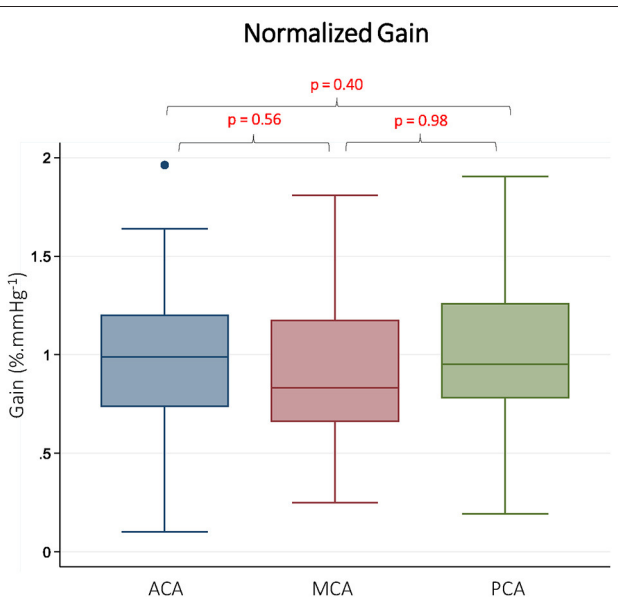

FIGURE 3 | Normalized gain in Different Vascular Territories. Normalized gain is presented from the low frequency band (0.07–0.2 Hz). ACA indicates anterior cerebral artery. MCA indicates middle cerebral artery. PCA indicates posterior cerebral artery. Reported *p*-values were calculated by paired *t*-tests.

reported in **Table 1**. The gain was different between vessels in all 3 frequency bands. In pairwise comparisons, gain was similar in the ACA and MCA, but significantly lower in the PCA. Representative data from the LF band are presented in **Figure 2**. Normalized gain, which accounts for differences in absolute CBFv, was similar across vessels (**Figure 3**). No difference between vessels was observed with respect to phase or coherence. Similarly, CBFv and BP spectral power was similar in each vessel (**Table 1**). These findings were consistent for all frequency bands.

DISCUSSION

In healthy volunteers, phase was similar in all cerebral vessels, indicating a consistent timing of the autoregulatory response. Lower gain in the posterior circulation raises the possibility of more tightly regulated CBF in this territory. However, after normalizing for differences in CBFv between vessels, this difference was no longer observed. While prior comparisons have been made between MCA and PCA in healthy and disease states (14, 15, 24–26), this study represents the first comparison across the ACA, MCA and PCA. Further, previous work comparing MCA and PCA dCA often fails to report both gain and

normalized gain across all frequency bands. The methodology we describe represents a thorough and easily reproducible protocol that can be used to quantify possible topographic heterogeneity in focal disease states such as stroke, subarachnoid hemorrhage, and PRES. Similarly, focal variant anatomy could be addressed in future work.

Anterior and Posterior Circulation

A difference between anterior and posterior circulation autoregulation is physiologically plausible, as these two territories receive different sources of flow (carotid vs vertebrobasilar system) and varying degrees of autonomic innervation (12). Results of prior studies have, however, been inconsistent. A study of young adults revealed similar MCA and PCA autoregulation (26), but greater autoregulatory properties have been reported in the cerebellar vasculature (16). It is unclear if this highlights a difference between anterior and posterior hemodynamics, or supratentorial and infratentorial hemodynamics. Rosengarten et al. observed more rapid regulation in the posterior circulation and smaller absolute changes in the posterior circulation, but this may be related to differences in baseline CBFv (14). On the other hand, Haubrich et al. observed higher gain in the PCA as compared to MCA in older adults (25). Age is an important consideration, as PCA gain may disproportionately increase with age (15). In the current study, very few older subjects were included, thus precluding a secondary age-based analysis.

Absolute and Normalized Gain

It is unclear if absolute gain ($cm.s^{-1}.mmHg^{-1}$) or normalized gain ($\%.\ mmHg^{-1}$) is more informative of autoregulatory function. Normalization is an appealing concept when comparing data from multiple subjects or multiple vessels with varying CBFv, but absolute changes in CBFv may also be physiologically relevant. For example, age has been observed to impact MCA absolute gain, but not normalized gain (27). On the other hand, patients with atrial fibrillation have higher normalized gain (LF band) than hypertensive patients, but this discrepancy is not seen in absolute gain (28). Absolute gain and normalized gain have diverging responses to changes in carbon dioxide (29). This is not to say that absolute gain is more informative than normalized gain, but rather that exclusive reporting of only relative or absolute gain may yield misleading results, thus highlighting the need for complete reporting of TFA results (18). Discrepancies may be particularly relevant in disease states, such as stroke, in which there may be large differences in CBFv.

Transfer Function Analysis

The TFA was performed over three standard frequency bands (VLF, LF, and HF). Trends in gain and phase were consistent across frequency bands. Spontaneous BP oscillations in the VLF and LF range are more likely driven by autonomic vascular tone, less confounded by the cardiac or respiratory cycle (30). Many investigators therefore focus on LF and/or VLF bands, but this leads to inconsistent reporting of dCA result in the literature (31). With increasing frequency, BP oscillations may also be modulated by cardiac and respiratory variables, thus complicating the interpretation of the BP-CBF relationship. Complete reporting of frequency bands, regardless of the interpretation, is critical to transparency and reproducibility (18). To that end, this study utilized a standardized TFA script and algorithm that is available through CARNet (www.car-net.org).

Finally, low-frequency spectral powers of hemodynamic signals have been proposed as biomarkers of neurovascular coupling and neural activity (22, 23). Originally developed for functional magnetic resonance imaging (fMRI) (23), a more recent paper used TCD to measure low-frequency power in CBFv signals in post cardiac arrest patients, in which a difference in spectral power was observed between survivors and non-survivors (32). The measured low-frequency spectral powers of hemodynamic signals reported herein in **Table 1** can be used to power future studies involving these biomarkers.

Limitations

There are limitations to this study. TCD data was collected unilaterally to optimize quality, assuming symmetry in this young, healthy cohort. Bilateral comparison could be particularly important in older subjects or focal disease states. TCD also provides a measure of CBFv rather than CBF. These two terms are proportional assuming the vessel trunk remains stable, which is a reasonable assumption during a brief study conducted at rest. The young age of the cohort limits the external validity when considering subjects of older age or with vascular risk factors. However, the objective was not to draw broad conclusions, but rather to report results for young, healthy adults and highlight a reproducible methodology that can easily be applied to additional populations in future work. A range of ages could be explored in a future healthy volunteer study before applying this protocol to older patient populations. Partial pressure of CO_2 impacts vascular tone and CBF, so it may confound our results, though it was assumed that during the monitoring period (15 min at rest), CO_2 remained stable, which has been the case in multiple prior studies (33). End-tidal CO_2 could be monitored in future work to ensure there is no confounding. Variant anatomy (e.g., fetal PCA) may impact hemodynamics, but cannot be accounted for in the current study because subjects do not have vessel imaging for review. Variant anatomy could be specifically considered in future work. The TFA methodology is somewhat limited by the assumption that CA is a linear control system. Nonetheless, it is a well-accepted approach to CA quantification.

CONCLUSION

Discriminating dynamic cerebral autoregulation between cerebrovascular territories is feasible with a TCD-based approach. In healthy young adults, the time delay of autoregulation is consistent across territories, but the magnitude of hemodynamic regulation is more tightly regulated in the posterior circulation. Importantly, typical flow velocities are

lower in the posterior circulation, so when considering percent hemodynamic changes, rather than absolute, no differences are observed between territories. Both absolute and normalized metrics contribute to the understanding of cerebrovascular physiology. The methodology described here can be easily reproduced and deployed to explore topographic characteristics of autoregulation in multiple disease states, in particular focal disease such as stroke.

DATA AVAILABILITY STATEMENT

The raw data supporting the conclusions of this article will be made available by the authors, without undue reservation.

ETHICS STATEMENT

The studies involving human participants were reviewed and approved by the University of Pennsylvania Institutional Review Board. The patients/participants provided their written informed consent to participate in this study.

AUTHOR CONTRIBUTIONS

NR performed data collection, and assisted in the data analysis, and contributed to manuscript preparation. SC assisted with data collection and contributed to manuscript preparation. MM assisted with study design, assisted with analysis, and contributed to manuscript preparation. WB assisted with data analysis and contributed to manuscript preparation. DK assisted with study design and contributed to manuscript preparation. WT assisted with data analysis and contributed to manuscript preparation. CF provided overall study design, assisted with data collection, performed primary analysis, and contributed to manuscript preparation. All authors contributed to the article and approved the submitted version.

FUNDING

This work was supported by National Institutes of Health Grant K23 NS110993 (CF); American Heart Association Grant 19CDA34630033 (CF); and The Thomas B. and Jeannette E. Laws McCabe Fund (CF).

REFERENCES

1. Aaslid R, Lindegaard KF, Sorteberg W, Nornes H. Cerebral autoregulation dynamics in humans. *Stroke.* (1989) 20:45–52.
2. Lassen NA. Autoregulation of cerebral blood flow. *Circ Res.* (1964) 15(Suppl):201–4.
3. Budohoski KP, Czosnyka M, Smielewski P, Kasprowicz M, Helmy A, Bulters D, et al. Impairment of cerebral autoregulation predicts delayed cerebral ischemia after subarachnoid hemorrhage: a prospective observational study. *Stroke.* (2012) 43:3230–7. doi: 10.1161/strokeaha.112.669788
4. Castro P, Azevedo E, Sorond F. Cerebral Autoregulation in Stroke. *Curr Atheroscler Rep.* (2018) 20:37. doi: 10.1007/s11883-018-0739-5
5. Radolovich DK, Aries MJ, Castellani G, Corona A, Lavinio A, Smielewski P, et al. Pulsatile intracranial pressure and cerebral autoregulation after traumatic brain injury. *Neurocrit Care.* (2011) 15:379–86. doi: 10.1007/s12028-011-9553-4
6. Guo ZN, Xing Y, Wang S, Ma H, Liu J, Yang Y. Characteristics of dynamic cerebral autoregulation in cerebral small vessel disease: Diffuse and sustained. *Sci Rep.* (2015) 5:15269. doi: 10.1038/srep15269
7. Claassen JA, Diaz-Arrastia R, Martin-Cook K, Levine BD, Zhang R. Altered cerebral hemodynamics in early Alzheimer disease: a pilot study using transcranial Doppler. *J Alzheimers Dis.* (2009) 17:621–9. doi: 10.3233/JAD-2009-1079
8. Reinhard M, Gerds TA, Grabiak D, Zimmermann PR, Roth M, Guschlbauer B, et al. Cerebral dysautoregulation and the risk of ischemic events in occlusive carotid artery disease. *J Neurol.* (2008) 255:1182–9. doi: 10.1007/s00415-008-0865-z
9. Silvestrini M, Paolino I, Vernieri F, Pedone C, Baruffaldi R, Gobbi B, et al. Cerebral hemodynamics and cognitive performance in patients with asymptomatic carotid stenosis. *Neurology.* (2009) 72:1062–8. doi: 10.1212/01.wnl.0000345015.35520.52
10. Zhao M, Amin-Hanjani S, Ruland S, Curcio AP, Ostergren L, Charbel FT. Regional cerebral blood flow using quantitative MR angiography. *AJNR Am J Neuroradiol.* (2007) 28:1470–3. doi: 10.3174/ajnr.A0582
11. Ito H, Yokoyama I, Iida H, Kinoshita T, Hatazawa J, Shimosegawa E, et al. Regional differences in cerebral vascular response to PaCO2 changes in humans measured by positron emission tomography. *J Cereb Blood Flow Metab.* (2000) 20:1264–70. doi: 10.1097/00004647-200008000-00011
12. Roloff EV, Tomiak-Baquero AM, Kasparov S, Paton JF. Parasympathetic innervation of vertebrobasilar arteries: is this a potential clinical target? *J Physiol.* (2016) 594:6463–85. doi: 10.1113/JP272450
13. Mazzilotta JC, Phelps ME, Miller J, Kuhl DE. Tomographic mapping of human cerebral metabolism: normal unstimulated state. *Neurology.* (1981) 31:503–16. doi: 10.1212/wnl.31.5.503
14. Rosengarten B, Kaps M. Cerebral autoregulation in middle cerebral artery territory precedes that of posterior cerebral artery in human cortex. *Cerebrovasc Dis.* (2002) 13:21–5. doi: 10.1159/000047741
15. Sorond FA, Khavari R, Serrador JM, Lipsitz LA. Regional cerebral autoregulation during orthostatic stress: age-related differences. *J Gerontol A Biol Sci Med Sci.* (2005) 60:1484–7. doi: 10.1093/gerona/60.11.1484
16. Reinhard M, Waldkircher Z, Timmer J, Weiller C, Hetzel A. Cerebellar autoregulation dynamics in humans. *J Cereb Blood Flow Metab.* (2008) 28:1605–12. doi: 10.1038/jcbfm.2008.48
17. van Beek AH, Claassen JA, Rikkert MG, Jansen RW. Cerebral autoregulation: an overview of current concepts and methodology with special focus on the elderly. *J Cereb Blood Flow Metab.* (2008) 28:1071–85. doi: 10.1038/jcbfm.2008.13
18. Claassen JA, Meel-van den Abeelen AS, Simpson DM, Panerai RB, international Cerebral Autoregulation Research N. Transfer function analysis of dynamic cerebral autoregulation: A white paper from the International Cerebral Autoregulation Research Network. *J Cereb Blood Flow Metab.* (2016) 36:665–80. doi: 10.1177/0271678X15626425
19. Intharakham K, Beishon L, Panerai RB, Haunton VJ, Robinson TG. Assessment of cerebral autoregulation in stroke: A systematic review and meta-analysis of studies at rest. *J Cereb Blood Flow Metab.* (2019) 39:2105–16. doi: 10.1177/0271678X19871013
20. Alexandrov AV, Sloan MA, Wong LK, Douville C, Razumovsky AY, Koroshetz WJ, et al. Practice standards for transcranial Doppler ultrasound: part I–test performance. *J Neuroimaging.* (2007) 17:11–8. doi: 10.1111/j.1552-6569.2006.00088.x
21. Schmidt EA, Piechnik SK, Smielewski P, Raabe A, Matta BF, Czosnyka M. Symmetry of cerebral hemodynamic indices derived from bilateral transcranial Doppler. *J Neuroimaging.* (2003) 13:248–54.
22. Garrett DD, Kovacevic N, McIntosh AR, Grady CL. Blood oxygen level-dependent signal variability is more than just noise. *J Neurosci.* (2010) 30:4914–21. doi: 10.1523/JNEUROSCI.5166-09.2010

23. Zang YF, He Y, Zhu CZ, Cao QJ, Sui MQ, Liang M, et al. Altered baseline brain activity in children with ADHD revealed by resting-state functional MRI. *Brain Dev.* (2007) 29:83–91. doi: 10.1016/j.braindev.2006.07.002
24. Reinhard M, Lorenz L, Sommerlade L, Allignol A, Urbach H, Weiller C, et al. Impaired dynamic cerebral autoregulation in patients with cerebral amyloid angiopathy. *Brain Res.* (2019) 1717:60–5. doi: 10.1016/j.brainres.2019.04.014
25. Haubrich C, Wendt A, Diehl RR, Klotzsch C. Dynamic autoregulation testing in the posterior cerebral artery. *Stroke.* (2004) 35:848–52. doi: 10.1161/01.STR.0000120729.99039.B6
26. Washio T, Watanabe H, Ogoh S. Dynamic cerebral autoregulation in anterior and posterior cerebral circulation during cold pressor test. *J Physiol Sci.* (2020) 70:1. doi: 10.1186/s12576-020-00732-7
27. Oudegeest-Sander MH, van Beek AH, Abbink K, Olde Rikkert MG, Hopman MT, Claassen JA. Assessment of dynamic cerebral autoregulation and cerebrovascular CO2 reactivity in ageing by measurements of cerebral blood flow and cortical oxygenation. *Exp Physiol.* (2014) 99:586–98. doi: 10.1113/expphysiol.2013.076455
28. Junejo RT, Braz ID, Lucas SJ, van Lieshout JJ, Phillips AA, Lip GY, et al. Neurovascular coupling and cerebral autoregulation in atrial fibrillation. *J Cereb Blood Flow Metab.* (2019) 40:1647–57. doi: 10.1177/0271678X19870770
29. Tzeng YC, Ainslie PN, Cooke WH, Peebles KC, Willie CK, MacRae BA, et al. Assessment of cerebral autoregulation: the quandary of quantification. *Am J Physiol Heart Circ Physiol.* (2012) 303:H658–71. doi: 10.1152/ajpheart.00328.2012
30. Julien C. The enigma of Mayer waves: Facts and models. *Cardiovasc Res.* (2006) 70:12–21. doi: 10.1016/j.cardiores.2005.11.008
31. Meel-van den Abeelen AS, van Beek AH, Slump CH, Panerai RB, Claassen JA. Transfer function analysis for the assessment of cerebral autoregulation using spontaneous oscillations in blood pressure and cerebral blood flow. *Med Eng Phys.* (2014) 36:563–75. doi: 10.1016/j.medengphy.2014.02.001
32. van den Brule JM, Vinke EJ, van Loon LM, van der Hoeven JG, Hoedemaekers CW. Low spontaneous variability in cerebral blood flow velocity in non-survivors after cardiac arrest. *Resuscitation.* (2017) 111:110–5. doi: 10.1016/j.resuscitation.2016.12.005
33. Eames PJ, Blake MJ, Dawson SL, Panerai RB, Potter JF. Dynamic cerebral autoregulation and beat to beat blood pressure control are impaired in acute ischaemic stroke. *J Neurol Neurosurg Psychiatry.* (2002) 72:467–72. doi: 10.1136/jnnp.72.4.467

Conflict of Interest: The authors declare that the research was conducted in the absence of any commercial or financial relationships that could be construed as a potential conflict of interest.

frontiers in Neurology

ORIGINAL RESEARCH
published: 13 April 2021
doi: 10.3389/fneur.2021.659890

Retinal Vessel Responses to Flicker Stimulation Are Impaired in $Ca_V2.3$-Deficient Mice—An *in-vivo* Evaluation Using Retinal Vessel Analysis (RVA)

*Felix Neumaier[1,2,3], Konstantin Kotliar[4], Roel Hubert Louis Haeren[5], Yasin Temel[5], Jan Niklas Lüke[6], Osama Seyam[4], Ute Lindauer[1,7], Hans Clusmann[1], Jürgen Hescheler[6], Gerrit Alexander Schubert[1], Toni Schneider[6] and Walid Albanna[1,6]**

[1] Department of Neurosurgery, RWTH Aachen University, Aachen, Germany, [2] Forschungszentrum Jülich GmbH, Institute of Neuroscience and Medicine, Nuclear Chemistry (INM-5), Jülich, Germany, [3] Institute of Radiochemistry and Experimental Molecular Imaging, Faculty of Medicine and University Hospital Cologne, University of Cologne, Cologne, Germany, [4] Department of Medical Engineering and Technomathematics, FH Aachen University of Applied Sciences, Aachen, Germany, [5] Department of Neurosurgery, Maastricht University Medical Center, Maastricht, Netherlands, [6] Institute for Neurophysiology, University of Cologne, Cologne, Germany, [7] Tranlational Neurosurgery and Neurobiology, RWTH Aachen University, Aachen, Germany

OPEN ACCESS

Edited by:
Chiara Robba,
University of Genoa, Italy

Reviewed by:
Eszter Farkas,
University of Szeged, Hungary
Cátia F. Lourenço,
University of Coimbra, Portugal

***Correspondence:**
Walid Albanna
walidalbanna@yahoo.de

Specialty section:
This article was submitted to Applied Neuroimaging, a section of the journal Frontiers in Neurology

Received: 28 January 2021
Accepted: 17 March 2021
Published: 13 April 2021

Citation:
Neumaier F, Kotliar K, Haeren RHL, Temel Y, Lüke JN, Seyam O, Lindauer U, Clusmann H, Hescheler J, Schubert GA, Schneider T and Albanna W (2021) Retinal Vessel Responses to Flicker Stimulation Are Impaired in $Ca_v2.3$-Deficient Mice—An in-vivo Evaluation Using Retinal Vessel Analysis (RVA). Front. Neurol. 12:659890. doi: 10.3389/fneur.2021.659890

Objective: Metabolic demand increases with neuronal activity and adequate energy supply is ensured by neurovascular coupling (NVC). Impairments of NVC have been reported in the context of several diseases and may correlate with disease severity and outcome. Voltage-gated Ca^{2+}-channels (VGCCs) are involved in the regulation of vasomotor tone. In the present study, we compared arterial and venous responses to flicker stimulation in $Ca_v2.3$-competent ($Ca_v2.3_{[+/+]}$) and -deficient ($Ca_v2.3_{[-/-]}$) mice using retinal vessel analysis.

Methods: The mice were anesthetized and the pupil of one eye was dilated by application of a mydriaticum. An adapted prototype of retinal vessel analyzer was used to perform dynamic retinal vessel analysis. Arterial and venous responses were quantified in terms of the area under the curve (AUC_{art}/AUC_{ven}) during flicker application, mean maximum dilation (mMD_{art}/mMD_{ven}) and time to maximum dilation (tMD_{art}/tMD_{ven}) during the flicker, dilation at flicker cessation (DFC_{art}/DFC_{ven}), mean maximum constriction (mMC_{art}/mMC_{ven}), time to maximum constriction (tMC_{art}/tMC_{ven}) after the flicker and reactive magnitude (RM_{art}/RM_{ven}).

Results: A total of 33 retinal scans were conducted in 22 $Ca_v2.3_{[+/+]}$ and 11 $Ca_v2.3_{[-/-]}$ mice. $Ca_v2.3_{[-/-]}$ mice were characterized by attenuated and partially reversed arterial and venous responses, as reflected in significantly lower AUC_{art} ($p = 0.031$) and AUC_{ven} ($p = 0.047$), a trend toward reduced DFC_{art} ($p = 0.100$), DFC_{ven} ($p = 0.100$), mMD_{ven} ($p = 0.075$), and RM_{art} ($p = 0.090$) and a trend toward increased tMD_{art} ($p = 0.096$).

Conclusion: To our knowledge, this is the first study using a novel, non-invasive analysis technique to document impairment of retinal vessel responses in VGCC-deficient mice. We propose that $Ca_v2.3$ channels could be involved in NVC and may contribute to the impairment of vasomotor responses under pathophysiological conditions.

Keywords: *in vivo* retinal vessel analysis, neurovascular coupling, voltage- gated Ca^{2+} channels, dynamic retinal vessel analysis, $Ca_v2.3$-deficient mice

INTRODUCTION

As brain tissue lacks significant energy reserves, proper global cerebral blood flow is critical for a constant supply of metabolic substrates, which is achieved through cerebral autoregulation, metabolic feedback mechanisms, and input from the autonomic nervous system (1). Much less is known about the exact mechanisms underlying neurovascular coupling (NVC), which mediates continuous adjustment of local cerebral blood flow to dynamic and regionally heterogeneous changes in neuronal activity and thus metabolic demand. NVC is accomplished by the so-called neurovascular unit (NVU), a subsumption of cell types with intimate anatomical and chemical relationship that comprises neuronal, glial, endothelial and vascular cells (2–5). Although still poorly understood, NVU function is increasingly recognized to be a complex multidimensional process that involves mediators released from the different cell types, which engage parallel signaling pathways across the entire cerebrovascular network (6, 7). In addition, there is strong evidence that dysfunctional signaling within the NVU (8) and in some cases even inversion of NVC (9) are involved in delayed cerebral ischemia and secondary brain damage after ischemic or hemorrhagic brain injury [reviewed in Guo and Lo (10)]. Voltage-gated Ca^{2+}-channels (VGCCs) are critical for Ca^{2+} influx into all types of cells in the NVU and almost certainly involved in NVC under physiological and pathophysiological conditions (11, 12). L-type VGCCs have traditionally been regarded as the main pathway for Ca^{2+} entry into vascular smooth muscle cells (11) and they remain the only approved target for prevention of cerebral vasospasm after subarachnoid hemorrhage by the Ca^{2+} channel antagonist nimodipine (13). However, while L-type channels predominate in large caliber proximal vessels, there is growing evidence for a role of non-L-type VGCCs in smaller diameter resistance vessels (11, 14, 15). Their exact identity and functional relevance remains controversial, which may reflect the existence of significant heterogeneity among different vascular beds, pathophysiological changes in the functional expression of different channels and/or the expression of these channels in other cell types of the NVU (11, 12). In addition, interpretation of experimental results on NVU function is complicated by the fact that many results from *in vitro* studies appear to be inconsistent (7), highlighting the importance of non-invasive *in vivo* approaches for valid studies on the mechanisms underlying NVC. One such approach is to analyze vascular responses in the retina, which is an embryological part of the central nervous system that can be assessed non-invasively, so that it provides a unique "window to the brain." Retinal vessel analysis (RVA) has been used in a number of clinical studies to assess microvascular responsiveness and to show that NVC is altered after ischemic or hemorrhagic stroke (16–18). In a previous, proof-of-principle study, we showed that RVA is also a feasible method for non-invasive assessment of vessel responses in the murine retina (19). In the present work, we used the same adapted prototype of a non-contact retinal vessel analyzer to investigate how genetic ablation of $Ca_v2.3$ voltage-gated calcium channels affects arterial and venous retinal responses in mice. These channels have previously been implicated in delayed cerebral vasospasm and impaired NVC after subarachnoid hemorrhage (20), but their exact role for microvascular function remains to be elucidated. Our results suggest that $Ca_v2.3$ channel dysfunction could be associated with altered NVC in the murine retina and demonstrate how RVA can be used for non-invasive *in vivo* studies on NVC in small animal models.

Abbreviations: AUC, area under the curve; AUC_{art}, arterial area under the curve during the flicker; AUC_{ven}, venous area under the curve during the flicker; DFC_{art}, arterial dilation at flicker cessation; DFC_{ven}, venous dilation at flicker cessation; DVA, dynamic vessel analyzer; ERG, electroretinographic; mMC_{art}, mean maximal arterial constriction after flicker cessation; mMC_{ven}, mean maximal venous constriction after flicker cessation; mMD_{art}, mean maximal arterial dilation in response to the flicker; mMD_{ven}, mean maximal venous dilation in response to the flicker; MU, arbitrary measuring units; NVC, neurovascular coupling; NVU, neurovascular unit; ONH, optic nerve head; RM_{art}, arterial reactive magnitude; RM_{ven}, venous reactive magnitude; RVA, retinal vessel analysis; SAH, subarachnoid hemorrhage; tMC_{art}, time to maximal arterial constriction after flicker cessation; tMC_{ven}, time to maximal venous constriction after flicker cessation; tMD_{art}, time to maximal arterial dilation during the flicker; tMD_{ven}, time to maximal venous dilation during the flicker; VGCCs, voltage-gated calcium channels.

MATERIALS AND METHODS

Animals

A total of 22 $Ca_v2.3$-competent ($Ca_v2.3_{[+/+]}$) and 11 $Ca_v2.3$-deficient ($Ca_v2.3_{[-/-]}$) male mice, aged 12–15 weeks, were used in the present study. Mice were housed in Makrolon type II cages at a constant temperature (20–22°C) with light on from 7 a.m. to 7 p.m. (light intensity at the surface of the animal cages was 5–10 lux) and *ad libitum* access to food and water. $Ca_v2.3_{[-/-]}$ mice were generated through deletion of exon 2 by Cre-mediated recombination (21). They are available from Mutant Mouse Resource and Research Centers (MMRRC) with the strain name B6J.129P2(Cg)-Cacna1etm1.1Tsch/Mmjax. Parallel breeding of parental inbred mouse lines of $Ca_v2.3_{[-/-]}$ and $Ca_v2.3_{[+/+]}$ mice ensured that they had the same mixed genetic background (C57Bl/6 × 129SvJ). The institutional

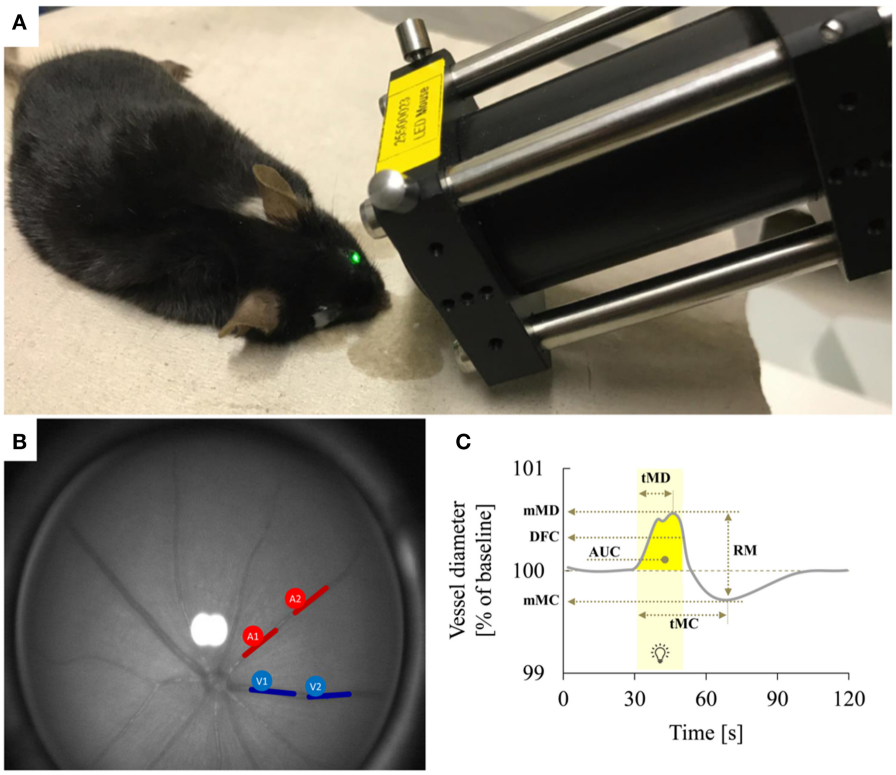

FIGURE 1 | Dynamic retinal vessel analysis. **(A)** Experimental setup showing the murine retinal vessel analyzer (RCrodent, IMEDOS Systems UG, Jena, Germany) in operation. **(B)** Murine retina as assessed with the retinal vessel analyzer. Proximal and distal arterial (A1 and A2) and venous (V1 and V2) segments are marked in red and blue, respectively, as described in detail in text. **(C)** Idealized representation of a retinal vessel response to flicker stimulation with the different parameters determined in the present study. The stimulation period is indicated by light yellow shading. Parameters used for quantification of the response comprised mean maximum dilation during the flicker (mMD), time to maximum dilation (tMD) relative to flicker initiation, dilation at flicker cessation (DFC), mean maximum constriction after the flicker (mMC), time to maximum constriction (tMC) relative to flicker initiation, the area under the curve (AUC) during the flicker (indicated by dark yellow shading) and the reactive magnitude (RM), determined as the difference between mean maximum dilation during the flicker and mean maximum constriction after the flicker. For additional information on these parameters see **Table 1**.

and governmental committees on animal care [Landesamt für Natur, Umwelt und Verbraucherschutz [LANUV] Nordrhein—Westfalen, Recklinghausen, Germany; 84-02.04.2016.A4555] approved all experiments described in the text, which were conducted in accordance with accepted standards of humane animal care, as reported in the UFAW handbook on the care and management of laboratory animals.

RCrodent Vessels Analysis

The device used for vessel analysis was an adapted prototype of the Dynamic Vessel Analyzer (DVA) (RCrodent, IMEDOS Systems UG, Jena, Germany) previously used for other preclinical and clinical applications (22), which enables murine retinal vessel analysis as a function of time by applying flicker light impulses at defined frequencies like also reported in rats (23) (**Figures 1A,B**). Prior to the experiments, mice were dark-adapted overnight (12 h), anesthetized by intraperitoneal injection of ketamine (66.7 mg/kg body weight; Ketanest, Parke-Davis/Pfizer, Berlin, Germany) and xylazine (6.7 mg/kg body weight, Rompun 2% Bayer Vital, Leverkusen, Germany) and positioned on a heating plate to maintain a constant body temperature of 37°C. The left eye was then dilated by application of a mydriatic agent (Tropicamide, Mydriaticum Stulln UD, Pharma Stulln GmbH, Stulln, Germany) and equipped with a dedicated polymethylmethacrylate mouse contact lens (Back Optic Zone Radius 1.7 mm, diameter 3.2 mm, zero dioptric from Cantor & Nissel, Brackley, UK) to protect the cornea. For the measurements, we used a light intensity of 30 lux and the standard 350 s measurement protocol by IMEDOS Systems for human studies (24). After baseline assessment for 50 s, measurements were performed by application of three consecutive cycles of monochromatic rectangular flicker stimulation (530 nm, 12.5 Hz, 20 s). To assess retinal vessel diameters, we used the standard protocol and application mode of the DVA, where the fundus is illuminated during the whole measurement and the illumination light is diminished during the flicker stimulation with an application frequency of 12.5 Hz (19). This mode differs from alternative paradigms of visual stimulation in murine studies, where the application of light or other visual stimuli is preceded and followed by a measurement with no illumination (25).

TABLE 1 | Definition of dynamic retinal vessel analysis parameters.

Parameter	Unit	Meaning
Arterial/Venous area under the curve during the flicker (AUC_{art}/AUC_{ven})	%*s	Area under the response curve during the 20 s flicker stimulation
Mean maximal arterial/venous dilation in response to the flicker (mMD_{art}/mMD_{ven})	% of baseline	Absolute maximum of the response to flicker stimulation
Time to maximal arterial/venous dilation during the flicker (tMD_{art}/tMD_{ven})	s	Time between flicker initiation and the absolute maximum response during the flicker
Arterial/venous dilation at flicker cessation (DFC_{art}/DFC_{ven})	% of baseline	Value of the response at the end of flicker stimulation
Mean maximal arterial/venous constriction after flicker cessation (mMC_{art}/mMC_{ven})	% of baseline	Absolute minimum of the response curve after flicker cessation
Time to maximal arterial/venous constriction after flicker cessation (tMC_{art}/tMC_{ven})	s	Time between flicker initiation and the absolute minimum response after flicker cessation
Arterial/venous reactive magnitude (RM_{art}/RM_{ven})	% of baseline	Difference between mean maximal dilation during the flicker and mean maximal constriction after flicker cessation

Retinal arteries and veins were selected arbitrarily for RVA assessment in the murine fundus. In order to improve signal-to-noise ratio of the assessment, each vessel type of a mouse was attempted to be measured in two locations: proximal and distal to the optic nerve head (ONH) (proximal: >0.3 and <2.5 ONH plexus diameters from the ONH plexus rim, distal: > 2.5 and < 5 ONH plexus diameters) as illustrated in **Figure 1B**. The individual retinal vessel parameters (**Table 1**) were then determined by taking the mean values from these proximal and distal measurements. This approach succeeded in 6/11 venous and 3/11 arterial vessels of $Ca_v2.3_{[-/-]}$ mice and in 18/22 venous and 6/22 arterial vessels of $Ca_v2.3_{[+/+]}$ mice. In the remaining cases, only one segment of each vessel type located in the area between 0.3 and 5 ONH plexus diameters from the rim could be assessed per animal.

In addition to the automated analysis performed by the commercial DVA software, further parameters of dynamic vascular response were derived and analyzed as described previously (26) using a template-set with macros (Microsoft Office Excel 2016, Californian, USA) to filter, process, and analyze numerical data from the original DVA-assessment (26, 27). Briefly, absolute vessel diameters within the retina were gauged by arbitrary measuring units (MU), where 1 MU corresponds to roughly 1 µm in the mouse eye. The conversion from the imaging system was adjusted to the size of the charge-coupled device (CCD) matrix and was calculated based on the size of a theoretical standard eye. For comparison of flicker responses between different animals, relative changes in vessel diameters were calculated in % of the individual baselines. To improve the signal-to-noise ratio for manual analysis, the three response curves obtained for each animal (30 s of baseline before flicker application, 20 s during flicker application and 80 s after flicker application) were averaged and smoothed using a running median with a time-window of 4 s and the corresponding back shift. The resulting curves were used to determine the parameters indicated in **Figure 1C** and **Table 1**.

Average time courses of vessel diameter changes in a given group were calculated according to a technique described previously (26, 28), where each time point of the average curve for the group is the median of all individual (relative) vessel diameters at this time point. The quality of DVA recordings was assessed semi-objectively using the cumulative scoring method described previously (27). The score ranged from 0 ("inadequate") to 5 ("excellent quality") and only DVA recordings with score values ≥ 2.0 were included in the analysis.

Statistical Analysis

Unless noted otherwise, all data are shown as median [1st quartile−3rd quartile]. Statistical comparisons with the Mann-Whitney-U-test were carried out in an explorative manner without correction for multiple comparisons in order to show tendencies and to identify potential differences for further investigation. Statistical significance was set at $p < 0.05$ and statistical results with $p \leq 0.1$ were considered as trend. All analyses and data presentation were performed with Excel (Microsoft Office Excel 2016, Californian, USA), SPSS v. 21 (IBM Chicago, Illinois, USA), and GraphPad Software (GraphPad Prism, Inc., La Jolla, USA). Boxplots show median values, 1st quartile and 3rd quartile (box), minimum and maximum values (whiskers), and individual data points (dots). Outliers were identified based on the definition by Turkey, where values below [1st quartile−1.5 * interquartile range (IQR)] or above [3rd quartile + 1.5 * IQR] are considered suspected outliers and values below [1st quartile−3 * IQR] or above [3rd quartile + 3 * IQR] are considered outliers.

RESULTS

The median body weight was 28.0 g (27.3 to 30.0 g) for $Ca_v2.3_{[+/+]}$ and 25.0 g (25.0 to 25.5 g) for $Ca_v2.3_{[-/-]}$ mice ($p = 0.001$).

The response characteristics and values of the retinal vessel analysis parameters in the two genotypes are summarized in **Tables 2**, **3**. The quality of the data was similar in both groups and sufficiently high for a comparative analysis (**Figure 2A**). There was no significant difference in median arterial [$Ca_v2.3_{[+/+]}$: 40.9

TABLE 2 | Response characteristics of retinal veins and arteries in $Ca_v2.3_{[+/+]}$ and $Ca_v2.3_{[-/-]}$ mice.

Response to flicker stimulation	$Ca_v2.3_{[+/+]}$ n (%)	$Ca_v2.3_{[-/-]}$ n (%)	*p*-value
Veins			**0.028**
No response	1 (5%)	3 (27%)	
Vasoconstriction	3 (14%)	4 (36%)	
Vasodilation	18 (82%)	4 (36%)	
All	22 (100%)	11 (100%)	
Arteries			**0.008**
No response	5 (23%)	0 (0%)	
Vasoconstriction	3 (14%)	7 (64%)	
Vasodilation	14 (64%)	4 (36%)	
All	22 (100%)	11 (100%)	

Bold values indicate p ≤ 0.1.

MU vs. $Ca_v2.3_{[-/-]}$: 43.9 MU, $p = 0.202$] or venous [$Ca_v2.3_{[+/+]}$: 55.5 MU vs. $Ca_v2.3_{[-/-]}$: 61.9 MU, $p = 0.285$] diameter between the two genotypes, although the values tended to be slightly higher in $Ca_v2.3_{[-/-]}$ mice (**Figure 2B**). As a measure for the retinal vascular density in both genotypes, we also calculated the overall number of vessels leaving the ONH in the murine fundus, which amounted to 10.0 (9.5 to 11.0) in $Ca_v2.3_{[+/+]}$ and 10.0 (10.0 to 10.0) in $Ca_v2.3_{[-/-]}$ mice ($p = 0.486$). Likewise, no difference was detected in the proportion of cases where one or more vessels branched in the near periphery to the ONH, which amounted to 86% in $Ca_v2.3_{[+/+]}$ compared to 82% in $Ca_v2.3_{[-/-]}$ mice ($p = 0.630$).

Figure 3 shows three representative examples of retinal arterial and venous reactions to monochromatic flickering light recorded in $Ca_v2.3_{[+/+]}$ (**Figure 3A**) or $Ca_v2.3_{[-/-]}$ (**Figure 3B**) mice. Venous responses could be recorded in all 22 $Ca_v2.3_{[+/+]}$ and 11 $Ca_v2.3_{[-/-]}$ mice included in the present study, while recording of arterial responses was technically feasible in 15 of the $Ca_v2.3_{[+/+]}$ and 10 of the $Ca_v2.3_{[-/-]}$ mice. Based on the venous area under the curve (AUC_{ven}), flicker stimulation evoked venous vasodilation (AUC_{ven} >2.5%*s), venous vasoconstriction (AUC_{ven} <-2.5%*s) or no response (−2.5<AUC_{ven} <2.5%*s) in 18 (82%), 3 (14%), or 1 (5%) of the $Ca_v2.3_{[+/+]}$ and 4 (36%), 4 (36%), or 3 (27%) of the $Ca_v2.3_{[-/-]}$ mice ($p = 0.028$, **Table 2**). In the arterial compartment, vasodilation, vasoconstriction or no response were observed in 14 (64%), 3 (14%) or 5 (23%) of the $Ca_v2.3_{[+/+]}$ and 4 (36%), 7 (64%), or 0 (0%) of the $Ca_v2.3_{[-/-]}$ mice ($p = 0.008$, **Table 2**). A comparison of average arterial and venous responses in the two genotypes is provided in **Figure 4**. Consistent with the results of our previous proof-of-principle study, retinal vessel responses in normal ($Ca_v2.3_{[+/+]}$) mice were smaller in magnitude than the corresponding responses observed in human subjects (17, 18, 26) but showed a similar biphasic shape with vasodilation during the flicker followed by vasoconstriction and gradual return to baseline or to a new steady-state after flicker cessation (**Figure 4A**).

On average, vessel dilation during the flicker was slower but more pronounced in the venous compartment, whereas vessel constriction after flicker cessation was stronger in the arterial compartment (**Figure 4A**). In addition, retinal vessel responses to flicker stimulation in both vascular compartments were altered in $Ca_v2.3$-deficient mice (**Figure 4B**), as described in more detail in the following sections.

Differences in Venous Responses to Flicker Stimulation

A comparison of average venous responses to flicker light measured in the two genotypes is provided in **Figure 5A**. Genetic ablation of $Ca_v2.3$ channels was associated with a pronounced decrease of venous responses during the flicker (**Figures 3B**, **5A**), as reflected in a significantly lower median venous AUC, which amounted to 0.5%*s (−3.9 to 5.8%*s) in $Ca_v2.3_{[-/-]}$ and 8.7%*s (5.0 to 13.2%*s) in $Ca_v2.3_{[+/+]}$ mice ($p = 0.047$, **Figure 5B**). There was also a tendency for maximum venous dilation in response to flicker to be reduced, with median values of 1.2% (0.7 to 1.8%) in $Ca_v2.3_{[+/+]}$ and 0.6% (0.2 to 0.9%) in $Ca_v2.3_{[-/-]}$ mice. However, because two of the $Ca_v2.3$-deficient mice actually showed an increased venous dilation during the flicker when compared to $Ca_v2.3$-competent mice (**Figure 5C**), the difference between both groups did not reach statistical significance ($p = 0.075$). Likewise, comparison of venous dilation at flicker cessation revealed no significant difference between the two genotypes ($p = 0.100$), even though relative vessel diameters were clearly reduced in all but two $Ca_v2.3_{[-/-]}$ mice (**Figure 5D**). On the other hand, there was little difference between the two genotypes with regard to the timing of venous dilation during the flicker ($p = 0.819$) or the magnitude ($p = 0.479$) and timing ($p = 0.268$) of venous constriction after flicker cessation (**Figure 5A**, **Table 3**).

Differences in Arterial Responses to Flicker Stimulation

As illustrated in **Figure 6A**, genetic ablation of $Ca_v2.3$ channels also resulted in alterations in retinal arterial responses, which consisted of a decrease and apparent initial reversal of vasodilation during the flicker. Quantitatively, this was reflected in a significant decrease of the arterial AUC during the flicker from a positive median value of 2.3% (−1.7 to 10.0%) in $Ca_v2.3_{[+/+]}$ to a negative median value of −4.5% (−7.3 to 1.9%) in $Ca_v2.3_{[-/-]}$ mice ($p = 0.031$, **Figure 6B**). The median time to maximal arterial dilation was also delayed from 10.0 s (8.0 to 14.3 s) in $Ca_v2.3_{[+/+]}$ to 15.0 s (10.8 to 25.3 s) in $Ca_v2.3_{[-/-]}$ mice, even though this difference did not reach statistical significance ($p = 0.096$, **Figure 6C**). In addition, arterial dilation at flicker cessation (**Figure 6D**) and the arterial reactive magnitude (**Table 3**) showed a tendency to be reduced in $Ca_v2.3$-deficient compared to $Ca_v2.3$-competent mice, although these differences remained below the threshold for statistical significance as well ($p = 0.100$ and $p = 0.090$, respectively).

DISCUSSION

Dynamic retinal vessel analysis is a powerful tool for non-invasive assessment of neurovascular coupling that remains to be widely adopted to experimental and preclinical murine animal models. Here, we used an adapted prototype of a non-contact retinal

TABLE 3 | Dynamic retinal vessel analysis parameters in $Ca_v2.3_{[+/+]}$ and $Ca_v2.3_{[-/-]}$ mice.

	$Ca_v2.3$[+/+] median (1.q–3.q)	$Ca_v2.3$[–/–] median (1.q–3.q)	*p*-value
General parameters:	***n* = 22**	***n* = 11**	
Age, [months]	4.7 (4.0 to 5.7)	4.9 (3.5 to 6.0)	0.592
Weight, [g]	28.0 (27.3 to 30.0)	25.0 (25.0 to 25.5)	**0.001**
Arterial parameters:	***n* = 15**	***n* = 10**	
Data quality, [subjective score 1.0 to 5.0]	4.5 (4.0 to 5.0)	4.5 (3.8 to 5.0)	0.246
Arterial diameter, [MU]	40.9 (35.5 to 50.9)	43.9 (39.0 to 59.2)	0.202
Mean maximal arterial dilation (mMD_{art}), [% baseline]	1.3 (0.6 to 2.2)	0.5 (0.2 to 1.2)	0.127
Time to maximal arterial dilation (tMD_{art}), [s]	10.0 (8.0 to 14.3)	15.0 (10.8 to 25.3)	**0.096**
Arterial dilation at flicker cessation (DFC_{art}), [% baseline]	0.3 (−0.4 to 0.5)	−0.1 (−0.7 to 0.1)	**0.100**
Arterial reactive magnitude (RM_{art}), [% baseline]	3.1 (2.4 to 3.7)	1.8 (1.4 to 2.9)	**0.090**
Arterial AUC during the flicker (AUC_{art}), [%*s]	2.3 (−1.7 to 10.0)	−4.5 (−7.3 to 1.9)	**0.031**
Mean maximal arterial constriction (mMC_{art}), [% baseline]	−0.3 (−1.0 to 0.6)	0.4 (−1.1 to 1.0)	0.396
Time to maximal arterial constriction (tMC_{art}), [s]	57.5 (40.5 to 65.3)	54.0 (38.5 to 62.5)	0.396
Venous parameters:	***n* = 22**	***n* = 11**	
Data quality, [subjective score 1.0 to 5.0]	4.5 (4.1 to 4.9)	4.0 (3.3 to 5.0)	0.435
Venous diameter, [MU]	55.5 (47.9 to 64.5)	61.9 (57.8 to 66.9)	0.285
Mean maximal venous dilation (mMD_{ven}), [% baseline]	1.2 (0.7 to 1.8)	0.6 (0.2 to 0.9)	**0.075**
Time to maximal venous dilation (tMD_{ven}), [s]	15.0 (10.6 to 20.6)	17.0 (7.5 to 18.3)	0.819
Venous dilation at flicker cessation (DFC_{ven}), [% baseline]	0.6 (0.0 to 0.8)	0.0 (−0.7 to 0.1)	**0.100**
Venous reactive magnitude (RM_{ven}), [% baseline]	2.1 (1.7 to 3.4)	1.8 (1.1 to 2.4)	0.236
Venous AUC during the flicker (AUC_{ven}), [%*s]	8.7 (5.0 to 13.2)	0.5 (−3.9 to 5.8)	**0.047**
Mean maximal venous constriction (mMC_{ven}), [% baseline]	−1.2 (−1.8 to −0.6)	−1.0 (−1.2 to −0.5)	0.479
Time to maximal venous constriction (tMC_{ven}), [s]	57.5 (50.3 to 76.8)	50.0 (42.3 to 63.0)	0.268

Bold values indicate p ≤ 0.1.

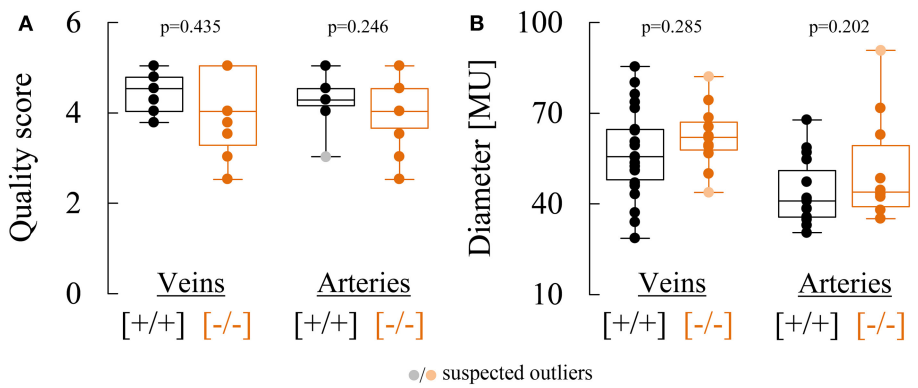

FIGURE 2 | Comparison of retinal vessel diameters and data quality in $Ca_v2.3_{[+/+]}$ and $Ca_v2.3_{[-/-]}$ mice. **(A)** Comparison of semi-objective cumulative quality scores for venous and arterial responses recorded in $Ca_v2.3_{[+/+]}$ (black) or $Ca_v2.3_{[-/-]}$ (orange) mice. **(B)** Comparison of venous (left) and arterial (right) diameters determined in $Ca_v2.3_{[+/+]}$ (black) or $Ca_v2.3_{[-/-]}$ (orange) mice and expressed in arbitrary measuring units (MU). One MU corresponds to roughly 1 μm.

vessel analyzer to compare the responses to flicker stimulation in $Ca_v2.3$-competent and -deficient mice.

Retinal Vessel Analysis in Mice

Our findings confirm and extent the results of a previous proof-of-concept study (19) by showing that non-invasive assessment of murine retinal vessel responses is feasible and that it can be used to analyze changes in genetically modified mice. Even though the signal-to-noise ratio (SNR) of individual responses to flicker stimulation remains to be improved by further technical and methodological refinements (see below), the variability of the parameter values obtained in wildtype mice was not excessive and in line with the relatively high (inter- and intra-subject) heterogeneity of microvascular responses observed in other studies (29–31). Moreover, while the shape of the individual responses was often not well-resolved, especially the average results obtained are in good agreement with the expected distinct pattern of retinal vessel responses to flicker stimulation (32).

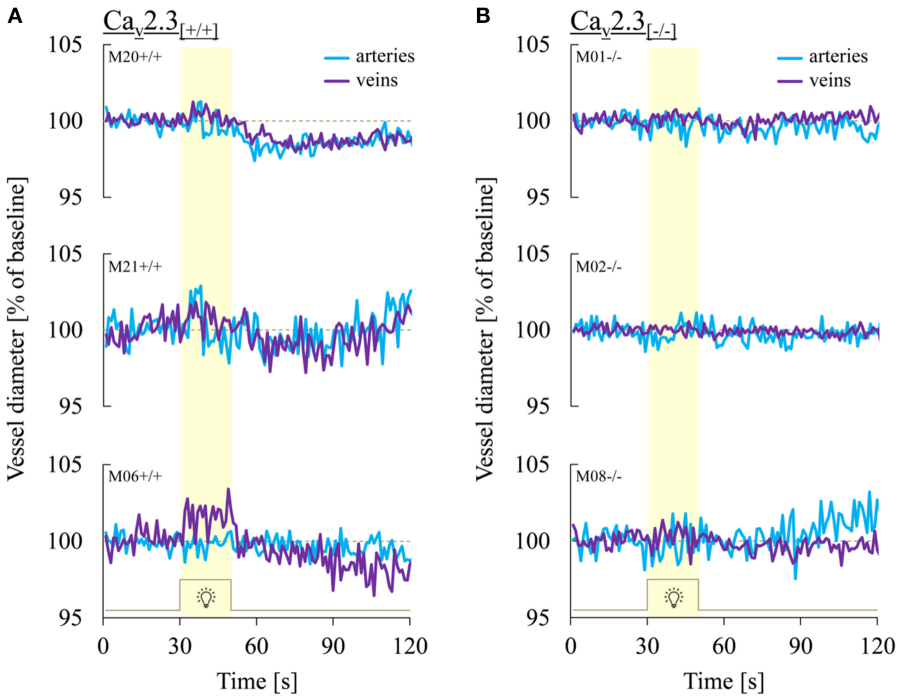

FIGURE 3 | Representative retinal vessel responses recorded in $Ca_v2.3_{[+/+]}$ and $Ca_v2.3_{[-/-]}$ mice. Shown are typical patterns of arterial (turquoise) and venous (purple) responses to flicker light recorded in **(A)** $Ca_v2.3$-competent ($Ca_v2.3_{[+/+]}$) and **(B)** $Ca_v2.3$-deficient ($Ca_v2.3_{[-/-]}$) mice. Note that both arterial and venous retinal vessel responses in $Ca_v2.3_{[-/-]}$ mice were consistently reduced or completely absent.

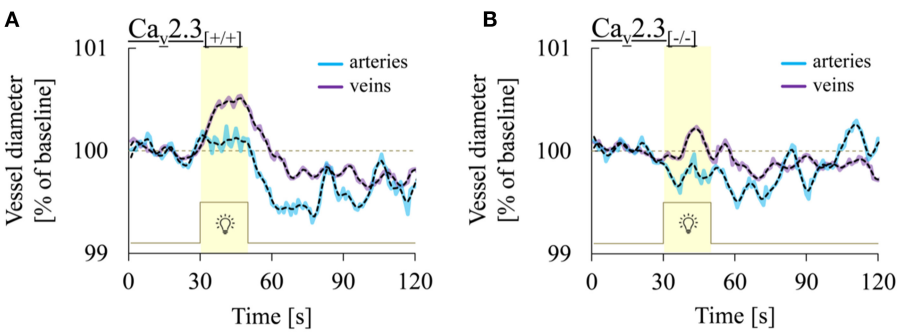

FIGURE 4 | Comparison of retinal arterial and venous responses in the two genotypes. Shown are average arterial (turquoise) and venous (purple) responses to flicker light recorded in **(A)** $Ca_v2.3$-competent [$Ca_v2.3_{[+/+]}$: $n = 15$ and 22 animals for arterial and venous responses, respectively] or **(B)** $Ca_v2.3$-deficient [$Ca_v2.3_{[-/-]}$: $n = 10$ and 11 animals for arterial and venous responses, respectively]. Black dotted lines show the same data after smoothing with a 2-points FFT filter (cut-of frequency: 0.25) to remove high-frequency noise. Note that venous dilation during the flicker was consistently more pronounced than arterial dilation and that average responses in both vascular compartments were reduced in $Ca_v2.3_{[-/-]}$ mice.

For example, previous studies in rats and human subjects have shown that retinal arteries exhibit rapid vasodilation on flicker initiation followed by a maintenance phase with little change before rapidly dropping below the baseline after flicker cessation and slowly returning back to their original value (31–37). While the maintenance phase in our average arterial responses appeared to have been obscured by the lower SNR in mouse recordings, wildtype mice clearly exhibited rapid vasodilation at stimulation onset, rapid and pronounced vasoconstriction after flicker cessation and a subsequent slow return of the vessel diameter to baseline (**Figure 6A**). Venous responses in the retina are typically characterized by much slower vasodilation during the flicker stimulation followed by a slow return to baseline after flicker cessation (31–37), which is in line with the average venous response we observed in wildtype mice (**Figure 5A**, but see below). That said, like in our previous study (19), the responses

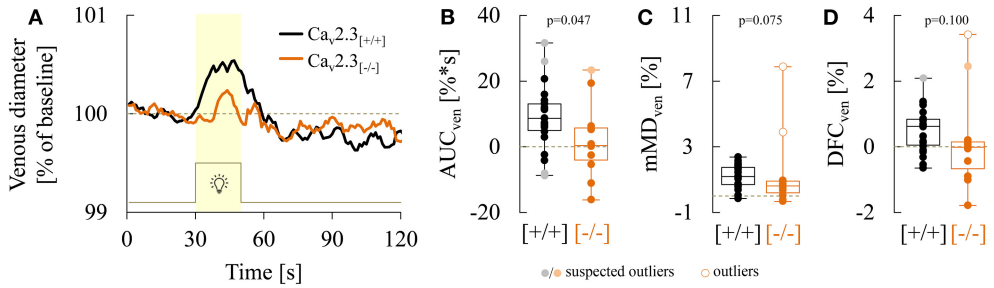

FIGURE 5 | Comparison of venous responses recorded in $Ca_v2.3_{[+/+]}$ and $Ca_v2.3_{[-/-]}$ mice. **(A)** Average venous responses to flicker stimulation in $Ca_v2.3$-competent ($Ca_v2.3_{[+/+]}$: black curve, $n = 22$ animals) and $Ca_v2.3$-deficient ($Ca_v2.3_{[-/-]}$: orange curve, $n = 11$ animals) mice. **(B–D)** Boxplots comparing **(B)** venous area under the curve (AUC_{ven}), **(C)** mean maximum venous dilation during the flicker (mMD_{ven}), and **(D)** venous dilation at flicker cessation (DFC_{ven}) in $Ca_v2.3_{[+/+]}$ (black) and $Ca_v2.3_{[-/-]}$ (orange) mice (same animals as in A). For remaining parameters see **Table 3**.

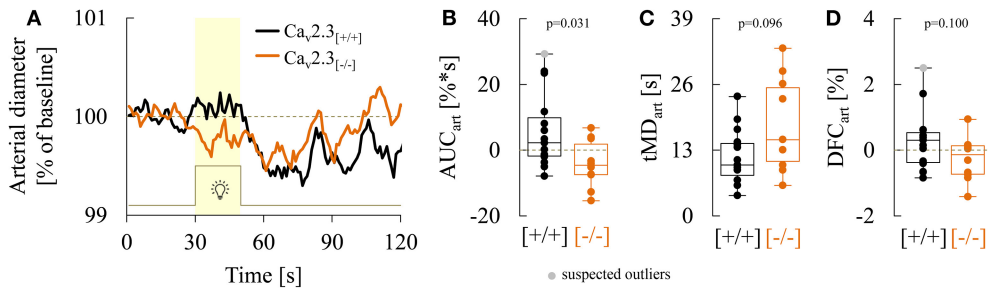

FIGURE 6 | Comparison of arterial responses recorded in $Ca_v2.3_{[+/+]}$ and $Ca_v2.3_{[-/-]}$ mice. **(A)** Average arterial responses to flicker stimulation in $Ca_v2.3$-competent [$Ca_v2.3_{[+/+]}$: black curve, $n = 15$ animals] and $Ca_v2.3$-deficient [$Ca_v2.3_{[-/-]}$: orange curve, $n = 10$ animals] mice. **(B–D)** Boxplots comparing **(B)** arterial area under the curve (AUC_{art}), **(C)** time of maximum arterial dilation during the flicker (tMD_{art}) and, **(D)** arterial dilation at flicker cessation (DFC_{ven}) in $Ca_v2.3_{[+/+]}$ (black) and $Ca_v2.3_{[-/-]}$ (orange) mice (same animals as in A). For remaining parameters see **Table 3**.

to flicker light stimulation appeared to be more consistent and pronounced in veins as compared to arteries, which would not be expected based on the dominant working model that arteries are the main effector of NVC and is in actual contrast to the small and inconsistent venous dilation previously observed in the rat retina (35). A possible explanation with regard to the latter could be differences in the anesthetic regimen, as common doses of many anesthetics have been shown to alter NVC and block vasodilation of veins in response to neuronal activity [reviewed in Gao et al. (38)]. While the aforementioned studies in rats were performed under α-chloralose anesthesia (35), which has been shown to reduce the metabolic rate in cortical neurons by 50% or more (39, 40), we used ketamine/xylazine at 2/3 of the common intraperitoneal dose, which might have contributed to the more pronounced venous responses observed in the present study. Moreover, even though arterial and venous responses in the human retina have often been reported to be comparable in magnitude (34, 41–43), more recent work by us and others has consistently demonstrated that the magnitude of venous responses actually exceeds the magnitude of arterial responses, and that these difference further increase with increasing age (31, 36, 37). Indeed, from a fluid mechanical point of view and assuming the same volumetric flow in both arteries and veins but a higher velocity in the arterial compartment, veins should dilate more to accommodate the same blood volume. Other factors that need to be considered with regard to the lower SNR in murine recordings are that veins are usually larger than arteries and that they appear darker, which increases their contrast to the background, makes venous responses less susceptible to erroneous diameter estimations and facilitates their separation from background noise. We intent to use fluorescent dyes to further improve the threshold for detection and resolution of arterial responses in the murine retina in future studies.

Another interesting observation of the present study is the fact that venous vasodilation during the flicker was often followed by vasoconstriction after flicker cessation, which was less marked than arterial vasoconstriction but still clearly evident in the average responses (**Figure 5A**). While this may seem to be at odds with the absence of vasoconstriction after flicker cessation usually observed in human retinal veins (34, 41–43), a recent study on the smallest vessels in the human retina found instances of constriction in venules as well (29), suggesting that their responses may at least in part be actively generated by contractile mural cells present at the vessel wall. In support of this assumption, the tone of porcine retinal veins without identifiable smooth muscle cells has previously been shown to be modulated by vasoconstricting and vasodilating agents (44–46). Interestingly, basal tone and its modulation by vasoactive agents were abolished in the absence of extracellular Ca^{2+}, while the

L-type VGCC antagonist nifedipine reduced basal tone but had no effect on venous vasoreactivity, possibly pointing to a role of Ca^{2+}-influx through non-L-type VGCCs (45). This makes it tempting to speculate that $Ca_v2.3$ channels could be involved in the processes underlying venous vasoreactivity (but see next section), even though further studies will clearly be required to firmly establish whether the responses of veins in the mouse retina are attributable to passive stretch secondary to arterial vasodilation or at least in part actively generated by contractile cells like pericytes.

Effects of $Ca_v2.3$ Channel Ablation on Retinal Vessel Responses

Our results also suggest that $Ca_v2.3$ channel dysfunction is associated with significantly reduced venous and possibly even inverted arterial responses to flicker stimulation. However, taking into account the limited SNR, further studies will be required to determine if the apparent inversion of arterial responses evident in **Figures 6A,B** was due to arterial vasoconstriction during the flicker or merely an artifact generated by background noise. That said, a reduction in the magnitude of vasodilation during flicker stimulation was clearly observed in both arteries and veins from $Ca_v2.3$-deficient compared to wildtype mice, while the timing of vasodilation or the magnitude and timing of vasoconstriction after flicker cessation appeared to be much less affected. Attenuated vessel responses could reflect reduced light-induced neuronal activity with an associated decrease in metabolic demand or alterations in the coupling of neuronal activity to local vessel responses (i.e., impaired NVC). Our present data are clearly insufficient to draw firm conclusions with regard to the underlying mechanisms. However, previous electroretinographic (ERG) recordings from the isolated murine and bovine retina indicate that genetic or pharmacological ablation of $Ca_v2.3$ channels produces no drastic neuronal dysfunction and actually increases the ERG b-wave, presumably due to reduced GABAergic feedback inhibition of rod bipolar cells (47–51). Also, while the decrease in retinal vessel dilation during flicker stimulation could be accounted for by reduced neuronal activity, the partial reversal of arterial responses in $Ca_v2.3$-deficient mice is more difficult to explain in terms of altered neuronal activity alone. As such, we propose that the observed reduction of retinal vessel responses reflects—at least in part—impaired NVC due to changes in one or more of the signaling pathways within the neurovascular unit. On first sight, this may appear difficult to reconcile with previous findings that Ca^{2+} influx through $Ca_v2.3$ channels in cerebral vessels actually contributes to vasoconstriction after experimental subarachnoid hemorrhage (SAH) (20). However, it has also been shown that $Ca_v2.3$ channels are not normally expressed in these vessels and that subarachnoid blood degradation products like hemoglobin may be required to induce their functional upregulation (12, 20, 52). As such, our findings could point to a role of $Ca_v2.3$ channels in neurons, astrocytes, capillary pericytes and/or endothelial cells for NVC. For example, $Ca_v2.3$ channels have been shown to be expressed in cultured astrocytes (53) and astrocyte Ca^{2+} signaling has implicated in the modulation of basal tone and pressure-induced vascular responses of retinal arteries and veins (54). The inversion of NVC after SAH has been linked to changes in astrocyte Ca^{2+} signaling (55) as well, and sustained exposure to pathophysiologically relevant concentrations of the hemoglobin degradation product bilirubin has been shown to impair $Ca_v2.3$ channel function (56), which could conceivably promote changes in NVC similar to those observed in the present study. This could have important clinical implications with regard to the proposed use of $Ca_v2.3$ channel antagonists for the treatment of cerebral vasospasm (20), as suppression of these channels in non-vascular cell types of the NVU could possibly further impair NVC. In any case, further studies on the role of $Ca_v2.3$ channels in different cell types belonging to the NVU will clearly be required to delineate their contribution to NVC under physiological and pathophysiological conditions. In particular, combination of RVA with techniques for assessment of inner retinal signaling could be used to confirm or refute our hypothesis that altered retinal vessel responses in $Ca_v2.3$-deficient mice cannot be accounted for by changes in neuronal activity alone. More broadly speaking, non-invasive assessment of murine retinal vessel responses by RVA represents a powerful tool for preclinical research on NVC, which could not only provide insight into the therapeutic action of currently used drugs like nimodipine (13) but also help to identify novel targets for improved treatment strategies. However, a potential limitation of RVA in its current form that should be mentioned is that evaluation of retinal vessel diameters and responses without a mydriaticum is not technically feasible, so that a (differential) effect of tropicamide application on $Ca_v2.3$-competent and –deficient mice cannot be excluded. Although previous studies indicate that pharmacologic mydriasis with tropicamide has no effect on retinal microcirculation in the macula and peripapillary region (57), we are currently working on a refined prototype with infrared cameras to overcome the need for mydriasis and further evaluate its impact on retinal vessel parameters.

CONCLUSION

To our knowledge, this is the first study using a novel, non-contact analysis technique to investigate retinal vessel responses in VGCC-deficient mice. The observed changes in mice lacking $Ca_v2.3$ VGCCs raise the possibility that these channels are involved in NVC and deserve further investigation.

DATA AVAILABILITY STATEMENT

The original contributions presented in the study are included in the article/supplementary material, further inquiries can be directed to the corresponding author/s.

ETHICS STATEMENT

The animal study was reviewed and approved by the institutional and governmental committees on animal care

(Landesamt für Natur, Umwelt und Verbraucherschutz [LANUV] Nordrhein—Westfalen, Recklinghausen, Germany; 84-02.04.2016.A4555) approved all experiments described in the text, which were conducted in accordance with accepted standards of humane animal care, as reported in the UFAW handbook on the care and management of laboratory animals.

AUTHOR'S NOTE

Part of this study was presented at the 72nd Annual Meeting of the German Society of Neurosurgery (DGNC), Joint Meeting with the Japan Neurosurgical Society (JNS), June 2020, Germany.

AUTHOR CONTRIBUTIONS

FN, TS, and WA conceived, designed, and performed the experiments. FN and WA first drafting of the manuscript and illustrations. FN, JL, WA, KK, and OS data acquisition. FN, KK, RHLH, YT, UL, GS, TS, WA, and OS analysis and interpretation of data. KK, RHLH, YT, UL, HC, JH, GS, and TS critical review of the manuscript. The final manuscript was critically revised and approved by all authors.

FUNDING

This work was supported by the START-Program of the Faculty of Medicine, RWTH Aachen, Germany (Grant no. 691540).

REFERENCES

1. Willie CK, Tzeng YC, Fisher JA, Ainslie PN. Integrative regulation of human brain blood flow. *J Physiol.* (2014) 592:841–59. doi: 10.1113/jphysiol.2013.268953
2. Petzold GC, Murthy VN. Role of astrocytes in neurovascular coupling. *Neuron.* (2011) 71:782–97. doi: 10.1016/j.neuron.2011.08.009
3. Stobart JLL, Lu L, Anderson HDI, Mori H, Anderson CM. Astrocyte-induced cortical vasodilation is mediated by D-serine and endothelial nitric oxide synthase. *Proc Natl Acad Sci USA.* (2013) 110:3149–54. doi: 10.1073/pnas.1215929110
4. Muoio V, Persson PB, Sendeski MM. The neurovascular unit - concept review. *Acta Physiol.* (2014) 210:790–8. doi: 10.1111/apha.12250
5. Chen BR, Kozberg MG, Bouchard MB, Shaik MA, Hillman EMC. A critical role for the vascular endothelium in functional neurovascular coupling in the brain. *J Am Heart Assoc.* (2014) 3. e000787. doi: 10.1161/JAHA.114.000787
6. Iadecola C. The neurovascular unit coming of age: a journey through neurovascular coupling in health and disease. *Neuron.* (2017) 96:17–42. doi: 10.1016/j.neuron.2017.07.030
7. Hosford PS, Gourine AV. What is the key mediator of the neurovascular coupling response? *Neurosci Biobehav Rev.* (2019) 96:174–81. doi: 10.1016/j.neubiorev.2018.11.011
8. Bo B, Li Y, Li W, Wang Y, Tong S. Neurovascular coupling impairment in acute ischemic stroke by optogenetics and optical brain imaging. In: *2020 42nd Annual International Conference of the IEEE Engineering in Medicine & Biology Society (EMBC)*. Montreal, QC: IEEE (2020). p. 3727–30. doi: 10.1109/EMBC44109.2020.9176641
9. Balbi M, Koide M, Wellman GC, Plesnila N. Inversion of neurovascular coupling after subarachnoid hemorrhage *in vivo*. *J Cereb Blood Flow Metab.* (2017) 37:3625–34. doi: 10.1177/0271678X16686595
10. Guo S, Lo EH. Dysfunctional cell-cell signaling in the neurovascular unit as a paradigm for central nervous system disease. *Stroke.* (2009) 40:S4–7. doi: 10.1161/STROKEAHA.108.534388
11. Cataldi M. The changing landscape of voltage-gated calcium channels in neurovascular disorders and in neurodegenerative diseases. *Curr Neuropharmacol.* (2013) 11:276–97. doi: 10.2174/1570159X11311030004
12. Ishiguro M, Wellman GC. Cellular basis of vasospasm: role of small diameter arteries and voltage-dependent Ca^{2+} channels. In: Steiger HJ, Kiris T, and Zhang JH, editors. *Cerebral Vasospasm. Acta Neurochirurgica Supplementum, Vol. 104*. Vienna: Springer Vienna (2008). p. 95–8. doi: 10.1007/978-3-211-75718-5_18
13. Dorhout Mees S, Rinkel GJ, Feigin VL, Algra A, van den Bergh WM, Vermeulen M, et al. Calcium antagonists for aneurysmal subarachnoid haemorrhage. *Cochrane Database Syst Rev.* (2007) 2007:CD000277. doi: 10.1002/14651858.CD000277.pub3
14. Kuo IY, Ellis A, Seymour V AL, Sandow SL, Hill CE. Dihydropyridine-insensitive calcium currents contribute to function of small cerebral arteries. *J Cereb Blood Flow Metab.* (2010) 30:1226–39. doi: 10.1038/jcbfm.2010.11
15. Navarro-Gonzalez MF, Grayson TH, Meaney KR, Cribbs LL, Hill CE. Non-L-type voltage-dependent calcium channels control vascular tone of the rat basilar artery. *Clin Exp Pharmacol Physiol.* (2009) 36:55–66. doi: 10.1111/j.1440-1681.2008.05035.x
16. Wu HQ, Wu H, Shi LL, Yu LY, Wang LY, Chen YL, et al. The association between retinal vasculature changes and stroke: a literature review and meta-analysis. *Int J Ophthalmol.* (2017) 10:109–14. doi: 10.18240/ijo.2017.01.18
17. Albanna W, Conzen C, Weiss M, Clusmann H, Fuest M, Mueller M, et al. Retinal vessel analysis (RVA) in the context of subarachnoid hemorrhage - A proof of concept study. *PLoS ONE.* (2016) 11:e0158781. doi: 10.1371/journal.pone.0158781
18. Conzen C, Albanna W, Weiss M, Kürten D, Vilser W, Kotliar K, et al. Vasoconstriction and impairment of neurovascular coupling after subarachnoid hemorrhage: a descriptive analysis of retinal changes. *Transl Stroke Res.* (2018) 9:284–93. doi: 10.1007/s12975-017-0585-8
19. Albanna W, Kotliar K, Lüke JN, Alpdogan S, Conzen C, Lindauer U, et al. Non-invasive evaluation of neurovascular coupling in the murine retina by dynamic retinal vessel analysis. *PLoS ONE.* (2018) 13:e0204689. doi: 10.1371/journal.pone.0204689
20. Ishiguro M, Wellman TL, Honda A, Russell SR, Tranmer BI, Wellman GC. Emergence of a R-type Ca^{2+} channel (Cav2.3) contributes to cerebral artery constriction after subarachnoid hemorrhage. *Circ Res.* (2005) 96:419–26. doi: 10.1161/01.RES.0000157670.49936.da
21. Pereverzev A, Mikhna M, Vajna R, Gissel C, Henry M, Hescheler J, et al. Disturbances in glucose-tolerance, insulin-release, and stress-induced hyperglycemia upon disruption of the Cav2.3 (a1E) subunit of voltage-gated Ca^{2+} channels. *Mol Endocrinol.* (2002) 16:884–95. doi: 10.1210/mend.16.4.0801
22. Czakó C, Kovács T, Ungvari Z, Csiszar A, Yabluchanskiy A, Conley S, et al. Retinal biomarkers for Alzheimer's disease and vascular cognitive impairment and dementia (VCID): implication for early diagnosis and prognosis. *GeroScience.* (2020) 42:1499–525. doi: 10.1007/s11357-020-00252-7
23. Link D, Strohmaier C, Seifert BU, Riemer T, Reitsamer HA, Haueisen J, et al. Novel non-contact retina camera for the rat and its application to dynamic retinal vessel analysis. *Biomed Opt Express.* (2011) 2:3094. doi: 10.1364/BOE.2.003094
24. Nagel E, Vilser W, Lanzl I. Age, blood pressure, and vessel diameter as factors influencing the arterial retinal flicker response. *Invest Ophthalmol Vis Sci.* (2004) 45:1486–92. doi: 10.1167/iovs.03-0667
25. van Veluw SJ, Hou SS, Calvo-Rodriguez M, Arbel-Ornath M, Snyder AC, Frosch MP, et al. Vasomotion as a driving force for paravascular clearance in the awake mouse brain. *Neuron.* (2020) 105:549–61.e5. doi: 10.1016/j.neuron.2019.10.033
26. Kotliar KE, Lanzl IM, Schmidt-Trucksäss A, Sitnikova D, Ali M, Blume K, et al. Dynamic retinal vessel response to flicker in obesity: a methodological approach. *Microvasc Res.* (2011) 81:123–8. doi: 10.1016/j.mvr.2010.11.007

27. Kotliar K, Hauser C, Ortner M, Muggenthaler C, Diehl-Schmid J, Angermann S, et al. Altered neurovascular coupling as measured by optical imaging: a biomarker for Alzheimer's disease. *Sci Rep.* (2017) 7:12906. doi: 10.1038/s41598-017-13349-5
28. Lanzl IM, Seidova SF, Maier M, Lohmann C, Schmidt-Trucksäss A, Halle M, et al. Dynamic retinal vessel response to flicker in age-related macular degeneration patients before and after vascular endothelial growth factor inhibitor injection. *Acta Ophthalmol.* (2011) 89:472–9. doi: 10.1111/j.1755-3768.2009.01718.x
29. Duan A, Bedggood PA, Bui BV, Metha AB. Evidence of flicker-induced functional hyperaemia in the smallest vessels of the human retinal blood supply. *PLoS ONE.* (2016) 11:e0162621. doi: 10.1371/journal.pone.0162621
30. Kneser M, Kohlmann T, Pokorny J, Tost F. Age related decline of microvascular regulation measured in healthy individuals by retinal dynamic vessel analysis. *Med Sci Monit.* (2009) 15:CR436–41.
31. Seshadri S, Ekart A, Gherghel D. Ageing effect on flicker-induced diameter changes in retinal microvessels of healthy individuals. *Acta Ophthalmol.* (2016) 94:e35–42. doi: 10.1111/aos.12786
32. Garhöfer G, Chua J, Tan B, Wong D, Schmidl D, Schmetterer L. Retinal neurovascular coupling in diabetes. *J Clin Med.* (2020) 9:2829. doi: 10.3390/jcm9092829
33. Heitmar R, Summers RJ. The time course of changes in retinal vessel diameter in response to differing durations of flicker light provocation. *Investig Opthalmology Vis Sci.* (2015) 56:7581–8. doi: 10.1167/iovs.15-17089
34. Polak K, Schmetterer L, Riva CE. Influence of flicker frequency on flicker-induced changes of retinal vessel diameter. *Invest Ophthalmol Vis Sci.* (2002) 43:2721–6.
35. Kornfield TE, Newman EA. Regulation of blood flow in the retinal trilaminar vascular network. *J Neurosci.* (2014) 34:11504–13. doi: 10.1523/JNEUROSCI.1971-14.2014
36. Kotliar KE, Mücke B, Vilser W, Lanzl I. Aging effects measured by retinal vessel analyzer. *Invest Ophthalmol Vis Sci.* (2005) 46:3916.
37. Kotliar KE, Mücke B, Vilser W, Lanzl IM. Age dependence of local retinal arterial reaction to monochromatic flicker light application. In: *103 Congress of the German Ophthalmological Society (DOG), and 15*. Berlin: SOE Congress (2005). p. 2509–10.
38. Gao Y-R, Ma Y, Zhang Q, Winder AT, Liang Z, Antinori L, et al. Time to wake up: studying neurovascular coupling and brain-wide circuit function in the un-anesthetized animal. *Neuroimage.* (2017) 153:382–8. doi: 10.1016/j.neuroimage.2016.11.069
39. Dudley RE, Nelson SR, Samson F. Influence of chloralose on brain regional glucose utilization. *Brain Res.* (1982) 233:173–80. doi: 10.1016/0006-8993(82)90938-6
40. Hyder F, Rothman DL, Shulman RG. Total neuroenergetics support localized brain activity: Implications for the interpretation of fMRI. *Proc Natl Acad Sci USA.* (2002) 99:10771–6. doi: 10.1073/pnas.132272299
41. Garhöfer G, Zawinka C, Resch H, Huemer KH, Dorner GT, Schmetterer L. Diffuse luminance flicker increases blood flow in major retinal arteries and veins. *Vision Res.* (2004) 44:833–8. doi: 10.1016/j.visres.2003.11.013
42. Hammer M, Vilser W, Riemer T, Liemt F, Jentsch S, Dawczynski J, et al. Retinal venous oxygen saturation increases by flicker light stimulation. *Investig Opthalmology Vis Sci.* (2011) 52:274–7. doi: 10.1167/iovs.10-5537
43. Noonan JE, Nguyen TT, Man REK, Best WJ, Wang JJ, Lamoureux EL. Retinal arteriolar dilation to flicker light is reduced on short-term retesting. *Investig Opthalmology Vis Sci.* (2013) 54:7764–8. doi: 10.1167/iovs.13-12525
44. Yu DY, Su EN, Cringle SJ, Morgan WH, McAllister IL, Yu PK. Local modulation of retinal vein tone. *Investig Opthalmology Vis Sci.* (2016) 57:412–9. doi: 10.1167/iovs.15-18358
45. Chen YL, Ren Y, Xu W, Rosa RH, Kuo L, Hein TW. Constriction of retinal venules to endothelin-1: obligatory roles of ET a receptors, extracellular calcium entry, and rho kinase. *Investig Opthalmology Vis Sci.* (2018) 59:5167–75. doi: 10.1167/iovs.18-25369
46. Chen YL, Xu W, Rosa RH, Kuo L, Hein TW. Hyperglycemia enhances constriction of retinal venules via activation of the reverse-mode sodium-calcium exchanger. *Diabetes.* (2019) 68:1624–34. doi: 10.2337/db19-0069
47. Lüke M, Henry M, Lingohr T, Maghsoodian M, Hescheler J, Weiergräber M, et al. A Ni^{2+}-sensitive component of the ERG b-wave from the isolated bovine retina is related to E-type voltage-gated Ca^{2+} channels. *Graefe's Arch Clin Exp Ophthalmol.* (2005) 243:933–41. doi: 10.1007/s00417-005-1145-6
48. Siapich SA, Banat M, Albanna W, Hescheler J, Lüke M, Schneider T. Antagonists of ionotropic -aminobutyric acid receptors impair the NiCl2-mediated stimulation of the electroretinogram b-wave amplitude from the isolated superfused vertebrate retina. *Acta Ophthalmol.* (2009) 87:854–65. doi: 10.1111/j.1755-3768.2008.01387.x
49. Alnawaiseh M, Albanna W, Chen CC, Campbell KP, Hescheler J, Lüke M, et al. Two separate Ni^{2+}-sensitive voltage-gated Ca^{2+} channels modulate transretinal signalling in the isolated murine retina. *Acta Ophthalmol.* (2011) 89:e579–90. doi: 10.1111/j.1755-3768.2011.02167.x
50. Siapich SA, Wrubel H, Albanna W, Alnawaiseh M, Hescheler J, Weiergräber M, et al. Effect of ZnCl2 and chelation of zinc ions by N,N-diethyldithiocarbamate (DEDTC) on the ERG b-wave amplitude from the isolated superfused vertebrate retina. *Curr Eye Res.* (2010) 35:322–34. doi: 10.3109/02713680903509410
51. Schneider T, Niklas Lüke J, Akhtar I, Neumaier F, Alexander Schubert G, Clusmann H, et al. Disturbances of transretinal signaling after ablation of CaV2.3 / R-type calcium channels. *Biophys J.* (2018) 114:39a—40a. doi: 10.1016/j.bpj.2017.11.267
52. Ishiguro M, Murakami K, Link T, Zvarova K, Tranmer BI, Morielli AD, et al. Acute and chronic effects of oxyhemoglobin on voltage-dependent ion channels in cerebral arteries. *Acta Neurochir Suppl.* (2008) 104:99–102. doi: 10.1007/978-3-211-75718-5_19
53. Latour I, Hamid J, Beedle AM, Zamponi GW, Macvicar BA. Expression of voltage-gated Ca^{2+} channel subtypes in cultured astrocytes. *Glia.* (2003) 41:347–53. doi: 10.1002/glia.10162
54. Li H, Bui BV, Cull G, Wang F, Wang L. Glial cell contribution to basal vessel diameter and pressure-initiated vascular responses in rat retina. *Investig Opthalmology Vis Sci.* (2017) 58:1–8. doi: 10.1167/iovs.16-20804
55. Pappas AC, Koide M, Wellman GC. Astrocyte Ca^{2+} signaling drives inversion of neurovascular coupling after subarachnoid hemorrhage. *J Neurosci.* (2015) 35:13375–84. doi: 10.1523/JNEUROSCI.1551-15.2015
56. Albanna W, Lüke JN, Schubert GA, Dibué-Adjei M, Kotliar K, Hescheler J, et al. Modulation of Cav2.3 channels by unconjugated bilirubin (UCB) – Candidate mechanism for UCB-induced neuromodulation and neurotoxicity. *Mol Cell Neurosci.* (2019) 96:35–46. doi: 10.1016/j.mcn.2019.03.003
57. Hohberger B, Müller M, Hosari S, Mardin CY. OCT-Angiography: mydriatic phenylephrine and tropicamide do not influence retinal microvasculature in macula and peripapillary region. *PLoS ONE.* (2019) 14:e0221395. doi: 10.1371/journal.pone.0221395

Conflict of Interest: The authors declare that the research was conducted in the absence of any commercial or financial relationships that could be construed as a potential conflict of interest.

frontiers in Neurology

BRIEF RESEARCH REPORT
published: 20 April 2021
doi: 10.3389/fneur.2021.662089

Physiologic Characteristics of Hyperosmolar Therapy After Pediatric Traumatic Brain Injury

Jeffrey Wellard[1], *Michael Kuwabara*[1,2], *P. David Adelson*[1,3] *and Brian Appavu*[1,3]*

[1] University of Arizona College of Medicine–Phoenix, Phoenix, AZ, United States, [2] Department of Radiology, Phoenix Children's Hospital, Phoenix, AZ, United States, [3] Department of Neurosciences, Barrow Neurological Institute at Phoenix Children's Hospital, Phoenix, AZ, United States

All work was performed at the Barrow Neurological Institute at Phoenix Children's Hospital.

Objective: Investigate injury severity, neuroimaging, physiology, and outcomes with bolus hyperosmolar therapy (HT) of 3% hypertonic saline or mannitol.

Methods: Retrospective cohort analysis was performed. Physiologic variables included intracranial pressure (ICP), arterial blood pressure (ABP), and heart rate (HR). Volume-pressure compensation (PVC) indices included ICP pulse amplitude (AMP) and correlation of AMP and ICP (RAP). Cerebrovascular pressure reactivity (CVPR) indices included pressure reactivity index (PRx), pulse amplitude index (PAx), wavelet PRx (wPRx), and correlation of AMP and cerebral perfusion pressure (RAC). Heart rate variability (HRV) indices included heart rate standard deviation (HRsd), heart rate root mean square of successive differences (HRrmssd) and low-high frequency ratio (LHF). Outcome was assessed using Glasgow Outcomes Scale Extended Pediatrics, 12-months post-injury. Generalized estimating equations was applied to investigate associations of physiologic changes and pre-treatment indices with HT efficacy. Repeated measures analysis of variance was applied to investigate changes after HT without intracranial hypertension (ICH). Wilcoxon rank-sum was applied to investigate HT responsiveness with age, injury severity, neuroimaging, and outcomes.

Results: Thirty children received bolus HT. ICH reduction after HT was associated with reduced ICP ($p = 0.0064$), ABP ($p = 0.0126$), PRx ($p = 0.0063$), increased HRsd ($p = 0.0408$), and decreased pretreatment RAC ($p = 0.0115$) and wPRx ($p = 0.0072$). HT-responsive patients were older and had improved outcomes ($p = 0.0394$). HT without ICH was associated with increased ICP ($P < 0.0001$) and ABP ($P < 0.0001$), increases in all HRV indices and decreases in all PVC indices.

Conclusion: After pediatric TBI, efficacious HT is associated with decreased ICP and ABP, pre-treatment indices suggesting efficient CVPR, and potentially improved outcomes.

Keywords: hyperosmolar therapy, hypertonic saline, mannitol, traumatic brain injury, pediatrics, cerebrovascular pressure reactivity, multimodality monitoring

OPEN ACCESS

Edited by:
Xiuyun Liu,
Johns Hopkins University,
United States

Reviewed by:
Syed Omar Shah,
Thomas Jefferson University,
United States
Mark Wainwright,
University of Washington,
United States

***Correspondence:**
Brian Appavu
bappavu@phoenixchildrens.com

Specialty section:
This article was submitted to Neurocritical and Neurohospitalist Care, a section of the journal Frontiers in Neurology

Received: *31 January 2021*
Accepted: *24 March 2021*
Published: *20 April 2021*

Citation:
Wellard J, Kuwabara M, Adelson PD and Appavu B (2021) Physiologic Characteristics of Hyperosmolar Therapy After Pediatric Traumatic Brain Injury. Front. Neurol. 12:662089. doi: 10.3389/fneur.2021.662089

INTRODUCTION

Traumatic brain injury (TBI) represents a leading cause of pediatric morbidity and mortality, affecting an estimated 280 per 100,000 children in the United States (1). Despite the significance of this condition, high-level recommendations are not available in current pediatric guidelines, with no level I evidence existing to guide clinical management (2). While most level II evidence focuses on therapies to avoid in care, level II evidence does exist to support bolus therapy of hypertonic saline (3%) for treatment of intracranial hypertension (ICH). Mannitol is also available as a hyperosmolar agent, but it has not been subjected to rigorous controlled clinical trials vs. placebo or other therapy in children. After TBI, ICH can arise from multiple sources including cerebral edema, increased cerebral arterial blood volume (CABV), increased cerebral sinus pressure, or obstructive hydrocephalus. While use of hyperosmolar therapy (HT) has been shown to reduce ICH, its putative pharmacological mechanisms focus on reduction of cerebral edema, yet this would make it potentially ineffective when ICH arises from other etiologies. Furthermore, concern has arisen that in patients with intact cerebrovascular pressure reactivity (CVPR), hypertonic saline may impair cerebral hemodynamics (3). For these reasons, further study and understanding of the mechanisms of actions of HT and real time responses to treatment are necessary.

Multimodality neurologic monitoring (MMM) represents an emerging technique to help clinicians understand complex physiologic states after TBI (4). This technique offers both data visualization of real-time physiology, as well as calculation of biomarkers of cerebral dynamics. Model-based indices of CVPR, such as the pressure reactivity index (PRx), have been developed to understand a patient's state of pressure-related cerebral autoregulation, and have been demonstrated to be a strong marker of injury severity after pediatric TBI (5–7). Other model-based indices of heart rate variability (HRV) and pressure-volume compensation (PVC) offer an opportunity to better characterize a patient's physiologic state (8–10). These calculated biomarkers, however, have not yet been recognized to offer effective and immediately actionable information to guide clinical care.

In this study, we wished to investigate physiologic changes associated with HT in pediatric TBI patients, as well as the association of HT efficacy for ICH with physiologic, patient-specific, and neuroimaging characteristics. We hypothesized that HT is associated with reduction of ICH. We also hypothesized that HT efficacy for ICH is associated with pre-treatment CVPR and that treatment efficacy is associated with changes in CVPR, PVC, HRV as well as improved functional outcomes.

MATERIALS AND METHODS

This was a retrospective study from a prospectively collected clinical database. The study was conducted at Phoenix Children's Hospital (Phoenix Arizona, USA) and was approved by the Institutional Review Board (17-469).

Children (<21 years of age) with TBI from a single pediatric intensive care unit who underwent continuous intraparenchymal intracranial pressure (ICP) monitoring and MMM were retrospectively analyzed from September 2014 to December 2019. Patients were managed according to institutional standard of care, which consisted of invasive arterial blood pressure (ABP) and invasive intracranial pressure monitoring with an intraparenchymal probe and sometimes an external ventricular drain (EVD). The decision to place an intraparenchymal probe and/or EVD was made based on the risk/benefit ratio by the neurosurgeon on call. Clinical care was implemented using an institutional protocol founded upon the most current pediatric TBI guidelines at the time (2, 11).

The primary aim of this study was to investigate physiologic changes associated with bolus HT. We classified patients who had evidence of ICH during the immediate hour prior to bolus HT, as well as patients who had no evidence of ICH during that period. Evidence of ICH was classified using a threshold of a dose of ICP > 20 mmHg within the hour preceding treatment that was >0 mmHg/h. We calculated dose of ICH using a previously described methodology accounting for cumulative extent and duration identified by the area under the curve above the threshold, ICP >20 mmHg over a 1 h period, obtaining measurements of mmHg/hour (12). In patients without pre-treatment evidence of ICH, we compared physiologic changes in the hour immediately after HT as compared to the hour immediately preceding treatment. In patients with evidence of ICH, we compared physiologic changes associated with treatment efficacy as compared to changes associated with treatment inefficacy. We also investigated the association of treatment efficacy with pre-treatment serum sodium levels and model-based indices of CVPR, PVC and HRV. Secondary aims of this study were to investigate whether treatment efficacy of HT was associated with patient characteristics such as injury severity, initial neuroimaging characteristics and global functional outcomes.

Patient Characteristics

Demographic patient information included age. Injury characteristics included Glasgow Coma Scale (GCS) score (13) at presentation in addition to the Pediatric Risk of Mortality III (PRISM III) score (14) on day of admission. GCS scores range from 1 to 8 with lower scores indicative of increased injury severity. PRISM III scores range from 0 to 74 with higher scores indicative of increased injury severity. Global functional outcome was measured using the Glasgow Outcome Score Extended-Pediatrics (GOSE-PEDs) score at 12 months after injury (15), GOSE-PEDs scores range from 1 to 8 with higher values representing worsened outcome.

Physiologic Data

Patients underwent MMM that included intraparenchymal ICP, invasive ABP (arterial blood pressure) and electrocardiogram (ECG) monitoring. Cerebral perfusion pressure (CPP) was calculated as the intraparenchymal ICP subtracted from the mean ICP. All patients also underwent continuous electroencephalography (cEEG) as part of MMM. Continuous physiologic data from all monitoring devices were collected and time-synchronized using an MMM device (CNS200; Moberg

ICU Solutions, Philadelphia, PA). ICM+ software (Cambridge, UK) was used to visualize and process MMM data to calculate model-based indices of CVPR, PVC, and HRV.

Cerebral hemodynamic variables collected for this study included intracranial pressure (ICP), arterial blood pressure (ABP) and heart rate (HR). Median dose of each hemodynamic variable was computed in the hour before and after bolus HT, and the difference after treatment was computed for each variable. Model-based indices utilized in this study were computed based upon each of these hemodynamic variables.

Model based indices of CVPR, PVC, and HRV are described in **Supplementary Table 1**. We classify model based indices as calculated values of two or more physiologic data captured from time series MMM signals that have been developed from conceptual models that describe physiologic states. Four different CVPR indices were explored, including the pressure reactivity index (PRx), pulse amplitude index (PAx), wavelet PRx (wPRx), and correlation of cerebral perfusion pressure and ICP pulse amplitude (RAC). A higher value for these indices signified impaired CVPR. PRx was calculated as a moving Pearson correlation coefficient between ABP and ICP within a 5-min averaging window (16). PAx was calculated similarly as a moving correlation coefficient between ABP and ICP pulse amplitude (17). RAC was calculated similarly as a moving correlation coefficient of ICP pulse amplitude and CPP (18). WPRx was calculated by taking the cosine of the wavelet transform phase shift between ABP and ICP (19). Physiologic indices of PVC included ICP pulse amplitude (AMP) and the correlation coefficient of AMP and ICP index (RAP). AMP represents the amplitude of the ICP waveform. RAP is calculated as a moving Pearson correlation coefficient between ICP within a 5-min averaging window (10). Indices of HRV included standard deviation of heart rate (HRsd), root-mean square of successive differences in heart rate (HRrmssd), and heart rate low-high frequency ratio (LHF). A lower value for these indices signifies impaired autonomic function. HRV variables were computed from time- and frequency-domain analyses according to international guidelines (8). For all HRV variables, a 30 s time series of R-R intervals was assessed from ECG that was updated every 10 s. HRsd and HRrmssd were computed from the time-domain signal. LHF was computed in the frequency domain, using Lomb-Scargle periodogram to calculate the spectral power of the RR time series in the low frequency range (0.04–0.15 Hz) and the high frequency range (0.15–0.4 Hz). To explore other physiologic biomarkers that may explain efficacy of HT based on its mechanism, we evaluated serum sodium levels acquired prior to HT.

Physiologic biomarkers investigated in relation to treatment efficacy were collected during the 1 h epoch immediately preceding and then proceeding bolus HT. The dose of ICH was also calculated in the 1 h immediately before and after bolus HT as the area under the curve during that time interval when ICP was >20 mmHg and was recorded in units of mmHg/hour, as done in previously described methods (12). Treatment efficacy was defined as a reduction in dose of ICP > 20 mmHg from the 1 h after initiation of bolus therapy as compared to the hour prior to bolus therapy. For example, a reduction from pre-treatment dose of ICH of 2.5 mmHg/h to a post-treatment dose of 1.8 mmHg/h would represent treatment efficacy. In contrast, a rise from a pre-treatment dose of ICH of 350.6 mmHg/h to a post-treatment dose of 355.6 mmHg/h would represent treatment inefficacy. The assessment of treatment efficacy was thus only evaluated for boluses which were preceded by ICP achieving a threshold dose of ICP >20 mmHg >0 mmHg/h. ICH Agents used for bolus dosing of HT included 3% hypertonic saline and mannitol. To characterize treatment responsiveness at the subject level, individual patients were considered responsive to HT if they experienced treatment efficacy to ≥50% of the bolus HT given to them during their monitoring.

Neuroimaging Characteristics

Initial computed tomography (CT) scans were reviewed by a neuroradiologist in their original digital form and graded according to the modified Marshall CT scan classification system (20). The neuroradiologist was blinded to MMM data or outcome measures at the time of analysis. Volumes of high- or mixed-density lesions consistent with intracranial hematomas were calculated by creating volumetric three-dimensional rendering using a commercially available region growing segmentation algorithm (Royal Phillips®, Best, Netherlands). Midline shift was measured in millimeters at the level of maximum deviation. The presence of basal cistern effacement was also described for each patient.

Statistical Analysis

Continuous and categorical variables were summarized with descriptive statistics including mean and standard deviation (SD) or median and interquartile range (IQR) of continuous variables, and frequencies of categorical variables. In patients with pre-treatment ICH, we employed generalized estimating equations (GEE), accounting for repeated measures (21), to test for the association of HT efficacy with differences in continuous physiologic variables. We also employed GEE in the same cohort to investigate the association of treatment efficacy with pre-treatment sodium levels and model-based indices of CVPR, PVC, and HRV. In patients without pre-treatment ICH, we employed one-way repeated measures analysis of variance (ANOVA) to test for changes in continuous physiologic variables before and after HT (22). Wilcoxon-rank sum test was used to investigate the association of continuous patient and neuroimaging characteristics with treatment responsiveness after HT. Fisher's exact test was used to test for the association of the presence or absence of basal cistern effacement or inflicted head trauma with treatment responsiveness. Findings were considered significant if the $p < 0.05$. Statistical analyses were performed using RStudio version 3.4.1.

RESULTS

Population

Seventy-nine children were identified with TBI undergoing MMM with ICP monitoring, among which seventy-four children (93.7%) underwent intraparenchymal ICP monitoring. Of those seventy-four children, thirty (40.5%) were identified to have

TABLE 1 | Patient characteristics.

Characteristic ($n = 30$)	Number (%) of patients
Female, number (%)	10 (33.3)
Mortality	3 (10.0)
3% Hypertonic saline, exclusively	17 (56.7)
Mannitol, exclusively	5 (16.7)
3% hypertonic saline and mannitol	8 (26.7%)
Treatment Responders	7 (23.3%)
Presence of basal cistern effacement	6 (27.3%)
	Median (IQR)
Age	6.5 (11.5)
Initial Glasgow Coma Score	6.5 (4.8)
Initial PRISM III Score	16.5 (7.0)
GOSE-PEDs, 12 months	5.0 (3.0)
Na level prior to therapy, mmol/L	148.0 (6.0)
CT Marshall Score	2.0 (4.0)
Intracranial Hematoma Volume (cm^3)	17.8 (25.8)
Midline shift (mm)	1.0 (2.8)
Bolus therapies per patient	3.0 (4.8)
3% Hypertonic saline dose, mL/kg	5.8 (2.5)
Mannitol dose, gm/kg	0.3 (0.1)
Timing of bolus hyperosmolar therapy after initial injury (days)	2.0 (3.0)

Note that values "prior to hyperosmolar therapy" reflect the 1 h prior to therapy. Abbreviations: N, count; Na, sodium; GOSE-PEDs, Glasgow Outcome Scale Extended Pediatrics; PRISM, Pediatric Risk of Mortality; CT, computed tomography, mL, milliliters; gm, grams; kg, kilograms; %, percent; IQR, interquartile range.

received distinct boluses of HT during their care with MMM. **Table 1** summarizes patient demographic data regarding TBI patients who received bolus HT. Ten patients (33.3%) were female. Ages ranged from 1 month to 16 years of age (median 6.5+/– interquartile range [IQR] 11.5). Nine of the thirty patients (30.0%) who underwent bolus HT had inflicted head injuries, among which five (55.6%) experiencing abusive head trauma and four (44.4%) experiencing gunshot wounds to the head. Initial GCS scores ranged from 3 to 15 (median 6.5 ± 4.8). Initial PRISM III scores ranged from 9 to 25 (median 16.5 ± 7.0). GOSE-PEDs scores at 12 months ranged from 1 to 8 (median 5.0 ± 3.0). Three patients (10.0%) experienced medically and surgically refractory ICH and died after withdrawal of life sustaining therapies. Serum sodium levels prior to bolus HT ranged from 138 to 175 mmol/L (median 148.0 ± 6.0). Twenty-two of the thirty patients (73.3%) receiving bolus HT had initial CT scans available for review. Initial CT Marshall scores ranged from 1 to 6 (median 2.0 ± 4.0). Intracranial hematoma volume ranged from 0 to 143.7 cm^3 (median 17.8 ± 25.8). Midline shift ranged from 0 to 21 mm (median 1.0 ± 2.8). Six patients (27.3%) demonstrated evidence of basal cistern effacement. All patients received intravenous Levetiracetam for seizure prophylaxis and nine patients (30.0%) experienced post-seizures, although seizures and antiepileptic treatment administration were not identified during the hour before or after HT for observed patients.

Characteristics of Bolus Hyperosmolar Therapy and Intracranial Hypertension

Characteristics are also summarized in **Table 1**. There were 148 boluses of HT identified during MMM, with each patient receiving between 1 and 21 distinct boluses of therapy (median 3.0 ± 4.8). Boluses of HT were obtained from 0 to 13 days after initial injury (median 2.0 ± 3.0). Seventeen patients (56.7%) received boluses exclusively with 3% hypertonic saline, five patients (16.7%) received boluses exclusively with mannitol, and eight patients (26.7%) received both mannitol and 3% hypertonic saline. Bolus dose of 3% hypertonic saline ranged from 0.6 to 13.3 mL/kg (median 5.8 ± 2.5). Bolus dose of mannitol ranged from 0.2 to 0.7 g/kg (median 0.3 ± 0.1). Of the 148 distinct boluses of HT, 78 boluses were preceded by evidence of ICH (52.7%) in the 1 h prior to treatment. Of these 78 treatments, 44 boluses (56.4%) were followed by reduction of ICH, representative of treatment efficacy. Seven patients (23.3%) had ≥50% treatment responsiveness and thus were considered responsive to HT.

Patient and Neuroimaging Characteristics Associated With Hyperosmolar Treatment Efficacy

Findings are summarized in **Table 2**. In patients with pre-treatment ICH, we observed that older age was associated with treatment efficacy (median 14.0±6.0 years; $p = 0.0194$) as compared to treatment inefficacy (median 4.0 ± 10.5 years). We did not observe associations of treatment efficacy with initial GCS or PRISM III scores, inflicted head trauma, CT Marshall scores, hematoma volume, midline shift, or the presence of basal cistern effacement. We did observe that patients who experienced treatment responsiveness had improved functional outcomes (median GOSE-PEDs 2.0 ± 3.5; $p = 0.0394$) at 12-months post-injury as compared to patients who did not experience treatment responsiveness (median GOSE-PEDs 5.0 ± 2.5).

Pre-treatment Sodium Levels and Model-Based Indices Associated With Hyperosmolar Treatment Efficacy

Findings are also summarized in **Table 2**. We observed that HT efficacy was associated with decreased pre-treatment median wPRx (0.05 $p = 0.0072$) and RAC ($p = 0.0115$) values. We did not observe that treatment efficacy was associated with pre-treatment serum sodium levels or values of PRx, PAx, RAP, AMP, HRsd, HRrmssd, or LHF Ratio.

Physiologic Changes After Hyperosmolar Treatment With Preceding Intracranial Hypertension

Findings are summarized in **Table 3**. As expected, we observed that HT efficacy for ICH was associated with decreased median ICP, whereas treatment inefficacy was associated with increased median ICP ($p = 0.0064$). We observed that treatment efficacy was associated with decreased median ABP, whereas treatment unresponsiveness was associated with increased ABP ($p = 0.0136$). In terms of indices of CVPR, we observed that treatment efficacy was associated with decreases in median PRx, whereas

TABLE 2 | Pre-treatment characteristics associated with reduction of intracranial hypertension after hyperosmolar therapy.

Biomarker	Effective [median (IQR)]	Ineffective [median (IQR)]	*p*-value
Age, years	**14.00 (6.00)**	**4.00 (10.50)**	**0.0194**
GCS score at presentation	4.00 (4.00)	7.00 (4.00)	0.2345
PRISM III score at presentation	15.00 (5.00)	17.00 (7.00)	0.9407
GOSE-PEDs, 12 months	**2.00 (3.50)**	**5.00 (2.50)**	**0.0394**
CT Marshall score	2.00 (2.00)	3.00 (4.00)	0.5907
Hematoma volume (cm^3)	19.50 (21.90)	16.00 (15.40)	0.8907
Midline shift (mm)	2.00 (2.50)	0.00 (3.00)	0.8794
Serum Na (mmol/L)	148.00 (6.00)	148.00 (6.00)	0.0885
PRx, median	0.04 (0.43)	0.21 (0.86)	0.1148
PAx, median	−0.30 (0.37)	−0.13 (0.52)	0.1071
wPRx, median	**−0.09 (0.28)**	**0.04 (0.71)**	**0.0064**
RAC, median	**−0.61 (0.38)**	**−0.55 (0.61)**	**0.0115**
RAP, median	0.81 (0.29)	0.76 (0.43)	0.1764
AMP, median	1.62 (1.65)	1.87 (1.72)	0.3239
HRsd, median	2.62 (2.60)	1.86 (2.98)	0.4606
HRrmssd, median	15.00 (16.11)	5.78 (18.21)	0.2517
LHF Ratio, median	2.11 (2.08)	1.56 (2.30)	0.9469
	Number (%) of patients	**Number (%) of patients**	
Presence of basal cistern effacement	6 (27.3%)	16 (72.7%)	0.1206
Inflicted head trauma	4 (25.0%)	5 (35.7%)	0.3932

Analysis of age, GCS, PRISM III, CT Marshall Score, hematoma volume, and midline shift performed using Wilcoxon rank sum test. Analysis of basal cistern effacement performed using Fisher's exact test. Analysis of all other variables performed using generalized estimating equations. Bold variables are representative of statistical significance. IQR, interquartile range; GCS, Glasgow Coma Scale; PRISM, Pediatric Risk of Mortality; GOSE-PEDs, Glasgow Outcome Scale –Extended Pediatrics; CT, computed tomography; cm, centimeters, mm, millimeters; Na, sodium; mmol/L, millimoles per liter; mmHg, millimeters of mercury; PRx, pressure reactivity index; wPRx, wavelet-pressure reactivity; PAx, pulse amplitude index; RAC, correlation coefficient between intracranial pressure pulse amplitude and cerebral perfusion pressure; RAP, correlation coefficient between intracranial pressure pulse amplitude and intracranial pressure; AMP, intracranial pressure pulse amplitude; HRsd, standard deviation of heart rate; HRrmssd, root mean square of successive differences of heart rate; LHF, low high frequency ratio.

TABLE 3 | Differences in cerebral physiology to bolus hyperosmolar therapy after intracranial hypertension.

Physiologic variable	Difference with treatment responsiveness [median (IQR)]	Difference with treatment unresponsiveness [median (IQR)]	*p*-value
ICP, median (mmHg)	**−1.66 (3.38)**	**+2.14 (2.910)**	**0.0064**
ABP, median (mmHg)	**−0.67 (4.19)**	**+0.31 (5.26)**	**0.0126**
HR, median (bpm)	−1.00 (7.64)	+0.32 (6.38)	0.8903
PRx, median	**−0.04 (0.22)**	**+0.02 (0.24)**	**0.0063**
PAx, median	−0.06 (0.25)	+0.02 (0.25)	0.0725
wPRx, median	−0.03 (0.27)	−0.01 (0.25)	0.2610
RAC, median	−0.01 (0.17)	−0.03 (0.19)	0.3672
RAP, median	−0.01 (0.31)	+0.03 (0.11)	0.0756
AMP, median	−0.10 (0.40)	+0.16 (0.46)	0.0795
HRsd, median	**−0.06 (0.83)**	**−0.03 (0.40)**	**0.0408**
HRrmssd, median	−0.38 (5.06)	+0.04 (2.56)	0.5242
LHF Ratio, median	+0.05 (1.08)	+0.00 (0.29)	0.8476

Analysis performed using generalized estimating equations. Bold variables are representative of statistical significance. ICP, intracranial pressure; ABP, arterial blood pressure; HR, heart rate; bpm, beats per minute; mmHg, millimeters of mercury; PRx, pressure reactivity index; PAx, pulse amplitude index; wPRx, wavelet-pressure reactivity; RAC, correlation coefficient between intracranial pressure pulse amplitude and cerebral perfusion pressure; RAP, correlation coefficient between intracranial pressure pulse amplitude and intracranial pressure; AMP, intracranial pressure pulse amplitude; HRsd, standard deviation of heart rate; HRrmssd, root mean square of successive differences of heart rate; LHF, low frequency-high frequency ratio.

treatment inefficacy was associated with increases in median PRx ($p = 0.0063$). We observed that treatment efficacy was associated with a greater decrease in median HRsd as compared to treatment inefficacy ($p = 0.0408$). We did not observe significant changes in relation to treatment responsiveness with regards to median HR, PAx, wPRx, RAC, RAP, AMP, HRrmssd, or LHF Ratio.

Physiologic Changes After Hyperosmolar Treatment Without Preceding Intracranial Hypertension

Findings are summarized in **Table 4**. In terms of physiologic vital signs, we observed that HT is associated with increases in ICP ($p < 0.0001$) and ABP ($p < 0.0001$) and decreases in HR ($p < 0.0001$). In terms of indices of CVPR, we observed that HT is associated with increases in PRx ($p < 0.0001$) and decreases in PAx ($p = 0.0005$), wPRx ($p < 0.0001$), and RAC ($p < 0.0001$). In terms of indices of PVC, we observed that HT is associated with increases in RAP ($p < 0.0001$) and AMP ($p < 0.0001$). In terms of HRV, we observed that HT is associated with increases in HRsd ($p < 0.0001$), HRrmssd ($p < 0.0001$), and LHF ratio ($p < 0.0001$).

DISCUSSION

We observed that HT efficacy against ICH is associated with reductions in ICP and ABP. We observed that pre-treatment evidence of efficient CVPR arising from two indices, wPRx and RAC, is associated with effective HT against ICH. In patients without ICH, HT led to increases in ICP and ABP, decreased PVC, and increased HRV.

HT is used against ICH for children with severe TBI. HT is thought to reduce ICH through two mechanisms (23). The first is the establishment of an osmotic gradient sufficient to draw cerebral edema from intraparenchymal tissue into cerebral circulation. The second involves plasma expansion resulting in decreased blood hematoma and reduced blood viscosity. If CVPR mechanisms are intact, this second response would lead to cerebral arteriolar vasoconstriction and a resultant decrease in CABV and ICP. If CVPR is impaired and an insufficient osmotic gradient is developed, HT carries risk of increasing CABV and worsening ICH and cerebral edema. In patients without evidence of ICH, it remains unclear how plasma expansion and the creation of osmotic gradients impacts CVPR, PVC and cerebral oxygen delivery.

TABLE 4 | Differences in cerebral physiology in relation to hyperosmolar therapy without intracranial hypertension.

Physiologic variable	Prior to treatment [mean (SD)]	After treatment [mean (SD)]	*p*-value
ICP, median (mmHg)	**11.06 (4.96)**	**12.81 (10.49)**	**<0.0001**
ABP, median (mmHg)	**77.78 (11.25)**	**78.57 (11.07)**	**<0.0001**
HR, median (bpm)	**99.87 (29.35)**	**97.22 (31.19)**	**<0.0001**
PRx, median	**0.09 (0.41)**	**0.10 (0.40)**	**<0.0001**
PAx, median	**−0.22 (0.37)**	**−0.24 (0.36)**	**0.0005**
wPRx, median	**0.04 (0.35)**	**0.03 (0.36)**	**<0.0001**
RAC, median	**−0.35 (0.42)**	**−0.38 (0.40)**	**<0.0001**
RAP, median	**0.46 (0.39)**	**0.48 (0.38)**	**<0.0001**
AMP, median	**1.21 (1.17)**	**1.26 (1.15)**	**<0.0001**
HRsd, median	**3.11 (1.82)**	**3.38 (2.39)**	**<0.0001**
HRrmssd, median	**18.75 (18.43)**	**20.89 (19.46)**	**<0.0001**
LHF Ratio, median	**1.59 (1.56)**	**2.95 (10.81)**	**<0.0001**

Analysis performed using one-way repeated-measures analysis of variance. Bold variables are representative of statistical significance. ICP, intracranial pressure; ABP, arterial blood pressure; HR, heart rate; bpm, beats per minute; mmHg, millimeters of mercury; PRx, pressure reactivity index; PAx, pulse amplitude index; wPRx, wavelet-pressure reactivity; RAC, correlation coefficient between intracranial pressure pulse amplitude and cerebral perfusion pressure; RAP, correlation coefficient between intracranial pressure pulse amplitude and intracranial pressure; AMP, intracranial pressure pulse amplitude; HRsd, standard deviation of heart rate; HRrmssd, root mean square of successive differences of heart rate; LHF, low frequency-high frequency ratio.

Our findings that efficacy of HT against ICH is associated with reduced ICP and ABP is consistent with putative mechanisms. Development of an osmotic gradient reduces intraparenchymal cerebral edema and ICP. Reduced ABP may reflect an appropriate CVPR response to cerebral circulation volume expansion resulting from HT. This is supported by our observation that HT efficacy is associated with lower pre-treatment wPRx and RAC values, reflective of efficient CVPR. We note that PRx values decrease after efficacious treatments and increase after ineffective treatments. This may reflect improved CVPR after efficacious HT, though no changes in other CVPR indices demonstrated significance. Increases in PRx after ineffective treatment likely reflects worsening CVPR. Prospective work investigating the effect of 23.5% hypertonic saline in poor grade subarachnoid hemorrhage patients suggests that it increases cerebral blood flow (24), and work examining mannitol suggests it does not acutely decrease CABV (25). PVC likely differs in young patients with open anterior fontanelles or smaller skulls as compared to older children who may reflect more similar dynamics to adults. Such changes in PVC may reflect changes in treatment efficacy across pediatric ages as we observed.

Our analysis of bolus HT in patients without ICH was performed to gain further insight regarding both the putative mechanisms and implications of HT. Use of bolus HT without ICH is a clinical decision which at our institution may occur to achieve goal serum sodium or osmolality levels desired by the treating team. HT without preceding ICH was associated with increases in ICP and ABP, with each moving oppositely from when HT improves ICH. In treatments without preceding ICH, there was also evidence of decreased HR, increased HRV (HRsd, HRrmssd and LHF Ratio) and decreasing PVC (increasing values of ABP and RAP). In these patients, there is likely insufficient cerebral edema for an osmotic gradient to shift sufficient cerebral edema toward cerebral circulation to reduce ICP. Rather, there is likely plasma expansion resulting in increased CABV, increased ICP and decreased PVC. An increase in ABP along with ICP may reflect impaired CVPR, but this is not clear. Whereas, PRx values increased in these situations, other indices of CVPR decreased. It should be noted that none of these indices of CVPR represent a gold standard for assessment of CVPR. Concern has been raised in prior work as to whether ineffective HT may impair CVPR (3). PRx, regardless of its accuracy in describing CVPR, has been validated as a marker of injury severity in children with TBI (6, 7), and our findings raise question as to whether inefficient use of HT carries risk of disrupting healthy cerebral dynamics and worsening outcomes.

Model-based indices of CVPR, PVC, and HRV derived from MMM data offer clinicians an opportunity to better understand real-time cerebral physiology. What has remained elusive in the implementation of MMM for clinical decision support is whether specific indices of CVPR, PVC, or HRV confer potential benefit for specific treatment strategies in clinical care. In this study, we investigate pre-treatment indices of CVPR, PVC, and HRV as factors that may confer benefit for HT. We observed that lower pre-treatment values for two CVPR indices, wPRx and RAC, that were indicative of efficient CVPR were associated with HT efficacy. PRx represents the most studied index of CA yet its calculation carries significant assumptions. PRx assumes cerebral blood volume as a surrogate of cerebral blood flow, relies on adequate transmission of cerebral blood volume into ICP, assumes that variability of ICP is purely due to extracranial sources, and assumes no incoherence between ABP and ICP. Inadequate transmission of cerebral blood volume into ICP may be common in infants with open anterior fontanelles or children after decompressive craniectomy. In patients with ICH related to malignant cerebral edema and decreasing CPP, ICP variability is related to intracranial sources. The wPRx index investigates wavelet transform phase shifts from ABP and ICP, deriving values when there is strong coherence. The RAC index relates ICP pulse amplitude with CPP, accounting for situations in which there is inadequate transmission of cerebral blood volume into ICP as well as situations in which ICP values are reflective of evolving cerebral edema. Our finding that lower values of wPRx and RAC are associated with treatment responsiveness for ICH suggests that efficient CVPR may confer benefit for HT, and that these indices may offer utility in these circumstances by overcoming unaddressed assumptions made by the PRx calculation.

HT for severe ICH represents the only level II recommendation to offer benefit for pediatric TBI patients. Existing studies that have helped formulate level II recommendations focus on reduction of ICH (26–29) and there are no studies to date demonstrating that HT, or any other therapy, improves functional outcomes. The reasons for the inability to demonstrate such benefit may lie in selection

of patients for whom therapy is considered. Existing clinical guidelines support use of HT as a tier II strategy (2, 30) in clinical care without a mechanistic understanding as to whether its use addresses etiologies of ICH at the individualized patient level. Its use focuses on the pathophysiology of cerebral edema, not accounting for circumstances in which ICH may more causally relate to increased CABV, obstructive hydrocephalus, increased metabolic demand, or poor venous drainage. The key component to demonstrating benefit in relation to functional outcomes may lie in the ability to use this therapeutic strategy in select patients demonstrating physiologic characteristics conferring potential to benefit. Our findings suggest that indices demonstrating efficient CVPR may identify those patients for whom HT will reduce ICH. Our findings also suggest that therapeutic benefit of HT in such patients may be associated with improved CVPR and functional outcomes.

This study is limited by a small sample size and its retrospective nature. HT occurred at varied time points in the course of TBI management, and we implemented a working cutoff of $\geq$50% of bolus HT efficacy to represent subject-level treatment responsiveness. For these reasons, we acknowledge limitations in extrapolating that treatment responsiveness is related to improved outcomes. The analysis methods employed in this study are exploratory techniques that serve for preliminary hypothesis generation. To account for small sample size, we aggregated data regarding both 3% hypertonic saline and mannitol and were unable to assess for differences in efficacy of either therapy. Our findings are limited given high variability of dosing employed for both agents. Because this is a single-center study, findings may not be generalizable across multiple centers. There is a need to conduct larger multi-center studies with standardized dosing and rigorous statistical methodologies to investigate whether model-based indices of CVPR, PVC and HRV may guide therapeutic targeting of HT to reduce ICH and improve functional outcomes.

CONCLUSION

After pediatric TBI, efficacy of bolus HT against ICH is associated with pre-treatment physiologic characteristics suggestive of efficient CVPR, and therapy leads to reduction of ICP and ABP. Bolus therapy of HT without preceding ICH may alter cerebral dynamics by increasing ICP and decreasing PVC.

DATA AVAILABILITY STATEMENT

The raw data supporting the conclusions of this article will be made available by the authors, without undue reservation.

ETHICS STATEMENT

The studies involving human participants were reviewed and approved by Phoenix Children's Hospital Institutional Review Board (IRB #17-469). Written informed consent from the participants' legal guardian/next of kin was not required to participate in this study in accordance with the national legislation and the institutional requirements.

AUTHOR CONTRIBUTIONS

JW, MK and BA contributed toward data analysis, preparation, development, and critical review of the manuscript. PA contributed toward preparation, development, and critical review of the manuscript. All authors contributed to the article and approved the submitted version.

FUNDING

This study was funded in part by the United States Department of Defense Congressionally Directed Medical Research Programs (W81XWH-19-1-0514).

ACKNOWLEDGMENTS

We thank Dr. M'hamed Temkit, Ph.D., for discussion of the statistical tests implemented in this study.

SUPPLEMENTARY MATERIAL

The Supplementary Material for this article can be found online at: https://www.frontiersin.org/articles/10.3389/fneur.2021.662089/full#supplementary-material

REFERENCES

1. Hawley CA, Ward AB, Long J, Owen DW, Magnay AR. Prevalence of traumatic brain injury amongst children admitted to hospital in one health district: a population-based study. *Injury.* (2003) 354:256–60. doi: 10.1016/s0020-1383(02)00193-6
2. Kochanek PM, Tasker RC, Carney N, Totten AM, Adelson PD, Selden NR, et al. Guidelines for the management of pediatric severe traumatic brain injury, third edition: update of the brain trauma foundation guidelines. *Pediatr Crit Care Med.* (2019) 20 (3 Suppl. 1):S1–82. doi: 10.1097/PCC.0000000000001735
3. Froese L, Dian J, Batson C, Gomez A, Unger B, Zeiler FA. The impact of hypertonic saline on cerebrovascular reactivity and compensatory reserve in traumatic brain injury: an exploratory analysis. *Acta Neurochir.* (2020) 162:2683–93. doi: 10.1007/s00701-020-04579-0
4. Appavu B, Burrows BT, Foldes S, Adelson PD. Approaches to multimodality monitoring in pediatric traumatic brain injury. *Front Neurol.* (2019) 10:1261. doi: 10.3389/fneur.2019.01261
5. Zeiler FA, Donnelly J, Calviello L, Smielewski P, Menon DK, Czosnyka M. Pressure autoregulation in measurement techniques in adult traumatic brain injury, part II: a scoping review of continuous methods. *J Neurotrauma.* (2017) 34:3227–37. doi: 10.1089/neu.2017.5086
6. Brady KM, Shaffner DH, Lee JK, Easley RB, Smielewski P, Czosnyka M, et al. Continuous monitoring of cerebrovascular pressure reactivity after traumatic brain injury in children. *Pediatrics.* (2009) 124:e1205–12. doi: 10.1542/peds.2009-0550
7. Lewis PM, Czosnyka M, Carter BG, Rosenfeld JV, Paul E, Singhal N, et al. Cerebrovascular pressure reactivity in children with traumatic brain injury. *Pediatr Crit Care Med.* (2015) 16:739–49. doi: 10.1097/PCC.0000000000000471

8. Task force of the European Society of Cardiology and the North American Society of Pacing and Electrophysiology. Heart rate variability. Standards of measurement, physiologic interpretation, clinical use. *Circulation.* (1996) 93:1043–65. doi: 10.1161/01.CIR.93.5.1043
9. Sykora E, Diedler J, Kasprowicz M, Budohoski KP, Haubrich C, Smielewski P, et al. Critical thresholds for cerebrovascular reactivity after traumatic brain injury. *Neurocrit Care.* (2012) 16:258–66. doi: 10.1007/s12028-011-9630-8
10. Balestreri M, Czosnyka M, Steiner LA, Schmidt E, Smielewski P, Matta B, et al. Intracranial hypertension: what additional information can be derived from ICP waveform after head injury? *Acta Neurochir.* (2004) 146:131–41. doi: 10.1007/s00701-003-0187-y
11. Kochanek PM, Carney N, Adelson PD, Ashwal S, Bell MJ, Bratton S, et al. Guidelines for the acute medical management of severe traumatic brain injury infants, children, and adolescents – second edition. *Pediatr Crit Care Med.* (2012) 13 (Suppl. 1):S1–82. doi: 10.1097/PCC.0b013e31823f435c
12. Lazardis C, Desantis SM, Smielewski P, Menon DK, Hutchinson P, Pickard JD, et al. Patient-specific thresholds of intracranial pressure in severe traumatic brain injury. *J Neurosurg.* (2014) 120:893–900. doi: 10.3171/2014.1.JNS131292
13. Teasdale G, Jennett B. Assessment of coma and impaired consciousness. A practical scale. *Lancet.* (1974) 13:2:81–4. doi: 10.1016/s0140-6736(74)91639-0
14. Pollack MM, Patel KM, Ruttiman UE. PRISM III: an updated pediatric risk of mortality score. *Crit Care Med.* (1996) 24:743–52. doi: 10.1097/00003246-199605000-00004
15. Beers SR, Wisniewski SR, Garcia-Filon P, Tian Y, Hahner T, Berger RP, et al. Validity of a pediatric version of the glasgow outcome scale – extended. *J Neurotrauma.* (2012) 29:1126–39. doi: 10.1089/neu.2011.2272
16. Steiner LA, Czosnyka M, Piechnik SK, Smielewski P, Chatfield D, Menon DK, et al. Continuous monitoring of cerebrovascular pressure reactivity allows determination of optimal cerebral perfusion in patients with traumatic brain injury. *Crit Care Med.* (2002) 30:733–8. doi: 10.1097/00003246-200204000-00002
17. Zeiler FA, Donnelly J, Calviello L, Lee JK, Smielewski P, Brady K, et al. Validation of pressure reactivity and pulse amplitude indices against the lower limit of autoregulation, part I: experimental intracranial hypertension. *J Neurotrauma.* (2018) 35:963–74. doi: 10.1089/neu.2017.5603
18. Zeiler FA, Donnelly J, Menon DK, Smielewski P, Hutchinson PGA, Czosnyka M. A description of a new continuous physiologic index in traumatic brain injury using the correlation between pulse amplitude of intracranial pressure and cerebral perfusion pressure. *J Neurotrauma.* (2018) 35:963–74. doi: 10.1089/neu.2017.5241
19. Liu X, Donnelly J, Czosnyka M, Aries MJH, Brady K, Cardim D, et al. Cerebrovascular pressure reactivity monitoring using wavelet analysis in traumatic brain injury patients: a retrospective study. *PLoS Med.* (2017) 2017:14:e1002348. doi: 10.1371/journal.pmed.1002348
20. Hiler M, Czosnyka M, Hutchinson P, Balestreri M, Smielewski P, Matta B, et al. Predictive value of initial computerized tomography scan, intracranial pressure, and state of autoregulation in patients with traumatic brain injury. *J Neurosurg.* (2006) 104:731–7. doi: 10.3171/jns.2006.104.5.731
21. Carr GJ, Chi EM. Analysis of variance for repeated measures. Data: a generalized estimating equations approach. *Stat Med.* (1992) 15: 1033–40. doi: 10.1002/sim.4780110805
22. Kim HY. Statistical notes for clinical researchers: a one-way repeated measures ANOVA for data with repeated observations. *Restor Dent Endod.* (2015) 40:91–5. doi: 10.5395/rde.2015.40.1.91
23. Knapp JM. Hyperosmolar therapy in the treatment of severe head injury in children: mannitol and hypertonic saline. *AACN Clin Issues.* (2005) 16:199–211. doi: 10.1097/00044067-200504000-00011
24. Tseng MY, Al-Rawi PG, Pickard PD, Rasulo FA, Kirkpatrick PJ. Effect of hypertonic saline on cerebral blood flow in poor-grade patients with subarachnoid hemorrhage. *Stroke.* (2003) 34:1389–96. doi: 10.1161/01.STR.0000071526.45277.44
25. Diringer MN, Scalfani MT, Zazulla AR, Videen TO, Dhar R, Powers WJ. Effect of mannitol on cerebral blood volume in patients with head injury. *Neurosurgery.* (2012) 70:1215–1219. doi: 10.1227/NEU.0b013e3182417bc2
26. Fisher B, Thomas D, Peterson B. Hypertonic saline lowers raised intracranial pressure in children after head trauma. *J Neurosurg Anesthesiol.* (1992) 4:4–10. doi: 10.1097/00008506-199201000-00002
27. Khanna S, Davis D, Peterson B, Fisher B, Tung H, O'Quigley J, et al. Use of hypertonic saline in the treatment of severe refractory post-traumatic intracranial hypertension in pediatric traumatic brain injury. *Crit Care Med.* (2000) 28:1144–51. doi: 10.1097/00003246-200004000-00038
28. Shein SL, Ferguson NM, Kochanek PM, Bayir H, Clark RS, Fink EL, et al. Effectiveness of pharmacological therapies for intracranial hypertension in children with severe traumatic brain injury – results from an automated data collection system time-synched to drug administration. *Pediatr Crit Care Med.* (2016) 17:236–45. doi: 10.1097/PCC.0000000000000610
29. Simma B, Burger R, Falk M, Sacher P, Fanconi S. A prospective, randomized, and controlled study of fluid management in children with severe head injury: lactated ringer's solution versus hypertonic saline. *Crit Care Med.* (1998) 26:1265–70. doi: 10.1097/00003246-199807000-00032
30. Kochanek PM, Tasker RC, Bell MJ, Adelson PD, Carney N, Vavilala M, et al. Management of pediatric severe traumatic brain injury: 2019 consensus and guidelines-based algorithm for first and second tier therapies. *Pediatr Crit Care Med.* (2019) 20:269–79. doi: 10.1097/PCC.0000000000001737

Conflict of Interest: The authors declare that the research was conducted in the absence of any commercial or financial relationships that could be construed as a potential conflict of interest.

frontiers in Neurology

ORIGINAL RESEARCH
published: 28 April 2021
doi: 10.3389/fneur.2021.662839

Wavelet Autoregulation Monitoring Identifies Blood Pressures Associated With Brain Injury in Neonatal Hypoxic-Ischemic Encephalopathy

*Xiuyun Liu[1], Aylin Tekes[2], Jamie Perin[3], May W. Chen[4], Bruno P. Soares[5], An N. Massaro[6,7,8], Rathinaswamy B. Govindan[6,7], Charlamaine Parkinson[4], Raul Chavez-Valdez[4], Frances J. Northington[4], Ken M. Brady[9] and Jennifer K. Lee[1]**

[1] Department of Anesthesiology and Critical Care Medicine, Johns Hopkins University, Baltimore, MD, United States, [2] Department of Radiology, Johns Hopkins University, Baltimore, MD, United States, [3] Department of Pediatrics, Center for Child and Community Health Research, Johns Hopkins University, Baltimore, MD, United States, [4] Division of Neonatology, Johns Hopkins University, Baltimore, MD, United States, [5] Department of Radiology, University of Vermont, Burlington, VT, United States, [6] Fetal Medicine Institute, Children's National Health System, Washington, DC, United States, [7] The George Washington University School of Medicine, Washington, DC, United States, [8] Division of Neonatology, Children's National Health System, Washington, DC, United States, [9] Department of Anesthesiology, Lurie Children's Hospital, Chicago, IL, United States

OPEN ACCESS

Edited by:
Chiara Robba,
University of Genoa, Italy

Reviewed by:
Benjamin Aaron Emanuel,
University of Southern California, United States
Denise Battaglini,
University of Barcelona, Spain

***Correspondence:**
Jennifer K. Lee
jklee@jhmi.edu

Specialty section:
This article was submitted to Neurocritical and Neurohospitalist Care, a section of the journal Frontiers in Neurology

Received: *01 February 2021*
Accepted: *22 March 2021*
Published: *28 April 2021*

Citation:
Liu X, Tekes A, Perin J, Chen MW, Soares BP, Massaro AN, Govindan RB, Parkinson C, Chavez-Valdez R, Northington FJ, Brady KM and Lee JK (2021) Wavelet Autoregulation Monitoring Identifies Blood Pressures Associated With Brain Injury in Neonatal Hypoxic-Ischemic Encephalopathy. Front. Neurol. 12:662839. doi: 10.3389/fneur.2021.662839

Dysfunctional cerebrovascular autoregulation may contribute to neurologic injury in neonatal hypoxic-ischemic encephalopathy (HIE). Identifying the optimal mean arterial blood pressure (MAPopt) that best supports autoregulation could help identify hemodynamic goals that support neurologic recovery. In neonates who received therapeutic hypothermia for HIE, we hypothesized that the wavelet hemoglobin volume index (wHVx) would identify MAPopt and that blood pressures closer to MAPopt would be associated with less brain injury on MRI. We also tested a correlation-derived hemoglobin volume index (HVx) and single- and multi-window data processing methodology. Autoregulation was monitored in consecutive 3-h periods using near infrared spectroscopy in an observational study. The neonates had a mean MAP of 54 mmHg (standard deviation: 9) during hypothermia. Greater blood pressure above the MAPopt from single-window wHVx was associated with less injury in the paracentral gyri ($p = 0.044$; $n = 63$), basal ganglia ($p = 0.015$), thalamus ($p = 0.013$), and brainstem ($p = 0.041$) after adjustments for sex, vasopressor use, seizures, arterial carbon dioxide level, and a perinatal insult score. Blood pressure exceeding MAPopt from the multi-window, correlation HVx was associated with less injury in the brainstem ($p = 0.021$) but not in other brain regions. We conclude that applying wavelet methodology to short autoregulation monitoring periods may improve the identification of MAPopt values that are associated with brain injury. Having blood pressure above MAPopt with an upper MAP of ~50–60 mmHg may reduce the risk of brain injury during therapeutic hypothermia. Though a cause-and-effect relationship cannot be inferred, the data support the need for randomized studies of autoregulation and brain injury in neonates with HIE.

Keywords: newborn, hypoxia, cerebrovascular circulation, brain, hypothermia, cerebral autoregulation

INTRODUCTION

Nearly one million neonatal deaths worldwide each year are related to hypoxic-ischemic encephalopathy (HIE) from intrapartum complications (1). Though therapeutic hypothermia has reduced mortality, additional treatments are needed to prevent the persistent moderate-to-severe neurologic disabilities that affect almost half of survivors who receive this therapy (2). Alterations in cerebrovascular blood pressure autoregulation, which holds blood flow stable across changes in perfusion pressure, may contribute to HIE-related brain injury. Neuroprotective hemodynamic goals for infants with HIE are unclear, and many clinicians base their blood pressure goals on the neonate's gestational age in weeks +5 (3). However, maintaining mean arterial blood pressure (MAP) above the gestational age+5 does not reduce neurologic injury in infants with HIE (4).

Autoregulation monitoring has the potential to clarify hemodynamic goals during recovery from brain injury. Blood pressures below the optimal MAP (MAPopt) at which autoregulation is most robust are associated with greater brain injury on MRI and worse neurocognitive outcomes in neonates with HIE (4–7). The pediatric traumatic brain injury guidelines recommend that clinicians consider monitoring autoregulation to reduce secondary injury (8). Unfortunately, similar recommendations cannot be made in neonatal medicine where autoregulation monitoring is challenged by the reliance on non-invasive cranial methods that often have high signal variability. More reliable techniques with less signal noise must be developed for neonatal autoregulation monitoring.

Mathematical algorithms that determine the relationship between blood pressure and cerebral blood volume can be used to assess autoregulation. The relative total tissue hemoglobin (rTHb) from near-infrared spectroscopy (NIRS) is a surrogate measure of cerebral blood volume during autoregulatory vasoreactivity (9). In theory, changes in cerebral metabolic rate, such as from temperature modulation, should have little effect on rTHb because rTHb measures oxygenated and deoxygenated hemoglobin. Indices derived from rTHb accurately measure autoregulation during therapeutic hypothermia (10).

The correlation between MAP and rTHb generates the hemoglobin volume index (HVx) (10). Though correlation is commonly used to assess autoregulation (4, 11), it can have considerable signal variability when applied to short monitoring periods. We therefore developed the wavelet hemoglobin volume index (wHVx) (12, 13) and a multi-window data processing method (14) to produce a more stable autoregulation index suitable for monitoring short time windows. Whether wHVx and multi-window processing can identify blood pressures associated with HIE brain injury is unknown. In this study, we tested wHVx and correlation HVx with single- and multi-window data processing in newborns with HIE. We hypothesized that blood pressure deviation from the MAPopt identified by wHVx would be associated with regional and global brain injury on MRI. We secondarily tested the MAPopt from correlation HVx and whether the multi-window technique improves MAPopt identification relative to the single-window technique.

MATERIALS AND METHODS

We measured autoregulatory vasoreactivity using NIRS in neonates who received therapeutic hypothermia for HIE in the Johns Hopkins neonatal intensive care unit (NICU). This prospective, observational study was approved by the Johns Hopkins Institutional Review Board. Before May 2013, written consent was obtained from neonates' parents for study participation. After that, NIRS became standard clinical care for HIE in our NICU, and the IRB waived the requirement for written consent. Sixty-six neonates in this study were reported in at least one of our past reports (4–7, 15–18). Four neonates contributed new data to the study.

Enrollment Criteria and Clinical Care

All neonates diagnosed with HIE were screened between September 2010 and November 2015. Study enrollment criteria included the receipt of therapeutic hypothermia, continuous arterial blood pressure monitoring, gestational age $\geq$35 weeks, and birth weight $\geq$1,800 g. Neonates without an arterial blood pressure cannula, who did not receive hypothermia, or who were transferred to another intensive care unit for potential extracorporeal membrane oxygenation were not eligible for the study.

Neonates were diagnosed with moderate or severe HIE at their birth hospital based on the National Institute of Child Health and Human Development (NICHD) Neonatal Research Network criteria as previously described (7, 19). Outborn neonates started passive cooling and were transported to our NICU for active therapeutic hypothermia. A modified Sarnat encephalopathy score (19, 20) was determined when they arrived at our NICU. Five neonates who were initially diagnosed with moderate HIE at the outside hospital were subsequently graded to have mild HIE at our institution during active cooling. The clinicians continued therapeutic hypothermia because perinatal acidosis increases the risk of persistent brain injury, even in mild encephalopathy (21), and the encephalopathy may rapidly evolve (22). These neonates met study criteria and therefore were enrolled.

We have reported our therapeutic hypothermia protocol (4, 6). Briefly, neonates underwent whole-body cooling to a goal rectal temperature of 33.5 $\pm$ 0.5°C for 72 h followed by rewarming at $\leq$0.5°C/h. For the study, the rewarming period was defined by a temperature increase from 34.1 to 36.4°C. The normothermia period was defined by a temperature $\geq$36.5°C. Clinicians followed routine clinical practice for blood pressure management, and they had access to the NIRS regional cerebral oxyhemoglobin data but not the HVx or wHVx. All neonates received morphine for sedation followed by as-needed fentanyl, hydromorphone, clonidine, or benzodiazepines. Dopamine was administered for hypotension, followed by dobutamine or epinephrine at the clinicians' discretion. Seizures were diagnosed by electroencephalogram and treated with phenobarbital. If the seizures persisted, neonates were administered levetiracetam, fosphenytoin, or topiramate. Hydrocortisone was administered for adrenal suppression or hypotension that was refractory to vasopressors. The neonates' partial pressure of arterial carbon dioxide ($PaCO_2$) levels were categorized into one of four

categories: (1) all 35–45 mmHg; (2) some <35 mmHg but none >45 mmHg; (3) none <35 mmHg but some >45 mmHg; and (4) some <35 mmHg and some >45 mmHg (4, 23).

We assigned each neonate a perinatal insult score based on common clinical criteria, including whether delivery was emergent, Apgar score at 10 min, first blood gas pH and base deficit, Sarnat stage, and need for mechanical ventilation (4, 24) (**Supplementary Table 1**). For outborn neonates, we used the Sarnat encephalopathy score that was obtained upon their arrival at our NICU. The purpose of the perinatal insult score, which is independently associated with HIE brain injury (24), is to provide a single variable that describes the neonate's clinical status soon after birth for multivariate analysis (4, 24). The investigator who assigned the perinatal insult scores (RC-V) was blinded to the autoregulation and MRI data.

Autoregulation Monitoring

A bedside laptop computer continuously monitored MAP from the arterial cannula and rTHb from bilateral cerebral NIRS (INVOS 5100; neonatal probes; Medtronic, Minneapolis, MN) during hypothermia, rewarming, and the first 3 h of normothermia. Data were sampled at 100 Hz with ICM+ software (University of Cambridge, Cambridge Enterprise, Cambridge, UK, https://icmplus.neurosurg.cam.ac.uk). The rTHb was detected by NIRS to obtain a surrogate measure of cerebral blood volume (9). (Additional information is provided in the **Supplementary Material**.) Artifacts in the arterial blood pressure tracing, including those from flushes and transducer adjustments, were filtered out manually. We averaged the MAP and rTHb data in consecutive, 10-s intervals to exclude high-frequency waveforms from respiration and pulse (**Figure 1A**). This filtering technique leaves slow-wave oscillation data from autoregulatory vasoreactivity (9). An investigator (XL) blinded to the neonate's temperature and brain MRI measures processed all of the autoregulation data.

HVx Calculation

HVx was calculated as the Pearson correlation coefficient between 10-s averages of MAP and rTHb from 30 paired samples in consecutive, 300-s epochs (**Figure 1B**). HVx is a continuous metric of autoregulatory vasoreactivity that ranges from −1 to +1. Negative or near-zero HVx indicates functional autoregulation because MAP and cerebral blood volume correlate negatively or not at all. When autoregulation becomes dysfunctional, HVx becomes increasingly positive and approaches +1 because MAP and cerebral blood volume correlate (10).

wHVx Calculation

Using methodology that we previously validated in piglets (12, 13), we calculated the wavelet transform phase shift between MAP and rTHb in the frequency range of 0.007–0.05 Hz. Intracranial slow waves from autoregulatory vasoreactivity are known to occur in this frequency range (9, 25). In brief, we calculated the wavelet transform phase shift at each scale-frequency point in 800-s data segments using a moving time window that was updated every 10 s and a wavelet transform coherence threshold of 0.46 (26) (**Supplementary Material**). This method assumes that data with good coherence represent true physiology whereas poorly coherent data are from signal noise.

Then, we calculated the wavelet semblance (the cosine of wavelet phase shift) to generate the wHVx. This process produced

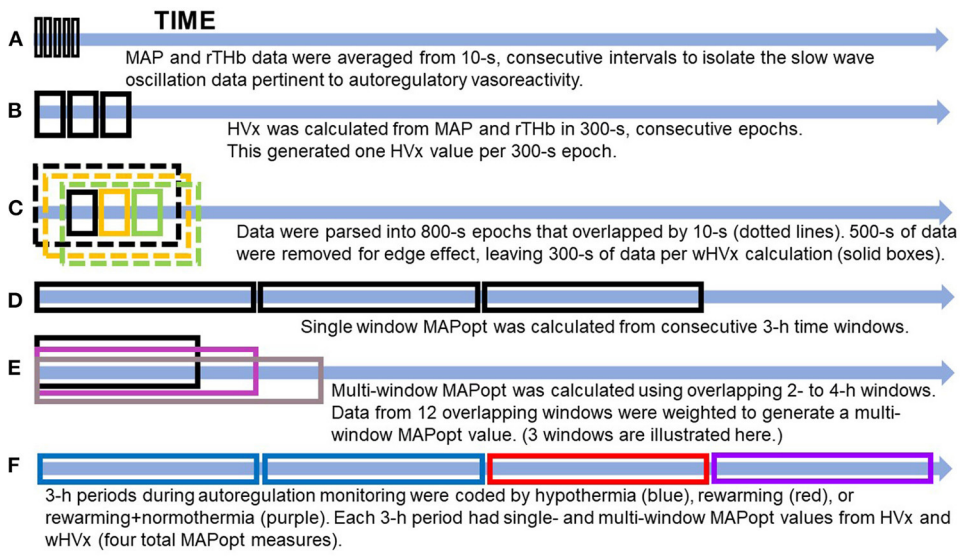

FIGURE 1 | Illustration of data processing. **(A)** The data were filtered to remove high-frequency waveforms, including those associated with pulse and respiration. **(B)** The hemoglobin volume index (HVx). **(C)** The wavelet hemoglobin volume index (wHVx). **(D)** Single-window, optimal mean arterial blood pressure (MAPopt). **(E)** Multi-window MAPopt. **(F)** MAPopt values were calculated in consecutive 3-hour periods that were coded by the neonate's core temperature. Boxes are not to scale. MAP, mean arterial blood pressure; rTHb, NIRS relative total tissue hemoglobin.

several wavelet semblances from 0.007 to 0.05 Hz at each time point. The wavelet semblance values were then averaged along the frequency domain to create one wHVx value for each time point. We chose an 800-s window length because an edge effect necessitated that we reject approximately 500 s of data (27), leaving 300 s of data to calculate wHVx. Therefore, both the wHVx and correlation HVx data were analyzed in 300-s epochs (**Figure 1C**) (**Supplementary Material**).

The wHVx is a continuous autoregulatory vasoreactivity index that ranges from −1 to +1. Functional autoregulation generates a high phase shift owing to the inverse correlation between MAP and rTHb (28). For example, when autoregulation is functional, increases in blood pressure cause the cerebral arterioles to constrict with a reduction in cerebral blood volume that is detected by rTHb. Perfect autoregulation causes a 180° phase shift between MAP and rTHb, thereby generating a wHVx of −1. When autoregulation is dysfunctional, increases in blood pressure cause the cerebral blood volume and rTHb to rise also. Complete pressure passivity generates a 0° phase shift between MAP and rTHb with a wHVx of +1. Thus, the wHVx and correlation HVx indices have the same directionality. Functional autoregulation is indicated by negative or near-zero wHVx and HVx. Dysfunctional autoregulation causes wHVx and HVx to become positive.

Identification of MAPopt

Graphs were generated by sorting each neonate's MAP into 3-mmHg bins on the x-axis and the mean HVx or wHVx of each bin on the y-axis. An automatic curve fitting method that used the smallest curve fitting error in ICM+ (13) generated a U-shaped curve with MAPopt at the nadir (**Figure 2**). Neonates without a nadir were coded as having an unidentifiable MAPopt.

We derived MAPopt from HVx and wHVx using single- and multi-window methods to generate four comparison indices. Single-window MAPopt was calculated in consecutive 3-h windows to generate one MAPopt per window (**Figures 1D**, **2**). Thus, every neonate had many single-window MAPopt values from HVx and wHVx across time.

The multi-window MAPopt was calculated by using a previously published method (14). Twelve 2-h to 4-h overlapping windows of data were updated every 10 min (**Figure 1E**) to generate 12 MAP-HVx and 12 MAP-wHVx graphs. A weighting process was applied based on curve fit error, curve shape, and window duration. Data with smaller curve fit errors that formed U-shapes and that were from shorter time windows were weighted heavily and contributed more to the MAPopt calculation (14). The weighted average from the 12 graphs generated the final multi-window MAPopt values from HVx and wHVx across time.

Finally, each neonate's autoregulation recording was divided into consecutive 3-h periods from the beginning of the recording. These were coded according to the neonate's rectal temperature (**Figure 1F**). Temperatures ≤34.0°C were considered hypothermia, and the rewarming period consisted of temperatures 34.1°C to 36.4°C. The rewarming+normothermia period included at least 15 min of rewarming plus normothermia, which was defined as ≥36.5°C. We did not analyze periods that contained a mixture of hypothermia and rewarming or only normothermia. One investigator (JKL) who was blinded to the autoregulation and MRI data coded the temperatures for each period. Ultimately, each neonate had four

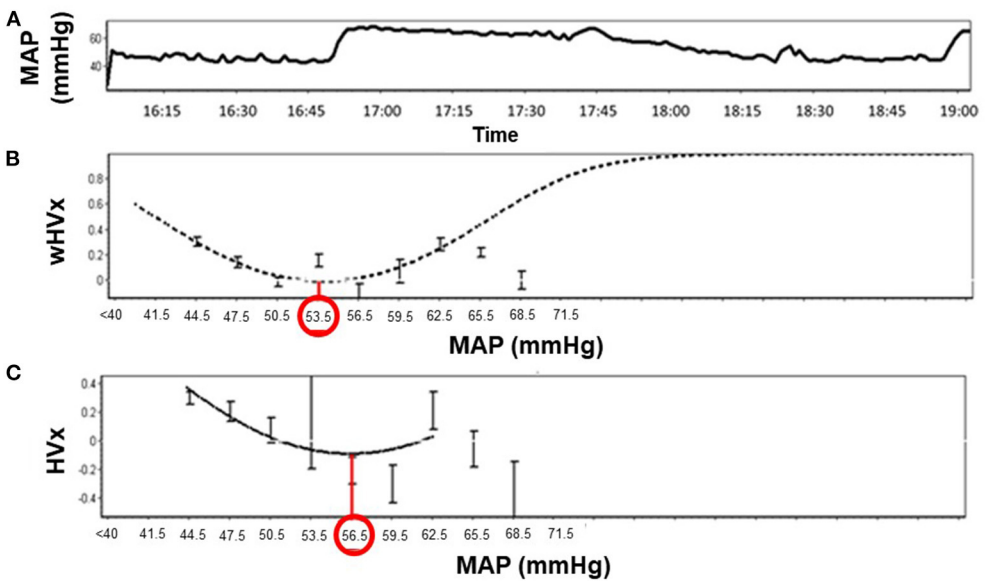

FIGURE 2 | Identification of optimal mean arterial blood pressure (MAPopt) by the hemoglobin volume index (HVx) and the wavelet hemoglobin volume index (wHVx) in an example neonate. **(A)** Mean arterial blood pressure; **(B)** Using wHVx, the curve fitting method identified MAPopt at 53.5 mmHg. **(C)** HVx identified MAPopt at 56.5 mmHg. The curved lines show the optimal curve fit applied by ICM+ software. The bars are standard deviations.

MAPopt values calculated by the single- and multi-window methods from HVx and wHVx in each 3-h period across hypothermia, rewarming, and the transition between rewarming and normothermia.

Brain MRI

Brain MRIs were obtained in neonates between 4 and 16 days of life on 1.5T (Avanto; Siemens, Erlangen, Germany) or 3T (Avanto; Siemens) clinical MRI scanners. All neonates were imaged without anesthesia during natural sleep. We reported our MRI methods previously (5–7). The neuroradiologists were blinded to the autoregulation indices and blood pressure data. An experienced pediatric neuroradiologist (AT) scored each MRI qualitatively as no, mild, moderate, or severe injury using T1, T2, and diffusion tensor imaging (DTI) in six regions: paracentral gyri, global white matter, thalamus, basal ganglia, posterior limb of the internal capsule, and brainstem (4).

Two pediatric neuroradiologists (AT, BS) also graded the T1 and T2 MRIs using the NICHD Neonatal Research Network score (2). This is a standardized score with categories of 0: no injury; **1A**: minimal cerebral lesions and no injury in the thalamus, basal ganglia, or internal capsule; **1B**: more extensive cerebral lesions without injury in the thalamus, basal ganglia, or internal capsule and no infarction; **2A**: any injury in thalamus, basal ganglia, or anterior or posterior limb of the internal capsule or watershed infarction; **2B**: same criteria as category **2A** with additional cerebral lesions; and **3**: cerebral hemispheric devastation. To test agreement in grading the MRIs, the two neuroradiologists independently interpreted 10 MRIs.

Statistical Analysis

Statistical analysis was conducted with R (www.r-project.org/). We used proportional odds logistic regression to examine the associations between autoregulation and brain injury in data stratified by three temperatures: hypothermia, rewarming, and rewarming + normothermia. Autoregulation was measured in each neonate by the maximal blood pressure above or below MAPopt. We also measured the area under the curve (AUC; min × mmHg/h) of time (minutes) with blood pressure above or below MAPopt and blood pressure (mmHg) above or below MAPopt normalized to the monitoring duration (hours) (4). These autoregulation measures were obtained in each 3-h period coded by temperature.

The associations between each neonate's autoregulation and brain injury parameters were additionally analyzed with adjustments for sex, $PaCO_2$ level, perinatal insult score, vasopressor use, and presence of electroencephalographic seizures. We selected these covariates because of their potential associations with autoregulation and brain injury (15, 23, 29–33).

We adjusted for multiple comparisons using Bonferroni corrections within each temperature and brain injury metric. For example, when analyzing the maximal blood pressure above MAPopt during hypothermia, 24 tests compared MAPopt from single- and multi-window wHVx and correlation HVx (four types of MAPopt) in 6 brain regions. Four additional tests compared maximal blood pressure above MAPopt with the NICHD global brain injury score. For the entire study encompassing the three temperatures (hypothermia, rewarming, and rewarming + normothermia), we performed 336 unadjusted and 336 adjusted comparisons. The Bonferroni correction controlled for the inflation of type 1 error caused by testing different MAPopt measures across time and in multiple brain

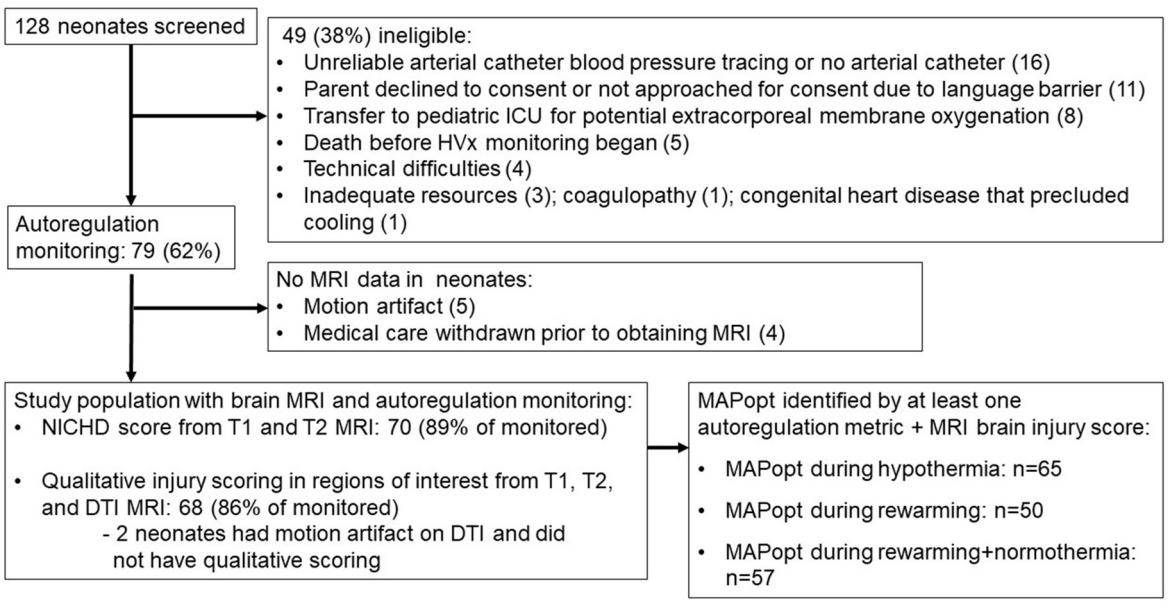

FIGURE 3 | Study screening and enrollment. ICU, intensive care unit; MRI, magnetic resonance imaging; NICHD, National Institute of Child Health and Human Development; DTI, diffusion tensor imaging; MAPopt, optimal mean arterial blood pressure.

TABLE 1 | Clinical descriptions of neonates ($n = 79$).

Characteristic	Mean (SD) or *n* (%)
Male sex	47 (59%)
Gestational age, weeks	39.1 (1.5)
Emergency delivery[a]	56 (71%)
Cesarean section	60 (76%)
10-min Apgar score	4.8 (2.2)
Vasopressor use	52 (66%)
Seizures[b]	31 (39%)
Required mechanical ventilation	41 (52%)
Sarnat encephalopathy score[c]	
1	5 (6%)
2	59 (75%)
3	15 (19%)
$PaCO_2$, mmHg	
All 35–45	6 (8%)
Some <35, all <45	16 (20%)
None <35, some >45	31 (39%)
Some <35, some >45	26 (33%)
pH of first arterial blood gas[d]	7.10 (0.16)
Base deficit of first arterial blood gas[e]	−16.1 (7.4)
Perinatal insult score	6 (1.4)

[a] *Defined as an unscheduled cesarean delivery for fetal distress.*
[b] *Diagnosed by electroencephalography.*
[c] *For neonates born at an outside hospital, the Sarnat score obtained after arrival to the Johns Hopkins neonatal intensive care unit is reported.*
[d] *Seventy seven neonates had pH values from their first arterial blood gas.*
[e] *Fifty four neonates had base deficit values from their first arterial blood gas.*
$PaCO_2$, partial pressure of arterial carbon dioxide.

regions (34). The 95% confidence intervals of the regression coefficients and the *p*-values were adjusted for multiple comparisons. $p < 0.05$ was considered statistically significant.

Sample Size Estimation

This is a secondary and exploratory analysis of data from our prior studies (4–7, 15–18). No other studies have calculated MAPopt using wavelet or multi-window autoregulation monitoring in HIE to our knowledge. Nonetheless, a separate study of HIE using a different wavelet autoregulation index showed that an approximate mean index difference of ≥0.25 identified neonates who died or suffered brain injury (35). Using these estimates, a sample of 17 newborns with brain injury and 17 without injury would have power >0.80 at the alpha 0.05 level (PS Power and Sample Size Calculations, v. 3.0) (36, 37).

RESULTS

Seventy-nine neonates were enrolled for autoregulation monitoring, and 70 (89%) received a brain MRI (**Figure 3**). The majority were delivered emergently by unscheduled cesarean section for documented fetal distress (**Table 1**). Autoregulation was monitored for a mean total of 54.4 h [standard deviation (SD): 21.7 h; 95% confidence interval (CI): 49.5, 59.1 h] in all neonates.

TABLE 2 | MRI interpretation by brain region and National Institute of Child Health and Human Development score.

Brain region[a]	*n* (%)
Paracentral gyri ($n = 68$)	
No injury	41 (60)
Mild injury	14 (21)
Moderate injury	6 (9)
Severe injury	7 (10)
White matter ($n = 68$)	
No injury	15 (22)
Mild injury	29 (43)
Moderate injury	11 (16)
Severe injury	13 (19)
Basal ganglia ($n = 68$)	
No injury	32 (47)
Mild injury	19 (28)
Moderate injury	10 (15)
Severe injury	7 (10)
Thalamus ($n = 68$)	
No injury	30 (44)
Mild injury	18 (27)
Moderate injury	11 (16)
Severe injury	9 (13)
Posterior limb of the internal capsule ($n = 68$)	
No injury	46 (68)
Mild injury	11 (16)
Moderate injury	6 (9)
Severe injury	5 (7)
Brainstem ($n = 68$)	
No injury	32 (47)
Mild injury	19 (28)
Moderate injury	10 (15)
Severe injury	7 (10)
NICHD score ($n = 70$)	
0	37 (53)
1A	6 (9)
1B	12 (17)
2A	6 (9)
2B	8 (11)
3	1 (1)

[a] *Seventy neonates had National Institute of Child Health and Human Development (NICHD) brain injury scoring on T1 and T2 MRI. The regional injury score, which required interpretation of T1, T2, and diffusion tensor imaging (DTI) MRI, was completed in only 68 neonates because two had motion artifact on DTI.*

The neuroradiologists had 100% agreement in grading injury on 10 MRIs. Most neonates had mild or no injury in the paracentral gyri, white matter, basal ganglia, thalamus, posterior limb of the internal capsule, and brain stem, with NICHD scores of 0, **1A**, or **1B** (**Table 2**). The white matter most commonly showed injury, whether mild, moderate, or severe, whereas gray matter and brainstem more often had no injury. White matter was also the most common region to have severe injury.

TABLE 3 | Mean optimal arterial blood pressure values identified by the autoregulation metrics.

Mathematical algorithm	Hypothermia mean (SD)		Rewarming mean (SD)		Rewarming + normothermia mean (SD)	
	n	mmHg	*n*	mmHg	*n*	mmHg
MAPopt_HVx (SW)	75	52 (6)	48	51 (9)	45	51 (8)
MAPopt_wHVx (SW)	74	52 (6)	45	52 (9)	47	54 (8)
MAPopt_HVx (MW)	76	53 (6)	50	51 (8)	52	51 (8)
MAPopt_wHVx (MW)	77	52 (5)	55	52 (7)	55	53 (7)

SD, standard deviation; HVx, hemoglobin volume index; wHVx, wavelet hemoglobin volume index; SW, single window; MW, multiple window; MAPopt, optimal mean arterial blood pressure.

Blood Pressure and MAPopt

Mean MAP was 54 mmHg (SD: 9; 95% CI: 52, 55) during hypothermia, 49 mmHg (SD: 8; 95% CI: 48, 50) during rewarming, and 49 mmHg (SD: 7; 95% CI: 48, 50) during rewarming+normothermia. Values for MAPopt differed by 0–3 mmHg between indices when all values were averaged across a temperature period (**Table 3**).

Wavelet HVx

Sixty-three neonates with MAPopt derived from single-window wHVx during hypothermia had regional brain injury scored on MRI. Greater maximal blood pressure above MAPopt was associated with less injury in the paracentral gyri ($\beta = -0.147$; 95% CI: −0.284, −0.010; $p = 0.044$), basal ganglia ($\beta = -0.142$; 95% CI: −0.261, −0.023; $p = 0.015$), thalamus ($\beta = -0.149$; 95% CI: −0.272, −0.026; $p = 0.013$), and brainstem ($\beta = -0.120$; 95% CI: −0.232, −0.009; $p = 0.041$) after adjusting for sex, vasopressors, seizures, $PaCO_2$, and the perinatal insult score. An example coefficient interpretation would be that for every 1 mmHg increase in maximal blood pressure above MAPopt, the odds ratio of increased paracentral gyri injury was 0.863 [exp(−0.147)] per increase in injury level (e.g., mild to moderate).

Blood pressure below the single-window wHVx MAPopt and the AUC during hypothermia were not related to regional brain injury ($p > 0.05$ for all comparisons, **Table 4**). Blood pressure relative to this MAPopt during rewarming and rewarming + normothermia was also not associated with regional injury.

NICHD global brain injury scores were graded in 65 neonates with MAPopt derived from single-window wHVx during hypothermia. Greater maximal blood pressure above this MAPopt was associated with less injury in the univariate analysis ($\beta = -0.084$; 95% CI: −0.160, −0.008; $p = 0.033$) but not in the multivariate analysis. The NICHD injury score was not related to blood pressure below this MAPopt or the AUC during hypothermia nor with any blood pressure metric during rewarming or rewarming + normothermia. The multi-window wHVx did not identify any relationships between blood pressure, MAPopt, and brain injury.

Correlation HVx

MAPopt during hypothermia was identified by the multi-window, correlation HVx in 64 neonates with regional brain injury measures. Higher blood pressure above this MAPopt was associated with less brainstem injury in the multivariate analysis ($\beta = -0.117$; 95% CI: −0.217, −0.009; $p = 0.021$). Blood pressure below this MAPopt and the AUC during hypothermia had no association with injury in any region. Moreover, regional brain injury was unrelated to blood pressure and MAPopt during rewarming or rewarming+normothermia. The NICHD score also was not associated with this MAPopt. Finally, single-window HVx did not identify any relationships between blood pressure, MAPopt, and brain injury.

DISCUSSION

Maintaining blood pressure within the range that optimizes autoregulation could mitigate brain injury in HIE (4–7, 16). We tested whether wHVx and correlation HVx, which we validated in piglets with HIE (13), and single- and multi-window methodology (14) identify MAPopt in short monitoring periods. Having blood pressure above the single-window wHVx-derived MAPopt during hypothermia was associated with less injury in the paracentral gyri, basal ganglia, thalamus, and brainstem after adjustments for sex, vasopressor use, seizures, $PaCO_2$, and perinatal insult score. Blood pressure that exceeded the MAPopt from multi-window, correlation HVx was associated with reduced injury in the brainstem only. We conclude that single-window wavelet methodology may increase accuracy in identifying MAPopt values that are associated with brain injury when using short monitoring periods. In neonates with an upper MAP of approximately 50–60 mmHg, having blood pressure above the MAPopt identified by single-window wHVx might be able to reduce the risk of neurologic injury.

MAPopt From Wavelet and Correlation HVx

Autoregulation is a frequency-dependent phenomenon. We theorized that our wavelet methodology, which is a time-frequency analysis, would detect physiologically relevant fluctuations in blood pressure and cerebral blood volume. Correlation HVx might detect signals that are unrelated to the frequency of autoregulation because it characterizes all of the frequency components. Accordingly, wHVx identified MAPopt values that were significantly related to brain injury in multiple regions, including the paracentral gyri, basal ganglia, thalamus, and brainstem. In contrast, correlation HVx identified MAPopt that was only associated with brainstem injury. The time-frequency analysis might be responsible for the superior

TABLE 4 | Comparisons of blood pressure relative to the MAPopt from wHVx during hypothermia.

	Maximal MAP above MAPopt (*n* = 63)		Maximal MAP below MAPopt (*n* = 63)		AUC above MAPopt (*n* = 63)		AUC below MAPopt (*n* = 63)	
	β	***P***	β	***P***	β	***P***	β	***P***
Single-window wHVx								
Paracentral gyri	−0.147	**0.044**	−0.019	1.000	−0.003	1.000	−0.002	1.000
White matter	−0.075	0.473	−0.004	1.000	−0.002	1.000	0.000	1.000
Basal ganglia	−0.142	**0.015**	0.003	1.000	−0.005	0.446	0.002	1.000
Thalamus	−0.149	**0.013**	−0.011	1.000	−0.005	0.439	0.001	1.000
Posterior limb of the internal capsule	−0.064	1.000	0.010	1.000	−0.004	1.000	0.000	1.000
Brainstem	−0.120	**0.041**	0.006	1.000	−0.004	1.000	0.002	1.000
	Maximal MAP above MAPopt (*n* = 65)		**Maximal MAP below MAPopt (*n* = 65)**		**AUC above MAPopt (*n* = 65)**		**AUC below MAPopt (*n* = 65)**	
	β	***P***	β	***P***	β	***P***	β	***P***
Multi-window wHVx								
Paracentral gyri	−0.069	1.000	0.006	1.000	−0.004	1.000	0.001	1.000
White matter	−0.037	1.000	0.004	1.000	−0.002	1.000	0.000	1.000
Basal ganglia	−0.085	0.216	−0.012	1.000	−0.004	1.000	0.002	1.000
Thalamus	−0.089	0.194	−0.021	1.000	−0.005	1.000	0.001	1.000
Posterior limb of the internal capsule	−0.040	1.000	0.019	1.000	−0.003	1.000	0.001	1.000
Brainstem	−0.089	0.139	−0.017	1.000	−0.003	1.000	0.001	1.000

Comparisons were adjusted for sex, partial pressure of arterial carbon dioxide, perinatal insult score, vasopressor use, and presence of electroencephalographic seizures. The analyses were also adjusted for multiple comparisons using Bonferroni corrections. Bold values are statistically significant p-values (p-values < 0.05).

MAP, mean arterial blood pressure; MAPopt, optimal mean arterial blood pressure; wHVx, wavelet hemoglobin volume index; AUC, area under the curve.

performance of wHVx relative to correlation HVx during short monitoring periods.

Neonates with greater blood pressure above the wHVx MAPopt had less brain injury than did neonates with lower blood pressure. This outcome agrees with our past findings that less paracentral gyri injury is associated with blood pressure exceeding MAPopt derived from correlation HVx (4). The risk of intraventricular hemorrhage in premature neonates is also reduced when blood pressure exceeds the MAPopt derived from a tissue oxygenation heart rate reactivity index (38). Moreover, we previously demonstrated that blood pressure below MAPopt relates to greater brain injury (4–6, 16). Though these findings suggest that higher blood pressure may be beneficial, extreme caution must be taken given the developing brain's fragile vascular anatomy and unique vulnerability (39). The neonates' MAP in our study had an upper 95% CI limit of 55 mmHg. We estimate that with an upper MAP limit of 50–60 mmHg, hypotension below MAPopt may be more deleterious than blood pressure above MAPopt.

MAPopt showed no association with white matter injury, even though white matter was the most commonly injured region. This finding contrasts with our past studies, which showed a relationship between white matter injury and autoregulation in long monitoring durations (4–6). Studies in preterm neonates show a link between periventricular white matter injury and hypotension (40). Less is known about cerebral blood flow–blood pressure regulation in subcortical and deep white matter in near-term or term newborns with HIE. It is possible that the gray matter is more sensitive to blood pressure deviation from MAPopt. Therapies beyond hemodynamic support may be needed to reduce white matter injury in HIE. Moreover, the 4–16-day age range in which the MRIs were obtained could have influenced the results because the neonates were imaged at different stages of evolving injury.

Single- and Multi-Window

We also tested single- and multi-window algorithms. In adults with traumatic brain injury, the multi-window method improved identification of the optimal cerebral perfusion pressure (CPPopt) with the most robust autoregulation. However, multi- and single-window CPPopt had comparable associations with neurologic outcome (14). In the current study, the single-window technique outperformed the multi-window technique with wHVx. Single-window wHVx identified MAPopt values associated with injury in the paracentral gyri, basal ganglia, thalamus, and brainstem in the multivariate analysis. The MAPopt from multi-window wHVx did not show any relationships with brain injury.

Clinical Considerations

Dysfunctional autoregulation is known to be associated with brain injury in newborns with HIE (35, 41, 42). We previously showed that having blood pressure below MAPopt is associated with greater brain injury on early MRI and poorer 2-year neurodevelopmental outcomes (4–6, 16). In those studies, we identified MAPopt using correlation HVx in 6–68-h recording durations. However, evolving brain injury (43, 44), cerebral edema (45), and hypercapnia (46) can shift the blood pressure limits of autoregulation. Averaging MAPopt across long periods of time might mask potential variation from acute clinical changes. Moreover, clinicians may need to identify MAPopt in neonates who have been monitored for only short periods. Therefore, we tested 3-h periods in the current study to advance the clinical potential of autoregulation monitoring. We also adjusted the analyses for sex, vasopressor use, seizures, $PaCO_2$, and the perinatal insult score because they affect autoregulation and brain injury (15, 23, 29–33).

Our study used a time-frequency decomposition method to calculate wHVx within a coherence spectrum between MAP and rTHb. Alternative wavelet autoregulation methods use frequency-only decomposition with only one coherence spectrum. The hemoglobin volume phase index (HVP) is one example of wavelet autoregulation monitoring that uses only frequency decomposition and a specific spectral coherence identified by multivariate autoregressive models. The HVP identified an association between dysfunctional autoregulation and brain injury on MRI, developmental delay, or death (35). Additional research is needed to identify potential prognostic differences between these related but different wavelet methods.

Because our study was observational, we cannot infer whether clinically targeting MAPopt would affect the risk of brain injury. We also cannot assume a cause-and-effect relationship between autoregulation and brain injury from our data. Hemodynamic instability from severe brain injury itself may be responsible for blood pressure instability around MAPopt. This is likely reflected in the association that we identified between brainstem injury and MAPopt. Randomized clinical studies are needed to test whether optimizing autoregulation reduces brain injury in neonates with HIE.

Most neonates had moderate HIE according to the modified Sarnat staging and no or mild regional brain injury on MRI. We included five neonates who were initially diagnosed with moderate HIE at an outside hospital but were later diagnosed with mild HIE upon transfer to our NICU and during active therapeutic hypothermia. Because the clinicians decided to continue administering therapeutic hypothermia, these neonates met study criteria. Additional research is needed in a more diverse and larger population with greater HIE severity.

LIMITATIONS

We acknowledge several limitations to our pilot study. This was a single-center study in a small cohort of neonates. Additional studies with a larger sample size are needed to study the neurologic effects of having blood pressure above or below MAPopt and to identify the best methods for finding MAPopt in neonates. The smaller sample sizes of neonates with MAPopt identified during rewarming and rewarming + normothermia and the limited number of infants with moderate to severe brain injury may have left us underpowered to detect differences. We used autoregulation indices derived from NIRS rTHb, which theoretically should be less affected by changes in cerebral metabolic rate than indices based solely on oxyhemoglobin.

Nonetheless, the predominant venous contribution to the NIRS signal limits the granularity of NIRS autoregulation monitoring. We only studied blood pressure autoregulation and could not account for additional factors that influence brain injury, including metabolic derangements and inflammation. Long-term neurodevelopmental outcome data were not available for all neonates. We adjusted our analyses for several clinical factors that are known to affect autoregulation and brain injury in HIE. Though we adjusted for seizures, we did not adjust for specific anti-epileptic medications.

Finally, our findings may not be generalizable because we studied a small sample size from a university-based NICU. Only neonates with arterial catheters could undergo autoregulation monitoring. Additional selection bias could also have occurred when cases were excluded because study consent was not obtained, the baby died before autoregulation monitoring or MRI, the baby was transferred to another intensive care unit for extracorporeal membrane oxygenation, or the MRI had motion artifact.

CONCLUSION

In neonates with HIE and upper MAP limits of approximately 50–60 mmHg during hypothermia, greater blood pressure above the MAPopt from single-window wHVx was associated with less injury in paracentral gyri, basal ganglia, thalamus, and brainstem. Wavelet HVx, which is a frequency-specific metric, improved the identification of neurologically relevant MAPopt values in short monitoring durations. Wavelet techniques have potential to improve neonatal autoregulation monitoring.

DATA AVAILABILITY STATEMENT

The raw data supporting the conclusions of this article will be made available by the authors, without undue reservation.

ETHICS STATEMENT

The studies involving human participants were reviewed and approved by the Johns Hopkins University Institutional Review Board. Written informed consent to participate in this study was provided by the participants' legal guardian through May 2013. After this date, the requirement for written consent was waived.

AUTHOR CONTRIBUTIONS

XL analyzed the data, interpreted the data, and wrote and edited the manuscript. AT and BS analyzed the brain MRIs, interpreted the data, and edited and approved the manuscript. JP conducted the data analysis, interpreted the data, and edited and approved the manuscript. AM, RG, and KB interpreted the data, and edited and approved the manuscript. RC-V, FN, MC, and CP assisted with data collection, data interpretation, and edited and approved the manuscript. JL designed the study, collected the data, interpreted the data analysis, and wrote the manuscript. All authors contributed to the article and approved the submitted version.

FUNDING

This study was supported by funding from the National Institutes of Health [R01NS107417 and R01NS109029 (JL); K08NS096115 (RC-V); R01HD070996 and R01HD086058 (FN); and R01NS107417 (AT)]; the American Heart Association Transformational Project Award [co-funded by the Lawrence J. and Florence A. DeGeorge Charitable Trust; 18TPA34170077 (JL)]; the American Heart Association Grant in Aid and the Johns Hopkins University-School of Medicine Clinician-Scientist Award (RC-V); and the Sutland-Pakula Endowment for Neonatal Research (RC-V).

ACKNOWLEDGMENTS

We thank Claire Levine, MS, ESL, for her editorial assistance.

SUPPLEMENTARY MATERIAL

The Supplementary Material for this article can be found online at: https://www.frontiersin.org/articles/10.3389/fneur.2021.662839/full#supplementary-material

REFERENCES

1. Lawn, J., Shibuya, K., and Stein, C. (2005). No cry at birth: global estimates of intrapartum stillbirths and intrapartum-related neonatal deaths. *Bulletin of the World Health Organization* 83, 409–417.
2. Shankaran, S., Pappas, A., Mcdonald, S.A., Vohr, B.R., Hintz, S.R., Yolton, K., Gustafson, K.E., Leach, T.M., Green, C., Bara, R., Petrie Huitema, C.M., Ehrenkranz, R.A., Tyson, J.E., Das, A., Hammond, J., Peralta-Carcelen, M., Evans, P.W., Heyne, R.J., Wilson-Costello, D.E., Vaucher, Y.E., Bauer, C.R., Dusick, A.M., Adams-Chapman, I., Goldstein, R.F., Guillet, R., Papile, L.A., Higgins, R.D., and Eunice Kennedy Shriver, N.N.R.N. (2012). Childhood outcomes after hypothermia for neonatal encephalopathy. *N Engl J Med* 366, 2085–2092.
3. Gretchen, C.B., and Rayannavar, A.S. (2015). "Cardiology," in *The Harriet Lane Handbook,* eds. B. Engorn & J. Flerlage. 20th ed: Saunders, an imprint of Elsevier Inc.), 127–171.
4. Lee, J.K., Poretti, A., Perin, J., Huisman, T., Parkinson, C., Chavez-Valdez, R., O'connor, M., Reyes, M., Armstrong, J., Jennings, J.M., Gilmore, M.M., Koehler, R.C., Northington, F.J., and Tekes, A. (2017). Optimizing Cerebral Autoregulation May Decrease Neonatal Regional Hypoxic-Ischemic Brain Injury. *Dev Neurosci* 39, 248–256.
5. Carrasco, M., Perin, J., Jennings, J.M., Parkinson, C., Gilmore, M.M., Chavez-Valdez, R., Massaro, A.N., Koehler, R.C., Northington, F.J., Tekes, A., and Lee, J.K. (2018). Cerebral Autoregulation and Conventional and Diffusion Tensor Imaging Magnetic Resonance Imaging in Neonatal Hypoxic-Ischemic Encephalopathy. *Pediatr Neurol* 82, 36–43.
6. Tekes, A., Poretti, A., Scheurkogel, M.M., Huisman, T.A., Howlett, J.A., Alqahtani, E., Lee, J.H., Parkinson, C., Shapiro, K., Chung, S.E., Jennings, J.M., Gilmore, M.M., Hogue, C.W., Martin, L.J., Koehler, R.C., Northington, F.J., and Lee, J.K. (2015). Apparent diffusion coefficient scalars correlate with near-infrared spectroscopy markers of cerebrovascular autoregulation in neonates

cooled for perinatal hypoxic-ischemic injury. *AJNR Am J Neuroradiol* 36, 188–193.
7. Howlett, J.A., Northington, F.J., Gilmore, M.M., Tekes, A., Huisman, T.A., Parkinson, C., Chung, S.E., Jennings, J.M., Jamrogowicz, J.J., Larson, A.C., Lehmann, C.U., Jackson, E., Brady, K.M., Koehler, R.C., and Lee, J.K. (2013). Cerebrovascular autoregulation and neurologic injury in neonatal hypoxic-ischemic encephalopathy. *Pediatr Res* 74, 525–535.
8. Kochanek, P.M., Tasker, R.C., Bell, M.J., Adelson, P.D., Carney, N., Vavilala, M.S., Selden, N.R., Bratton, S.L., Grant, G.A., Kissoon, N., Reuter-Rice, K.E., and Wainwright, M.S. (2019). Management of Pediatric Severe Traumatic Brain Injury: 2019 Consensus and Guidelines-Based Algorithm for First and Second Tier Therapies. *Pediatr Crit Care Med* 20, 269–279.
9. Lee, J.K., Kibler, K.K., Benni, P.B., Easley, R.B., Czosnyka, M., Smielewski, P., Koehler, R.C., Shaffner, D.H., and Brady, K.M. (2009). Cerebrovascular reactivity measured by near-infrared spectroscopy. *Stroke* 40, 1820–1826.
10. Larson, A.C., Jamrogowicz, J.L., Kulikowicz, E., Wang, B., Yang, Z.J., Shaffner, D.H., Koehler, R.C., and Lee, J.K. (2013). Cerebrovascular autoregulation after rewarming from hypothermia in a neonatal swine model of asphyxic brain injury. *J Appl Physiol (1985)* 115, 1433–1442.
11. Czosnyka, M., Smielewski, P., Kirkpatrick, P., Laing, R.J., Menon, D., and Pickard, J.D. (1997). Continuous assessment of the cerebral vasomotor reactivity in head injury. *Neurosurgery* 41, 11–17; discussion 17–19.
12. Liu, X., Czosnyka, M., Donnelly, J., Cardim, D., Cabeleira, M., Hutchinson, P.J., Hu, X., Smielewski, P., and Brady, K. (2018). Wavelet pressure reactivity index: a validation study. *J Physiol* 596, 2797–2809.
13. Liu, X., Hu, X., Brady, K.M., Koehler, R., Smielewski, P., Czosnyka, M., Donnelly, J., and Lee, J.K. (2020). Comparison of wavelet and correlation indices of cerebral autoregulation in a pediatric swine model of cardiac arrest. *Sci Rep* 10, 5926.
14. Liu, X.Y., Maurits, N.M., Aries, M.J.H., Czosnyka, M., Ercole, A., Donnelly, J., Cardim, D., Kim, D.J., Dias, C., Cabeleira, M., and Smielewski, P. (2017). Monitoring of Optimal Cerebral Perfusion Pressure in Traumatic Brain Injured Patients Using a Multi-Window Weighting Algorithm. *Journal of Neurotrauma* 34, 3081–3088.
15. Gilmore, M.M., Tekes, A., Perin, J., Parkinson, C., Spahic, H., Chavez-Valdez, R., Northington, F.J., and Lee, J.K. (2020). Later cooling within 6 h and temperatures outside 33-34 degrees C are not associated with dysfunctional autoregulation during hypothermia for neonatal encephalopathy. *Pediatr Res*. 89:223–30.
16. Burton, V.J., Gerner, G., Cristofalo, E., Chung, S.E., Jennings, J.M., Parkinson, C., Koehler, R.C., Chavez-Valdez, R., Johnston, M.V., Northington, F.J., and Lee, J.K. (2015). A pilot cohort study of cerebral autoregulation and 2-year neurodevelopmental outcomes in neonates with hypoxic-ischemic encephalopathy who received therapeutic hypothermia. *BMC Neurol* 15, 209.
17. Chavez-Valdez, R., O'connor, M., Perin, J., Reyes, M., Armstrong, J., Parkinson, C., Gilmore, M., Jennings, J., Northington, F.J., and Lee, J.K. (2017). Associations between cerebrovascular blood pressure autoregulation and cardiopulmonary injury may be sex-specific in neonates treated with therapeutic hypothermia for hypoxic-ischemic encephalopathy. *Pediatr. Res.* 81, 759–766.
18. Lee, J.K., Perin, J., Parkinson, C., O'connor, M., Gilmore, M.M., Reyes, M., Armstrong, J., Jennings, J.M., Northington, F.J., and Chavez-Valdez, R. (2017). Relationships between cerebral autoregulation and markers of kidney and liver injury in neonatal encephalopathy and therapeutic hypothermia. *Journal of Perinatology* 37, 938–942.
19. Shankaran, S., Laptook, A.R., Ehrenkranz, R.A., Tyson, J.E., Mcdonald, S.A., Donovan, E.F., Fanaroff, A.A., Poole, W.K., Wright, L.L., Higgins, R.D., Finer, N.N., Carlo, W.A., Duara, S., Oh, W., Cotten, C.M., Stevenson, D.K., Stoll, B.J., Lemons, J.A., Guillet, R., Jobe, A.H., National Institute of Child, H., and Human Development Neonatal Research, N. (2005). Whole-body hypothermia for neonates with hypoxic-ischemic encephalopathy. *N Engl J Med* 353, 1574–1584.
20. Sarnat, H.B., and Sarnat, M.S. (1976). Neonatal encephalopathy following fetal distress. A clinical and electroencephalographic study. *Arch Neurol* 33, 696–705.
21. Dupont, T.L., Chalak, L.F., Morriss, M.C., Burchfield, P.J., Christie, L., and Sanchez, P.J. (2013). Short-term outcomes of newborns with perinatal acidemia who are not eligible for systemic hypothermia therapy. *J. Pediatr.* 162, 35–41.
22. Olsen, S.L., Dejonge, M., Kline, A., Liptsen, E., Song, D., Anderson, B., and Mathur, A. (2013). Optimizing therapeutic hypothermia for neonatal encephalopathy. *Pediatrics* 131, e591–603.
23. Pappas, A., Shankaran, S., Laptook, A.R., Langer, J.C., Bara, R., Ehrenkranz, R.A., Goldberg, R.N., Das, A., Higgins, R.D., Tyson, J.E., Walsh, M.C., Eunice Kennedy Shriver National Institute of Child, H., and Human Development Neonatal Research, N. (2011). Hypocarbia and adverse outcome in neonatal hypoxic-ischemic encephalopathy. *J Pediatr* 158, 752–7 58 e751.
24. Gilmore, M.M., Stone, B.S., Shepard, J.A., Czosnyka, M., Easley, R.B., and Brady, K.M. (2011). Relationship between cerebrovascular dysautoregulation and arterial blood pressure in the premature infant. *J Perinatol* 31, 722–729.
25. Fraser, C.D., 3rd, Brady, K.M., Rhee, C.J., Easley, R.B., Kibler, K., Smielewski, P., Czosnyka, M., Kaczka, D.W., Andropoulos, D.B., and Rusin, C. (2013). The frequency response of cerebral autoregulation. *J Appl Physiol (1985)* 115, 52–56.
26. Liu, X.Y., Donnelly, J., Czosnyka, M., Aries, M.J.H., Brady, K., Cardim, D., Robba, C., Cabeleira, M., Kim, D.J., Haubrich, C., Hutchinson, P.J., and Smielewski, P. (2017). Cerebrovascular pressure reactivity monitoring using wavelet analysis in traumatic brain injury patients: A retrospective study. *Plos Medicine* 14, e1002348.
27. Addison, P.S. (2002). *The Illustrated Wavelet Transform Handbook: Introductory Theory and Applications in Science, Engineering, Medicine and Finance.* Boca Raton: CRC Press.
28. Brady, K.M., Easley, R.B., Kibler, K., Kaczka, D.W., Andropoulos, D., Fraser, C.D., 3rd, Smielewski, P., Czosnyka, M., Adams, G.J., Rhee, C.J., and Rusin, C.G. (2012). Positive end-expiratory pressure oscillation facilitates brain vascular reactivity monitoring. *J Appl Physiol (1985)* 113, 1362–1368.
29. Armstead, W.M., Riley, J., and Vavilala, M.S. (2013). Dopamine Prevents Impairment of Autoregulation After Traumatic Brain Injury in the Newborn Pig Through Inhibition of Up-regulation of Endothelin-1 and Extracellular Signal-Regulated Kinase Mitogen-Activated Protein Kinase. *Pediatric Critical Care Medicine* 14, E103–E111.
30. Massaro, A.N., Murthy, K., Zaniletti, I., Cook, N., Digeronimo, R., Dizon, M., Hamrick, S.E., Mckay, V.J., Natarajan, G., Rao, R., Smith, D., Telesco, R., Wadhawan, R., Asselin, J.M., Durand, D.J., Evans, J.R., Dykes, F., Reber, K.M., Padula, M.A., Pallotto, E.K., Short, B.L., and Mathur, A.M. (2015). Short-term outcomes after perinatal hypoxic ischemic encephalopathy: a report from the Children's Hospitals Neonatal Consortium HIE focus group. *J Perinatol* 35, 290–296.
31. Monrad, P., Sannagowdara, K., Bozarth, X., Bhosrekar, S., Hecox, K., Nwosu, M., Schwabe, M., Meyer, M., Szabo, A., Prigge, J., Lemke, R., Horn, B., and Whelan, H.T. (2015). Haemodynamic response associated with both ictal and interictal epileptiform activity using simultaneous video electroencephalography/near infrared spectroscopy in a within-subject study. *Journal of near Infrared Spectroscopy* 23, 209–218.
32. Murden, S., Borbelyova, V., Lastuvka, Z., Myslivecek, J., Otahal, J., and Riljak, V. (2019). Gender differences involved in the pathophysiology of the perinatal hypoxic-ischemic damage. *Physiol Res* 68, S207–S217.
33. Lingappan, K., Kaiser, J.R., Srinivasan, C., Gunn, A.J., and Grp, C.S. (2016). Relationship between PCO2 and unfavorable outcome in infants with moderate-to-severe hypoxic ischemic encephalopathy. *Pediatric Research* 80, 204–208.
34. Sedgwick, P. (2012). STATISTICAL QUESTION Multiple significance tests: the Bonferroni correction. *British Medical Journal* 344, e509.
35. Massaro, A.N., Lee, J.K., Vezina, G., Glass, P., O'kane, A., Li, R., Chang, T., Brady, K., and Govindan, R. (2020). Exploratory Assessment of the Relationship Between Hemoglobin Volume Phase Index, Magnetic Resonance Imaging, and Functional Outcome in Neonates with Hypoxic-Ischemic Encephalopathy. *Neurocrit Care*. doi: 10.1007/s12028-020-01150-8. [Epub ahead of print].
36. Dupont, W.D., and Plummer, W.D., Jr. (1998). Power and sample size calculations for studies involving linear regression. *Control Clin Trials* 19, 589–601.

37. Dupont, W.D., and Plummer, W.D., Jr. (1990). Power and sample size calculations. A review and computer program. *Control Clin Trials* 11, 116–128.
38. Da Costa, C.S., Czosnyka, M., Smielewski, P., and Austin, T. (2018). Optimal Mean Arterial Blood Pressure in Extremely Preterm Infants within the First 24 Hours of Life. *J Pediatr* 203, 242–248.
39. Rorke, L.B. (1992). Anatomical features of the developing brain implicated in pathogenesis of hypoxic-ischemic injury. *Brain Pathol* 2, 211–221.
40. Børch, K., Lou, H.C., and Greisen, G. (2010). Cerebral white matter blood flow and arterial blood pressure in preterm infants. *Acta Paediatr* 99, 1489–1492.
41. Massaro, A.N., Govindan, R.B., Vezina, G., Chang, T., Andescavage, N.N., Wang, Y., Al-Shargabi, T., Metzler, M., Harris, K., and Du Plessis, A.J. (2015). Impaired cerebral autoregulation and brain injury in newborns with hypoxic-ischemic encephalopathy treated with hypothermia. *J Neurophysiol* 114, 818–824.
42. Chalak, L.F., Tian, F., Adams-Huet, B., Vasil, D., Laptook, A., Tarumi, T., and Zhang, R. (2017). Novel Wavelet Real Time Analysis of Neurovascular Coupling in Neonatal Encephalopathy. *Sci Rep* 7, 45958.
43. Gunn, A.J., and Thoresen, M. (2006). Hypothermic neuroprotection. *NeuroRx* 3, 154–169.
44. Wassink, G., Gunn, E.R., Drury, P.P., Bennet, L., and Gunn, A.J. (2014). The mechanisms and treatment of asphyxial encephalopathy. *Front Neurosci* 8, 40.
45. Brady, K.M., Lee, J.K., Kibler, K.K., Easley, R.B., Koehler, R.C., Czosnyka, M., Smielewski, P., and Shaffner, D.H. (2009). The lower limit of cerebral blood flow autoregulation is increased with elevated intracranial pressure. *Anesth Analg* 108, 1278–1283.
46. Nusbaum, D.M., Brady, K.M., Kibler, K.K., and Blaine Easley, R. (2016). Acute hypercarbia increases the lower limit of cerebral blood flow autoregulation in a porcine model. *Neurol Res* 38, 196–204.

Conflict of Interest: JL, FN, and RC-V received research support from Medtronic for a separate study. JL was previously a paid consultant for Medtronic and JL is currently a paid consultant for Edwards Life Sciences. These arrangements have been reviewed and approved by the Johns Hopkins University in accordance with its conflict of interest policies. Medtronic and Edwards Life Sciences had no role in the design of the current study, collection or analysis of the data, interpretation of the results, manuscript writing, or our decision to submit this manuscript for publication. Some methods used to measure and monitor autoregulation as described in this manuscript were patented by The Johns Hopkins University, listing KB as a co-inventor. These patents are exclusively licensed to Medtronic Inc. and KB received a portion of the licensing fee.

The remaining authors declare that the research was conducted in the absence of any commercial or financial relationships that could be construed as a potential conflict of interest.

frontiers in Neurology

ORIGINAL RESEARCH
published: 17 May 2021
doi: 10.3389/fneur.2021.667842

An Audit and Comparison of pH, Measured Concentration, and Particulate Matter in Mannitol and Hypertonic Saline Solutions

Christopher J. Carr[1], Jonathan Scoville[2], James Ruble[3], Chad Condie[3], Gary Davis[3], Candace L. Floyd[4], Logan Kelly[3], Ken Monson[3], Ethan Reichert[2], Buse Sarigul[5] and Gregory W. J. Hawryluk[6,7]*

[1] Department of Neurosurgery, Tulane University/Ochsner Clinic Foundation, New Orleans, LA, United States, [2] Department of Neurosurgery, University of Utah School of Medicine, Salt Lake City, UT, United States, [3] Department of Pharmacotherapy, University of Utah School of Medicine, Salt Lake City, UT, United States, [4] Department of Physical Medicine and Rehabilitation, University of Utah School of Medicine, Salt Lake City, UT, United States, [5] Department of Neurosurgery, Okmeydani Education Hospital, Istanbul, Turkey, [6] Section of Neurosurgery, Department of Surgery, University of Manitoba, Health Sciences Centre, Winnipeg, MB, Canada, [7] Brain Trauma Foundation, Palo Alto, CA, United States

OPEN ACCESS

Edited by:
Xiuyun Liu,
Johns Hopkins University,
United States

Reviewed by:
Jian-Xin Zhou,
Capital Medical University, China
Guoyi Gao,
Shanghai General Hospital, China

***Correspondence:**
Christopher J. Carr
christopher.carr1984@gmail.com

Specialty section:
This article was submitted to Neurocritical and Neurohospitalist Care, a section of the journal Frontiers in Neurology

Received: *14 February 2021*
Accepted: *19 April 2021*
Published: *17 May 2021*

Citation:
Carr CJ, Scoville J, Ruble J, Condie C, Davis G, Floyd CL, Kelly L, Monson K, Reichert E, Sarigul B and Hawryluk GWJ (2021) An Audit and Comparison of pH, Measured Concentration, and Particulate Matter in Mannitol and Hypertonic Saline Solutions. Front. Neurol. 12:667842. doi: 10.3389/fneur.2021.667842

Background: The preferred hyperosmolar therapy remains controversial. Differences in physical properties such as pH and osmolality may be important considerations in hyperosmolar agent selection. We aimed to characterize important physical properties of commercially available hyperosmolar solutions.

Methods: We measured pH and concentration in 37 commonly-used hyperosmolar solutions, including 20 and 25% mannitol and 3, 5, 14.6, and 23.4% hypertonic saline. pH was determined digitally and with litmus paper. Concentration was determined by freezing point and vapor pressure osmometry. Salinity/specific gravity was measured with portable refractometry. Particulate matter was analyzed with filtration and light microscopy and with dynamic light scattering nephelometry.

Results: pH of all solutions was below physiological range (measured range 4.13–6.80); there was no correlation between pH and solution concentration ($R^2 = 0.005$, $p = 0.60$). Mannitol (mean 5.65, sd 0.94) was less acidic than hypertonic saline (5.16, 0.60). 14/59 (24%) pH measurements and 85/111 concentration measurements were outside manufacturer standards. All 36/36 mannitol concentration measurements were outside standards vs. 48/72 (67%) hypertonic saline ($p < 0.0001$). All solutions examined on light microscopy contained crystalline and/or non-crystalline particulate matter up to several hundred microns in diameter. From nephelometry, particulate matter was detected in 20/22 (91%) solutions.

Conclusion: We present a novel characterization of mannitol and hypertonic saline. Further research should be undertaken, including research examining development of acidosis following hyperosmolar therapy, the relevance of our findings for dose-response, and the clinical relevance of particulate matter in solution.

Keywords: hyperosmolar therapy, audit, acid-base imbalance, pH, hypertonic saline, intracranial hypertension, mannitol, particulate matter

INTRODUCTION

Hyperosmolar solutions are critical therapeutics in modern neurocritical care, and they have a long history of use. In 1919, changes were demonstrated in cat brain volume following intravenous administration of hyperosmolar and hypoosmolar solutions (1). The following year, the use of hypertonic saline to decrease brain edema caused by tumors was reported (2). In the 1950s, urea became the first agent in widespread use for reducing intracranial pressure (3). Mannitol has long been a workhorse treatment for intracranial hypertension and was the recommended agent in the Brain Trauma Foundation's (BTF's) original *Guidelines for the Management of Severe Head Injury*, published in 1996 (4). In the current, 4th edition guidelines, mannitol remains the sole agent recommended; nevertheless, the BTF judged there to be insufficient evidence to support the superiority of any specific hyperosmolar agent (5–7). In contrast, the more recent *Guidelines for the Acute Treatment of Cerebral Edema in Neurocritical Care Patients* from the Neurocritical Care Society acknowledge recently published evidence in favor of hypertonic saline (8). Despite this new evidence, however, there remains uncertainty as to which agent is preferable overall and whether one agent may be preferred in specific clinical circumstances (8–30).

Despite the critical role of hyperosmolar therapy, we are unaware of any prior effort to systematically measure the physical properties of commercially available mannitol and hypertonic saline solutions that can be administered to patients. Differences in physical properties such as pH and concentration may be important considerations in selecting a specific agent, and a better understanding of precisely what is administered is anticipated to inform patient care. Per manufacturer specifications, a remarkably wide range of physical properties is permissible: for instance, pH may range from 4.5 to 7.0; measured solution concentration may contain labeled concentration ±5%. Given this, we were interested in auditing how variable measured properties of these solutions actually are and how these change with labeled concentration. We were also interested in determining whether solutions contain particulate matter given the potential for mannitol and hypertonic saline to crystalize. Finally, we were interested in determining whether generalizable differences in these properties exist between various labeled concentrations of mannitol and hypertonic saline.

MATERIALS AND METHODS

We measured pH and concentration in 37 solutions from 4 different manufacturers and 13 different lots of commercially available solutions of 20 and 25% mannitol; 3, 5, 14.6, and 23.4% sodium chloride saline; and sterile water. Solutions were obtained by the Neuro ICU pharmacist through normal supply chain distribution. None of these samples or lots had been related to any FDA recalls. Proper storage and transportation was confirmed in accordance with usual clinical practices. Solutions were confirmed to be intact and unexpired, determined to be free from crystals or contaminants on visual inspection, and progressively labeled A through AK. All testing was conducted at a normal room temperature range of 20–25 degrees Celsius. All machines were calibrated and used in accordance with manufacturer specifications. All assays were performed at the University of Utah between September 2017 and February 2019.

pH was determined digitally (Orion 8103BNUWP Ultra pH probe with Orion 3-Star benchtop meter, Thermo Fisher Scientific Inc, West Valley City, Utah) and verified with litmus paper (pHydrion, Micro Essential Laboratory, Brooklyn, New York). Two investigators recorded measurements independently. Osmolality was determined by freezing point osmometry (model 3320, Advanced Instruments, Inc., Norwood, MA) and verified by vapor pressure osmometry (Vapro, ELITechGroup, Logan, Utah). Salinity/specific gravity was determined using portable refractometry (ETvalley, Shenzhen, China).

To visualize particulate matter, we pushed 1 mL of solutions A through V through 0.8-micron filter paper (Merck Millipore, Billerica, Massachusetts) and examined the dried filter under light microscopy. We corroborated these results using nephelometry with dynamic light scattering instrumentation (DynaPro Plate Reader II, Wyatt Technology, Santa Barbara, CA). With this technique, a laser is passed through a sample at an angle, and the intensity of scattered light is measured to determine the size-distribution of dissolved particles.

For all tests, a minimum of three measurements were taken. A one-way ANOVA with Tukey's *post-hoc* test to compare means across multiple groups was conducted in SAS version 9.4. Linear regression was conducted using GraphPad to assess labeled concentration-dependent trends. Fisher's exact test was conducted to evaluate proportions. Alpha was taken as 0.05 for all tests.

RESULTS

Our ANOVA model incorporated solution contents (i.e., 14.6% saline), type (i.e., saline), manufacturer, lot, and labeled concentration. Calculated p-value for this model was <0.0001. Sample characteristics and results are summarized in **Table 1**.

pH of all solutions was below physiological range (digital range 4.13–6.80). For digital pH measurements, mannitol (mean 5.65, standard deviation 0.94) was significantly less acidic than hypertonic saline (5.16, 0.60). 20% mannitol (5.82, 1.00) was less acidic than all other solutions, including 25% mannitol (5.13, 0.63), 3% (5.10, 0.46), 5% (5.38, 0.23), 14.6% (5.78, 0.06), and 23.4% (4.84, 0.89) saline, and sterile water (mean 5.23). Litmus testing results were concordant with digital pH results. Although all solutions were more acidic than physiological pH, there was no apparent correlation between pH and the specified solution concentration ($R^2 = 0.005$, $p = 0.60$, **Figure 1**).

14/59 (24%) pH measurements conducted fell outside of manufacturer standards (4.5–7.0, per package inserts). In all 14/14 instances, measured pH was below 4.5. 0/18 mannitol pH measurements were outside of manufacturer range vs. 14/39 (36%) hypertonic saline, $p = 0.0025$. 2/23 (9%) pH measurements for manufacturer A were out of standards vs. 3/24 (13%) for B, 6/9 (67%) for C, and 3/3 for D, $p < 0.0001$.

TABLE 1 | Measured solution physical properties.

ID	Contents	Type	Maker	Lot	Digital pH	Fp osmolality	Bp osmolality	Salinity/sg (%)
A	Sterile water	Control	A	1	5.23	0 (0)	4.6 (0)	0 (0)
B	5% saline	Saline	A	2	5.26	1,597 (1,548–1,712)	1,576 (1,548–1,712)	4.65 (4.75–5.25)
C	5% saline	Saline	A	2	5.23	1,607 (1,548–1,712)	1576.8 (1,548–1,712)	4.65 (4.75–5.25)
D	5% saline	Saline	A	2	5.64	1,616 (1,548–1,712)	1570.8 (1,548–1,712)	4.6 (4.75–5.25)
E	20% mannitol	Mannitol	B	3	5.82	1,367 (869–961)	1287.4 (869–961)	15.6 (19–21)
F	20% mannitol	Mannitol	B	3	6.32	1,345 (869–961)	1285.2 (869–961)	16 (19–21)
G	20% mannitol	Mannitol	B	3	6.51	1,407 (869–961)	1281.2 (869–961)	15.8 (19–21)
H	3% saline	Saline	A	4	5.21	950 (947–1,047)	938.8 (947–1,047)	2.7 (2.85–3.15)
I	3% saline	Saline	A	4	5.38	955 (947–1,047)	937.6 (947–1,047)	2.7 (2.85–3.15)
J	3% saline	Saline	A	4	5.39	946 (947–1,047)	937.6 (947–1,047)	2.75 (2.85–3.15)
K	20% mannitol	Mannitol	B	5	6.65	1,347 (869–961)	1,278 (869–961)	15.5 (19–21)
L	20% mannitol	Mannitol	B	5	6.80	1,356 (869–961)	1258.6 (869–961)	15.8 (19–21)
M	20% mannitol	Mannitol	B	5	6.64	1,334 (869–961)	1,278 (869–961)	16 (19–21)
N	23.4% saline	Saline	C	6	5.56	7,150 (6,164–6,814)	7483.2 (6,164–6,814)	21.6 (22.2–24.6)
O	23.4% saline	Saline	C	6	5.68	5,914 (6,164–6,814)	7482.4 (6,164–6,814)	21.6 (22.2–24.6)
P	23.4% saline	Saline	C	6	5.68	8,022 (6,164–6,814)	7487.2 (6,164–6,814)	21.4 (22.2–24.6)
Q	14.6% saline	Saline	B	7	5.85	4,880 (4,144–4,582)	4553.2 (4,144–4,582)	13.5 (13.8–15.3)
R	14.6% saline	Saline	B	7	5.75	4,387 (4,144–4,582)	4,516 (4,144–4,582)	13.4 (13.8–15.3)
S	14.6% saline	Saline	B	7	5.74	5,979 (4,144–4,582)	4616.4 (4,144–4,582)	15.7 (13.8–15.3)
T	3% saline	Saline	A	8	5.65	961 (947–1,047)	934.2 (947–1,047)	2.7 (2.85–3.15)
U	3% saline	Saline	A	8	5.42	960 (947–1,047)	936.4 (947–1,047)	2.7 (2.85–3.15)
V	3% saline	Saline	A	8	5.52	960 (947–1,047)	935.8 (947–1,047)	2.7 (2.85–3.15)
W	3% saline	Saline	A	9	5.01	944 (947–1,047)	944 (947–1,047)	2.8 (2.85–3.15)
X	3% saline	Saline	A	9	5.30	943.7 (947–1,047)	944 (947–1,047)	2.85 (2.85–3.15)
Y	3% saline	Saline	A	9	5.19	940.7 (947–1,047)	943 (947–1,047)	2.85 (2.85–3.15)
Z	3% saline	Saline	D	10	4.40	942 (947–1,047)	944 (947–1,047)	2.9 (2.85–3.15)
AA	3% saline	Saline	D	10	4.39	960.7 (947–1,047)	941 (947–1,047)	2.9 (2.85–3.15)
AB	3% saline	Saline	D	10	4.37	944 (947–1,047)	940 (947–1,047)	2.9 (2.85–3.15)
AC	25% mannitol	Mannitol	B	11	5.81	1475.7 (1,043–1,153)	1,422 (1,043–1,153)	20.1 (23.7–26.3)
AD	25% mannitol	Mannitol	B	11	4.57	1381 (1,043–1,153)	1,428 (1,043–1,153)	21 (23.7–26.3)
AE	25% mannitol	Mannitol	B	11	5.01	1,374 (1,043–1,153)	1,416 (1,043–1,153)	22.2 (23.7–26.3)
AF	23.4% saline	Saline	C	12	4.13	7,502 (6,164–6,814)	7,374 (6,164–6,814)	23.1 (22.2–24.6)
AG	23.4% saline	Saline	C	12	4.30	7,492 (6,164–6,814)	7,386 (6,164–6,814)	23.4 (22.2–24.6)
AH	23.4% saline	Saline	C	12	3.71	7,514 (6,164–6,814)	7,380 (6,164–6,814)	23.1 (22.2–24.6)
AI	20% mannitol	Mannitol	B	13	4.60	1,349 (869–961)	1,140 (869–961)	18 (19–21)
AJ	20% mannitol	Mannitol	B	13	4.51	1,308 (869–961)	1,146 (869–961)	16.8 (19–21)
AK	20% mannitol	Mannitol	B	13	4.51	1,317 (869–961)	1,170 (869–961)	18 (19–21)

Industry standard pH for all solutions is 4-5-7.0. Industry standards for osmolality and salinity/specific gravity are labeled concentration ±5%. These are specified in parentheses following the measured parameter. ID, solution identifier; fp, freezing point; vp, vapor pressure; sg, specific gravity.

For osmolality as measured by freezing point depression, 20% mannitol (1349.22, 22.86) was significantly less concentrated than 14.6% (5082.00, 815.00) and 23.4% (7265.67, 718.49) saline; 25% mannitol (1410.33, 56.98), 3% saline (952.17, 8.33), and 5% saline (1613.00, 5.57) were less concentrated than 14.6 and 23.4% saline. As expected, osmolality as measured by freezing point depression increased with increasing labeled concentration ($R^2 = 0.29$, $p = 0.0006$, **Figure 2**).

For osmolality as measured by vapor point elevation, all solutions were significantly different from each other. These were, from low to high concentration: sterile water (4.60), 3% saline (939.70, 3.49), 20% mannitol (1236.04, 64.05), 25% mannitol (1422.00, 6.00), 5% (1574.53, 3.26), 14.6% (4561.87, 50.76), and 23.4% saline (7432.13, 57.26). As expected, osmolality as measured by vapor point elevation increased with increasing labeled concentration ($R^2 = 0.29$, $p = 0.0005$, **Figure 3**). These vapor point elevation results were concordant with osmolality as measured by freezing point depression.

For salinity/specific gravity as measured by portable refractometry, all solutions were significantly different from each other, including: 20% (16.39, 0.99) and 25% (21.10, 1.05) mannitol; 3% (2.79, 0.09), 5% (4.63, 0.03), 14.6% (14.20, 1.30), and 23.4% (22.37, 0.92) hypertonic saline; and sterile

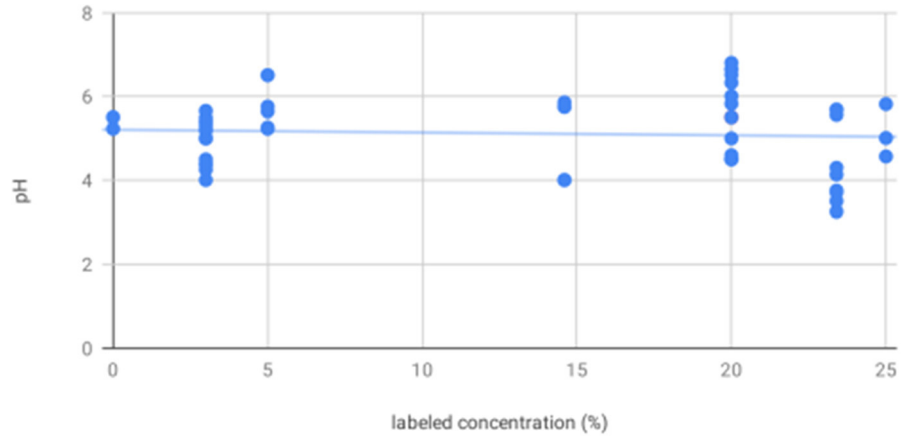

FIGURE 1 | There is no association between labeled solution concentration and pH—scatter plot showing pH as measured by digital pH meter and litmus paper for all solutions shows no significant trend in pH as a function of increasing labeled solution concentration.

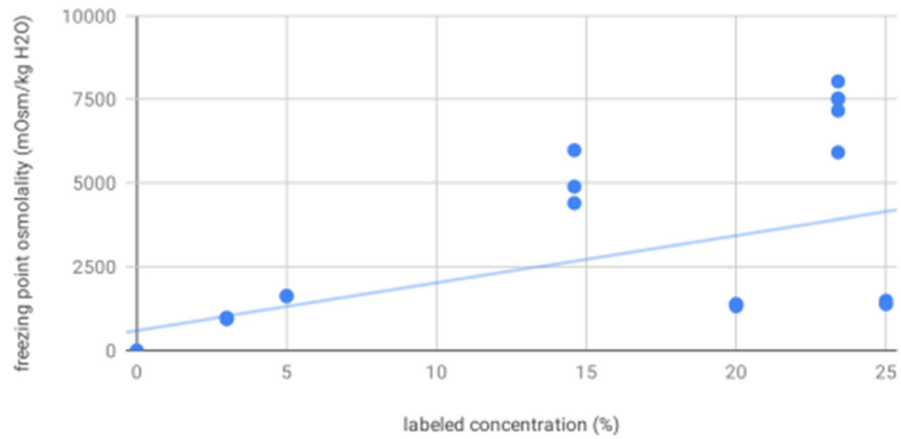

FIGURE 2 | Freezing point osmolality increases with increasing labeled solution concentration—scatter plot showing osmolality as measured by freezing point depression for all solutions increases as a function of increasing labeled solution concentration, as expected.

water (0.00). As expected, salinity/specific gravity as measured by portable refractometry increased with increasing labeled concentration ($R^2 = 0.98$, $p < 0.0001$, **Figure 4**).

Measured concentration—including both osmometry and refractometry—differed significantly from labeled concentration, and there was a great deal of variability with measurements. 85/111 (77%) total concentration measurements fell out of manufacturer standards (published parameter ±5%). All 36/36 mannitol concentration measurements were out of standards vs. 48/72 (67%) for hypertonic saline, $p < 0.0001$. All mannitol specific gravity measurements were below the standard range and all mannitol osmolality measurements were above the standard range, which may suggest solvent evaporation or presence of impurities, intermediates, or breakdown products. 23/39 (59%) concentration measurements for manufacturer A were out of standards vs. 42/45 (93%) for B, 15/18 (83%) for C, and 5/9 (56%) for D, $p = 0.0004$.

4/22 (18%) comparisons between solutions with the same contents from the same manufacturer from different lots were statistically significantly different, whereas 3/12 (25%) comparisons between solutions with the same contents from different manufacturers were statistically significantly different; the statistical comparison between these proportions was not statistically significantly different, $p = 0.68$. These results may be underpowered given our small sample size, or they may suggest our findings are independent of manufacturer and lot.

All solutions examined on light microscopy—including sterile water, mannitol, and hypertonic saline solutions—were found to contain crystalline and/or non-crystalline particulate matter up to several hundred microns in diameter (**Figure 5**). From nephelometry, particulate matter was detected in 20/22 (91%) solutions, with mean particle diameter ranging from 0.1 to 96.3 microns. Based on standard classification used in this technique, 6/20 (30%) particulate matter containing solutions were highly

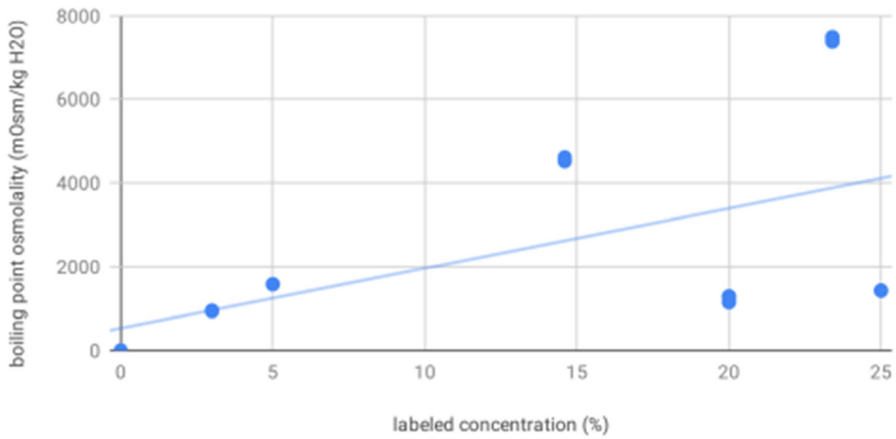

FIGURE 3 | Boiling point osmolality increases with increasing labeled solution concentration—scatter plot showing osmolality as measured by vapor point elevation for all solutions increases as a function of increasing labeled solution concentration, as expected.

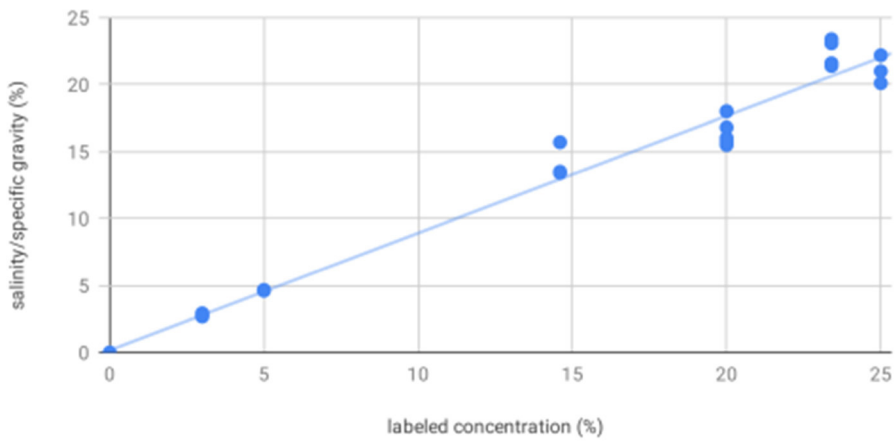

FIGURE 4 | Salinity/specific gravity increases with increasing labeled solution concentration—scatter plot showing salinity/specific gravity as measured by portable refractometer for all solutions increases as a function of increasing labeled solution concentration, as expected. These results showed measured values consistently and proportionally less than labeled concentration by a weighted mean difference of 18% for mannitol and 6% for hypertonic saline. This may be a result of crystallization. As with freezing point depression and vapor point elevation, there was increased variability at higher concentrations.

monodisperse (homogeneous mixtures); 12/20 (60%) solutions were monodisperse and 2/20 (10%) solutions were polydisperse (heterogeneous mixtures). Nephelometry results are presented in further detail in **Table 2**.

DISCUSSION

Though mannitol has long-been the workhorse hyperosmolar therapy, a growing body of literature suggests that hypertonic saline is also effective in treating elevated intracranial pressure from a variety of causes (12). Although it has been suggested that hypertonic saline may be superior to mannitol in terms of rate, duration, effect size, and side effect profile, controversy remains (13–19). It may be reasonably inferred that hypertonic saline has the same osmotic effect as mannitol (20–22), yet crucial key differences may exist for additional mechanisms of action that have yet to be fully explored, and there may be particular circumstances or indications that favor one agent over the other (23–30).

Through our investigations of pH, osmolality, and salinity/specific gravity, we were able to detect many significant differences in physical properties among commercially available mannitol and hypertonic saline solutions taken from our ICU that may inform the decision of which hyperosmolar therapy to use for a particular patient. In summary, we found the following:

pH of all Hyperosmolar Solutions Was Considerably Below Physiological Range

We detected pH values considerably below physiological range (7.35–7.45)—and manufacturer standards (4.5–7.0)—across multiple solution contents, types, manufacturers, lots, and

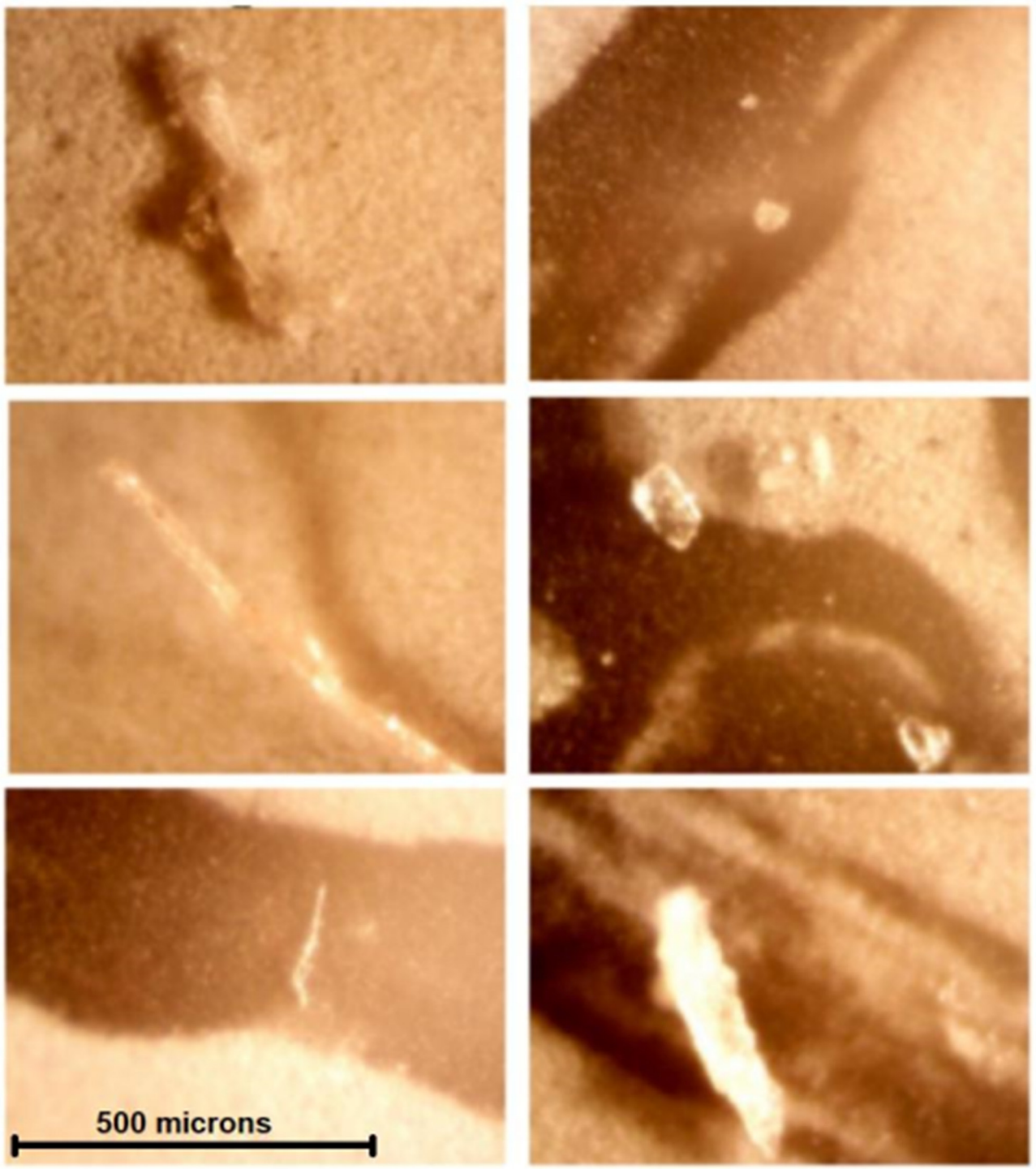

FIGURE 5 | Contaminants or crystals were found in all solutions examined by light microscopy—All images were obtained at the same magnification. Noncrystalline contaminants or crystals visualized are considerably larger than human capillary beds (5–10 microns). These are, clockwise, from top left, solutions A (sterile water), B (5% saline), I (3% saline), G (20% mannitol), L (20% mannitol), and P (23.4% saline).

labeled concentrations, using multiple measurement modalities. The effect of hyperosmolar infusion on acid/base homeostasis is poorly understood. The differences we detected may be relevant, especially for acidotic patients. More research is needed on this matter, including correlation of measured solution properties with clinical and laboratory outcomes.

TABLE 2 | Dynamic light scattering nephelometry data for solutions A through V.

ID	Contents	Mean particle diameter (μm)	% Polydispersity	Polydispersity index
A	Sterile water	0	0	0
B	5% NaCl	45.6	2.02	0.02
C	5% NaCl	83.9	15.32	0.15
D	5% NaCl	35.3	13.74	0.14
E	20% mannitol	43.0	22.11	0.22
F	20% mannitol	55.2	8.75	0.09
G	20% mannitol	0.1	8.27	0.08
H	3% NaCl	0.1	0.00	0.00
I	3% NaCl	0	0.00	0.00
J	3% NaCl	0.068	3.99	0.04
K	20% mannitol	20.2	0.00	0.00
L	20% mannitol	0.6	9.49	0.09
M	20% mannitol	0.2	12.15	0.12
N	23.4% NaCl	0.1	6.60	0.07
O	23.4% NaCl	0.1	3.59	0.04
P	23.4% NaCl	0.3	18.21	0.18
Q	14.6% NaCl	75.7	9.41	0.09
R	14.6% NaCl	12.2	17.49	0.17
S	14.6% NaCl	43.6	13.94	0.14
T	3% NaCl	96.3	10.08	0.10
U	3% NaCl	57.7	6.36	0.06
V	3% NaCl	0.6	22.96	0.23

Here we include a measure of central tendency as mean particle size and a measure of variance as polydispersity. Polydispersity describes the width of the Gaussian distribution. The percent polydispersity may be used to broadly characterize a solution as monodisperse (<20%) or polydisperse (≥20%). The polydispersity index is a dimensionless and scaled number that is calculated from correlated data. It has been used to indicate the fitness of the sample for analysis by dynamic light scattering nephelometry. Solution samples with polydispersity indices between 0.05 and 0.7 are typically good candidates for DLS analysis. Values > 0.7 indicate a broad diversity of particle size ranges. Mean particle sizes varied widely between the solutions, ranging from 0 μm (solutions A and I) to 96.3 μm (solution T). In accordance with their percent polydispersity, solutions E (22.11%) and V (22.96%) would be characterized as polydisperse; all other solutions are monodisperse. Solutions B, H, I, J, K, and O, have a polydispersity index below 0.05. Values <0.05 are rarely seen and usually indicate highly monodisperse standard solutions. Nevertheless, the average particle sizes in these 6 highly monodisperse solutions range from 0 to 45.6 μm. It is possible that because many of these particle sizes are in the micron range rather than nano range, the machine may have had some difficulty in analysis.

Mannitol Was Less Acidic Than Hypertonic Saline

Our results showed mannitol was less acidic than hypertonic saline. Previous investigations have shown the development of hyperchloremic metabolic acidosis after large saline infusions (31–34). This has been shown to be an independent risk factor for mortality in critically ill patients (35–37). Among studies of neurocritical care patients in particular, Riha et al. observed increased in-hospital mortality among patients with moderate hyperchloremia during 3% hypertonic saline infusion (38). Sadan et al. showed a strong association between hyperchloremia and acute kidney injury and between acute kidney injury and mortality in subarachnoid hemorrhage patients (39). Finally, Huang et al. demonstrated that hyperchloremia and increasing serum chloride were associated with increased odds of 30-day mortality and poor outcome after 6-months in a population of critically ill stroke patients (40). While none of these studies demonstrates a causal relationship between hypertonic saline infusion and poor clinical outcomes in neurocritical care patients, it may be preferable to choose mannitol over hypertonic saline in patients with concerning acidosis who require hyperosmolar therapy. In any case, one should be conscious of the propensity for such patients to develop hyperchloremic metabolic acidosis and the effects this can have on clinical outcomes and monitor accordingly. Our results suggest that further direct investigation of this question is warranted.

Measured Concentration Differed From Labeled Concentrations

Osmolality and salinity/specific gravity measurements were inconsistent with labeled concentrations across multiple solution contents, types, manufacturers, and lots using multiple measurement modalities. This suggests the presence of occult crystallization, evaporation, or impurities, intermediates, or breakdown products in solution. More research should be undertaken to investigate how variance in hyperosmolar solution contents may explain variant clinical responses and outcomes. In the meantime, our results suggest that clinicians may want to be cautious in administering the minimum effective dose of hyperosmolar therapy in conjunction with real-time monitoring for treatment effects and adverse effects such as those that may be caused by over- or under-diuresis or end-organ damage.

Mannitol Was More Likely to Be Out of the Specified Concentration Range Compared to Hypertonic Saline

Mannitol may be supersaturated at room temperature, and manufacturer labels state that it should be warmed before use if crystallization has occurred. We were unable to find any such recommendation for hypertonic saline, as the concentration at which aqueous sodium chloride becomes supersaturated is above that of the solutions we tested. Our tests were all conducted at room temperature, and no crystals were identified on gross visual inspection. If crystallization occurred, our results may suggest a need to warm solutions even without gross evidence of crystallization. Our results add to the existing literature demonstrating an inconsistent dose-response relationship between hyperosmolar solutions and intracranial pressure (41–43). While we cannot comment specifically on results of past studies or infer any effect on intracranial pressure from our data, our results suggest that future investigations of the dose-response relationship between hyperosmolar solutions and intracranial pressure may wish to consider validating their own findings by directly measuring the physical properties of the solutions given.

Large Particulate Matter Was Found in all Solutions we Examined

All solutions were found to contain particulate matter on both light microscopy and nephelometry. Nephelometry is an

analytical chemistry method to measure intensity of scattered light and extrapolate particle size distribution within a solution. Nevertheless, this technique is limited to size analysis and does not discern specific chemical identity. We were therefore unable to definitively determine if particulate matter in our samples was due to crystallization, contamination, or both. Although speculative, the presence of non-degradable contaminants such as microplastics, which are now ubiquitous in the environment (44), in intravenous fluids would be a concerning finding warranting aggressive additional investigation.

Many solutions contained particles considerably larger than human capillary beds (5–10 μm). Such particulate matter in the bloodstream may be thrombogenic or obstruct blood vessels (45–47), thereby depriving the tissues of oxygen or other nutrients or impeding the expeditious diuresis that is the very purpose of hyperosmolar therapy. Furthermore, direct injury to body tissues including the lung, kidney, and brain may result from crystal or contaminant deposition, which may be compounded by a patent foramen ovale. It should be noted that intravenous fluids undergo sterile processing and are not filtered during manufacturing.

Study Limitations

There are many studies that examine clinical outcomes or surrogate endpoints (such as effect on intracranial pressure) in patients undergoing mannitol or hypertonic saline therapy. Likewise, there are many basic science studies involving the administration of hyperosmolar solutions under idealized laboratory conditions that rely on precise compounding and controlled experiment. We believe this is the first study that interrogates the physical properties of commercially-available hyperosmolar solutions as they actually exist in the ICU—that is to say, what actually gets infused into patients. While these solutions are manufactured and tested under tightly regulated systems of quality control, we found that, despite a remarkably wide range of values permitted, a large number of solutions fell out of that wide range when subjected to our own rigorous testing. We were able to corroborate our results using multiple complementary techniques—i.e., both digital and litmus paper measurement of pH; precise freezing point depression and boiling point elevation methods for determining osmolality along with an analog technique for determining salinity/specific gravity. Our divergent results do not speak directly to whether manufacturer standards and quality control are flawed, nor can we attribute causality to storage or transportation factors. Nevertheless, the high degree of variance in pH and concentration, along with evidence of widespread particulate matter, that we found in hyperosmolar solutions obtained through our normal supply chain distribution is concerning and should prompt additional investigation.

Our study also has several weaknesses: since our study is a novel characterization, we were not certain what we would find. Although the 37 solutions from 4 manufacturers and 13 lots that we did evaluate represents the widest range we were able to procure over a period of several months, perhaps due to supply chain difficulties, overall we did not investigate a large number of solutions, and our results were likely affected by this small sample size. More solutions from different manufacturers and lots must be sampled to more accurately characterize manufacturer- and lot-specific central tendency and variance. Additionally, we conducted our experiments at room temperature, rather than at body temperature. As mentioned above, mannitol may be supersaturated at room temperature, and manufacturer labels state that it should be warmed before use if crystallization has occurred. Nevertheless, no crystals were identified on gross visual inspection. Hyperosmolar solutions are often used emergently, and it is our experience that mannitol solutions are seldom warmed before use if there is no gross evidence of crystallization. It was our aim to recapitulate as faithfully as possible the conditions under which these solutions are actually administered. One would expect the solutions to warm in the body, but the rapidity and extent of crystals dissolving is uncertain in this circumstance. It would have been a useful investigation to warm the solutions to body temperature before passing them through filters or interrogating them using nephelometry with dynamic light scattering instrumentation in order to determine the effect of temperature on our detection of particulate matter. Furthermore, there are no recommendations for warming hypertonic saline; nevertheless, particulate matter was ubiquitous in all solutions and solution types. This warrants future investigation. Likewise, while solution package inserts allow for buffering to ensure the recommended pH range, it is our experience that pH of solutions is seldom checked before infusion, particularly in the emergent situations that may call for mannitol or hypertonic saline. If the patient experiences an acidosis following hyperosmolar therapy, it may be attributed to underlying disease rather than the possibility that it may be iatrogenic. As stipulated above, our findings confirm that clinicians should be particularly mindful if a patient develops a hyperchloremic metabolic acidosis following hypertonic saline infusion. Finally, our study is hypothesis generating: it is basic science conducted in a laboratory and cannot be directly extrapolated to patient care. Additional clinical or pathological research involving patients—i.e., causal investigations involving acidosis and alkalosis or deposition of crystal or non-crystalline contaminants in tissues following hyperosmolar therapy—is necessary to establish the clinical relevance of our findings.

CONCLUSION

In conclusion, our purpose was to present a novel and practical characterization of commercially available hyperosmolar solutions used for critically ill patients—including various concentrations of mannitol and hypertonic saline. Even with the remarkably broad range permitted for the physical properties of hyperosmolar solutions, values for many solutions fell outside of these permitted ranges. We found that pH of all hyperosmolar solutions was considerably below physiological range, although mannitol was less acidic than hypertonic saline. This finding may be relevant for patients with acid/base disturbances. Future clinical studies should investigate the development of acidosis following treatment with either agent. Measured solution concentrations differed considerably from labeled concentrations, suggesting occult crystallization or non-uniformity and potentially reduced effectiveness or potential for harm; mannitol was more likely to be outside of concentration standards compared to hypertonic saline. Crystalline and

non-crystalline particulate matter was also observed in all solutions, even those that are not known to crystallize at room or physiological temperatures. Further research is needed to characterize manufacturer and lot effects and to determine if particulate matter in these solutions can induce thrombogenesis or occlude the microvasculature.

DATA AVAILABILITY STATEMENT

The raw data supporting the conclusions of this article will be made available by the authors upon request.

AUTHOR CONTRIBUTIONS

CCa: conceptualization, data curation, formal analysis, investigation, methodology, project administration, software, writing—original draft, and visualization. JS: conceptualization, data curation, formal analysis, investigation, methodology, project administration, software, and writing—original draft. JR: conceptualization, data curation, formal analysis, investigation, methodlogy, project administration, resources, software, supervision, and writing—original draft. CCo, GD, CF, LK, and KM: methodology, resources, and writing—reviewing and editing. ER: methodology, project administration, resources, and writing—reviewing and editing. BS: writing—reviewing and editing. GH: conceptualization, funding acquisition, methodology, project administration, resources, supervision, and writing—review and editing. All authors contributed to the article and approved the submitted version.

FUNDING

Funding for this project was provided by the Department of Neurosurgery, University of Utah.

REFERENCES

1. Weed LH, McKibben PS. Experimental alteration of brain bulk. *Am J Physiol Legacy Content.* (1919) 48:531–58. doi: 10.1152/ajplegacy.1919.48.4.531
2. Cushing H, Foley FEB. Alterations of intracranial tension by salt solutions in the alimentary canal. *Exp Biol Med.* (1920) 17:217–8. doi: 10.3181/00379727-17-120
3. Otvos B, Kshettry VR, Benzel EC. The history of urea as a hyperosmolar agent to decrease brain swelling. *Neurosurg Focus.* (2014) 36:E3. doi: 10.3171/2014.1.FOCUS13558
4. Guidelines for the management of severe head injury. Introduction. *J Neurotrauma.* (1996) 13:643–45. doi: 10.1089/neu.1996.13.643
5. The use of mannitol in severe head injury. Brain Trauma Foundation. *J Neurotrauma.* (1996). 13:705–9. doi: 10.1089/neu.1996.13.705
6. Bratton SL, Chestnut RM, Ghajar J, McConnell Hammond FF, Harris OA, Hartl R, et al. Guidelines for the management of severe traumatic brain injury. II. hyperosmolar therapy. *J Neurotrauma.* (2007) 24(Suppl. 1):S14–20. doi: 10.1089/neu.2007.9994
7. Carney N, Totten AM, O'Reilly C, Ullman JS, Hawryluk GW, Bell MJ, et al. Guidelines for the management of severe traumatic brain injury, fourth edition. *Neurosurgery.* (2017) 80:6–15. doi: 10.1227/NEU.0000000000001432
8. Cook AM, Morgan Jones G, Hawryluk GWJ, Mailloux P, McLaughlin D, Papangelou A, et al. Guidelines for the acute treatment of cerebral edema in neurocritical care patients. *Neurocrit Care.* (2020) 32:647–66. doi: 10.1007/s12028-020-00959-7
9. Mendelow AD, Teasdale GM, Russell T, Flood J, Patterson J, Murray GD. Effect of mannitol on cerebral blood flow and cerebral perfusion pressure in human head injury. *J Neurosurg.* (1985) 63:43–8. doi: 10.3171/jns.1985.63.1.0043
10. Feig PU, McCurdy DK. The hypertonic state. *N Engl J Med.* (1977) 297:1444–54. doi: 10.1056/NEJM197712292972608
11. The Brain Trauma Foundation. The American Association of Neurological Surgeons. The Joint Section on Neurotrauma and Critical Care. Use of mannitol. *J Neurotrauma.* (2000) 17:521–5. doi: 10.1089/neu.2000.17.521
12. Chen H, Song Z, Dennis JA. Hypertonic saline versus other intracranial pressure-lowering agents for people with acute traumatic brain injury. *Cochrane Database Syst Rev.* (2020) 1:CD010904. doi: 10.1002/14651858.CD010904.pub3
13. Boone MD, Oren-Grinberg A, Robinson TM, Chen CC, Kasper EM. Mannitol or hypertonic saline in the setting of traumatic brain injury: what have we learned? *Surg Neurol Int.* (2015) 6:177. doi: 10.4103/2152-7806.170248
14. Yozova ID, Howard J, Henke D, Dirkmann D, Adamik KN. Comparison of the effects of 7.2% hypertonic saline and 20% mannitol on whole blood coagulation and platelet function in dogs with suspected intracranial hypertension - a pilot study. *BMC Vet Res.* (2017) 13:185. doi: 10.1186/s12917-017-1108-2
15. Mangat HS, Chiu YL, Gerber LM, Alimi M, Ghajar J, Härtl R. Hypertonic saline reduces cumulative and daily intracranial pressure burdens after severe traumatic brain injury. *J Neurosurg.* (2015) 122:202–10. doi: 10.3171/2014.10.JNS132545
16. Upadhyay P, Tripathi VN, Singh RP, Sachan D. Role of hypertonic saline and mannitol in the management of raised intracranial pressure in children: a randomized comparative study. *J Pediatr Neurosci.* (2010) 5:18–21. doi: 10.4103/1817-1745.66673
17. Mirski AM, Denchev ID, Schnitzer SM, Hanley FD. Comparison between hypertonic saline and mannitol in the reduction of elevated intracranial pressure in a rodent model of acute cerebral injury. *J Neurosurg Anesthesiol.* (2000) 12:334–44. doi: 10.1097/00008506-200010000-00006
18. Shackford SR, Bourguignon PR, Wald SL, Rogers FB, Osler TM, Clark DE. Hypertonic saline resuscitation of patients with head injury: a prospective, randomized clinical trial. *J Trauma.* (1998) 44:50–8. doi: 10.1097/00005373-199801000-00004
19. Qureshi AI, Suarez JI, Castro A, Bhardwaj A. Use of hypertonic saline/acetate infusion in treatment of cerebral edema in patients with head trauma: experience at a single center. *J Trauma.* (1999) 47:659–65. doi: 10.1097/00005373-199910000-00009
20. Doyle JA, Davis DP, Hoyt DB. The use of hypertonic saline in the treatment of traumatic brain injury. *J Trauma.* (2001) 50:367–83. doi: 10.1097/00005373-200102000-00030
21. Ogden AT, Mayer SA, Connolly ES Jr. Hyperosmolar agents in neurosurgical practice: the evolving role of hypertonic saline. *Neurosurgery.* (2005) 57:207–15. doi: 10.1227/01.NEU.0000166533.79031.D8
22. Starke RM, Dumont AS. The role of hypertonic saline in neurosurgery. *World Neurosurg.* (2014) 82:1040–2. doi: 10.1016/j.wneu.2013.03.019
23. Barry KG, Cohen A, Knochel JP, Whelan TJ Jr, Beisel WR, Vargas CA, et al. Mannitol infusion. II. The prevention of acute functional renal failure during resection of an aneurysm of the abdominal aorta. *N Engl J Med.* (1961) 264:967–71. doi: 10.1056/NEJM196105112641902
24. James HE. Methodology for the control of intracranial pressure with hypertonic mannitol. *Acta Neurochir.* (1980) 51:161–72. doi: 10.1007/BF01406742
25. McGraw CP, Howard G. Effect of mannitol on increased intracranial pressure. *Neurosurgery.* (1983) 13:269–71. doi: 10.1227/00006123-198309000-00009
26. Cruz J, Miner ME, Allen SJ, Alves WM, Gennarelli TA. Continuous monitoring of cerebral oxygenation in acute brain injury: injection of mannitol during hyperventilation. *J Neurosurg.* (1990) 73:725–30. doi: 10.3171/jns.1990.73.5.0725

27. Marshall LF, SMith RW, Rauscher LA, Shapiro HM. Mannitol dose requirements in brain-injured patients. *J Neurosurg.* (1978) 48:169–72. doi: 10.3171/jns.1978.48.2.0169
28. Brain Trauma Foundation; American Association of Neurological Surgeons; Congress of Neurological Surgeons; Guidelines for the management of severe traumatic brain injury. II. Hyperosmolar therapy. *J Neurotrauma.* (2007) 24 (Suppl. 1):S14–20.
29. Muizelaar JP, Wei EP, Kontos HA, Becker DP. Mannitol causes compensatory cerebral vasoconstriction and vasodilation in response to blood viscosity changes. *J Neurosurg.* (1983) 59:822–8. doi: 10.3171/jns.1983.59.5.0822
30. Kim MY, Park JH, Kang NR, Jang HR, Lee JE, Huh W, et al. Increased risk of acute kidney injury associated with higher infusion rate of mannitol in patients with intracranial hemorrhage. *J Neurosurg.* (2014) 120:1340–8. doi: 10.3171/2013.12.JNS13888
31. Scheingraber S, Rehm M, Sehmisch C, Finsterer U. Rapid saline infusion produces hyperchloremic acidosis in patients undergoing gynecologic surgery. *Anesthesiology.* (1999) 90:1265–70. doi: 10.1097/00000542-199905000-00007
32. O'Dell E, Tibby SM, Durward A, Murdoch IA. Hyperchloremia is the dominant cause of metabolic acidosis in the postresuscitation phase of pediatric meningococcal sepsis. *Crit Care Med.* (2007) 35:2390–4. doi: 10.1097/01.CCM.0000284588.17760.99
33. Yunos NM, Bellomo R, Story D, Kellum J. Bench-to-bedside review: chloride in critical illness. *Crit Care.* (2010) 14:226. doi: 10.1186/cc9052
34. Ke L, Calzavacca P, Bailey M, Li WQ, Bellomo R, May CN. Acid-base changes after fluid bolus: sodium chloride vs. sodium octanoate. *Intensive Care Med Exp.* (2013) 1:23. doi: 10.1186/2197-425X-1-4
35. Boniatti MM, Cardoso PR, Castilho RK, Vieira SR. Is hyperchloremia associated with mortality in critically ill patients? A prospective cohort study. *J Crit Care.* (2011) 26:175–9. doi: 10.1016/j.jcrc.2010.04.013
36. Shaw AD, Raghunathan K, Peyerl FW, Munson SH, Paluszkiewicz SM, Schermer CR. Association between intravenous chloride load during resuscitation and in-hospital mortality among patients with SIRS. *Intensive Care Med.* (2014) 40:1897–905. doi: 10.1007/s00134-014-3505-3
37. Neyra JA, Canepa-Escaro F, Li X, Manllo J, Adams-Huet B, Yee J, et al. Association of hyperchloremia with hospital mortality in critically ill septic patients. *Crit Care Med.* (2015) 43:1938–44. doi: 10.1097/CCM.0000000000001161
38. Riha HM, Erdman MJ, Vandigo JE, Kimmons LA, Goyal N, Davidson KE, et al. Impact of moderate hyperchloremia on clinical outcomes in intracerebral hemorrhage patients treated with continuous infusion hypertonic saline: a pilot study. *Crit Care Med.* (2017) 45:e947–53. doi: 10.1097/CCM.0000000000002522
39. Sadan O, Singbartl K, Kandiah PA, Martin KS, Samuels OB. Hyperchloremia is associated with acute kidney injury in patients with subarachnoid hemorrhage. *Crit Care Med.* (2017) 45:1382–8. doi: 10.1097/CCM.0000000000002497
40. Huang K, Hu Y, Wu Y, Ji Z, Wang S, Lin Z, et al. Hyperchloremia is associated with poorer outcome in critically ill stroke patients. *Front Neurol.* (2018) 9:485. doi: 10.3389/fneur.2018.00485
41. Sorani MD, Manley GT. Dose-response relationship of mannitol and intracranial pressure: a metaanalysis. *J Neurosurg.* (2008) 108:80–87. doi: 10.3171/JNS/2008/108/01/0080
42. Francony G, Fauvage B, Falcon D, Canet C, Dilou H, Lavagne P, et al. Equimolar doses of mannitol and hypertonic saline in the treatment of increased intracranial pressure. *Crit Care Med.* (2008) 36:795–800. doi: 10.1097/CCM.0B013E3181643B41
43. Cottenceau V, Masson F, Mahamid E, Petit L, Shik V, Sztark F, et al. Comparison of effects of equiosmolar doses of mannitol and hypertonic saline on cerebral blood flow and metabolism in traumatic brain injury. *J Neurotrauma.* (2011) 28:2003–12. doi: 10.1089/neu.2011.1929
44. Koelmans AA, Mohamed Nor NH, Hermsen E, Kooi M, Mintenig SM, De France J. Microplastics in freshwaters and drinking water: critical review and assessment of data quality. *Water Res.* (2019) 155:410–22. doi: 10.1016/j.watres.2019.02.054
45. Walpot H, Franke RP, Burchard WG, Agternkamp C, Müller FG, Mittermayer C, et al. Partikuläre Verunreinigung von Infusionslösungen und Medikamentenzusätzen im Rahmen einer Langzeit-Intensiv-Therapie. Teil 2. Tiermodell [Particulate contamination of infusion solutions and drug additives in the framework of long-term intensive therapy. 2. an animal model]. *Anaesthesist.* (1989) 38:617–21.
46. Lehr HA, Brunner J, Rangoonwala R, Kirkpatrick CJ. Particulate matter contamination of intravenous antibiotics aggravates loss of functional capillary density in postischemic striated muscle. *Am J Respir Crit Care Med.* (2002) 165:514–20. doi: 10.1164/ajrccm.165.4.2108033
47. Benlabed M, Martin Mena A, Gaudy R, Perez M, Genay S, Hecq JD, et al. Analysis of particulate exposure during continuous drug infusion in critically ill adult patients: a preliminary proof-of-concept *in vitro* study. *Intensive Care Med Exp.* (2018) 6:38. doi: 10.1186/s40635-018-0205-2

Conflict of Interest: The authors declare that the research was conducted in the absence of any commercial or financial relationships that could be construed as a potential conflict of interest.

frontiers in Neurology

ORIGINAL RESEARCH
published: 14 June 2021
doi: 10.3389/fneur.2021.690183

Non-invasive Assessment of Neurovascular Coupling After Aneurysmal Subarachnoid Hemorrhage: A Prospective Observational Trial Using Retinal Vessel Analysis

Walid Albanna[1,2†], Catharina Conzen[1†], Miriam Weiss[1], Katharina Seyfried[1], Konstantin Kotliar[3], Tobias Philip Schmidt[1], David Kuerten[4], Jürgen Hescheler[2], Anne Bruecken[5], Arno Schmidt-Trucksäss[6], Felix Neumaier[1], Martin Wiesmann[7], Hans Clusmann[1] and Gerrit Alexander Schubert[1]*

[1] Department of Neurosurgery, RWTH Aachen University, Aachen, Germany, [2] Institute for Neurophysiology, University of Cologne, Cologne, Germany, [3] Department of Medical Engineering and Technomathematics, FH Aachen University of Applied Sciences, Aachen, Germany, [4] Department of Ophthalmology, RWTH Aachen University, Aachen, Germany, [5] Department of Intensive Care and Intermediate Care, RWTH Aachen University, Aachen, Germany, [6] Department of Exercise and Health Sciences, University of Basel, Basel, Switzerland, [7] Department of Diagnostic and Interventional Neuroradiology, RWTH Aachen University, Aachen, Germany

OPEN ACCESS

Edited by:
Chiara Robba, University of Genoa, Italy

Reviewed by:
Masayo Koide, University of Vermont, United States
Alessandra Splendiani, University of L'Aquila, Italy

***Correspondence:**
Walid Albanna
WalidAlbanna@yahoo.de

[†]These authors have contributed equally to this work

Specialty section:
This article was submitted to Neurocritical and Neurohospitalist Care, a section of the journal Frontiers in Neurology

Received: *02 April 2021*
Accepted: *18 May 2021*
Published: *14 June 2021*

Citation:
Albanna W, Conzen C, Weiss M, Seyfried K, Kotliar K, Schmidt TP, Kuerten D, Hescheler J, Bruecken A, Schmidt-Trucksäss A, Neumaier F, Wiesmann M, Clusmann H and Schubert GA (2021) Non-invasive Assessment of Neurovascular Coupling After Aneurysmal Subarachnoid Hemorrhage: A Prospective Observational Trial Using Retinal Vessel Analysis. Front. Neurol. 12:690183. doi: 10.3389/fneur.2021.690183

Objective: Delayed cerebral ischemia (DCI) is a common complication after aneurysmal subarachnoid hemorrhage (aSAH) and can lead to infarction and poor clinical outcome. The underlying mechanisms are still incompletely understood, but animal models indicate that vasoactive metabolites and inflammatory cytokines produced within the subarachnoid space may progressively impair and partially invert neurovascular coupling (NVC) in the brain. Because cerebral and retinal microvasculature are governed by comparable regulatory mechanisms and may be connected by perivascular pathways, retinal vascular changes are increasingly recognized as a potential surrogate for altered NVC in the brain. Here, we used non-invasive retinal vessel analysis (RVA) to assess microvascular function in aSAH patients at different times after the ictus.

Methods: Static and dynamic RVA were performed using a Retinal Vessel Analyzer (IMEDOS Systems GmbH, Jena) in 70 aSAH patients during the early (d_{0-4}), critical (d_{5-15}), late (d_{16-23}) phase, and at follow-up (f/u > 6 weeks) after the ictus. For comparison, an age-matched cohort of 42 healthy subjects was also included in the study. Vessel diameters were quantified in terms of the central retinal arterial and venous equivalent (CRAE, CRVE) and the retinal arterio-venous-ratio (AVR). Vessel responses to flicker light excitation (FLE) were quantified by recording the maximum arterial and venous dilation (MAD, MVD), the time to 30% and 100% of maximum dilation ($tMAD_{30}$, $tMVD_{30}$; tMAD, tMVD, resp.), and the arterial and venous area under the curve (AUC_{art}, AUC_{ven}) during the FLE. For subgroup analyses, patients were stratified according to the development of DCI and clinical outcomes after 12 months.

Results: Vessel diameter (CRAE, CRVE) was significantly smaller in aSAH patients and showed little change throughout the whole observation period ($p < 0.0001$ vs. control for all time periods examined). In addition, aSAH patients exhibited impaired arterial but not venous responses to FLE, as reflected in a significantly lower MAD [2.2 (1.0–3.2)% vs. 3.6 (2.6–5.6)% in control subjects, $p = 0.0016$] and AUC_{art} [21.5 (9.4–35.8)%*s vs. 51.4 (32.5–69.7)%*s in control subjects, $p = 0.0001$] on d_{0-4}. However, gradual recovery was observed during the first 3 weeks, with close to normal levels at follow-up, when MAD and AUC_{art} amounted to 3.0 [2.0–5.0]% ($p = 0.141$ vs. control, $p = 0.0321$ vs. d_{5-15}) and 44.5 [23.2–61.1]%*s ($p = 0.138$ *vs.* control, $p < 0.01$ vs. d_{0-4} & d_{5-15}). Finally, patients with clinical deterioration (DCI) showed opposite changes in the kinetics of arterial responses during early and late phase, as reflected in a significantly lower $tMAD_{30}$ on d_{0-4} [4.0 (3.0–6.8) s vs. 7.0 (5.0–8.0) s in patients without DCI, $p = 0.022$) and a significantly higher tMAD on d_{16-23} (24.0 (21.0–29.3) s *vs.* 18.0 (14.0–21.0) s in patients without DCI, $p = 0.017$].

Conclusion: Our findings confirm and extend previous observations that aSAH results in sustained impairments of NVC in the retina. DCI may be associated with characteristic changes in the kinetics of retinal arterial responses. However, further studies will be required to determine their clinical implications and to assess if they can be used to identify patients at risk of developing DCI.

Trial Registration: ClinicalTrials.gov Identifier: NCT04094155.

Keywords: aneurysmal subarachnoid hemorrhage, cerebral infarction, delayed cerebral ischemia, microvascular function, neurovascular coupling, retinal vessel analysis

INTRODUCTION

Aneurysmal subarachnoid hemorrhage (aSAH) due to sudden rupture of a cerebral aneurysm is responsible for only 5–7% of all stroke events (1) but is associated with a fatality rate of almost 50%, accounting for up to 20% of all cerebrovascular-related deaths (2). Owing to a complex pathophysiology that involves early and delayed forms of brain injury, a significant number of patients surviving aSAH remain disabled with or without compromise detected on detailed neuropsychological testing. Only 10% of patients recover completely. The most common complication responsible for long-term impairments is delayed cerebral ischemia (DCI), which is typically observed during the first two or at most 3 weeks after aSAH onset and is associated with the appearance of a new focal neurologic deficit or a persistent decline in the patient's Glasgow Coma Scale score (3). Although traditionally attributed to vasoconstriction of large caliber proximal vessels (i.e., angiographic vasospasm) secondary to degradation of subarachnoid blood and intrathecal immune activation, more recent findings also point to a critical role of microvascular dysfunction (4–7). In particular, several studies performed in animal models have demonstrated a progressive impairment and partial inversion of cerebral neurovascular coupling (NVC) (8–10), the process responsible for adjusting local cerebral blood flow (CBF) to regionally heterogeneous changes in metabolic demand due to neuronal activation. While there is evidence for similar impairment in human aSAH patients (11–13), clinical assessment of NVC remains a diagnostic challenge that is usually achieved through invasive CBF measurements or highly specialized and expensive functional imaging techniques. An alternative approach to evaluate NVC is to measure microvascular responses in the retina, an embryological part of the central nervous system that can be assessed non-invasively by retinal vessel analysis (RVA). Because cerebral and retinal microvasculature bear a close anatomical correlation and are governed by common regulatory mechanisms, retinal vascular changes are increasingly recognized as potential screening option for altered NVC in the brain (14, 15). For example, a potential role of RVA for predicting cerebrovascular changes has previously been shown in elderly adults (16, 17), after coarctation repair (18) and in patients with diabetes (19) or Alzheimer's disease (20). During aSAH, the sudden rise of intracranial pressure often forces subarachnoid blood into the pre-retinal space (21), which may expose retinal micro-vessels to the same blood degradation products and inflammatory cytokines thought to be responsible for microvascular dysfunction in the brain. In addition, recent discovery of a cerebral and retinal glymphatic system (22) argues for the existence of perivascular pathways through which vasoactive agents formed in the subarachnoid space may also directly reach the retinal microvasculature. We have previously demonstrated the feasibility of RVA in aSAH patients (23) and provided first evidence for retinal vasoconstriction and signs of impaired NVC in these patients compared to healthy control

subjects (11). In this prospective study on a larger cohort of aSAH patients, we sought to validate our previous findings and evaluate the relationship between potential changes in NVC as detected by RVA and the occurrence of DCI and long-term clinical outcome.

MATERIALS AND METHODS

Patients with aSAH admitted to the Department of Neurosurgery at the RWTH Aachen University Hospital between July 2015 and December 2019 were considered for enrollment into the present study. Patients were selected based on the following inclusion criteria: (1) age $\geq$ 18 years, (2) aneurysmal origin of SAH as confirmed by computed tomography (CT) angiography and/or digital subtraction angiography (DSA), (3) absence of intraocular comorbidities or contraindications that would have precluded application of mydriatic agents, and (4) absence of Terson syndrome unless it did not interfere with the analysis of selected retinal vessels. Before enrolment, written informed consent according to the Declaration of Helsinki was obtained from all patients or their legal representatives and the study protocol was approved by the local Research Ethics Committee of the RWTH Aachen University (EK 069/15).

A total of 70 patients with aSAH were prospectively recruited, in whom measurements were performed 0–4 days (early phase: d_{0-4}), 5–15 days (critical phase: d_{5-15}), 16–23 days (late phase: d_{16-23}) and more than 6 weeks (follow-up: f/u) after the ictus. If more than one measurement was available for a given patient in a given phase, all measurements in this phase were averaged to calculate a mean valued. For comparison, an age-matched cohort of 42 healthy subjects who were measured by RVA at the Department of Exercise and Health Sciences at the University of Basel was also included in the study.

The clinical severity of aSAH on admission was assessed according to the Hunt and Hess (HH) grading scale and the degree of aneurysmal bleeding was scored according to the modified Fischer (mFS) scale based on CT scans. Patients were treated according to current multidisciplinary consensus guidelines (3, 24, 25). The aneurysm was secured by neurosurgical clipping or endovascular coiling based on an interdisciplinary consensus. Patients received prophylactic nimodipine therapy (180–360 mg per day) unless precluded by hemodynamic instability. All patients were continuously monitored for complications such as delayed cerebral ischemia (DCI), which was considered as a neurological worsening according to the definition by Vergouwen et al. (3) or territorial or watershed hypoperfusion on perfusion CT scans. In analgosedated patients, deterioration in cerebral microdialysis (71 high cut-off catheter, μdialysis, Stockholm, Sweden) or cerebral tissue oxygen saturation (Neurovent PTO, Raumedic AG, Helmbrechts, Germany) were used as surrogates to trigger CT perfusion. First-tier treatment in case of DCI consisted of induced hypertension (>180 mmHg systolic blood pressure) as per institutional protocol. In refractory cases without clinical or neuromonitoring improvement but confirmed misery perfusion on CTA or DSA, second-tier rescue therapy by balloon dilatation and/or continuous intra-arterial infusion of nimodipine was considered based on angiographic findings (26, 27). Clinical outcome after 12 months according to the extended Glasgow Outcome Scale (GOS-E) was assessed by an independent investigator based on a telephone interview, clinical investigation in the outpatient clinic or clinical status compiled from the medical reports. A summary of the demographic and clinical data obtained on admission or during in-hospital treatment is provided in **Table 1**.

TABLE 1 | Demographic and clinical data of control and aSAH patients.

Patient characteristic	Patients, *n* (%)	Control, *n* (%)
All patients	70 (100%)	42 (100%)
Gender		
Female	51 (73%)	20 (48%)
Male	19 (27%)	22 (52%)
Age		
	51 [48–59] yrs	50 [43–59] yrs
Aneurysm location		
Anterior circulation	53 (76%)	
Posterior circulation	16 (23%)	
Both	1 (1%)	
Hunt and hess (HH) grade		
Good grade (HH_{1-3})	56 (80%)	
Poor grade (HH_{4-5})	14 (20%)	
Modified fisher (mFS) scale		
Thin blood (mFS_{0-2})	34 (49%)	
Thick blood (mFS_{3-4})	36 (51%)	
Treatment modality		
Clipping	24 (34%)	
Coiling	44 (63%)	
Both	2 (3%)	
Delayed cerebral ischemia (DCI)		
DCI	23 (32%)	
DCI-related infarction	1 (1%)	
Outcome		
Favorable (GOS-E_{5-8})	64 (92%)	
Unfavorable (GOS-E_{1-4})	6 (8%)	

Retinal Vessel Analysis

Static and dynamic retinal vessel analyses were performed using a maneuverable Retinal Vessel Analyzer (IMEDOS Systems GmbH, Jena, Germany) as described previously (11, 23). Briefly, after unilateral application of a mydriatic agent (Tropicamide, Mydriaticum Stulln UD, Pharma Stulln GmbH, Stulln, Germany), conscious patients were examined in a sitting position while analgo-sedated patients were examined in supine position with the head and torso partially turned. For assessment of NVC, retinal veins and arteries were focused and the vessel diameters recorded continuously in operator-selected regions of interest located equidistant to the papilla. Measurements were performed with a standard 350 s dynamic vessel analysis protocol comprised of 50 s of baseline recording and three cycles of flicker-light excitation (FLE). For extended analysis the recorded

vessel diameters were expressed as percentage of the baseline diameter and plotted as a function of time as described in detail elsewhere (20, 28). To improve the signal-to-noise ratio, the individual response curves obtained for each subject during the three successive cycles of FLE were averaged. In healthy subjects, the typical arterial response curves thus obtained feature primary vasodilation upon initiation of FLE, which reaches a maximum after a characteristic latency and is followed, after termination of the stimulus, by a reflectory vasoconstriction (29). The general shape and amplitude of the response curve provide an index for the integrity of NVC, and were quantified by calculating maximum arterial and venous dilatation (MAD, MVD), the arterial and venous area-under-the-curve (AUC_{art}, AUC_{ven}) and the time to reach 30% ($tMAD_{30}$, $tMVD_{30}$) and 100% (tMAD, tMVD) of MAD and MVD after flicker initiation (**Figure 1A**). Following the dynamic analysis, monochromatic fundus images for static retinal vessel analysis (**Figure 1B**) were obtained at a 30° camera angle with the optic nerve centered and processed using a dedicated software tool (VisualIS, IMEDOS Systems GmbH., Jena, Germany). Central retinal arterial and venous equivalents (CRAE and CRVE, respectively), and arterio-venous ratio (AVR) were calculated as described previously (30, 31). All dynamic and static examinations were routinely paralleled by multimodal monitoring of mean arterial blood pressure (MAP), heart rate, blood gases, oxygenation and intracranial pressure (ICP), ensuring physiological conditions at the time of image acquisition. Measurement was aborted in case of hemodynamic or ventilatory instability.

Statistical Analysis

Normal distribution was tested using the Kolmogorow-Smirnow normality test. Quantitative parameter values are presented as mean ± standard deviation (SD) or as median [1 quartile−3 quartile], and as percentage in case of nominal data. Differences between two groups were analyzed using the two-sided student *t*-test, Mann–Whitney-test or Chi-Square test, respectively. For subgroup analyses with regard to DCI and outcome, all patients were stratified into groups according to the development of DCI (DCI *vs.* no DCI) and clinical outcome after 12 months (unfavorable: GOS-E_{1-4} *vs.* favorable: GOS-E_{5-8}), respectively (see **Supplementary Tables 1, 2**). For analysis of the influence of nimodipine, all measurements (see **Supplementary Table 3**) or all patients (see **Supplementary Table 4**) were stratified into groups according to oral nimodipine treatment (measurements in nimodipine-treated patients *vs.* measurements in patients with no nimodipine treatment for at least 24 h). Statistical significance was set at $p<0.05$; statistical results with $p<0.1$ were accepted as a trend. All analyses were performed using Excel (Microsoft Office Excel 2010, Californian, USA), SPSS v. 21 (IBM Chicago, Illinois, USA), Numbers®, Apple Inc., Cupertino, USA, GraphPad Prism® and GraphPad Software, Inc., La Jolla, USA.

RESULTS

The demographic data of patients included in this study are summarized in **Table 1** In total, the aSAH cohort comprised 70 patients with a median age of 51 [48–59] years, of whom 51 (73%) were female and 19 (27%) were male. Twenty-three (32%) of the patients developed delayed cerebral ischemia (DCI), which progressed to infarction in one patient. The clinical outcome after 12 months was favorable (GOS-E_{5-8}) in 64 (92%) and unfavorable (GOS-E_{1-4}) in 6 (8%) of the patients. Retinal vessel analysis (RVA) could be performed in 32, 53, 23, and 40 patients during the early (d_{0-4}), critical (d_{5-15}), late (d_{16-23}) phase, and follow-up, respectively. For comparison, a cohort of 42 healthy subjects with a median age of 50 [43–59] years, of whom 20 (48%) were female and 22 (52%) were male, was also included in the study (**Table 1**).

Vessel Diameters

When compared to control subjects, the arterial diameter, expressed as central retinal arterial equivalent (CRAE), was significantly reduced immediately after aSAH and remained so throughout the whole observation period ($p < 0.0001$ for all time periods examined), with only a minor, non-significant increase in vessel diameters observed in measurements performed at follow-up (f/u) more than 6 weeks after the ictus (**Figure 2A, Table 2**). Likewise, the central retinal venous equivalent (CRVE) was significantly reduced in aSAH patients compared to control subjects ($p < 0.0001$ for all time periods examined) and showed little change during the observation period (**Figure 2B, Table 3**). For relative assessment of vessel dimensions and to account for systematic variations in measurements, the retinal arterio-venous-ratio (AVR) was also calculated. As illustrated in **Figure 2C**, the AVR showed very similar changes, although the difference to the control subjects only reached statistical significance during the early phase (d_{0-4}, $p = 0.0396$) and after more than 6 weeks (f/u, $p = 0.0050$).

Neurovascular Coupling

Dynamic retinal vessel analysis revealed dramatic and sustained impairments in the arterial response of aSAH patients to flicker light stimulation when compared to the control subjects (**Figure 3A**). In particular, aSAH patients exhibited an acute reduction in arterial vasodilation during the flicker, as reflected in a significantly lower MAD [2.2 (1.0–3.2)% vs. 3.8 (2.6–5.6)% in control subjects, $p = 0.0016$] and AUC_{art} [21.5 (9.4–35.8)%*s vs. 51.4 (32.5–69.7)%*s in control subjects, $p = 0.0001$] during the early phase (d_{0-4}, **Figures 3B,C**), while the timing of the response (i.e., tMAD and $tMAD_{30}$) appeared to be largely unaffected (**Table 2**). Unlike the changes in arterial diameter and AVR, both MAD and AUC_{art} showed a gradual recovery toward healthy controls, with a significant reduction only during the first 3 weeks after the ictus (**Figures 3B,C**). For example, AUC_{art} increased to 22.4 [12.6–45.0]%*s ($p < 0.0001$ vs. Control) during the critical (d_{5-15}) and 30.5 [3.2–53.9]%*s ($p = 0.0033$ vs. Control) during the late (d_{16-23}) phase (**Figure 3C**). In measurements performed at follow-up more than 6 weeks after the ictus, AUC_{art} already amounted to 44.5 [23.2–61.1]%*s, which is close to the value of 51.4 [32.5–69.7]%*s ($p = 0.1380$) observed in the control subjects and significantly higher than the values observed during the early [21.5 (9.4–35.8)%*s, $p = 0.0066$] and critical [22.4 (12.6–45.0)%*s, $p = 0.0047$] phase (**Figure 3C**).

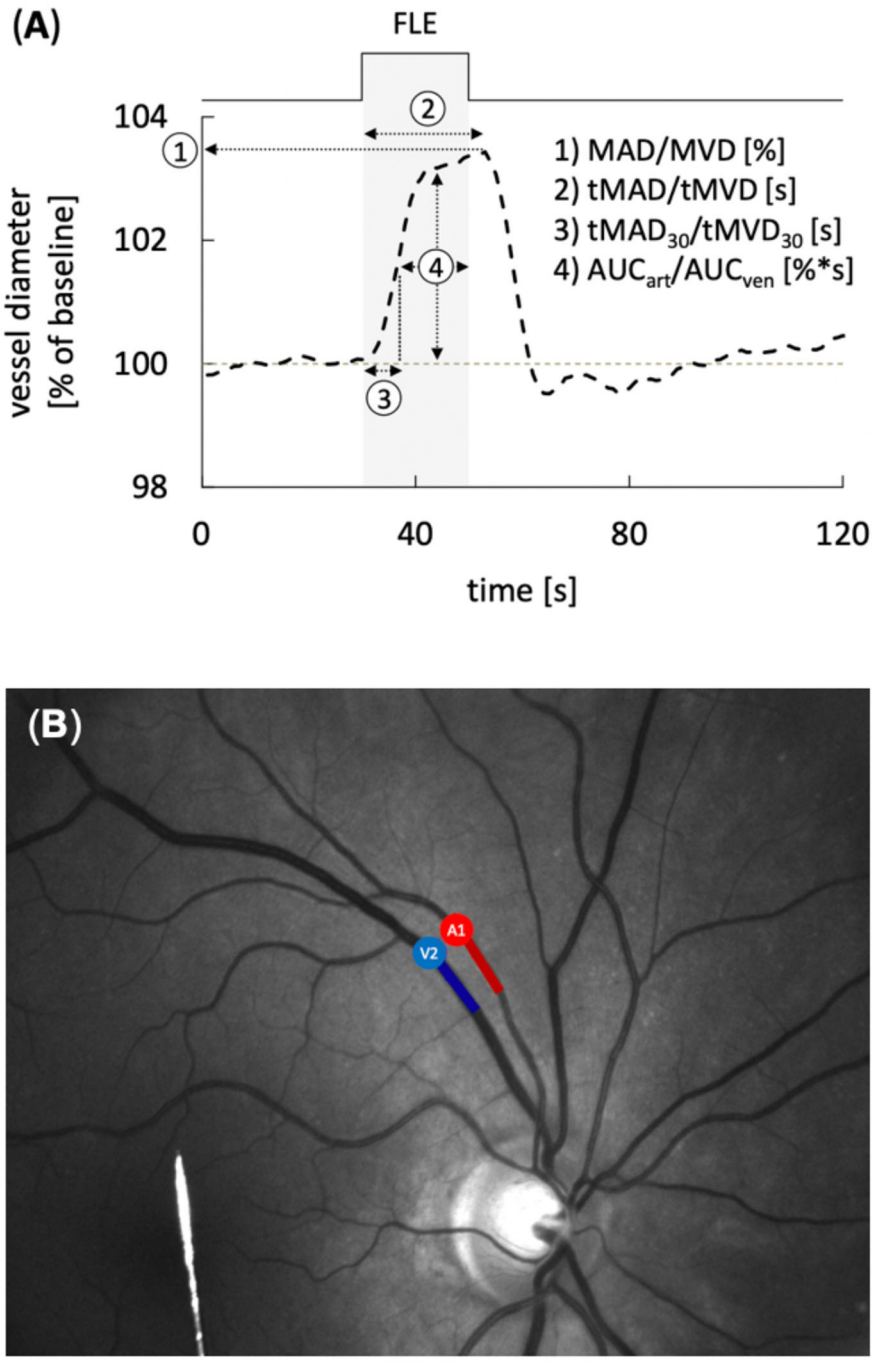

FIGURE 1 | Static and dynamic retinal vessel analysis (RVA). **(A)** Average retinal vessel response to flicker light excitation (FLE) in healthy subjects with the different parameters determined for dynamic RVA. The stimulation period is indicated above and by light gray shading. Parameters used for quantification of the response comprised maximum arterial or venous dilation (MAD/MVD), time to maximum arterial or venous dilation (tMAD/tMVD) relative to flicker initiation, time to 30% of the maximum arterial or venous dilation ($tMAD_{30}/tMVD_{30}$) relative to flicker initiation, and arterial or venous area under the curve (AUC_{art}/AUC_{ven}) during the FLE. **(B)** Example of a monochromatic fundus image used for RVA. Arterial (A) and venous (V) segments are indicated in red and blue, respectively.

Analysis of venous responses to flicker light revealed much less marked differences (**Figure 3D, Table 3**). In particular, neither MVD (**Figure 3E**) nor the timing of venous responses (**Table 3**) showed significant differences compared to control subjects. Moreover, there was only a tendency for AUC_{ven} during the early phase to be reduced when compared to control subjects

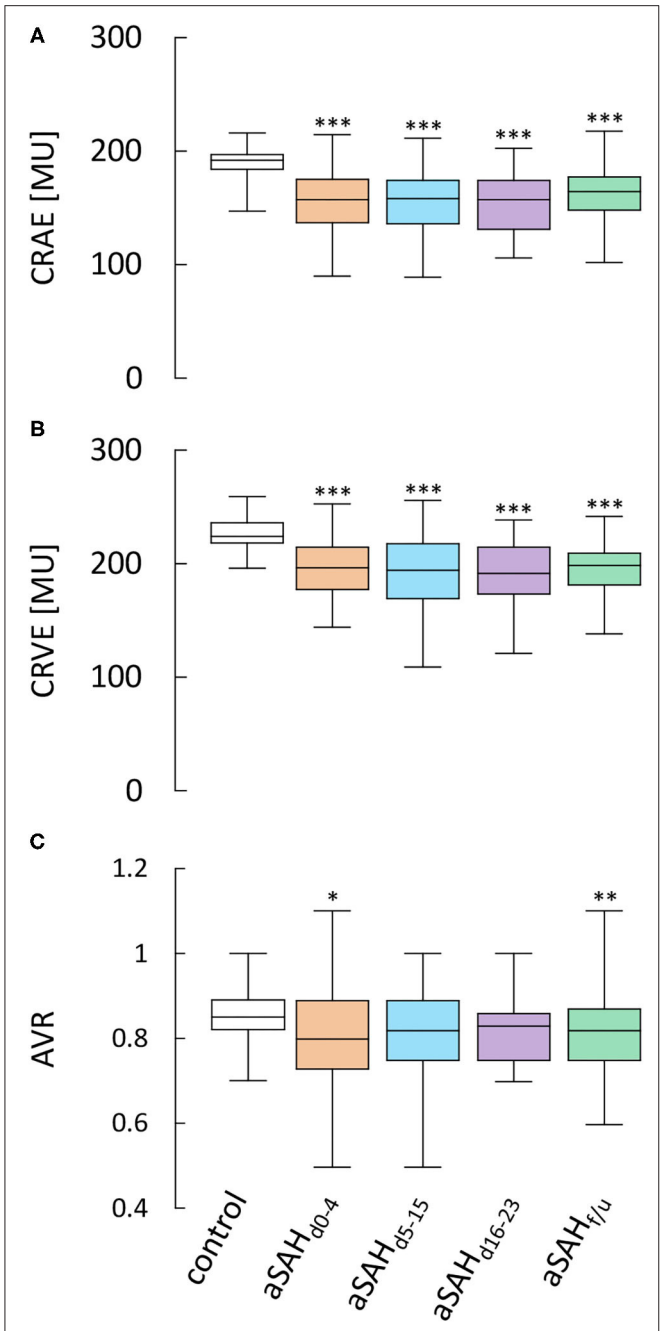

FIGURE 2 | Results from static RVA in aSAH patients and control subjects. Comparison of **(A)** central retinal arterial equivalent (CRAE) as a measure of arterial diameter, **(B)** central retinal venous equivalent (CRVE) as a measure of venous diameter and **(C)** retinal arterio-venous-ratio (AVR) in control subjects and aSAH patients during the early ($aSAH_{d0-4}$), critical ($aSAH_{d5-15}$) and late ($aSAH_{d16-23}$) phase and at follow-up more than 6 weeks after the ictus ($aSAH_{f/u}$). ***$p < 0.001$ vs. control; **$p < 0.01$ vs. control; *$p < 0.05$ vs. control.

[41.3 (16.4–46.8)%*s vs. 45.7 (31.2–62.2)%*s in control subjects, $p = 0.0610$], although a significant difference was detected when compared to the corresponding value at follow-up [41.3 (16.4–46.8)%*s vs. 52.4 (34.2–61.7)%*s at follow-up, $p = 0.0205$; **Figure 3F**].

Subgroup Analyses With Regard to Cardiovascular Risk Factors

Cardiovascular risk factors like diabetes mellitus have been shown to alter retinal vessel diameters and/or responses to stimulation (32) and could thus act as important confounding factors. There was only one patient with diabetes in our study, excluding further analysis of its potential as a confounding factor. However, to address the role of other cardiovascular risk factors like arterial hypertension, obesity and smoking, we examined their potential association with RVA parameters determined during the early phase. There was no difference in any of the parameters between patients stratified according to smoking status, but a tendency for AUC_{ven} to be lower in patients in hypertension [36.1 (12.8–43.2)%*s vs. 44.4 (27.6–56.5)%*s in normotensive patients, $p = 0.0818$], which may have contributed to the difference in AUC_{ven} between aSAH and control patients during the early phase described above. In addition, while AUC_{art} tended to be lower in patients with BMI $\geq$ 30 [8.1 (−10.1–12.5)%*s vs. 26.9 (11.6–36.6)%*s in patients with BMI < 30, $p = 0.062$], it actually tended to be higher in patients with arterial hypertension [27.8 (14.9–44.8)%*s vs. 11.9 (4.1–32.0)%*s in normotensive patients, $p = 0.0502$], although none of these differences reached statistical significance (for details see **Supplementary Table 1**).

Subgroup Analyses With Regard to DCI and Long-Term Clinical Outcome

To examine if differences in retinal vessel responses could facilitate early detection of patients at risk of complications and delayed brain injury, we also analyzed data stratified according to the occurrence of DCI and long-term clinical outcome. While most parameters were independent of the subgroup (**Supplementary Tables 2, 3**), there were some subtle but significant kinetic differences between arterial responses in patients with and without DCI. In particular, patients that developed DCI showed faster vasodilation on flicker initiation during the early phase (**Figure 4A**), which was most evident when the average responses in both groups were normalized by their maximum amplitude (inset and arrow in **Figure 4A**). Quantitatively, this difference was reflected in a significantly lower $tMAD_{30}$ (**Figure 4B**), which amounted to 4.0 [3.0–6.8] s in patients with DCI ($n = 10$) vs. 7.0 [5.0–8.0] s ($p = 0.022$) in patients without DCI ($n = 13$). There was also a tendency for a lower tMAD in patients with DCI, but the difference was much less pronounced and did not reach statistical significance ($p = 0.254$, **Figure 4C**). Interestingly, these differences appeared to be restricted to the early phase and their direction actually reversed during the late phase (**Figure 4D**), where patients with DCI exhibited a higher $tMAD_{30}$ (**Figure 4E**) and a significantly higher tMAD [24.0 (21.0–29.3) s, $n = 6$ vs. 18.0 (14.0–21.0) s in patients without DCI, $n = 17$, $p = 0.017$, **Figure 4F**]. In contrast, no significant differences were observed in venous retinal vessel parameters between patients with and without DCI

(**Supplementary Table 2**). Comparison of results with regard to the clinical outcome after 12 months was hampered by the fact that RVA could only be performed in a total of six patients with a poor clinical outcome. However, patients with an unfavorable outcome were characterized by a tendency for lower arterial and venous diameters throughout the whole observation period (**Supplementary Table 3**), and the CRVE in these patients during the critical phase [d_{5-15}: 171 (144–187) MU, $n = 4$] was significantly ($p = 0.045$) lower than the corresponding value in patients with a favorable outcome [199 (170–220) MU, $n = 43$]. Arterial and venous parameters from dynamic retinal vessel analysis on the other hand either showed no significant differences or the number of patients with a poor outcome was simply too small for statistical testing (**Supplementary Table 3**).

Effects of Nimodipine Treatment

Finally, to examine if retinal vessel diameters or their response to flicker stimulation were affected by treatment with the L-type Ca^{2+} channel antagonist nimodipine, we compared data obtained during nimodipine treatment and data obtained while no nimodipine was administered (**Supplementary Table 4**). However, neither static nor dynamic retinal vessel parameters appeared to be affected by nimodipine. For example, in 51 static measurements performed during nimodipine treatment, arterial and venous diameters (CRAE & CRVE) were 158 [136–174] MU and 199 [171–214] MU, while the corresponding values in 30 measurements performed while no nimodipine was administered were 162 [133–178] MU ($p = 0.4868$) and 200 [174–209] MU ($p = 0.9692$). Likewise, maximum arterial and venous dilation upon stimulation (MAD and MVD) amounted to 2.2 [1.4–3.6]% and 3.6 [2.6–5.0]% during nimodipine treatment as compared to 2.9 [1.2–4.6]% ($p = 0.4343$) and 3.7 [2.4–4.7]% ($p = 0.8484$) in measurements performed while no nimodipine was administered (**Figures 5A,B**, for remaining parameters see **Supplementary Table 4**). Similar results were obtained when the same analysis was performed after stratification of the patients according to the occurrence of DCI (see **Supplementary Table 4**). Finally, to ensure that this was not due to differences in the time-frame of measurements performed with and without nimodipine treatment, we also compared data obtained during early, critical and late phase respectively (**Figures 5C–H**, **Supplementary Table 6**). However, neither retinal vessel diameters (**Figures 5C,D**), nor the maximum amplitude (**Figures 5E,F**), AUC (**Supplementary Table 6**), or time-course (**Figures 5G,H**) of vasodilation in response to flicker light stimulation during any of the phases appeared to be affected by nimodipine treatment.

DISCUSSION

The exact pathophysiological cascades underlying delayed cerebral ischemia (DCI) and other complications in aSAH patients surviving the initial bleed are still poorly understood. Evidence from animal models indicates that a mismatch between metabolic demand and local CBF due to impaired NVC could contribute to DCI, but the clinical relevance of these findings has remained elusive as there is still a lack of methods for non-invasive assessment of NVC in human subjects. A promising approach to evaluate NVC in aSAH patients is to measure microvascular responses in the retina, an embryological part of the central nervous system and possibly exposed to the same vasoactive hemoglobin metabolites and inflammatory cytokines as small cerebral vessels. Thus, recent discovery of a cerebral and retinal glymphatic system (22) indicates that there are perivascular pathways through which vasoactive agents formed in the subarachnoid space could directly reach the retinal microvasculature. Here, we used static and dynamic retinal vessel analysis (RVA) in aSAH patients to detect changes in basal diameter and responsiveness of retinal vessels to flicker light stimulation, both of which have been proposed as potential candidates for early detection of cerebrovascular dysfunction (14, 15).

Static RVA and Retinal Vessel Diameters After aSAH

Vasoconstriction of large caliber proximal vessels (i.e., angiographic vasospasm) is a common complication after aSAH and was long regarded as the main cause of DCI and poor clinical outcomes, but more recent studies have questioned this concept and proposed a more important role of microvascular changes (4, 5). Our present findings point to a sustained reduction in the diameter of retinal microvessels after aSAH compared to control subjects, which appeared to be more pronounced in the arterial compartment, as reflected in a parallel and significant decrease of the arterio-venous-ratio (AVR) during the early phase and at follow-up. The latter would be consistent with the general view that veins have only limited capability for active vasoconstriction and our previous proposal that the reduced venule diameter in the retina after aSAH is at least partly mediated by constriction of upstream arterioles and a resulting reduction in blood flow (11). In any case, the observed microvascular changes resemble aSAH-induced changes in large caliber vessels, namely early cerebral artery vasoconstriction and an associated reduction in cerebral perfusion which may contribute to DCI in some patients (33–35). Considering that increased intracranial pressure during the acute phase of aSAH forces subarachnoid blood into the preretinal space, a significant reduction in retinal vessel diameters observed during the early phase after aSAH is in line with previous *in vitro* and *in vivo* animal studies showing that blood-filled cerebrospinal fluid enhances constriction of both, the retinal (36) and cerebral (37) microvasculature. Interestingly and in contrast to angiographic vasospasm, which usually dissolves by week 2 after the ictus (34), however, there was almost no return of arterial and venous diameters toward the control level during the first 3 weeks after aSAH and only a partial, non-significant recovery at follow-up more than 6 weeks later. A possible explanation for these observations is that part of the reduced basal vessel diameter reflects pathophysiological mechanisms that are not readily reversible and outlast the impairments in vessel responsiveness to stimulation. This would be in line with the results from animal studies indicating that, at least in large caliber vessels, the initial

TABLE 2 | Arterial RVA parameters in control and aSAH patients.

Parameter	Median [q1–q3]	*n*	*p*-value (vs. Control)	*p*-value (vs. $aSAH_{f/u}$)
CRAE [MU]				
Control	192 [184–197]	42	–	–
$aSAH_{d0-4}$	157 [137–175]	32	**<0.0001**	0.2214
$aSAH_{d5-15}$	158 [136–174]	53	**<0.0001**	0.3996
$aSAH_{d16-23}$	157 [131–174]	23	**<0.0001**	0.5614
$aSAH_{f/u}$	164 [148–177]	40	**<0.0001**	–
AVR				
Control	0.85 [0.82–0.89]	42	**–**	–
$aSAH_{d0-4}$	0.80 [0.73–0.89]	32	**0.0396**	0.8626
$aSAH_{d5-15}$	0.82 [0.75–0.89]	53	0.0802	0.4305
$aSAH_{d16-23}$	0.83 [0.75–0.86]	23	0.0986	0.7186
$aSAH_{f/u}$	0.82 [0.75–0.87]	40	**0.0050**	–
MAD [%]				
Control	3.8 [2.6–5.6]	42	–	–
$aSAH_{d0-4}$	2.2 [1.0–3.2]	32	**0.0016**	0.0521
$aSAH_{d5-15}$	2.1 [1.4–3.6]	53	**0.0002**	**0.0321**
$aSAH_{d16-23}$	2.9 [1.6–4.2]	23	**0.0189**	0.2623
$aSAH_{f/u}$	3.0 [2.0–5.0]	40	0.1410	–
tMAD [s]				
Control	19.0 [17.0–21.0]	42	–	–
$aSAH_{d0-4}$	17.0 [14.0–22.0]	32	0.2638	0.6574
$aSAH_{d5-15}$	18.0 [14.8–19.8]	53	0.1295	0.7246
$aSAH_{d16-23}$	20.0 [17.3–21.8]	23	0.7620	0.0907
$aSAH_{f/u}$	18.0 [12.3–20.0]	40	0.0830	–
$tMAD_{30}$ [s]				
Control	5.0 [4.1–5.5]	42	–	–
$aSAH_{d0-4}$	5.0 [4.0–8.0]	32	0.1762	**0.0266**
$aSAH_{d5-15}$	5.0 [3.0–7.0]	53	0.8656	0.1599
$aSAH_{d16-23}$	5.0 [3.0–6.0]	23	0.8524	0.3451
$aSAH_{f/u}$	4.0 [2.5–5.5]	40	0.0680	–
AUC_{art} [%*s]				
Control	51.4 [32.5–69.7]	42	–	–
$aSAH_{d0-4}$	21.5 [9.4–35.8]	32	**0.0001**	**0.0066**
$aSAH_{d5-15}$	22.4 [12.6–45.0]	53	**<0.0001**	**0.0047**
$aSAH_{d16-23}$	30.5 [3.2–53.9]	23	**0.0033**	0.0890
$aSAH_{f/u}$	44.5 [23.2–61.1]	40	0.1380	–

AUC_{art}, arterial area under the curve during flicker stimulation; AVR, retinal arterio-venous-ratio; CRAE, central retinal arterial equivalent; f/u, follow-up (>6 weeks after ictus); MAD, maximum arterial dilation; RVA, retinal vessel analysis; tMAD, time to maximum arterial dilation; $tMAD_{30}$, time to 30% of maximum arterial dilation. Bold values indicate $p < 0.05$.

arterial narrowing by vasoactive substances after aSAH leads to tissue damage and structural changes with an associated long-term alteration of the arterial tone (38, 39). In this context, it is also interesting to note that perivascular enlargement in the brain, a putative imaging biomarker for microvascular brain damage (40), has recently been demonstrated to be associated with narrower arterial calibers in the retina (41).

Dynamic RVA and Neurovascular Coupling After aSAH

Adequate NVC is critical for continuous adjustment of local CBF to regionally heterogeneous changes in metabolic demand but may be compromised by the pathophysiological cascades initiated during bleeding into the subarachnoid space. Our present findings demonstrate a sustained decrease of retinal arterial vasodilation with partial recovery in response to flicker light stimulation in aSAH patients, as reflected in a significantly reduced maximum amplitude and area under the response curve compared to control subjects. Unlike the changes in vessel diameters, arterial responsiveness in aSAH patients showed a gradual recovery during the first 3 weeks and reached almost normal levels at follow-up more than 6 weeks after the ictus. Given that complications like DCI and DCI-related infarctions, which have been proposed to be the result of microvascular

TABLE 3 | Venous RVA parameters in control and aSAH patients.

Parameter	Median [q1–q3]	*n*	*p*-value (vs. Control)	*p*-value (vs. $aSAH_{f/u}$)
CRVE [MU]				
Control	224 [218–236]	42	–	–
$aSAH_{d0-4}$	196 [177–214]	32	**<0.0001**	0.2909
$aSAH_{d5-15}$	194 [169–217]	53	**<0.0001**	0.4043
$aSAH_{d16-23}$	191 [173–214]	23	**<0.0001**	0.2454
$aSAH_{f/u}$	198 [181–209]	40	**<0.0001**	–
AVR				
Control	0.85 [0.82–0.89]	42	**–**	–
$aSAH_{d0-4}$	0.80 [0.73–0.89]	32	**0.0396**	0.8626
$aSAH_{d5-15}$	0.82 [0.75–0.89]	53	0.0802	0.4305
$aSAH_{d16-23}$	0.83 [0.75–0.86]	23	0.0986	0.7186
$aSAH_{f/u}$	0.82 [0.75–0.87]	40	**0.0050**	–
MVD [%]				
Control	3.9 [3.0–5.8]	42	–	–
$aSAH_{d0-4}$	3.7 [2.9–4.7]	32	0.3179	0.1432
$aSAH_{d5-15}$	4.1 [2.7–5.2]	53	0.4165	0.2388
$aSAH_{d16-23}$	4.3 [2.6–5.4]	23	0.6356	0.5304
$aSAH_{f/u}$	4.5 [3.4–5.4]	40	0.7270	–
tMVD [s]				
Control	20.5 [19.0–22.0]	42	–	–
$aSAH_{d0-4}$	22.0 [20.0–24.0]	32	0.1872	**0.0235**
$aSAH_{d5-15}$	21.0 [19.0–22.5]	53	0.9903	0.0761
$aSAH_{d16-23}$	22.0 [20.0–24.0]	23	0.4663	**0.0110**
$aSAH_{f/u}$	19.0 [18.0–22.0]	40	0.2040	–
$tMVD_{30}$ [s]				
Control	7.0 [6.0–8.4]	42	–	–
$aSAH_{d0-4}$	6.0 [5.0–8.0]	32	0.1269	0.6026
$aSAH_{d5-15}$	7.0 [6.0–8.0]	53	0.7015	0.3347
$aSAH_{d16-23}$	7.0 [7.0–8.0]	23	0.0720	0.1297
$aSAH_{f/u}$	6.5 [5.5–8.0]	40	0.1530	–
AUC_{ven} [%*s]				
Control	45.7 [31.3–62.2]	42	–	–
$aSAH_{d0-4}$	41.3 [16.4–46.8]	32	0.0610	**0.0205**
$aSAH_{d5-15}$	45.0 [27.5–60.8]	53	0.3833	0.1464
$aSAH_{d16-23}$	44.5 [20.2–60.9]	23	0.3054	0.1853
$aSAH_{f/u}$	52.4 [34.2–61.7]	40	0.6030	–

AUC_{ven}, venous area under the curve during flicker stimulation; AVR, retinal arterio-venous-ratio; CRVE, central retinal venous equivalent; f/u, follow-up (>6 weeks after ictus); MVD, maximum venous dilation; RVA, retinal vessel analysis; tMVD, time to maximum venous dilation; $tMVD_{30}$, time to 30% of maximum venous dilation. Bold values indicate $p < 0.05$.

dysfunction in the brain, are typically restricted to the first two or at most 3 weeks after the ictus as well, these findings support the assumption that retinal vessels could serve as a surrogate marker for changes in cerebral small vessels after aSAH. The observed time-course also matches the pathophysiological cascades traditionally thought to be responsible for vascular dysfunction after aSAH, namely hemolysis of subarachnoid blood and intrathecal immune activation during the early phase, secondary immune infiltration and formation of various vasoactive hemoglobin metabolites during the critical phase and their gradual clearance during the late phase (42–44). Further support for the idea comes from recent discovery of cerebral and retinal glymphatic systems (22), which could provide a perivascular pathway through which vasoactive agents formed during the critical phase reach the retinal microvasculature. If this turns out to be the case, dynamic RVA could not only provide a unique tool to monitor their impact on microvascular function in a relatively simple manner but also a read-out of disease- or treatment-related changes in cerebral small vessels that are otherwise difficult or impossible to assess directly and

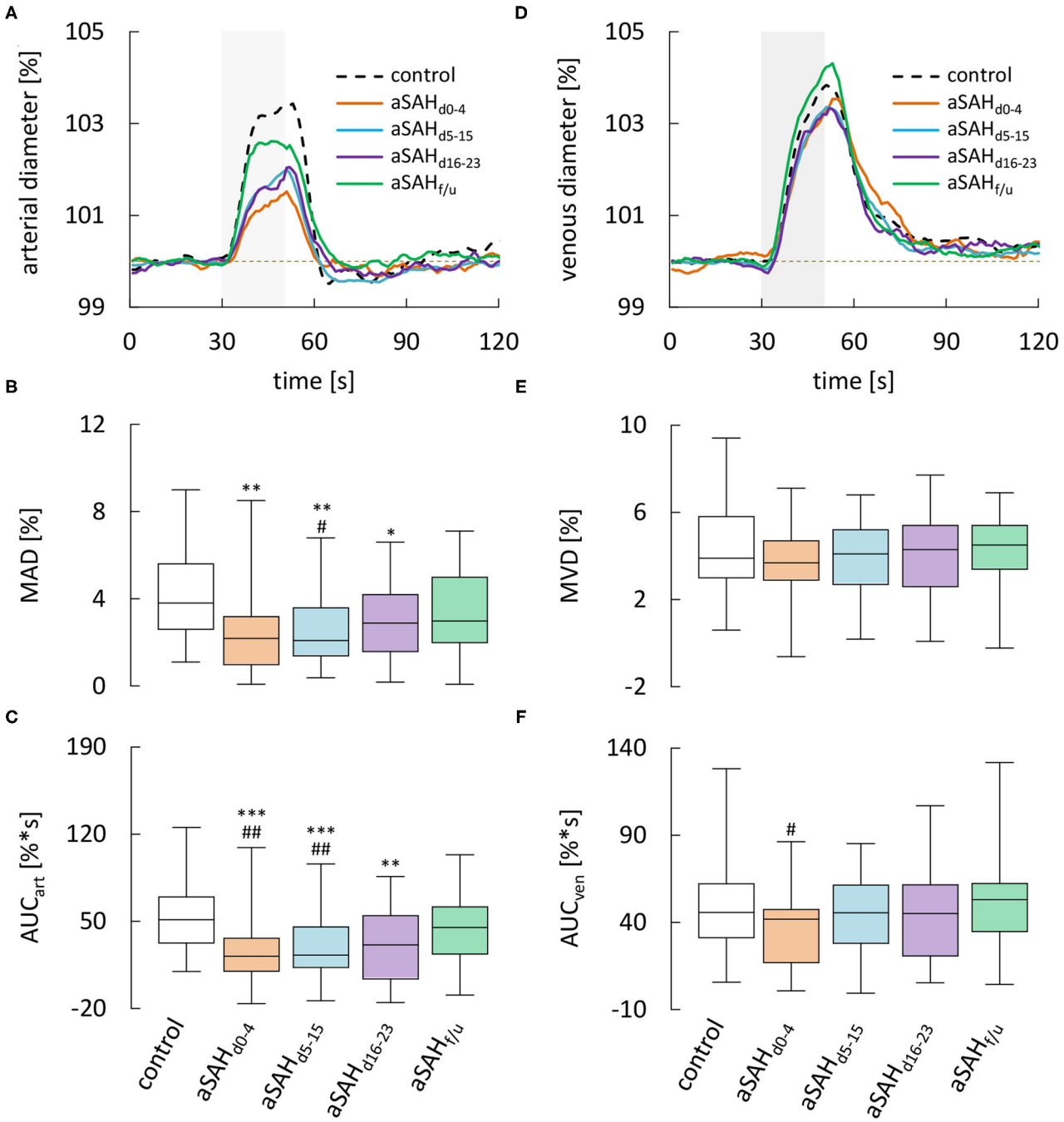

FIGURE 3 | Results from dynamic RVA in aSAH patients and control subjects. **(A)** Average relative retinal arterial responses to flicker light stimulation measured in control subjects and aSAH patients during the early ($aSAH_{d0-4}$), critical ($aSAH_{d5-15}$), and late ($aSAH_{d16-23}$) phase and at follow-up more than 6 weeks after the ictus ($aSAH_{f/u}$). Stimulation period is indicated by light gray shading. **(B)** Maximum arterial dilation (MAD) quantified from data shown in A. **(C)** Arterial area under the curve (AUC_{art}) quantified from the data shown in A. **(D)** Average retinal venous responses to flicker light stimulation measured in control subjects and aSAH patients at the same times as in A. **(E)** Maximum venous dilation (MVD) quantified from the data shown in D. **(F)** Venous area under the curve (AUC_{ven}) quantified from the data shown in A. $^{***}p < 0.001$ vs. control; $^{**}p < 0.01$ vs. control; $^{*}p = 0.05$ vs. control; $^{\#\#}p < 0.01$ vs. $aSAH_{f/u}$; $^{\#}p < 0.05$ vs. $aSAH_{f/u}$.

non-invasively. For example, our present findings suggest that nimodipine, the only FDA-approved pharmacological treatment for delayed cerebral vasospasm after aSAH (45), neither affects the basal diameter nor the responsiveness of retinal microvessels to stimulation, although this remains to be confirmed it future studies.

Likewise, further study will be required to evaluate the sensitivity of RVA with regard to the early detection of DCI.

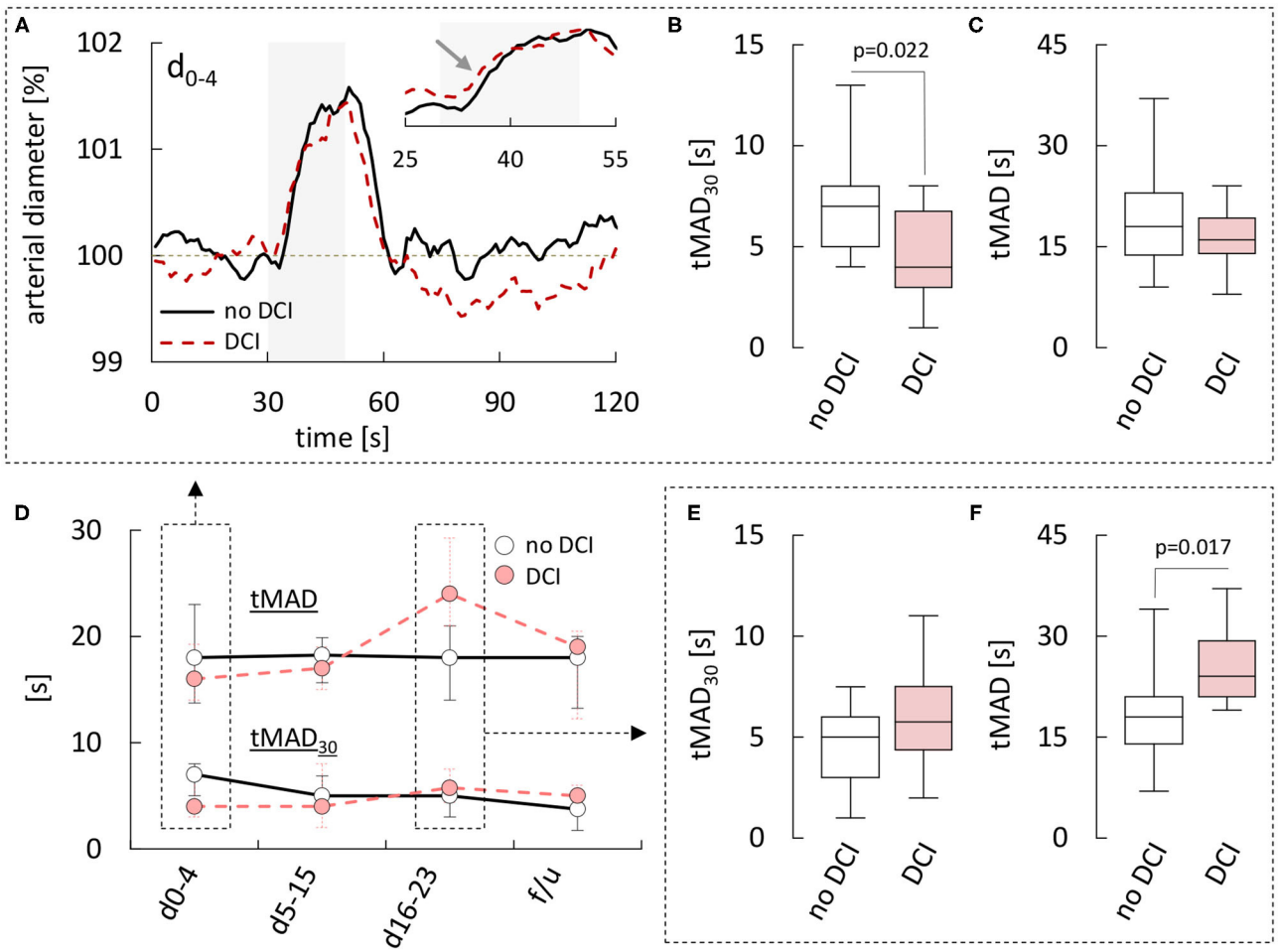

FIGURE 4 | Comparison of retinal arterial responses in aSAH patients with and without DCI. **(A)** Average relative retinal arterial responses to flicker light stimulation measured during the early phase (days 0–4) in aSAH patients with or without delayed cerebral ischemia (DCI). Stimulation period is indicated by light gray shading. Inset shows the rising phase on an expanded time-scale and after scaling the responses to the same amplitude to highlight kinetic changes. **(B)** Time to 30% of the maximum arterial dilation ($tMAD_{30}$) and **(C)** time to maximum arterial dilation (tMAD) determined during the early phase in patients with and without DCI. **(D)** Time-course of changes in median [q1–q3] $tMAD_{30}$ (bottom) and tMAD (top) observed in patients with or without DCI. **(E)** $tMAD_{30}$ and **(F)** tMAD determined during the late phase (days 16–23) in patients with and without DCI. For a summary of all parameters and *p*-values see **Supplementary Table 2**.

Limitations and Confounding Factors

There are several confounding factors that have to be taken into account when interpreting our results. First and foremost, although adaptation of our current imaging technique allowed us to also recruit some more severely affected, analgo-sedated patients, cases with mild aSAH, good clinical grade (HH_{1-3}), and/or good clinical outcome were still clearly overrepresented in our cohort, which may have biased the observed changes, likely toward milder alterations. To overcome this limitation, which is mainly brought about by the limited maneuverability of the required funduscope in supine patients, we are currently working on a miniaturized, wearable device for RVA that is comparable to commercially available "smartglasses" and should facilitate bedside testing of immobilized and sedated patients (46). That said, given the complexity of blood flow regulation and NVC, it is likely that numerous factors, some of which may still be unknown, can influence retinal vessel diameters and their responsiveness to stimulation. In order to reduce potential confounding factors and ensure standardized, physiological conditions at the time of image acquisition, our measurements were routinely paralleled by multimodal monitoring of mean arterial blood pressure (MAP), heart rate, blood gases, oxygenation, and intracranial pressure (ICP). In addition, our analysis indicates that there was no effect of nimodipine treatment on any of the parameters evaluated. With regard to static RVA, it is also important to keep in mind that direct comparison of CRAE and CRVE values between control and aSAH patients may have been influenced by the fact that measurements were performed using devices at two different facilities.

It is also worth noting that cardiovascular risk factors like diabetes or arterial hypertension could act as confounding

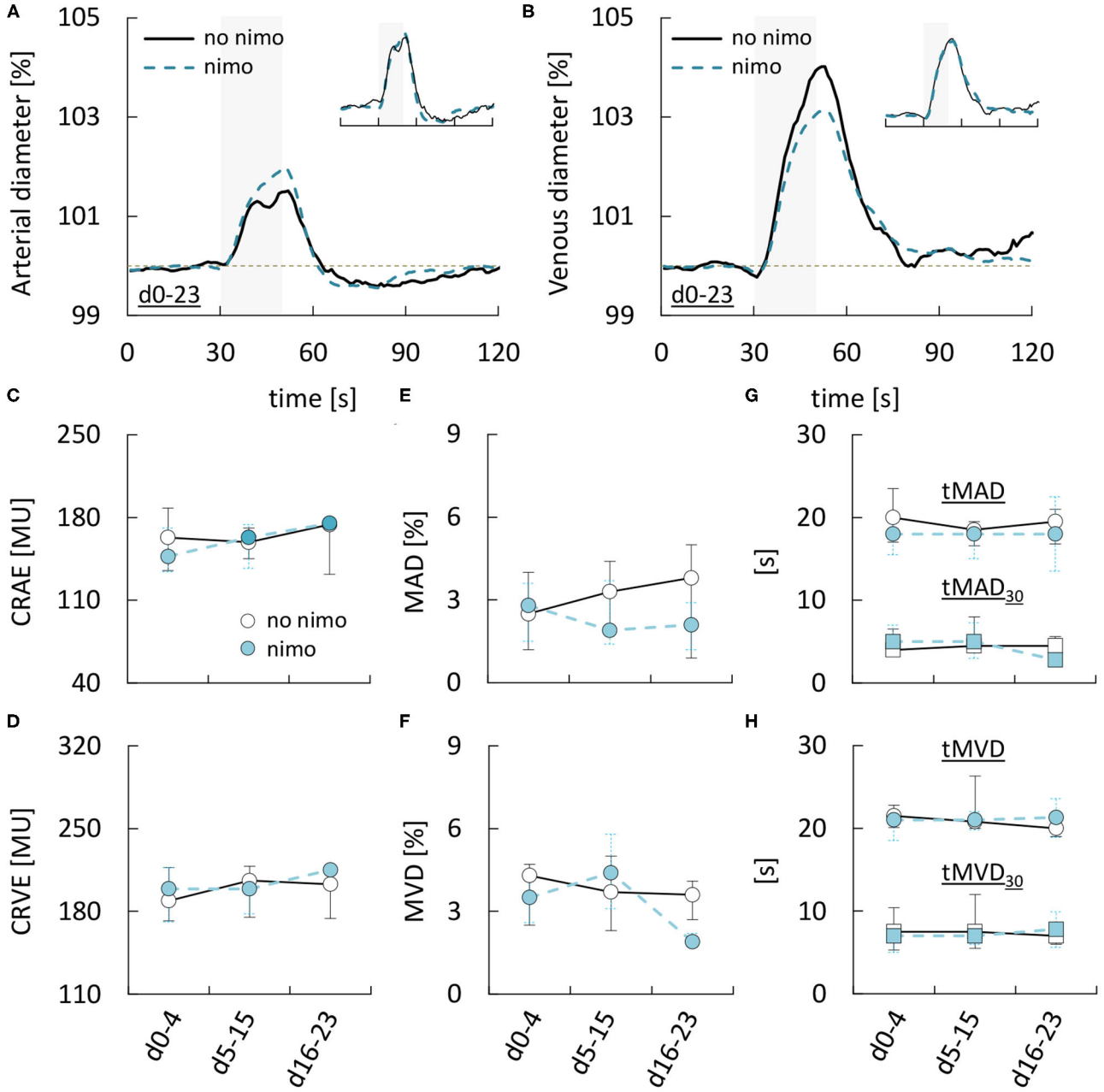

FIGURE 5 | Dependence of retinal vessel properties in aSAH patients on nimodipine treatment. **(A)** Average relative arterial responses to flicker light stimulation measured with or without nimodipine (nimo) treatment. Inset shows the same data but scaled to the same amplitude for comparison of response kinetics. Stimulation period is indicated by light gray shading. **(B)** Average relative venous responses to flicker light stimulation measured with or without nimodipine (nimo) treatment. Inset shows the same data but scaled to the same amplitude for comparison of response kinetics. Stimulation period is indicated by light gray shading. **(C–H)** Comparison of **(C)** central retinal arterial equivalent (CRAE), **(D)** central retinal venous equivalent (CRVE), **(E)** maximum arterial dilation (MAD), **(F)** maximum venous dilation (MVD), **(G)** time to 30 and 100% of maximum arterial dilation ($tMAD_{30}$ & tMAD), and **(H)** time to 30 and 100% of maximum venous dilation ($tMVD_{30}$ & tMVD) in aSAH patients with or without nimodipine treatment during the early ($aSAH_{d0-4}$), critical ($aSAH_{d5-15}$), and late ($aSAH_{d16-23}$) phase.

factors and complicate the use of RVA in the context of aSAH. For example, in the present study, there was a tendency for AUC_{art} to be higher in patients with arterial hypertension, which could partly mask the decrease of this parameter after aSAH. Consistent with previous studies (32), these differences were relatively subtle and they did not reach statistical significance, but further studies on the role of these and other cardiovascular risk factors will clearly be required before RVA can be reliably used for diagnostic applications in the context of aSAH.

Finally, it should be noted that in contrast to our previous study, we observed no significant effects of aSAH on the latency of arterial or venous responses, which could reflect the fact that these parameters are more sensitive to inherent technical limitations such as the finite signal-to-noise ratio. As such, our present findings that patients with DCI exhibit a reduced arterial latency ($tMAD_{30}$) during the early but increased arterial latency (tMAD) during the late phase should be interpreted with care as well-until they can be confirmed in future studies.

In particular, given the subtle nature of these differences, it seems unlikely that they would allow for reliable prediction and/or confirmation of DCI in the clinical setting. However, based on the small number of patients we evaluated, future studies with larger patient populations may be able to identify more robust correlations between RVA parameters and DCI. Considering that DCI remains one of the main preventable causes of poor clinical outcomes after aSAH, such studies will almost certainly be performed in the near future and their results should help to conclusively rate the clinical value of RVA in this setting.

CONCLUSIONS

Our findings confirm and extend the results from previous studies that aSAH is associated with sustained vasoconstriction and impairments of NVC in retinal vessels. Retinal vessel responses may differ between patients with and without DCI. Although their clinical relevance remains to be firmly established, these findings suggest that RVA could be a unique tool for monitoring microvascular function in aSAH patients in a simple and non-invasive manner.

DATA AVAILABILITY STATEMENT

The original contributions presented in the study are included in the article/**Supplementary Material**, further inquiries can be directed to the corresponding author/s.

ETHICS STATEMENT

All procedures involving human participants were performed in accordance with the ethical standards of the institutional and/or national research committee and with the 1964 Helsinki declaration and its later amendments or comparable ethical standards. Reference Number EK 069/15. The patients/participants provided their written informed consent to participate in this study.

AUTHOR CONTRIBUTIONS

WA, CC, MWe, KS, DK, and GS: conceived, designed, and performed the experiments. WA: first drafting of the manuscript. WA and FN: illustrations. WA, CC, MWe, KS, KK, and GS: data acquisition. WA, CC, KK, and GS: analysis and interpretation of data. WA, CC, TS, JH, AB, AS-T, FN, MWi, HC, and GS: critical review of the manuscript. All authors were critically revised and approved by the final manuscript.

FUNDING

WA was supported by funding from the German Society of Neurointensive and Emergency Medicine (Junior research award 2017). CC was supported by the START-Program of the Faculty of Medicine (RWTH Aachen University, Grant No. 691545) and by the Foundation of Neurosurgical Research (German Society of Neurosurgery, 2016).

SUPPLEMENTARY MATERIAL

The Supplementary Material for this article can be found online at: https://www.frontiersin.org/articles/10.3389/fneur.2021.690183/full#supplementary-material

REFERENCES

1. Kaptain GJ, Lanzino G, Kassell NF. Subarachnoid haemorrhage: epidemiology, risk factors, and treatment options. *Drugs Aging.* (2000) 17:183–99. doi: 10.2165/00002512-200017030-00003
2. Weaver JP, Fisher M. Subarachnoid hemorrhage: an update of pathogenesis, diagnosis and management. *J Neurol Sci.* (1994) 125:119–31. doi: 10.1016/0022-510X(94)90024-8
3. Vergouwen MDI, Vermeulen M, van Gijn J, Rinkel GJE, Wijdicks EF, Muizelaar JP, et al. Definition of delayed cerebral ischemia after aneurysmal subarachnoid hemorrhage as an outcome event in clinical trials and observational studies: proposal of a multidisciplinary research group. *Stroke.* (2010) 41:2391–5. doi: 10.1161/STROKEAHA.110.589275
4. Meyers PM, Connolly ES. Disappointing results for clazosentan in CONSCIOUS-2. *Nat Rev Neurol.* (2011) 7:660–1. doi: 10.1038/nrneurol.2011.168
5. Naraoka M, Matsuda N, Shimamura N, Asano K, Ohkuma H. The role of arterioles and the microcirculation in the development of vasospasm after aneurysmal SAH. *Biomed Res Int.* (2014) 2014:253746. doi: 10.1155/2014/253746
6. Geraghty JR, Davis JL, Testai FD. Neuroinflammation and microvascular dysfunction after experimental subarachnoid hemorrhage: emerging components of early brain injury related to outcome. *Neurocrit Care.* (2019) 31:373–89. doi: 10.1007/s12028-019-00710-x
7. Suzuki H, Kanamaru H, Kawakita F, Asada R, Fujimoto M, Shiba M. Cerebrovascular pathophysiology of delayed cerebral ischemia after aneurysmal subarachnoid hemorrhage. *Histol Histopathol.* (2021) 36:143–58. doi: 10.14670/HH-18-253
8. Balbi M, Koide M, Wellman GC, Plesnila N. Inversion of neurovascular coupling after subarachnoid hemorrhage in vivo. *J Cereb Blood Flow Metab.* (2017) 37:3625–34. doi: 10.1177/0271678X16686595
9. Balbi M, Vega MJ, Lourbopoulos A, Terpolilli NA, Plesnila N. Long-term impairment of neurovascular coupling following experimental subarachnoid hemorrhage. *J Cereb Blood Flow Metab.* (2020) 40:1193–202. doi: 10.1177/0271678X19863021
10. Koide M, Bonev AD, Nelson MT, Wellman GC. Inversion of neurovascular coupling by subarachnoid blood depends on large-conductance Ca2+-activated K+ (BK) channels. *Proc Natl Acad Sic USA.* (2012) 109:E1387–95. doi: 10.1073/pnas.1121359109

11. Conzen C, Albanna W, Weiss M, Kürten D, Vilser W, Kotliar K, et al. Vasoconstriction and impairment of neurovascular coupling after subarachnoid hemorrhage: a descriptive analysis of retinal changes. *Transl Stroke Res.* (2018) 9:284–93. doi: 10.1007/s12975-017-0585-8
12. Winkler MKL, Chassidim Y, Lublinsky S, Revankar GS, Major S, Kang E-J, et al. Impaired neurovascular coupling to ictal epileptic activity and spreading depolarization in a patient with subarachnoid hemorrhage: possible link to blood-brain barrier dysfunction. *Epilepsia.* (2012) 53:22–30. doi: 10.1111/j.1528-1167.2012.03699.x
13. da Costa L, Fierstra J, Fisher JA, Mikulis DJ, Han JS, Tymianski M. BOLD MRI and early impairment of cerebrovascular reserve after aneurysmal subarachnoid hemorrhage. *J Magn Reson Imaging.* (2014) 40:972–9. doi: 10.1002/jmri.24474
14. Cabrera DeBuc D, Somfai GM, Koller A. Retinal microvascular network alterations: Potential biomarkers of cerebrovascular and neural diseases. *Am J Physiol Circ Physiol.* (2017) 312:H201–12. doi: 10.1152/ajpheart.00201.2016
15. Patton N, Aslam T, MacGillivray T, Pattie A, Deary IJ, Dhillon B. Retinal vascular image analysis as a potential screening tool for cerebrovascular disease: a rationale based on homology between cerebral and retinal microvasculatures. *J Anat.* (2005) 206:319–48. doi: 10.1111/j.1469-7580.2005.00395.x
16. Lipecz A, Csipo T, Tarantini S, Hand RA, Ngo BTN, Conley S, et al. Age-related impairment of neurovascular coupling responses: a dynamic vessel analysis (DVA)-based approach to measure decreased flicker light stimulus-induced retinal arteriolar dilation in healthy older adults. *GeroScience.* (2019) 41:341–9. doi: 10.1007/s11357-019-00078-y
17. Golzan SM, Goozee K, Georgevsky D, Avolio A, Chatterjee P, Shen K, et al. Retinal vascular and structural changes are associated with amyloid burden in the elderly: ophthalmic biomarkers of preclinical Alzheimer's disease. *Alzheimers Res Ther.* (2017) 9:13. doi: 10.1186/s13195-017-0239-9
18. Pressler A, Esefeld K, Scherr J, Ali M, Hanssen H, Kotliar K, et al. Structural alterations of retinal arterioles in adults late after repair of aortic isthmic coarctation. *Am J Cardiol.* (2010) 105:740–4. doi: 10.1016/j.amjcard.2009.10.070
19. Bettermann K, Slocomb J, Shivkumar V, Quillen D, Gardner TW, Lott ME. Impaired retinal vasoreactivity: an early marker of stroke risk in diabetes. *J Neuroimaging.* (2017) 27:78–84. doi: 10.1111/jon.12412
20. Kotliar K, Hauser C, Ortner M, Muggenthaler C, Diehl-Schmid J, Angermann S, et al. Altered neurovascular coupling as measured by optical imaging: a biomarker for Alzheimer's disease. *Sci Rep.* (2017) 7:12906. doi: 10.1038/s41598-017-13349-5
21. Fountas KN, Kapsalaki EZ, Lee GP, Machinis TG, Grigorian AA, Robinson JS, et al. Terson hemorrhage in patients suffering aneurysmal subarachnoid hemorrhage: predisposing factors and prognostic significance. *J Neurosurg.* (2008) 109:439–44. doi: 10.3171/JNS/2008/109/9/0439
22. Wostyn P, De Groot V, Van Dam D, Audenaert K, De Deyn PP, Killer HE. The glymphatic system: a new player in ocular diseases? *Investig Opthalmology Vis Sci.* (2016) 57:5426. doi: 10.1167/iovs.16-20262
23. Albanna W, Conzen C, Weiss M, Clusmann H, Fuest M, Mueller M, et al. Retinal vessel analysis (RVA) in the context of subarachnoid hemorrhage–a proof of concept study. *PLoS ONE.* (2016) 11:e0158781. doi: 10.1371/journal.pone.0158781
24. Le Roux P, Menon DK, Citerio G, Vespa P, Bader MK, Brophy GM, et al. Consensus summary statement of the international multidisciplinary consensus conference on multimodality monitoring in neurocritical care. *Intensive Care Med.* (2014) 40:1189–1209. doi: 10.1007/s00134-014-3369-6
25. Hutchinson P, O'Phelan K. International multidisciplinary consensus conference on multimodality monitoring: cerebral metabolism. *Neurocrit Care.* (2014) 21:148–58. doi: 10.1007/s12028-014-0035-3
26. Albanna W, Weiss M, Müller M, Brockmann MA, Rieg A, Conzen C, et al. Endovascular rescue therapies for refractory vasospasm after subarachnoid hemorrhage: a prospective evaluation study using multimodal, continuous event neuromonitoring. *Neurosurgery.* (2017) 80:942–9. doi: 10.1093/neuros/nyw132
27. Weiss M, Conzen C, Mueller M, Wiesmann M, Clusmann H, Albanna W, et al. Endovascular rescue treatment for delayed cerebral ischemia after subarachnoid hemorrhage is safe and effective. *Front Neurol.* (2019) 10:136. doi: 10.3389/fneur.2019.00136
28. Kotliar KE, Lanzl IM, Schmidt-Trucksäss A, Sitnikova D, Ali M, Blume K, et al. Dynamic retinal vessel response to flicker in obesity: a methodological approach. *Microvasc Res.* (2011) 81:123–28. doi: 10.1016/j.mvr.2010.11.007
29. Polak K. Evaluation of the zeiss retinal vessel analyser. *Br J Ophthalmol.* (2000) 84:1285–90. doi: 10.1136/bjo.84.11.1285
30. Nagel E, Vilser W, Fink A, Riemer T. Statische Gefäßanalyse in nonmydriatischen und mydriatischen Bildern. *Klin Monbl Augenheilkd.* (2007) 224:411–6. doi: 10.1055/s-2007-963093
31. Hubbard LD, Brothers RJ, King WN, Clegg LX, Klein R, Cooper LS, et al. Methods for evaluation of retinal microvascular abnormalities associated with hypertension/sclerosis in the atherosclerosis risk in communities study. *Ophthalmology.* (1999) 106:2269–80. doi: 10.1016/S0161-6420(99)90525-0
32. Heitmar R, Lip GYH, Ryder RE, Blann AD. Retinal vessel diameters and reactivity in diabetes mellitus and/or cardiovascular disease. *Cardiovasc Diabetol.* (2017) 16:56. doi: 10.1186/s12933-017-0534-6
33. Bederson JB, Levy AL, Hong Ding W, Kahn R, DiPerna CA, Jenkins AL, et al. Acute vasoconstriction after subarachnoid hemorrhage. *Neurosurgery.* (1998) 42:352–62. doi: 10.1097/00006123-199802000-00091
34. Weir B, Grace M, Hansen J, Rothberg C. Time course of vasospasm in man. *J Neurosurg.* (1978) 48:173–8. doi: 10.3171/jns.1978.48.2.0173
35. Ferguson S, Macdonald RL. Predictors of cerebral infarction in patients with aneurysmal subarachnoid hemorrhage. *Neurosurgery.* (2007) 60:658–67. doi: 10.1227/01.NEU.0000255396.23280.31
36. Liu Z, Li Q, Cui G, Zhu G, Tang W, Zhao H, et al. Blood-filled cerebrospinal fluid-enhanced pericyte microvasculature contraction in rat retina: a novel *in vitro* study of subarachnoid hemorrhage. *Exp Ther Med.* (2016) 12:2411–6. doi: 10.3892/etm.2016.3644
37. Wang KC, Tang SC, Lee JE, Tsai JC, Lai DM, Lin WC, et al. Impaired microcirculation after subarachnoid hemorrhage in an in vivo animal model. *Sci Rep.* (2018) 8:13315. doi: 10.1038/s41598-018-31709-7
38. Vorkapic P, Bevan JA, Bevan RD. Longitudinal in vivo and in vitro time-course study of chronic cerebrovasospasm in the rabbit basilar artery. *Neurosurg Rev.* (1991) 14:215–9. doi: 10.1007/BF00310660
39. Peeyush Kumar T, McBride DW, Dash PK, Matsumura K, Rubi A, Blackburn SL. Endothelial cell dysfunction and injury in subarachnoid hemorrhage. *Mol Neurobiol.* (2019) 56:1992–2006. doi: 10.1007/s12035-018-1213-7
40. Groeschel S, Chong WK, Surtees R, Hanefeld F. Virchow-Robin spaces on magnetic resonance images: normative data, their dilatation, and a review of the literature. *Neuroradiology.* (2006) 48:745–754. doi: 10.1007/s00234-006-0112-1
41. Mutlu U, Adams HHH, Hofman A, Lugt A van der, Klaver CCW, Vernooij MW, et al. Retinal microvascular calibers are associated with enlarged perivascular spaces in the brain. *Stroke.* (2016) 47:1374–6. doi: 10.1161/STROKEAHA.115.012438
42. Clark JF, Sharp FR. Bilirubin oxidation products (BOXes) and their role in cerebral vasospasm after subarachnoid hemorrhage. *J Cereb Blood Flow Metab.* (2006) 26:1223–33. doi: 10.1038/sj.jcbfm.9600280
43. Kikuchi T, Okuda Y, Kaito N, Abe T. Cytokine production in cerebrospinal fluid after subarachnoid haemorrhage. *Neurol Res.* (1995) 17:106–8. doi: 10.1080/01616412.1995.11740296
44. Roa JA, Sarkar D, Zanaty M, Ishii D, Lu Y, Karandikar NJ, et al. Preliminary results in the analysis of the immune response after aneurysmal subarachnoid hemorrhage. *Sci Rep.* (2020) 10:11809. doi: 10.1038/s41598-020-68861-y

45. Maruhashi T, Higashi Y. An overview of pharmacotherapy for cerebral vasospasm and delayed cerebral ischemia after subarachnoid hemorrhage. *Expert Opin Pharmacother.* (2021) 1–14. doi: 10.1080/14656566.2021.1912013
46. Albanna W. Retinal vessel analysis for acute neurovascular diseases: timely realization of a wearable prototype by unorthodox means. *Int J Ophthalmic Pathol.* (2019) 8.

Conflict of Interest: IMEDOS Systems GmbH provided the Retinal Vessel Analyzer for research purposes only. The company did not have any additional role in the study design, data collection and analysis, decision to publish, or preparation of the manuscript.

The authors declare that the research was conducted in the absence of any commercial or financial relationships that could be construed as a potential conflict of interest.

frontiers in Neurology

ORIGINAL RESEARCH
published: 16 June 2021
doi: 10.3389/fneur.2021.674466

Early Effects of Passive Leg-Raising Test, Fluid Challenge, and Norepinephrine on Cerebral Autoregulation and Oxygenation in COVID-19 Critically Ill Patients

Chiara Robba[1,2], Antonio Messina[3,4], Denise Battaglini[2], Lorenzo Ball[1,2], Iole Brunetti[2], Matteo Bassetti[5,6], Daniele R. Giacobbe[5,6], Antonio Vena[6], Nicolo' Patroniti[1,2], Maurizio Cecconi[3,4], Basil F. Matta[7], Xiuyun Liu[8], Patricia R. M. Rocco[9], Marek Czosnyka[10] and Paolo Pelosi[1,2]*

[1] Department of Surgical Sciences and Integrated Diagnostics (DISC), University of Genoa, Genoa, Italy, [2] San Martino Policlinico Hospital, Istituto di Ricovero e Cura a Carattere Scientifico for Oncology and Neuroscience, Genoa, Italy, [3] Humanitas Clinical and Research Center-Istituto di Ricovero e Cura a Carattere Scientifico, Milan, Italy, [4] Department of Biomedical Sciences, Humanitas University, Milan, Italy, [5] Department of Health Sciences (DISSAL), University of Genoa, Genoa, Italy, [6] Infectious Diseases Unit, San Martino Policlinico Hospital, Genoa, Italy, [7] Neurocritical Care Unit, Addenbrookes Hospital, Cambridge, United Kingdom, [8] Department of Anesthesiology and Critical Care Medicine, John Hopkins University, Baltimore, MD, United States, [9] Laboratory of Pulmonary Investigation, Carlos Chagas Filho Institute of Biophysics, Rio de Janeiro, Brazil, [10] Brain Physics Laboratory, Department of Clinical Neurosciences, University of Cambridge, Cambridge, United Kingdom

OPEN ACCESS

Edited by:
William Armstead, University of Pennsylvania, United States

Reviewed by:
Thomas Scheeren, University Medical Center Groningen, Netherlands
Ryan Matthew Martin, University of California, Davis, United States

***Correspondence:**
Chiara Robba
kiarobba@gmail.com

Specialty section:
This article was submitted to Neurocritical and Neurohospitalist Care, a section of the journal Frontiers in Neurology

Received: *01 March 2021*
Accepted: *29 April 2021*
Published: *16 June 2021*

Citation:
Robba C, Messina A, Battaglini D, Ball L, Brunetti I, Bassetti M, Giacobbe DR, Vena A, Patroniti N, Cecconi M, Matta BF, Liu X, Rocco PRM, Czosnyka M and Pelosi P (2021) Early Effects of Passive Leg-Raising Test, Fluid Challenge, and Norepinephrine on Cerebral Autoregulation and Oxygenation in COVID-19 Critically Ill Patients. Front. Neurol. 12:674466. doi: 10.3389/fneur.2021.674466

Background: Coronavirus disease 2019 (COVID-19) patients are at high risk of neurological complications consequent to several factors including persistent hypotension. There is a paucity of data on the effects of therapeutic interventions designed to optimize systemic hemodynamics on cerebral autoregulation (CA) in this group of patients.

Methods: Single-center, observational prospective study conducted at San Martino Policlinico Hospital, Genoa, Italy, from October 1 to December 15, 2020. Mechanically ventilated COVID-19 patients, who had at least one episode of hypotension and received a passive leg raising (PLR) test, were included. They were then treated with fluid challenge (FC) and/or norepinephrine (NE), according to patients' clinical conditions, at different moments. The primary outcome was to assess the early effects of PLR test and of FC and NE [when clinically indicated to maintain adequate mean arterial pressure (MAP)] on CA (CA index) measured by transcranial Doppler (TCD). Secondary outcomes were to evaluate the effects of PLR test, FC, and NE on systemic hemodynamic variables, cerebral oxygenation (rSo_2), and non-invasive intracranial pressure (nICP).

Results: Twenty-three patients were included and underwent PLR test. Of these, 22 patients received FC and 14 were treated with NE. The median age was 62 years (interquartile range = 57–68.5 years), and 78% were male. PLR test led to a low CA index [58% (44–76.3%)]. FC and NE administration resulted in a CA index of 90.8% (74.2–100%) and 100% (100–100%), respectively. After PLR test, nICP based on pulsatility index and nICP based on flow velocity diastolic formula was

increased [18.6 (17.7–19.6) vs. 19.3 (18.2–19.8) mm Hg, $p = 0.009$, and 12.9 (8.5–18) vs. 15 (10.5–19.7) mm Hg, $p = 0.001$, respectively]. PLR test, FC, and NE resulted in a significant increase in MAP and rSo_2.

Conclusions: In mechanically ventilated severe COVID-19 patients, PLR test adversely affects CA. An individualized strategy aimed at assessing both the hemodynamic and cerebral needs is warranted in patients at high risk of neurological complications.

Keywords: fluid challenge, norepinephrine, passive leg raising test, cerebral oxygenation, cerebral autoregulation

INTRODUCTION

Severe hypoxemic respiratory failure is the main reason for intensive care unit (ICU) admission in coronavirus disease 2019 (COVID-19) patients (1–3).

However, COVID-19 is a multisystemic disease (4), with significant implications for the brain (5–7). Different mechanisms related to neurological damage have been proposed, such as a direct viral neurotropism, hypercoagulable state, and systemic complications including hypoxia and hypotension (8). Therefore, it seems logical that in order to protect the brain, with optimized cerebral perfusion and oxygenation, hemodynamic stability should be maintained (6).

The current target of mean arterial pressure (MAP) commonly used in the general ICU population (>65 mm Hg) (7) may not always be sufficient to ensure adequate cerebral perfusion, as the brain might potentially require higher values of MAP to optimize cerebral perfusion pressure (CPP) and maintain cerebral autoregulation (CA) (9, 10), especially in the COVID-19 patients who often present altered cerebrovascular dynamics (5). A commonly used functional hemodynamic test to assess fluid responsiveness is the passive leg raising (PLR) test, which causes a shift of intravascular fluids from the legs to the abdominal compartment. Methods proposed to optimize MAP have different pathophysiological mechanisms and include a quick infusion of a small amount of fluids [the so-called fluid challenge (FC)], which provides an extrinsic increase in intravascular volume, and vasopressors, such as norepinephrine (NE), generally used in fluids non-responders, which increase vascular tone.

As no data are available regarding the effect of PLR test on cerebral function and in particular autoregulation in mechanically ventilated severe COVID-19 patients, we conducted a prospective observational study; the primary outcome was to assess the early effect of PLR test and of FC and/or NE—when clinically indicated—on static CA [CA index measured by transcranial Doppler (TCD)]. Secondary outcomes were to evaluate the effects of PLR test, FC, and NE on systemic hemodynamic variables, cerebral oxygenation [regional cerebral oxygen saturation (rSO_2)], and non-invasive intracranial pressure (nICP).

Abbreviations: ABP, arterial blood pressure; CA, cerebral autoregulation; COVID-19, coronavirus disease 2019; CPP, cerebral perfusion pressure; $ETCO_2$, end-tidal carbon dioxide; FC, fluid challenge; FIO_2, fraction of inspired oxygen; FVd, diastolic flow velocity; FVm, mean flow velocity; FVs, systolic flow velocity; Hb, hemoglobin; ICU, intensive care unit; MAP, mean arterial pressure; MCAs, middle cerebral arteries; nCPP, non-invasive cerebral perfusion pressure; NE, norepinephrine; nICP, non-invasive intracranial pressure; NIRS, near-infrared spectroscopy; $PaCO_2$, partial pressure of carbon dioxide; PEEP, positive end-expiratory pressure; Pi, perfusion index; PI, pulsatility index; PLR test, passive leg raising test; Pplat, plateau pressure; rSO_2, cerebral oxygenation; SpO_2, peripheral saturation of oxygen; TCD, transcranial Doppler.

MATERIALS AND METHODS

A single-center, prospective observational study was conducted at Policlinico San Martino, IRCCS for Oncology and Neuroscience, Genoa, Italy. This study is reported according to the Strengthening the Reporting of Observational Studies in Epidemiology statement guidelines for observational cohort studies (**Supplementary Material 1**) (11). The local ethical review board approved the protocol (Comitato Etico Regione Liguria, protocol n. CER Liguria: 23/2020). Mechanically ventilated patients admitted to ICU during the second wave of COVID-19 pandemic (from the October 1 to December 15, 2020) were included. COVID-19 patients were defined with a confirmed SARS-CoV-2 (severe acute respiratory syndrome coronavirus 2) polymerase chain reaction using nasopharyngeal swab or bronchoalveolar lavage. Inclusion criteria were (1) ≥18 years old; (2) mechanically ventilated severe COVID-19 patients requiring a PLR test as well as FC and/or NE administration, according to the indications of the attending physician, during the occurrence of hypotension [defined as MAP ≤65 mm Hg and/or systolic blood pressure (SBP) ≤90 mm Hg]; and (3) patients undergoing multimodal neuromonitoring [including cerebral oxygenation using near-infrared spectroscopy (NIRS) and TCD].

Exclusion criteria were (1) patients with a limited acoustic window for TCD assessment, which might have led to a non-precise measurement of the cerebral flow velocities; and (2) patients with known neurological conditions before or during ICU admission, which might have impaired CA (stroke, trauma, intracerebral masses, etc.).

Data Collection

Data were reviewed and collected by physicians trained in critical care patients' electronic medical records. Baseline characteristics, including demographic and clinical data, were collected at ICU admission. Patients' data have been partially previously presented Robba et al. (12). Data collection included age, gender, Sequential Organ Failure Assessment, body mass index, comorbidities (hypertension, diabetes mellitus, chronic kidney injury, chronic

respiratory disease, previous neurological disease, liver failure, chronic cardiac disease), laboratory parameters [blood test, D-dimer, C-reactive protein, procalcitonin, creatinine, hemoglobin (Hb)], and ventilatory parameters [tidal volume (V_T), fraction of inspired oxygen (FIO_2), respiratory rate (RR), positive end-expiratory pressure (PEEP), plateau pressure (Pplat), and respiratory system compliance].

General Management in ICU

Patients were sedated with a combination of propofol, midazolam, and fentanyl and mechanically ventilated using pressure-controlled ventilation, aimed at maintaining Pplat <28 cm H_2O, using a V_T of 4–8 mL/kg of predicted body weight. FIO_2 and PEEP were titrated in order to achieve peripheral saturation of oxygen (SpO_2) 88–92%, and RR was set to maintain arterial partial pressure of carbon dioxide ($PaCO_2$) = 35–45 mm Hg. Permissive hypercapnia was allowed as long as arterial pH was maintained $\geq$7.35. Specific ventilatory management has been previously described in Robba et al. (12). Invasive arterial blood pressure (ABP), heart rate (HR), and end-tidal carbon dioxide ($ETCO_2$) were continuously measured. Using a Masimo root device with pulse CO–oximetry sensors connected to Rainbow devices, total Hb, perfusion index (Pi), and pleth variability index were non-invasively measured.

Hemodynamic Management

PLR test was performed to assess fluid responsiveness during episodes of hypotension. With the patient seated at 45° in a head-up semirecumbent position ($T0_{PLR}$), patient's upper body was then lowered to a horizontal position with legs passively raised at 45°, for 30–90 s. At the end of the procedure, before repositioning patient's legs, $T1_{PLR}$ was defined (13–15). We considered a positive PLR test with 5% of $ETCO_2$ increase in Delta $ETCO_2$ from $T0_{PLR}$ to $T1_{PLR}$ (16, 17), as a surrogate of 10% increase in stroke volume (cardiac output monitor) (13). As this study is observational and did not change our practice, we did not have the possibility during the pandemic to use a more advanced hemodynamic tool in all our patients. Despite $ETCO_2$ is not the criterion standard for PLR test evaluation, it has been previously used, and it demonstrated to be strongly associated with stroke volume changes, and therefore, it is now widely acceptable (13, 14, 17). According to the $ETCO_2$ response to the PLR test as well as recommendation of the attending physician, patients received FC [crystalloids (4 mL/kg over 20 min)] (14, 15, 18) or NE infusion (central venous at a controlled rate using an infusion pump with an initial dose of 0.05 μg/kg per minute). NE infusion was then eventually started in PLR non-responding patients, or after FC, according to recommendation of attending physician if another episode of hypotension occurred. $T0_{FC}$ and $T0_{NE}$ were evaluated at the beginning of FC and NE infusion, whereas $T1_{FC}$ and $T1_{NE}$ were considered at the end of FC administration or at timepoints of 5 min after the beginning of NE, when the NE dosage was titrated (starting with a dose of 0.05 μg/kg per minute) to maintain an MAP >65 mm Hg. A complete hemodynamic assessment (HR, ABP, MAP, Hb, SpO_2, Pi, and PVI) and neuromonitoring evaluation (TCD- and NIRS-derived indices) were obtained at timepoints T0 and T1 of FC and NE administration. No other interventions (such as mechanical ventilation settings changes, repositioning of the patient) were performed between T0 and T1.

Neuromonitoring Data

During the second wave of the pandemic, we started to use neuromonitoring tools in all our patients as routine, at least in the early phases from ICU admission, as we noticed a high number of neurological complications (5).

Cerebral Oxygenation

Masimo Root monitor® (USA) was used for the continuous measurement of rSO_2 through bilateral sensors applied to the frontotemporal area. Different indices derived were obtained including (1) rSO_2, which represents the total regional cerebral oxygen saturation value; (2) variation of O_2Hbi, ΔO_2Hbi, which represents the modifications of the oxygenated (arterial) component of the Hb of the total rSO_2, whereas $\Delta HHbi$ defines the variation of the deoxygenated (venous) component of Hb of the total value of rSO_2; (3) $\Delta cHbi$, which is the sum of the values of ΔO_2Hbi and $\Delta HHbi$; and (4) ΔSpO_2-rSO_2 which represents the differences between the value of systemic and cerebral oxygenation. Final values were calculated as the mean between the right and left frontotemporal sensors.

Calculation of Static CA

CA index was measured using TCD. Percentage change in estimated cerebrovascular resistance (CVR_e) in relation to the change in ABP over the entire period of time needed for an MAP increase from baseline (T0) to the higher level (T1) was calculated as CVR_e = MAP/(cerebral blood flow velocity) (19). We calculated CA index as CA = (% ΔCVR_e/% ΔMAP) × 100% as previously described (19). We expressed the CA index as a percentage of full autoregulatory capacity. A change in CVR, which would fully compensate for the drop in MAP, would yield a static CA of 100%, whereas no response of CVR, after ABP changes, would yield a static CA of 0%.

nICP Assessment

Transcranial color duplex Doppler technique (Philips, Bothell, WA, USA) was performed with a low-frequency (2 MHz) echographic micro convex through a temporal window to assess bilateral middle cerebral arteries (MCAs). Systolic, diastolic, and mean flow velocity (FVs, FVd, and FVm, respectively) were obtained bilaterally from the MCA.

nICP was measured using two different formulas:

(1) FVd formula (nICPFVd) (20, 21):

$$nCPP = MAP^*(FVd/FVm) + 14,$$

where nCPP is non-invasive cerebral perfusion pressure and then

$$nICP = MAP - nCPP,$$

(2) Pulsatility index (PI)–based nICP (nICPPI):

PI was measured according to the Gosling formula (22):

$$PI = (FVs - FVd)/Fm,$$

Estimation based on TCD-derived PI was based on the linear regression among known values of ICP and PI previously analyzed by Budohoski et al. (23):

$$\text{nICPPI} = 4.47^{*}\text{PI} + 12.68$$

The final nICPPI was calculated using the mean of the right and left PI, whereas nICPFVd was calculated using the mean flow velocity of both MCAs.

Statistical Analysis

No data on cerebral oxygenation after PLR test, FC, and NE are available in COVID-19 patients. Therefore, a formal sample size calculation was not feasible *a priori*. However, the achieved sample size was comparable to other physiologic studies in the field (24). The Shapiro–Wilk test was used to test the normality of the distribution of the results. Data are reported as median and interquartile range (IQR = 25th−75th percentiles), if not otherwise specified. Comparisons between different variables at T0 and T1 were performed by paired *t*-test, whereas non-normally distributed variables were compared by Wilcoxon signed rank test. One-way repeated-measures analysis of variance and Friedman test, followed by Bonferroni *post-hoc* test, were used for parametric and non-parametric data, respectively. Correlations between cerebral and systemic oxygenation were evaluated using Pearson or Spearman test. Correlations with repeated measurements were computed according to the Bland and Altman method (25). All statistical analyses were performed using SPSS 21® (IBM Corp., USA). $p < 0.05$ was considered statistically significant.

RESULTS

Baseline characteristics of the patients are presented in **Table 1**. The median age of the population was 62 years (IQR = 57–68.5 years), and 78% of the patients were male. **Table 2** presents the hemodynamic and neuromonitoring parameters analyzed in the different subgroups [PLR ($n = 23$), FC ($n = 22$), and NE ($n = 14$)]. In all cases, PLR test was positive, and in 22 cases, FC was used as first-line treatment. In one patient, who presented with important fluid overload and respiratory failure, NE was started even with a positive PLR, based on the recommendation of ICU physician and patient's clinical conditions. After FC administration, despite a good initial response of MAP, 14 patients also required NE following another episode of hypotension (range between 0.05 and 1.5 μg/kg per minute).

TABLE 1 | Characteristics of the patients included in the study.

Characteristics of patients	All patients ($n = 23$)
Demographics	
Gender, male, *n* (%)	18 (78.3)
Age (years), median (IQR)	62 (57–68.5)
BMI (kg/m^2), median (IQR)	26 (24.7–29)
PBW (kg), median (IQR)	70 (61–75)
Comorbidities	
Respiratory disease, *n* (%)	3 (13.4)
Cardiovascular disease, *n* (%)	5 (21.7)
Cancer, *n* (%)	0 (0)
Moderate/severe liver disease, *n* (%)	1 (4.3)
End-stage kidney injury, *n* (%)	0 (0)
Hypertension, *n* (%)	13 (56.5)
Diabetes mellitus, *n* (%)	3 (13)
ICU characteristics at admission	
SOFA score, median (IQR)	5 (4–7)
Pao_2/Fio_2, median (IQR)	81 (65–83)
PEEP, median (IQR)	11 (9–12)
V_T (mL), median (IQR)	434 (370–560)
Pplat,rs (cm H_2O), median (IQR)	26.5 (25–28)
Crs (mL/cm H_2O), median (IQR)	24 (22–30)
D-Dimer (ng/mL), median (IQR)	1794 (1251–6252)
C-reactive protein (mg/dL), median (IQR)	108.5 (60–135)
Procalcitonin (ng/mL), median (IQR)	0.6 (0.18–1.76)
Interleukin 6 (pg/dL), median (IQR)	39 (31–83.3)
Creatinine (mg/dL), median (IQR)	0.7 (0.6–1.1)
Heart rate (bpm), median (IQR)	85 (72–97)
Mean arterial pressure (mm Hg), median (IQR)	78 (73–85)
ICU discharge characteristics	
Dead, *n* (%)	13 (56.5)
Alive, *n* (%)	10 (43.5)

IQR, interquartile range; n, number; BMI, body mass index; PBW, predicted body weight; SOFA, Sequential Organ Failure Assessment; ICU, intensive care unit; Pao_2/Fio_2, arterial oxygen partial pressure/fraction of inspired oxygen; PEEP, positive end expiratory pressure; V_T, tidal volume; Pplat,rs, respiratory system plateau pressure; Crs, respiratory system compliance.

Effect of PLR Test, FC, and NE on CA

PLR test resulted in a CA index of 58% (44–76.3%), whereas FC and NE of 90.8% (74.2–100%) and 98% (96–100%), respectively. CA index did not differ between FC and NE ($p = 0.169$) (**Figure 1**). nICPPI ($p = 0.542$), nICPFVd ($p = 0.529$), and nCPP ($p = 0.722$) did not differ significantly between FC and NE (**Supplementary Figures 1–3**). NE yielded higher values of rSo_2 compared to FC (**Supplementary Figure 4**) (NE vs. FC; $p = 0.043$).

Effect of PLR Test, FC, and NE on Systemic Hemodynamics, Cerebral Oxygenation, and nICP

PLR Test

After PLR test, MAP was increased [63 (59–64.5) vs. 69 (67.5–71.5) mm Hg, $p < 0.001$] and rSo_2 [52% (51–59.5%) vs. 57% (54–63.5%), $p < 0.001$], as well as nICPPI and nICPFVd [18.6 (17.7–19.6) vs. 19.3 (18.2–19.8) mm Hg, $p = 0.009$, and 12.9 (8.5–18) vs. 15 (10.5–19.7) mm Hg, $p = 0.001$, respectively (**Table 2**)].

Fluid Challenge

Fluid administration resulted in a significant increase in MAP [61 (59–65) vs. 69 (67–72) mm Hg, $p < 0.001$], rSo_2 [55 (52–60) vs. 58 (56–65)%, $p < 0.001$], and nICPFVd [10.9 (6.7–15.7) vs. 14.4 (5.6- 21.1) mm Hg, $p = 0.004$] but not nICPPI [19.6 (14.8–21.1) vs. 18.2 (16.4–19.1) mm Hg, $p = 0.153$] (**Table 2**).

TABLE 2 | Hemodynamic and neuromonitoring variables before (T0) and after (T1) passive leg raising test, fluid challenge, and norepinephrine.

	Passive leg raising test ($n = 23$)			Fluid challenge ($n = 22$)			Norepinephrine ($n = 14$)		
Parameter	**T0**	**T1**	***p*-Value**	**T0**	**T1**	***p*-Value**	**T0**	**T1**	***p*-Value**
Hemodynamics									
MAP (mm Hg)	63 (59–64.5)	69 (67.5–71.5)	<0.001*	61 (59–65)	69 (67–72)	<0.001*	63.5 (61–64)	69 (66–71)	<0.001*
HR (bpm)	76 (66.5–88.5)	77 (67–86)	0.822	75.5 (67–89)	75 (67–92)	0.910	76.5 (65–87)	78.5 (67–87)	0.239
Hb (g/dL)	7.9 (7.6–8.4)	8.2 (7.9–8.4)	0.132	7.7 (7.1–8.6)	8.5 (8.1–8.8)	0.434	8.3 (7.8–8.4)	8.8 (8.2–9)	0.432
PVI	20 (16–24)	15.5 (12–19)	<0.001*	20 (16–24)	16 (12–19)	<0.001*	19 (16–23)	19 (15–23)	0.324
Pi	3 (3–4)	4 (4–5)	<0.001*	3 (3–4)	4 (4–5)	<0.001*	3 (3–4)	4 (3–4)	0.046*
Neuromonitoring									
rSo_2 (%)	52 (51–59.5)	57 (54–63.5)	<0.001*	55 (52–60)	58 (56–65)	<0.001*	54.5 (53–62)	61.5 (61–66)	0.001*
ΔcHbi	4.7 (3.6–6.6)	6 (5–8)	<0.001*	5.3 (3.1–7)	6.6 (4.5–8.4)	<0.001*	5.3 (4.3–8.1)	7.3 (5.4–10.5)	0.001*
ΔO_2Hbi	3.8 (2.8–4.5)	4.1 (3.2–5)	<0.001*	3.5 (2.8–4.6)	3.9 (3.2–5.6)	<0.001*	3.9 (3.2–4.3)	5.7 (3.9–7.1)	0.001*
ΔHHbi	1.1 (0.8–1.9)	2.1 (1.8–2.9)	<0.001*	1.2 (0.4–2.1)	2.4 (1.4–3.1)	<0.001*	1.8 (0.7–2.9)	1.9 (0.9–3)	0.143
nICPPI (mm Hg)	18.6 (17.7–19.6)	19.3 (18.2–19.8)	0.009*	19.6 (14.8–21.1)	18.2 (16.4–19.1)	0.153	17.6 (16.5–20.3)	17.5 (16.5–19.9)	0.216
nICPFVd (mm Hg)	12.9 (8.5–18)	15 (10.5–19.7)	0.001*	10.9 (6.7–15.7)	14.4 (5.6 (21.1)	0.004*	10 (6.9–21.3)	12.2 (5.5–22.6)	0.022*
nCPP (mm Hg)	49.9 (42.1–53.8)	54.5 (49.3–59.6)	<0.001*	49.6 (44.8–61.1)	54.9 (50.7–65)	<0.001*	53.5 (41.2–60.5)	57.4 (45.3–62.5)	<0.001*
CVR (mm Hg/cm per second)	1.1 (1–1.2)	1.2 (1.1–1.4)	<0.001*	1.1 (1–1.2)	1.2 (1.1–1.3)	<0.001*	1.2 (1.1–1.2)	1.2 (1.2–1.3)	0.001*
Others									
$ETCO_2$ (mm Hg)	43 (40–47)	46 (43–52.5)	0.001*	43 (38–51)	46.5 (44–50)	0.047*	43.5 (38–47)	45 (41–55)	0.001*
Spo_2 (%)	90 (88–92)	91 (88–92)	0.854	90 (89–92)	91 (89–92)	0.357	89.5 (87–94)	89.5 (87–94)	0.317
DeltaSpo_2-rSo_2 (%)	36 (32–38.5)	32 (28–35.5)	<0.001*	35 (30–37)	32 (27–35)	<0.001*	33 (29–37)	26 (25–32)	0.001*

*Values are expressed as median and interquartile range if not otherwise specified. Hemodynamic and neuromonitoring variables before (T0) and after (T1) passive leg raising test, fluid challenge, and norepinephrine. Values are expressed as median and interquartile range if not otherwise specified. rSo_2, cerebral oxygenation saturation; Delta O_2Hbi (ΔO_2Hbi), variation of the oxygenated component of the hemoglobin (Hb); Delta HHbi (ΔHHbi), variations of the deoxygenated component of Hb; Delta cHbi (ΔcHbi), sum of the values of ΔO_2Hbi and ΔHHbi in the calculation of rSo_2 value (ΔcHbi = ΔHHbi + ΔO_2Hbi); ΔSpo_2-rSo_2, difference between the value of Spo_2 and rSo_2; N, number; MAP, mean arterial pressure; HR, heart rate; Pi, perfusion index; PVI, pleth variability index; $ETCO_2$, end-tidal carbon dioxide; nCPP, non-invasive cerebral perfusion pressure; nICPPI, non-invasive intracranial pressure (ICP) based on pulsatility index; nICPFVd, non-invasive ICP based on flow velocity diastolic (FVd) formula; CVR, cerebrovascular resistance. *$p < 0.05$.*

Norepinephrine

The administration of NE led to a significant increase in MAP [63.5 (61–64) vs. 69 (66–71) mm Hg, $p < 0.001$] and of rSo_2 [54.5% (53–62%) vs. 61.5% (61–66%), $p = 0.001$] (**Table 2**), but only the arterial component improved [ΔO_2Hbi = 3.9 (3.2–4.3) vs. 5.7 (3.9–7.1), $p = 0.001$]. nICPFVd slightly increased [10 (6.9–21.3) vs. 12.2 (5.5–22.6) mm Hg, $p = 0.022$], but not nICPPI [17.6 (16.5–20.3) vs. 17.5 (16.5–19.9) mm Hg, $p = 0.216$].

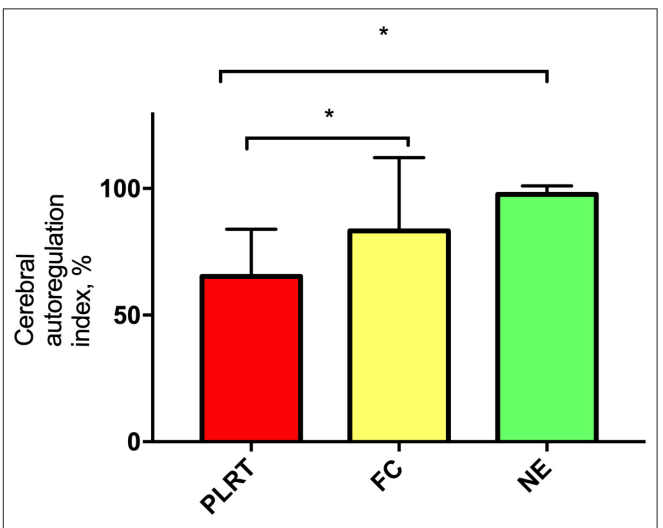

FIGURE 1 | Percentage of cerebral autoregulation index. Data are expressed as mean, standard deviation. PLRT, passive leg raising test; FC, fluid challenge; NE, norepinephrine.

DISCUSSION

In the present study, we investigated the effects of PLR test, FC, and NE on cerebral physiology in mechanically ventilated patients with severe COVID-19 pneumonia. We found that (1) PLR test is associated with impaired CA; (2) FC and NE yield increased MAP, CPP, and rSo_2. However, rSo_2 is significantly higher after NE therapy compared to FC.

This is the first study exploring the effects of hemodynamic changes on cerebral hemodynamics in critically ill COVID-19 patients undergoing mechanical ventilation. This topic is of clinical importance, but not sufficiently highlighted in the literature. Patients with COVID-19 are at high risk of hemodynamic instability, because of sedation, mechanical ventilation, and eventually sepsis with direct negative effect on cardiac function, yielding cardiological complications (26–28). Maintenance of hemodynamic stability and the prompt treatment of hypotensive events are fundamental in this cohort of

patients, to provide systemic organ perfusion and an appropriate CPP to the brain (29). In fact, COVID-19 patients are at risk of short- and long-term neurological complications (5, 8). The occurrence of stroke is increased in this population (30), and it appears to be greater in patients with COVID-19 when compared to those with influenza (1.6 vs. 0.2%, respectively, with odds ratio 7.6) (31). This higher incidence has been attributed to the increased incidence of both venous and arterial thromboembolism. In this context, it is well-known that hemodynamic instability and in particular hypotension and altered autoregulation are important risk factors for cerebral damage and secondary brain injury (6, 29, 32, 33). Although COVID-19 patients are not primarily brain-injured patients, recent evidence suggests that the cerebrovascular dynamics are impaired in this cohort of patients, with altered intracranial pressure and pupillometer indexes in most cases (8, 10, 34). Moreover, impaired CA is associated with poor outcome not only in brain-injured patients, but also in several other groups of patients, such as sepsis and cardiac arrest (6, 34, 35). PLR test is often used in the clinical practice as a test to assess the need for fluids and to help in the decision of starting fluid therapy or vasopressors; however, PLR test causes an intrinsic increase in intravascular volume, with shift of intravascular fluids from the legs to the abdominal compartment. This may increase intra-abdominal and intrathoracic pressures (36), yielding impaired cerebral hemodynamics and for this reason has been often discouraged in patients at risk of intracranial complications (37). There are few previous studies including a minority of ICU patients with brain injury who underwent PLR test [i.e., two of 34 patients in the study by Biais et al. (38), six of 71 patients in the study by Monnet et al. (39)], and no specific data on this subpopulation are available. The best hemodynamic strategy to optimize cerebral perfusion and autoregulation remains unclear. Fluid therapy is often used as first-line therapy in critically ill patients with hypotension (36), inducing a transient increase in cardiac preload consequent to extrinsic increase in intravascular volume, whereas vasopressors are started to improve MAP acting on vasomotor tone. The choice to use PLR test in these patients and treat them with fluids or vasopressors should depend on both lung and cerebral needs, which are often in conflict (40, 41). Our results suggest that PLR test may significantly decrease the cerebral autoregulatory system function of COVID-19 patients. PLR test can also increase ICP, suggesting that it may not be appropriate in patients at risk of cerebral complications. FC and NE were able to increase MAP and CPP, but NE seems to have a better effect on cerebral oxygenation and autoregulation, even though no differences in MAP and CPP between the three strategies were observed at T1.

The impact of vasopressors and FC on CA is not completely understood. Klein et al. (42) recently found in a cohort of 91 traumatic brain injury and 13 stroke patients that dynamic intracranial pressure–based measurements of cerebrovascular reactivity are not affected by NE. Similarly, Johnston et al. (43) suggested that CPP augmentation with NE, but not with dopamine, resulted in a significant reduction in arterial–venous oxygen difference (37 ± 11 vs. 33 ± 12 mL/L) and a significant increase in brain tissue oxygen (2.6 ± 1.1 vs. 3.0 ± 1.1 kPa).

The mechanism according to which NE—compared to fluids—could potentially better preserve autoregulation and cerebral oxygenation might be related to a greater effect of NE on the arterial component of rSO_2, ΔO_2Hbi, compared to FC. Furthermore, this could be related to specific characteristics of NE and the brain-blood barrier (BBB), which contains monoaminoxidase, thus allowing preserving cerebral vessels from its potential vasoconstrictor effects. Indeed, previous evidence confirms that NE has neuroprotective effects and improves CA (44) and oxygenation (43), leading to a significant increase in cerebral blood flow, in both conditions when BBB is intact or experimentally opened (45). No data are available regarding the effect of FC on CA so far, but potentially changes in plasma osmolarity and vascular content might have less protective effect on cerebral hemodynamics and BBB.

Limitations

This study presents several limitations. First, the sample size of the patients included is small, especially considering each subgroup; however, no data are available in COVID-19 patients on this topic. Moreover, the number of patients in the current study is higher than that in similar studies on brain-injured patients (46). Second, the response to PLR test was defined according to changes of $ETCO_2$, which is not the criterion standard (36, 47); the $ETCO_2$ has been already used in patients with acute respiratory distress syndrome and NE infusion showing a better performance, as compared to systemic pressure (48). To the best of our knowledge, no data are available so far in COVID-19 patients regarding this use; however, we considered the performance of this surrogate good enough in a context of paucity of resources. Third, our results would have been strengthened by the availability of more specific data on physiological parameters including invasive neurologic, respiratory, and hemodynamic monitoring to assess the changes consequent to the application of the different hemodynamic strategies. In particular, the use of invasive ICP and oxygenation would have been of extreme utility, but no indications are available for their use in non-primarily brain-injured patients. Also, our population represents a specific subgroup with peculiar characteristics, and therefore, our results may not be applicable in other clinical settings. Fourth, PLR is a test, whereas FC and NE administration are two types of clinical interventions, and therefore, these are not comparable. The decision whether to avoid PLR test in patients at risk of cerebral complications should take into account patients' needs and clinical conditions, and further larger studies are warranted to clarify this issue. In addition, as some patients received both FC and NE, we cannot exclude a cumulative effect of these techniques. Finally, we evaluated the early effects of PLR test on static CA, and no information is provided from our results on a long-term effect of this technique.

CONCLUSIONS

In mechanically ventilated severe COVID-19 patients, PLR test results in a reduction of cerebral autoregulatory function. PLR test, FC, and NE increased cerebral oxygenation, but NE seemed to have the major beneficial effect on cerebral oxygenation compared to FC. An individualized strategy aimed at assessing both the hemodynamic and cerebral needs is warranted in COVID-19 patients at high risk of neurological complications.

DATA AVAILABILITY STATEMENT

The raw data supporting the conclusions of this article will be made available by the authors, without undue reservation.

ETHICS STATEMENT

The studies involving human participants were reviewed and approved by University of Genoa, Policlinico San Martino. The patients/participants provided their written informed consent to participate in this study.

AUTHOR CONTRIBUTIONS

CR: conceived of the study, designed the study, interpretation of the data, and drafted the manuscript. DB: acquired the data, interpretation of the data, and critical revision of the manuscript. AM and PP: interpretation of the data, critical revision of the manuscript, and final approval. LB, IB, NP, MCe, BM, XL, PR, MCz, DG, AV, and MB: critical revision of the manuscript and final approval. All authors read and approved the final manuscript.

SUPPLEMENTARY MATERIAL

The Supplementary Material for this article can be found online at: https://www.frontiersin.org/articles/10.3389/fneur.2021.674466/full#supplementary-material

REFERENCES

1. Bassetti M, Vena A, Giacobbe DR. The novel Chinese coronavirus (2019-nCoV) infections: challenges for fighting the storm. *Eur J Clin Invest.* (2020) 50:e13209. doi: 10.1111/eci.13209
2. Goyal P, Choi JJ, Pinheiro LC, Schenck EJ, Chen R, Jabri A, et al. Clinical characteristics of Covid-19 in New York City. *N Engl J Med.* (2020) 382:2372–4. doi: 10.1056/NEJMc2010419
3. Wu Z, McGoogan JM. Characteristics of and important lessons from the coronavirus disease 2019 (COVID-19) outbreak in China. *JAMA*. (2020) 323:1239. doi: 10.1001/jama.2020.2648
4. Robba C, Battaglini D, Pelosi P, Rocco RMP. Multiple organ dysfunction in SARS-CoV-2: MODS-CoV-2. *Expert Rev Respir Med.* (2020) 14:865–8. doi: 10.1080/17476348.2020.1778470
5. Battaglini D, Santori G, Chandraptham K, Iannuzzi F, Bastianello M, Tarantino F, et al. Neurological complications and noninvasive multimodal neuromonitoring in critically ill mechanically ventilated COVID-19 patients. *Front Neurol.* (2020) 11:602114. doi: 10.3389/fneur.2020.602114
6. Robba C, Crippa IA, Taccone FS. Septic encephalopathy. *Curr Neurol Neurosci Rep.* (2018) 18:82. doi: 10.1007/s11910-018-0895-6
7. Levy MM, Evans LE, Rhodes A. The surviving sepsis campaign bundle: 2018 update. *Intensive Care Med.* (2018) 44:925–8. doi: 10.1007/s00134-018-5085-0
8. Battaglini D, Brunetti I, Anania P, Fiaschi P, Zona G, Ball L, et al. Neurological manifestations of severe SARS-CoV-2 infection: potential mechanisms and implications of individualized mechanical ventilation settings. *Front Neurol.* (2020) 11:845. doi: 10.3389/fneur.2020.00845
9. Beqiri E, Smielewski P, Robba C, Czosnyka M, Cabeleira MT, Tas J, et al. Feasibility of individualised severe traumatic brain injury management using an automated assessment of optimal cerebral perfusion pressure: the COGiTATE phase II study protocol. *BMJ Open.* (2019) 9:e030727. doi: 10.1136/bmjopen-2019-030727
10. Donnelly J, Czosnyka M, Adams H, Robba C, Steiner LA, Cardim D, et al. Individualizing thresholds of cerebral perfusion pressure using estimated limits of autoregulation. *Crit Care Med.* (2017) 45:1464–71. doi: 10.1097/CCM.0000000000002575
11. Elm E von, Altman DG, Egger M, Pocock SJ, Gøtzsche PC, Vandenbroucke JP. Strengthening the reporting of observational studies in epidemiology (STROBE) statement: guidelines for reporting observational studies. *BMJ.* (2007) 335:806–8. doi: 10.1136/bmj.39335.541782.AD
12. Robba C, Ball L, Battaglini D, Cardim D, Moncalvo E, Brunetti I, et al. Early effects of ventilatory rescue therapies on systemic and cerebral oxygenation in mechanically ventilated COVID-19 patients with acute respiratory distress syndrome: a prospective observational study. *Crit Care.* (2021) 25:111. doi: 10.1186/s13054-021-03537-1
13. Monnet X, Marik PE, Teboul JL. Prediction of fluid responsiveness: an update. *Ann Intensive Care.* (2016) 6:111. doi: 10.1186/s13613-016-0216-7
14. Vincent JL, Cecconi M, De Backer D. The fluid challenge. *Crit Care.* (2020) 24:703. doi: 10.1186/s13054-020-03443-y
15. Vincent JL, Weil MH. Fluid challenge revisited. *Crit Care Med.* (2006) 34:1333–7. doi: 10.1097/01.CCM.0000214677.76535.A5
16. Xiao-ting W, Hua Z, Da-wei L, Hong-min Z, Huai-wu H, Yun L, et al. Changes in end-tidal CO_2 could predict fluid responsiveness in the passive leg raising test but not in the mini-fluid challenge test: a prospective and observational study. *J Crit Care.* (2015) 30:1061–6. doi: 10.1016/j.jcrc.2015.05.019
17. Monge García MI, Gil Cano A, Gracia Romero M, Monterroso Pintado R, Pérez Madueño V, Díaz Monrové JC. Non-invasive assessment of fluid responsiveness by changes in partial end-tidal CO_2 pressure during a passive leg-raising maneuver. *Ann Intensive Care.* (2012) 2:9. doi: 10.1186/2110-5820-2-9
18. Toscani L, Aya HD, Antonakaki D, Bastoni D, Watson X, Arulkumaran N, et al. What is the impact of the fluid challenge technique on diagnosis of fluid responsiveness? A systematic review and meta-analysis. *Crit Care.* (2017) 21:207. doi: 10.1186/s13054-017-1796-9
19. Tiecks FP, Lam AM, Aaslid R, Newell DW. Comparison of static and dynamic cerebral autoregulation measurements. *Stroke.* (1995) 26:1014–9. doi: 10.1161/01.STR.26.6.1014
20. Rasulo FA, Bertuetti R, Robba C, Lusenti F, Cantoni A, Bernini M, et al. The accuracy of transcranial Doppler in excluding intracranial hypertension following acute brain injury: a multicenter prospective pilot study. *Crit Care.* (2017) 21:44. doi: 10.1186/s13054-017-1632-2
21. Robba C, Donnelly J, Bertuetti R, Cardim D, Sekhon MS, Aries M, et al. Doppler non-invasive monitoring of ICP in an animal model of acute intracranial hypertension. *Neurocrit Care.* (2015) 23:419–26. doi: 10.1007/s12028-015-0163-4
22. Gosling R, King D. Arterial assessment by Doppler-shift ultrasound. *Proc R Soc Med.* (1974) 67:447–9.
23. Budohoski KP, Schmidt B, Smielewski P, Kasprowicz M, Plontke R, Pickard JD, et al. Non-invasively estimated ICP pulse amplitude strongly correlates with outcome after TBI. *Acta Neurochir Suppl.* (2012) 114:121–5. doi: 10.1007/978-3-7091-0956-4_22
24. Pickard JD, Hutchinson PJ, Coles JP, Steiner LA, Johnston AJ, Fryer TD, et al. Imaging of cerebral blood flow and metabolism in brain injury

in the ICU. *Acta Neurochir Suppl.* (2005) 95:459–64. doi: 10.1007/3-211-32318-X_94
25. Bland JM, Altman DG. Statistics notes: calculating correlation coefficients with repeated observations: part 1–correlation within subjects. *BMJ.* (1995) 310:446–6. doi: 10.1136/bmj.310.6977.446
26. Zhou C, Pei H, Gao Y, Zhang Y, Cao L, Fang Z, et al. Optimal cut-off value of elevated cardiac troponin concentrations for myocardial injury predicts clinical outcomes in adult patients with COVID-19: a dose–response analysis protocol for systematic review. *BMJ Open.* (2021) 11:e046575. doi: 10.1136/bmjopen-2020-046575
27. Palazzuoli A, Ruocco G, Tecson KM, McCullough PA. Screening, detection, and management of heart failure in the SARS-CoV2 (COVID-19) pandemic. *Heart Fail Rev.* (2021) 6:1–7. doi: 10.1007/s10741-020-10068-4
28. Li YL, Zheng JB, Jin Y, Tang R, Li M, Xiu CH, et al. Acute right ventricular dysfunction in severe COVID-19 pneumonia. *Rev Cardiovasc Med.* (2020) 21:635–41. doi: 10.31083/j.rcm.2020.04.159
29. Volpi PC, Robba C, Rota M, Vargiolu A, Citerio G. Trajectories of early secondary insults correlate to outcomes of traumatic brain injury: results from a large, single centre, observational study. *BMC Emerg Med.* (2018) 18:52. doi: 10.1186/s12873-018-0197-y
30. Baracchini C, Pieroni A, Viaro F, Cianci V, Cattelan AM, Tiberio I, et al. Acute stroke management pathway during coronavirus-19 pandemic. *Neurol Sci.* (2020) 41:1003–5. doi: 10.1007/s10072-020-04375-9
31. Merkler AE, Parikh NS, Mir S, Gupta A, Kamel H, Lin E, et al. Risk of ischemic stroke in patients with coronavirus disease 2019 (COVID-19) vs patients with influenza. *JAMA Neurol.* (2020) 77:1366. doi: 10.1001/jamaneurol.2020.2730
32. Chesnut RM, Marshall LF, Klauber MR, Blunt BA, Baldwin N, Eisenberg HM, et al. The role of secondary brain injury in determining outcome from severe head injury. *J Trauma Inj Infect Crit Care.* (1993) 34:216–22. doi: 10.1097/00005373-199302000-00006
33. Chesnut RM, Marshall SB, Piek J, Blunt BA, Klauber MR, Marshall LF. Early and late systemic hypotension as a frequent and fundamental source of cerebral ischemia following severe brain injury in the traumatic coma data bank. In: *Monitoring of Cerebral Blood Flow and Metabolism in Intensive Care*. Vienna: Springer (1993). p. 121–5. doi: 10.1007/978-3-7091-9302-0_21
34. Donnelly J, Budohoski KP, Smielewski P, Czosnyka M. Regulation of the cerebral circulation: bedside assessment and clinical implications. *Crit Care.* (2016) 20:129. doi: 10.1186/s13054-016-1293-6
35. Cardim D, Griesdale DE, Ainslie PN, Robba C, Calviello L, Czosnyka M, et al. A comparison of non-invasive versus invasive measures of intracranial pressure in hypoxic ischaemic brain injury after cardiac arrest. *Resuscitation.* (2019) 137:221–8. doi: 10.1016/j.resuscitation.2019.01.002
36. Minini A, Abraham P, Malbrain MLNG. Predicting fluid responsiveness with the passive leg raising test: don't be fooled by intra-abdominal hypertension! *Ann Transl Med.* (2020) 8:799. doi: 10.21037/atm.2019.12.14
37. Monnet X, Teboul J-L. Assessment of volume responsiveness during mechanical ventilation: recent advances. *Crit Care.* (2013) 17:217. doi: 10.1186/cc12526
38. Biais M, Vidil L, Sarrabay P, Cottenceau V, Revel P, Sztark F. Changes in stroke volume induced by passive leg raising in spontaneously breathing patients: comparison between echocardiography and Vigileo^{TM}/FloTrac^{TM} device. *Crit Care.* (2009) 13:R195. doi: 10.1186/cc8195
39. Monnet X, Rienzo M, Osman D, Anguel N, Richard C, Pinsky MR, et al. Passive leg raising predicts fluid responsiveness in the critically ill. *Crit Care Med.* (2006) 34:1402–7. doi: 10.1097/01.CCM.0000215453.11735.06
40. van Mourik N, Metske HA, Hofstra JJ, Binnekade JM, Geerts BF, Schultz MJ, et al. Cumulative fluid balance predicts mortality and increases time on mechanical ventilation in ARDS patients: an observational cohort study. *PLoS ONE.* (2019) 14:e0224563. doi: 10.1371/journal.pone.0224563
41. Seitz KP, Caldwell ES, Hough CL. Fluid management in ARDS: an evaluation of current practice and the association between early diuretic use and hospital mortality. *J Intensive Care.* (2020) 8:78. doi: 10.1186/s40560-020-00496-7
42. Klein SP, Fieuws S, Meyfroidt G, Depreitere B. Effects of norepinephrine, propofol, and hemoglobin concentration on dynamic measurements of cerebrovascular reactivity in acute brain injury. *J Neurotrauma.* (2020) 35:506–12. doi: 10.1089/neu.2020.7160
43. Johnston AJ, Steiner LA, Chatfield DA, Coles JP, Hutchinson PJ, Al-Rawi PG, et al. Effect of cerebral perfusion pressure augmentation with dopamine and norepinephrine on global and focal brain oxygenation after traumatic brain injury. *Intensive Care Med.* (2004) 30:791–7. doi: 10.1007/s00134-003-2155-7
44. Froese L, Dian J, Batson C, Gomez A, Alarifi N, Unger B, et al. The impact of vasopressor and sedative agents on cerebrovascular reactivity and compensatory reserve in traumatic brain injury: an exploratory analysis. *Neurotrauma Rep.* (2020) 1:157–68. doi: 10.1089/neur.2020.0028
45. MacKenzie E, McCulloch J, O'Kean M, Pickard J, Harper A. Cerebral circulation and norepinephrine: relevance of the blood-brain barrier. *Am J Physiol Content.* (1976) 231:483–8. doi: 10.1152/ajplegacy.1976.231.2.483
46. James HE, Schneider S. Effects of acute isotonic saline administration on serum osmolality, serum electrolytes, brain water content and intracranial pressure. In: *Mechanisms of Secondary Brain Damage*. Vienna: Springer. p. 89–93. doi: 10.1007/978-3-7091-9266-5_13
47. Cherpanath TGV, Hirsch A, Geerts BF, Lagrand WK, Leeflang MM, Schultz MJ, et al. Predicting fluid responsiveness by passive leg raising. *Crit Care Med.* (2016) 44:981–91. doi: 10.1097/CCM.0000000000001556
48. Monnet X, Bataille A, Magalhaes E, Barrois J, Le Corre M, Gosset C, et al. End-tidal carbon dioxide is better than arterial pressure for predicting volume responsiveness by the passive leg raising test. *Intensive Care Med.* (2013) 39:93–100. doi: 10.1007/s00134-012-2693-y

Conflict of Interest: The authors declare that the research was conducted in the absence of any commercial or financial relationships that could be construed as a potential conflict of interest.

frontiers in Neurology

REVIEW
published: 23 July 2021
doi: 10.3389/fneur.2021.688362

Cerebral Autoregulation in Subarachnoid Hemorrhage

Darcy Lidington[1,2], *Hoyee Wan*[1,2] *and Steffen-Sebastian Bolz*[1,2,3]*

[1] *Department of Physiology, University of Toronto, Toronto, ON, Canada,* [2] *Toronto Centre for Microvascular Medicine at the Ted Rogers Centre for Heart Research Translational Biology and Engineering Program, University of Toronto, Toronto, ON, Canada,* [3] *Heart & Stroke/Richard Lewar Centre of Excellence for Cardiovascular Research, University of Toronto, Toronto, ON, Canada*

Subarachnoid hemorrhage (SAH) is a devastating stroke subtype with a high rate of mortality and morbidity. The poor clinical outcome can be attributed to the biphasic course of the disease: even if the patient survives the initial bleeding emergency, delayed cerebral ischemia (DCI) frequently follows within 2 weeks time and levies additional serious brain injury. Current therapeutic interventions do not specifically target the microvascular dysfunction underlying the ischemic event and as a consequence, provide only modest improvement in clinical outcome. SAH perturbs an extensive number of microvascular processes, including the "automated" control of cerebral perfusion, termed "*cerebral autoregulation.*" Recent evidence suggests that disrupted cerebral autoregulation is an important aspect of SAH-induced brain injury. This review presents the key clinical aspects of cerebral autoregulation and its disruption in SAH: it provides a mechanistic overview of cerebral autoregulation, describes current clinical methods for measuring autoregulation in SAH patients and reviews current and emerging therapeutic options for SAH patients. Recent advancements should fuel optimism that microvascular dysfunction and cerebral autoregulation can be rectified in SAH patients.

Keywords: stroke, microvascular dysfunction, cerebral blood flow, cystic fibrosis transmembrane conductance regulator, delayed ischemia

OPEN ACCESS

Edited by:
Xiuyun Liu,
Johns Hopkins University, United States

Reviewed by:
Adel Helmy,
University of Cambridge, United Kingdom
Masayo Koide,
University of Vermont, United States

***Correspondence:**
Steffen-Sebastian Bolz
sts.bolz@utoronto.ca

Specialty section:
This article was submitted to Stroke, a section of the journal Frontiers in Neurology

Received: *30 March 2021*
Accepted: *25 June 2021*
Published: *23 July 2021*

Citation:
Lidington D, Wan H and Bolz S-S (2021) Cerebral Autoregulation in Subarachnoid Hemorrhage. Front. Neurol. 12:688362. doi: 10.3389/fneur.2021.688362

INTRODUCTION

Cerebral aneurysms are common [1–5% prevalence (1, 2)] and pose a "silent risk" of severe brain injury. When an aneurysm ruptures, blood rapidly enters into the subarachnoid space: this event is termed aneurysmal subarachnoid hemorrhage (SAH) (1, 3, 4). In severe cases, intracranial pressure (ICP) elevates to levels that cause cerebrovascular arrest and death quickly ensues. As one might expect, SAH has a high case fatality rate (32–67%); of those that survive the initial bleed, 30-50% will suffer long-term disability as a result of serious brain injury (3–5). In terms of productive life years lost, SAH closely rivals more common forms of stroke due to its early age of onset (1, 6): thus, SAH incurs a disproportionately heavy cost (7), despite being a relatively rare form of stroke (∼10 in 100,000 persons per year) (8–10). The interventions to halt ruptured aneurysm bleeding and prevent subsequent re-bleeds are frequently successful: thus, if the patient survives the initial bleeding event, which depends on the severity of bleeding and how quickly emergency medical attention is initiated, most of the *treatable* mortality and morbidity in SAH occurs during neurointensive care. In this regard, a pronounced secondary ischemic event, termed "*delayed cerebral ischemia (DCI)*" emerges 3–14 days following SAH. DCI is a significant cause of death and disability in SAH patients who survive the initial aneurysm rupture (1, 11, 12).

Until recently, DCI was attributed to radiographically visible large artery constriction, known as *angiographic vasospasm*, as this common complication often occurs concomitantly with the ischemic event (13). Consequently, the majority of research efforts focused on developing therapeutic interventions to curtail angiographic vasospasm, in the hopes that this would significantly improve patient outcome (4, 14). These efforts culminated in the disappointing CONSCIOUS clinical trials involving the endothelin-1 receptor antagonist clazosentan, which successfully reduced the incidence of large artery constriction, but failed to improve clinical outcome (15–18). This failure necessitated a shift in attention from the radiographically visible angiographic vasospasm to the radiographically invisible cerebral microcirculation. Indeed, given that the microcirculation is the primary determinant of cerebrovascular resistance (19), microcirculatory dysfunction is more aptly positioned to drive ischemic injury than large artery vasoconstriction. There are an extensive number of processes governed by the microcirculation; of these processes, the "automated" control of cerebral perfusion, termed "*cerebral autoregulation,*" appears to be an important aspect of SAH-induced brain injury, as it is clearly impaired following SAH (20–24) and it is a strong independent predictor of both DCI and negative outcome (22–24).

For physicians caring for SAH patients, this review summarizes the key clinical aspects of cerebral autoregulation and its disruption in the context of SAH. Our review is segmented into three primary subsections: (1) an overview of cerebral autoregulation, its mechanistic basis and predictions on how SAH alters autoregulatory function, (2) clinical measures of autoregulation and their relationship to patient outcomes, and (3) current therapeutic interventions for SAH in the context of autoregulation, which explains why alternative approaches are desperately required. In our subsequent discussion, we will examine some emerging therapeutic options that may be capable of correcting dysfunctional autoregulation in SAH.

Cerebral Blood Flow Autoregulation

C*erebral blood flow autoregulation* is a regulatory mechanism that maintains constant brain perfusion over a relatively wide range of cerebral perfusion pressures (CPPs). This mechanism originates within the cerebral microcirculation, where resistance arteries actively match their level of constriction and hence, vascular resistance, to the prevalent perfusion pressure (25). Neils Lassen is credited with introducing the concept of cerebral blood flow autoregulation in 1959, after reviewing and integrating several human studies examining the effects of controlled hypotension on cerebral perfusion (26). However, the concept's roots date much further back, as the underlying myogenic mechanism had been identified by Sir William Bayliss in 1902 (27) and autoregulation had already been established within the renal microcirculation as early as 1946 (28).

Lassen's curve visually presents cerebral autoregulation as a correlation between cerebral blood flow against mean arterial pressure (MAP; **Figure 1**) (26). Technically, CPP (i.e., the difference between MAP and intracranial pressure) is the more appropriate x-axis ordinate, but there is generally a tight relationship between MAP and CPP in normal settings, since ICP is generally constant. The autoregulatory curve possesses three key regions: a central plateau flanked by two inflection points that define the lower and upper limits of autoregulatory activity (**Figure 1**). The region at and below the lower limit is a state of maximal dilation within the microcirculation and consequently, reductions in CPP within this region result in reductions in blood flow. While the lower limit of autoregulation is considered a critical clinical benchmark, the brain is generally able to tolerate blood flow reductions of 30–60% before the onset of ischemic symptoms (29, 30). In essence, the brain enjoys a degree of "luxury perfusion," known clinically as the "cerebrovascular reserve capacity." Thus, the MAP at which ischemic symptoms typically arise may be substantially lower than the MAP that defines the lower limit of autoregulation. As an important caveat, SAH patients may have reduced or exhausted cerebrovascular reserve capacity (31) and thus, are likely to be more vulnerable to hypotension than healthy individuals. On the other side of Lassen's curve, the region at and above the upper limit of autoregulation represents a state of maximal microcirculatory constriction and at high pressures, an inability to maintain constriction (i.e., "forced dilation"). This poses a different threat to the brain's viability, including pressure-induced microcirculatory damage (32, 33), blood brain barrier disruption (34–36), and vasogenic edema formation (36, 37). Since blood brain barrier disruption and cerebrovascular edema are predictive for poor neurological outcome in SAH (38, 39), the upper limit of autoregulation is as clinically significant as the lower limit.

Since there are no systematic assessments defining the entire autoregulatory range in humans, the generally accepted range is 50-150 mmHg, as originally described by Lassen (25, 26). However, there are several key aspects of Lassen's work and our current understanding of autoregulation that are frequently overlooked (40). First, Lassen combined 11 different subject groups across 7 independent studies, regardless of patient health status or medication/anesthetic use: thus, the curve is highly prone to error, as it is composed of inter-subject means from uncontrolled and heterogenous conditions (26). As reviewed by Drummond (40), several subsequent studies specifically targeting the lower limit of autoregulation in humans suggest that the lower limit is actually much closer to a MAP of 70 mmHg. Second, the same studies reviewed by Drummond demonstrate remarkable inter-subject variability and consequently, the "one-size-fits-all" representation of the autoregulatory curve is considerably misleading: no single range can be broadly applied to a given patient (40). Third, the plateau of autoregulation is likely not perfectly flat, as there is evidence that autoregulatory responses to MAP elevation are more effective than responses to MAP reductions (41–44): thus, some degree of pressure passivity may be normal in healthy individuals and is not necessarily indicative of dysfunction (45). Finally, autoregulation is a physiologically fragile mechanism that is perturbed by many pathologies: thus, the autoregulatory range may be very different in SAH patients compared to healthy subjects and Lassen's curve (46–48). In summary, while the fundamental concept of autoregulation has withstood the test

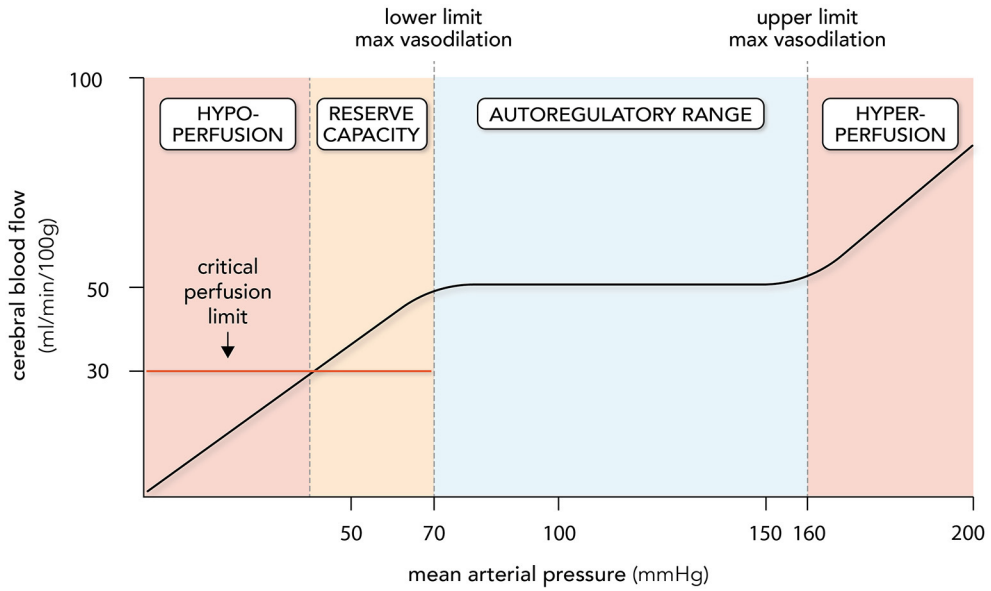

FIGURE 1 | Cerebral autoregulation. Cerebral autoregulation is plotted as a relationship between cerebral blood flow (CBF) and mean arterial pressure (MAP). The autoregulatory range is defined by MAP levels that elicit maximal myogenic vasodilation (lower limit; ∼70 mmHg) and myogenic vasoconstriction (upper limit; ∼160 mmHg): CBF remains relatively stable as MAP changes within this range. Perfusion decreases when MAP drops below the lower limit; however, overt symptoms are not observed until a critical perfusion threshold is reached, usually 40–60% below normal levels. The MAP range where perfusion drops without symptoms is termed the cerebrovascular reserve capacity. Hypoperfusion and ischemia occur at MAP levels below the reserve capacity; hyperperfusion and vasogenic edema occur at MAP levels above the upper limit. It must be stressed that the lower and upper limits of autoregulation, the size of the cerebrovascular reserve capacity and the level of perfusion maintained by autoregulation all display variation. Thus, the plot represents regularly quoted values.

of time, the absolute values of Lassen's curve are outdated, and additional data derived from SAH patients is required in order to provide more effective guidance.

It must also be emphasized that pressure autoregulation is not the sole determinant of cerebral perfusion: in addition to automatically adjusting microvascular resistance to pressure, vascular smooth muscle cells also sense and integrate a variety of metabolic signals, which superimpose on autoregulation to elicit regional perfusion changes in response to heightened local metabolic demand (49–52). Examples of these metabolic signals include, but are certainly not limited to, pH, O_2 and CO_2 tensions, lactate, adenosine, nitric oxide, potassium ions, and vasoactive neurotransmitters (e.g., dopamine and acetylcholine) (49–52). These localized influences are most often termed "*neurovascular coupling*" (49–52), although "*metabolic autoregulation*" (i.e., the matching of perfusion to metabolic demand) has also been used (53). To avoid confusion, the present review refers to pressure autoregulation when the singular term "autoregulation" is used.

In pathological settings, autoregulatory dysfunction undoubtedly incorporates both intrinsic changes to how smooth muscle cells sense and respond to pressure and their vasomotor responses to the metabolic signals emanating from the external environment. Isolating the effects of SAH on the intrinsic pressure-sensitive mechanisms can only be effectively achieved with an *in vitro* experimental system that directly characterizes a resistance artery's response to pressure in a controlled external environment where confounding metabolic and neural inputs are eliminated.

The Myogenic Response

Sir William Bayliss introduced the concept that intravascular pressure significantly modulates vascular tone in 1902, publishing a set of elegant *in situ* and *in vitro* (i.e., excised arteries) experiments that demonstrated pressure-dependent vasoconstriction and vasodilation (27). Since Bayliss could not attribute these responses to neuronal (i.e., responses persisted despite severed nerves and artery excision) or metabolic (stable *in vitro* conditions) inputs, he deemed these responses to be *myogenic* in nature (i.e., "myocyte origin") (27). Indeed, Bayliss noted that "*The muscular coat of the arteries reacts, like smooth muscle in other situations, to stretching force by contraction… it also reacts to diminution of tension by relaxation, shown, of course, only when in a state of tone.*" (27). Remarkably, Bayliss' discovery was largely ignored for 45 years (54), in part because another prominent physiologist, Gleb von Anrep, failed to reproduce Bayliss' results in similar experiments and instead attributed the constrictions and dilations to neuronal (adrenaline) and metabolic influences, respectively (55). Although several subsequent studies by others largely supported Bayliss' original conclusion (54), the mechanism did not rise to prominence until (i) blood flow autoregulation was shown to be due to a non-neural, pressure-dependent mechanism (56) and (ii) myogenic mechanisms were demonstrated to significantly alter vascular resistance *in vivo* (57, 58).

As a functional definition, the myogenic response is vasoconstriction in response to an increase in transmural pressure (i.e., the pressure across the vessel wall) and vasodilation in response to a decrease in transmural pressure. Small cerebral arteries (<300 μm in diameter) are myogenically active (19, 59–62) and given that these arteries account for ∼80% of the cerebrovascular resistance (i.e., between the systemic circulation and the cerebral capillaries) (19), they are the prime determinants of cerebral perfusion. It must be highlighted, however, that large cerebral arteries (∼ 1 mm or more) (62, 63), including middle cerebral, basilar and pial arteries (64, 65), are also myogenically active. This is not typically observed in other tissues: in skeletal muscle, for example, only the smaller resistance arteries are myogenically active, whereas larger arteries appear to have minimal myogenic reactivity and a limited role in autoregulation within that tissue (19, 66). This point highlights a key danger of generalizations, based on observations from other vascular beds. In the cerebral circulation, there is clearly a gradient in myogenic reactivity, with smaller vessels developing more myogenic tone than larger vessels (62). Larger arteries may engage their myogenic mechanisms predominantly at higher pressures (>120 mmHg) (59, 67), which could be a means of increasing autoregulatory range. Specifically, to prevent small resistance arteries from reaching their maximal myogenic vasoconstriction limit at high pressures, cerebrovascular resistance increases upstream to attenuate the downstream pressures, thereby permitting the small resistance arteries to retain a high degree of perfusion control (59, 67). As mentioned previously, regional differences in autoregulation exist, indicating that myogenic reactivity and segmental activity within different regions of the brain is not uniform (59). Thus, different regions of the brain are likely to respond differently to SAH and systemic interventions.

At the molecular level, the myogenic response is the conversion of a mechanical stimulus (i.e., wall tension) into an intracellular biochemical signal; however, reviews over the last 20 years attest to the enormous complexity and mechanistic diversity of myogenic mechanisms (32, 54, 68–75). It is also noteworthy that mechanistic variations across species, biological sex, developmental status, vascular bed, and artery branch order have been identified (74). With this in mind, our review will provide only a simplified and abbreviated overview of selected key mechanisms driving myogenic signaling.

Depolarization is the critical initiator of the myogenic response: vascular wall tension is sensed by mechanosensitive ion channels (76–78) and/or other mechanosensitive elements (79–81), eliciting depolarization, L-type calcium channel activation, and calcium influx (82). Other voltage and ion-sensitive channels are subsequently engaged by the depolarization and ion influx, for example voltage gated (K_v) and calcium-activated large conductance (BK) potassium channels, which play important roles in modulating the depolarization response (83, 84). Elevated cytosolic calcium levels stimulate *calcium-dependent vasoconstriction*, a process that involves the calcium/calmodulin-dependent activation of myosin light chain kinase and subsequent phosphorylation of myosin light chain 20: this phosphorylation event activates actin-myosin filament interaction and gliding (71). While extracellular calcium influx is generally considered to be the key source of calcium driving calcium-dependent vasoconstriction, calcium released from intracellular stores also plays a key role in mediating the constriction response (85, 86). In addition, calcium-independent mechanisms work in concert to increase *calcium sensitization*, which amplifies calcium-dependent responses by inhibiting the phosphatase that directly antagonizes the activity of myosin light chain kinase (i.e., myosin light chain phosphatase) (69, 71). In a previous review, we detailed a number of signaling entities that have been demonstrated to enhance calcium sensitivity in the context of the myogenic response (75): notable examples include sphingosine-1-phosphate (S1P) signaling (86, 87), 20-hydroxyeicosatetraenoic acid (20-HETE) signaling (72, 88), Rho kinase (89, 90), and protein kinase C (91, 92).

Only a handful of studies have utilized cannulated resistance arteries *ex vivo* to investigate the effects of SAH on myogenic reactivity (**Table 1**). As demonstrated in mouse olfactory (87, 93) and middle cerebral (94), rat parenchymal (95, 96) and middle cerebral (97), canine basilar (98), and rabbit cerebellar and posterior cerebral resistance arteries (99, 100), these studies are unanimous in concluding that SAH augments cerebral resistance artery myogenic reactivity. Through the use of endothelial denudation (95), smooth muscle cell specific gene deletion (87) and studies on freshly isolated artery myocytes (96, 100), this pathological effect can be attributed to a change in smooth muscle cell function. One common thread appears to be an enhancement of calcium-dependent signaling, which was either directly shown (95, 96, 100) or can be inferred (87, 93), based on previous studies (86, 90). Calcium sensitization is also likely to be enhanced, since the S1P-dependent signals characterized by Yagi et al., are known to enhance calcium sensitivity (69, 74, 86, 90). At the molecular level, (i) changes in potassium channel expression (96, 100) augment pressure-dependent depolarization and calcium influx (95), while (ii) augmented S1P signaling (87) further mobilizes intracellular calcium stores and increases calcium sensitization (86, 90). In summary, SAH appears to broadly increase myogenic reactivity throughout the cerebral microcirculation: since the basis of cerebral autoregulation is the myogenic response, these studies imply that autoregulation must also change in response to SAH.

Autoregulatory Changes in Response to Augmented Myogenic Reactivity

In clinical practice, it would be risky to assume that SAH does not alter the shape or position of the autoregulatory curve: thus, in order to properly interpret clinical measurements of autoregulation, we need to make predictions about how augmented myogenic vasoconstriction will affect autoregulation. Here, we will consider 3 potential scenarios involving microvascular and macrovascular constriction: (i) microcirculatory vasoconstriction (i.e., augmented myogenic vasoconstriction) in the absence of angiographic vasospasm, (ii) angiographic vasospasm alone, and (iii) both microcirculatory and large artery vasoconstriction. We propose the following effects on autoregulation:

TABLE 1 | Research studies utilizing pressure myography to assess the effect of experimental subarachnoid hemorrhage on myogenic reactivity.

References	Citation	Species	Cerebral artery	Critical observations
Yagi et al., 2015	(87)	Mouse	Olfactory	SAH augments myogenic reactivity and reduces CBF. Etanercept (TNF inhibitor) and JTE-013 (S1P2 receptor antagonist) normalize myogenic reactivity and reduce neurological injury in SAH; etanercept improves CBF in SAH.
Lidington et al., 2019	(93)	Mouse	Olfactory	SAH augments myogenic reactivity and reduces CBF. Lumacaftor (CFTR corrector therapeutic) normalizes myogenic reactivity, improves CBF and reduces neurological injury in SAH.
Deng et al., 2018	(94)	Mouse	Middle Cerebral	Hemolyzed blood reversibly augments myogenic tone *in vitro* and *in vivo*. Superoxide scavenging (Tempol) prevents myogenic tone augmentation *in vitro* and *in vivo*.
Nystoriak et al., 2011	(95)	Rat	Parenchymal	SAH augments pressure-dependent membrane depolarization, calcium influx and vasoconstriction.
Wellman and Koide, 2013	(96)	Rat	Parenchymal	SAH augments potassium currents and myogenic tone.
Gong et al., 2019	(97)	Rat	Middle Cerebral	SAH increases TRMP4 expression/activity, resulting in augmented depolarization and vascular tone. Blockade of TRMP4 (9-phenanthrol) significantly improves vascular tone and CBF in SAH.
Harder et al., 1987	(98)	Dog	Basilar	SAH reduces basilar artery potassium conductance and induces basilar artery vasospasm. Inhibiting potassium efflux (nicorandil) reduces basilar artery constriction *in vitro* and *in vivo*.
Ishiguro et al., 2002	(99)	Rabbit	Basilar, Posterior and Cerebellar	SAH augments posterior and cerebellar artery myogenic tone. SAH augments basilar artery constriction *in vivo* (measured angiographically).
Koide et al., 2011	(100)	Rabbit	Posterior and Cerebellar	SAH augments arterial wall depolarization, calcium influx and myogenic tone. SAH reduces calcium spark frequency, suggesting reduced BK channel activity.

A blood injection model of SAH was used in all publications. BK, calcium activated large conductance potassium channels; CBF, cerebral blood flow; S1P2, Sphingosine-1-phosphate receptor 2; SAH, Subarachnoid hemorrhage; TRMP4, Transient receptor potential melastatin-4.

Our first scenario (**Figure 2A**) is consistent with observations that DCI occurs in SAH patients in the absence of angiographic vasospasm (101–107). Augmented myogenic vasoconstriction reduces CBF and depending on the extent of the augmented myogenic reactivity, CBF may fall below the critical perfusion threshold, resulting in ischemia. The upper limit of autoregulation shifts to the left as a consequence of the enhanced constriction, assuming that the maximal constriction level for the artery is not altered. This is a reasonable conjecture, as the isolated artery studies found that SAH does not affect maximal artery diameter or enhance vasoconstriction to non-myogenic stimuli (87, 93, 95). One might speculate that the lower limit would also shift to the left, but there are two lines of evidence that suggest this would not occur. First, the pressure at which arteries lack wall tension (i.e., become slack) is very close to the lower limit of autoregulation: therefore, it is unlikely that mechanotransductive processes operate below the lower limit (108). Second, using hypocapnia as a means of inducing microvascular vasoconstriction and reducing CBF, Artru and Lam determined that the lower limit of autoregulation does not shift leftward as a result of enhanced vasoconstriction (109). Scenario 1 (**Figure 2A**) has been elegantly demonstrated in an experimental mouse model, where SAH induces (i) a marked reduction in CBF (ii) throughout a narrowed autoregulatory range that (iii) possesses a reduced upper limit and unchanged lower limit (110).

Because autoregulation maintains constant CBF at reduced levels, perfusion will not increase unless the CPP passes the upper limit of autoregulation. In severe cases (i.e., where ischemic symptoms are present), the autoregulatory range may be small enough that the upper limit can be passed with "moderate elevations" in systemic blood pressure [e.g., an elevation of mean arterial pressure to 140 mmHg (46); **Figure 2A**]. Since elevated blood pressure is common in SAH patients (111), some patients who do not have ischemic symptoms may have CPPs above the upper limit that would be identified as abnormal autoregulation.

In our second scenario (**Figure 2B**), large artery vasoconstriction (i.e., angiographic vasospasm) would increase upstream resistance, thereby lowering the intravascular pressure sensed by the microvascular resistance arteries. In response, the resistance arteries would dilate to maintain CBF, until the lower limit of autoregulation is reached. Thus, the primary effect large artery vasoconstriction is a rightward shift in the autoregulatory curve, but not a change in the perfusion level. In severe angiographic vasospasm, the autoregulatory curve may shift far enough that CPP falls below the lower limit and reductions in perfusion are observed; however, some patients will remain in the reserve capacity zone and therefore, not suffer ischemic injury as a result (112). This scenario is consistent with observations

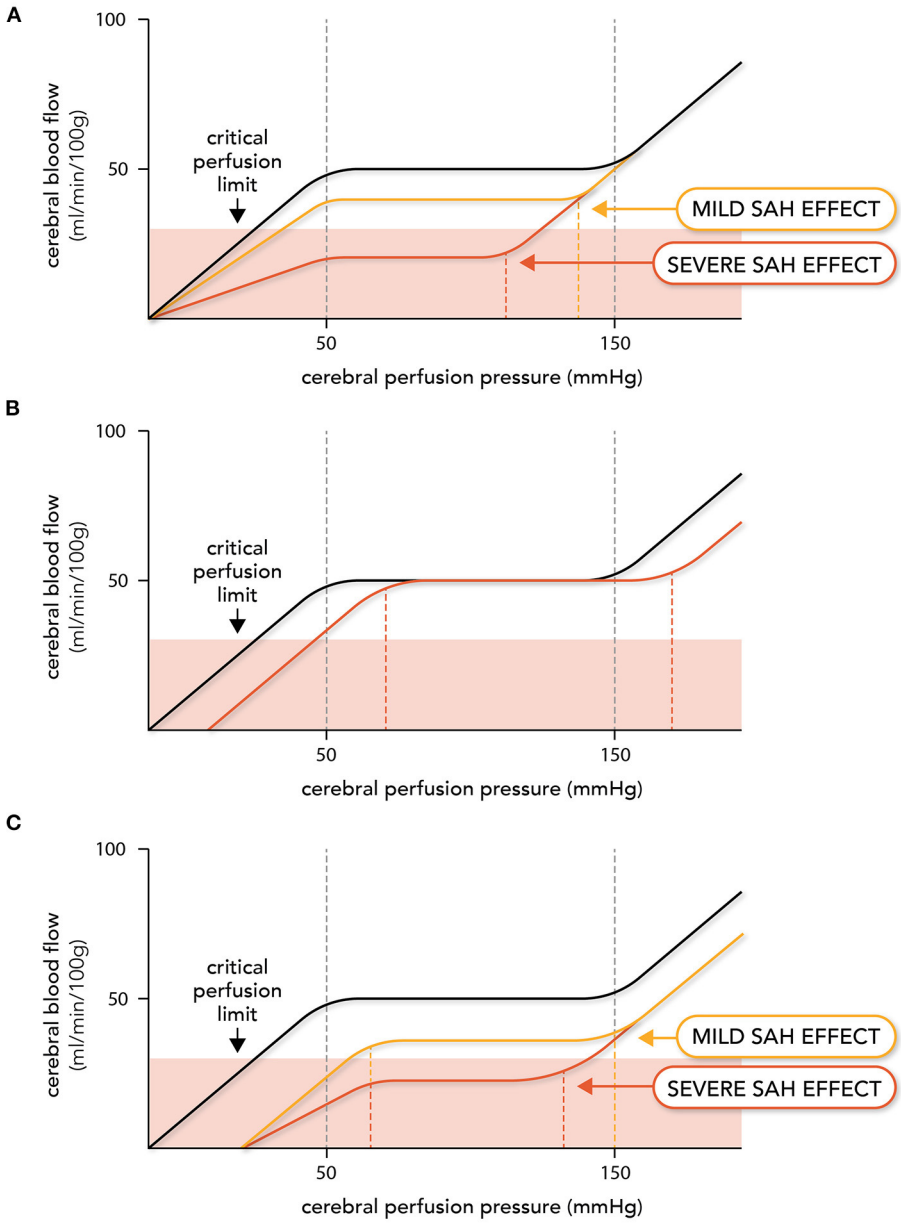

FIGURE 2 | Expected effects of subarachnoid hemorrhage on autoregulation. Altered vascular reactivity in subarachnoid hemorrhage (SAH) can have three hypothetical effects on cerebral autoregulation. Note that in this figure, cerebral autoregulation is plotted as the relationship between cerebral blood flow (CBF) and cerebral perfusion pressure (i.e., the difference between mean arterial pressure and intracranial pressure): this was done because intracranial pressure varies in SAH patients, thereby adding a variable to consider when relating CBF to mean arterial pressure in this pathological setting. The autoregulation curve in black represents the normal, non-pathological situation, while the red and yellow lines represent altered autoregulation. In **(A)**, augmented myogenic reactivity (i.e., microvascular constriction) reduces perfusion, shifts the upper limit of autoregulation leftward and narrows the autoregulatory range. In severe cases, cerebral blood flow drops below the critical perfusion limit. In **(B)**, upstream large artery constriction (i.e., angiographic vasospasm) reduces the perfusion pressure entering the microcirculation. This stimulates a right-ward shift in the autoregulatory curve, but perfusion deficits do not occur until the new lower limit is reached. In **(C)**, both microvascular and larger artery constriction occur, creating a hybrid of **(A)** and **(B)**.

that many patients with severe angiographic vasospasm do not suffer significant neurological decline (14, 112). Scenario 2 (**Figure 2B**) has been demonstrated in an experimental rabbit model associated with significant vasospasm: in this model, SAH profoundly compromises the lower limit of autoregulation, with CBF eventually reaching control levels at higher mean arterial pressures (113).

Our final scenario (**Figure 2C**) combines both of these elements: cerebral perfusion is reduced; the autoregulatory range narrows due to a leftward shift in the upper limit; and the

autoregulatory curve shifts to the right due to the large artery constriction decreasing the "apparent" intravascular pressure sensed by the microcirculation. This represents a potentially dangerous scenario for SAH patients, as the rightward shift in the autoregulatory curve has the potential to shift the patient's CPP below the lower limit, thereby further reducing perfusion. Curtailing angiographic vasospasm may or may not increase cerebral perfusion in this scenario; even if perfusion increases, it may not sufficiently rise to prevent ischemic injury. This scenario provides a possible explanation for why therapeutically targeting angiographic vasospasm failed to deliver benefit (15, 16).

CLINICAL DATA ON CEREBRAL AUTOREGULATION

Cerebral autoregulation has been a focus of clinical assessment in SAH patients for over 50 years. In this subsection, we present distilled descriptions of the most frequently used methods to measure autoregulation in SAH patients, including the key principles, caveats, and conclusions.

Static Autoregulation Measurement

Direct cerebral blood flow measurements require lengthy time scales and consequently, provide only a snapshot of autoregulation in steady state settings (114). Fantini et al. provide a comprehensive review of the techniques utilized to quantitatively measure cerebral blood flow, which notably includes ^{133}Xe clearance, positron emission tomography, thermal diffusion, magnetic resonance imaging arterial spin labeling, and perfusion computed tomography (114). Utilizing these approaches for autoregulation studies generally requires pharmacological interventions to persistently alter blood pressure, although positional changes can also be used. Transcranial Doppler (TCD) has been extensively used to assess static autoregulation in shorter time periods (41), but measuring blood flow velocity (BFV) as a surrogate for blood flow is error-prone, due to the poor assumption that the insonified artery's diameter does not change in response to the pharmacological intervention (113, 115, 116). The emergence of color-coded duplex ultrasonography (CDUS), which simultaneously measures BFV and arterial diameter, provides a superior ultrasound alternative to the standard TCD approach (115).

Static autoregulation measurements generally provide quantitative measures of the overall performance of autoregulation, in many cases with a high spatial resolution. In fact, Lassen's iconic autoregulatory curve was the result of combining 7 human studies with static measurements of cerebral blood flow and MAP (26). However, the approach is not without limitations, especially in SAH patients: (i) pharmacologically inducing blood pressure changes can be dangerous in critically ill SAH patients, (ii) sequential monitoring can require lengthy periods of time and therefore, it is not practical to routinely monitor static autoregulation, (iii) certain methods, such as ^{133}Xe clearance, are invasive (intra-arterial injection) (114), (iv) anesthetics (e.g., halothane) and certain vasoactive agents very likely alter autoregulation, thereby incorporating a potential confound and (v) most measurements require non-bedside equipment.

Although autoregulation responds to both increases (vasoconstriction) and reductions (vasodilation) in perfusion pressure, running both protocols in SAH patients is logistically challenging. Thus, studies generally measure responses after a single stimulus in SAH patients, almost always a reduction in blood pressure (20, 101, 117–121). In some cases, a hypertensive stimulus has been utilized (122, 123) and in others no stimulus was utilized (124, 125). In this latter case, autoregulatory failure is inferred when angiographic vasospasm reduces downstream perfusion, due to an assumption that compensatory downstream vasodilation should engage (124). It is worth noting that the majority of static autoregulation studies are rather dated and that the standard of care for SAH patients has evolved considerably since.

Given that ischemia and perfusion deficits are common in SAH patients, it is not surprising that these studies largely confirm that SAH compromises autoregulation in many SAH patients (**Table 2**) (20, 101, 117–125). There is little and disparate data regarding the temporal profile of autoregulatory perturbation, with one study indicating that the initial phase displays the greatest autoregulatory disruption (<7 days) (20), while another suggests that significant deterioration occurs within the window of delayed ischemia (>7 days) (121). Similarly, there is little data relating these measures to outcome, with one study indicating that highly-disrupted autoregulation associates with poor Glasgow outcome score (117), while another found no autoregulatory differences between patients who develop symptomatic vasospasm vs. those who do not (121). Intriguingly, two studies indicate that autoregulatory dysfunction is heterogeneous and consequently, systemic interventions intended to increase blood flow within ischemic regions can paradoxically reduce perfusion in that region and/or others (101, 122). This raises concerns that empirically deploying systemic therapies may have serious unintended consequences.

Dynamic Autoregulation Measurement

Dynamic autoregulation assessment refers to a relatively simple TCD-based method that evaluates the autoregulatory response to a transient reduction in perfusion pressure. In brief, middle cerebral artery (MCA) BFV is continuously measured by TCD. Autoregulatory responses are then measured following an alteration in CPP (the transmural pressure sensed by myogenic mechanisms): this is typically achieved in SAH patients by compressing the carotid artery ipsilateral to the insonified MCA (126–131), although in some cases, a bilateral thigh cuff is utilized (132, 133). Compression of the carotid artery (tailored to yield ∼30% reduction in MCA BFV) decreases CPP: after a brief period (usually 3–5 s), the compression is released. When autoregulation is behaving normally, the microcirculation dilates in response to the reduced perfusion pressure: consequently, when pressure is rapidly restored, a brief hyperemic response occurs. Hence, the test is frequently referred to as a ***Transient Hyperemic Response Test (THRT)***. The test is scored as a binary measure (intact/perturbed), depending on whether the transient

TABLE 2 | Clinical studies assessing cerebral blood flow autoregulation in subarachnoid hemorrhage patients.

References	Citation	Study size	SAH grade	CBF method	Critical observations
Dernbach et al., 1988	(20)	SAH - 14/Unruptured - 10	Hunt-Hess 1-4	Thermal Probe	Patients with Hunt-Hess 1-2 scores display perturbed autoregulation when operated on within 7 days of SAH (n = 6). After 7 days post-SAH ictus (n = 8), perturbed autoregulation was not evident.
Heilbrun et al., 1972	(101)	SAH - 10	Hunt-Hess 2-5	Intra-arterial ^{133}Xe CT	4/9 SAH patients displayed a global loss of autoregulation. 4/5 patients with intact autoregulation had satisfactory outcomes, while 3/4 patients with disrupted autoregulation had poor outcomes.
Tenjin et al., 1988	(117)	SAH - 9/Unruptured - 3	WFNS 1-4	Thermal Probe	SAH severity predicts perturbed autoregulation (n = 2 WFNS 3-4 vs. n = 7 WFNS 1-2); perturbed autoregulation predicts outcome (n = 4 GOS 3-5 vs. n = 5 GOS 1-2).
Muench et al., 2005	(118)	SAH - 10	Hunt-Hess 2-5	TD-rCBF	Pathological values of autoregulation index were observed in the patient population. Reductions in mean arterial pressure result in decreased cerebral blood flow.
Nornes et al., 1977	(119)	SAH - 21	Hunt-Hess 1-3	Flow Probe	Grade 3 SAH (n = 9) induces a rightward shift in the lower limit of autoregulation (∼76 mmHg), compared to grades 1-2 (n = 12; ∼62 mmHg).
Pickard et al., 1980	(120)	SAH - 20	Hunt-Hess 1-3	Intra-venous ^{133}Xe CT	Halothane-induced hypotension increased CBF in 15/20 patients, with 1 developing neurological deficits; 5/20 had reduced CBF during hypotension, with 4 developing neurological deficits.
Cossu et al., 1999	(121)	SAH - 77	WFNS 1-5	Thermal Probe	WFNS grade 1-2 patients (n = 23) had a better autoregulatory index than WFNS 4-5 patients (n = 19). In WFNS grade 1-2 patients, better autoregulation was observed within 0–2 days post-SAH compared to 3–7 days and >7 days.
Darby et al., 1994	(122)	SAH - 13	Hunt-Hess 1-5	Inhaled ^{133}Xe CT	Dopamine-induced hypertension (90–110 mmHg) does not alter overall CBF; however, ischemic territories increase CBF while high perfusion territories decrease CBF.
Muizelaar et al., 1986	(123)	4 SAH Case Reports	Hunt-Hess 2-5	^{133}Xe CT	Phenylephrine-induced hypertension (17–50 mmHg) increases CBF. 3/4 patient MAPs were within the normal autoregulatory range prior to (90–98 mmHg) and following intervention (112–126 mmHg).
Hattingen et al., 2008	(124)	SAH - 51/Healthy - 15	Hunt-Hess 1-5	MRI Spin Labeling	SAH patients have reduced CBF compared to controls. Vasospasm reduces CBF in downstream region. Impaired autoregulation is inferred by lack of compensatory vasodilation, as measured by CBV.
Diringer et al., 2016	(125)	SAH - 25	WFNS 2-5	^{15}O PET	Normal mean autoregulatory index following phenylephrine treatment. However, data values were highly variable, with many points outside "normal" range.

CBF, cerebral blood flow; CBV, cerebral blood volume; CT, computed tomography; GOS, Glasgow outcome score; MAP, mean arterial pressure; MRI, magnetic resonance imaging; PET, positron emission tomography; SAH, Subarachnoid hemorrhage; TD-rCBF, Transcranial Doppler relative CBF measurement; WFNS, World Federation of Neurosurgical Societies scale.

hyperemic BFV is 10% higher than the pre-compression BFV. In the thigh cuff approach, thigh cuffs are inflated to 200 mmHg for 2 min and then rapidly released, resulting in a negative step change in CPP. The autoregulatory BFV response is then mapped to 10 theoretical traces incorporating autoregulatory dynamic gain, a dampening factor and a time constant (134). Each curve represents a different degree of autoregulatory impairment, known as the ***Autoregulation Index (ARI)***, with 0 indicating no autoregulation and 9 indicating "perfect" autoregulation.

Although the methods are relatively simple, non-invasive and use readily available TCD equipment, there are some general caveats and limitations: (i) the measurements are highly prone to inconsistency, most likely due to short-term variations in autoregulatory activity, the influence of other physiological variables and noise in the system, (ii) there is an assumption that MCA diameter does not change as a result of the interventions, and (iii) the THRT is graded against a somewhat arbitrary present/absent threshold that oversimplifies the outcome.

SAH patients frequently display abnormal THRT results (**Table 3**) (126–131). Two studies show a timeline following SAH ictus, based on the proportion of patients with negative/abnormal THRT results: while these studies show variable proportions of negative results early after ictus (0–3 days post-SAH), there is a clear peak between days 7–10, after which point the proportion of negative THRT results declines (128, 129). This peak fits well with the timeline for development of DCI. Negative THRT results are frequently, but not always, a good predictor for the emergence of angiographic vasospasm (126, 127, 129, 130) and poor THRT results are clearly more prevalent in patients who develop cerebral infarction (129, 131), have poor neurological

status (e.g., WFNS Score >2 or Glasgow Coma Score <6) (126–129, 131) and ultimately have poor outcomes (e.g., Glasgow Outcome Score ≤3 or modified Rankin Scale ≥4 at 6 months) (126, 128, 131). Likewise, the thigh cuff/ARI approach appears capable of segregating patients who will develop angiographic vasospasm, rapid neurological deterioration, and suffer poor outcome (132, 133). ARI is consistently reduced in SAH patients (ARI scores of 4–6 in good outcome and 1–4 in poor outcome) and generally increase over time (i.e., over 0-10 days post-SAH) in patients who improve and decline in those who deteriorate (132, 133).

Continuous Autoregulation Measurement

There are several practical considerations that hinder the routine measurement of static and dynamic cerebral autoregulation in critically ill patients: (i) static autoregulation measures require the use of vasoactive drugs or mechanical maneuvers that are often contraindicated in critically ill patients, (ii) assessments can be time consuming and consequently, frequent/routine assessment would add a substantial workload burden to neurocritical care staff, and (iii) assessments can be prohibitively expensive, especially if MRI-based methods are used. In a critical care setting, cerebral autoregulation assessments should be fast and inexpensive, minimally disturb the patient and ideally, utilize data that is already collected as part of neurocritical monitoring. Continuous autoregulation measurements largely meet these criteria, as they rely on endogenous variations in blood pressure and utilize continuous monitoring data from widely available equipment.

The ***Pressure Reactivity Index (PRx)***, first described in 1997 by Czosnyka et al. (135, 136), measures the association between slow waves in arterial blood pressure (ABP) and ICP, where ABP serves as a surrogate for CPP and ICP as a surrogate for vascular reactivity. The latter is predicated on the fact that vasomotor responses globally change cerebrovascular volume and consequently, ICP (as per the Monro-Kellie doctrine). In a setting with intact autoregulation, there is an inverse relationship between ABP and ICP: increases in ABP stimulate myogenic vasoconstriction, which decreases ICP *via* a blood volume reduction. The PRx index is calculated using a moving Pearson correlation; when PRx is subsequently plotted against CPP (i.e., CPP=ABP-ICP), a U-shaped relationship is observed (137), with the autoregulatory range defined by near-zero or slightly negative values and the progressive loss of autoregulation as increasingly positive values (i.e., increased ICP resulting from the transmission of ABP into the microcirculation).

Although measuring PRx requires is invasive (i.e., ventricular or intraparenchymal transducer), these parameters may be measured in SAH patients who are subject to continuous ICP monitoring. However, PRx measurements in SAH patients possesses key caveats: (i) ABP must be a reliable correlate of CPP, which may be problematic in patients with high ICP levels, putatively due to compression of intracranial veins and consequent increase in venous resistance (138, 139); (ii) slow waves in ICP must be solely dependent on blood volume changes, as experimentally validated in non-pathological settings (140); (iii) craniospinal compliance (i.e., the capacity to compensate for added intracranial volume) must not substantially increase following decompressive craniotomy (141, 142) or with the use of external ventricular drains (143), as this will alter PRx values regardless of autoregulatory status [decompressive craniotomy likely invalidates PRx measurements (142)]; and (iv) as a global measure, PRx measurements assume that all vascular beds within the cerebral microcirculation behave similarly with respect to pressure reactivity, which is probably true at normal perfusion pressures, but not at the extremes (144). It should also be noted that since the CPP estimation incorporates the ICP (i.e., CPP=ABP-ICP), there is a statistical bias in the U-shaped PRx/CPP relationship, owing to the fact that PRx and CPP share a common parameter, resulting in a degree of "autocorrelation" (145). Without correction, this bias likely distorts the true autoregulatory window and consequently, the estimates of appropriate perfusion pressures (145).

PRx measurements are more firmly established as a prognostic indicator for traumatic brain injury patients than they are for SAH patients (136, 146). Nevertheless, there are several informative PRx studies in SAH patients (**Table 4**) (46, 143, 147–151). The vast majority of SAH patients display abnormally positive PRx values (i.e., perturbed cerebral autoregulation) (46, 143, 147–149); as anomalies, one small study (21 patients) failed to show disrupted autoregulation in SAH patients (151) and another (42 patients) found normal autoregulation in patients who survived for 3 months, while non-survivors displayed significantly higher PRx values (150). A subset of studies measured PRx over a prolonged time course (i.e., within 1 day to 14 days post-SAH) (46, 147, 149): as a general trend, PRx values were highly positive initially, declined between days 1–3 and then rebounded to higher levels over the next 7-10 days (46, 147). The acutely elevated PRx levels (days 0–3) may indicate (or contribute to) the extent of early brain injury (152), while the delayed rise in PRx on day 4 and beyond is consistent with the timeframe that DCI clinically emerges (11).

The prognostic value of PRx measurements in SAH patients is not yet established. While several studies observe an association between higher PRx values and outcome parameters (46, 147, 150), others have not (148, 149, 151). Small numbers, variations in SAH severity and therapeutic interventions, different threshold values for abnormal PRx, technical differences (e.g., probe placement) and PRx calculation differences [e.g., signal averaging (149)] likely contribute to these discrepancies. In a 242 patient retrospective cohort study (46), higher PRx levels at 6.5–10 days post-SAH independently associate with unfavorable extended Glasgow outcome scores (GOS-E ≥4 at 12 months); interestingly, CPP levels *below* 90 mmHg (normal CPP target is 60-70 mmHg) also associated with unfavorable outcome. This potentially identifies a clinically significant augmentation of myogenic vasoconstriction, which would simultaneously induce a leftward shift in the upper limit of autoregulation (resulting in higher PRx values) and reduce perfusion (promoting ischemia at CPP levels of 60-70 mmHg). In support of this conclusion, Johnson et al., stratified SAH patients into high and low PRx values (≤0.1 vs. >1) and found that the high PRx group associated with lower CBF, despite the fact that both groups possessed similar/normal CPP and ICP levels (148). Interestingly,

TABLE 3 | Clinical studies utilizing the Transient Hyperemic Response Test (THRT) in subarachnoid hemorrhage patients.

References	Citation	Study size	SAH grade	Critical observations
Smielewski et al., 1995	(126)	52	WFNS 1-5	Negative THRT result (<1.09) correlated with worse WFNS grade and GOS.
Lam et al., 2000	(127)	20	WFNS 1-4	6/20 patients displayed a negative THRT result (<1.09) 1 day after surgery: 5 developed DIDs. 6/14 remaining patients had a negative THRT result 3–7 days post-surgery: none developed DIDs.
Rätsep and Asser, 2001	(128)	55	WFNS 1-5	A negative THRT result (<1.10) was found in 22–35% of assessments over 0–19 days post-SAH ictus. Negative THRT results peaked at 0–3 and 7–14 days. Negative THRT associated with unfavorable GOS (1-2).
Rätsep et al., 2002	(129)	50	WFNS 1-5	Negative THRT results (<1.10) were found in 33% of assessments over 0–18 days post-SAH ictus. Negative THRT results peaked at 0–3 and 7–14 days post-SAH. Negative THRT result associated with poor initial WFNS grade (>2), vasospasm and impaired consciousness.
Al-Jehani et al., 2018	(130)	15	Hunt-Hess 1-5	7/15 patients had a negative THRT result (<1.09). A negative THRT result predicts the development of symptomatic vasospasm (5/6).
Rynkowski et al., 2019	(131)	40	Not Defined	19/40 patients had a negative THRT result (<1.09). Negative THRT result correlated with Hunt-Hess score ≥4, higher APACHE II scores (12 vs. 3.5) and unfavorable outcome (mRS ≥4 at 6 months).

These studies included SAH patients only. In Rynkowski et al., Hunt-Hess scores were obtained for 11/40 patients. APACHE II, Acute Physiology And Chronic Health Evaluation II; DIDs, Delayed ischemic deficits; GOS, Glasgow outcome score; mRS, Modified Rankin score; SAH, Subarachnoid hemorrhage; THRT, Transient hyperemic response test; WFNS, World Federation of Neurosurgical Societies scale.

TABLE 4 | Clinical studies utilizing Pressure Reactivity Index (PRx) measurements in subarachnoid hemorrhage patients.

References	Citation	Study size	SAH grade	Critical observations
Svedung Wettervik et al., 2021	(46)	242	WFNS 1-5	PRx was >0 in SAH patients and tended to increase at 3–4 days post-ictus in patients with unfavorable outcome (GOS-E 1-4 at 12 months). High PRx values independently associate with unfavorable outcome.
Howells et al., 2017	(143)	129	Hunt-Hess 1-5	80/129 patients had an extraventricular drain opened during ICP/PRx measurements. An open drain did not corrupt ICP signal and conferred small, but significant improvements in PRx.
Gaasch et al., 2018	(147)	43	Hunt-Hess 2-5	PRx values are highest at day 0 post-ictus (0.31), decline and then rise at 4–10 days post-ictus. Patients with DCI and poor outcome (mRS 3-5 at 3 months) had higher PRx values compared to those without. High PRx values over 0–3 days post-ictus (0.21 vs. 0.08) associated with DCI and poor outcome.
Johnson et al., 2016	(148)	47	Hunt-Hess 1-5	Patients with PRx >1 had lower CBF than PRx ≤1 patients over 14 day assessment period. Dichotomized PRx groups did not associate with Hunt-Hess score or predict the development of DCI.
Eide et al., 2012	(149)	94	Hunt-Hess 1-5	PRx was higher (0.28) in patients who die (mRS 6), compared to mRS 0-2 (0.16) and mRS 3-5 (0.12) patients. PRx could not differentiate mRS 0-2 and mRS 3-5 patients. Amplitude correlation was a better predictor than PRx.
Bijlenga et al., 2012	(150)	42	WFNS 4-5	PRx at 0–2 days post-ictus was higher in patients who died within 3 months (0.10; 9/25) vs. survivors (−0.17; 16/25). PRx did not predict the development of vasospasm; PRx values were not significantly affected by vasospasm.
Barth et al., 2010	(151)	21	Hunt-Hess 2-4	PRx values were not statistically different between patients who developed infarcts (0.06; 8/21) vs. those who did not develop infarcts (0.10; 13/15). PRx did not correlate with ORx or FRx indies.

These studies included SAH patients only. With the exception of Eide et al., all studies were retrospective. DCI, delayed cerebral ischemia; FRx, flow reactivity index; GOS-E, Glasgow outcome score-extended; ICP, intracranial pressure; mRS, Modified Rankin score; ORx, oxygen reactivity index; PRx, Pressure reactivity index; SAH, Subarachnoid hemorrhage; WFNS, World Federation of Neurosurgical Societies scale.

neither of these studies found a significant relation between PRx or CBF and development of symptomatic DCI (46, 148).

Of the other continuous methods for determining cerebral autoregulation, it is worth elaborating on the TCD-based ***Systolic Reactivity Index (Sx)*** and ***Mean Reactivity Index (Mx)***, as these are non-invasive alternatives to PRx. Both Sx and Mx are similar to PRx, in that they correlate slow waves in CPP and CBF surrogates. For Sx and Mx, systolic blood pressure (Sx) and mean blood pressure (Mx) serve as surrogates of CPP, while MCA BFV serves as a surrogate of CBF. In a setting with intact autoregulation, CBF remains constant despite changes in blood pressure and consequently, MCA BFV remains constant; when autoregulation is compromised, CBF increases with pressure and hence, BFV in the MCA concomitantly increases. Like PRx, the Sx and Mx indices are calculated using a moving Pearson correlation, yielding a U-shaped autoregulatory relationship.

Although measuring Sx or Mx is non-invasive, the method has several caveats and limitations: (i) the technique is highly operator-dependent and requires expertise for reliable and reproducible measurements (153); (ii) the measurement is applicable only to the territories perfused by the MCA; (iii) although TCD equipment is readily available in critical care settings, TCD monitoring in critically ill patients is cumbersome and generally time-limited to 1 h (138, 142); (iv) like PRx, Mx and Sx are impacted by high ICP, presumably due to compression of intracranial veins (138); and (v) BFV only serves as a reliable surrogate for CBF if the MCA diameter remains constant during the course of measurement. Since the Mx and Sx measurements do not rely on absolute BFV measurements, MCA vasospasm does not disrupt the measurement and thus, Mx, Sx and the presence of MCA vasospasm (profoundly accelerated flow velocity) can be derived from the same recordings (21). Interestingly, PRx and Mx only display a modest correlation to each other ($r = 0.36$ to 0.58), which likely reflects territorial differences (i.e., global vs. regional), measurement susceptibility to ICP and differences in model assumptions (138, 142).

Only a handful of studies have used Mx or Sx in SAH patients (**Table 5**) (21, 154–156). In these studies, the majority of SAH possessed elevated Mx or Sx values (21, 154, 155), although in one study, the elevated values were only found in patients who developed DCI (154). Only one study completed daily measurements over an extended time course and observed that Sx increased between days 2 and 8 in patients who develop DCI and then decline thereafter (154). Both Sx and Mx increase in the presence of vasospasm, indicating compromised autoregulation within the downstream microcirculation. In terms of prognostic value, Sx or Mx measurements in SAH patients successfully predict DCI (22, 154, 155); no studies have attempted to associate Sx or Mx values to longitudinal outcome scores in SAH patients. Taken together, these data show reasonable agreement with PRx in terms of the prevalence and time course of disrupted autoregulation and correlation to negative outcomes.

It should be mentioned that slow waves in blood pressure and TCD-based MCA BFV have been also analyzed with a transfer function analysis, instead of the moving Pearson correlation that generates the Mx and Sx values. Simplistically, a transfer function is Fourier decomposition of input and output signals that are transformed into sinusoids with the same frequency, but a different amplitude (gain) and a latency (shift in time; phase); a coherence function identifies conditions where estimates of gain and phase are reliable (157). When cerebral autoregulation is intact, the resistance arteries prevent/dampen the transmission of pressure fluctuations into cerebral flow (low gain and high phase). In contrast, when autoregulation is compromised, pressure fluctuations are rapidly transmitted as flow responses (high gain and low phase). Otite et al. demonstrate that higher transfer function gain and phase in SAH patients associates with angiographic vasospasm and DCI (158).

Of the remaining continuous autoregulation measures available, the ***Oxygen Reactivity Index*** (correlation between slow waves in oxygen saturation and blood pressure) (114) deserves a brief mention. ORx has been assessed in SAH patients, using either an invasive oxygen probe (23, 24) or by minimally invasive near infra-red spectroscopy (NIRS) (154, 159). Budohoski et al. (154) conducted Sx measurements in parallel with ORx measures and found a similar time course for autoregulation impairment and predictive value for DCI. Oxygen reactivity measures appear to predict the development of DCI (154, 159), delayed infarction (24) and unfavorable Glasgow outcome score (GOS $\leq$3) (23) in SAH; however, the invasiveness and/or availability of NIRS equipment likely prohibits the widespread use of this method in a clinical setting.

Summary of Clinical Data

Collectively, a large body of clinical data strongly support the conclusion that cerebral blood flow autoregulation is perturbed in SAH patients: this is not necessarily a surprising revelation. However, many issues hamper the overall interpretation of the literature and the utility of autoregulatory assessment as a prognostic indicator. Most notable among these issues are (i) the absence of a "gold standard" autoregulation measurement, (ii) the sparsity of studies utilizing multiple assessment techniques, and (iii) the diversity in patient populations and outcome measures. It can be argued that there is no "gold standard" method for measuring cerebral autoregulation, as every method has limitations (**Table 6**). Yet, the vast majority of clinical studies rely on a single approach to measure autoregulation, with ease-of-collection (or more accurately, the ability to collect data with minimal patient disturbance) moving to the forefront of practical considerations. With this in mind, it is worth acknowledging some of the key challenges and knowledge gaps with respect to clinical autoregulation measurements and its clinical use.

First, static, dynamic, and continuous measurement assess different aspects and timescales of autoregulation: these may not be equally affected in pathological settings (160, 161). Comparing different methodologies, therefore, is impossible until we better define how the different assessment methods interrelate. Second, the brain has significant regional differences in vascular architecture and metabolic demand: thus, it is not surprising that regional differences in cerebral autoregulation exist in both normal (59) and pathological settings (101, 122). To add to this complexity, metabolic factors such as CO_2 can profoundly alter autoregulation through direct actions on vascular reactivity (162): these effects would also

TABLE 5 | Clinical studies utilizing Mean Flow Velocity Index (Mx) or Systolic Flow Velocity Index (Sx) measurements in subarachnoid hemorrhage patients.

References	Citation	Study size	SAH grade	Critical observations
Soehle et al., 2004	(21)	32	WFNS 1-5	Baseline Mx and Sx values in SAH patients were similar to previously reported values for healthy volunteers. Vasospasm (15/32 patients) significantly increased both Mx and Sx values.
Budohoski et al., 2012	(154)	96	WFNS 1-5	Sx values are higher in patients who develop DCI (0.09; 32/98) vs. those who do not (0.00; 66/98). Higher Sx values at days 0–5 post-ictus independently predict DCI, but not vasospasm.
Calviere et al., 2015	(155)	30	WFNS 1-3	Mx within 4 days and at 7 days post-SAH ictus, but not at 14 days post-ictus, is higher compared to previously reported values for healthy volunteers. Mx alone did not predict the development of DCI. Worsening Mx, combined with the presence of vasospasm, predicted the development of DCI.
Zweifel et al., 2010	(156)	27	WFNS 2-5	13/51 individual Mx measurements indicated disturbed autoregulation (Mx >0.15). Mx correlated with TOx measurements when both recordings time-averaged over the recording interval. Non-averaged correlations were highly variable.

These studies included SAH patients only. DCI, delayed cerebral ischemia; Mx, Mean flow velocity index; SAH, Subarachnoid hemorrhage; Sx, Systolic flow velocity index; TOx, Tissue oxygenation index; WFNS, World Federation of Neurosurgical Societies scale.

be regional, as they should be more pronounced in ischemic regions compared to non-ischemic regions. Methodologies with limited spatial resolution will be unable to resolve regional and focal differences in autoregulation, thereby reducing their sensitivity and predictive capabilities. Third, determining the time course of autoregulatory impairment in different SAH patient populations (i.e., different severities) and more firmly establishing its relationship to DCI and other outcomes would require a significant, multi-center research undertaking; however, this information is critical for enabling accurate risk stratification that would direct clinical management. Finally, while identifying autoregulatory perturbation may indicate that an intervention is required, it does not inform the clinician with respect to *how to respond*. Thus, there is a clear need to elucidate the molecular mechanisms that perturb autoregulation in SAH. Without this knowledge, interventions will remain "blunt instruments" with some, but limited efficacy.

CLINICAL INTERVENTIONS FOR ISCHEMIA IN SAH

In the distant past (45–50 years ago and beyond), aneurysmal rebleeding was the primary cause of mortality and morbidity in SAH patients who survived the initial aneurysmal rupture. The development of aneurysm clips and effective microsurgical techniques (163, 164), pioneered in 1911 by Harvey Cushing's invention of the silver clip (165), significantly improved aneurysmal rebleeding rates. More recently, endovascular coiling has emerged as a less invasive alternative to surgical clipping: the aneurysm is accessed with a microcatheter and platinum coils are deployed into the aneurysm, stimulating the formation of a clot that permanently occludes the aneurysm (166, 167). Although re-bleeding remains a significant risk for SAH patients (11), cerebrovascular constriction and ischemia has now become the primary cause of death and disability in SAH patients who survive the initial rupture (1, 11, 12). This ischemic event is commonly termed DCI or "*delayed ischemic neurological deficit,*" due to its emergence 3–14 days post-SAH ictus (11, 12). It may also be referred to as "*symptomatic vasospasm*" or "*clinical vasospasm,*" due to its overlap with the emergence of angiographic vasospasm (13). Regardless of the term used, the clinical criteria for diagnosing DCI is "*the occurrence of focal neurological impairment (e.g., hemiparesis, aphasia, apraxia, hemianopia, or neglect), or a decrease of at least 2 points on the Glasgow Coma Scale (either on the total score or on one of its individual components [eye, motor on either side, verbal]) that lasts for at least 1 h, is not apparent immediately after aneurysm occlusion and cannot be attributed to other causes by means of clinical assessment, CT or MRI scanning of the brain, and appropriate laboratory studies.*" At present, there are only 2 interventions used to treat DCI: hyperdynamic therapy and the calcium channel antagonist nimodipine (168).

Hyperdynamic Therapy

Hyperdynamic therapy endeavors to alleviate ischemia by increasing the CPP, sometimes in combination with altered blood rheology (169). The combined therapy is referred to as "*Triple H Therapy,*" as it includes *hypertension*, *hypervolemia,* and *hemodilution* as core elements (169, 170). Vasopressors, typically phenylephrine, norepinephrine or dopamine, are used to induce hypertension. Hypervolemia is induced using colloid solutions containing albumin, hexastarch, dextrans, or gelatins and serves two functions: it adds to the hypertension and induces a state of hemodilution (i.e., reduced hematocrit). There are two distinct rationales underpinning these interventions: (i) the hypertension aspect assumes that cerebral autoregulation is absent or profoundly dysfunctional in ischemic regions and thus, flow will increase in a manner proportional to CPP; and (ii) according to the Hagen–Poiseuille law, flow should increase following hemodilution, because blood viscosity decreases.

The use of hypertension for treating neurological symptoms has a long history. In 1951, Denny-Brown recognized that

TABLE 6 | Comparison of clinically utilized techniques to measure cerebral autoregulation in subarachnoid hemorrhage patients.

		CBF Measurement Properties				
Technique	**Invasiveness**	**Spatial resolution**	**Relative/ Absolute**	**Snapshot/ Continuous**	**Significant limitations**	**References**
Thermal Conductivity Probe	Invasive	Regional level	Absolute	Continuous	Measurements limited to cranial surgeries. Measurement are not completed at bedside.	(20, 117)
Carotid Artery Flow Probe	Invasive	Low/Global level	Absolute	Continuous	Measurements limited to cranial surgeries. Requires surgical implantation of flow probes. Measurements are not completed at bedside.	(119)
^{133}Xe Computed Tomography	Minimally or Non-Invasive	High/Local level	Absolute	Snapshot	Rapid washout limits the number of views/projections per trial. Soft tissue may attenuate signals, especially in anterior images. Method requires specialized equipment. Measurements are not completed at bedside.	(101, 120, 122, 123)
Magnetic Resonance Imaging (MRI)	Minimally Invasive	High/Local level	Absolute	Snapshot	Long scan times required to obtain measurements. Very expensive equipment required. Measurements are not completed at bedside.	(124)
^{15}O Positron Emission Tomography	Minimally Invasive	High/Local level	Absolute	Snapshot	Long scan times required to obtain measurements. Very expensive equipment required. Measurements are not completed at bedside.	(125)
Transcranial Doppler	Minimally Invasive	Regional level	Relative	Continuous	Assumes that insonified artery diameter remains constant. Not a reliable measure of CBF.	(118)
Transient Hyperemic Response Test	Minimally Invasive	Regional level	Relative	Snapshot	Highly prone to inconsistency. Assumes that MCA diameter remains constant.	(126–131)
Pressure Reactivity Index (PRx)	Invasive	Low/Global level	Relative	Continuous	ICP measurements are invasive, but may already be included in standard of care. Decompressive craniotomy or ventricular drains may compromise ICP measurements. Measurements when ICP is high are likely unreliable	(46, 143, 147–151)
Systolic Flow Velocity Index (Sx) or Mean Flow Velocity Index (Mx)	Non-invasive	Regional level	Relative	Continuous	Assumes that insonified artery diameter remains constant. Not a reliable measure of CBF. Requires a highly-qualified operator. Cumbersome to complete at bedside.	(21, 154–156)

In this table, invasive techniques require surgical access, while minimally invasive techniques require injections (intravenous or intraarterial). CBF, cerebral blood flow; ICP, intracranial pressure; MCA, middle cerebral artery.

hypotension caused rapid neurological deterioration in patients suffering from cerebral artery disease: consequently, he proposed that raising systemic blood pressure would alleviate the cerebrovascular insufficiency and hence, the symptoms (171). Denny-Brown's postulate was not acted upon until 1967, when Farhat and Schneider used hypertension to successfully treat hemiparesis in a case series of 4 patients with cerebrovascular insufficiency (172). In some cases, a modest blood pressure elevation was sufficient to reverse ischemic symptoms (from 110/70 to 150/100 mmHg), while in other patients, rather extreme levels of hypertension were utilized (250/120 mmHg) (172). The major impediment to using hypertension in SAH patients was the significant risk of rebleeding; however, advancements in surgical methods to definitively occlude the aneurysm (i.e., clipping) opened the door for this therapeutic approach. In 1976, Kosnik and Hunt demonstrated that hypertension improved DCI symptoms in 6 of 7 surgically clipped SAH patients (173), setting the stage for what would ultimately become its routine use in SAH.

Neither Triple H therapy, nor any of its individual components, have ever been subjected to large prospective randomized clinical trials and consequently, the evidence of benefit is limited to small studies or case reports that are frequently uncontrolled and utilize different protocols. Gathier et al. planned a 240 patient randomized trial to assess the effect of hypertension on patients presenting clinical symptoms of DCI; however, the trial was prematurely halted due to slow enrollment (174). Several prior studies, however, suggested that the treatment outcomes with hypertensive or Triple H therapy are better than not intervening at all (123, 175–189). As examples: in 9 studies reporting the clinical response to hypertension in 187 SAH patients, improvement of neurological deficits ranged

from 50 to 100%, with most studies reporting improvement in around 80% of patients (123, 173, 175, 176, 181–185); in 5 studies reporting long-term functional outcome at 2 to 6 months (141 patients), a good functional outcome was seen in 38 to 54% of the patients (181, 186–189). Thus, there was an impetus to incorporate the procedure into the standard of care, despite the lack of rigorous data. As documented in the 1994 and 2009 AHA guidelines for managing SAH patients (190, 191), the use of Triple-H therapy was recommended as "*a reasonable approach for treating symptomatic vasospasm*" until relatively recently. The hypervolemia component has since fallen out of favor in revised AHA therapy guidelines (168). Hypervolemia is a physiological stressor that is associated with a high incidence of adverse side effects, including: profound diuresis (176), electrolyte abnormalities (192), reflexive bradycardia (176), pulmonary edema (169, 193), dilutional coagulopathy (194), renal dysfunction (194), and cardiac failure due to fluid overload (169). Not surprisingly, some studies now indicate that positive fluid balance is associated with negative functional outcomes in SAH patients (189, 195). The revised AHA guidelines (2012) recommend (i) maintaining euvolemia and normal circulating blood volume; and (ii) inducing hypertension in patients with delayed ischemia, unless blood pressure is elevated at baseline or cardiac status precludes it (168). Interestingly, Triple H therapy, which includes the adverse effect-prone hypervolemia aspect, is still used in some clinical settings (46). The 2012 guidelines (168) remain the current standard (196), despite: (i) several recent studies challenging the notion that hyperdynamic therapy confers benefit to SAH patients suffering ischemia (197–201); (ii) systematic reviews concluding that the available evidence, which is rated "moderate-to-low grade," does not support a recommendation (202–205); (iii) a relatively high rate of serious complications, such as cardiac arrhythmia, pulmonary edema, hemorrhagic transformation, and intracranial bleeding (181, 185); and (iv) the risk of cerebral edema developing in response to induced hypertension (39).

In the context of autoregulation, hyperdynamic therapy faces a number of significant challenges. First, as discussed previously in section 2.1, there is high inter-subject variability in the upper and lower limits of autoregulation (40); in SAH patients, this is coupled with a variable degree of perturbation (**Figure 2**). Hence, there is no "universal threshold" that can adequately guide clinicians with respect to effective and/or safe hypertension limits. In the absence of a reliable, real-time CBF measurement, titrating hyperdynamic therapy would require incrementally increasing pressure until neurological benefit is achieved (i.e., presumably by monitoring conscious SAH patients). Pragmatically, clinicians simply use a target pressure, with the assumption *and hope* that this will translate into improved perfusion (204).

Second, cerebral autoregulation is not uniform throughout the brain under normal conditions (59), and autoregulatory dysfunction in SAH is clearly heterogenous (101, 122). Thus, the systemic nature of hyperdynamic therapy undoubtedly elicits variable effects in different brain regions: under-perfused regions may enjoy an increase in CBF (if the hypertension is sufficient to do so), but other regions may become hyperperfused (i.e., above the upper limit of autoregulation) and prone to injury from the high pressure (206–209). These conditions, which include posterior reversible encephalopathy syndrome (PRES) and reversible leukoencephalopathy (RLS) are both causes of altered neurological function during hyperdynamic therapy that may mimic worsening DCI (206–209). This raises an interesting conundrum: since PRES and RLS are not widely reported as complications of hyperdynamic therapy, continued neurological deterioration may be interpreted as uncorrected hypoperfusion and provoke even more aggressive blood pressure augmentation, which would only further exacerbate injury. On a similar note, in cases of severe microcirculatory constriction (**Figure 2A**), it is possible that the only means of increasing perfusion is to breach the upper limit of autoregulation, potentially setting the stage for vasogenic edema (39). Thus, hyperdynamic therapy may benefit some SAH patients suffering from cerebral ischemia, but in many cases, the improper titration of the therapy and regional variability makes it likely that it simply substitutes another form of brain injury in the place of ischemic injury. This may partially explain why recent meta-analyses generally fail to identify improvement or harm resulting from the therapeutic intervention (202–205).

Finally, there is a presumption that the vasopressors used to induce hypertension do not appreciably alter cerebrovascular tone. Under non-pathological conditions, systemic catecholamines do not cross the blood-brain barrier and hence, increasing systemic blood pressure with norepinephrine or epinephrine does not increase CBF (210), until the upper limit of autoregulation is passed. In SAH, the blood-brain barrier is likely to be disrupted (211), permitting systemically-applied vasopressors access to the cerebrovascular smooth muscle cells, where they can then exert direct effects. This is one possible explanation for the observations by Darby et al., where certain non-ischemic regions paradoxically decreased perfusion in response hyperdynamic therapy (a potential *intracerebral steal phenomenon*) (122).

In summary, hyperdynamic therapy is a "last resort" intervention, because the underlying mechanisms causing the microcirculatory constriction are not understood. Thus, there are few options available to increase CBF when symptoms of ischemic injury occur. Hyperdynamic therapy, therefore, attempts to override the constriction with high pressure: this may increase CBF, but with risks of both systemic and central nervous system injury. The evidence supporting hyperdynamic therapy as an intervention is weak (196, 202–205) and the methods and manner of administrating the therapy are highly variable (212). Nevertheless, hyperdynamic therapy appears destined to remain a routine intervention for DCI, until a clearly superior alternative is discovered.

Nimodipine

Nimodipine is the only FDA-approved medication for use in SAH: it belongs to the dihydropyridine (DHP) class of calcium channel blockers that inhibit L-type, voltage-sensitive calcium channels. The blockade of voltage-gated L-type calcium channels strongly impacts depolarization-stimulated vasoconstriction (213, 214), a core requirement for myogenic

vasoconstriction (68). Nimodipine is rapidly absorbed from the gastrointestinal tract following oral administration and reaches peak plasma concentrations within 1 h. However, nimodipine undergoes extensive first-pass metabolism in the liver and its bioavailability following oral administration is reported to be ∼13% (215, 216). Due to metabolism, nimodipine is rapidly eliminated, with an initial half-life of ∼1-2 h (215, 216). Hence, nimodipine must be administered frequently (every 4 h orally) or through continuous intravenous infusion.

In order to increase cerebral perfusion, cerebrovascular resistance must decrease relative to systemic resistance. Nimodipine is characterized as a "preferential cerebrovascular dilator," with several reports demonstrating that nimodipine stimulates an increase in cerebral blood flow at concentrations that either do not alter systemic blood pressure or elicit only modest reductions (217–220). This cerebrovascular dilatory action is preferentially exerted on small vessels (<70 μm) and there is no obvious effect on veins (220–223). Several aspects may contribute to this preferential effect:

First, nimodipine is more lipophilic than most other DHP antagonists and other calcium channel blockers, which enables it to cross the blood brain barrier: this is an obvious prerequisite for cerebrovascular efficacy. Although nimodipine crosses the blood-brain barrier, its concentration in cerebrospinal fluid (CSF) is much lower than in plasma (10-250x lower in CSF relative to plasma) (224–226). It is generally assumed, therefore, that nimodipine does not significantly bind to CSF proteins [95% of plasma nimodipine is protein-bound (215)] and is therefore absorbed by membrane structures or neuroglia within the brain. While membrane nimodipine concentrations may indeed be higher than CSF levels, the idea that nimodipine *accumulates* in cerebral cell membranes is largely not supported by available evidence: nimodipine possesses a relatively low partition coefficient, can easily wash out of membranes and has a short clinical half-life (227); radiolabeling distribution patterns show low concentrations in the brain (228). Nimodipine's cerebrovascular preference, therefore, is not likely due to a preferential distribution to the brain.

In the absence of a distribution effect (i.e., higher nimodipine concentrations in the brain), the cerebrovascular preference might entail a higher sensitivity to L-type calcium channel inhibition relative to peripheral arteries. This conclusion is primarily based on comparisons of agonist-stimulated responses (e.g., serotonin) in basilar and saphenous arteries (213, 214). However, the evidence that myogenically active cerebral resistance arteries are more sensitive to L-type calcium channel inhibition due to its ion channel composition is not clear. A systematic comparison of peripheral and cerebral artery channel expression that could more definitively address this issue is lacking.

Finally, the myogenic response is highly dependent on membrane potential, voltage-gated calcium channels, and calcium influx (68, 229, 230). Thus, vascular beds that have a high degree of autoregulation may be more susceptible to L-type calcium channel blockade, due to a more profound effect on its myogenic mechanism. Consistent with this premise, nimodipine preferentially increases both cerebral and coronary blood flow in rabbits (218): both are highly autoregulated vascular beds. Nimodipine's vasodilative effect is more pronounced in smaller arteries, which are more myogenically active than larger vessels (221, 222).

The FDA approved nimodipine for use in SAH in 1988. At the time, many of the studies supporting the use of nimodipine were "non-comparative" and relied on historical data to drive conclusions regarding the effect of nimodipine. Some notable examples of these non-comparative studies include Ljunggren et al. (231) and Auer et al. (232). While these studies generally supported the use of nimodipine therapy, their reliance on historical data as a comparator rendered them incapable of providing sound data pertaining to the overall efficacy of the nimodipine treatment. There were, however, 6 randomized placebo-controlled trials that clearly demonstrated an improvement in either neurological outcome or mortality (225, 233–237); an additional small trial that directly compared treated and untreated patients also demonstrated benefit (238) (**Table 7**). Long term survival assessments indicate that nimodipine reduces 3-month mortality and cerebral infarction in SAH patients (239, 243).

Since nimodipine possesses vasodilatory properties, a vascular mechanism was presumed. However, there is scant evidence for an effect on cerebral perfusion in SAH patients. Only 2 of the controlled trials (1 placebo controlled) that preceded FDA approval conducted CBF measurements: neither found evidence that nimodipine increased cerebral perfusion (235, 238). In 4 studies, angiographic vasospasm was assessed: in 1 trial, nimodipine reduced the severity of angiographic vasospasm in patients with severe neurological outcomes (225); however, the remaining trials showed no difference in the incidence or severity of angiographic vasospasm (233–235). In summary, the FDA approved nimodipine based on solid evidence that it improves neurological outcomes and mortality after SAH across all grades, except perhaps for the most severe cases (244); however, there is minimal-to-no evidence that nimodipine improves cerebral perfusion as its mechanism of action (**Table 7**). It is also notable that nimodipine is not an effective treatment for acute ischemic stroke (245) or traumatic brain injury (246), both of which involve ischemic injury as a component of the pathologies.

Only a handful of studies have examined the effect of nimodipine on cerebral autoregulation in humans and animal models (240, 247–249): the majority of these studies found that nimodipine has no effect on CBF autoregulation; in one experimental study, nimodipine improved cerebral autoregulation in rats following SAH (measured by ^{133}Xe clearance) (250). For obvious reasons, nimodipine has not been rigorously trialed against a placebo in SAH patients to determine its mechanism of action. While there is some evidence that nimodipine treatment increases cerebral perfusion in healthy volunteers (219, 247), only a handful of studies have attempted to determine whether nimodipine increases cerebral perfusion in SAH patients (235, 238, 240–242): these trials are difficult to interpret, due to the lack of an untreated control. Of the trials that use reasonably reliable CBF measurement methods (e.g., ^{133}Xe clearance), the results are generally unsupportive of a perfusion effect (**Table 7**).

TABLE 7 | Clinical studies involving nimodipine treatment in subarachnoid hemorrhage patients.

References	Citation	SAH grade	Study size	Nimodipine dose	Placebo?	Primary endopoints	CBF measured?	Critical observations
Allen et al., 1983	(225)	Not Defined	116 (56 treated)	0.35 mg/kg/4 h	YES	Neurologic, Radiographic	NO	Nimodipine reduced the incidence of severe neurological deficits, including death. Nimodipine reduced vasospasm in patients with severe outcomes, but not normal outcomes.
Philippon et al., 1986	(233)	Hunt-Hess 1-3	70 (31 treated)	60 mg/4 h	YES	Neurologic, Radiographic	NO	Nimodipine reduced neurological deficit severity when vasospasm was present. Nimodipine did not affect the incidence of neurologial deficits or vasospasm.
Petruk et al., 1988	(234)	Hunt-Hess 3-5	154 (72 treated)	90 mg/4 h	YES	Neurologic, Radiographic	NO	Nimodipine improved Glasgow Outcome Scores in Hunt-Hess 3-4 patients. Nimodipine significantly reduced neurological deficits associated with vasospasm. Nimodipine did not influence incidence or severity of vasospasm.
Mee et al., 1988	(235)	All Grades on	50 (25 treated)	60 mg/4 h	YES	Neurologic, Radiographic, CBF	**YES**	Nimodipine reduced mortality, but did not change the proportion of good/poor outcomes.
		Custom Scale						Nimodipine did not affect the incidence of vasospasm and did not change CBF.
Jan et al., 1988	(236)	Hunt-Hess 1-5	127 (73 treated)	0.03 mg/kg/h	YES	Neurologic	NO	Nimodipine improved neurological outcome in patients with vasospasm.
Pickard et al., 1989	(237)	Hunt-Hess 1-5	554 (278 treated)	60 mg/4 h	YES	Neurologic, Infarction	NO	Nimodipine reduced cerebral infarcts and poor outcomes; there was a strong tendency for reduced mortality.
Messeter et al., 1987	(238)	Hunt-Hess 1-3	20 (13 treated)	topical/i.v.	NO	Neurologic, CBF	**YES**	Nimodipine did not alter CBF, but it improved neurological outcome.
Ohman et al., 1991	(239)	Hunt-Hess 1-3	213 (109 treated)	0.03 mg/kg/h	YES	Neurologic, Infarction	NO	Nimodipine reduced mortality, but did not change the proportion of good/poor outcome.
								Nimodipine reduced the incidence of cerebral infarcts and DCI.
Rasmussen et al., 1999	(240)	Hunt-Hess 3-5	8 (pre/post)	0.03 mg/kg/h	NO	CBF, autoregulation, $CRMO_2$	**YES**	Nimodipine did not alter CBF or autoregulation. Nimodipine may improve $CRMO_2$ during hypotension.
Choi et al., 2012	(241)	Hunt-Hess 3-5	16	30–60 mg/4 h	NO	MAP, CBF	**YES**	Each nimodipine dose caused small decreases in MAP and CBF.
Hänggi et al., 2008	(242)	WFNS 1-4	26 (pre/post)	Intra-arterial	NO	CBF, radiographic	**YES**	In patients with severe vasospasm refractory to systemic nimodipine, intra-arterial nimodipine transiently reduced vasospasm and increased perfusion.

These studies included SAH patients only. CBF, Cerebral blood flow; $CRMO_2$, cerebral metabolic rate of oxygen; DCI, delayed cerebral ischemia; MAP, mean arterial pressure; SAH, Subarachnoid hemorrhage; WFNS, World Federation of Neurosurgical Societies scale.

Rasmussen et al. measured CBF in patients with severe SAH prior to and following nimodipine treatment and observed no effect on CBF or cerebral autoregulation (240). Choi et al. measured CBF following successive nimodipine dosing and generally found marginal reductions in CBF with each dose, concomitant with reductions in MAP (241). Hänggi et al. demonstrated that intra-arterial administration of nimodipine improved perfusion in patients with refractory vasospasm, but only transiently (242).

The absence of a clear vascular effect has spurred the search for non-vascular mechanisms of action that could explain nimodipine's beneficial effect in SAH. The attenuation of cortical spreading depolarizations is one potential non-vascular mechanism that has received significant attention (251). Spreading depolarizations are slow propagating waves of neuronal and glial mass depolarization that can occur when brain tissue is exposed to noxious stimuli following neurological injury (251). Under normal conditions, the depolarization is associated with a contaminant increase in regional CBF, to match the increased metabolic demand. However, after SAH and ischemic stroke, the oligemic response is converted to a ischemic response, resulting in paradoxical vasoconstriction and spreading

ischemia. Since neurons express high levels of L-type calcium channels (252), nimodipine could directly protect neurons by inhibiting these spontaneous depolarizations. In support of this potential mechanism of action, spreading depolarizations are known to occur in SAH patients and are associated with delayed ischemic injury (253, 254); subarachnoid blood can acutely trigger spreading depolarizations that cause infarctions (255); and nimodipine is capable of attenuating spreading depolarizations (256, 257). Nimodipine can directly protect neurons from ischemic damage by this mechanism (258, 259) and could prevent electrical changes in response to oxygen/glucose deprivation (260). Taken together, there is a reasonable basis to propose that direct neuroprotection explains nimodipine's positive effect in SAH.

While a neuroprotective mechanism can confer benefit during ischemic episodes in SAH, directly targeting the perfusion deficit (i.e., the original intent of the treatment) would undoubtedly be more effective. However, globally targeting the cerebral microcirculation with a vasodilator has many of the same shortcomings as hyperdynamic therapy. Specifically, there is both normal or pathological heterogeneity in autoregulatory status within the cerebral microcirculation: thus, global treatment could undermine autoregulation in regions where it functions properly, potentially leading to hyperperfusion, edema and/or potentially, a *steal phenomenon*. It should also be noted that since the myogenic response, the basis of autoregulation, depends on L-type calcium channels (68, 229, 230), careful titration would be required to maintain autoregulatory function. As an illustration, Hockel et al. delivered nimodipine as a continuous intra-arterial infusion *via* the carotid artery, in order to maximally deliver a high nimodipine dose to the cerebral microcirculation (261). The authors measured an increase in PRx and oxygen tension, suggesting a vascular effect, albeit the overall effect was transient (6 h) (261). The increase in PRx value indicates deteriorated autoregulation, which should not occur unless the treatment compromises autoregulation as a whole (i.e., the myogenic mechanism may be ablated in some regions).

In summary, it appears unlikely that orally administered nimodipine elicits significant and sustained cerebrovascular dilation and increased perfusion. As a consequence, a neuroprotective mechanism is now favored. While it would be preferable to target the vascular mechanism, the global use of vasodilators is problematic and there are currently no alternative approaches available.

DISCUSSION

Cerebral autoregulation is a crucial homeostatic mechanism: its disruption in SAH can profoundly compromise cerebral perfusion and consequently, cause ischemic injury. Autoregulatory status can be measured in a clinical setting: while these measures are generally predictive of outcome, future efforts need to establish a "gold standard" procedure with sufficient numbers in order provide appropriate diagnostic and prognostic guidance. However, the absence of interventions that can correct perturbed autoregulation is a dire problem: a substantial research investment is required on this front, as the number of interventional options at the clinician's disposal is limited.

As reviewed by Daou et al., an array of pharmacological interventions have been tested for efficacy in SAH (262). Many of these interventions displayed early promise in reducing ischemic injury in SAH, only to later fail in larger trials: some notable examples include clazosentan (endothelin-1 receptor blocker) (15–18), nicardipine (263), magnesium (voltage-dependent calcium channel blocker) (264, 265), statins (pleiotropic vascular and neuroprotective effects) (266, 267), tirilizad (antioxidant) (268), and erythropoietin (pleiotropic vascular and neuroprotective effects) (269, 270). Given that the mechanisms underlying SAH-induced microvascular dysfunction have not been adequately defined, these interventions were predicated on their known vascular effects and/or their successful use in other pathological settings. However, since the etiology of microvascular dysfunction in SAH is largely uncharacterized and probably multifactorial, the failure to properly target a causal mechanism undoubtedly contributed to these interventions' lack of efficacy.

There are few studies that systematically investigate how myogenic reactivity, the underlying basis of autoregulation, changes in SAH (87, 93, 95, 96, 98–100). Isolating and cannulating small resistance arteries that are 0.1 mm in diameter and 0.5–0.8 mm in length is time consuming and technically demanding work; it is difficult to conduct biochemical assessments on artery samples, as the tissue amounts are highly limited; and molecular manipulations are generally limited to testing arteries from gene deletion models. As a consequence, only a small number of researchers utilize pressure myography as a core research technique and from there, only a small proportion of these researchers study SAH, as it is considered an orphan disease. In the current research climate, where high-throughput projects are favored for funding, it is hard to attract new researchers into this challenging discipline, despite the desperate need.

Based on the available myogenic reactivity studies utilizing SAH models, several potential therapeutic targets have been proposed (**Figure 3**), including Kv channels, tumor necrosis factor (TNF), S1P receptor subtype 2 ($S1P_2R$), Rho-associated protein kinase (ROCK) and the cystic fibrosis transmembrane conductance regulator (CFTR). It is worth considering how these might fare as interventions (**Table 8**).

Several studies using isolated cerebral arteries (98) and/or primary smooth muscle cells derived from cerebral arteries (96, 98, 271) demonstrate that SAH reduces potassium currents, leading to enhanced depolarization and calcium entry in response to pressure (96, 100, 271). These results are buttressed by experiments demonstrating that oxyhemoglobin reduces potassium channel expression *in vitro* (272–274). The specific potassium channel types/subtypes affected have not been fully defined and may involve $K_v1.5$, $K_v2.1$, $K_v2.2$, K_v7, or BK channels (100, 271, 275, 276). Both K_v channel activators (e.g., retigabine) (276) and BK channel activators (e.g., zonisamide) (277, 278) are clinically available and have been used in experimental SAH settings; however, to our knowledge, these therapeutics

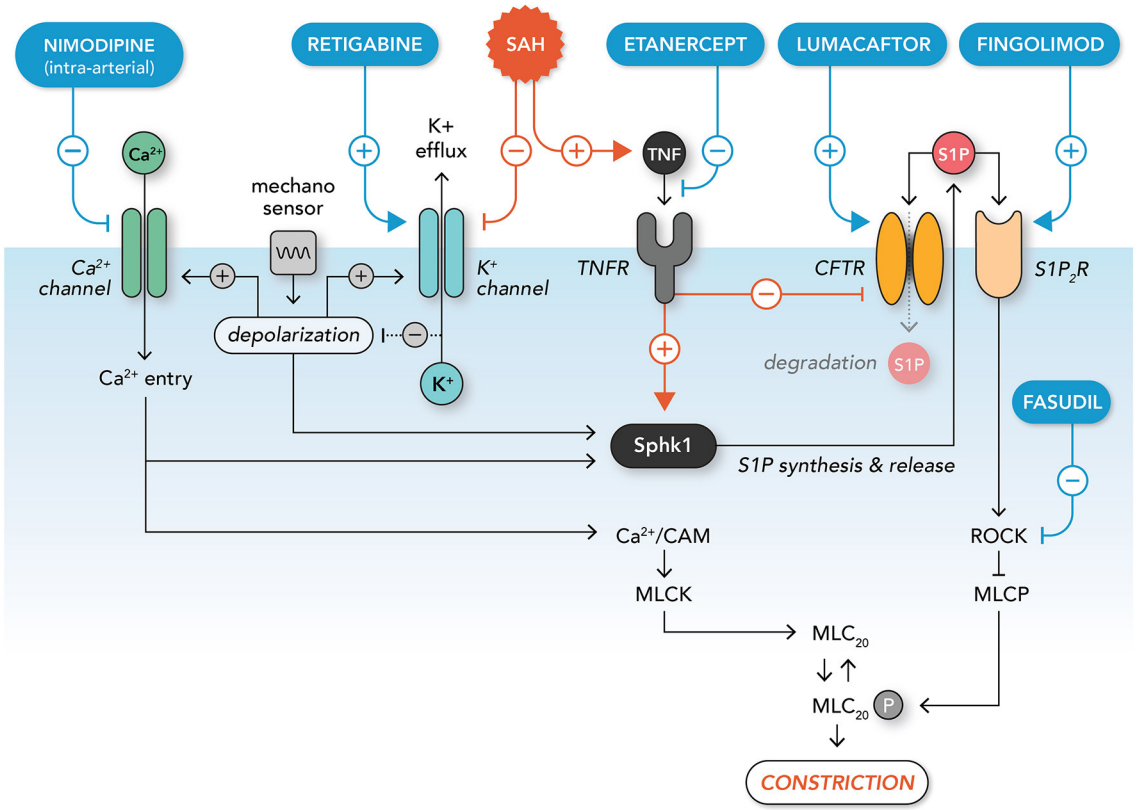

FIGURE 3 | Molecular mechanisms augmenting microvascular constriction in subarachnoid hemorrhage and potential interventions. A mechanosensitive complex initiates myogenic vasoconstriction *via* membrane potential depolarization: this leads to calcium entry *via* opening of voltage-gated calcium channels; voltage gated potassium channels also open, leading to hyperpolarizing potassium efflux that limits the extent of depolarization (negative feedback). Intracellular calcium activates calmodulin (CAM), myosin light chain kinase (MLCK) and the contraction apparatus. In addition, calcium entry and depolarization lead to the activation of sphingosine kinase 1 (Sphk1), which synthesizes and releases sphingosine-1-phosphate (S1P) into the extracellular compartment. Extracellular S1P activates the S1P2 receptor subtype ($S1P_2R$), thereby activating the Rho-associated protein kinase (ROCK) signaling pathway. ROCK signaling inhibits myosin light chain phosphatase (MLCP), which enhances MLCK's activation of the contractile apparatus. Extracellular S1P is sequestered from $S1P_2R$ by the cystic fibrosis transmembrane conductance regulator (CFTR), which transports S1P across the plasma membrane for degradation. In subarachnoid hemorrhage (SAH), potassium channels are down-regulated, leading to enhanced depolarization through disinhibition. SAH also stimulates inflammatory tumor necrosis factor signaling, which down-regulates CFTR expression and enhances the activation of Sphk1. This increases pro-constrictive S1P / $S1P_2R$ / ROCK signaling, which enhances constriction *via* the inhibition of MLCP. Therapeutics targeting these pathological processes include: (i) intra-arterially-delivered nimodipine (calcium channel blocker; limits calcium entry), (ii) retigabine (potassium channel activator; reduces depolarization), (iii) etanercept (inhibits TNF signaling; reduces S1P synthesis and increases S1P degradation), (iv) lumacaftor (increases CFTR expression; increases S1P degradation), (v) fingolimod (stimulates S1P receptor internalization; inhibits ROCK activation), and (vi) fasudil (ROCK inhibitor; limits inhibition of MLCP).

have not been utilized to clinically treat SAH. Both retigabine and zonisamide are typically used as anti-seizure medications and are associated with several adverse central nervous system effects, including somnolence, dizziness and confusion (279, 280). Further, Kv and BK channels are expressed in neurons and many other excitable cell types and thus, widespread adverse effects could occur. These issues probably preclude their use clinical use in SAH.

The remaining targets (TNF, S1P, $S1P_2R$, CFTR, and ROCK) may all be functionally linked into a pathological signaling chain (75). Briefly, our previous work shows that soluble TNF [i.e., TNF released *via* shedding (281–283)] enhances S1P signaling in cerebral arteries following SAH, by augmenting S1P synthesis and preventing S1P degradation (87, 93). Specifically, TNF enhances S1P synthesis *via* sphingosine kinase 1 activation (284); simultaneously, it reduces S1P degradation, *via* the down-regulation of CFTR protein expression (87, 93), a critical S1P transporter (285, 286) that sequesters S1P from its receptors (287). In cerebral vessels, S1P significantly enhances vascular tone and myogenic vasoconstriction (87, 285, 288–291), primarily *via* the $S1P_2R$ subtype (87). Mechanistically, $S1P_2R$ activation enhances calcium sensitivity (i.e., yielding more constriction for a given increase in intracellular calcium) *via* the activation of the ROCK signaling cascade (292).

There are several lines of evidence supporting TNF's role in SAH: (i) cerebrospinal TNF levels rise and peak 4–10 days post-SAH ictus (293–295), the timeframe when delayed autoregulatory disruption and ischemia generally occurs; (ii)

TABLE 8 | Potential interventions for treating dysfunctional autoregulation in subarachnoid hemorrhage.

Molecular target	Target function	Pathological mechanism	Intervention	Mechanism of action and potential negative effects on autoregulation
Potassium channels (Kv and BK)	Counteracts depolarization with a hyperpolarizing current	Channels are downregulated in SAH resulting in enhanced depolarization	Retigabine Zonisamide	Intervention activates potassium channels, thereby reducing cellular excitability. Overdosing potentially abolishes myogenic reactivity, thereby eliminating autoregulation. Intervention is not specific to myogenic reactivity or autoregulation.
Calcium channels (L-Type)	Permits extracellular calcium entry, which activates molecular effectors of cellular contraction.	Calcium influx is augmented in SAH due to enhanced depolarization	Nimodipine	Intervention attenuates depolarization-dependent calcium influx. Overdosing potentially abolishes myogenic reactivity, thereby eliminating autoregulation. Intervention is not specific to myogenic reactivity or autoregulation
$S1P_2R$	Enhances calcium sensitivity *via* ROCK-dependent inhibition of MLCP	Calcium sensitivity is augmented in SAH *via* enhanced S1P signaling	Fingolimod	Intervention reduces calcium sensitivity by antagonizing $S1P_2R$ signaling. Strong $S1P_2R$ antagonism may abolish myogenic reactivity, thereby eliminating autoregulation. Intervention is immunosuppressive.
ROCK	Enhances calcium sensitivity *via* MLCP inhibition	Calcium sensitivity is augmented in SAH *via* enhanced S1P signaling	Fasudil	Intervention reduces calcium sensitivity by inhibiting ROCK. Strong ROCK inhibition may abolish myogenic reactivity, thereby eliminating autoregulation.
TNF	Pathological mechanism only. Stimulates S1P production and downregulates CFTR expression.	Enhanced S1P signaling augments calcium influx and calcium sensitivity	Etanercept	Intervention normalizes myogenic reactivity and autoregulation by eliminating the pathological enhancement of S1P signaling. Intervention is immunosuppressive.
CFTR	Antagonizes $S1P_2R$ signaling by sequestering S1P away from receptors	Calcium sensitivity is augmented in SAH *via* enhanced S1P signaling	Lumacaftor	Intervention normalizes myogenic reactivity and autoregulation by eliminating the pathological enhancement of $S1P_2R$ signalling.

BK, calcium activated large conductance potassium channels; CFTR, Cystic fibrosis transmembrane conductance regulator; Kv, Voltage-gated potassium channel; MLCP, myosin light chain phosphatase; ROCK, Rho-associated protein kinase; SAH, subarachnoid hemorrhage; S1P, Sphingosine-1-phosphate; $S1P_2R$, Sphingosine-1-phosphate receptor 2; TNF, Tumor necrosis factor.

TNF levels associate with perturbed cerebral flow velocities and poor outcomes (293, 296, 297); and (iii) anti-TNF therapy (i.e., etanercept or adalimumab) reduces vascular constriction and/or neurological injury in experimental SAH (298–300). Likewise, cerebrospinal S1P levels are also substantially elevated in SAH patients (301) and attenuating S1P receptor activity, either with an $S1P_2R$ antagonist (JTE-013) (87) or fingolimod (stimulates S1P receptor internalization) (302, 303), improves perfusion and outcomes in experimental SAH. The ROCK inhibitor fasudil, which inhibits the downstream signals associated with $S1P_2R$ activation, is currently used prophylactically in Japan and China, with some clinical studies demonstrating evidence of benefit (304–306). Collectively, these data strongly support that SAH activates a pro-constrictive TNF/S1P signaling axis. It should be noted, however, that there is limited clinical trial data from which to draw from and the purported benefits of fasudil remain to be confirmed in large randomized controlled clinical trials (307).

There are no clinically approved $S1P_2R$ antagonists. Fingolimod is approved to treat multiple sclerosis (308) and has been clinically tested in small trials involving acute cerebral stroke (309) and intracerebral hemorrhage (310). While these stroke trials did not observe adverse effects associated with treatment (309, 310), fingolimod is known to be immunosuppressive and is associated with several adverse effects, including infections, elevated liver enzymes, central nervous system effects [e.g., headache, dizziness and in some cases, leukoencephalopathy (311)] and cardiac effects (bradycardia and atrioventricular block) (308). The immunosuppression and known adverse effects have likely deterred fingolimod's use in SAH clinical trials. Like fingolimod, TNF antagonists (e.g., etanercept, adalimumab) are also immunosuppressive and bear a high risk of permitting opportunistic infections (312); additionally, the large physical size of the therapeutics (∼150 kDa) would necessitate a compromised blood-brain barrier or intrathecal delivery in order to reach its targets within the brain. The immunosuppressive effects and risk of secondary infection probably deter the use of anti-TNF therapeutics. Fasudil appears to have reasonable safety in SAH patients (313). One possible drawback to fasudil treatment is that it likely

requires proper titration, as strong ROCK inhibition would compromise myogenic reactivity altogether (90); fasudil may also compromise myogenic responses in cerebral vessels that are not perturbed by SAH. As stated previously, fasudil's efficacy has not been conclusively ascertained (307), as no large, randomized controlled clinical studies have been undertaken.

This narrows the already short list of candidates to one intriguing entity: CFTR therapeutics (75). Experimentally, the CFTR "corrector" therapeutic lumacaftor (314) increases wild-type CFTR expression in cerebral arteries by a proteostatic mechanism (93, 315): this modification normalizes the augmented myogenic reactivity in cerebral arteries derived from mice with experimental SAH, but has no apparent effect in control/sham arteries (93). Not surprisingly, lumacaftor successfully increases cerebral perfusion and protects against neuronal injury in experimental SAH (93). Additionally, skeletal muscle resistance arteries do not appear to appreciably express CFTR (93, 316): since these peripheral arteries would not be affected by the CFTR therapeutics, the chances of developing hypotension in response to treatment appears to be limited. Collectively, this represents the quintessential "magic bullet" scenario, where the therapeutic specifically targets a pathological cerebrovascular mechanism.

CFTR therapeutics are generally considered safe and are well-tolerated, although this pertains to its use in cystic fibrosis patients. There is limited safety data available for non-cystic fibrosis patients; however, CFTR therapeutics have been shown to be well-tolerated in a small cohort of healthy volunteers (317) and smokers with chronic obstructive pulmonary disease (318). There are two important caveats to the use of CFTR therapeutics in SAH patients: first and foremost, there is a large translational gap between animals and human subjects and it remains to be determined whether CFTR is a regulator of cerebrovascular tone in humans. On this note, our previous translational work comparing human/mouse mesenteric and skeletal muscle artery CFTR expression and function displayed excellent comparability (316), providing reasonable grounds to predict that human cerebral arteries will be modulated by CFTR therapeutics. Nevertheless, proof-of-principle clinical trials are needed. The second caveat pertains to the cost of the medication. Because cystic fibrosis is a rare disease, the medications are very expensive: this is necessary in order for the drug companies to recoup the heavy costs invested into their clinical trials. Since SAH is itself a rare disease, short-term use (i.e., a week to a few months) may incur a tolerable expense; it will be much more cost effective when the medications can be repurposed after they are off-patent.

CONCLUSION

Reliably improving cerebral perfusion in SAH patients has proven challenging: while many pathological mechanisms have been proposed, understanding why vascular reactivity changes in SAH remains a serious knowledge deficiency. Consequently, there have been no therapeutic interventions developed within the last 35 years that conclusively ameliorate ischemia in SAH, with the notable exception of nimodipine (which probably works by a different mechanism than intended). Myogenic reactivity and its systemic counterpart, cerebral autoregulation, are crucial homeostatic mechanisms that are perturbed in SAH. Understanding the molecular basis for this microvascular dysfunction, coupled with advances in clinical monitoring of autoregulation, will provide the best prospect of identifying new interventions that successfully restore autoregulation and perfusion in SAH patients.

AUTHOR CONTRIBUTIONS

DL wrote the first draft of this article. All authors contributed equally to the conceptualization, literature research, and revision of the final manuscript.

FUNDING

Funding for publication charges was provided by The Brain Aneurysm Foundation (Thomas J. Tinlin Chair of Research Award) and a *Ted Rogers Centre for Heart Research* (University of Toronto) research grant. S-SB receives stipend support from a Heart and Stroke Foundation of Ontario Mid-Career Investigator award.

ACKNOWLEDGMENTS

We thank Alexandra Erin Papaelias for graphic design.

REFERENCES

1. van Gijn J, Kerr RS, Rinkel GJE. Subarachnoid haemorrhage. *Lancet.* (2007) 369:306–18. doi: 10.1016/S0140-6736(07)60153-6
2. Wiebers DO. Unruptured intracranial aneurysms: natural history, clinical outcome, and risks of surgical and endovascular treatment. *Lancet.* (2003) 362:103–10. doi: 10.1016/S0140-6736(03)13860-3
3. Hop JW, Rinkel GJE, Algra A, van Gijn J. Case-fatality rates and functional outcome after subarachnoid hemorrhage: a systematic review. *Stroke.* (1997) 28:660–4. doi: 10.1161/01.STR.28.3.660
4. Solenski NJ, Haley EC, Kassell NF, Kongable G, Germanson T, Truskowski L, et al. Medical complications of aneurysmal subarachnoid hemorrhage: a report of the multicenter, cooperative aneurysm study. Participants of the multicenter cooperative aneurysm study. *Crit Care Med.* (1995) 23:1007–17. doi: 10.1097/00003246-199506000-00004
5. Galea JP, Dulhanty L, Patel HC. UK and Ireland subarachnoid hemorrhage database collaborators. Predictors of outcome in aneurysmal subarachnoid hemorrhage patients: observations from a multicenter data set. *Stroke.* (2017) 48:2958–63. doi: 10.1161/STROKEAHA.117.017777
6. Johnston SC, Selvin S, Gress DR. The burden, trends, and demographics of mortality from subarachnoid hemorrhage. *Neurology.* (1998) 50:1413–8. doi: 10.1212/WNL.50.5.1413
7. Modi S, Shah K, Schultz L, Tahir R, Affan M, Varelas P. Cost of hospitalization for aneurysmal subarachnoid hemorrhage in the United States. *Clin Neurol Neurosurg.* (2019) 182:167–70. doi: 10.1016/j.clineuro.2019.05.018

8. Linn FHH, Rinkel GJE, Algra A, van Gijn J. Incidence of subarachnoid hemorrhage: role of region, year, and rate of computed tomography: a meta-analysis. *Stroke.* (1996) 27:625–9. doi: 10.1161/01.STR.27.4.625
9. de Rooij NK, Linn FHH, van der Plas JA, Algra A, Rinkel GJE. Incidence of subarachnoid haemorrhage: a systematic review with emphasis on region, age, gender and time trends. *J Neurol Neurosurg Psychiatry.* (2007) 78:1365–72. doi: 10.1136/jnnp.2007.117655
10. Etminan N, Chang H-S, Hackenberg K, de Rooij NK, Vergouwen MDI, Rinkel GJE, et al. Worldwide incidence of aneurysmal subarachnoid hemorrhage according to region, time period, blood pressure, and smoking prevalence in the population: a systematic review and meta-analysis. *JAMA Neurol.* (2019) 76:588–97. doi: 10.1001/jamaneurol.2019.0006
11. Brilstra EH, Rinkel GJE, Algra A, van Gijn J. Rebleeding, secondary ischemia, and timing of operation in patients with subarachnoid hemorrhage. *Neurology.* (2000) 55:1656–60. doi: 10.1212/WNL.55.11.1656
12. Macdonald RL. Delayed neurological deterioration after subarachnoid haemorrhage. *Nat Rev Neurol.* (2014) 10:44–58. doi: 10.1038/nrneurol.2013.246
13. Stein SC, Levine JM, Nagpal S, LeRoux PD. Vasospasm as the sole cause of cerebral ischemia: how strong is the evidence? *Neurosurg Focus.* (2006) 21:1–7. doi: 10.3171/foc.2006.21.3.2
14. Vergouwen MDI, Ilodigwe D, Macdonald RL. Cerebral infarction after subarachnoid hemorrhage contributes to poor outcome by vasospasm-dependent and -independent effects. *Stroke.* (2011) 42:924–9. doi: 10.1161/STROKEAHA.110.597914
15. Macdonald RL, Higashida RT, Keller E, Mayer SA, Molyneux A, Raabe A, et al. Clazosentan, an endothelin receptor antagonist, in patients with aneurysmal subarachnoid haemorrhage undergoing surgical clipping: a randomised, double-blind, placebo-controlled phase 3 trial (CONSCIOUS-2). *Lancet Neurol.* (2011) 10:618–25. doi: 10.1016/S1474-4422(11)70108-9
16. Macdonald RL, Higashida RT, Keller E, Mayer SA, Molyneux A, Raabe A, et al. Randomized trial of clazosentan in patients with aneurysmal subarachnoid hemorrhage undergoing endovascular coiling. *Stroke.* (2012) 43:1463–9. doi: 10.1161/STROKEAHA.111.648980
17. Macdonald RL, Kassell NF, Mayer S, Ruefenacht D, Schmiedek P, Weidauer S, et al. Clazosentan to overcome neurological ischemia and infarction occurring after subarachnoid hemorrhage (CONSCIOUS-1): randomized, double-blind, placebo-controlled phase 2 dose-finding trial. *Stroke.* (2008) 39:3015–21. doi: 10.1161/STROKEAHA.108.519942
18. Etminan N, Vergouwen MD, Ilodigwe D, Macdonald RL. Effect of pharmaceutical treatment on vasospasm, delayed cerebral ischemia, and clinical outcome in patients with aneurysmal subarachnoid hemorrhage: a systematic review and meta-analysis. *J Cereb Blood Flow Metab.* (2011) 31:1443–51. doi: 10.1038/jcbfm.2011.7
19. Mulvany MJ, Aalkjaer C. Structure and function of small arteries. *Physiol Rev.* (1990) 70:921–61.
20. Dernbach PD, Little JR, Jones SC, Ebrahim ZY. Altered cerebral autoregulation and CO2 reactivity after aneurysmal subarachnoid hemorrhage. *Neurosurgery.* (1988) 22:822–6. doi: 10.1227/00006123-198805000-00003
21. Soehle M, Czosnyka M, Pickard JD, Kirkpatrick PJ. Continuous assessment of cerebral autoregulation in subarachnoid hemorrhage. *Anesth Analg.* (2004) 98:1133–9. doi: 10.1213/01.ane.0000111101.41190.99
22. Budohoski KP, Czosnyka M, Kirkpatrick PJ, Smielewski P, Steiner LA, Pickard JD. Clinical relevance of cerebral autoregulation following subarachnoid haemorrhage. *Nat Rev Neurol.* (2013) 9:152–63. doi: 10.1038/nrneurol.2013.11
23. Jaeger M, Soehle M, Schuhmann MU, Meixensberger J. Clinical significance of impaired cerebrovascular autoregulation after severe aneurysmal subarachnoid hemorrhage. *Stroke.* (2012) 43:2097–101. doi: 10.1161/STROKEAHA.112.659888
24. Jaeger M, Schuhmann MU, Soehle M, Nagel C, Meixensberger J. Continuous monitoring of cerebrovascular autoregulation after subarachnoid hemorrhage by brain tissue oxygen pressure reactivity and its relation to delayed cerebral infarction. *Stroke.* (2007) 38:981–6. doi: 10.1161/01.STR.0000257964.65743.99
25. Paulson OB, Strandgaard S, Edvinsson L. Cerebral autoregulation. *Cerebrovasc Brain Metab Rev.* (1990) 2:161–92.
26. Lassen NA. Cerebral blood flow and oxygen consumption in man. *Physiol Rev.* (1959) 39:183–238. doi: 10.1152/physrev.1959.39.2.183
27. Bayliss WM. On the local reactions of the arterial wall to changes of internal pressure. *J Physiol.* (1902) 28:220–31. doi: 10.1113/jphysiol.1902.sp000911
28. Selkurt EE. The relation of renal blood flow to effective arterial pressure in the intact kidney of the dog. *Am J Physiol.* (1946) 147:537–49. doi: 10.1152/ajplegacy.1946.147.3.537
29. Baron JC. Perfusion thresholds in human cerebral ischemia: historical perspective and therapeutic implications. *Cerebrovasc Dis.* (2001) 11(Suppl. 1):2–8. doi: 10.1159/000049119
30. Njemanze PC. Critical limits of pressure-flow relation in the human brain. *Stroke.* (1992) 23:1743–7. doi: 10.1161/01.str.23.12.1743
31. Reinprecht A, Czech T, Asenbaum S, Podreka I, Schmidbauer M. Low cerebrovascular reserve capacity in long-term follow-up after subarachnoid hemorrhage. *Surg Neurol.* (2005) 64:116–21. doi: 10.1016/j.surneu.2004.12.017
32. Bidani AK, Griffin KA, Williamson G, Wang X, Loutzenhiser R. Protective importance of the myogenic response in the renal circulation. *Hypertension.* (2009) 54:393–8. doi: 10.1161/HYPERTENSIONAHA.109.133777
33. Kono M, Belyantseva IA, Skoura A, Frolenkov GI, Starost MF, Dreier JL, et al. Deafness and stria vascularis defects in S1P2 receptor-null mice. *J Biol Chem.* (2007) 282:10690–6. doi: 10.1074/jbc.M700370200
34. Mansour A, Rashad S, Niizuma K, Fujimura M, Tominaga T. A novel model of cerebral hyperperfusion with blood-brain barrier breakdown, white matter injury, and cognitive dysfunction. *J Neurosurg.* (2019) 133:1–13. doi: 10.3171/2019.7.JNS19212
35. Sokrab T-EO, Johansson BB, Kalimo H, Olsson Y, A. transient hypertensive opening of the blood-brain barrier can lead to brain damage. *Acta Neuropathol.* (1988) 75:557–65. doi: 10.1007/BF00686200
36. Tiebosch IACW, van den Bergh WM, Bouts MJRJ, Zwartbol R, van der Toorn A, Dijkhuizen RM. Progression of brain lesions in relation to hyperperfusion from subacute to chronic stages after experimental subarachnoid hemorrhage: a multiparametric MRI study. *Cerebrovasc Dis.* (2013) 36:167–72. doi: 10.1159/000352048
37. van Mook WNKA, Rennenberg RJMW, Schurink GW, van Oostenbrugge RJ, Mess WH, Hofman PAM, et al. Cerebral hyperperfusion syndrome. *Lancet Neurol.* (2005) 4:877–88. doi: 10.1016/S1474-4422(05)70251-9
38. Lublinsky S, Major S, Kola V, Horst V, Santos E, Platz J, et al. Early blood-brain barrier dysfunction predicts neurological outcome following aneurysmal subarachnoid hemorrhage. *EBioMedicine.* (2019) 43:460–72. doi: 10.1016/j.ebiom.2019.04.054
39. Claassen J, Carhuapoma JR, Kreiter KT, Du EY, Connolly ES, Mayer SA. Global cerebral edema after subarachnoid hemorrhage: frequency, predictors, and impact on outcome. *Stroke.* (2002) 33:1225–32. doi: 10.1161/01.str.0000015624.29071.1f
40. Drummond JC. Blood pressure and the brain: how low can you go? *Anesth Analg.* (2019) 128:759–71. doi: 10.1213/ANE.0000000000004034
41. Numan T, Bain AR, Hoiland RL, Smirl JD, Lewis NC, Ainslie PN. Static autoregulation in humans: a review and reanalysis. *Med Eng Phys.* (2014) 36:1487–95. doi: 10.1016/j.medengphy.2014.08.001
42. Schmidt B, Klingelhöfer J, Perkes I, Czosnyka M. Cerebral autoregulatory response depends on the direction of change in perfusion pressure. *J Neurotrauma.* (2009) 26:651–6. doi: 10.1089/neu.2008.0784
43. Aaslid R, Blaha M, Sviri G, Douville CM, Newell DW. Asymmetric dynamic cerebral autoregulatory response to cyclic stimuli. *Stroke.* (2007) 38:1465–9. doi: 10.1161/STROKEAHA.106.473462
44. Tzeng Y-C, Willie CK, Atkinson G, Lucas SJE, Wong A, Ainslie PN. Cerebrovascular regulation during transient hypotension and hypertension in humans. *Hypertension.* (2010) 56:268–73. doi: 10.1161/HYPERTENSIONAHA.110.152066
45. Lucas SJE, Tzeng YC, Galvin SD, Thomas KN, Ogoh S, Ainslie PN. Influence of changes in blood pressure on cerebral perfusion and oxygenation. *Hypertension.* (2010) 55:698–705. doi: 10.1161/HYPERTENSIONAHA.109.146290

46. Svedung Wettervik T, Howells T, Lewén A, Ronne-Engström E, Enblad P. Temporal dynamics of ICP, CPP, PRx, and CPPopt in high-grade aneurysmal subarachnoid hemorrhage and the relation to clinical outcome. *Neurocrit Care.* (2021) 34:390–402. doi: 10.1007/s12028-020-01162-4
47. Budohoski KP, Czosnyka M, Smielewski P, Varsos GV, Kasprowicz M, Brady KM, et al. Cerebral autoregulation after subarachnoid hemorrhage: comparison of three methods. *J Cereb Blood Flow Metab.* (2013) 33:449–56. doi: 10.1038/jcbfm.2012.189
48. Handa Y, Hayashi M, Takeuchi H, Kubota T, Kobayashi H, Kawano H. Time course of the impairment of cerebral autoregulation during chronic cerebral vasospasm after subarachnoid hemorrhage in primates. *J Neurosurg.* (1992) 76:493–501. doi: 10.3171/jns.1992.76.3.0493
49. Girouard H, Iadecola C. Neurovascular coupling in the normal brain and in hypertension, stroke, and Alzheimer disease. *J Appl Physiol (1985).* (2006) 100:328–35. doi: 10.1152/japplphysiol.00966.2005
50. Lecrux C, Hamel E. The neurovascular unit in brain function and disease. *Acta Physiol.* (2011) 203:47–59. doi: 10.1111/j.1748-1716.2011.02256.x
51. Phillips AA, Chan FH, Zheng MMZ, Krassioukov AV, Ainslie PN. Neurovascular coupling in humans: physiology, methodological advances and clinical implications. *J Cereb Blood Flow Metab.* (2016) 36:647–64. doi: 10.1177/0271678X15617954
52. Freeman RD Li B. Neural–metabolic coupling in the central visual pathway. *Philos Trans R Soc Lond B Biol Sci.* (2016) 371:20150357. doi: 10.1098/rstb.2015.0357
53. Muizelaar JP, Schröder ML. Overview of monitoring of cerebral blood flow and metabolism after severe head injury. *Can J Neurol Sci.* (1994) 21:S6–11. doi: 10.1017/S0084255900003685
54. Davis MJ, Hill MA. Signaling mechanisms underlying the vascular myogenic response. *Physiol Rev.* (1999) 79:387–423. doi: 10.1152/physrev.1999.79.2.387
55. von Anrep G. On local vascular reactions and their interpretation. *J Physiol.* (1912) 45:318–27. doi: 10.1113/jphysiol.1912.sp001554
56. Folkow B. Intravascular pressure as a factor regulating the tone of the small vessels. *Acta Physiol Scand.* (1949) 17:289–310. doi: 10.1111/j.1748-1716.1949.tb00576.x
57. Johnson PC. Myogenic nature of increase in intestinal vascular resistance with venous pressure elevation. *Circ Res.* (1959) 7:992–9. doi: 10.1161/01.res.7.6.992
58. Selkurt EE, Johnson PC. Effect of acute elevation of portal venous pressure on mesenteric blood volume, interstitial fluid volume and hemodynamics. *Circ Res.* (1958) 6:592–9. doi: 10.1161/01.res.6.5.592
59. Baumbach GL, Heistad DD. Regional, segmental, and temporal heterogeneity of cerebral vascular autoregulation. *Ann Biomed Eng.* (1985) 13:303. doi: 10.1007/BF02584248
60. Harraz OF, Visser F, Brett SE, Goldman D, Zechariah A, Hashad AM, et al. Welsh DG. CaV12/CaV3x channels mediate divergent vasomotor responses in human cerebral arteries. *J Gen Physiol.* (2015) 145:405–18. doi: 10.1085/jgp.201511361
61. Wallis SJ, Firth J, Dunn WR. Pressure-induced myogenic responses in human isolated cerebral resistance arteries. *Stroke.* (1996) 27:2287–91. doi: 10.1161/01.str.27.12.2287
62. Thorin-Trescases N, Bartolotta T, Hyman N, Penar PL, Walters CL, Bevan RD, et al. Diameter dependence of myogenic tone of human pial arteries. Possible relation to distensibility. *Stroke.* (1997) 28:2486–92. doi: 10.1161/01.str.28.12.2486
63. Vinall PE, Simeone FA. Cerebral autoregulation: an *in vitro* study. *Stroke.* (1981) 12:640–2. doi: 10.1161/01.str.12.5.640
64. Bevan RD, Vijayakumaran E, Gentry A, Wellman T, Bevan JA. Intrinsic tone of cerebral artery segments of human infants between 23 weeks of gestation and term. *Pediatr Res.* (1998) 43:20–7. doi: 10.1203/00006450-199801000-00004
65. Miller CA, Yashon D, Locke G, Hunt WE. Autonomous activity in the human basilar artery: Relationship to cerebral vascular spasm. *Neurology.* (1971) 21:1249. doi: 10.1212/WNL.21.12.1249
66. de Wit C, Jahrbeck B, Schäfer C, Bolz SS, Pohl U. Nitric oxide opposes myogenic pressure responses predominantly in large arterioles *in vivo*. *Hypertension.* (1998) 31:787–94. doi: 10.1161/01.hyp.31.3.787
67. Kontos HA, Wei EP, Navari RM, Levasseur JE, Rosenblum WI, Patterson JL. Responses of cerebral arteries and arterioles to acute hypotension and hypertension. *Am J Physiol.* (1978) 234:H371–83. doi: 10.1152/ajpheart.1978.234.4.H371
68. Hill MA, Zou H, Potocnik SJ, Meininger GA, Davis MJ. Invited review: arteriolar smooth muscle mechanotransduction: Ca(2+) signaling pathways underlying myogenic reactivity. *J Appl Physiol.* (2001) 91:973–83. doi: 10.1152/jappl.2001.91.2.973
69. Schubert R, Lidington D, Bolz S-S. The emerging role of Ca^{2+} sensitivity regulation in promoting myogenic vasoconstriction. *Cardiovasc Res.* (2008) 77:8–18. doi: 10.1016/j.cardiores.2007.07.018
70. Hill MA, Meininger GA, Davis MJ, Laher I. Therapeutic potential of pharmacologically targeting arteriolar myogenic tone. *Trends Pharmacol Sci.* (2009) 30:363–74. doi: 10.1016/j.tips.2009.04.008
71. Cole WC, Welsh DG. Role of myosin light chain kinase and myosin light chain phosphatase in the resistance arterial myogenic response to intravascular pressure. *Arch Biochem Biophys.* (2011) 510:160–73. doi: 10.1016/j.abb.2011.02.024
72. Harder DR, Narayanan J, Gebremedhin D. Pressure-induced myogenic tone and role of 20-HETE in mediating autoregulation of cerebral blood flow. *Am J Physiol Heart Circ Physiol.* (2011) 300:H1557–65. doi: 10.1152/ajpheart.01097.2010
73. Davis MJ. Perspective: physiological role(s) of the vascular myogenic response. *Microcirculation.* (2012) 19:99–114. doi: 10.1111/j.1549-8719.2011.00131.x
74. Lidington D, Schubert R, Bolz S-S. Capitalizing on diversity: an integrative approach towards the multiplicity of cellular mechanisms underlying myogenic responsiveness. *Cardiovasc Res.* (2013) 97:404–12. doi: 10.1093/cvr/cvs345
75. Lidington D, Kroetsch JT, Bolz S-S. Cerebral artery myogenic reactivity: the next frontier in developing effective interventions for subarachnoid hemorrhage. *J Cereb Blood Flow Metab.* (2018) 38:17–37. doi: 10.1177/0271678X17742548
76. Spassova MA, Hewavitharana T, Xu W, Soboloff J, Gill DL, A. common mechanism underlies stretch activation and receptor activation of TRPC6 channels. *Proc Natl Acad Sci USA.* (2006) 103:16586–91. doi: 10.1073/pnas.0606894103
77. Welsh DG, Morielli AD, Nelson MT, Brayden JE. Transient receptor potential channels regulate myogenic tone of resistance arteries. *Circ Res.* (2002) 90:248–50. 11861411
78. Wang Y, Deng X, Hewavitharana T, Soboloff J, Gill DL. Stim, ORAI and TRPC channels in the control of calcium entry signals in smooth muscle. *Clin Exp Pharmacol Physiol.* (2008) 35:1127–33. doi: 10.1111/j.1440-1681.2008.05018.x
79. Martinez-Lemus LA, Crow T, Davis MJ, Meininger GA. alphavbeta3- and alpha5beta1-integrin blockade inhibits myogenic constriction of skeletal muscle resistance arterioles. *Am J Physiol Heart Circ Physiol.* (2005) 289:H322–9. doi: 10.1152/ajpheart.00923.2003
80. Sun Z, Martinez-Lemus LA, Hill MA, Meininger GA. Extracellular matrix-specific focal adhesions in vascular smooth muscle produce mechanically active adhesion sites. *Am J Physiol Cell Physiol.* (2008) 295:C268–78. doi: 10.1152/ajpcell.00516.2007
81. Kroetsch JT, Levy AS, Zhang H, Aschar-Sobbi R, Lidington D, Offermanns S, et al. Constitutive smooth muscle tumour necrosis factor regulates microvascular myogenic responsiveness and systemic blood pressure. *Nat Commun.* (2017) 8:14805. doi: 10.1038/ncomms14805
82. Knot HJ, Nelson MT. Regulation of arterial diameter and wall $[Ca^{2+}]$ in cerebral arteries of rat by membrane potential and intravascular pressure. *J Physiol.* (1998) 508 (Pt 1):199–209. doi: 10.1111/j.1469-7793.1998.199br.x
83. Faraci FM, Sobey CG. Role of potassium channels in regulation of cerebral vascular tone. *J Cereb Blood Flow Metab.* (1998) 18:1047–63. doi: 10.1097/00004647-199810000-00001
84. Knot HJ, Standen NB, Nelson MT. Ryanodine receptors regulate arterial diameter and wall $[Ca^{2+}]$ in cerebral arteries of rat *via* Ca^{2+}-dependent K+ channels. *J Physiol.* (1998) 508 (Pt 1):211–21. doi: 10.1111/j.1469-7793.1998.211br.x

85. Kotecha N, Hill MA. Myogenic contraction in rat skeletal muscle arterioles: smooth muscle membrane potential and Ca(2+) signaling. *Am J Physiol Heart Circ Physiol.* (2005) 289:H1326–34. doi: 10.1152/ajpheart.00323.2005
86. Lidington D, Peter BF, Meissner A, Kroetsch JT, Pitson SM, Pohl U, et al. The phosphorylation motif at serine 225 governs the localization and function of sphingosine kinase 1 in resistance arteries. *Arterioscler Thromb Vasc Biol.* (2009) 29:1916–22. doi: 10.1161/ATVBAHA.109.194803
87. Yagi K, Lidington D, Wan H, Fares JC, Meissner A, Sumiyoshi M, et al. Therapeutically targeting tumor necrosis factor-α/sphingosine-1-phosphate signaling corrects myogenic reactivity in subarachnoid hemorrhage. *Stroke.* (2015) 46:2260–70. doi: 10.1161/STROKEAHA.114.006365
88. Berg RMG. Myogenic and metabolic feedback in cerebral autoregulation: putative involvement of arachidonic acid-dependent pathways. *Med Hypotheses.* (2016) 92:12–7. doi: 10.1016/j.mehy.2016.04.024
89. Johnson RP, El-Yazbi AF, Takeya K, Walsh EJ, Walsh MP, Cole WC. Ca^{2+} sensitization *via* phosphorylation of myosin phosphatase targeting subunit at threonine-855 by Rho kinase contributes to the arterial myogenic response. *J Physiol.* (2009) 587:2537–53. doi: 10.1113/jphysiol.2008.168252
90. Bolz S-S, Vogel L, Sollinger D, Derwand R, Boer C, Pitson SM, et al. Sphingosine kinase modulates microvascular tone and myogenic responses through activation of RhoA/Rho kinase. *Circulation.* (2003) 108:342–7. doi: 10.1161/01.CIR.0000080324.12530.0D
91. Korzick DH, Laughlin MH, Bowles DK. Alterations in PKC signaling underlie enhanced myogenic tone in exercise-trained porcine coronary resistance arteries. *J Appl Physiol. (1985).* (2004) 96:1425–32. doi: 10.1152/japplphysiol.01077.2003
92. Dessy C, Matsuda N, Hulvershorn J, Sougnez CL, Sellke FW, Morgan KG. Evidence for involvement of the PKC-alpha isoform in myogenic contractions of the coronary microcirculation. *Am J Physiol Heart Circ Physiol.* (2000) 279:H916–23. doi: 10.1152/ajpheart.2000.279.3.H916
93. Lidington D, Fares JC, Uhl FE, Dinh DD, Kroetsch JT, Sauvé M, et al. CFTR therapeutics normalize cerebral perfusion deficits in mouse models of heart failure and subarachnoid hemorrhage. *JACC Basic Transl Sci.* (2019) 4:940–58. doi: 10.1016/j.jacbts.2019.07.004
94. Deng W, Kandhi S, Zhang B, Huang A, Koller A, Sun D. Extravascular blood augments myogenic constriction of cerebral arterioles: implications for hemorrhage-induced vasospasm. *J Am Heart Assoc.* (2018) 7:e008623. doi: 10.1161/JAHA.118.008623
95. Nystoriak MA, O'Connor KP, Sonkusare SK, Brayden JE, Nelson MT, Wellman GC. Fundamental increase in pressure-dependent constriction of brain parenchymal arterioles from subarachnoid hemorrhage model rats due to membrane depolarization. *Am J Physiol Heart Circ Physiol.* (2011) 300:H803–12. doi: 10.1152/ajpheart.00760.2010
96. Wellman GC, Koide M. Impact of subarachnoid hemorrhage on parenchymal arteriolar function. *Acta Neurochir Suppl.* (2013) 115:173–7. doi: 10.1007/978-3-7091-1192-5_33
97. Gong Y, Du M-Y, Yu H-L, Yang Z-Y, Li Y-J, Zhou L, et al. Increased TRPM4 activity in cerebral artery myocytes contributes to cerebral blood flow reduction after subarachnoid hemorrhage in rats. *Neurotherapeutics.* (2019) 16:901–11. doi: 10.1007/s13311-019-00741-4
98. Harder DR, Dernbach P, Waters A. Possible cellular mechanism for cerebral vasospasm after experimental subarachnoid hemorrhage in the dog. *J Clin Invest.* (1987) 80:875–80. doi: 10.1172/JCI113146
99. Ishiguro M, Puryear CB, Bisson E, Saundry CM, Nathan DJ, Russell SR, et al. Enhanced myogenic tone in cerebral arteries from a rabbit model of subarachnoid hemorrhage. *Am J Physiol Heart Circ Physiol.* (2002) 283:H2217–25. doi: 10.1152/ajpheart.00629.2002
100. Koide M, Nystoriak MA, Brayden JE, Wellman GC. Impact of subarachnoid hemorrhage on local and global calcium signaling in cerebral artery myocytes. *Acta Neurochir Suppl.* (2011) 110:145–50. doi: 10.1007/978-3-7091-0353-1_25
101. Heilbrun MP, Olesen J, Lassen NA. Regional cerebral blood flow studies in subarachnoid hemorrhage. *J Neurosurg.* (1972) 37:36–44. doi: 10.3171/jns.1972.37.1.0036
102. Dhar R, Scalfani MT, Blackburn S, Zazulia AR, Videen T, Diringer M. Relationship between angiographic vasospasm and regional hypoperfusion in aneurysmal subarachnoid hemorrhage. *Stroke.* (2012) 43:1788–94. doi: 10.1161/STROKEAHA.111.646836
103. Kelly PJ, Gorten RJ, Grossman RG, Eisenberg HM. Cerebral perfusion, vascular spasm, and outcome in patients with ruptured intracranial aneurysms. *J Neurosurg.* (1977) 47:44–9. doi: 10.3171/jns.1977.47.1.0044
104. Schubert GA, Seiz M, Hegewald AA, Manville J, Thomé C. Acute hypoperfusion immediately after subarachnoid hemorrhage: a xenon contrast-enhanced CT study. *J Neurotrauma.* (2009) 26:2225–31. doi: 10.1089/neu.2009.0924
105. Géraud G, Tremoulet M, Guell A, Bes A. The prognostic value of noninvasive CBF measurement in subarachnoid hemorrhage. *Stroke.* (1984) 15:301–5.
106. Ohkuma H, Suzuki S, Kudo K, Islam S, Kikkawa T. Cortical blood flow during cerebral vasospasm after aneurysmal subarachnoid hemorrhage: three-dimensional N-isopropyl-p-[(123)I]iodoamphetamine single photon emission CT findings. *AJNR Am J Neuroradiol.* (2003) 24:444–50.
107. Naidech AM, Drescher J, Tamul P, Shaibani A, Batjer HH, Alberts MJ. Acute physiological derangement is associated with early radiographic cerebral infarction after subarachnoid haemorrhage. *J Neurol Neurosurg Psychiatry.* (2006) 77:1340–4. doi: 10.1136/jnnp.2006.089748
108. Osol G, Brekke JF, McElroy-Yaggy K, Gokina NI. Myogenic tone, reactivity, and forced dilatation: a three-phase model of *in vitro* arterial myogenic behavior. *Am J Physiol Heart Circ Physiol.* (2002) 283:H2260–7. doi: 10.1152/ajpheart.00634.2002
109. Artru AA, Katz RA, Colley PS. Autoregulation of cerebral blood flow during normocapnia and hypocapnia in dogs. *Anesthesiology.* (1989) 70:288–92. doi: 10.1097/00000542-198902000-00018
110. Koide M, Ferris HR, Nelson MT, Wellman GC. Impaired cerebral autoregulation after subarachnoid hemorrhage: a quantitative assessment using a mouse model. *Front Physiol.* (2021) 12:688468. doi: 10.3389/fphys.2021.688468
111. Qureshi AI, Ezzeddine MA, Nasar A, Suri MFK, Kirmani JF, Hussein HM, et al. Prevalence of elevated blood pressure in 563,704 adult patients with stroke presenting to the ED in the United States. *Am J Emerg Med.* (2007) 25:32–8. doi: 10.1016/j.ajem.2006.07.008
112. Dankbaar JW, Rijsdijk M, van der Schaaf IC, Velthuis BK, Wermer MJH, Rinkel GJE. Relationship between vasospasm, cerebral perfusion, and delayed cerebral ischemia after aneurysmal subarachnoid hemorrhage. *Neuroradiology.* (2009) 51:813–9. doi: 10.1007/s00234-009-0575-y
113. Nelson RJ, Perry S, Hames TK, Pickard JD. Transcranial Doppler ultrasound studies of cerebral autoregulation and subarachnoid hemorrhage in the rabbit. *J Neurosurg.* (1990) 73:601–10. doi: 10.3171/jns.1990.73.4.0601
114. Fantini S, Sassaroli A, Tgavalekos KT, Kornbluth J. Cerebral blood flow and autoregulation: current measurement techniques and prospects for noninvasive optical methods. *Neurophoton.* (2016) 3:031411. doi: 10.1117/1.NPh.3.3.031411
115. Liu J, Zhu Y-S, Hill C, Armstrong K, Takashi T, Timea H, et al. Cerebral autoregulation of blood velocity and volumetric flow during steady-state changes in arterial pressure. *Hypertension.* (2013) 62:973–9. doi: 10.1161/HYPERTENSIONAHA.113.01867
116. Manno EM, Gress DR, Schwamm LH, Diringer MN, Ogilvy CS. Effects of induced hypertension on transcranial Doppler ultrasound velocities in patients after subarachnoid hemorrhage. *Stroke.* (1998) 29:422–8. doi: 10.1161/01.str.29.2.422
117. Tenjin H, Hirakawa K, Mizukawa N, Yano I, Ohta T, Uchibori M, et al. Dysautoregulation in patients with ruptured aneurysms: cerebral blood flow measurements obtained during surgery by a temperature-controlled thermoelectrical method. *Neurosurgery.* (1988) 23:705–9. doi: 10.1227/00006123-198812000-00003
118. Muench E, Bauhuf C, Roth H, Horn P, Phillips M, Marquetant N, et al. Effects of positive end-expiratory pressure on regional cerebral blood flow, intracranial pressure, and brain tissue oxygenation. *Crit Care Med.* (2005) 33:2367–72. doi: 10.1097/01.ccm.0000181732.37319.df
119. Nornes H, Knutzen HB, Wikeby P. Cerebral arterial blood flow and aneurysm surgery: Part 2: Induced hypotension and autoregulatory capacity. *J Neurosurg.* (1977) 47:819–27. doi: 10.3171/jns.1977.47.6.0819
120. Pickard JD, Matheson M, Patterson J, Wyper D. Prediction of late ischemic complications after cerebral aneurysm surgery by the intraoperative

measurement of cerebral blood flow. *J Neurosurg.* (1980) 53:305–8. doi: 10.3171/jns.1980.53.3.0305
121. Cossu M, Gennaro S, Rossi A, Balestrero MA, Cella F, Viale GL. Autoregulation of cortical blood flow during surgery for ruptured intracranial aneurysms. *J Neurosurg Sci.* (1999) 43:99–105.
122. Darby JM, Yonas H, Marks EC, Durham S, Snyder RW, Nemoto EM. Acute cerebral blood flow response to dopamine-induced hypertension after subarachnoid hemorrhage. *J Neurosurg.* (1994) 80:857–64. doi: 10.3171/jns.1994.80.5.0857
123. Muizelaar JP, Becker DP. Induced hypertension for the treatment of cerebral ischemia after subarachnoid hemorrhage. Direct effect on cerebral blood flow. *Surg Neurol.* (1986) 25:317–25. doi: 10.1016/0090-3019(86)90205-3
124. Hattingen E, Blasel S, Dettmann E, Vatter H, Pilatus U, Seifert V, et al. Perfusion-weighted MRI to evaluate cerebral autoregulation in aneurysmal subarachnoid haemorrhage. *Neuroradiology.* (2008) 50:929. doi: 10.1007/s00234-008-0424-4
125. Diringer MN, Dhar R, Scalfani M, Zazulia AR, Chicoine M, Powers WJ, et al. Effect of high-dose simvastatin on cerebral blood flow and static autoregulation in subarachnoid hemorrhage. *Neurocrit Care.* (2016) 25:56–63. doi: 10.1007/s12028-015-0233-7
126. Smielewski P, Czosnyka M, Iyer V, Piechnik S, Whitehouse H, Pickard J. Computerised transient hyperaemic response test–a method for the assessment of cerebral autoregulation. *Ultrasound Med Biol.* (1995) 21:599–611. doi: 10.1016/0301-5629(94)00154-6
127. Lam JMK, Smielewski P, Czosnyka M, Pickard JD, Kirkpatrick PJ. Predicting delayed ischemic deficits after aneurysmal subarachnoid hemorrhage using a transient hyperemic response test of cerebral autoregulation. *Neurosurgery.* (2000) 47:819–26. doi: 10.1097/00006123-200010000-00004
128. Rätsep T, Asser T. Cerebral hemodynamic impairment after aneurysmal subarachnoid hemorrhage as evaluated using transcranial Doppler ultrasonography: relationship to delayed cerebral ischemia and clinical outcome. *J Neurosurg.* (2001) 95:393–401. doi: 10.3171/jns.2001.95.3.0393
129. Rätsep T, Eelmäe J, Asser T. Routine utilization of the transient hyperaemic response test after aneurysmal subarachnoid haemorrhage. In: Czosnyka M, Pickard JD, Kirkpatrick PJ, Smielewski P, Hutchinson P, editors. *Intracranial Pressure and Brain Biochemical Monitoring Acta Neurochirurgica Supplements*. Vienna: Springer (2002). p. 121–4. doi: 10.1007/978-3-7091-6738-0_31
130. Al-Jehani H, Angle M, Marcoux J, Teitelbaum J. Early abnormal transient hyperemic response test can predict delayed ischemic neurologic deficit in subarachnoid hemorrhage. *Crit Ultrasound J.* (2018) 10:1–6. doi: 10.1186/s13089-017-0079-7
131. Rynkowski CB, de Oliveira Manoel AL, dos Reis MM, Puppo C, Worm PV, Zambonin D, et al. Early transcranial doppler evaluation of cerebral autoregulation independently predicts functional outcome after aneurysmal subarachnoid hemorrhage. *Neurocrit Care.* (2019) 31:253–62. doi: 10.1007/s12028-019-00732-5
132. Fontana J, Moratin J, Ehrlich G, Scharf J, Weiß C, Schmieder K, et al. Dynamic autoregulatory response after aneurysmal subarachnoid hemorrhage and its relation to angiographic vasospasm and clinical outcome. *Neurocrit Care.* (2015) 23:355–63. doi: 10.1007/s12028-014-0104-7
133. Fontana J, Wenz H, Schmieder K, Barth M. Impairment of dynamic pressure autoregulation precedes clinical deterioration after aneurysmal subarachnoid hemorrhage. *J Neuroimaging.* (2016) 26:339–45. doi: 10.1111/jon.12295
134. Mahdi A, Nikolic D, Birch AA, Olufsen MS, Panerai RB, Simpson DM, et al. Increased blood pressure variability upon standing up improves reproducibility of cerebral autoregulation indices. *Med Eng Phys.* (2017) 47:151–8. doi: 10.1016/j.medengphy.2017.06.006
135. Czosnyka M, Smielewski P, Kirkpatrick P, Laing RJ, Menon D, Pickard JD. Continuous assessment of the cerebral vasomotor reactivity in head injury. *Neurosurgery.* (1997) 41:11–9. doi: 10.1097/00006123-199707000-00005
136. Czosnyka M, Czosnyka Z, Smielewski P. Pressure reactivity index: journey through the past 20 years. *Acta Neurochir.* (2017) 159:2063–5. doi: 10.1007/s00701-017-3310-1
137. Steiner LA, Czosnyka M, Piechnik SK, Smielewski P, Chatfield D, Menon DK, et al. Continuous monitoring of cerebrovascular pressure reactivity allows determination of optimal cerebral perfusion pressure in patients with traumatic brain injury. *Crit Care Med.* (2002) 30:733–8. doi: 10.1097/00003246-200204000-00002
138. Budohoski KP, Czosnyka M, de Riva N, Smielewski P, Pickard JD, Menon DK, et al. The relationship between cerebral blood flow autoregulation and cerebrovascular pressure reactivity after traumatic brain injury. *Neurosurgery.* (2012) 71:652–61. doi: 10.1227/NEU.0b013e318260feb1
139. Panerai RB. Assessment of cerebral pressure autoregulation in humans - a review of measurement methods. *Physiol Meas.* (1998) 19:305. doi: 10.1088/0967-3334/19/3/001
140. Lee JK, Kibler KK, Benni PB, Easley ER, Czosnyka M, Smielewski P, et al. Cerebrovascular reactivity measured by near-infrared spectroscopy. *Stroke.* (2009) 40:1820–6. doi: 10.1161/STROKEAHA.108.536094
141. Timofeev I, Czosnyka M, Nortje J, Smielewski P, Kirkpatrick P, Gupta A, et al. Effect of decompressive craniectomy on intracranial pressure and cerebrospinal compensation following traumatic brain injury. *J Neurosurg.* (2008) 108:66–73. doi: 10.3171/JNS/2008/108/01/0066
142. Zweifel C, Lavinio A, Steiner LA, Radolovich D, Smielewski P, Timofeev I, et al. Continuous monitoring of cerebrovascular pressure reactivity in patients with head injury. *Neurosurg Focus.* (2008) 25:E2. doi: 10.3171/FOC.2008.25.10.E2
143. Howells T, Johnson U, McKelvey T, Ronne-Engström E, Enblad P. The effects of ventricular drainage on the intracranial pressure signal and the pressure reactivity index. *J Clin Monit Comput.* (2017) 31:469–78. doi: 10.1007/s10877-016-9863-3
144. MacKenzie E T, Farrar J K, Fitch W, Graham D I, Gregory P C, Harper A M. Effects of hemorrhagic hypotension on the cerebral circulation. I Cerebral blood flow and pial arteriolar caliber. *Stroke.* (1979) 10:711–8. doi: 10.1161/01.STR.10.6.711
145. Kelly S, Bishop SM, Ercole A. Statistical signal properties of the pressure-reactivity index (PRx). *Acta Neurochir Suppl.* (2018) 126:317–20. doi: 10.1007/978-3-319-65798-1_62
146. Copplestone S, Welbourne J, A. narrative review of the clinical application of pressure reactiviy indices in the neurocritical care unit. *Br J Neurosurg.* (2018) 32:4–12. doi: 10.1080/02688697.2017.1416063
147. Gaasch M, Schiefecker AJ, Kofler M, Beer R, Rass V, Pfausler B, et al. Cerebral autoregulation in the prediction of delayed cerebral ischemia and clinical outcome in poor-grade aneurysmal subarachnoid hemorrhage patients. *Crit Care Med.* (2018) 46:774–80. doi: 10.1097/CCM.0000000000003016
148. Johnson U, Engquist H, Howells T, Nilsson P, Ronne-Engström E, Lewén A, et al. Bedside Xenon-CT shows lower CBF in SAH patients with impaired CBF pressure autoregulation as defined by pressure reactivity index (PRx). *Neurocrit Care.* (2016) 25:47–55. doi: 10.1007/s12028-016-0240-3
149. Eide PK, Sorteberg A, Bentsen G, Marthinsen PB, Stubhaug A, Sorteberg W. Pressure-derived versus pressure wave amplitude–derived indices of cerebrovascular pressure reactivity in relation to early clinical state and 12-month outcome following aneurysmal subarachnoid hemorrhage: clinical article. *J Neurosurg.* (2012) 116:961–71. doi: 10.3171/2012.1.JNS111313
150. Bijlenga P, Czosnyka M, Budohoski KP, Soehle M, Pickard JD, Kirkpatrick PJ, et al. "Optimal cerebral perfusion pressure" in poor grade patients after subarachnoid hemorrhage. *Neurocrit Care.* (2010) 13:17–23. doi: 10.1007/s12028-010-9362-1
151. Barth M, Woitzik J, Weiss C, Muench E, Diepers M, Schmiedek P, et al. Correlation of clinical outcome with pressure-, oxygen-, and flow-related indices of cerebrovascular reactivity in patients following aneurysmal SAH. *Neurocrit Care.* (2010) 12:234–43. doi: 10.1007/s12028-009-9287-8
152. Conzen C, Becker K, Albanna W, Weiss M, Bach A, Lushina N, et al. The Acute Phase of experimental subarachnoid hemorrhage: intracranial pressure dynamics and their effect on cerebral blood flow and autoregulation. *Transl Stroke Res.* (2019) 10:566–82. doi: 10.1007/s12975-018-0674-3
153. Nicoletto HA, Burkman MH. Transcranial Doppler series part II: performing a transcranial Doppler. *Am J Electroneurodiagnostic Technol.* (2009) 49:14–27. doi: 10.1080/1086508X.2009.11079700
154. Budohoski KP, Czosnyka M, Smielewski P, Kasprowicz M, Helmy A, Bulters D, et al. Impairment of cerebral autoregulation predicts delayed cerebral ischemia after subarachnoid hemorrhage: a prospective observational study. *Stroke.* (2012) 43:3230–7. doi: 10.1161/STROKEAHA.112.669788
155. Calviere L, Nasr N, Arnaud C, Czosnyka M, Viguier A, Tissot B, et al. Prediction of delayed cerebral ischemia after subarachnoid hemorrhage

using cerebral blood flow velocities and cerebral autoregulation assessment. *Neurocrit Care.* (2015) 23:253–8. doi: 10.1007/s12028-015-0125-x
156. Zweifel C, Castellani G, Czosnyka M, Carrera E, Brady KM, Kirkpatrick PJ, et al. Continuous assessment of cerebral autoregulation with near-infrared spectroscopy in adults after subarachnoid hemorrhage. *Stroke.* (2010) 41:1963–8. doi: 10.1161/STROKEAHA.109.577320
157. Claassen JA. Meel-van den Abeelen AS, Simpson DM, Panerai RB. Transfer function analysis of dynamic cerebral autoregulation: a white paper from the International Cerebral Autoregulation Research Network. *J Cereb Blood Flow Metab.* (2016) 36:665–80. doi: 10.1177/0271678X15626425
158. Otite F, Mink S, Tan CO, Puri A, Zamani AA, Mehregan A, et al. Impaired cerebral autoregulation is associated with vasospasm and delayed cerebral ischemia in subarachnoid hemorrhage. *Stroke.* (2014) 45:677–82. doi: 10.1161/STROKEAHA.113.002630
159. Liu G, Guo Z, Sun X, Chai W, Qi L, Li H, et al. Monitoring of the effect of cerebral autoregulation on delayed cerebral ischemia in patients with aneurysmal subarachnoid hemorrhage. *World Neurosurg.* (2018) 118:e269–75. doi: 10.1016/j.wneu.2018.06.170
160. Dawson SL, Blake MJ, Panerai RB, Potter JF. Dynamic but not static cerebral autoregulation is impaired in acute ischaemic stroke. *Cerebrovasc Dis.* (2000) 10:126–32. doi: 10.1159/000016041
161. van der Scheer JW, Kamijo Y-I, Leicht CA, Millar PJ, Shibasaki M, Goosey-Tolfrey VL, et al. comparison of static and dynamic cerebral autoregulation during mild whole-body cold stress in individuals with and without cervical spinal cord injury: a pilot study. *Spinal Cord.* (2018) 56:469–77. doi: 10.1038/s41393-017-0021-7
162. Meng L, Gelb AW. Regulation of cerebral autoregulation by carbon dioxide. *Anesthesiology.* (2015) 122:196–205. doi: 10.1097/ALN.0000000000000506
163. Lai LT, O'Neill AH. History, evolution, and continuing innovations of intracranial aneurysm surgery. *World Neurosurg.* (2017) 102:673–81. doi: 10.1016/j.wneu.2017.02.006
164. Louw DF, Asfora WT, Sutherland GR, A. brief history of aneurysm clips. *Neurosurg Focus.* (2001) 11:E4. doi: 10.3171/foc.2001.11.2.5
165. Cushing H. The control of bleeding in operations for brain tumors: with the description of silver "clips" for the occlusion of vessels inaccessible to the ligature. *Ann Surg.* (1911) 54:1–19. doi: 10.1097/00000658-191107000-00002
166. Campos JK, Lien BV, Wang AS, Lin L-M. Advances in endovascular aneurysm management: coiling and adjunctive devices. *Stroke Vasc Neurol.* (2020) 5:14–21. doi: 10.1136/svn-2019-000303
167. Liu A, Huang J. Treatment of intracranial aneurysms: clipping versus coiling. *Curr Cardiol Rep.* (2015) 17:73. doi: 10.1007/s11886-015-0628-2
168. Connolly ES, Rabinstein AA, Carhuapoma JR, Derdeyn CP, Dion J, Higashida RT, et al. Guidelines for the management of aneurysmal subarachnoid hemorrhage: a guideline for healthcare professionals from the American Heart Association/American Stroke Association. *Stroke.* (2012) 43:1711–37. doi: 10.1161/STR.0b013e3182587839
169. Sen J, Belli A, Albon H, Morgan L, Petzold A, Kitchen N. Triple-H therapy in the management of aneurysmal subarachnoid haemorrhage. *Lancet Neurol.* (2003) 2:614–21. doi: 10.1016/S1474-4422(03)00531-3
170. Lee KH, Lukovits T, Friedman JA. "Triple-H" therapy for cerebral vasospasm following subarachnoid hemorrhage. *Neurocrit Care.* (2006) 4:68–76. doi: 10.1385/NCC:4:1:068
171. Denny-Brown D. The treatment of recurrent cerebrovascular symptoms and the question of "vasospasm." *Med Clin North Am.* (1951) 35:1457–74. doi: 10.1016/S0025-7125(16)35234-8
172. Farhat SM, Schneider RC. Observations on the effect of systemic blood pressure on intracranial circulation in patients with cerebrovascular insufficiency. *J Neurosurg.* (1967) 27:441–5. doi: 10.3171/jns.1967.27.5.0441
173. Kosnik EJ, Hunt WE. Postoperative hypertension in the management of patients with intracranial arterial aneurysms. *J Neurosurg.* (1976) 45:148–54. doi: 10.3171/jns.1976.45.2.0148
174. Gathier CS, van den Bergh WM, van der Jagt M, Verweij BH, Dankbaar JW, Müller MC, et al. Induced hypertension for delayed cerebral ischemia after aneurysmal subarachnoid hemorrhage: a randomized clinical trial. *Stroke.* (2018) 49:76–83. doi: 10.1161/STROKEAHA.117.017956
175. Awad IA, Carter LP, Spetzler RF, Medina M, Williams FC. Clinical vasospasm after subarachnoid hemorrhage: response to hypervolemic hemodilution and arterial hypertension. *Stroke.* (1987) 18:365–72. doi: 10.1161/01.str.18.2.365
176. Kassell NF, Peerless SJ, Durward QJ, Beck DW, Drake CG, Adams HP. Treatment of ischemic deficits from vasospasm with intravascular volume expansion and induced arterial hypertension. *Neurosurgery.* (1982) 11:337–43. doi: 10.1227/00006123-198209000-00001
177. Yano K, Kuroda T, Tanabe Y, Yamada H. Preventive therapy against delayed cerebral ischaemia after aneurysmal subarachnoid haemorrhage: trials of thromboxane A2 synthetase inhibitor and hyperdynamic therapy. *Acta Neurochir.* (1993) 125:15–9. doi: 10.1007/BF01401822
178. Pritz MB, Giannotta SL, Kindt GW, McGillicuddy JE, Prager RL. Treatment of patients with neurological deficits associated with cerebral vasospasm by intravascular volume expansion. *Neurosurgery.* (1978) 3:364–8. doi: 10.1227/00006123-197811000-00006
179. Giannotta SL, McGillicuddy JE, Kindt GW. Diagnosis and treatment of postoperative cerebral vasospasm. *Surg Neurol.* (1977) 8:286–90.
180. Origitano TC, Wascher TM, Reichman OH, Anderson DE. Sustained increased cerebral blood flow with prophylactic hypertensive hypervolemic hemodilution ("triple-H" therapy) after subarachnoid hemorrhage. *Neurosurgery.* (1990) 27:729–39; discussion 739–40. doi: 10.1097/00006123-199011000-00010
181. Roy B, McCullough LD, Dhar R, Grady J, Wang Y-B, Brown RJ. Comparison of initial vasopressors used for delayed cerebral ischemia after aneurysmal subarachnoid hemorrhage. *Cerebrovasc Dis.* (2017) 43:266–71. doi: 10.1159/000458536
182. Touho H, Karasawa J, Ohnishi H, Shishido H, Yamada K, Shibamoto K. Evaluation of therapeutically induced hypertension in patients with delayed cerebral vasospasm by xenon-enhanced computed tomography. *Neurol Med Chir.* (1992) 32:671–8. doi: 10.2176/nmc.32.671
183. Aiyagari V, Cross DT, Deibert E, Dacey RG, Diringer MN. Safety of hemodynamic augmentation in patients treated with Guglielmi detachable coils after acute aneurysmal subarachnoid hemorrhage. *Stroke.* (2001) 32:1994–7. doi: 10.1161/hs0901.094621
184. Miller JA, Dacey RG, Diringer MN. Safety of hypertensive hypervolemic therapy with phenylephrine in the treatment of delayed ischemic deficits after subarachnoid hemorrhage. *Stroke.* (1995) 26:2260–6. doi: 10.1161/01.str.26.12.2260
185. Otsubo H, Takemae T, Inoue T, Kobayashi S, Sugita K. Normovolaemic induced hypertension therapy for cerebral vasospasm after subarachnoid haemorrhage. *Acta Neurochir.* (1990) 103:18–26. doi: 10.1007/BF01420187
186. Murphy A, de Oliveira Manoel AL, Macdonald RL, Baker A, Lee T-Y, Marotta T, et al. Changes in cerebral perfusion with induced hypertension in aneurysmal subarachnoid hemorrhage: a pilot and feasibility study. *Neurocrit Care.* (2017) 27:3–10. doi: 10.1007/s12028-017-0379-6
187. Frontera JA, Fernandez A, Schmidt JM, Claassen J, Wartenberg KE, Badjatia N, et al. Clinical response to hypertensive hypervolemic therapy and outcome after subarachnoid hemorrhage. *Neurosurgery.* (2010) 66:35–41. doi: 10.1227/01.NEU.0000359530.04529.07
188. Qureshi AI, Suarez JI, Bhardwaj A, Yahia AM, Tamargo RJ, Ulatowski JA. Early predictors of outcome in patients receiving hypervolemic and hypertensive therapy for symptomatic vasospasm after subarachnoid hemorrhage. *Crit Care Med.* (2000) 28:824–9. doi: 10.1097/00003246-200003000-00035
189. Raabe A, Beck J, Keller M, Vatter H, Zimmermann M, Seifert V. Relative importance of hypertension compared with hypervolemia for increasing cerebral oxygenation in patients with cerebral vasospasm after subarachnoid hemorrhage. *J Neurosurg.* (2005) 103:974–81. doi: 10.3171/jns.2005.103.6.0974
190. Bederson JB, Connolly ES, Batjer HH, Dacey RG, Dion JE, Diringer MN, et al. Guidelines for the management of aneurysmal subarachnoid hemorrhage: a statement for healthcare professionals from a special writing Group of the Stroke Council, American Heart Association. *Stroke.* (2009) 40:994–1025. doi: 10.1161/STROKEAHA.108.191395
191. Mayberg MR, Batjer HH, Dacey R, Diringer M, Haley EC, Heros RC, et al. Guidelines for the management of aneurysmal subarachnoid hemorrhage. A statement for healthcare professionals from a special writing group of the

Stroke Council, American Heart Association. *Circulation.* (1994) 90:2592–605. doi: 10.1161/01.cir.90.5.2592
192. Brown RJ, Epling BP, Staff I, Fortunato G, Grady JJ, McCullough LD. Polyuria and cerebral vasospasm after aneurysmal subarachnoid hemorrhage. *BMC Neurol.* (2015) 15:201. doi: 10.1186/s12883-015-0446-6
193. Corsten L, Raja A, Guppy K, Roitberg B, Misra M, Alp MS, et al. Contemporary management of subarachnoid hemorrhage and vasospasm: the UIC experience. *Surg Neurol.* (2001) 56:140–8. doi: 10.1016/S0090-3019(01)00513-4
194. Nearman HS, Herman ML. Toxic effects of colloids in the intensive care unit. *Crit Care Clin.* (1991) 7:713–23.
195. Kissoon NR, Mandrekar JN, Fugate JE, Lanzino G, Wijdicks EFM, Rabinstein AA. Positive fluid balance is associated with poor outcomes in subarachnoid hemorrhage. *J Stroke Cerebrovasc Dis.* (2015) 24:2245–51. doi: 10.1016/j.jstrokecerebrovasdis.2015.05.027
196. Maher M, Schweizer TA, Macdonald RL. Treatment of spontaneous subarachnoid hemorrhage: guidelines and gaps. *Stroke.* (2020) 51:1326–32. doi: 10.1161/STROKEAHA.119.025997
197. Lennihan L, Mayer SA, Fink ME, Beckford A, Paik MC, Zhang H, et al. Effect of hypervolemic therapy on cerebral blood flow after subarachnoid hemorrhage : a randomized controlled trial. *Stroke.* (2000) 31:383–91. doi: 10.1161/01.str.31.2.383
198. Egge A, Waterloo K, Sjøholm H, Solberg T, Ingebrigtsen T, Romner B. Prophylactic hyperdynamic postoperative fluid therapy after aneurysmal subarachnoid hemorrhage: a clinical, prospective, randomized, controlled study. *Neurosurgery.* (2001) 49:593–605. doi: 10.1097/00006123-200109000-00012
199. Gathier CS, Dankbaar JW, van der Jagt M, Verweij BH, Oldenbeuving AW, Rinkel GJE, et al. Effects of induced hypertension on cerebral perfusion in delayed cerebral ischemia after aneurysmal subarachnoid hemorrhage: a randomized clinical trial. *Stroke.* (2015) 46:3277–81. doi: 10.1161/STROKEAHA.115.010537
200. Togashi K, Joffe AM, Sekhar L, Kim L, Lam A, Yanez D, et al. Randomized pilot trial of intensive management of blood pressure or volume expansion in subarachnoid hemorrhage (IMPROVES). *Neurosurgery.* (2015) 76:125–34; discussion 134–5; quiz 135. doi: 10.1227/NEU.0000000000000592
201. Tagami T, Kuwamoto K, Watanabe A, Unemoto K, Yokobori S, Matsumoto G, et al. Effect of triple-H prophylaxis on global end-diastolic volume and clinical outcomes in patients with aneurysmal subarachnoid hemorrhage. *Neurocrit Care.* (2014) 21:462–9. doi: 10.1007/s12028-014-9973-z
202. Treggiari MM, Walder B, Suter PM, Romand J-A. Systematic review of the prevention of delayed ischemic neurological deficits with hypertension, hypervolemia, and hemodilution therapy following subarachnoid hemorrhage. *J Neurosurg.* (2003) 98:978–84. doi: 10.3171/jns.2003.98.5.0978
203. Loan JJM, Wiggins AN, Brennan PM. Medically induced hypertension, hypervolaemia and haemodilution for the treatment and prophylaxis of vasospasm following aneurysmal subarachnoid haemorrhage: systematic review. *Br J Neurosurg.* (2018) 32:157–64. doi: 10.1080/02688697.2018.1426720
204. Myburgh JA. "Triple h" therapy for aneurysmal subarachnoid haemorrhage: real therapy or chasing numbers? *Crit Care Resusc.* (2005) 7:206–12.
205. Dankbaar JW, Slooter AJ, Rinkel GJ, Schaaf I. Effect of different components of triple-H therapy on cerebral perfusion in patients with aneurysmal subarachnoid haemorrhage: a systematic review. *Crit Care.* (2010) 14:R23. doi: 10.1186/cc8886
206. Madaelil TP, Dhar R. Posterior reversible encephalopathy syndrome with thalamic involvement during vasopressor treatment of vertebrobasilar vasospasm after subarachnoid hemorrhage. *J Neurointerv Surg.* (2016) 8:e45–e45. doi: 10.1136/neurintsurg-2015-012103.rep
207. Sepideh A-H, Schwartz RB, Sathi S, Stieg PE. Hypertensive encephalopathy as a complication of hyperdynamic therapy for vasospasm: report of two cases. *Neurosurgery.* (1999) 44:1113–6. doi: 10.1097/00006123-199905000-00097
208. Jang HW, Lee HJ. Posterior reversible leukoencephalopathy due to "triple H" therapy. *J Clin Neurosci.* (2010) 17:1059–61. doi: 10.1016/j.jocn.2009.10.006
209. Wartenberg KE, Parra A, CT. and CT-perfusion findings of reversible leukoencephalopathy during triple-H therapy for symptomatic subarachnoid hemorrhage-related vasospasm. *J Neuroimaging.* (2006) 16:170–5. doi: 10.1111/j.1552-6569.2006.00031.x
210. Myburgh JA, Upton RN, Grant C, Martinez A, A. Comparison of the effects of norepinephrine, epinephrine, and dopamine on cerebral blood flow and oxygen utilisation. *Acta Neurochir Suppl.* (1998) 71:19–21. doi: 10.1007/978-3-7091-6475-4_6
211. Amoo M, Henry J, Pender N, Brennan P, Campbell M, Javadpour M. Blood-brain barrier permeability imaging as a predictor for delayed cerebral ischaemia following subarachnoid haemorrhage. A narrative review. *Acta Neurochir.* (2021) 163:1457–67. doi: 10.1007/s00701-020-04670-6
212. Meyer R, Deem S, Yanez ND, Souter M, Lam A, Treggiari MM. Current practices of triple-H prophylaxis and therapy in patients with subarachnoid hemorrhage. *Neurocrit Care.* (2011) 14:24–36. doi: 10.1007/s12028-010-9437-z
213. Towart R. The selective inhibition of serotonin-induced contractions of rabbit cerebral vascular smooth muscle by calcium-antagonistic dihydropyridines. An investigation of the mechanism of action of nimodipine. *Circ Res.* (1981) 48:650–7. doi: 10.1161/01.res.48.5.650
214. Kazda S, Towart R. Nimodipine: a new calcium antagonistic drug with a preferential cerebrovascular action. *Acta Neurochir.* (1982) 63:259–65. doi: 10.1007/bf01728880
215. Scriabine A, Battye R, Hoffmeister F, Kazda S, Towart R, Garthoff B, et al. Nimodipine. *Cardiovasc Drug Rev.* (1985) 3:197–218. doi: 10.1111/j.1527-3466.1985.tb00479.x
216. Rämsch KD, Graefe KH, Scherling D, Sommer J, Ziegler R. Pharmacokinetics and metabolism of calcium-blocking agents nifedipine, nitrendipine, and nimodipine. *Am J Nephrol.* (1986) 6(Suppl. 1):73–80. doi: 10.1159/000167224
217. Harper AM, Craigen L, Kazda S. Effect of the calcium antagonist, nimodipine, on cerebral blood flow and metabolism in the primate. *J Cereb Blood Flow Metab.* (1981) 1:349–56. doi: 10.1038/jcbfm.1981.38
218. Haws CW, Gourley JK, Heistad DD. Effects of nimodipine on cerebral blood flow. *J Pharmacol Exp Ther.* (1983) 225:24–8.
219. Canova D, Roatta S, Micieli G, Bosone D. Cerebral oxygenation and haemodynamic effects induced by nimodipine in healthy subjects. *Funct Neurol.* (2012) 17:169–76.
220. Langley MS, Sorkin EM. Nimodipine. A review of its pharmacodynamic and pharmacokinetic properties, and therapeutic potential in cerebrovascular disease. *Drugs.* (1989) 37:669–99. doi: 10.2165/00003495-198937050-00004
221. Tanaka K, Gotoh F, Muramatsu F, Fukuuchi Y, Okayasu H, Suzuki N, et al. Effect of nimodipine, a calcium antagonist, on cerebral vasospasm after subarachnoid hemorrhage in cats. *Arzneimittelforschung.* (1982) 32:1529–34.
222. Tanaka K, Gotoh F, Muramatsu F, Fukuuchi Y, Amano T, Okayasu H, et al. Effects of nimodipine (Bay e 9736) on cerebral circulation in cats. *Arzneimittelforschung.* (1980) 30:1494–7.
223. Auer LM, Oberbauer RW, Schalk HV. Human pial vascular reactions to intravenous Nimodipine-infusion during EC-IC bypass surgery. *Stroke.* (1983) 14:210–3. doi: 10.1161/01.str.14.2.210
224. Rämsch KD, Ahr G, Tettenborn D, Auer LM. Overview on pharmacokinetics of nimodipine in healthy volunteers and in patients with subarachnoid hemorrhage. *Neurochirurgia.* (1985) 28 (Suppl. 1):74–8. doi: 10.1055/s-2008-1054107
225. Allen GS, Ahn HS, Preziosi TJ, Battye R, Boone SC, Boone SC, et al. Cerebral arterial spasm–a controlled trial of nimodipine in patients with subarachnoid hemorrhage. *N Engl J Med.* (1983) 308:619–24. doi: 10.1056/NEJM198303173081103
226. Albanna W, Weiss M, Conzen C, Clusmann H, Schneider T, Reinsch M, et al. Systemic and cerebral concentration of nimodipine during established and experimental vasospasm treatment. *World Neurosurg.* (2017) 102:459–65. doi: 10.1016/j.wneu.2017.03.062
227. Herbette LG, Trumbore M, Chester DW, Katz AM. Possible molecular basis for the pharmacokinetics and pharmacodynamics of three membrane-active drugs: propranolol, nimodipine and amiodarone. *J Mol Cell Cardiol.* (1988) 20:373–8. doi: 10.1016/s0022-2828(88)80128-7
228. Suwelack D, Weber H, Maruhn D. Pharmacokinetics of Nimodipine. II Communication: distribution, elimination and placental transfer in rats following single and multiple doses of [14C]nimodipine. *Arzneimittelforschung.* (1985) 35:1787–94.

229. Schubert R, Mulvany MJ. The myogenic response: established facts and attractive hypotheses. *Clin Sci.* (1999) 96:313–26.
230. Hill MA, Davis MJ, Meininger GA, Potocnik SJ, Murphy TV. Arteriolar myogenic signalling mechanisms: Implications for local vascular function. *Clin Hemorheol Microcirc.* (2006) 34:67–79.
231. Ljunggren BC, Brandt JL, Säveland HG. Outcome in patients subjected to early aneurysm operation and intravenous nimodipine. *Minerva Med.* (1986) 77:1087–92.
232. Auer LM, Brandt L, Ebeling U, Gilsbach J, Groeger U, Harders A, et al. Nimodipine and early aneurysm operation in good condition SAH patients. *Acta Neurochir.* (1986) 82:7–13. doi: 10.1007/bf01456313
233. Philippon J, Grob R, Dagreou F, Guggiari M, Rivierez M, Viars P. Prevention of vasospasm in subarachnoid haemorrhage. A controlled study with nimodipine. *Acta Neurochir.* (1986) 82:110–4. doi: 10.1007/BF01456369
234. Petruk KC, West M, Mohr G, Weir BK, Benoit BG, Gentili F, et al. Nimodipine treatment in poor-grade aneurysm patients. Results of a multicenter double-blind placebo-controlled trial. *J Neurosurg.* (1988) 68:505–17. doi: 10.3171/jns.1988.68.4.0505
235. Mee E, Dorrance D, Lowe D, Neil-Dwyer G. Controlled study of nimodipine in aneurysm patients treated early after subarachnoid hemorrhage. *Neurosurgery.* (1988) 22:484–91.
236. Jan M, Buchheit F, Tremoulet M. Therapeutic trial of intravenous nimodipine in patients with established cerebral vasospasm after rupture of intracranial aneurysms. *Neurosurgery.* (1988) 23:154–7. doi: 10.1227/00006123-198808000-00004
237. Pickard JD, Murray GD, Illingworth R, Shaw MD, Teasdale GM, Foy PM, et al. Effect of oral nimodipine on cerebral infarction and outcome after subarachnoid haemorrhage: british aneurysm nimodipine trial. *BMJ.* (1989) 298:636–42. doi: 10.1136/bmj.298.6674.636
238. Messeter K, Brandt L, Ljunggren B, Svendgaard NA, Algotsson L, Romner B, et al. Prediction and prevention of delayed ischemic dysfunction after aneurysmal subarachnoid hemorrhage and early operation. *Neurosurgery.* (1987) 20:548–53. doi: 10.1227/00006123-198704000-00007
239. Ohman J, Servo A, Heiskanen O. Long-term effects of nimodipine on cerebral infarcts and outcome after aneurysmal subarachnoid hemorrhage and surgery. *J Neurosurg.* (1991) 74:8–13. doi: 10.3171/jns.1991.74.1.0008
240. Rasmussen G, Bergholdt B, Dalh B, Sunde N, Cold G, Voldby B. Effect of nimodipine on cerebral blood flow and cerebrovascular reactivity after subarachnoid haemorrhage. *Acta Neurol Scand.* (1999) 99:182–6. doi: 10.1111/j.1600-0404.1999.tb07341.x
241. Choi HA, Ko S-B, Chen H, Gilmore E, Carpenter AM, Lee D, et al. Acute effects of nimodipine on cerebral vasculature and brain metabolism in high grade subarachnoid hemorrhage patients. *Neurocrit Care.* (2012) 16:363–7. doi: 10.1007/s12028-012-9670-8
242. Hänggi D, Turowski B, Beseoglu K, Yong M, Steiger HJ. Intra-arterial nimodipine for severe cerebral vasospasm after aneurysmal subarachnoid hemorrhage: influence on clinical course and cerebral perfusion. *AJNR Am J Neuroradiol.* (2008) 29:1053–60. doi: 10.3174/ajnr.A1005
243. Karinen P, Koivukangas P, Ohinmaa A, Koivukangas J, Ohman J. Cost-effectiveness analysis of nimodipine treatment after aneurysmal subarachnoid hemorrhage and surgery. *Neurosurgery.* (1999) 45:780–4; discussion 784–5. doi: 10.1097/00006123-199910000-00009
244. Velat GJ, Kimball MM, Mocco JD, Hoh BL. Vasospasm after aneurysmal subarachnoid hemorrhage: review of randomized controlled trials and meta-analyses in the literature. *World Neurosurg.* (2011) 76:446–54. doi: 10.1016/j.wneu.2011.02.030
245. Zhang J, Yang J, Zhang C, Jiang X, Zhou H, Liu M. Calcium antagonists for acute ischemic stroke. *Cochrane Database Syst Rev.* (2012) 2:CD001928. doi: 10.1002/14651858.CD001928.pub2
246. Langham J, Goldfrad C, Teasdale G, Shaw D, Rowan K. Calcium channel blockers for acute traumatic brain injury. *Cochrane Database Syst Rev.* (2003) 4:CD000565. doi: 10.1002/14651858.CD000565
247. Schmidt JF, Waldemar G. Effect of nimodipine on cerebral blood flow in human volunteers. *J Cardiovasc Pharmacol.* (1990) 16:568–71. doi: 10.1097/00005344-199010000-00007
248. Höllerhage HG, Gaab MR, Zumkeller M, Walter GF. The influence of nimodipine on cerebral blood flow autoregulation and blood-brain barrier. *J Neurosurg.* (1988) 69:919–22. doi: 10.3171/jns.1988.69.6.0919
249. Stånge K, Lagerkranser M, Sollevi A. Nimodipine does not affect the cerebral autoregulatory response in the anesthetized pig. *J Neurosurg Anesthesiol.* (1994) 6:116–21. doi: 10.1097/00008506-199404000-00007
250. Hauerberg J, Rasmussen G, Juhler M, Gjerris F. The effect of nimodipine on autoregulation of cerebral blood flow after subarachnoid haemorrhage in rat. *Acta Neurochir (Wien).* (1995) 132:98–103. doi: 10.1007/bf01404855
251. Dreier JP. The role of spreading depression, spreading depolarization and spreading ischemia in neurological disease. *Nat Med.* (2011) 17:439–47. doi: 10.1038/nm.2333
252. Ricci A, Sabbatini M, Tomassoni D, Mignini F, Petrelli C, Amenta F. Neuronal populations of rat cerebral cortex and hippocampus expressed a higher density of L-type Ca 2+ channel than corresponding cerebral vessels. *Clin Exp Hypertens.* (2002) 24:715–26. 12450246
253. Dreier JP, Woitzik J, Fabricius M, Bhatia R, Major S, Drenckhahn C, et al. Delayed ischaemic neurological deficits after subarachnoid haemorrhage are associated with clusters of spreading depolarizations. *Brain.* (2006) 129:3224–37. doi: 10.1093/brain/awl297
254. Sarrafzadeh A, Santos E, Wiesenthal D, Martus P, Vajkoczy P, Oehmchen M, et al. Cerebral glucose and spreading depolarization in patients with aneurysmal subarachnoid hemorrhage. *Acta Neurochir Suppl.* (2013) 115:143–7. doi: 10.1007/978-3-7091-1192-5_28
255. Hartings JA, York J, Carroll CP, Hinzman JM, Mahoney E, Krueger B, et al. Subarachnoid blood acutely induces spreading depolarizations and early cortical infarction. *Brain.* (2017) 140:2673–90. doi: 10.1093/brain/awx214
256. Richter F, Ebersberger A, Schaible H-GG. Blockade of voltage-gated calcium channels in rat inhibits repetitive cortical spreading depression. *Neurosci Lett.* (2002) 334:123–6. doi: 10.1016/s0304-3940(02)01120-5
257. Szabó Í, Tóth MO, Török Z, Varga DP, Menyhárt Á, Frank R, et al. The impact of dihydropyridine derivatives on the cerebral blood flow response to somatosensory stimulation and spreading depolarization. *Br J Pharmacol.* (2019) 176:1222–34. doi: 10.1111/bph.14611
258. Nuglisch J, Karkoutly C, Mennel HD, Roßberg C, Krieglstein J. Protective effect of nimodipine against ischemic neuronal damage in rat hippocampus without changing postischemic cerebral blood flow. *J Cereb Blood Flow Metab.* (1990) 10:654–9. doi: 10.1038/jcbfm.1990.118
259. Di Mascio R, Marchioli R, Tognoni G. From pharmacological promises to controlled clinical trials to meta-analysis and back: the case of nimodipine in cerebrovascular disorders. *Clin Trials Metaanal.* (1994) 29:57–79.
260. Pisani A, Calabresi P, Tozzi A, D'Angelo V, Bernardi G. L-type Ca^{2+} channel blockers attenuate electrical changes and Ca^{2+} rise induced by oxygen/glucose deprivation in cortical neurons. *Stroke.* (1998) 29:196–201; discussion 202.
261. Hockel K, Diedler J, Steiner J, Birkenhauer U, Ernemann U, Schuhmann MU. Effect of intra-arterial and intravenous nimodipine therapy of cerebral vasospasm after subarachnoid hemorrhage on cerebrovascular reactivity and oxygenation. *World Neurosurg.* (2017) 101:372–8. doi: 10.1016/j.wneu.2017.02.014
262. Daou BJ, Koduri S, Thompson BG, Chaudhary N, Pandey AS. Clinical and experimental aspects of aneurysmal subarachnoid hemorrhage. *CNS Neurosci Ther.* (2019) 25:1096–112. doi: 10.1111/cns.13222
263. Haley EC, Kassell NF, Torner JC, A. randomized controlled trial of high-dose intravenous nicardipine in aneurysmal subarachnoid hemorrhage. A report of the Cooperative Aneurysm Study. *J Neurosurg.* (1993) 78:537–47. doi: 10.3171/jns.1993.78.4.0537
264. Wong GKC, Poon WS, Chan MTV, Boet R, Gin T, Ng SCP, et al. Intravenous magnesium sulphate for aneurysmal subarachnoid hemorrhage (IMASH): a randomized, double-blinded, placebo-controlled, multicenter phase III trial. *Stroke.* (2010) 41:921–6. doi: 10.1161/STROKEAHA.109.571125
265. Leijenaar JF, Mees SMD, Algra A, Van Den Bergh WM, Rinkel GJE. Effect of magnesium treatment and glucose levels on delayed cerebral ischemia in patients with subarachnoid hemorrhage: a substudy of the Magnesium in Aneurysmal Subarachnoid Haemorrhage trial (MASH-II). *Int J Stroke.* (2015) 10:108–12. doi: 10.1111/ijs.12621
266. Vergouwen MD, Meijers JC, Geskus RB, Coert BA, Horn J, Stroes ES, et al. Biologic effects of simvastatin in patients with aneurysmal subarachnoid hemorrhage: a double-blind, placebo-controlled randomized trial. *J Cereb Blood Flow Metab.* (2009) 29:1444–53. doi: 10.1038/jcbfm.2009.59

267. Kirkpatrick PJ, Turner CL, Smith C, Hutchinson PJ, Murray GD. Simvastatin in aneurysmal subarachnoid haemorrhage (STASH): a multicentre randomised phase 3 trial. *Lancet Neurol.* (2014) 13:666–75. doi: 10.1016/S1474-4422(14)70084-5
268. Zhang S, Wang L, Liu M, Wu B. Tirilazad for aneurysmal subarachnoid haemorrhage. *Cochrane Database Syst Rev.* (2010) 2:CD006778. doi: 10.1002/14651858.CD006778.pub2
269. Güresir E, Vasiliadis N, Konczalla J, Raab P, Hattingen E, Seifert V, et al. Erythropoietin prevents delayed hemodynamic dysfunction after subarachnoid hemorrhage in a randomized controlled experimental setting. *J Neurol Sci.* (2013) 332:128–35. doi: 10.1016/j.jns.2013.07.004
270. Helbok R, Shaker E, Beer R, Chemelli A, Sojer M, Sohm F, et al. High dose erythropoietin increases brain tissue oxygen tension in severe vasospasm after subarachnoid hemorrhage. *BMC Neurol.* (2012) 12:32. doi: 10.1186/1471-2377-12-32
271. Jahromi BS, Aihara Y, Ai J, Zhang Z-D, Nikitina E, Macdonald RL. Voltage-gated K+ channel dysfunction in myocytes from a dog model of subarachnoid hemorrhage. *J Cereb Blood Flow Metab.* (2008) 28:797–811. doi: 10.1038/sj.jcbfm.9600577
272. Ishiguro M, Morielli AD, Zvarova K, Tranmer BI, Penar PL, Wellman GC. Oxyhemoglobin-induced suppression of voltage-dependent K+ channels in cerebral arteries by enhanced tyrosine kinase activity. *Circ Res.* (2006) 99:1252–60. doi: 10.1161/01.RES.0000250821.32324.e1
273. Koide M, Wellman GC. SAH-induced MMP activation and K V current suppression is mediated *via* both ROS-dependent and ROS-independent mechanisms. *Acta Neurochir Suppl.* (2015) 120:89–94. doi: 10.1007/978-3-319-04981-6_15
274. Koide M, Wellman GC. SAH-induced suppression of voltage-gated K(+) (K (V)) channel currents in parenchymal arteriolar myocytes involves activation of the HB-EGF/EGFR pathway. *Acta Neurochir Suppl.* (2013) 115:179–84. doi: 10.1007/978-3-7091-1192-5_34
275. Aihara Y, Jahromi BS, Yassari R, Nikitina E, Agbaje-Williams M, Macdonald RL. Molecular profile of vascular ion channels after experimental subarachnoid hemorrhage. *J Cereb Blood Flow Metab.* (2004) 24:75–83. doi: 10.1097/01.WCB.0000095803.98378.D8
276. Mani BK, O'Dowd J, Kumar L, Brueggemann LI, Ross M, Byron KL. Vascular KCNQ (Kv7) potassium channels as common signaling intermediates and therapeutic targets in cerebral vasospasm. *J Cardiovasc Pharmacol.* (2013) 61:51–62. doi: 10.1097/FJC.0b013e3182771708
277. Bentzen BH, Olesen S-P, Rønn LCB, Grunnet M, BK. channel activators and their therapeutic perspectives. *Front Physiol.* (2014) 5:389. doi: 10.3389/fphys.2014.00389
278. Demirci AY, Seckin H, Besalti O, Arikok AT, Yigitkanli T, Caliskan M, et al. Study the effects of zonisamide on fine structure of rabbit basilar artery and hippocampus in rabbit subarachnoid hemorrhage model. *Acta Neurochir.* (2013) 155:1531–7. doi: 10.1007/s00701-013-1726-9
279. Sarkis RA, Goksen Y, Mu Y, Rosner B, Lee JW. Cognitive and fatigue side effects of anti-epileptic drugs: an analysis of phase III add-on trials. *J Neurol.* (2018) 265:2137–42. doi: 10.1007/s00415-018-8971-z
280. Plosker GL, Scott LJ. Retigabine: in partial seizures. *CNS Drugs.* (2006) 20:601–8. doi: 10.2165/00023210-200620070-00005
281. Bazzoni F, Beutler B. The tumor necrosis factor ligand and receptor families. *N Engl J Med.* (1996) 334:1717–25. doi: 10.1056/NEJM199606273342607
282. Hehlgans T, Männel DN. The TNF-TNF receptor system. *Biol Chem.* (2002) 383:1581–5. doi: 10.1515/BC.2002.178
283. Calligaris M, Cuffaro D, Bonelli S, Spanò DP, Rossello A, Nuti E, et al. Strategies to target ADAM17 in disease: from its discovery to the iRhom revolution. *Molecules.* (2021) 26:944. doi: 10.3390/molecules26040944
284. Pitson SM, Moretti PAB, Zebol JR, Lynn HE, Xia P, Vadas MA, et al. Activation of sphingosine kinase 1 by ERK1/2-mediated phosphorylation. *EMBO J.* (2003) 22:5491–500. doi: 10.1093/emboj/cdg540
285. Meissner A, Yang J, Kroetsch JT, Sauvé M, Dax H, Momen A, et al. Tumor necrosis factor-α-mediated downregulation of the cystic fibrosis transmembrane conductance regulator drives pathological sphingosine-1-phosphate signaling in a mouse model of heart failure. *Circulation.* (2012) 125:2739–50. doi: 10.1161/CIRCULATIONAHA.111.047316
286. Boujaoude LC, Bradshaw-Wilder C, Mao C, Cohn J, Ogretmen B, Hannun YA, et al. Cystic fibrosis transmembrane regulator regulates uptake of sphingoid base phosphates and lysophosphatidic acid: modulation of cellular activity of sphingosine 1-phosphate. *J Biol Chem.* (2001) 276:35258–64. doi: 10.1074/jbc.M105442200
287. Peter BF, Lidington D, Harada A, Bolz HJ, Vogel L, Heximer S, et al. Role of sphingosine-1-phosphate phosphohydrolase 1 in the regulation of resistance artery tone. *Circ Res.* (2008) 103:315–24. doi: 10.1161/CIRCRESAHA.108.173575
288. Yang J, Hossein Noyan-Ashraf M, Meissner A, Voigtlaender-Bolz J, Kroetsch JT, Foltz W, et al. Proximal cerebral arteries develop myogenic responsiveness in heart failure *via* tumor necrosis factor-α-dependent activation of sphingosine-1-phosphate signaling. *Circulation.* (2012) 126:196–206. doi: 10.1161/CIRCULATIONAHA.111.039644
289. Lim M, Choi S-K, Cho Y-E, Yeon S-I, Kim E-C, Ahn D-S, et al. The role of sphingosine kinase 1/sphingosine-1-phosphate pathway in the myogenic tone of posterior cerebral arteries. *PLoS ONE.* (2012) 7:e35177. doi: 10.1371/journal.pone.0035177
290. Salomone S, Soydan G, Ip PC-T, Hopson KMP, Waeber C. Vessel-specific role of sphingosine kinase 1 in the vasoconstriction of isolated basilar arteries. *Pharmacol Res.* (2010) 62:465–74. doi: 10.1016/j.phrs.2010.09.002
291. Tosaka M, Okajima F, Hashiba Y, Saito N, Nagano T, Watanabe T, et al. Sphingosine 1-phosphate contracts canine basilar arteries *in vitro* and *in vivo*: possible role in pathogenesis of cerebral vasospasm. *Stroke.* (2001) 32:2913–9. doi: 10.1161/hs1201.099525
292. Watterson KR, Ratz PH, Spiegel S. The role of sphingosine-1-phosphate in smooth muscle contraction. *Cell Signal.* (2005) 17:289–98. doi: 10.1016/j.cellsig.2004.09.013
293. Fassbender K, Hodapp B, Rossol S, Bertsch T, Schmeck J, Schütt S, et al. Inflammatory cytokines in subarachnoid haemorrhage: association with abnormal blood flow velocities in basal cerebral arteries. *J Neurol Neurosurg Psychiatry.* (2001) 70:534–7. doi: 10.1136/jnnp.70.4.534
294. Mathiesen T, Edner G, Ulfarsson E, Andersson B. Cerebrospinal fluid interleukin-1 receptor antagonist and tumor necrosis factor-alpha following subarachnoid hemorrhage. *J Neurosurg.* (1997) 87:215–20. doi: 10.3171/jns.1997.87.2.0215
295. Hanafy KA, Grobelny B, Fernandez L, Kurtz P, Connolly ES, Mayer SA, et al. Brain interstitial fluid TNF-alpha after subarachnoid hemorrhage. *J Neurol Sci.* (2010) 291:69–73. doi: 10.1016/j.jns.2009.12.023
296. Lad SP, Hegen H, Gupta G, Deisenhammer F, Steinberg GK. Proteomic biomarker discovery in cerebrospinal fluid for cerebral vasospasm following subarachnoid hemorrhage. *J Stroke Cerebrovasc Dis.* (2012) 21:30–41. doi: 10.1016/j.jstrokecerebrovasdis.2010.04.004
297. Hanafy KA, Stuart RM, Khandji AG, Connolly ES, Badjatia N, Mayer SA, et al. Relationship between brain interstitial fluid tumor necrosis factor-α and cerebral vasospasm after aneurysmal subarachnoid hemorrhage. *J Clin Neurosci.* (2010) 17:853–6. doi: 10.1016/j.jocn.2009.11.041
298. Vecchione C, Frati A, Di Pardo A, Cifelli G, Carnevale D, Gentile MT, et al. Tumor necrosis factor-alpha mediates hemolysis-induced vasoconstriction and the cerebral vasospasm evoked by subarachnoid hemorrhage. *Hypertension.* (2009) 54:150–6. doi: 10.1161/HYPERTENSIONAHA.108.128124
299. Toguşlu G, Erdi MF, Araç D, Keskin F, Kilinç I, Cüce G. Ameliorating the effects of Adalimumab on rabbits with experimental cerebral vasospasm after subarachnoid hemorrhage. *Ulus Travma Acil Cerrahi Derg.* (2020) 26:847–52. doi: 10.14744/tjtes.2019.52504
300. Zhang B, Song J, Ma X, Zhao Y, Liu Z, Li Y, et al. Etanercept alleviates early brain injury following experimental subarachnoid hemorrhage and the possible role of tumor necrosis factor-α and c-Jun N-terminal kinase pathway. *Neurochem Res.* (2015) 40:591–9. doi: 10.1007/s11064-014-1506-9
301. Männer A, Thomas D, Wagner M, Konczalla J, Steinmetz H, Brunkhorst R, et al. Sphingosine 1-phosphate levels in cerebrospinal fluid after subarachnoid hemorrhage. *Neurol Res Pract.* (2020) 2:49. doi: 10.1186/s42466-020-00093-x
302. Wang Y, Zhou S, Han Z, Yin D, Luo Y, Tian Y, et al. Fingolimod administration improves neurological functions of mice with subarachnoid hemorrhage. *Neurosci Lett.* (2020) 736:135250. doi: 10.1016/j.neulet.2020.135250

303. Xu H-L, Pelligrino DA, Paisansathan C, Testai FD. Protective role of fingolimod (FTY720) in rats subjected to subarachnoid hemorrhage. *J Neuroinflammation.* (2015) 12:16. doi: 10.1186/s12974-015-0234-7
304. Zhao J, Zhou D, Guo J, Ren Z, Zhou L, Wang S, et al. Efficacy and safety of fasudil in patients with subarachnoid hemorrhage: final results of a randomized trial of fasudil versus nimodipine. *Neurol Med Chir.* (2011) 51:679–83. doi: 10.2176/nmc.51.679
305. Zhao J, Zhou D, Guo J, Ren Z, Zhou L, Wang S, et al. Effect of fasudil hydrochloride, a protein kinase inhibitor, on cerebral vasospasm and delayed cerebral ischemic symptoms after aneurysmal subarachnoid hemorrhage. *Neurol Med Chir.* (2006) 46:421–8. doi: 10.2176/nmc.46.421
306. Shibuya M, Suzuki Y, Sugita K, Saito I, Sasaki T, Takakura K, et al. Effect of AT877 on cerebral vasospasm after aneurysmal subarachnoid hemorrhage. Results of a prospective placebo-controlled double-blind trial. *J Neurosurg.* (1992) 76:571–7. doi: 10.3171/jns.1992.76.4.0571
307. Liu GJ, Wang ZJ, Wang YF, Xu LL, Wang XL, Liu Y, et al. Systematic assessment and meta-analysis of the efficacy and safety of fasudil in the treatment of cerebral vasospasm in patients with subarachnoid hemorrhage. *Eur J Clin Pharmacol.* (2012) 68:131–9. doi: 10.1007/s00228-011-1100-x
308. Yoshii F, Moriya Y, Ohnuki T, Ryo M, Takahashi W. Neurological safety of fingolimod: an updated review. *Clin Exp Neuroimmunol.* (2017) 8:233–43. doi: 10.1111/cen3.12397
309. Fu Y, Zhang N, Ren L, Yan Y, Sun N, Li Y-J, et al. Impact of an immune modulator fingolimod on acute ischemic stroke. *Proc Natl Acad Sci USA.* (2014) 111:18315–20. doi: 10.1073/pnas.1416166111
310. Fu Y, Hao J, Zhang N, Ren L, Sun N, Li Y-J, et al. Fingolimod for the treatment of intracerebral hemorrhage: a 2-arm proof-of-concept study. *JAMA Neurol.* (2014) 71:1092–101. doi: 10.1001/jamaneurol.2014.1065
311. Maass F, von Gottberg P, Franz J, Stadelmann C, Bähr M, Weber MS. Case report: findings suggestive of paraclinical progressive multifocal leukoencephalopathy and lung cancer-derived brain metastases in an MS patient treated with fingolimod. *Front Neurol.* (2021) 12:561158. doi: 10.3389/fneur.2021.561158
312. Murdaca G, Spanò F, Contatore M, Guastalla A, Penza E, Magnani O, et al. Infection risk associated with anti-TNF-α agents: a review. *Expert Opin Drug Saf.* (2015) 14:571–82. doi: 10.1517/14740338.2015.1009036
313. Suzuki Y, Shibuya M, Satoh S, Sugimoto Y, Takakura K, A. postmarketing surveillance study of fasudil treatment after aneurysmal subarachnoid hemorrhage. *Surg Neurol.* (2007) 68:126–32. doi: 10.1016/j.surneu.2006.10.037
314. Boyle MP, Bell SC, Konstan MW, McColley SA, Rowe SM, Rietschel E, et al. corrector (lumacaftor) and a CFTR potentiator (ivacaftor) for treatment of patients with cystic fibrosis who have a phe508del CFTR mutation: a phase 2 randomised controlled trial. *Lancet Respir Med.* (2014) 2:527–38. doi: 10.1016/S2213-2600(14)70132-8
315. Okiyoneda T, Veit G, Dekkers JF, Bagdany M, Soya N, Xu H, et al. Mechanism-based corrector combination restores ΔF508-CFTR folding and function. *Nat Chem Biol.* (2013) 9:444–54. doi: 10.1038/nchembio.1253
316. Hui S, Levy AS, Slack DL, Burnstein MJ, Errett L, Bonneau D, et al. Sphingosine-1-phosphate signaling regulates myogenic responsiveness in human resistance arteries. *PLoS ONE.* (2015) 10:e0138142. doi: 10.1371/journal.pone.0138142
317. Marigowda G, Liu F, Waltz D. Effect of bronchodilators in healthy individuals receiving lumacaftor/ivacaftor combination therapy. *J Cyst Fibros.* (2017) 16:246–9. doi: 10.1016/j.jcf.2016.11.001
318. Solomon GM, Hathorne H, Liu B, Raju SV, Reeves G, Acosta EP, et al. Pilot evaluation of ivacaftor for chronic bronchitis. *Lancet Respir Med.* (2016) 4:e32–3. doi: 10.1016/S2213-2600(16)30047-9

Conflict of Interest: DL is a consultant for Qanatpharma AG (Stans, Switzerland). SS-B is executive board member of Qanatpharma AG and Aphaia Pharma AG (Zug, Switzerland). Neither Qanatpharma AG nor Aphaia Pharma AG had any financial or intellectual involvement in this article.

The remaining author declares that the research was conducted in the absence of any commercial or financial relationships that could be construed as a potential conflict of interest.

Publisher's Note: All claims expressed in this article are solely those of the authors and do not necessarily represent those of their affiliated organizations, or those of the publisher, the editors and the reviewers. Any product that may be evaluated in this article, or claim that may be made by its manufacturer, is not guaranteed or endorsed by the publisher.

frontiers in Neurology

REVIEW
published: 16 August 2021
doi: 10.3389/fneur.2021.692207

Association Between Processed Electroencephalogram-Based Objectively Measured Depth of Sedation and Cerebrovascular Response: A Systematic Scoping Overview of the Human and Animal Literature

Logan Froese[1], Joshua Dian[2], Alwyn Gomez[2,3], Carleen Batson[3], Amanjyot Singh Sainbhi[1] and Frederick A. Zeiler[1,2,3,4,5]*

[1] Biomedical Engineering, Faculty of Engineering, University of Manitoba, Winnipeg, MB, Canada, [2] Section of Neurosurgery, Department of Surgery, Rady Faculty of Health Sciences, University of Manitoba, Winnipeg, MB, Canada, [3] Department of Human Anatomy and Cell Science, Rady Faculty of Health Sciences, University of Manitoba, Winnipeg, MB, Canada, [4] Centre on Aging, University of Manitoba, Winnipeg, MB, Canada, [5] Division of Anaesthesia, Department of Medicine, Addenbrooke's Hospital, University of Cambridge, Cambridge, United Kingdom

OPEN ACCESS

Edited by:
Xiuyun Liu,
Johns Hopkins University,
United States

Reviewed by:
Teodor Mikael Svedung Wettervik,
Uppsala University, Sweden
Gyaninder Pal Singh,
All India Institute of Medical Sciences, India

***Correspondence:**
Logan Froese
log.froese@gmail.com

Specialty section:
This article was submitted to Neurocritical and Neurohospitalist Care, a section of the journal Frontiers in Neurology

Received: *07 April 2021*
Accepted: *21 July 2021*
Published: *16 August 2021*

Citation:
Froese L, Dian J, Gomez A, Batson C, Sainbhi AS and Zeiler FA (2021) Association Between Processed Electroencephalogram-Based Objectively Measured Depth of Sedation and Cerebrovascular Response: A Systematic Scoping Overview of the Human and Animal Literature. Front. Neurol. 12:692207. doi: 10.3389/fneur.2021.692207

Background: Current understanding of the impact that sedative agents have on neurovascular coupling, cerebral blood flow (CBF) and cerebrovascular response remains uncertain. One confounding factor regarding the impact of sedative agents is the depth of sedation, which is often determined at the bedside using clinical examination scoring systems. Such systems do not objectively account for sedation depth at the neurovascular level. As the depth of sedation can impact CBF and cerebral metabolism, the need for objective assessments of sedation depth is key. This is particularly the case in traumatic brain injury (TBI), where emerging literature suggests that cerebrovascular dysfunction dominates the burden of physiological dysfunction. Processed electroencephalogram (EEG) entropy measures are one possible solution to objectively quantify depth of sedation. Such measures are widely employed within anesthesia and are easy to employ at the bedside. However, the association between such EEG measures and cerebrovascular response remains unclear. Thus, to improve our understanding of the relationship between objectively measured depth of sedation and cerebrovascular response, we performed a scoping review of the literature.

Methods: A systematically conduced scoping review of the existing literature on objectively measured sedation depth and CBF/cerebrovascular response was performed, search multiple databases from inception to November 2020. All available literature was reviewed to assess the association between objective sedation depth [as measured through processed electroencephalogram (EEG)] and CBF/cerebral autoregulation.

Results: A total of 13 articles, 12 on adult humans and 1 on animal models, were identified. Initiation of sedation was found to decrease processed EEG entropy and

CBF/cerebrovascular response measures. However, after this initial drop in values there is a wide range of responses in CBF seen. There were limited statistically reproduceable associations between processed EEG and CBF/cerebrovascular response. The literature body remains heterogeneous in both pathological states studied and sedative agent utilized, limiting the strength of conclusions that can be made.

Conclusions: Conclusions about sedation depth, neurovascular coupling, CBF, and cerebrovascular response are limited. Much further work is required to outline the impact of sedation on neurovascular coupling.

Keywords: bispectral index, cerebrovascular autoregulation, cerebrovascular response, depth of sedation, entropy index

INTRODUCTION

The near ubiquitous use of sedation throughout a variety of critical care illnesses and its ability to help mediate the cascading secondary injury pathways in the setting of acute neurological injuries (1), highlights sedation as an important aspect of patient care in the intensive care unit (ICU). Despite the widespread use of sedation, the correlation between objectively measured depth of sedation, neurovascular coupling and cerebrovascular response/cerebral blood flow (CBF) is limited (2–5). To date, most assessments of sedation depth in the ICU occur using bedside clinical examination scoring systems, which are confounded by inter- and intra-assessor heterogeneity (6–8). In addition, such clinical exam scores do not objectively measure sedation depth at the neurological level but merely utilize the patient's response to stimuli as a surrogate for sedation depth. Moreover, there is still a major concern with overuse of sedatives as emerging evidence demonstrates an association between sedative dosing exposure and worse overall 6 month outcomes (9–12).

In specific critical illnesses, the impact that sedation has on cerebrovascular response is of paramount interest. Such is the case in the treatment of moderate/severe traumatic brain injuries (TBI), where sedation is used for its ability to reduce cerebral metabolic activity and conserve CBF with the hopes that it will maintain healthy homeostasis and reduce secondary injury (13, 14). However, recent comprehensive reviews evaluating the impact of various commonly utilized sedative agents in TBI care, and their corresponding impact on CBF/cerebrovascular response, have demonstrated conflicting results (3, 4, 15). Studies identified in these reviews failed to record objectively measured sedation depth, and only commented on the sedative agent type and dosing. Similarly, two recent works evaluating continuously measured cerebrovascular reactivity in TBI patients, in response to fluctuations in sedative agent doses, found that sedative dose change resulted in little-to-no impact on cerebrovascular reactivity (5, 16). However, again, no objective measures of sedation depth were utilized in these works. Thus, it remains unknown if there is an optimal depth of sedation in each individual patient which would promote recovery while preserving neurovascular coupling and a healthy cerebrovascular state.

Processed electroencephalogram (EEG) is a commonly utilized technology in the operating room, to objectively assess sedation depth during anesthesia. Bispectral index (BIS) monitoring is the most common processed EEG method to assess sedation depth objectively, with the Entropy index monitoring less prevalent. Both of these indices leverage primarily superficial EEG signals from the frontal lobe (17, 18). However, BIS and Entropy Index adoption for routine monitoring in the ICU has been limited. Furthermore, the association between BIS/Entropy metrics and CBF/cerebrovascular response is uncertain. Though recent work from our laboratory suggests there is the presence of individual patient optimal sedation levels in TBI as measured through BIS (16), such findings are still preliminary and exploratory in nature. Thus, if we are to adopt BIS for continuous assessment of sedation depth in critical and neurocritical care, we require clarity regarding any link between its metrics, neurovascular coupling and CBF/cerebrovascular response. As such, the goal of this study was to perform a systematically conducted scoping review of the literature, assessing for any documented association between BIS and CBF/cerebrovascular reactivity, in humans or animal models.

MATERIALS AND METHODS

A systematically conducted scoping review of the available literature was conducted using the methodology outlined in the Cochrane Handbook for Systematic Reviewers (19). The data was reported in line with the Preferred Reporting Items for Systematic Reviews and Meta-Analyses (PRISMA) (20). Appendix A of the **Supplementary Materials** provides the PRISMA checklist. Search strategy and methodology is similar to other scoping reviews published by our group (3, 21, 22).

The review questions and search strategy were decided upon by the supervisor (F.A.Z.) and primary author (L.F.).

Search Question, Population, and Inclusion and Exclusion Criteria

The question posed for systematic review was: What is the association between objectively measured depth of sedation, as assessed with processed EEG (i.e., BIS), and the CBF/cerebrovascular response? All studies, either prospective or retrospective, of any size were included. We also included both

human and animal studies, to be comprehensive in our scoping overview of the literature.

The primary outcome measure was the association between processed EEG measures and CBF or the cerebrovascular responsiveness, as documented by any neuroimaging technique (i.e., magnetic resonance imaging, computed tomography, PET) or continuous CBF/cerebrovascular monitoring (i.e., laser-Doppler flow probe, transcranial Doppler or any other objective means of CBF determination). Similarly, studies evaluating BIS and cerebral autoregulation/cerebrovascular reactivity, in response to sedation administration, we also included. Secondary outcomes included any other associated physiologic responses to BIS that were documented.

All studies whether prospective or retrospective, of all sizes, human subject or animal models, and with the use of processed EEG (i.e., BIS or Entropy Index) with formal documentation of cerebrovascular response/CBF were eligible for inclusion in this review. Exclusion criteria were the following: being non-English, using non-processed EEG (i.e., not BIS or Entropy Index), or lacking documentation of the association between processed EEG metrics and CBF/cerebrovascular response.

Search Strategy

MEDLINE, BIOSIS, EMBASE, Global Health, SCOPUS, and Cochrane Library from inception to November 2020 were searched using individualized search strategies for each database. The search strategy for MEDLINE can be seen in Appendix B of the **Supplementary Materials**, with a similar search strategy used for the other databases. Finally, the reference lists of review articles on the cerebrovascular/CBF response to sedation were examined to ensure no references were left out.

Study Selection

Using 2 reviewers (LF and JD), a 2-step review of all articles returned by our search strategies was performed. First, the reviewers independently screened all titles and abstracts of the returned articles to decide whether they met the inclusion criteria. Second, full text of the chosen articles was assessed to confirm whether they met the inclusion criteria and that the primary outcome of documented association between processed EEG and CBF/cerebrovascular response. Any discrepancies between the 2 reviewers were resolved by a third party (FZ).

Data Collection

Data was extracted from the selected articles and stored in multiple electronic databases to ensure data integrity.

Human Studies

Data fields included the following: number of patients, study type, mean age, patient characteristics, goal of the study, sedation dose and duration, technique to measure CBF/cerebrovascular assessment, CBF/cerebrovascular response, other outcomes and conclusion (i.e., regarding association between BIS and CBF/cerebrovascular response).

Animal Studies

Data fields included the following: type of models and model characteristics, goal of the study, sedation dose, technique to measure CBF/cerebrovascular assessment, CBF/cerebrovascular response, other outcomes, and conclusion (i.e., regarding association between BIS and CBF/cerebrovascular response).

Bias Assessment

Given the goal of this review was to provide a comprehensive scoping overview of the available literature, a formal bias assessment was not conducted.

Statistical Analysis

A meta-analysis was not performed in this study because of the heterogeneity of study designs and data.

RESULTS

Search Results and Study Characteristics

The results of the search strategy across all databases and other sources are summarized in **Figure 1**. Overall, a total of 8,707 articles were identified from the databases searched. A total of 2,747 articles were removed because of duplicated references, leaving 5,960 to review. By applying the inclusion/exclusion criteria to the title and abstract of these articles, we identified 72 articles that fit these criteria. Three articles were added from reference sections of pertinent review articles, leaving a total of 75 full papers to review. On applying the inclusion/exclusion criteria to the full-text documents, only 13 articles were found eligible for inclusion in the systematic review. Articles were excluded because they either did not report details around the association between processed EEG and CBF/cerebrovascular response, were review articles, or were non-relevant. Twelve articles described human adult patients, and the other 1 used animal models. All were original studies, with none describing patients under the age of 18.

Tables 1, **2** show the 12 articles that had human patients and documented the association between processed EEG and CBF/cerebrovascular response (23–34). All articles used the BIS methodology, except for one which used the Entropy Index (23). Patients were either under deep sedation or varying levels of sedation (23, 26, 27), or sleeping (in one study) (24). In order to characterize CBF and vasculature response, the following techniques were used: Positron Emission Tomography (PET) (23, 24, 26–28), transcranial Doppler (25, 31–34) and laser Doppler flowmetry (29, 30). In the human studies, the following cohorts were studied: 7 studies used healthy patients (23–28, 34), two used patients undergoing a craniotomy (29, 30), one used TBI patients (31), one used patients with spinal or maxillofacial disorders (32), and one used patients undergoing carotid endarterectomy (33). The majority of these studies controlled partial carbon dioxide pressure (P_{CO2}) through mechanical ventilation (29, 30). **Appendix C** shows the study that used deeply sedated animal models with BIS recording (35). The animal model study failed to comment on P_{CO2} (35).

BIS Human CBF Response

Overall there was limited direct correlation with BIS and CBF or cerebral blood flow velocity (CBFv), with many studies either demonstrating no correlation (26, 27, 29, 30) or a wide variation

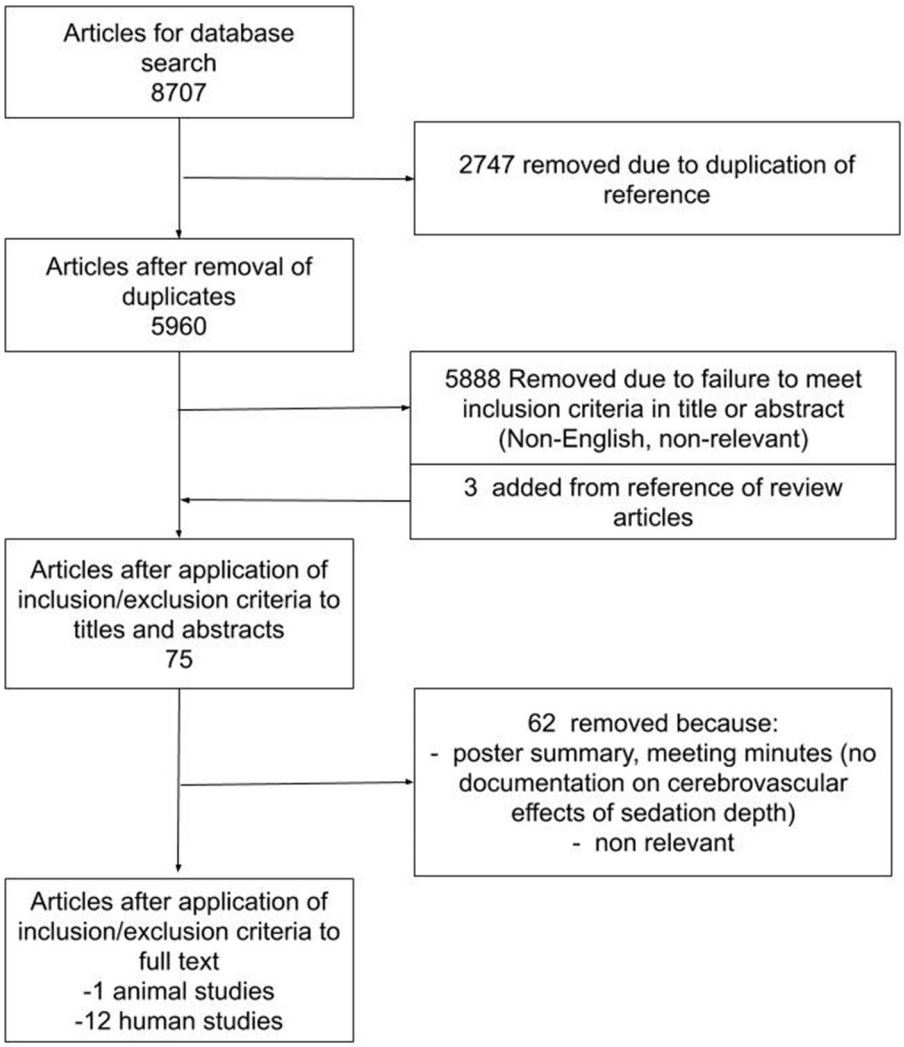

FIGURE 1 | PRISMA Flow Diagram. PRISMA, Preferred Reporting In Systematic Reviews and Meta-Analysis.

in response (24, 25, 28, 34). One study demonstrated BIS having a linear correlation with CBFv and propofol (34), though the variation in CBFv response was significant. Furthermore, *in situations* where consciousness was measured throughout the awake and sedated states, there was a consistent initial decrease in both BIS and CBF/CBFv from the conscious to unconscious state, with sevoflurane (26), propofol (28, 31, 32), or midazolam (25). However, after this initial drop in BIS and CBF/CBFv, there was a wide variation in CBF/CBFv response to similar BIS levels across the population. Of note, one study used midazolam as the initial agent to induce sedation after which flumazenil was used to reverse the sedative effects of midazolam, this increased BIS but did not change CBFv (25). Many of these studies measured various states of consciousness, as evaluated by different levels of BIS, with all having a wide individual variation in CBF/CBFv response at each level (26, 28, 29, 32, 34).

Within the study that evaluated the relationship between CBF and sleep stages, there was a linear correlation between regional CBF and BIS (24). Finally, in a single study that used cross clamping of the carotid artery to modify blood flow, a strong positive correlation between BIS and CBFv was found (33).

BIS Correlation With Cerebral Vessels and Regional Responses

Only two studies evaluated the capillary venous blood flow response (the blood flow assessed through the capillary bed of the brain) through the use of a laser Doppler flow and spectroscopy. Both studies found that there was limited connection with BIS and cerebrovascular response (29, 30). Three drugs were used to achieve BIS levels of 50 and 21; sevoflurane (29), propofol (30) and remifentanil (30). With each agent there was varying change in blood flow. However, propofol did have a significant

TABLE 1 | Human included studies–general characteristics and study goals.

References	No. patients	study type	Mean age (y)	Patient characteristics	Primary and secondary goal of study
Healthy patients					
Maksimow et al. (23)	16	Prospective study	20–30	Healthy male volunteers	Primary: Evaluate the correlation between EEG Entropy and rCBF
Noirhomme et al. (24)	6	Prospective study	20–30	Healthy male volunteers	Primary: Assess the correlation between BIS and rCBF
Ogawa et al. (25)	16	Prospective study	20–26	Healthy young males	Primary: Assess the cerebral circulatory effects of flumazenil after midazolam sedation
Schlünzen et al. (26)	9	Prospective study	21–25	Healthy volunteers	Primary: Evaluate the rCBF effect of sevoflurane Secondary: Differences for sub-anesthesia and anesthesia dose
Schlünzen et al. (27)	9	Prospective study	Not mentioned	Healthy volunteers	Primary: Evaluate the dose-dependent effects of isoflurane on CBF
Veselis et.al. (28)	10	Prospective study	35 ± 10	Healthy male volunteers	Primary: Assess the effects of thiopental and propofol on regions of the brain
Craniectomy					
Klein et al. (29, 30)	20	Prospective study	Not mentioned	Patients undergoing a craniotomy	Primary: Assess the effect sevoflurane induced BIS reduction on cerebral microcirculation
Klein et al. (29, 30)	21	Prospective study	35–61	Patients undergoing a craniotomy	Primary: Effect of cerebral microcirculation during propofol infusion
Head injury					
Skytioti et al. (31)	17	Prospective study	23–76	ASA physical status of I or II	Primary: ICA flow response to anesthesia, pneumoperitoneum and head-up tilt
Other adult surgery populations					
Conti et al. (32)	40	Prospective study	18–65	Patients undergoing treatment for spinal or maxillofacial disorders	Primary: Effect of cerebral hemodynamics after propofol-remifentanil or sevoflurane infusions
Dahaba et al. (33)	20	Prospective study	62.2 ± 9.7	Patients undergoing carotid Endarterectomy	Primary: Detection of CBFv using BIS
Ludbrook et al. (34)	7	Prospective study	18–50	Healthy subjects undergoing elective orthopedic surgery	Primary: Evaluate the effects of Propofol on the Brain

ASA, American society of anesthesiologist; BIS, bispectral index; CBF, cerebral blood flow; CBFv, cerebral blood flow velocity; CPP, cerebral perfusion pressure; EEG, electroencephalogram; ICA, internal carotid artery; rCBF, regional cerebral blood flow; TBI, traumatic brain injury.

increase in regional oxygen saturation by 20% (30). Sevoflurane at high doses (over 0.7%) caused significant decrease to CBF of cerebellum at over 18%, as measured through PET (26). Similarly, in the cortical areas there was a distinct decrease in CBF with a large dose of sevoflurane (over 0.7%) and propofol (over 12.5 ug/ml) (23).

Entropy Index Human CBF Response

In the single study that used the Entropy Index to assess depth of sedation, there was a wide variation in CBFv response (23). Within this study there were examples of the Entropy Index having a linear correlation with CBFv, during sevoflurane or propofol-remifentanil infusions, when the patient transitioned from awake to sedated states.

Animal Models

The single animal study used pigs with systemic arterial hypotension and liver trauma. This study found a slight positive correlation between CBFv and BIS, though this lacked statistical significance (35). Coupled with this, BIS was also linked with cerebral tissue oxygenation as measured through near infrared spectroscopy within these models.

DISCUSSION

Though the literature lacked consistent significant correlations between processed EEG/depth of sedation and cerebrovascular response/CBF, they are undoubtedly associated. This was depicted in all studies that measured BIS or Entropy Index values and CBF/CBFv response, from a conscious to unconscious state. Such studies found that all sedatives caused a decrease in processed EEG values and CBF/CBFv, while mean arterial pressure (MAP) was maintained (23, 25, 26, 28, 31, 32). Furthermore in the one study that clamped the carotid arteries, they found BIS to be correlated with a decrease in CBFv caused through the clamping (33). Though these are limited connections, it highlights that there exists some correlation between objectively measured sedation depth using processed EEG, neurovascular coupling and CBF.

TABLE 2 | Human treatment and cerebrovascular response–study details.

References	Dose	Mean duration of dose administration	Technique to measure cerebrovascular response	Cerebrovascular response	Other outcome	Conclusions
Healthy patients						
Maksimow et al. (23)	• Sevoflurane: 0.4, 0.7, and 2% • Propofol: 7.6, 12.5 and 19 ug/ml	Not mentioned	• rCBF: PET • Depth of Sedation: EEG Entropy Index	• Both drugs initially decreased BIS and rCBF though after the initial decrease (~5 ml/100 g/min) there was a wide range in BIS and rCBF response • Heavy sedation indicated by BIS did correlate with the lowest rCBF values • P_{CO2} maintained through ventilation	Cortical areas of the most significant associations were remarkably similar for the two drugs	Despite the EEG and rCBF correlation at the extreme end of the spectrum there is a vast amount of internal variations
Noirhomme et al. (24)	Sleep stages		• rCBF: PET • Depth of Sedation: BIS	Linear correlation with rCBF and BIS of up to 0.57 were found at various sleep stages, however BIS values varied widely in both sleep stages and CBF levels		Though the level of rCBF and BIS correlated, there was massive variance within BIS response to sleep stages
Ogawa et al. (25)	• Midazolam: 0.5 mg every 2 min until OAA of 3 • After which flumazenil was administered at 0.2 mg until a OAA of 5	2 H	• CBFv: Transcranial Doppler • $ETCO_2$: Pulse oximeter • Depth of Sedation: BIS 4 channel	• For both sedation, BIS and CBFv decreased from baseline values (68 to 64 ± 13 cm/s) with limited change to $ETCO_2$ • Despite the increase in BIS level after Flumazenil infusion CBFv still decreased both alone and after midazolam to 61 ± 11 cm/s	Flumazenil reversed the BIS drop of Midazolam without effecting CBFv	Despite the fluctuation in BIS, CBFv remained reduced after sedation, this indicates limited correlation between these values
Schlünzen et al. (26)	Sevoflurane at 0.4, 0.7, and 2%	Not mentioned	• rCBF: PET • Depth of Sedation: BIS	• Sevoflurane decreased the BIS values dose dependently from (96.8 to 38.5 ± 5) • No significant change in global CBF was observed • rCBF increased in the anterior cingulate (17–21%) and decreased in the cerebellum (18–35%), this was identified at all three levels of sedation compared to baseline • P_{CO2} maintained through ventilation		At sevoflurane concentrations at 0.7% and 2.0% a significant decrease in rCBF with dose-dependent decreases to BIS
Schlünzen et al. (27)	Isoflurane: 0.2, 0.4, and 1 MAC	Not mentioned	• rCBF: PET • Depth of Sedation: BIS	• Dose-dependent decrease to BIS (from 96 to 34 ± 6) with Isoflurane infusion but no significant change to global CBF seen • rCBF increased in anterior cingulate and decreased in the cerebellum • P_{CO2} maintained through ventilation		Little correlation with BIS and global CBF
Veselis et.al. (28)	• Propofol: 1.2–2.7 ug/ml • Thiopental: 4.8–10.6 ug/ml	2 H	• rCBF: SPM 99 analysis of PET • Depth of Sedation: BIS • Oxygenation: pulse oximeter	• BIS decreased similar in both sedations, however limited change to rCBF • P_{CO2} maintained through ventilation	Hypnosis drastically reduced BIS level to 70	There is no clear correlation between CBF and BIS

(Continued)

TABLE 2 | Continued

References	Dose	Mean duration of dose administration	Technique to measure cerebrovascular response	Cerebrovascular response	Other outcome	Conclusions
Craniectomy						
Klein et al. (29, 30)	Sevoflurane 1.5–2.5% vol/vol	Not mentioned	• Capillary venous blood flow and rSO_2: Laser-Doppler flowmetry and spectroscopy • Depth of Sedation: BIS	Limited fluctuation from BIS levels of 50–25 had little change to rCBF or rSO_2		Cerebral microcirculation and oxygenation remains unaltered by sevoflurane-induced changes in BIS
Klein et al. (29, 30)	• Propofol: 4–10 mg/kg/h • Remifentanil: 0.1–0.4 μg/kg/min	Not mentioned	• Capillary venous blood flow and rSO_2: Laser-Doppler flowmetry and spectroscopy • Depth of Sedation: BIS	• The reduction of BIS from 40 to 21 in both groups had limited results to capillary venous blood flow but propofol had a 20% increase in rSO_2		Changes in BIS do not seem to influence regional capillary blood flow
Head injury						
Skytioti et al. (31)	Propofol: 5.8 to 7.9 mg/kg/h	Not mentioned	• CBFv: Transcranial Doppler Ultrasound • Depth of Sedation: BIS • $ETCO_2$: Breath samples • MAP: Finapres	• CBFv and BIS decreased with the introduction of propofol (~100 ml/min) and remained low in both after pneumoperitoneum and head up tilt at 200 ml/min • P_{CO2} maintained through ventilation		Limited correlation from BIS to CBFv as the true measured EEG effects were not commented on
Other adult surgery populations						
Conti et al. (32)	Sevoflurane and propofol-remifentanil injected to induce BIS values of 50 and 35	Not mentioned	• CBFv: Transcranial Doppler • Depth of Sedation: BIS • THRR: Calculated from blood flow	• At BIS level of 50 both drugs decreased CBFv (over −10 cm/s) however at BIS 35 sevoflurane saw a slight increase, though this was still less then awake ($p < 0.05$) • Sevoflurane BIS value of 35 had a decrease in THRR to 1.1, propofol-remifentanil had a slight increase to 1.3 baseline was 1.2 • P_{CO2} maintained through ventilation	BIS at level 35 demonstrated similar response as hypercapnia	Propofol–remifentanil demonstrated preservation pressure-flow relationship by inducing a dose-dependent low-flow state Sevoflurane had differing effect on cerebral autoregulation at different concentrations Despite the BIS and CBFv coupling it is still unclear if this decrease in CBFv is associated with EEG or rather the drug's influence on cerebral circulation
Dahaba et al. (33)	• Propofol: 4 ± 0.2 μg/ml • Rocuronium: 600 ug/kg • Phenylephrine: 50 ug	Not mentioned	• CBFv: Transcranial doppler • Depth of Sedation: BIS • MAP: Controlled with vasopressin	• There was a correlation between BIS and CBFv with a higher correlation after cross clamping of the carotid artery on either side ($p = 0.112$) • Good correlation (r=0.763) between ipsilateral BIS-Vista and CBFv • BIS-Vista decline with CBFv decline both 40% • P_{CO2} maintained through ventilation		• BIS and CBFv had a measurable correlation responsive to lateral influence on the blood flow • BIS-Vista had a discriminative power of depicting a CBFv decline however it cannot be considered a reliable indicator of cerebral ischemia/hypoperfusion.
Ludbrook et al. (34)	Propofol: 110 mg/min for 5 min then 10 mg/min for 20 min	25 Min	• MAP and blood samples: Arterial catheter • CBFv: Transcranial Doppler • Depth of sedation: BIS	• Propofol rapidly dropped BIS after 6.5 min which correlated with low CBFv at 60% of baseline however BIS did carry heavy patient variation • P_{CO2} maintained through ventilation	MAP also had a significant drop at 6.5 min	Propofol and BIS had close relationship together but limited correlation to CBFv

BIS, bispectral index; CA, cerebral autoregulation; CBF, cerebral blood flow; CBFv, cerebral blood flow velocity; $CMRO_2$, cerebral metabolic rate of oxygen; EEG, electroencephalogram; $ETCO_2$, end tidal carbon dioxide; MAP, mean arterial pressure; N_2O, nitrous oxide; P_{CO2}, partial pressure of carbon dioxide; PET, positron emission tomography; rCBF, regional cerebral blood flow; rSO_2, regional oxygen saturation; THRR, transient hyperemic response ratio.

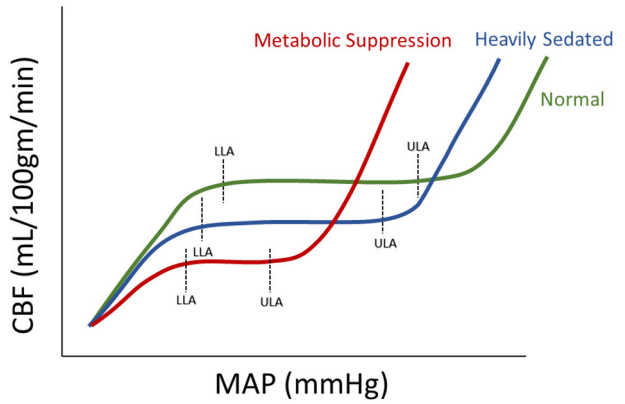

FIGURE 2 | Theoretical Autoregulation curve for Normal, Heavily Sedated, and Metabolically Suppressed Patients. The figure shows three therotical autoregulatory curves for three patient types: normal, heavily sedated and metabolically supressed. a.u., arbitray units; CBF, cerebral blood flow; LLA, lower limit of autoregulation; MAP, mean arterial blood pressure; ml/100 gm/min, milliliter per 100 grams per minute; mmHg, millimeters of mercury; ULA, upper limit of autoregulation.

Within this review, depth of sedation (as measure through BIS or Entropy Index) failed to be clearly linearly associated with CBF. However, this should not be a surprise given CBF is under the control of the innate cerebral autoregulatory function of the pre-capillary arterioles (36). CBF has been shown to follow an S-shaped curve in association with changes in systemic arterial blood pressure, allowing for maintenance of CBF during wide fluctuations of blood pressure. Yet, beyond certain points in MAP, CBF becomes pressure passive. Thus, with escalating sedative doses, corresponding to changes in BIS, there is the potential that we could alter the autoregulatory curve for a given patient, leading to a non-linear relationship between CBF and sedation depth. The influence of sedation on cerebral autoregulation has been demonstrated in past studies (37, 38), and we have illustrated some theoretical responses to sedation in **Figure 2**. In general, with the introduction of sedation, one would expect lower overall MAP and CBF levels, this would in turn indicate that the plateau of the Lassen curve would be lower than an awake patient. Furthermore, the lower limit of autoregulation would be reduced (emerge at a lower MAP) due to a less exhausted vasodilatory reserve caused through a decrease in metabolic demand (39), with the upper limit of autoregulation being more susceptible to metabolically demanding changes in MAP. There are presumed instances of metabolic suppression where the Lassen curve is greatly deteriorated and thus the lower and upper limits of autoregulation are significantly deranged (40). In such cases, the plateau wave would be greatly reduced or even absent.

This concept is further supported by recent work from our group, that continuously assessed BIS and cerebrovascular reactivity (using the pressure reactivity index) in high-frequency in TBI patients (16). This exploratory work found that there is a parabolic distribution between BIS and cerebrovascular reactivity, which is patient specific (see **Figure 3** for example). We were able to demonstrate deterioration in cerebrovascular reactivity during both light sedation and heavy sedation (i.e., near burst suppression levels) states. Further, these findings in theory could lead to targeted sedation to optimize cerebral autoregulation and reduce secondary insult (16). This is in corollary to such advances seen with individualized optimal cerebral perfusion pressure physiologic targets using cerebrovascular reactivity (41, 42). In this way BIS could be coupled with other forms of cerebral autoregulatory treatment methods to achieve cerebral homeostasis, thus highlighting the impact that processed EEG metric may play in TBI. Furthermore, aside from TBI care, such optimized sedation targets in other critical illnesses may lead to improved cognitive outcomes in general critical care populations though this has yet to be explored.

However, the relationship between objective depth of sedation and CBF or cerebrovascular reactivity is not that simple. This review highlights a vast heterogeneity within the sedative agent used and, as the previous discrepancy of the literate illustrates, each agent may play a different role in cerebral response (3, 4). Thus the limited BIS and CBF connection demonstrated in this heterogeneous body of literature, could be related to disparities in medication type utilized. This was affirmed by the different cerebral responses seen in studies that used two sedative agents to achieve similar BIS values (23, 28, 30). Therefore, the full extent that each sedative agent has on BIS, neurovascular coupling, and CBF/cerebrovascular reactivity is still largely unknown, requiring further investigation.

Limitations

First, the literature uncovered was very heterogeneous in design, and results had a limited cross-sectional relationship based on the variation of sedative agent used. Second, most studies focused on small patient populations, with limited ability to extrapolate findings. Third, different CBF and cerebral vessel response methods were utilized, which further limits the ability to compare between studies, populations and extrapolate beyond the works identified in this review. Fourth, the disparity in response seen in CBF to changes in processed EEG metrics limits our ability to confidently state the correlation between processed EEG and CBF, highlighting the need for further investigation in this area. Fifth, most studies focused on low-resolution physiology data, in assessing the relationship between processed EEG and CBF/cerebrovascular reactivity. Such data is limited in its ability to explore the temporal profile of objective sedation depth changes, using BIS, and CBF/cerebrovascular response. This highlights the need for continuous high-fidelity data sets, with BIS and multi-modal cerebral physiologic monitoring to properly comment on any associations.

Future Directions

Despite the identified limitations of our review and the knowledge gap in the literature, there are essential avenues for future investigation highlighted by this work. First, metrics that focus on processed EEG like BIS or Entropy Index, use targeted algorithms to reduce the highly variable and vastly complex EEG output of the superficial area of the frontal

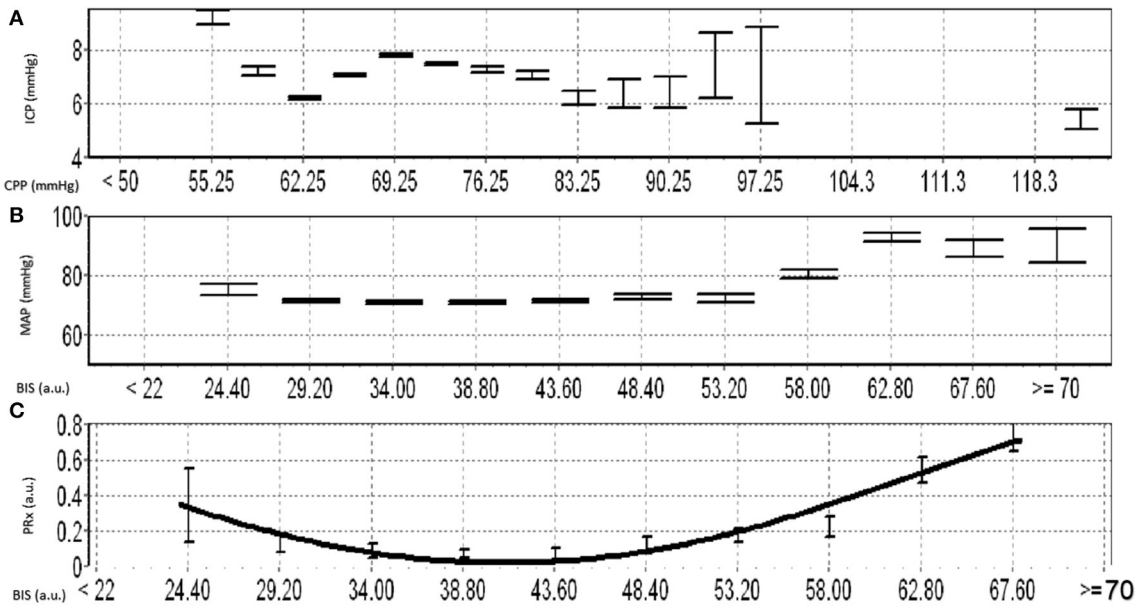

FIGURE 3 | Example of Optimal Depth of Sedation Based on BIS and PRx. **(A)** shows the error bar plot for ICP vs. CPP, **(B)** shows the error bar plot of MAP vs. BIS, **(C)** shows the error bar plot of PRx and different BIS values and demostrates the parabolic relationship between BIS and PRx. a.u., arbitray units; BIS, bisprectal index; CPP, cerebral perfusion pressure; ICP, intracraintal pressure; MAP, mean arterial pressure; mmHg, millimeters of mercury; PRx, pressure reactivity index.

lobe. Thus, if these metrics are implemented to help evaluate CBF or autoregulation the clinician must be aware that any change to the normal electrical impedance of the fontal cortex or the areas of interest are elsewhere, the results would have impeded accuracy. Therefore, studies will require high-frequency data streams of processed EEG metrics, linked with multi-modal cerebral physiologic monitoring to expose the more consistent physiological response and reduce confounding factors. Spatial resolution on EEG entropy index assessments could be improved with large EEG arrays, with signals process for each channel. Similarly, as PRx is derived from a focal pressure monitoring, future improvements in spatial resolution for autoregulation assessments may be facilitated by multi-channel functional near infrared spectroscopy or bilateral transcranial Doppler assessments.

The analysis of these continuous variables in conjunction with processed EEG, will allow the researcher to comment on the multiple factors that influence BIS like MAP, severe cerebral ischemia, impaired autoregulation and P_{CO2}. Along with this, devices like near infrared spectroscopy or parenchymal brain tissue oxygen probes would both potentially offer both the assessment of regional cerebral oxygen delivery, in concert with sedation depth and cerebral autoregulation.

Additionally, multi-modal cerebral physiologic data linked with medication dosing information in time-series would also aid in the understanding of various sedative agents and their subsequent impact on physiology and BIS. As well, by pairing the dosing regimen the researcher can account for the influence of other confounding factors in these agents like MAP or the metabolic coupling effect. Furthermore, targeted sedation strategies using propofol or barbiturates that have similar effects globally throughout the brain (3, 43) would better isolate discrepancy between BIS response and outside confounding factors.

Finally, when assessing the parabolic relationship between BIS and PRx, the use of time connected high frequency physiological data would provide better insight as to the true impairment of the Lassen curve and optimal BIS values. Current literature assessing cerebral autoregulation and metabolic suppression is limited, and is hampered by global assumption about BIS response and sedation. Factors like subdural hemorrhage causing fluctuations to regional electrical impedance, ischemia/systemic vasopressors/blood gas levels causing metabolic fluctuations or other systemic stimuli triggering increase brain activity, all result in derangements to BIS values. Thus, continuous data sets would allow the analysis of separate physiological responses and patient states throughout treatment. Opening the opportunity to comment on the interconnected nature of processed EEG to other cerebral states.

All of this information will need large multi-center data sets with, studying a variety of critical illness states, healthy patients undergoing elective surgery, and awake volunteers. Such comprehensive data collection strategies will highlight the relationships between sedation depth and cerebrovascular response. The findings here will better delineate the role of processed EEG in routine monitoring for patients with critical illness and potentially the role of individualized sedation metrics to advance personalized medicine approaches in critical care (16). Such work is the focus of our lab, the Winnipeg Acute TBI Laboratories, and various research collaboratives (16, 44–47).

CONCLUSIONS

This review highlights the potential for processed EEG metrics to provide information regarding CBF/cerebrovascular response. The literature demonstrates that initiation of sedation will decrease BIS/Entropy Index, CBF and CBFv, highlighting processed EEG's potential to quantify neurovascular coupling. However, after this initial decrease there is a wide range of response between BIS and CBF/CBFv seen, both within and between patient cohorts. Thus, any conclusion about sedation and its role on neurovascular coupling and cerebrovascular response is uncertain. Variation in responses may be related to the differential effects of sedative agents on individual subject's autoregulatory function and/or patient's depth of sedation. Future research with high frequency datasets is required to evaluate processed EEG/BIS and its correlation with CBF/cerebral autoregulation.

AUTHOR CONTRIBUTIONS

LF was responsible for design, analysis and manuscript composition. JD was responsible for article screening and manuscript composition. AG, CB, and AS were responsible for manuscript composition. FZ was responsible for concept, design, analysis, manuscript composition, and supervision. All authors contributed to the article and approved the submitted version.

FUNDING

FZ receives research support from the Manitoba Public Insurance (MPI) Neuroscience/TBI Research Endowment, the Health Sciences Center Foundation Winnipeg, the United States National Institutes of Health (NIH) through the National Institute of Neurological Disorders and Stroke (NINDS)(Grant #: R03NS114335-01), the Canadian Institutes of Health Research (CIHR)(Grant #: 432061), the Canada Foundation for Innovation (CFI)(Project #: 38583), Research Manitoba (Grant #: 3906), the University of Manitoba VPRI Research Investment Fund (RIF), the University of Manitoba Center on Aging, and the University of Manitoba Rudy Falk Clinician-Scientist Professorship. LF was supported through the University of Manitoba–Department of Surgery GFT Research Grant, and the University of Manitoba Office of Research Services (ORS)—University Research Grant Program (URGP). AG was supported through the University of Manitoba Clinician Investigator Program. CB was support through the Center on Aging at the University of Manitoba.

SUPPLEMENTARY MATERIAL

The Supplementary Material for this article can be found online at: https://www.frontiersin.org/articles/10.3389/fneur.2021.692207/full#supplementary-material

REFERENCES

1. Oddo M, Crippa IA, Mehta S, Menon D, Payen J-F, Taccone FS, et al. Optimizing sedation in patients with acute brain injury. *Crit Care.* (2016) 20:128. doi: 10.1186/s13054-016-1294-5
2. Carney N, Totten AM, O'Reilly C, Ullman JS, Hawryluk GWJ, Bell MJ, et al. Guidelines for the management of severe traumatic brain injury, fourth edition. *Neurosurgery.* (2017) 80:6–15. doi: 10.1227/NEU.0000000000001432
3. Froese L, Dian J, Batson C, Gomez A, Unger B, Zeiler FA. Cerebrovascular response to propofol, fentanyl, and *Midazolam* in moderate/severe traumatic brain injury: a scoping systematic review of the human and animal literature. *Neurotrauma Rep.* (2020) 1:100–12. doi: 10.1089/neur.2020.0040
4. Zeiler FA, Sader N, Gillman LM, Teitelbaum J, West M, Kazina CJ. The cerebrovascular response to ketamine: a systematic review of the animal and human literature. *J Neurosurg Anesthesiol.* (2016) 28:123–40. doi: 10.1097/ANA.0000000000000234
5. Froese L, Dian J, Batson C, Gomez A, Alarifi N, Unger B, et al. The impact of vasopressor and sedative agents on cerebrovascular reactivity and compensatory reserve in traumatic brain injury: an exploratory analysis. *Neurotrauma Rep.* (2020) 1:157–68. doi: 10.1089/neur.2020.0028
6. Nies RJ, Müller C, Pfister R, Binder PS, Nosseir N, Nettersheim FS, et al. Monitoring of sedation depth in intensive care unit by therapeutic drug monitoring? A prospective observation study of medical intensive care patients. *J Intensive Care.* (2018) 6:62. doi: 10.1186/s40560-018-0331-7
7. Arevalo JJ, Brinkkemper T, van der Heide A, Rietjens JA, Ribbe M, Deliens L, et al. Palliative sedation: reliability and validity of sedation scales. *J Pain Symptom Manage.* (2012) 44:704–14. doi: 10.1016/j.jpainsymman.2011.11.010
8. Hogg LH, Bobek MB, Mion LC, Legere BM, Banjac S, VanKerkhove K, et al. Interrater reliability of 2 sedation scales in a medical intensive care unit: a preliminary report. *Am J Crit Care Off Publ Am Assoc Crit-Care Nurses.* (2001) 10:79–83. doi: 10.4037/ajcc2001.10.2.79
9. Porhomayon J, El-Solh AA, Adlparvar G, Jaoude P, Nader ND. Impact of sedation on cognitive function in mechanically ventilated patients. *Lung.* (2016) 194:43–52. doi: 10.1007/s00408-015-9820-9
10. Girard TD. Sedation, delirium, and cognitive function after critical illness. *Crit Care Clin.* (2018) 34:585–98. doi: 10.1016/j.ccc.2018.06.009
11. Menon DK, Young Y, Tew DN, Bacon PJ. New horizons in ICU sedation: exploring non-sedative effects of ICU sedation. *Clin Intensive Care Int J Crit Coron Care Med.* (1994) 5:22–6.
12. Roberts DJ, Hall RI, Kramer AH, Robertson HL, Gallagher CN, Zygun DA. Sedation for critically ill adults with severe traumatic brain injury: a systematic review of randomized controlled trials. *Crit Care Med.* (2011) 39:2743–51. doi: 10.1097/CCM.0b013e318228236f
13. Urwin SC, Menon DK. Comparative tolerability of sedative agents in head-injured adults. *Drug Saf.* (2004) 27:107–33. doi: 10.2165/00002018-200427020-00003
14. Flower O, Hellings S. Sedation in traumatic brain injury. *Emerg Med Int.* (2012) 2012:637171. doi: 10.1155/2012/637171
15. Froese L, Batson C, Gomez A, Dian J, Zeiler FA. The limited impact of current therapeutic interventions on cerebrovascular reactivity in traumatic brain injury: a narrative overview. *Neurocrit Care.* (2020) 34:325–35. doi: 10.1007/s12028-020-01003-4
16. Froese L, Dian J, Gomez A, Zeiler FA. Sedation and cerebrovascular reactivity in traumatic brain injury: another potential for personalized approaches in neurocritical care? *Acta Neurochir.* (2021) 163:1383–9. doi: 10.1007/s00701-020-04662-6
17. Singh S, Bansal S, Kumar G, Gupta I, Thakur JR. Entropy as an indicator to measure depth of anaesthesia for laryngeal mask airway (LMA) insertion during sevoflurane and propofol anaesthesia. *J Clin Diagn Res.* (2017) 11:UC01–3. doi: 10.7860/JCDR/2017/27316.10177
18. *Frequently Asked Questions: BIS™ Brain Monitoring Technology.* Available online at: https://hcpresources.medtronic.com/blog/frequently-asked-questions-bis-brain-monitoring-technology (accessed June 10, 2021]).
19. Higgins J, Thomas J. *Cochrane Handbook for Systematic Reviews of Interventions.* Available online at: /handbook/current (accessed January 5, 2020).

20. Moher D, Liberati A, Tetzlaff J. Preferred reporting items for systematic reviews and meta-analysis: the PRISMA statement. *AnnIntern Med.* (2009) 151:264–9. doi: 10.7326/0003-4819-151-4-200908180-00135
21. Froese L, Dian J, Gomez A, Unger B, Zeiler FA. Cerebrovascular response to phenylephrine in traumatic brain injury: a scoping systematic review of the human and animal literature. *Neurotrauma Rep.* (2020) 1:46–62. doi: 10.1089/neur.2020.0008
22. Froese L, Dian J, Gomez A, Unger B, Zeiler FA. The cerebrovascular response to norepinephrine: a scoping systematic review of the animal and human literature. *Pharmacol Res Perspect.* (2020) 8:e00655. doi: 10.1002/prp2.655
23. Maksimow A, Kaisti K, Aalto S, Mäenpää M, Jääskeläinen S, Hinkka S, et al. Correlation of EEG spectral entropy with regional cerebral blood flow during sevoflurane and propofol anaesthesia*. *Anaesthesia.* (2005) 60:862–9. doi: 10.1111/j.1365-2044.2005.04289.x
24. Noirhomme Q, Boly M, Bonhomme V, Boveroux P, Phillips C, Peigneux P, et al. Bispectral index correlates with regional cerebral blood flow during sleep in distinct cortical and subcortical structures in humans. *Arch Ital Biol.* (2009) 147:51–7.
25. Ogawa Y, Iwasaki K, Aoki K, Yanagida R, Ueda K, Kato J, et al. The effects of flumazenil after midazolam sedation on cerebral blood flow and dynamic cerebral autoregulation in healthy young males. *J Neurosurg Anesthesiol.* (2015) 27:275–81. doi: 10.1097/ANA.0000000000000156
26. Schlünzen L, Vafaee MS, Cold GE, Rasmussen M, Nielsen JF, Gjedde A. Effects of subanaesthetic and anaesthetic doses of sevoflurane on regional cerebral blood flow in healthy volunteers. A positron emission tomographic study. *Acta Anaesthesiol Scand.* (2004) 48:1268–76. doi: 10.1111/j.1399-6576.2004.00505.x
27. Schlünzen L, Cold GE, Rasmussen M, Vafaee MS. Effects of dose-dependent levels of isoflurane on cerebral blood flow in healthy subjects studied using positron emission tomography. *Acta Anaesthesiol Scand.* (2006) 50:306–12. doi: 10.1111/j.1399-6576.2006.00954.x
28. Veselis RA, Feshchenko VA, Reinsel RA, Beattie B, Akhurst TJ. Propofol and thiopental do not interfere with regional cerebral blood flow response at sedative concentrations. *Anesthesiology.* (2005) 102:26–34. doi: 10.1097/00000542-200501000-00008
29. Klein KU, Schramm P, Werner C, Engelhard K. Sevoflurane-induced reduction of bispectral index does not affect human cerebral microcirculation. *Eur J Anaesthesiol EJA.* (2016) 33:152–4. doi: 10.1097/EJA.0000000000000278
30. Klein KU, Fukui K, Schramm P, Stadie A, Fischer G, Werner C, et al. Human cerebral microcirculation and oxygen saturation during propofol-induced reduction of bispectral index. *Br J Anaesth.* (2011) 107:735–41. doi: 10.1093/bja/aer227
31. Skytioti M, Elstad M, Søvik S. Internal carotid artery blood flow response to anesthesia, pneumoperitoneum, and head-up tilt during laparoscopic cholecystectomy. *Anesthesiology.* (2019) 131:512–20. doi: 10.1097/ALN.0000000000002838
32. Conti A, Iacopino DG, Fodale V, Micalizzi S, Penna O, Santamaria LB. Cerebral haemodynamic changes during propofol-remifentanil or sevoflurane anaesthesia: transcranial doppler study under bispectral index monitoring. *Br J Anaesth.* (2006) 97:333–9. doi: 10.1093/bja/ael169
33. Dahaba AA, Xue JX, Hua Y, Liu QH, Xu GX, Liu YM, et al. The utility of using the bispectral index–vista for detecting cross-clamping decline in cerebral blood flow velocity. *Oper Neurosurg.* (2010) 67:ons102–7. doi: 10.1227/01.NEU.0000383152.50183.81
34. Ludbrook GL, Visco E, Lam AM. Propofol: relation between brain concentrations, electroencephalogram, middle cerebral artery blood flow velocity, and cerebral oxygen extraction during induction of anesthesia. *Anesthesiology.* (2002) 97:1363–70. doi: 10.1097/00000542-200212000-00006
35. Cavus E, Meybohm P, Doerges V, Hoecker J, Betz M, Hanss R, et al. Effects of cerebral hypoperfusion on bispectral index: a randomised, controlled animal experiment during haemorrhagic shock. *Resuscitation.* (2010) 81:1183–9. doi: 10.1016/j.resuscitation.2010.05.018
36. Lassen NA. Control of cerebral circulation in health and disease. *Circ Res.* (1974) 34:749–60. doi: 10.1161/01.RES.34.6.749
37. Ogawa Y, Iwasaki K, Aoki K, Gokan D, Hirose N, Kato J, et al. The different effects of midazolam and propofol sedation on dynamic cerebral autoregulation. *Anesth Analg.* (2010) 111:1279–84. doi: 10.1213/ANE.0b013e3181f42fc0
38. Dagal A, Lam AM. Cerebral autoregulation and anesthesia. *Curr Opin Anesthesiol.* (2009) 22:547–52. doi: 10.1097/ACO.0b013e32833020be
39. Nusbaum DM, Brady KM, Kibler KK, Easley RB. Acute hypercarbia increases the lower limit of cerebral blood flow autoregulation in a porcine model. *Neurol Res.* (2016) 38:196–204. doi: 10.1179/1743132815Y.0000000094
40. Gingrich KJ. Neuroanesthesia: handbook of clinical and physiologic essentials. *Arch Neurol.* (1992) 49:680. doi: 10.1001/archneur.1992.00530310018002
41. Zeiler FA, Ercole A, Cabeleira M, Carbonara M, Stocchetti N, Menon DK, et al. Comparison of performance of different optimal cerebral perfusion pressure parameters for outcome prediction in adult traumatic brain injury: a collaborative european neurotrauma effectiveness research in traumatic brain injury (CENTER-TBI) study. *J Neurotrauma.* (2019) 36:1505–17. doi: 10.1089/neu.2018.6182
42. Aries MJ, Czosnyka M, Budohoski K, Steiner L, Lavinio A, Kolias A, et al. Continuous determination of optimal cerebral perfusion pressure in traumatic brain injury*. *Crit Care Med.* (2012) 40:2456–63. doi: 10.1097/CCM.0b013e3182514eb6
43. Slupe AM, Kirsch JR. Effects of anesthesia on cerebral blood flow, metabolism, and neuroprotection. *J Cereb Blood Flow Metab.* (2018) 38:2192–208. doi: 10.1177/0271678X18789273
44. Zeiler FA, Ercole A, Beqiri E, Cabeleira M, Aries M, Zoerle T, et al. Cerebrovascular reactivity is not associated with therapeutic intensity in adult traumatic brain injury: a CENTER-TBI analysis. *Acta Neurochir.* (2019) 161:1955–64. doi: 10.1007/s00701-019-03980-8
45. Zeiler FA, Unger B, West M, Kazina CJ, Berrington N, Ellis M. Manitoba cranial neurotrauma research – past, present and future. *J Neurotrauma.* (2018) 35:1999–2001.
46. Bernard F, Gallagher C, Griesdale D, Kramer A, Sekhon M, Zeiler FA. The CAnadian high-resolution traumatic brain injury (CAHR-TBI) research collaborative. *Can J Neurol Sci J Can Sci Neurol.* (2020) 47:551–6. doi: 10.1017/cjn.2020.54
47. Thelin EP, Raj R, Bellander B-M, Nelson D, Piippo-Karjalainen A, Siironen J, et al. Comparison of high versus low frequency cerebral physiology for cerebrovascular reactivity assessment in traumatic brain injury: a multi-center pilot study. *J Clin Monit Comput.* (2019) 34:971–94. doi: 10.1007/s10877-019-00392-y

Conflict of Interest: The authors declare that the research was conducted in the absence of any commercial or financial relationships that could be construed as a potential conflict of interest.

Publisher's Note: All claims expressed in this article are solely those of the authors and do not necessarily represent those of their affiliated organizations, or those of the publisher, the editors and the reviewers. Any product that may be evaluated in this article, or claim that may be made by its manufacturer, is not guaranteed or endorsed by the publisher.

frontiers in Neurology

OPINION
published: 03 September 2021
doi: 10.3389/fneur.2021.720770

Cerebral Autoregulation and Neurovascular Coupling in Acute and Chronic Stroke

Lucy C. Beishon[1]* *and Jatinder S. Minhas*[1,2]

[1] Department of Cardiovascular Sciences, University of Leicester, Leicester, United Kingdom, [2] National Institute for Health Research (NIHR) Leicester Biomedical Research Centre, British Heart Foundation Cardiovascular Research Centre, Glenfield Hospital, Leicester, United Kingdom

Keywords: cerebral blood flow, dynamic cerebral autoregulation, cerebrovascular accident, cerebral haemodynamics, ischaemic stroke, intracerebral haemorrhage

OPEN ACCESS

Edited by:
Xiuyun Liu,
Johns Hopkins University,
United States

Reviewed by:
Yi Yang,
First Affiliated Hospital of Jilin University, China
Fenghua Tian,
University of Texas at Arlington,
United States

***Correspondence:**
Lucy C. Beishon
lb330@le.ac.uk

Specialty section:
This article was submitted to Stroke, a section of the journal Frontiers in Neurology

Received: *04 June 2021*
Accepted: *11 August 2021*
Published: *03 September 2021*

Citation:
Beishon LC and Minhas JS (2021) Cerebral Autoregulation and Neurovascular Coupling in Acute and Chronic Stroke. Front. Neurol. 12:720770. doi: 10.3389/fneur.2021.720770

INTRODUCTION

Stroke is currently the second leading cause of death worldwide, and results in significant morbidity, and poorer quality of life for those affected (1). Stroke can be classified under two major sub-types: ischaemic and haemorrhagic. Ischaemic stroke accounts for ∼70% of all stroke, and results from arterial occlusion, usually through embolism or small vessel thrombosis (2). Haemorrhagic stroke is a result of arterial rupture in the brain (2). However, the two sub-types frequently co-exist, with similar risk factors (e.g., hypertension), and overlap in pathological mechanisms (3).

Although stroke incidence has declined in high-income countries, it remains a prevalent issue amongst low and middle-income countries, disproportionately affecting a younger, working age population in these areas (1). The treatment of acute ischaemic stroke (AIS) has advanced over recent decades. Notably, the advent of both thrombolysis and mechanical thrombectomy has revolutionised the management of AIS, associated with reduced mortality, and improved functional outcome (2, 4, 5). Despite these advances, the management of haemorrhagic stroke has lagged behind, and treatment options are largely confined to reversal of anticoagulants and intensive blood pressure (BP) lowering (2). Conversely, in AIS, the target for BP management remains uncertain, and trials have largely shown equivalence (6, 7), or harm (8), associated with aggressive BP management strategies. To understand the mechanistic implications of BP lowering in AIS, studies have investigated the temporal changes in cerebral autoregulation (CA) following stroke (9). In healthy states, CA maintains a constant cerebral perfusion, despite fluctuations in systemic BP (10). However, the ability of the brain maintain CA may be compromised in the acute phase of stroke, increasing the vulnerability of the brain to hypoperfusion with intensive BP management strategies (11, 12). Conversely, surges in BP during this vulnerable phase may risk haemorrhagic transformation of the infarct, resulting in poorer outcomes (11, 12). Thus, understanding the temporal nature of CA in the acute phase of stroke could provide important mechanistic insights to guide BP management strategies in the clinical setting.

A related concept to CA is the physiological mechanism of neurovascular coupling (NVC). Under healthy conditions, neuronal activity is tightly coupled to cerebral blood flow (CBF), such that increases in neuronal activity will result in increases in CBF to ensure the metabolic demands of the brain are met. Intact NVC is integral to maintain optimal cognitive function, and thus may be an important physiological mechanism in the chronic or rehabilitation phase of stroke. The following sections consider the evidence to support a role for CA and NVC as important mechanistic factors in the acute and chronic phases of stroke, and the key clinical and research implications going forward.

CA

Dynamic cerebral autoregulation (dCA) has now been carefully characterised at rest in AIS (13), acute intracerebral haemorrhage (ICH) (14) and chronic stroke (15) states. Furthermore, several studies have modelled the relationship between arterial CO_2 ($PaCO_2$), cerebral blood flow and dynamic cerebral autoregulation (16, 17). Hypercapnia causes vasodilation and deteriorates CA, with hypocapnia conversely causing vasoconstriction and an improvement in CA status (16, 17). Meta-analyses, albeit with significant heterogeneity, have demonstrated transfer function analysis parameter [phase and autoregulation index (ARI)] impairment in large and small artery AIS, lower phase in ICH and "rebounding phase" in chronic stroke (13). Unfortunately, limitations of existing transcranial Doppler based haemodynamic studies include low assessment frequency post stroke [particularly lacking data in ultra-acute (hours) and medium to longer term (weeks to months)] and clarification of dCA "cut-points" for impairment. Until very recently, there was a lack of dCA data peri- mechanical thrombectomy (MT), however, recent studies have shown worse dCA in the first 24 h associated with higher rates of haemorrhagic transformation and lower rates of recanalization (18). Specific learnings from this data suggest incomplete recanalisation of large-vessel occlusion, with impaired autoregulation status confer complication—raising the importance of adequate blood pressure control in this context (18). Whilst there are confounders to consider when assessing dCA pre-, during or post- MT including blood pressure (19, 20), end-tidal carbon dioxide level (21) and mode of anaesthesia (22)—their behaviour and interactions are yet to be determined. Higher end-tidal CO_2 levels in those with incomplete recanalisation, especially beyond 72 h post large-vessel occlusion (LVO) is of significant interest (18). In ICH, the storey differs, with severe hypocapnia (low arterial CO_2 levels) associated with poor prognosis (23). Furthermore, lowering BP during acute hypertensive states during ICH, in the setting of low arterial CO_2 levels, leads to a greater risk of ischaemic lesions on MRI imaging (23). These differences in acute haemodynamics between stroke sub-types could be explained by nature of structural lesion (infarct vs. haematoma), existence of pre-existing chronic hypertension or differing responses to blood pressure lowering. Given personalised autoregulation-based BP targets are now possible in both a ward based stroke setting (24) and neurocritical care (25). Unfortunately, there still remains an inability to quantify the potential modulation of dCA by chronic hypertension before, during and immediately after acute stroke. The perceived "rightward shift" in the dCA curve is yet to be proven in acute (within 96 h) and sub-acute (7 to 14 days) contexts with ongoing hypertension or antihypertensive treatment being administered (26).

Recent advancements have further highlighted the need to recognise inter-subject variability (27) and responders vs. non-responders (28). There is evidence to suggest dCA impairment is greatest in regions with critically reduced perfusion (greatest volume of viable tissue), though dCA impairment can be present across the entire hemisphere to varying degrees (27). In ICH, through routinely obtained MRI scans in the first 7 days post-event, initial BP, nadir BP, and arterial CO_2 were independent predictors of diffusion-restricted lesion incidence (23). Pooled individual patient data meta-analyses from the ATACH-2 and MISTIE III trials demonstrated in a heterogeneous cohort of patients with ICH, diffusion-weighted imaging (DWI) lesions were associated with 2.5-fold heightened risk of stroke among ICH survivors—with elevated risk persisting for AIS but not for recurrent ICH (29). In order to determine whether ischaemic lesions noted on DWI are preventable, or indeed governed by therapeutic variation in BP approaches (30)—mechanistic dCA studies at time of BP lowering, with continuous end-tidal CO_2 measurement are needed, with MRI DWI assessment at 7 days. White matter ischaemic change may be attributed to by high blood pressure variability in addition to adverse adaptations of CA. In hypertensives without acute stroke disease, dCA (assessed using ARI) and CO_2 reactivity were not related to white matter lesions—however, relationships with duration of hypertension and nocturnal BP dipping were shown (31). Ultimately, there exists a complex interdependent relationship between acute and chronic hypertensive states, dCA, and chronic cerebrovascular ischaemic injury. Crucially, we have evidence to support the hypothesis that carbon dioxide change in the acute setting post-stroke may modify risk, through interaction with BP lowering and dCA status, increasing the ischaemic stroke risk post ICH (23).

In both AIS and ICH, there exist adverse pathophysiologically driven complications including vasogenic oedema and haematoma expansion, respectively. The behaviour of cerebrovascular tone (critical closing pressure, CrCP) and resistance (resistance area product, RAP) is less well-understood. There is debate as to the sensitivity of CrCP to variation in intracranial pressure (ICP) (32). However, the presence of a haematoma in ICH as compared to controls, during normocapnic and hypocapnic conditions, showed significant differences in CrCP and RAP (33). Beyond common indices of dCA, there is limited knowledge of tone and resistance parameters in acute cerebrovascular states as compared to the traumatic brain injury literature.

NVC

To date, the majority of studies have focussed on changes in CA in the acute, subacute, and chronic phases of stroke, with fewer studies investigating the effects on NVC (34). Animal models suggest that NVC is impaired early after stroke as a result of the reduction in neural activity which drives increases in CBF via feed forward mechanisms under normal conditions (35). In a mouse model of stroke, NVC processes were disrupted early after small-scale stroke, with disturbances peaking in the subacute period post-infarction, and remaining in the chronic phase (8 weeks post-event) (36). Impairments have been found to be widespread, occurring beyond the site of initial infarction (35, 36), and recovery of neural activity lags behind the restoration of perfusion (36). Perfusion in the acute phase was found to be

predictive of neuronal outcome and recovery, in keeping with clinical studies discussed below (36).

In a systematic review, sixteen studies investigated changes in brain activation using transcranial Doppler or positron emission tomography based imaging (34). The review found mixed findings, with variable changes in response in both the affected and unaffected hemispheres (34). However, studies varied in the paradigm used to evoke CBF responses (sensorimotor, word finding, object recognition, word repetition and reading tasks), the phase of stroke studied, and the imaging modality used (34). Thus, it remains unclear to what extent these mixed findings are as a result of the heterogeneity in the methods used to assess NVC in stroke (34). Salinet et al. found NVC responses were reduced bilaterally to a passive motor paradigm within 48 h of stroke onset, and this correlated with stroke severity, and poorer functional outcome at 3 months (37). In a separate analysis, this was found to be as a result of myogenic, rather than metabolic impairment in NVC mechanisms (38). In a functional magnetic resonance imaging (MRI) study of chronic stroke patients, motor activity was associated with increases in CBF and cerebral blood volume (CBV) on arterial spin labelling, but with no discernible blood-oxygen level dependent response (39). However, CBF and CBV responses were attenuated when compared to healthy adults suggesting persistent abnormalities in NVC in chronic stroke, but these were dependent on the imaging modality used (39). The effects of thrombolysis on NVC processes are not fully understood, but may be as a result of effects on endothelial N-methyl-D-Aspartate receptor signalling (40, 41). However, function at the neurovascular unit has been suggested as one mechanism for the variability in inter-individual outcome with thrombolysis (42). In particular, patency of the microvasculature is essential to the recovery of neuronal function, and the level of injury in the unit determines the outcome with thrombolytic therapy (42).

To date, the majority of human studies have been cross-sectional, and longitudinal studies investigating the temporal evolution of NVC changes post-stroke are lacking. In particular, the role of NVC in the pathogenesis and outcome in haemorrhagic stroke has not been researched. Available evidence suggests NVC disruption in the early phases is predictive of functional outcome in ischaemic stroke (36, 37, 43), however cognitive outcomes have not been widely studied. The majority of human studies have focussed on sensori-motor rather than cognitive paradigms (34), which may be more relatable to recovery of motor rather than cognitive function. Importantly, up to one third of patients after stroke will experience long terms problems with memory and cognition, and severe stroke can bring forward the onset of dementia by up to 25 years (44). However, the relationship between cognitive function and NVC disruption remains under-researched. Thus, significant gaps remain in our understanding, particularly concerning how NVC process may be modulated to enhance functional and cognitive recovery in patients after stroke.

NVC AND CA RECOMMENDATIONS

Given the evolution of the field and the desire to utilise haemodynamic studies to deduce treatment response, prognostic indices and optimise physiological profiles—there is an ever-increasing individualised approach. However, gaps have emerged across both NVC and CA lines of investigation, offering an opportunity to highlight necessary short- and medium-term study recommendations:

- What is the longitudinal behaviour of NVC beyond sub-acute stroke and into chronic stroke states?
- Does NVC behaviour differ post ICH as compared to AIS?
- Can NVC be modulated to enhance functional and cognitive recovery in patients post stroke?
- Is there a longitudinal relationship between CO_2 change post stroke and development of white matter lesions?
- To what extent does BP lowering cause harm due to its interaction with hypocapnia in AIS and ICH?

In order to address these pending research questions, multi-modality and inter-disciplinary studies are necessary. In addition, pooling of existing datasets to minimise research data waste and to maximise validity and statistical power is essential. There already exist multi-centre efforts to this effect, across cerebrovascular (45) and non-cerebrovascular (46) disease states. We encourage those working within the field to support these initiatives.

AUTHOR CONTRIBUTIONS

LB and JM prepared and wrote this manuscript through equal contribution to all aspects of its delivery.

FUNDING

LB was a research training fellow funded by the Dunhill Medical Trust (RTF180627). JM was an NIHR Clinical Lecturer in Older People and Complex Health Needs.

REFERENCES

1. Johnson W, Onuma O, Owolabi M, Sachdev S. Stroke: a global response is needed. *Bull World Health Organ.* (2016) 94:634A. doi: 10.2471/BLT.16.181636
2. Campbell BCV, Khatri P. Stroke. *Lancet.* (2020) 396:129–42. doi: 10.1016/S0140-6736(20)31179-X
3. Fisher M, Vasilevko V, Cribbs DH. Mixed cerebrovascular disease and the future of stroke prevention. *Transl Stroke Res.* (2012) 3:39–51. doi: 10.1007/s12975-012-0185-6
4. Mistry EA, Mistry AM, Nakawah MO, Chitale RV, James RF, Volpi JJ, et al. Mechanical thrombectomy outcomes with and without intravenous thrombolysis in stroke patients. *Stroke.* (2017) 48:2450–6. doi: 10.1161/STROKEAHA.117.017320
5. Muruet W, Rudd A, Wolfe CDA, Douiri A. Long-Term survival after intravenous thrombolysis for ischemic stroke: a propensity

score-matched cohort with up to 10-year follow-up. *Stroke.* (2018) 49:607–13. doi: 10.1161/STROKEAHA.117.019889
6. ENOS Investigators. Efficacy of nitric oxide, with or without continuing antihypertensive treatment, for management of high blood pressure in acute stroke (ENOS): a partial-factorial randomised controlled trial. *Lancet.* (2015) 385:617–28. doi: 10.1016/S0140-6736(14)61121-1
7. Anderson CS, Huang Y, Lindley RI, Chen X, Arima H, Chen G, et al. Intensive blood pressure reduction with intravenous thrombolysis therapy for acute ischaemic stroke (ENCHANTED): an international, randomised, open-label, blinded-endpoint, phase 3 trial. *Lancet.* (2019) 393:877–88. doi: 10.1016/S0140-6736(19)30038-8
8. Sandset EC, Bath PMW, Boysen G, Jatuzis D, Kõrv J, Lüders S, et al. The angiotensin-receptor blocker candesartan for treatment of acute stroke (SCAST): a randomised, placebo-controlled, double-blind trial. *Lancet.* (2011) 377:741–50. doi: 10.1016/S0140-6736(11)60104-9
9. Nogueira RC, Beishon L, Bor-Seng-Shu E, Panerai RB, Robinson TG. Cerebral autoregulation in ischemic stroke: from pathophysiology to clinical concepts. *Brain Sci.* (2021) 11:511. doi: 10.3390/brainsci11040511
10. Panerai RB. Cerebral autoregulation: from models to clinical applications. *Cardiovasc Eng.* (2008) 8:42–59. doi: 10.1007/s10558-007-9044-6
11. Anderson CS, Arima H, Lavados P, Billot L, Hackett ML, Olavarría VV, et al. Cluster-Randomized, crossover trial of head positioning in acute stroke. *N Engl J Med.* (2017) 376:2437–47. doi: 10.1056/NEJMoa1615715
12. Anderson CS, Olavarría VV. Head positioning in acute stroke. *Stroke.* (2019) 50:224–8. doi: 10.1161/STROKEAHA.118.020087
13. Intharakham K, Beishon L, Panerai RB, Haunton VJ, Robinson TG. Assessment of cerebral autoregulation in stroke: a systematic review and meta-analysis of studies at rest. *J Cereb Blood Flow Metab.* (2019) 39:2105–16. doi: 10.1177/0271678X19871013
14. Minhas JS, Panerai RB, Ghaly G, Divall P, Robinson TG. Cerebral autoregulation in hemorrhagic stroke: a systematic review and meta-analysis of transcranial doppler ultrasonography studies. *J Clin Ultrasound.* (2019) 47:14–21. doi: 10.1002/jcu.22645
15. Aoi MC, Hu K, Lo MT, Selim M, Olufsen MS, Novak V. Impaired cerebral autoregulation is associated with brain atrophy and worse functional status in chronic ischemic stroke. *PLoS ONE.* (2012) 7:e46794. doi: 10.1371/journal.pone.0046794
16. Minhas JS, Panerai RB, Robinson TG. Modelling the cerebral haemodynamic response in the physiological range of $PaCO_2$. *Physiol Meas.* (2018) 39:065001. doi: 10.1088/1361-6579/aac76b
17. Meng L, Gelb AW. Regulation of cerebral autoregulation by carbon dioxide. *Anesthesiology.* (2015) 122:196–205. doi: 10.1097/ALN.0000000000000506
18. Sheriff F, Castro P, Kozberg M, Larose S, Monk A, Azevedo E, et al. dynamic cerebral autoregulation post endovascular thrombectomy in acute ischemic stroke. *Brain Sci.* (2020) 10:641. doi: 10.3390/brainsci10090641
19. Minhas JS, Wang X, Lindley RI, Delcourt C, Song L, Woodward M, et al. Comparative effects of intensive-blood pressure versus standard-blood pressure-lowering treatment in patients with severe ischemic stroke in the ENCHANTED trial. *J Hypertens.* (2021) 39:280–5. doi: 10.1097/HJH.0000000000002640
20. Robinson TG, Minhas JS, Miller J. Review of major trials of acute blood pressure management in stroke. *J Cereb Blood Flow Metab.* (2021) 271678X211004310. doi: 10.1177/0271678X211004310. [Epub ahead of print].
21. Salinet ASM, Minhas JS, Panerai RB, Bor-Seng-Shu E, Robinson TG. Do acute stroke patients develop hypocapnia? A systematic review and meta-analysis. *J Neurol Sci.* (2019) 402:30–9. doi: 10.1016/j.jns.2019.04.038
22. Minhas JS, Rook W, Panerai RB, Hoiland RL, Ainslie PN, Thompson JP, et al. Pathophysiological and clinical considerations in the perioperative care of patients with a previous ischaemic stroke: a multidisciplinary narrative review. *Br J Anaesth.* (2020) 124:183–96. doi: 10.1016/j.bja.2019.10.021
23. Hextrum S, Minhas JS, Liotta EM, Sorond FA, Naidech AM, Maas MB. Hypocapnia, ischemic lesions, and outcomes after intracerebral hemorrhage. *J Neurol Sci.* (2020) 418:117139. doi: 10.1016/j.jns.2020.117139
24. Petersen NH, Silverman A, Strander SM, Kodali S, Wang A, Sansing LH, et al. Fixed compared with autoregulation-oriented blood pressure thresholds after mechanical thrombectomy for ischemic stroke. *Stroke.* (2020) 51:914–21. doi: 10.1161/STROKEAHA.119.026596
25. Czosnyka M, Hutchinson P, Smielewski P. Treatment targets based on autoregulation parameters in neurocritical care patients. *Curr Opin Crit Care.* (2020) 26:109–14. doi: 10.1097/MCC.0000000000000704
26. Dawson SL, Panerai RB, Potter JF. Serial changes in static and dynamic cerebral autoregulation after acute ischaemic stroke. *Cerebrovasc Dis.* (2003) 16:69–75. doi: 10.1159/000070118
27. Hecht N, Schrammel M, Neumann K, Müller MM, Dreier JP, Vajkoczy P, et al. Perfusion-Dependent cerebral autoregulation impairment in hemispheric stroke. *Ann Neurol.* (2021) 89:358–68. doi: 10.1002/ana.25963
28. Minhas JS, Panerai RB, Swienton D, Robinson TG. Feasibility of improving cerebral autoregulation in acute intracerebral hemorrhage (BREATHE-ICH) study: results from an experimental interventional study. *Int J Stroke.* (2020) 15:627–37. doi: 10.1177/1747493019873690
29. Murthy SB, Zhang C, Gupta A, Cho SM, Rivera-Lara L, Avadhani R, et al. Diffusion-Weighted imaging lesions after intracerebral hemorrhage and risk of stroke: a MISTIE III and ATACH-2 analysis. *Stroke.* (2021) 52:595–602. doi: 10.1161/STROKEAHA.120.031628
30. Kadicheeni M, Robinson TG, Divall P, Parry-Jones AR, Minhas JS. Therapeutic variation in lowering blood pressure: effects on intracranial pressure in acute intracerebral haemorrhage. *High Blood Press Cardiovasc Prev.* (2021) 28:115–28. doi: 10.1007/s40292-021-00435-z
31. Birns J, Jarosz J, Markus HS, Kalra L. Cerebrovascular reactivity and dynamic autoregulation in ischaemic subcortical white matter disease. *J Neurol Neurosurg Psychiatry.* (2009) 80:1093–8. doi: 10.1136/jnnp.2009.174607
32. Czosnyka M, Smielewski P, Piechnik S, Al-Rawi PG, Kirkpatrick PJ, Matta BF, et al. Critical closing pressure in cerebrovascular circulation. *J Neurol Neurosurg Psychiatry.* (1999) 66:606–11. doi: 10.1136/jnnp.66.5.606
33. Ince J, Mankoo AS, Kadicheeni M, Swienton D, Panerai RB, Robinson TG, et al. Cerebrovascular tone and resistance measures differ between healthy control and patients with acute intracerebral haemorrhage: exploratory analyses from the BREATHE-ICH study. *Physiol Meas.* (2021) 42. doi: 10.1088/1361-6579/abf7da
34. Salinet AS, Haunton VJ, Panerai RB, Robinson TG. A systematic review of cerebral hemodynamic responses to neural activation following stroke. *J Neurol.* (2013) 260:2715–21. doi: 10.1007/s00415-013-6836-z
35. Girouard H, Iadecola C. Neurovascular coupling in the normal brain and in hypertension, stroke, Alzheimer disease. *J Appl Physiol.* (2006) 100:328–35. doi: 10.1152/japplphysiol.00966.2005
36. He F, Sullender CT, Zhu H, Williamson MR, Li X, Zhao Z, et al. Multimodal mapping of neural activity and cerebral blood flow reveals long-lasting neurovascular dissociations after small-scale strokes. *Sci Adv.* (2020) 6:eaba1933. doi: 10.1126/sciadv.aba1933
37. Salinet AS, Silva NC, Caldas J, De Azevedo DS, De-Lima-Oliveira M, Nogueira RC, et al. Impaired cerebral autoregulation and neurovascular coupling in middle cerebral artery stroke: influence of severity? *J Cereb Blood Flow Metab.* (2018) 39:2277–85. doi: 10.1177/0271678X18794835
38. Salinet AS, Robinson TG, Panerai RB. Cerebral blood flow response to neural activation after acute ischemic stroke: a failure of myogenic regulation? *J Neurol.* (2013) 260:2588–95. doi: 10.1007/s00415-013-7022-z
39. Blicher JU, Stagg CJ, O'shea J, Østergaard L, Macintosh BJ, Johansen-Berg H, et al. Visualization of altered neurovascular coupling in chronic stroke patients using multimodal functional MRI. *J Cereb Blood Flow Metab.* (2012) 32:2044–54. doi: 10.1038/jcbfm.2012.105
40. Park L, Gallo EF, Anrather J, Wang G, Norris EH, Paul J, et al. Key role of tissue plasminogen activator in neurovascular coupling. *Proc Natl Acad Sci USA.* (2008) 105:1073–8. doi: 10.1073/pnas.0708823105
41. Anfray A, Drieu A, Hingot V, Hommet Y, Yetim M, Rubio M, et al. Circulating tPA contributes to neurovascular coupling by a mechanism involving the endothelial NMDA receptors. *J Cereb Blood Flow Metab.* (2020) 40:2038–54. doi: 10.1177/0271678X19883599
42. Del Zoppo GJ. The neurovascular unit in the setting of stroke. *J Intern Med.* (2010) 267:156–71. doi: 10.1111/j.1365-2796.2009.02199.x
43. Wu D, Liu X, Gadhoumi K, Pu Y, Hemphill JC, Zhang Z, et al. Causal relationship between neuronal activity and cerebral hemodynamics in patients with ischemic stroke. *J Neural Eng.* (2020) 17:026006. doi: 10.1088/1741-2552/ab75af
44. Pendlebury ST, Rothwell PM. Incidence and prevalence of dementia associated with transient ischaemic attack and stroke: analysis of the

population-based oxford vascular study. *Lancet Neurol.* (2019) 18:248–58. doi: 10.1016/S1474-4422(18)30442-3

45. Beishon L, Minhas JS, Nogueira R, Castro P, Budgeon C, Aries M, et al. INFOMATAS multi-center systematic review and meta-analysis individual patient data of dynamic cerebral autoregulation in ischemic stroke. *Int J Stroke.* (2020) 15:807–12. doi: 10.1177/1747493020907003
46. Tas J, Beqiri E, Van Kaam CR, Ercole A, Bellen G, Bruyninckx D, et al. An update on the COGiTATE phase II study: feasibility and safety of targeting an optimal cerebral perfusion pressure as a patient-tailored therapy in severe traumatic brain injury. *Acta Neurochir Suppl.* (2021) 131:143–7. doi: 10.1007/978-3-030-59436-7_29

Author Disclaimer: The views expressed in this publication are those of the author(s) and not necessarily those of the NHS, the National Institute for Health Research, or the Department of Health, or the authors' respective organisations.

Conflict of Interest: The authors declare that the research was conducted in the absence of any commercial or financial relationships that could be construed as a potential conflict of interest.

Publisher's Note: All claims expressed in this article are solely those of the authors and do not necessarily represent those of their affiliated organizations, or those of the publisher, the editors and the reviewers. Any product that may be evaluated in this article, or claim that may be made by its manufacturer, is not guaranteed or endorsed by the publisher.

frontiers in Neurology

BRIEF RESEARCH REPORT
published: 10 September 2021
doi: 10.3389/fneur.2021.695705

Near-Infrared Spectroscopy-Derived Dynamic Cerebral Autoregulation in Experimental Human Endotoxemia—An Exploratory Study

Nick Eleveld[1], Cornelia W. E. Hoedemaekers[2], C. Ruud van Kaam[2], Guus P. Leijte[2,3], Judith M. D. van den Brule[2], Peter Pickkers[2,3], Marcel J. H. Aries[4], Natasha M. Maurits[1] and Jan Willem J. Elting[1]*

[1] Department of Neurology, University Medical Center Groningen, University of Groningen, Groningen, Netherlands, [2] Department of Intensive Care Medicine, Radboud University Medical Center, Radboud University, Nijmegen, Netherlands, [3] Radboud Center for Infectious Diseases (RCI), Radboud University Medical Center, Radboud University, Nijmegen, Netherlands, [4] Department of Intensive Care Medicine, School of Mental Health and NeuroSciences (MHeNS), University Medical Center Maastricht (MUMC+), Maastricht University, Maastricht, Netherlands

OPEN ACCESS

Edited by:
Dong Ming,
Tianjin University, China

Reviewed by:
Kirsten Møller,
Rigshospitalet, Denmark
Xiuyun Liu,
Johns Hopkins University, United States

***Correspondence:**
Nick Eleveld
n.eleveld@umcg.nl

Specialty section:
This article was submitted to Neurocritical and Neurohospitalist Care, a section of the journal Frontiers in Neurology

Received: *15 April 2021*
Accepted: *11 August 2021*
Published: *10 September 2021*

Citation:
Eleveld N, Hoedemaekers CWE, van Kaam CR, Leijte GP, van den Brule JMD, Pickkers P, Aries MJH, Maurits NM and Elting JWJ (2021) Near-Infrared Spectroscopy-Derived Dynamic Cerebral Autoregulation in Experimental Human Endotoxemia—An Exploratory Study. Front. Neurol. 12:695705. doi: 10.3389/fneur.2021.695705

Cerebral perfusion may be altered in sepsis patients. However, there are conflicting findings on cerebral autoregulation (CA) in healthy participants undergoing the experimental endotoxemia protocol, a proxy for systemic inflammation in sepsis. In the current study, a newly developed near-infrared spectroscopy (NIRS)-based CA index is investigated in an endotoxemia study population, together with an index of focal cerebral oxygenation.

Methods: Continuous-wave NIRS data were obtained from 11 healthy participants receiving a continuous infusion of bacterial endotoxin for 3 h (ClinicalTrials.gov NCT02922673) under extensive physiological monitoring. Oxygenated–deoxygenated hemoglobin phase differences in the (very)low frequency (VLF/LF) bands and the Tissue Saturation Index (TSI) were calculated at baseline, during systemic inflammation, and at the end of the experiment 7 h after the initiation of endotoxin administration.

Results: The median (inter-quartile range) LF phase difference was 16.2° (3.0–52.6°) at baseline and decreased to 3.9° (2.0–8.8°) at systemic inflammation ($p = 0.03$). The LF phase difference increased from systemic inflammation to 27.6° (12.7–67.5°) at the end of the experiment ($p = 0.005$). No significant changes in VLF phase difference were observed. The TSI (mean ± SD) increased from 63.7 ± 3.4% at baseline to 66.5 ± 2.8% during systemic inflammation ($p = 0.03$) and remained higher at the end of the experiment (67.1 ± 4.2%, $p = 0.04$). Further analysis did not reveal a major influence of changes in several covariates such as blood pressure, heart rate, $PaCO_2$, and temperature, although some degree of interaction could not be excluded.

Discussion: A reversible decrease in NIRS-derived cerebral autoregulation phase difference was seen after endotoxin infusion, with a small, sustained increase in TSI. These findings suggest that endotoxin administration in healthy participants reversibly impairs CA, accompanied by sustained microvascular vasodilation.

Keywords: near-infrared spectroscopy, human endotoxemia model, dynamic cerebral autoregulation, sepsis, cerebral perfusion

INTRODUCTION

Sepsis is defined as life-threatening organ dysfunction caused by a dysregulated host response to infection (1). Apart from systemic effects, sepsis patients may experience cerebral complications. Sepsis-associated encephalopathy (SAE) is a severe complication in sepsis (2) and is associated with increased mortality and long-term cognitive impairment. The pathophysiology of SAE is multifactorial, and inflammatory cytokines, alterations in cerebral metabolism, and blood–brain-barrier compromise have been described as etiological factors for the development of SAE (2). In addition, there is increasing evidence for alteration of the cerebral (micro-)circulation and cerebral autoregulation (CA) during sepsis, which may play an important role in SAE pathogenesis (3, 4).

The experimental human endotoxemia model is a standardized reproducible model in which healthy volunteers are challenged with endotoxin (lipopolysaccharide, LPS) to induce a systemic inflammatory response. This model can be used to study systemic inflammation and has been used to investigate several phenomena associated with sepsis, including cerebral perfusion, cerebral (micro-) vascular function, and SAE (5–9). In general, although alterations in CA are seen in patients with SAE, there are conflicting findings regarding CA in healthy participants undergoing experimental endotoxemia. Three studies have estimated the dynamic cerebral autoregulation (DCA) with transfer function analysis (TFA), in which the temporal relation was determined between oscillations in arterial blood pressure (ABP) and cerebral blood flow velocity (CBFv) measured with transcranial Doppler (TCD). DCA is quantified with "gain" and "phase difference". Two earlier studies reported an improvement in DCA (reduced gain and increased phase difference) upon infusion of 2 ng/kg bacterial LPS (7, 10). In a recent study, Van den Brule et al. investigated DCA in an endotoxemia study with a continuous infusion of, in total, 4 ng/kg bacterial LPS. No changes in gain or phase difference were found (5).

CA has also been assessed with measurements of ABP and near-infrared spectroscopy (NIRS), a non-invasive technique that uses near-infrared light to calculate the concentration of hemoglobin (Hb) in the cerebral cortex (11, 12). Recently, a new DCA measurement model that employs only high-frequency continuous-wave NIRS measurements on the frontotemporal scalp was developed (13). In short, the temporal relation between the concentration of oxygenated (OxyHb) and deoxygenated hemoglobin (HHb) is determined with TFA, which results in phase difference values analogous to TFA for ABP and CBFv. Correction for transit time and blood flow/blood volume (TT-BF/BV) oscillations for phase difference values is needed, after which NIRS-derived DCA phase difference values were similar to the phase difference values obtained *via* the classic TCD- and ABP-based method in healthy volunteers during rest and hypercapnia (13).

The NIRS technique to assess DCA has several advantages over the technique using TCD and ABP: it requires little operator experience, is more comfortable for the participant, and allows for long-term measurements. These advantages could provide a higher signal-to-noise ratio for the NIRS compared to the TCD/ABP method. Further studies in clinically relevant populations are therefore warranted. In the current study, unilateral, frontotemporal NIRS measurements obtained from the same healthy participants that were studied by Van den Brule et al. during experimental endotoxemia (5) were analyzed to explore the temporal dynamics of NIRS-derived CA. We hypothesized that possible changes in CA can be detected more easily with NIRS than with TCD and ABP due to the aforementioned advantages of the NIRS-CA technique.

We compared the temporal dynamics of NIRS-derived dynamic cerebral autoregulation as characterized by TFA phase difference before, during, and after administration of endotoxin. Furthermore, we investigated the dynamics of the Tissue Saturation Index (TSI), a more common and clinically used NIRS measure of cerebral oxygenation, as the TSI is thought to be susceptible to changes in cerebral blood volume (CBV) or cerebral blood flow (CBF).

Lastly, the relation was explored between phase difference and TSI, and several potential confounders that have been described to influence cerebral perfusion and DCA: mean arterial pressure (MAP), $PaCO_2$, pH, temperature, heart rate, inflammatory cytokine concentrations, and power in ABP and NIRS oscillations (14, 15).

MATERIALS AND METHODS

Participants and Study Protocol

NIRS data from 11 participants were used from an existing dataset of healthy adult males undergoing an experimental human endotoxemia study [ClinicalTrials.gov NCT02922673 (16)]. Of the original 13 datasets, two participants were excluded because of the insufficient quality of NIRS data resulting from excessive movement artifacts.

A comprehensive study protocol for the study has been published previously (5, 16). A summary of the study protocol is provided here. A continuous infusion of bacterial LPS was employed under extensive vital sign monitoring, with additional NIRS measurements. A schematic description of the protocol is provided in **Figure 1**. Data on age, body mass index (BMI), resting heart rate, MAP, and (tympanic) body temperature were obtained at baseline ($T = -60$ min). All participants received pre-hydration with 1.5 L of 2.5% glucose/0.45% saline solution in the hour before LPS administration, followed by 150-ml/h continuous hydration until the end of the experiment (5). Purified LPS (lipopolysaccharide, *E. coli Type O113*, lot no. 94332B4; List Biological Laboratories, Campbell, USA) was dissolved in normal saline (0.9%). An intravenous loading bolus of 1 ng/kg body weight was administered, followed by a continuous infusion of 1 ng/kg body weight/hour for a period of 3 h (5).

Monitoring and Data Collection

Monitoring of clinical parameters included continuous invasive ABP, electrocardiography, arterial oxygen saturation (SpO_2), intermittent tympanic temperature, TCD-derived cerebral blood flow velocity in the middle cerebral artery (MCA), arterial blood gas, and inflammatory cytokine concentrations (5, 16).

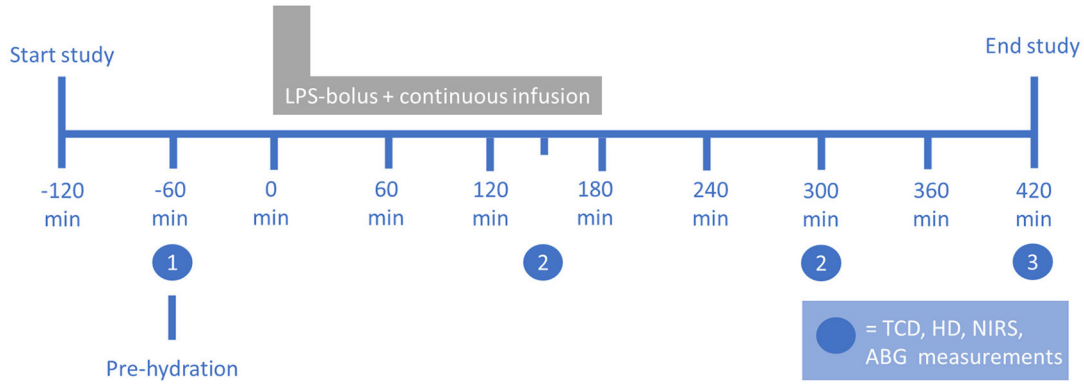

FIGURE 1 | Setup of the human endotoxemia trial. The numbers indicate the measurements at (1) baseline, (2) systemic inflammation, and (3) the end of the experiment. ABG, arterial blood gas; HD, hemodynamic; LPS, lipopolysaccharide; NIRS, near-infrared spectroscopy; TCD, transcranial Doppler. Figure reproduced with permission from Figure 1 in Van den Brule et al., *Shock* (2018), doi: 10.1097/SHK.0000000000001003.

NIRS recordings were performed at four time points: 60 min before LPS administration (baseline), during systemic inflammation at 150 and 300 min after the initiation of LPS administration, and at the end of the experiment, 420 min after the initiation of LPS administration. A continuous-wave NIRS device (Portalite, Artinis Medical Systems, Elst, The Netherlands) was placed on the frontotemporal forehead. Near-infrared light was transmitted with wavelengths of 760 and 850 nm by a light-emitting diode and was received by a photodiode at 35-mm inter-optode distance. Data were obtained at 50-Hz sampling frequency with device-specific acquisition software (Oxysoft, Artinis Medical Systems, Elst, The Netherlands). Changes in OxyHb and HHb were derived using the modified Beer–Lambert Law (17).

All OxyHb and HHb data were systematically inspected for artifacts and noise with in-house developed Labview data visualization and correction software (Labview 2015, National Instruments, Austin, TX, United States), which has been used before by our group (13). The artifacts were visually identified and removed by linear interpolation as recommended by the international Cerebral Autoregulation Research Network (CARNet) (18). For longer artifacts (>5 s), artifact containing data were removed. A second reviewer visually inspected the resulting data for any remaining artifacts. At least 5 min of high-quality data were required for each time point as is recommended (18).

The mean cerebral TSI was calculated from the artifact-corrected OxyHb and HHb data using spatially resolved spectroscopy in Oxysoft, following the method of Matcher et al. (19, 20).

Non-invasive, NIRS-Only-Derived Dynamic Cerebral Autoregulation

The relationship between OxyHb and HHb was determined with TFA following CARNet recommendations (18). Power spectral density and cross-spectral density estimates were determined using Welch's method (100-s epochs, 50% window overlap). Coherence, gain, and phase difference were computed and trichotomized into one of three frequency bands: very low frequency (VLF): 0.02–0.07 Hz, low frequency (LF): 0.07–0.2 Hz, and high frequency (HF): 0.2–0.5 Hz. Gain and phase difference values were excluded if the corresponding coherence values were below the window-dependent coherence threshold as defined in the CARNet White Paper (18).

The capillary TT-BF/BV correction method developed by our group was applied to the phase difference values after TFA calculation (13). In short, a linear trend line was fitted to the HF band phase difference values. Only data sections that yielded at least five consecutive frequency bins with significant coherence were used for line fitting, thereby avoiding inclusion of bins with significant coherence that arose by chance. Subsequently, this trend line was subtracted from the LF/VLF phase difference values, thereby obtaining the NIRS-derived TT-BF/BV-corrected CA estimation. NIRS-derived CA estimates were defined as TT-BF/BV-corrected VLF and LF phase differences. These were calculated for each time point for which NIRS data were available.

Data Pooling

For the measurements at 150 min after the initiation of endotoxin administration, movement-related artifacts were prominent in some of the NIRS data (healthy volunteers getting sicker), so for this time point, data from only $n = 7$ participants were available. Although there was a difference in inflammatory response as measured by plasma cytokine concentration between 150 and 300 min after the initiation of endotoxin administration, inflammation at both time points was markedly higher than at baseline or at the end of the experiment as was reported previously (5). We therefore decided to pool the data at these two time points by averaging to obtain one "intra-inflammatory" measurement for each participant. If measurements were only available at either 150 or 300 min, these data were used. For further analysis, data were therefore obtained from three time points: (1) baseline (−60 min), (2) systemic inflammation, and (3) at the end of the experiment (420 min).

TABLE 1 | Hemodynamic and clinical parameters of the participants ($n = 11$) for each time point.

		Time point 1 baseline	Time point 2 systemic inflammation	Time point 3 end of experiment	*p*-value TP1 vs. TP2	*p*-value TP1 vs. TP3	*p*-value TP2 vs. TP3
MAP (mmHg)	Mean ± SD	86.1 ± 10.7	76.6 ± 6.6	73.3 ± 6.5	0.0103	0.0032	0.2168
Heart rate (/min)	Mean ± SD	61.5 ± 6.9	88.7 ± 13.5	84.1 ± 10.7	0.0000	0.000	0.0427
Temperature (°C)	Median (IQR)	36.8 (36–36.8)	38.3 (37.9–38.6)	37.8 (37.5–38.1)	0.0010	0.0010	0.0186
SpO_2 (%)	Median (IQR)	100 (100)	98.5 (98.0–99.5)	99 (98 - 100)	0.0020	0.0547	0.2891
pH	Median (IQR)	7.38 (7.37–7.39)	7.43 (7.42–7.45)	7.42 (7.41–7.45)	0.0010	0.0020	0.6563
PaO_2 (kPa)	Mean ± SD	14.0 ± 1.2	12.5 ± 1.7	13.7 ± 1.0	N.S.	N.S.	N.S.
$PaCO_2$ (kPa)	Median (IQR)	5.41 (4.73–5.69)	4.85 (4.36–5.09)	4.79 (4.65–5.47)	0.0020	0.042	0.4131
IL-6 (ng/ml)	Median (IQR)	9.9 (3.2–30.4)	395 (134–1467)	17.2 (10.3–24.2)	0.0010	0.4131	0.0010
TNFα (pg/ml)	Median (IQR)	11.7 (7.3–17.7)	243 (131–476)	43.8 (31.6–54.4)	0.0010	0.0029	0.0010

IL, interleukin; IQR, inter-quartile range; MAP, mean arterial pressure; N.S., repeated-measures test statistic not significant; PaO_2/$PaCO_2$, arterial partial pressure of oxygen/carbon dioxide; p-value, post-hoc test p-value for difference between time points; SpO_2, arterial saturation of oxygen; SD, population standard deviation; TNFα, tumor necrosis factor alpha; TP, time point.

Statistical Analysis

Data distribution was assessed for normality using histograms and the Shapiro–Wilk W-test and for sphericity using Mauchly's test. For normally distributed data, the between-time point differences were determined using a repeated-measures analysis of variance (rm-ANOVA). For non-normally distributed data, the non-parametric Friedman test was used. Paired t-tests and Wilcoxon signed rank tests were used for *post-hoc* testing in case of normally and non-normally distributed data, respectively. The significance level was set at $\alpha = 0.05$. Pearson's correlation coefficient with Benjamini–Hochberg correction was used to explore the relation between the change in phase difference and TSI between different time points and changes in hemodynamic confounders related to cerebral perfusion and CA. Statistical analyses were performed using Stata/SE 16 (StataCorp., College Station, TX) and MATLAB 2019b (The MathWorks, Inc., Natick, MA).

RESULTS

Baseline Characteristics and Hemodynamic Parameters

The participants were healthy young adults (22.4 ± 1.6 years old) with a BMI of 24.2 ± 2.4 kg/m^2 and normal baseline physiological measurements as can be seen in **Table 1**. The hemodynamic parameters at each time point are provided in **Table 1** and **Figure 2**. A sustained decrease in MAP and a reversible decrease in $PaCO_2$ was observed, respectively. Heart rate, temperature, and pH showed a reversible increase.

NIRS-Derived Cerebral Autoregulation

The NIRS measurement duration was 20.9 ± 7.4 min (mean ± SD). After the application of TT-BF/BV correction, phase difference values were obtained in the VLF and LF bands (data on coherence, gain, and phase difference for all frequency bands can be found in the **Supplementary Material**). Phase difference values are provided for each participant at each time point for both the VLF and LF frequency bands in **Figures 3A,B**, respectively. No statistically significant differences in VLF phase difference values were found between the different time points ($\chi^2 = 5.10$, $p = 0.08$, Friedman test), although a trend toward lower values at time point 2 could be observed. For the LF band, a statistically significant difference in phase difference values between the time points was found ($\chi^2 = 7.82$, $p = 0.02$). Median (IQR) LF phase difference values decreased from time point 1 (16.2°, 3.0–52.6°) to time point 2 (3.9°, 2.0–8.8°; $Z = 2.13$, $p = 0.03$). The LF phase difference values were also higher at time point 3 (27.6°, 12.7–67.5°) than at time point 2 ($Z = -2.67$, $p = 0.005$, all Wilcoxon signed rank tests). No significant difference between time points 1 and 3 was found ($Z = -1.78$, $p = 0.08$).

No correlation was found between changes in LF phase difference between the time points and changes in the following variables: LF band power spectral density (PSD) in OxyHb, HHb, or ABP or $PaCO_2$, pH, and IL-6 or TNFα concentrations (all $R^2 < 0.25$, $p > 0.1$; see **Supplementary Material** for details). A positive correlation was found between changes in LF phase difference between time points 1 and 2 and changes in MAP ($R^2 = 0.50$, $p = 0.015$). A negative correlation was found between changes in LF phase difference between time points 2 and 3 and changes in heart rate ($R^2 = 0.45$, $p = 0.024$) and temperature ($R^2 = 0.65$, $p = 0.003$). Only the latter correlation remained statistically significant after correcting for multiple comparisons.

Tissue Saturation Index

TSI values are provided for each participant at each time point in **Figure 3C**. There was a significant difference in TSI between time points ($F = 4.78$, $p = 0.02$, rm-ANOVA). *Post-hoc* testing indicated that the TSI was higher at time points 2 (66.5 ± 2.8%) and 3 (67.1 ± 4.2%) than at time point 1 (63.7 ± 3.4%) [$t_{(10)} = -2.46$, $p = 0.03$ and $t_{(10)} = -2.40$, $p = 0.04$, respectively]. No significant differences between time points 2 and 3 were found [$t_{(10)} = -0.68$, $p = 0.51$].

No correlation was found between changes in TSI between the time points and changes in the following variables: LF band PSD in OxyHb, HHb, or ABP, $PaCO_2$, temperature, heart rate, and IL-6 or TNFα concentrations (all $R^2 < 0.25$, $p > 0.1$) (**Supplementary Material**). A weak, negative correlation was

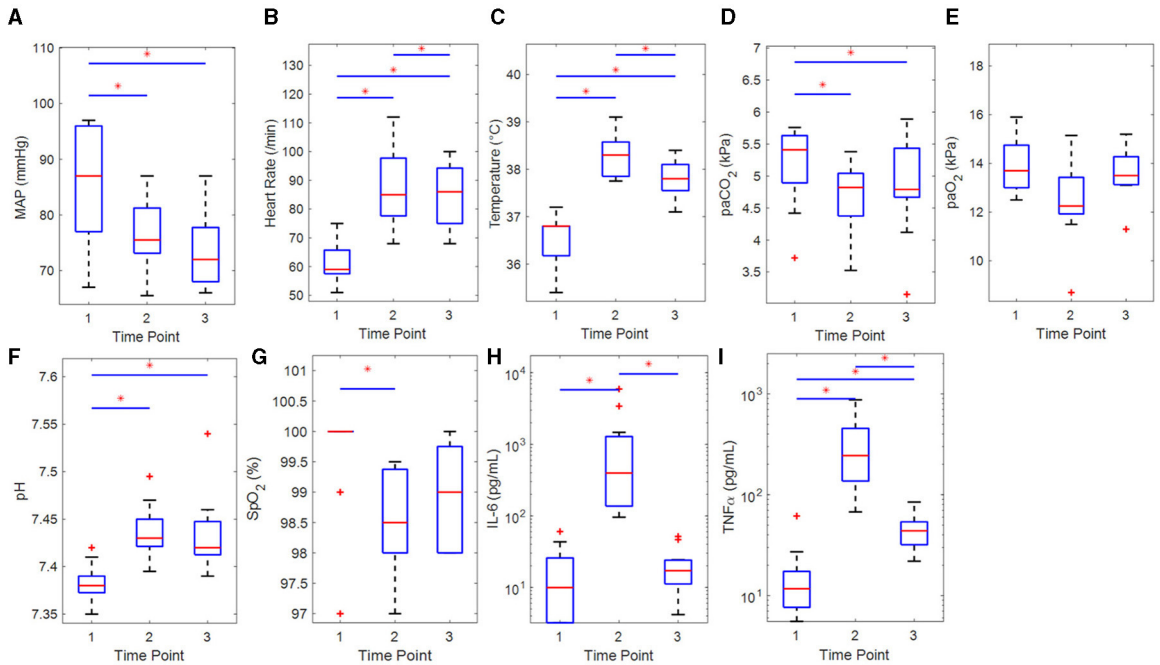

FIGURE 2 | Boxplots of hemodynamic and clinical parameters of the participants ($n = 11$) for each time point with results of the statistical comparisons. **(A)** Mean arterial pressure (rm-ANOVA), **(B)** heart rate (rm-ANOVA), **(C)** temperature (Sign. Rnk), **(D)** PaCO2 (Sign. Rnk), **(E)** PaO2 (Sign. Rnk), **(F)** pH (Sign. Rnk), **(G)** SpO2 (Sign. Rnk), **(H)** IL-6 (Sign. Rnk), and **(I)** TNFα (Sign. Rnk). IL, interleukin; MAP, mean arterial pressure; $PaO_2/PaCO_2$, arterial partial pressure of oxygen/carbon dioxide; rm-ANOVA, repeated-measures analysis of variance; Sign. Rnk, Wilcoxon's signed rank test; SpO_2, arterial saturation of oxygen; TNFα, tumor necrosis factor alpha. *$p < 0.05$ for difference between time points.

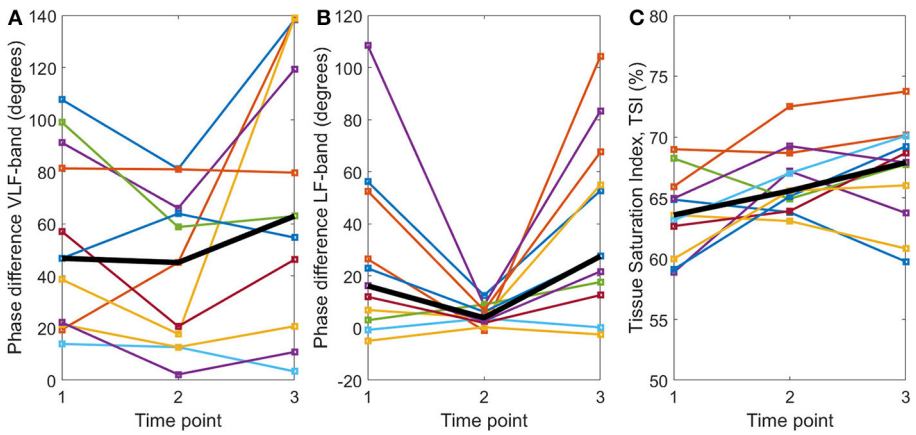

FIGURE 3 | TT-BF/BV-corrected phase differences (degrees) between OxyHb and HHb for the **(A)** very low frequency and **(B)** low frequency bands and **(C)** mean tissue saturation index (%) calculated with spatially resolved spectroscopy at three time points: (1) baseline, (2) systemic inflammation, and (3) at the end of the experiment. The per time point group median is shown by the black line.

found between changes in TSI between time points 1 and 2 and pH ($R^2 = 0.40$, $p = 0.04$).

DISCUSSION

Interpretation of the Results

In this study, NIRS-derived DCA estimations were obtained during experimental human endotoxemia with a continuous infusion of bacterial LPS. The TT-BF/BV-corrected phase difference values in the LF band were significantly lower during systemic inflammation compared with baseline and at the end of the experiment. In addition, the TSI increased significantly during systemic inflammation compared with baseline and remained significantly higher at the end of the experiment.

We found a reversible decrease in LF phase difference measured with NIRS, which suggests impaired CA during endotoxemia in healthy volunteers. The extensive physiological changes resulting from endotoxin administration could

theoretically underlie the observed NIRS changes, but after extensive analysis, we found no unambiguous explanation for the observed decrease in LF phase difference measured with NIRS.

A decrease in LF phase difference between time points 1 (baseline) and 2 (systemic inflammation) correlated with a decrease in MAP, although this was not significant after correcting for multiple comparisons. Furthermore, although the LF phase difference increased between time points 2 and 3 (end of the experiment), MAP did not, attenuating the interpretation of a major influence of MAP changes on LF phase. Furthermore, an increase in LF phase correlated with a decrease in heart rate and temperature, although only the latter remained statistically significant after correcting for multiple comparisons and only between time points 2 and 3. There was no correlation with temperature and heart rate changes between time points 1 and 2, supporting the interpretation that these changes may not be an important confounder. Other potential confounders that we analyzed were changes in inflammatory cytokines (IL-6 and TNFα) and $PaCO_2$. All these variables did not correlate with the changes in LF phase. Note that the absence of correlations with potential confounders in our small sample should not be interpreted as proof of the absence of any such relationship: it could be that there actually is a (weak) relationship that could be identified in larger samples.

Previous data by Brassard and colleagues support the idea that the improvement in dynamic CA that they found during experimental endotoxemia correlated with a decrease in carbon dioxide tension (7). The relation between hypocapnia and DCA phase difference is well recognized (21, 22). In our study, relative hypocapnia and alkalosis were also present, which are expected to induce an increase in LF band DCA phase difference. The opposite was observed (decrease in LF band phase). It could be that the effect of hypocapnia is masked in part by other physiological changes that occurred in our endotoxemia population, among others the decrease in MAP or a higher inflammatory response. Indeed the population studied by Brassard et al. had no decrease in MAP upon a lower bolus administration of 2 ng/kg of endotoxin.

The small but sustained increase in TSI that was observed may have resulted from microvascular vasodilatation, with concomitant increases in CBV and/or CBF. We could not further clarify this phenomenon based on our data, as we found only a weak, non-significant relation between the increase in TSI between time points 1 and 2 and an increase in pH. However, both an increase in TSI and a decrease in LF phase difference measured with NIRS are consistent with the interpretation of cerebral microvascular vasodilatation in response to endotoxin infusion.

No significant changes in VLF phase difference were found. We hypothesize that this is due to the limited reproducibility of VLF phase difference values using TFA (15, 23). A variation in LF phase difference values was seen between the participants showing an evident reversible decrease during endotoxin-induced systemic inflammation and the participants with consistently low phase difference values with limited variation. We hypothesize that CA was consistently "off" in the latter group, given the known non-stationarity of CA function, also in healthy participants (14).

Comparison With TCD- and ABP-Derived DCA

The reversible decrease in NIRS-derived LF phase difference observed in this study has not been found with TFA using TCD and ABP measurements as reported previously (5). It could be that the autoregulatory dysfunction observed upon endotoxin administration mainly demonstrates itself in a patchy distribution in the cortical microvasculature, the effects of which cannot be easily found in TCD-based CBF velocity in the MCA. Another possibility is that some of the CA effects of endotoxin administration occur at the level of pre-capillary sphincters and not only at the level of the cerebral arterioles themselves (13, 24, 25). The NIRS measurements could be sensitive to both microvascular regulators. The OxyHb and HHb components are present proximal and distal to both regulators, making NIRS suitable for the detection of alterations in the function of both the arterioles and the pre-capillary sphincters. The TCD-derived CBFv could be only sensitive to the upstream resistance effects of the arterioles. Another explanation may be methodological. The variation in TFA analysis has been shown to decrease with measurement duration (23). In our study, the mean ± SD duration of the NIRS measurements was 20.9 ± 7.4 min, compared with 5 min as previously reported for TCD and ABP (5).

Limitations

We recognize several limitations of our study. The sample size of 11 participants prevents an extensive, multivariate analysis of the data, and it may limit the external validity of the results. Furthermore, we pooled the NIRS parameters from two measurements ($T = 150$ and 300 min) due to movement artifacts in some measurements. This allowed an "intra-inflammatory" measurement for each participant, and it limited the number of statistical comparisons. We consider this justified and advisable, as the concentration of pro-inflammatory cytokines was high at both time points as published previously, indicating the systemic inflammatory response (5). Longer (>30 min) measurements would allow for more artifact-free data, but this was unfeasible in the current endotoxemia setup. The cerebral origin of the NIRS-only DCA measurements has previously been confirmed by comparison against TCD/ABP-derived DCA during rest and hypercapnia. However, we cannot exclude the confounding effects of changes in extracerebral perfusion that may have resulted from systemic microvascular vasodilation in the febrile phase of systemic inflammation in the current study. It should be mentioned that one participant was in a consistent hyperventilation (hypocapnic) state during the entire experiment ($3.15 < PaCO_2 < 3.72$ kPa) but was not excluded from the analysis to prevent selection bias. Lastly, the NIRS measurements are sensitive to movement artifacts, which was exemplified in our study as we had to exclude measurements from two participants. Movement-related artifacts may however be less pronounced

in clinical target populations, including sedated patients in the ICU.

Future Perspective

The NIRS-only technique is a non-invasive, easy-to-use modality for the measurement and monitoring of CA. This study provides first insights that NIRS-only-derived DCA changes during experimental human endotoxemia. It provides indications for an influence of bacterial endotoxin on DCA, which warrants further investigation in larger endotoxemia studies. Moreover, it could be interesting to investigate NIRS-derived DCA in a sepsis population, as the systemic inflammatory response in sepsis is higher, longer, and has a stronger hemodynamic effect than during experimental endotoxemia, and there is more variability in (cerebrovascular) outcome.

CONCLUSION

Our findings suggest that endotoxin administration in healthy volunteers results in changes in cerebral microvascular autoregulation and microvascular vasodilation.

DATA AVAILABILITY STATEMENT

The raw data supporting the conclusions of this article will be made available by the authors, without undue reservation.

ETHICS STATEMENT

The studies involving human participants were reviewed and approved by Commissie Mensgebonden Onderwoek regio Arnhem—Nijmegen. The patients/participants provided their written informed consent to participate in this study.

AUTHOR CONTRIBUTIONS

CH, PP, GL, and JB contributed to conception and design of the study. GL, JB, and CH performed the measurements. JE, NE, and NM performed the data-analysis and statistical analysis. NE drafted the manuscript. CH, GL, CvK, JvB, MA, JE, NE, and NM wrote sections of the manuscript. All authors contributed to the manuscript revision, read, and approved the submitted version.

FUNDING

Graduate School of Medical Sciences, University of Groningen: Research grant NE.

SUPPLEMENTARY MATERIAL

The Supplementary Material for this article can be found online at: https://www.frontiersin.org/articles/10.3389/fneur.2021.695705/full#supplementary-material

REFERENCES

1. Singer M, Deutschman CS, Seymour C, Shankar-Hari M, Annane D, Bauer M, et al. The third international consensus definitions for sepsis and septic shock (sepsis-3). *JAMA.* (2016) 315:801–10. doi: 10.1001/jama.2016.0287
2. Gofton TE, Young GB. Sepsis-associated encephalopathy. *Nat Rev Neurol.* (2012) 8:557–66. doi: 10.1038/nrneurol.2012.183
3. Taccone FS, Castanares-Zapatero D, Peres-Bota D, Vincent J-L, Berre' J, Melot C. Cerebral autoregulation is influenced by carbon dioxide levels in patients with septic shock. *Neurocrit Care.* (2010) 12:35–42. doi: 10.1007/s12028-009-9289-6
4. Ferlini L, Su F, Creteur J, Taccone FS, Gaspard N. Cerebral autoregulation and neurovascular coupling are progressively impaired during septic shock: an experimental study. *Intensive Care Med Exp.* (2020) 8:44. doi: 10.1186/s40635-020-00332-0
5. van den Brule JMD, van Kaam CR, Leijte GP, Stolk R, Pickkers P, van der Hoeven JG, et al. Dynamic cerebral autoregulation and critical closing pressure in experimental human endotoxemia and sepsis patients. *Med One.* (2019) 4:e190009. doi: 10.20900/mo.20190009
6. Møller K, Strauss GI, Qvist J, Fonsmark L, Knudsen GM, Larsen FS, et al. Cerebral blood flow and oxidative metabolism during human endotoxemia. *J Cereb Blood Flow Metab.* (2002) 22:1262–70. doi: 10.1097/01.WCB.0000037999.34930.CA
7. Brassard P, Kim YS, Van Lieshout J, Secher NH, Rosenmeier JB. Endotoxemia reduces cerebral perfusion but enhances dynamic cerebrovascular autoregulation at reduced arterial carbon dioxide tension. *Crit Care Med.* (2012) 40:1873–8. doi: 10.1097/CCM.0b013e3182474ca7
8. Pollard V, Prough DS, Deyo DJ, Conroy B, Uchida T, Daye A, et al. Cerebral blood flow during experimental endotoxemia in volunteers. *Crit Care Med.* (1997) 25:1700–6. doi: 10.1097/00003246-199710000-00020
9. Lowry SF. Human endotoxemia: a model for mechanistic insight and therapeutic targeting. *Shock.* (2005) 24(Suppl. 1):94–100. doi: 10.1097/01.shk.0000191340.23907.a1
10. Berg RMG, Plovsing RR, Ronit A, Bailey DM, Holstein-Rathlou NH, Møller K. Disassociation of static and dynamic cerebral autoregulatory performance in healthy volunteers after lipopolysaccharide infusion and in patients with sepsis. *Am J Physiol Regul Integr Comp Physiol.* (2012) 303:R1127–35. doi: 10.1152/ajpregu.00242.2012
11. Liu X, Akiyoshi K, Nakano M, Brady K, Bush B, Nadkarni R, et al. Determining thresholds for three indices of autoregulation to identify the lower limit of autoregulation during cardiac surgery. *Crit Care Med.* (2021) 49:650–60. doi: 10.1097/CCM.0000000000004737
12. Lee JK, Kibler KK, Benni PB, Easley RB, Czosnyka M, Smielewski P, et al. Cerebrovascular reactivity measured by near-infrared spectroscopy. *Stroke.* (2009) 40:1820–6. doi: 10.1161/STROKEAHA.108.536094
13. Elting JWJ, Tas J, Aries MJH, Czosnyka M, Maurits NM. Dynamic cerebral autoregulation estimates derived from near infrared spectroscopy and transcranial Doppler are similar after correction for transit time and blood flow and blood volume oscillations. *J Cereb Blood Flow Metab.* (2020) 40:135–49. doi: 10.1177/0271678X18806107
14. Panerai RB. Nonstationarity of dynamic cerebral autoregulation. *Med Eng Phys.* (2014) 36:576–84. doi: 10.1016/j.medengphy.2013.09.004
15. Sanders ML, Elting JWJ, Panerai RB, Aries M, Bor-Seng-Shu E, Caicedo A, et al. Dynamic cerebral autoregulation reproducibility is affected by physiological variability. *Front Physiol.* (2019) 10:865. doi: 10.3389/fphys.2019.00865
16. Leijte GP, Kiers D, Van Der Heijden W, Jansen A, Gerretsen J, Boerrigter V, et al. Treatment with acetylsalicylic acid reverses endotoxin tolerance in humans *in vivo*: a randomized placebo-controlled study. *Crit Care Med.* (2019) 47:508–16. doi: 10.1097/CCM.0000000000003630
17. Wyatt JS, Cope M, Delpy DT, Richardson CE, Edwards AD, Wray S, et al. Quantitation of cerebral blood volume in human infants by near-infrared spectroscopy. *J Appl Physiol.* (1990) 68:1086–91. doi: 10.1152/jappl.1990.68.3.1086
18. Claassen JA, Meel-Van Den Abeelen AS, Simpson DM, Panerai RB, Caicedo Dorado A, Mitsis GD, et al. Transfer function analysis of dynamic

cerebral autoregulation: a white paper from the international cerebral autoregulation research network. *J Cereb Blood Flow Metab.* (2015) 36:665–80. doi: 10.1177/0271678X15626425

19. Matcher SJ, Kirkpatrick PJ, Nahid K, Cope M, Delpy DT. Absolute quantification methods in tissue near-infrared spectroscopy. In: *Optical Tomography, Photon Migration, and Spectroscopy of Tissue and Model Media: Theory, Human Studies, and Instrumentation.* (1995). p. 486–95
20. Matcher SJ, Cope M, Delpy DT. *In vivo* measurements of the wavelength dependence of tissue-scattering coefficients between 760 and 900 nm measured with time-resolved spectroscopy. *Appl Opt*. (1997) 36:386–96. doi: 10.1364/AO.36.000386
21. Aaslid R, Lindegaard KF, Sorteberg W, Nornes H. Cerebral autoregulation dynamics in humans. *Stroke.* (1989) 20:45–52. doi: 10.1161/01.STR.20.1.45
22. Panerai RB, Deverson ST, Mahony P, Hayes P, Evans DH. Effect of CO2 on dynamic cerebral autoregulation measurement. *Physiol Meas.* (1999) 20:265–75. doi: 10.1088/0967-3334/20/3/304
23. Elting JW, Sanders ML, Panerai RB, Aries M, Bor-Seng-Shu E, Caicedo A, et al. Assessment of dynamic cerebral autoregulation in humans: is reproducibility dependent on blood pressure variability? *PLoS ONE.* (2020) 15:e0227651. doi: 10.1371/journal.pone.0227651
24. Hudetz AG. Blood flow in the cerebral capillary network: a review emphasizing observations with intravital microscopy. *Microcirculation.* (1997) 4:233–52. doi: 10.3109/10739689709146787
25. Hall CN, Reynell C, Gesslein B, Hamilton NB, Mishra A, Sutherland BA, et al. Capillary pericytes regulate cerebral blood flow in health and disease. *Nature.* (2014) 508:55–60. doi: 10.1038/nature 13165

Conflict of Interest: The authors declare that the research was conducted in the absence of any commercial or financial relationships that could be construed as a potential conflict of interest.

Publisher's Note: All claims expressed in this article are solely those of the authors and do not necessarily represent those of their affiliated organizations, or those of the publisher, the editors and the reviewers. Any product that may be evaluated in this article, or claim that may be made by its manufacturer, is not guaranteed or endorsed by the publisher.

frontiers in Neurology

REVIEW
published: 05 October 2021
doi: 10.3389/fneur.2021.740185

Perspective on Cerebral Autoregulation Monitoring in Neonatal Cardiac Surgery Requiring Cardiopulmonary Bypass

Jared M. Spilka[1*†], *Conor P. O'Halloran*[2†], *Bradley S. Marino*[3‡] *and Kenneth M. Brady*[1‡]

[1] *Division of Cardiac Anesthesia, Department of Anesthesiology, Ann and Robert H. Lurie Children's Hospital of Chicago, Chicago, IL, United States,* [2] *Division of Cardiology, Department of Pediatrics, Ann and Robert H. Lurie Children's Hospital of Chicago, Chicago, IL, United States,* [3] *Department of Pediatric Cardiology, Cleveland Clinic, Cleveland, OH, United States*

OPEN ACCESS

Edited by:
Dong Ming,
Tianjin University, China

Reviewed by:
Erik Dirk Gommer,
Maastricht University Medical Centre, Netherlands
David Simpson,
University of Southampton, United Kingdom
Alexey Trofimov,
Privolzhsky Research Medical University (PIMU), Russia

***Correspondence:**
Jared M. Spilka
jspilka@luriechildrens.org

†These authors share first authorship

‡These authors share senior authorship

Specialty section:
This article was submitted to Neurocritical and Neurohospitalist Care, a section of the journal Frontiers in Neurology

Received: *22 July 2021*
Accepted: *09 September 2021*
Published: *05 October 2021*

Citation:
Spilka JM, O'Halloran CP, Marino BS and Brady KM (2021) Perspective on Cerebral Autoregulation Monitoring in Neonatal Cardiac Surgery Requiring Cardiopulmonary Bypass. Front. Neurol. 12:740185. doi: 10.3389/fneur.2021.740185

The autoregulation of cerebral blood flow protects against brain injury from transient fluctuations in arterial blood pressure. Impaired autoregulation may contribute to hypoperfusion injury in neonates and infants. Monitoring cerebral autoregulation in neonatal cardiac surgery as a guide for arterial blood pressure management may reduce neurodevelopmental morbidity. Cerebral autoregulation monitoring has been validated in animal models and in an adult trial autoregulation monitoring during bypass improved postoperative delirium scores. The nuances of pediatric cardiac disease and congenital heart surgery make simply applying adult trial findings to this unique population inappropriate. Therefore, dedicated pediatric clinical trials of cerebral autoregulation monitoring are indicated.

Keywords: cerebral autogregulation, congenital heart disease, neonate, autoregulation monitoring, pediatrics, neurological injury, cardiopulmonary bypass

THE BURDEN OF NEUROLOGIC INJURY AFTER NEONATAL HEART SURGERY

Neurological injury occurs in roughly half of newborns undergoing cardiac surgery using cardiopulmonary bypass (CPB) (1). MRI studies reveal that stroke occurs in about 10% of this population (2) secondary to both ischemic and thromboembolic events. However, white matter injury (WMI) occurs at a much higher rate, affecting over 50% of neonates undergoing cardiac surgery with CPB +/- deep hypothermic circulatory arrest (DHCA) vs. only 4% in infants who require similar surgical procedures (3). The potential causes of inadequate perfusion instigating WMI are myriad. Neonates with critical congenital heart disease have oxygen delivery vulnerabilities *in utero,* preoperatively, intraoperatively, and postoperatively. Highly sensitive oligodendrocytes occupy a watershed region in the neonatal brain, and this is thought to contribute to the high incidence of white matter injury reminiscent of preterm periventricular leukomalacia (4). The duration of CPB, use and duration of DHCA, low arterial blood pressure (ABP), and hypoxemia in the first 48 post-operative hours are all associated with WMI (3, 5). The most complex congenital cardiac lesions require repair by a series of staged surgeries, potentially compounding injury over time through multiple episodes of CPB. The magnitude of disability associated with WMI is not yet established and cannot be studied without following cohorts to teenage and adult years. A recent, large meta-analysis of neurodevelopmental outcome after neonatal cardiac surgery

showed a disappointing magnitude of impairment in both the psychomotor and cognitive indices of the Bayley Scale of Infant Development (78 and 88% of normative means on average). (6) Improved understanding of neonatal brain perfusion and interventions to reduce neurological injury have high potential impact for neonates who require heart surgery and CPB.

Watershed Injuries in the White Matter Suggest Vulnerability to Inadequate Cerebral Blood Flow

Neonates, especially preterm neonates, lack the robust, redundant cerebral vasculature that is present in infants and adults. Poor vascular redundancy in the deep white matter may enhance the risk of watershed injury during cerebral dysautoregulation. Fragile vascular overgrowth in the germinal matrix is a risk factor for hemorrhage for the preterm neonate, but germinal matrix hemorrhage is a less common injury after CPB than watershed WMI. (7) Congenital heart disease is associated with increased risk of abnormal brain development, independent of the finding of brain injury during surgical or procedural interventions. Neonates with congenital heart disease have small, relatively immature brains, perturbations in brain structural integrity and metabolism, regional growth differences, and an overall decrease in cerebral blood flow (8–12). The immaturity of the neurovascular system in neonates with congenital heart disease may contribute to both dysautoregulation of cerebral blood flow, and vulnerability to injury from dysautoregulation. Prevention of the dysautoregulated state by maintaining ABP within the limits of autoregulation is a modifiable care practice that may prevent or mitigate WMI in this population.

Hypotension, and Optimal ABP for Neonates With Heart Disease Are Unknown

The goal of autoregulation monitoring in neonates with congenital heart disease is to delineate the lower limit of autoregulation (LLA), providing a target for ABP management. (7) Maintaining ABP above LLA is hoped to protect watershed regions of the neonatal brain from fluctuations of cerebral blood flow that occur in the dysautoregulated state. (13) The limits of autoregulation for neonates, and the inter-subject variability of these limits are not known. Criteria for hypotension in neonates are poorly defined and best treatments of "hypotension" (fluid, vasopressors, ionotropes) are debated (14) Current ABP management is based solely on experiential knowledge rather than individualized physiological goals (7). Further, there is a dichotomy of physiological goals which occurs in the setting of neonatal cardiac pathology, which benefits from low ABP and maintaining cerebral autoregulation, which may require higher ABP. When the neonatal heart is weakened by surgery and critical illness, lowered systemic vascular resistance (SVR) improves stroke volume and cardiac output. There is no effective measure of SVR, stroke volume or cardiac output for neonates, so lowered ABP is used as a primary surrogate. Strict SVR control has improved outcomes for neonates with the most critical heart lesions (13, 15, 16). However, the brain is dependent on ABP, not cardiac output for perfusion, so this highly effective ABP lowering strategy may improve survival at the expense of an increase in brain injury.

In principle the maintenance of ABP above LLA during neonatal cardiac surgery may prevent neurological injury and improve neurodevelopmental outcomes. This remains as an only partially tested hypothesis which requires further study (13). Cerebral autoregulation monitoring during CPB in adults has shown improvement in neurological outcomes (17, 18). The uniqueness of neonatal physiology and the requirement for strict SVR control when heart disease is present are factors that elevate the importance of studying the limits of autoregulation in this population.

Technical Considerations for Autoregulation Monitoring in the Cardiac OR

The concept of autoregulation pre-dates the technical ability to measure autoregulation in real time. Conceptually, a real time autoregulation monitor requires a measure of arterial blood pressure (ABP) or cerebral perfusion pressure (CPP), a measure of cerebral blood flow (CBF) or a proxy, and a mathematical approach to determine if cerebral blood flow is passive to blood pressure (19).

The first modern attempts to monitor autoregulation in real time are typified by Czosnyka et al. in 2 seminal papers (20, 21). These methods utilized transcranial Doppler (the mean velocity index or Mx) or intracranial pressure (the pressure reactivity index or PRx). Czosnyka et al. explained that the positive correlation between middle cerebral artery flow velocity and CPP (i.e., positive Mx) was evidence of pressure passive cerebral blood flow (i.e., decreased ABP leads to decreased CBF) which defines disturbed autoregulation. Utilizing the same cohort and study design, ICP was used as a surrogate for cerebral blood volume to quantify vasoreactivity as passivity of blood volume to ABP (20). During normal cerebral vasoreactivity, a negative relationship between ABP and ICP should be observed (lower ABP leads to vasodilation, leads to higher blood volume, leads to higher ICP). Conversely, dysfunctional vasoreactivity renders a positive relationship between ABP and ICP (lower ABP, vascular tone does not change, blood volume decreases due to lower distending pressure, ICP decreases). These methods are ideal for patients with head trauma, but trans-cranial Doppler insonation under a surgical drape is difficult during neonatal heart surgery, and invasive intracranial pressure monitoring is not possible.

Two Requirements for the Cardiac OR: Hands-Free and Non-Invasive

The feasibility of less invasive monitors of cerebral pressure autoregulation using reflectance near infrared spectroscopy (NIRS) was established in a series of experiments in neonatal piglets (22, 23). In these experiments a "gold standard" autoregulation curve was established using invasive laser Doppler flow probes. Relative total hemoglobin (rTHb) was measured using NIRS as the inverse of the recovery of light isosbestic to the hemoglobin species. Whereas PRx correlates ABP with

ICP, Hemoglobin Volume Index (HVx) correlated ABP with NIRS measure of total hemoglobin, which is a proxy for cerebral vascular tone and ICP. rTHb measured in this way served as a proxy for cerebral vascular tone to render a NIRS-based analog of the PRx, the Hemoglobin-Volume Index, or HVx. Additionally, standard, commercially available measures of cerebral tissue oxygenation were used as a proxy for CBF to render a NIRS-based analog of the Mx, the Cerebral Oximetry Index, or COx. Both the HVx and the COx were compared against the gold standard LLA. Receiver operator curves (ROC) describing the ability of HVx and COx to distinguish autoregulation from dysregulation were created.

Two relevant observations came from these experiments. First, rTHb showed high coherence (relatedness in the frequency domain) with ICP at the slow wave frequency. This observation inadvertently validated the assumption that ICP slow waves are the result of fluctuating CBV, which is an assumption inherent to the PRx. Second, non-invasive measures of autoregulation (COx) and cerebral vasoreactivity (HVx) effectively differentiate periods of cerebral autoregulation from dysregulation with similar performance to invasive measures (i.e., PRx). For example, the area under the curve (AUC) of the ROC for HVx was 0.85, compared to an AUC of 0.88 for the invasive measure PRx. HVx had a sensitivity of 77% and specificity of 84%. COx had an AUC of 0.89, sensitivity of 83%, and specificity of 75%.

Why Frequency Matters?

In their pioneering work, Czosnyka et al. discussed the importance of examining the correct frequency of waveform when monitoring cerebral autoregulation. ABP fluctuates over each second due to cardiac systole/diastole, every few seconds due to respirations, and over minutes to hours due to changes in clinical status. In addition, ABP fluctuates every 30 seconds to few minutes in a phenomenon termed slow waves. These waves were first described in the ICP pressure tracing and were termed B waves (early observations of cerebral autoregulation were seen by visual comparison of ABP and ICP tracings at the B wave frequency) (24). Slow waves are ideal for measuring autoregulation because they are naturally occurring blood pressure fluctuations that occur at a frequency that engages the autoregulation mechanism. By contrast, the ABP pulse due to cardiac systole/diastole occurs too rapidly and is not buffered by cerebral autoregulation. The respiratory cycle in ABP is also too rapid for reliable engagement of the autoregulation mechanism, especially at rapid respiratory rates seen in neonates. Therefore, slow wave oscillations in ABP have been used to measure autoregulation and vasoreactivity in most attempts to quantify autoregulation in real time. The use of slow waves dictates the refresh rate of autoregulation monitoring, and is the rate-limiter for time to delineate the lower limit of autoregulation. Current methods are estimated to require 15 to 30 min of monitoring to delineate the lower limit of autoregulation in the neonatal cardiac operating room.

Too Many Options: How Do We Validate Them?

The number of proposed measures of autoregulation and vasoreactivity has increased in the last decade, with varying levels of evidence to support their utilization. All metrics share 3 fundamental components (25):

1) **Changes in ABP must occur and be measured.** Measurement of ABP is straight forward using intra-arterial catheters which are standard practice in intensive care units. Most attempts to measure autoregulation have focused on the slow wave oscillations in ABP described above.
2) **Changes in CBF or CBV must be measured.** A number of different non-invasive monitors of CBF or CBV have been proposed, most of which rely on measuring blood flow by doppler effect, or oximetry and blood volume based on the light absorption of hemoglobin.
3) **The relationship between ABP and CBF/CBV must be quantified to identify periods when CBF/CBV are passive to changes in ABP.** Of the three components this is the least intuitive to most clinicians. Conceptually all measures of relatedness can be divided into time-domain and frequency-domain measures. Time domain measures of relatedness determine if and to what extent two variables "move together" over time. The Pearson correlation coefficient is the most commonly used time-domain metric. Alternatively, complex biologic signals such as ABP or cerebral tissue oxygenation can be broken down into combinations of waves of different frequencies and magnitudes. In an oversimplification, frequency domain measures determine if and to what degree the component waves that make up more complex signals are shared between different signals (i.e., between ABP and cerebral oxygenation).

Although the NIRS based measures utilizing correlation or phase shift have performed well in animal validation, there are several other potential measures of CBF/CBV and mathematical approaches to assessing passivity to blood pressure. This leads to an essentially endless list of possible combinations. With so many measures of autoregulation (and more likely to be developed), it is important to consider the evidence burden needed to compare and optimize these potential tools. The following three requirements have been proposed (26):

1) Validate the candidate index against an accepted gold standard measure of autoregulation (in pediatric cardiac surgery population, this would be an autoregulation curve calculated from laser doppler probe and arterial blood pressure). Given that gold standard measures of cerebral blood flow are invasive, this criterium is likely to require animal study.
2) Show strong relatedness of a candidate index to outcome reproducibly in prospective studies of humans.
3) Demonstrate feasibility of using actionable data from a candidate index, such that clinicians can optimize clinical care and minimize morbidity.

Surprisingly Poor Performances in Some Published Metrics When Studied Methodically

Utilizing the piglet experimental construct described above, a large number of candidate indices were compared with each other and to the gold standard LLA (19). The available

measures included tissue oxygenation measured by NIRS (rSO2), total hemoglobin measured by NIRS (THb, measured using the isosbestic wavelength method), laser doppler flow (LDF), ICP, and mean arterial blood pressure (MAP). Four mathematical approaches (correlation, phase shift, gain of transfer and coherence) were applied to 6 variable pairs to create 24 indices of autoregulation. Receiver operator curves were created for each index (using the gold standard LLA) and area under the curves estimated to allow comparisons. These receiver operator curves determine the ability of each index to correctly discriminate between times within the ABP bounds of autoregulation (as determined by laser doppler probe-ABP relationship) and times outside the ABP bounds of autoregulation. Eight indices appeared to outperform the other metrics. This tedious, but important analysis showed that correlation and phase- based indices clearly outperformed those based on either gain of transfer or coherence. NIRS-derived measures of cerebral oximetry and blood volume (ie rTHb) performed as well as invasive ICP and out-performed direct flow measurements with laser-Doppler. Any new method to measure autoregulation, either by novel interrogation of the brain vasculature or novel mathematic assessment of passivity to ABP needs to undergo a similar evaluation as many published methods failed to delineate LLA when critically examined this way.

NIRS Can Measure Autoregulation. Is It Feasible in the Neonatal Cardiac OR?

HVx and COx are candidate indices that meet the requirements of being hands-free and non-invasive. Both performed well in the animal validation study. However, neither has been studied adequately in the clinical environment to demonstrate feasibility or efficacy to prevent neurologic injury in the neonatal cardiac population. As a start to this effort, the feasibility NIRS-based methods to measure autoregulation during cardiac surgery in children was demonstrated in a prospective observational pilot study of 54 children (13). The LLA was estimated using a COx threshold of 0.4 (extrapolated from the piglet data) and was able to be determined for 77% of the subjects during surgery. The average LLA was 42 mmHg but ranged from 20 to 55 mmHg (including non-neonates). This study demonstrated that LLA could be estimated in the clinical environment, but did not demonstrate relatedness to outcome, and did not demonstrate true feasibility: ie, if the LLA is known, is it actionable? How long did it take to delineate LLA? Can the burden of hypotension be reduced by knowing the LLA? One true demonstration of autoregulation monitoring feasibility using the mean velocity index (Mx) has been done in an adult population. Hogue et al. significantly reduced, by nearly half, the magnitude and duration of ABP below LLA when LLA was revealed to the care team with real time monitoring (18). The area-under-curve variable used in that study quantifies the burden of hypotension below LLA and is ideal for studying feasibility of autoregulation monitoring for the neonatal cardiac surgical population. If LLA can be known in a timely manner, and if the care team has options to raise ABP above LLA, then the hypotension exposure will be lower.

Safety Concerns in the Neonatal Population

As described above, function of the neonatal heart is negatively impacted by afterload in the perioperative window. Raising ABP to exceed LLA is an expected intervention from showing LLA to care providers with autoregulation monitoring. Options include increasing pump flow rates, contractility, preload, and systemic vascular resistance. Each of these has the potential for harm. Does optimizing perfusion of the brain also optimize cardiac performance and perfusion of the visceral organs? It seems unlikely given that the brain is dependent on ABP for perfusion while the viscera are dependent on cardiac output (27, 28). If ABP maintenance comes at the expense of cardiac output, then higher rates of acute kidney injury, bowel injury, acidosis, heart failure and pulmonary edema may occur. In the case of the adult cardiac population, maintenance of ABP above LLA was associated with improved multi-organ outcomes (18), but this cannot be applied to the neonatal case due to differences in neonatal myocardium and peculiarities related to shunted circulation in newborns with congenital heart disease.

Neonates undergoing cardiac surgery are at risk of a distinct low cardiac output state/syndrome (LCOS) about 6–18 h post-operatively. When LCOS is accompanied by high SVR cardiovascular collapse can result. This was noted in the Norwood procedure for hypoplastic left heart syndrome which historically had perioperative morbidity of 50% within the first 48 h of surgery (29). The initiation of afterload reduction via phenoxybenzamine (a vasodilator) during Norwood procedure resulted in lower indexed SVR, higher SVO_2 via internal jugular oximetric measurements, decreased arteriovenous O_2 content differences, and improved systemic blood flow (30, 31). Study has shown that freedom from circulatory collapse at 72 h was increased with phenoxybenzamine (95 vs. 69% without phenoxybenzamine (16). The PRIMACORP study in 2003 showed that milrinone (a vasodilator) also decreased the incidence of LCOS after biventricular repair with CPB (32). The need to reduce SVR to prevent LCOS and the need to raise SVR to achieve ABP above the LLA are diametrically opposed clinical goals in the neonates with cardiac disease. Understanding the effect of optimizing ABP based on LLA vs. the rate of LCOS and reduced survival cannot be inferred from adult trials.

The Challenge of Demonstrating Efficacy of Brain Protection in Neonates

If the burden of hypotension can be effectively reduced by autoregulation monitoring, will the burden of neurologic injury be similarly reduced, and how can that be demonstrated? In the adult RCT of autoregulation monitoring for cardiac surgery, multiple outcomes were evaluated. While MRI differences were not observed, patients with autoregulation monitoring experienced a 45% reduction in post-operative delirium compared to controls. (38 vs. 53%, $p = 0.04$) (17, 18).

The outcomes of adult studies cannot serve as a template for neonatal studies. MRI findings in adults are largely embolic while MRI findings in neonates after cardiopulmonary bypass are primarily watershed white matter injuries (WMI) (3, 4). It is not surprising that autoregulation monitoring did not change the incidence of embolic events, but it is conceivable that maintaining ABP above LLA would reduce ischemic WMI. Therefore, MRI will be important outcome measure for the neonatal population. To date, no intervention has reduced WMI seen on MRI in this population.

Overt neurologic injury is uncommonly seen in neonates, even with substantial MRI injury. Therefore, neurologic exam is likely too insensitive to use as an outcome. Delirium cannot be measured with the same precision in neonatal populations as in adult populations, so it is unlikely that a neonatal study could replicate the adult finding of reduced delirium.

Seizure activity occurs in nearly 10% of neonates after cardiac surgery, is most often clinically silent, and is strongly associated with developmental outcome (33, 34). Seizure activity is an attractive outcome for studying efficacy of autoregulation monitoring because the data are low cost and obtained immediately after surgery. Post-operative EEG should be included in any trial of neonatal autoregulation monitoring during cardiac surgery. With a baseline incidence of 10%, a multi-center trial with large sample size would be required to show a reduction in rate of post-operative seizure.

The gold standard neurologic outcome for neonates with neurologic risk is the developmental exam. Any study that collects data for 5 yr and then requires a 5 yr follow up developmental exam becomes a 10-yr study. The most impactful developmental study of neonates with cardiac disease is the Boston circulatory arrest trial, which followed serial developmental exams into the late teen years (35). Even if a substantial neonatal cohort could be recruited in 5 yr with randomization of autoregulation monitoring, the results of developmental testing at 15 yr would require 20 yr of effort. Extensive work done to date on developing autoregulation monitors for neonatal cardiac surgery is little more than foundation for the efforts of a subsequent generation of clinician-scientists.

CONCLUSION AND A LOOK TO THE FUTURE

Teams that care for neonates with cardiac disease have made substantial progress in achieving survival for complex and delicate surgical disease with very little room for error. The current frontier is the unacceptably high rate of neurologic injury in the survivors of neonatal heart surgery. Given the multifactorial vulnerabilities of the neonatal brain perfused by a malformed circulation, it is not likely that any single intervention will eliminate brain injury. Autoregulation monitoring stands at the front of the line with these interventions because low ABP is needed for survival of neonatal heart surgery, and we do not currently know how low we can lower ABP and still perfuse the brain. The most logical way to answer this question is to measure LLA with autoregulation monitoring.

Dynamic autoregulation monitoring has been developed with adequate validity to reliably delineate optimal perfusion pressure for patients with traumatic brain injury. These concepts have been applied to develop non-invasive methods using reflectance NIRS, and the NIRS-based measures have been validated against gold standard measures of LLA in animal models. What remains is clinical translation specific to the neonatal population, demonstrating feasibility, safety, and efficacy. We have outlined challenges peculiar to neonates with heart disease for each of these clinical research steps.

If feasibility cannot be demonstrated with current methods to measure autoregulation, one can ask if this is inability to modulate blood pressure in the setting of cardiac surgery, or if the autoregulation data is coming to slow to delineate LLA in a practical way. In the latter case, the challenge to making autoregulation monitoring faster has been the fundamental frequency of the autoregulation mechanism which acts as a high pass filter for ABP waves having a period of 30 seconds or longer (36). One promising effort to speed up autoregulation monitoring is the co-trending method put forward by Medtronic, Inc. (37). Another approach is to increase the precision of each measure of autoregulation (thereby decreasing the time to reliable LLA determination). This can be done with inducing low frequency blood pressure waves which can be done with a variety of minimal physiologic perturbations (38).

Safety was not only demonstrated in the adult data, but major morbidity including AKI (acute kidney injury) was lower in patients when ABP was above LLA. It is not clear that the same pattern will hold true in neonates. If SVR crisis, renal or bowel injury, respiratory failure, heart failure, arrhythmia or death are higher in study groups where ABP is kept above LLA, then the specific interventions used to manage ABP will have to be examined. Any method to raise ABP in this population has the potential to cause some combination of these complications. Autoregulation monitoring will only prove beneficial and safe if the intervention can maintain ABP above LLA without causing complication related to low cardiac output.

Once feasibility and safety are demonstrated, sample size required to document efficacy can be calculated. It is anticipated that such a trial will be multi-center, and that the outcomes will be a combination of MRI, seizure activity, and developmental follow-up. The stamina required to complete such a study is non-trivial and would likely span two decades of work. Although this study is the optimal pathway to apply evidence-based medicine to clinical practice, there is very little precedent for successful randomized trials of monitoring technologies. Most standard monitoring was adopted despite a failure of trials to demonstrate outcome benefit (39). Perhaps, given the success of the adult trial of autoregulation monitoring, this pattern will be broken, and proper evidence will be obtained for the rollout of a technology with potential to benefit such a vulnerable population.

AUTHOR CONTRIBUTIONS

All authors contributed to the article and approved the submitted version.

FUNDING

This research was supported by grant from Additional Ventures: Single Ventricle Research Fund 2020.

REFERENCES

1. Andropoulos DB, Hunter JV, Nelson DP, Stayer SA, Stark AR, McKenzie ED, et al. Brain immaturity is associated with brain injury before and after neonatal cardiac surgery with high-flow bypass and cerebral oxygenation monitoring. *J Thorac Cardiovasc Surg.* (2010) 139:543–56. doi: 10.1016/j.jtcvs.2009.08.022
2. Chen J, Zimmerman RA, Jarvik GP, Nord AS, Clancy RR, Wernovsky G, et al. Perioperative stroke in infants undergoing open heart operations for congenital heart disease. *Ann Thorac Surg.* (2009) 88:823–9. doi: 10.1016/j.athoracsur.2009.03.030
3. Galli KK, Zimmerman RA, Jarvik GP, Wernovsky G, Kuypers MK, Clancy RR, et al. Periventricular leukomalacia is common after neonatal cardiac surgery. *J Thorac Cardiovasc Surg.* (2004) 127:692–704. doi: 10.1016/j.jtcvs.2003.09.053
4. McQuillen PS, Barkovich AJ, Hamrick SEG, Perez M, Ward P, Glidden DV, et al. Temporal and anatomic risk profile of brain injury with neonatal repair of congenital heart defects. *Stroke.* (2007) 38:736–41. doi: 10.1161/01.STR.0000247941.41234.90
5. Beca J, Gunn JK, Coleman L, Hope A, Reed PW, Hunt RW, et al. New white matter brain injury after infant heart surgery is associated with diagnostic group and the use of circulatory arrest. *Circulation.* (2013) 127:971–9. doi: 10.1161/CIRCULATIONAHA.112.001089
6. Gaynor JW, Stopp C, Wypij D, Andropoulos DB, Atallah J, Atz AM, et al. Neurodevelopmental outcomes after cardiac surgery in infancy. *Pediatrics.* (2015) 135:816–25. doi: 10.1542/peds.2014-3825
7. Rhee CJ, da Costa CS, Austin T, Brady KM, Czosnyka M, Lee JK. Neonatal cerebrovascular autoregulation. *Pediatr Res.* (2018) 84:602–10. doi: 10.1038/s41390-018-0141-6
8. Licht DJ, Shera DM, Clancy RR, Wernovsky G, Montenegro LM, Nicolson SC, et al. Brain maturation is delayed in infants with complex congenital heart defects. *J Thorac Cardiovasc Surg.* (2009) 137:529–36. doi: 10.1016/j.jtcvs.2008.10.025
9. Dimitropoulos A, McQuillen PS, Sethi V, Moosa A, Chau V, Xu D, et al. Brain injury and development in newborns with critical congenital heart disease. *Neurology.* (2013) 81:241–8. doi: 10.1212/WNL.0b013e31829bfdcf
10. Miller SP, McQuillen PS, Hamrick S, Xu D, Glidden DV, Charlton N, et al. Abnormal brain development in newborns with congenital heart disease. *N Engl J Med.* (2007) 357:1928–38. doi: 10.1056/NEJMoa067393
11. Ortinau C, Beca J, Lambeth J, Ferdman B, Alexopoulos D, Shimony JS, et al. Regional alterations in cerebral growth exist preoperatively in infants with congenital heart disease. *J Thorac Cardiovasc Surg.* (2012) 143:1264–70. doi: 10.1016/j.jtcvs.2011.10.039
12. Licht DJ, Wang J, Silvestre DW, Nicolson SC, Montenegro LM, Wernovsky G, et al. Preoperative cerebral blood flow is diminished in neonates with severe congenital heart defects. *J Thorac Cardiovasc Surg.* (2004) 128:841–9. doi: 10.1016/S0022-5223(04)01066-9
13. Brady KM, Mytar JO, Lee JK, Cameron DE, Vricella LA, Thompson WR, et al. Monitoring cerebral blood flow pressure autoregulation in pediatric patients during cardiac surgery. *Stroke.* (2010) 41:1957–62. doi: 10.1161/STROKEAHA.109.575167
14. Al-Aweel I, Pursley DM, Rubin LP, Shah B, Weisberger S, Richardson DK. Variations in prevalence of hypotension, hypertension, and vasopressor use in NICUs. *J Perinatol.* (2001) 21:272–8. doi: 10.1038/sj.jp.7210563
15. Furck AK, Hansen JH, Uebing A, Scheewe J, Jung O, Kramer H-H. The impact of afterload reduction on the early postoperative course after the Norwood operation - a 12-year single-centre experience. *Eur J Cardiothorac Surg.* (2010) 37:289–95. doi: 10.1016/j.ejcts.2009.07.051
16. De Oliveira NC, Ashburn DA, Khalid F, Burkhart HM, Adatia IT, Holtby HM, et al. Prevention of early sudden circulatory collapse after the Norwood operation. *Circulation.* (2004) 110:II133–138. doi: 10.1161/01.CIR.0000138399.30587.8e
17. Brown CH, Neufeld KJ, Tian J, Probert J, LaFlam A, Max L, et al. Effect of targeting mean arterial pressure during cardiopulmonary bypass by monitoring cerebral autoregulation on postsurgical delirium among older patients: a nested randomized clinical trial. *JAMA Surg.* (2019) 154:819–26. doi: 10.1001/jamasurg.2019.1163
18. Hogue CW, Brown CH, Hori D, Ono M, Nomura Y, Balmert LC, et al. Personalized blood pressure management during cardiac surgery with cerebral autoregulation monitoring: a randomized trial. *Semin Thorac Cardiovasc Surg.* (2020) 33:429–38. doi: 10.1053/j.semtcvs.2020.09.032
19. Govindan RB, Brady KM, Massaro AN, Perin J, Jennings JM, DuPlessis AJ, et al. Comparison of frequency- and time-domain autoregulation and vasoreactivity indices in a piglet model of hypoxia-ischemia and hypothermia. *Dev Neurosci.* (2019) 40:547–59. doi: 10.1159/000499425
20. Czosnyka M, Smielewski P, Kirkpatrick P, Laing RJ, Menon D, Pickard JD. Continuous assessment of the cerebral vasomotor reactivity in head injury. *Neurosurgery.* (1997) 41:11–7. doi: 10.1097/00006123-199707000-00005
21. Czosnyka M, Smielewski P, Kirkpatrick P, Menon DK, Pickard JD. Monitoring of cerebral autoregulation in head-injured patients. *Stroke.* (1996) 27:1829–34. doi: 10.1161/01.STR.27.10.1829
22. Lee JK, Kibler KK, Benni PB, Easley RB, Czosnyka M, Smielewski P, et al. Cerebrovascular reactivity measured by near-infrared spectroscopy. *Stroke.* (2009) 40:1820–6. doi: 10.1161/STROKEAHA.108.536094
23. Brady KM, Lee JK, Kibler KK, Smielewski P, Czosnyka M, Easley RB, et al. Continuous time-domain analysis of cerebrovascular autoregulation using near-infrared spectroscopy. *Stroke.* (2007) 38:2818–25. doi: 10.1161/STROKEAHA.107.485706
24. Lundberg N. Continuous recording and control of ventricular fluid pressure in neurosurgical practice. *Acta Psychiatr Scand Suppl.* (1960) 36:1–193.
25. Brady K, Andropoulos DB, Kibler K, Easley RB. A new monitor of pressure autoregulation: what does it add? *Anesth Analg.* (2015) 121:1121–3. doi: 10.1213/ANE.0000000000000952
26. Brady KM, Mery CM. Cerebral autoregulation: making sense of the nonsensical. *J Thorac Cardiovasc Surg.* (2017) 154:1045–6. doi: 10.1016/j.jtcvs.2017.05.074
27. Schwartz AE, Sandhu AA, Kaplon RJ, Young WL, Jonassen AE, Adams DC, et al. Cerebral blood flow is determined by arterial pressure and not cardiopulmonary bypass flow rate. *Ann Thorac Surg.* (1995) 60:165–9. doi: 10.1016/S0003-4975(95)00357-6
28. Rhee CJ, Kibler KK, Easley RB, Andropoulos DB, Czosnyka M, Smielewski P, et al. Renovascular reactivity measured by near-infrared spectroscopy. *J Appl Physiol.* (2012) 113:307–14. doi: 10.1152/japplphysiol.00024.2012
29. Mahle WT, Spray TL, Wernovsky G, Gaynor JW, Clark BJ. Survival after reconstructive surgery for hypoplastic left heart syndrome: a 15-year experience from a single institution. *Circulation.* (2000) 102:III136–141. doi: 10.1161/01.CIR.102.suppl_3.III-136
30. Hoffman GM, Tweddell JS, Ghanayem NS, Mussatto KA, Stuth EA, Jaquis RDB, et al. Alteration of the critical arteriovenous oxygen saturation relationship by sustained afterload reduction after the Norwood procedure. *J Thorac Cardiovasc Surg.* (2004) 127:738–45. doi: 10.1016/S0022-5223(03)01315-1
31. Tweddell JS, Hoffman GM, Fedderly RT, Berger S, Thomas JP, Ghanayem NS, et al. Phenoxybenzamine improves systemic oxygen delivery after the Norwood procedure. *Ann Thorac Surg.* (1999) 67:161–7. doi: 10.1016/S0003-4975(98)01266-1
32. Hoffman TM, Wernovsky G, Atz AM, Kulik TJ, Nelson DP, Chang AC, et al. Efficacy and safety of milrinone in preventing low cardiac output syndrome in infants and children after corrective surgery for congenital heart disease. *Circulation.* (2003) 107:996–1002. doi: 10.1161/01.CIR.0000051365.81920.28
33. Naim MY, Gaynor JW, Chen J, Nicolson SC, Fuller S, Spray TL, et al. Subclinical seizures identified by postoperative electroencephalographic

monitoring are common after neonatal cardiac surgery. *J Thorac Cardiovasc Surg.* (2015) 150:169–78. doi: 10.1016/j.jtcvs.2015.03.045
34. Nathan M. Seizure prediction after neonatal cardiac surgery: the search continues. *Ann Thorac Surg.* (2021) 111:2048–9. doi: 10.1016/j.athoracsur.2020.06.092
35. Bellinger DC, Wypij D, Rivkin MJ, DeMaso DR, Robertson RL, Dunbar-Masterson C, et al. Adolescents with d-transposition of the great arteries corrected with the arterial switch procedure: neuropsychological assessment and structural brain imaging. *Circulation.* (2011) 124:1361–9. doi: 10.1161/CIRCULATIONAHA.111.026963
36. Fraser CD, Brady KM, Rhee CJ, Easley RB, Kibler K, Smielewski P, et al. The frequency response of cerebral autoregulation. *J Appl Physiol.* (2013) 115:52–6. doi: 10.1152/japplphysiol.00068.2013
37. Montgomery D, Brown C, Hogue CW, Brady K, Nakano M, Nomura Y, et al. Real-time intraoperative determination and reporting of cerebral autoregulation state using near-infrared spectroscopy. *Anesth Analg.* (2020) 131:1520–8. doi: 10.1213/ANE.0000000000004614
38. Brady KM, Easley RB, Kibler K, Kaczka DW, Andropoulos D, Fraser CD, et al. Positive end-expiratory pressure oscillation facilitates brain vascular reactivity monitoring. *J Appl Physiol.* (2012) 113:1362–8. doi: 10.1152/japplphysiol.00853.2012
39. Pedersen T, Nicholson A, Hovhannisyan K, Møller AM, Smith AF, Lewis SR. Pulse oximetry for perioperative monitoring. *Cochrane Database Syst Rev.* (2014). doi: 10.1002/14651858.CD002013.pub3

Conflict of Interest: The authors declare that the research was conducted in the absence of any commercial or financial relationships that could be construed as a potential conflict of interest.

Publisher's Note: All claims expressed in this article are solely those of the authors and do not necessarily represent those of their affiliated organizations, or those of the publisher, the editors and the reviewers. Any product that may be evaluated in this article, or claim that may be made by its manufacturer, is not guaranteed or endorsed by the publisher.

frontiers in Neurology

ORIGINAL RESEARCH
published: 11 November 2021
doi: 10.3389/fneur.2021.745770

Neurovascular Reactivity in the Aging Mouse Brain Assessed by Laser Speckle Contrast Imaging and 2-Photon Microscopy: Quantification by an Investigator-Independent Analysis Tool

Fatma Burcu Seker[1]*, *Ziyu Fan*[1], *Benno Gesierich*[1], *Malo Gaubert*[1], *Rebecca Isabella Sienel*[1] and *Nikolaus Plesnila*[1,2]*

[1] Institute for Stroke and Dementia Research, Munich University Hospital and University of Munich, Munich, Germany, [2] Munich Cluster for Systems Neurology (SyNergy), Munich, Germany

OPEN ACCESS

Edited by:
Dong Ming,
Tianjin University, China

Reviewed by:
Hirac Gurden,
Université de Paris, France
Hongyang Lu,
Medtronic Inc, Ireland

***Correspondence:**
Fatma Burcu Seker
burcu.seker@med.uni-muenchen.de
Nikolaus Plesnila
nikolaus.plesnila@med.uni-muenchen.de

Specialty section:
This article was submitted to Applied Neuroimaging, a section of the journal Frontiers in Neurology

Received: 22 July 2021
Accepted: 08 October 2021
Published: 11 November 2021

Citation:
Seker FB, Fan Z, Gesierich B, Gaubert M, Sienel RI and Plesnila N (2021) Neurovascular Reactivity in the Aging Mouse Brain Assessed by Laser Speckle Contrast Imaging and 2-Photon Microscopy: Quantification by an Investigator-Independent Analysis Tool. Front. Neurol. 12:745770. doi: 10.3389/fneur.2021.745770

The brain has a high energy demand but little to no energy stores. Therefore, proper brain function relies on the delivery of glucose and oxygen by the cerebral vasculature. The regulation of cerebral blood flow (CBF) occurs at the level of the cerebral capillaries and is driven by a fast and efficient crosstalk between neurons and vessels, a process termed neurovascular coupling (NVC). Experimentally NVC is mainly triggered by sensory stimulation and assessed by measuring either CBF by laser Doppler fluxmetry, laser speckle contrast imaging (LSCI), intrinsic optical imaging, BOLD fMRI, near infrared spectroscopy (NIRS) or functional ultrasound imaging (fUS). Since these techniques have relatively low spatial resolution, diameters of cerebral vessels are mainly assessed by 2-photon microscopy (2-PM). Results of studies on NVC rely on stable animal physiology, high-quality data acquisition, and unbiased data analysis, criteria, which are not easy to achieve. In the current study, we assessed NVC using two different imaging modalities, i.e., LSCI and 2-PM, and analyzed our data using an investigator-independent Matlab-based analysis tool, after manually defining the area of analysis in LSCI and vessels to measure in 2-PM. By investigating NVC in 6–8 weeks, 1-, and 2-year-old mice, we found that NVC was maximal in 1-year old mice and was significantly reduced in aged mice. These findings suggest that NVC is differently affected during the aging process. Most interestingly, specifically pial arterioles, seem to be distinctly affected by the aging. The main finding of our study is that the automated analysis tool works very efficiently in terms of time and accuracy. In fact, the tool reduces the analysis time of one animal from approximately 23 h to about 2 s while basically making no mistakes. In summary, we developed an experimental workflow, which allows us to reliably measure NVC with high spatial and temporal resolution in young and aged mice and to analyze these data in an investigator-independent manner.

Keywords: neurovascular coupling, hypercapnia, laser speckle contrast imaging, two-photon microscopy, aging, investigator-independent analysis

INTRODUCTION

Since the brain stores very little energy, proper neuronal function depends on a constant supply of glucose and oxygen via cerebral blood flow. During increased neuronal activity, the need for nutrients increases and the necessary excess energy is delivered via a tightly regulated redistribution of blood flow to these active areas by dilation of cerebral blood vessels. This regulation of cerebral blood flow (CBF) by the crosstalk between neurons and cerebral vessels is called "neurovascular coupling" or NVC (1, 2). NVC responses can be utilized as an indicator of neuronal activity. Under pathological conditions, NVC may be used to detect dysfunctions of the cerebrovascular system (3–5).

To investigate NVC *in vivo*, three different steps are needed: (1) a stimulation paradigm, (2) a fast technique to measure CBF or to visualize cerebral vessel reactivity, and (3) an unbiased and reliable method for data analysis. The first step depends on which region of the brain is studied. Typically, odor and visual cues, electrical or tactile sensory stimulations of the whiskers or the paws are used (6–9). The second prerequisite can be achieved using non-invasive optical methods based on the speckle pattern of moving red blood cells (Laser Speckle Contrast Imaging, LSCI). LSCI is a very powerful imaging tool for the 2-D visualization of perfusion dynamics in tissues (10–12). Another imaging method for visualizing the dynamics of the cerebral vasculature is two-photon microscopy (2-PM) (13–15). 2-PM is a state-of-the-art confocal scanning microscopy technique with a high spatial and temporal resolution able to visualize pial vessels, penetrating arterioles, and deep cortical microvessels *in vivo*. The final, but equally critical step is data analysis. The software provided with commercially available LSCI units has mainly been developed for data acquisition in single human subjects and has therefore only limited analysis capabilities. This is particularly true when it comes to the analysis of data sets acquired at different time points and in whole groups of subjects. Therefore, commercially available LSCI analysis solutions are not entirely suitable for research purposes. Also analyzing images obtained by 2-PM is a time-consuming manual process prone to investigator bias. Therefore, the main aim of the current study is to present a novel tool for the analysis of LSCI and 2-PM data to establish a flexible, software-based analysis pipeline for an automated and investigator-independent analysis of the obtained data sets.

To test our new experimental workflow, we used a model of physiological aging, a paradigm well-known to be associated with an age-related decrease in NVC. The world population is aging and over 30% of the people in western countries will be older than 65 years of age by 2050 (16). Aging causes significant structural changes in brain volume, in the dendritic arbor, spine and synapse numbers, and vasculature (17, 18). Among this population, cognitive impairments related to vascular changes are responsible for at least 20% of all dementia cases (19). Surely, NVC as a key homeostatic regulator is inevitably affected by these vascular changes (20). Sensory-evoked NVC responses are indirect measures of neuronal activation and any alteration in NVC can predict underlying pathology (21, 22). A substantial number of publications from various laboratories suggests impaired NVC in aged humans and experimental animals (23–27). It has been shown that age strongly alters CBF regulation in humans, specifically steady-state CBF decreases progressively during the aging process concomitant with an increase in CBF pulsatility after midlife (28). Also, structurally, cerebrovascular pathologies involving small arteries and arterioles are very common in the aged brain (29–31). Therefore a deep understanding of how NVC changes during aging is an important prerequisite in order to decipher the mechanisms underlying cerebrovascular disease, dementia, and neurodegeneration (32–34). Aging affects the normal structure and function of the neurovascular unit (NVU). Aged mice show decreased astrocyte end-feet density, reduced pericyte coverage in the hippocampus, more activated microglia, and reduced CBF as compared to young mice (35). Moreover, aging and concomitant metabolic disorders such as obesity impair NVC in animals and humans thereby making the aging brain more vulnerable to age-related neurodegenerative disorders such as Alzheimer's and Parkinson's Disease (4, 36, 37). Therefore, deciphering how NVC is affected by aging may lead to new therapeutic strategies for these disorders.

MATERIALS AND METHODS

Experimental Animals

All experimental procedures were conducted according to institutional guidelines of the University of Munich and were approved by the Government of Upper Bavaria (animal protocol number: Vet_2-15-196). In all parts of the experiments, 6–8 weeks old C57BL/6N mice were purchased from Charles River Laboratories (Sulzfeld, Germany). Mice at the age of 6–8 weeks were categorized as young and mice at the age of 1 year and 2 years were categorized as aged. The mice were aged in the animal facility of the Institute of Stroke and Dementia Research. All mice were housed in groups of five in isolated ventilated HEPA filtered cages with a 12-h light/dark cycle with *ad libitum* access to food and water. All cages had standard enrichment.

Chronic Cranial Window Implantation

A chronic cranial window was implanted over the left somatosensory cortex between the coronal and the sagittal suture. The rostromedial corner of the window was placed as close as possible to Bregma. Mice received buprenorphine (0.1 mg/kg) 30 min before surgery for analgesia and anesthesia was induced with 5% isoflurane and maintained with 2% isoflurane in 70% room air and 30% O_2 during surgery. A feedback-controlled heating pad was used to maintain body temperature at 37°C. Animals were fixed in a stereotactic frame using a nose clamp and the scalp was incised along the midline. Lidocaine (2%) was applied topically onto the skull as a local anesthetic and a round craniotomy with a diameter of 4 mm was performed above the somatosensory cortex and covered with a glass window. A plastic ring (diameter: 1 cm; weight: 0.1 g) was glued on top of the cranial window to form a water reservoir. After surgery, mice were placed in a pre-heated wake-up box (32°C) until all vital functions recovered. All mice received buprenorphine

and enrofloxacin (10 mg/kg s.c.) once daily for three days after surgery .

Whisker Stimulation

Three weeks after window implantation, mice received medetomidine (0.05 mg/kg, sc) for light sedation. After 10 min animals were anesthetized with 2% isoflurane and placed in a stereotactic frame. Afterwards, isoflurane was gradually reduced to 0.5–0.75% (in 70/30% Air/O_2) and whisker stimulation was performed over one minute by manually or mechanically stroking the contralateral (right) vibrissae with a brush at a frequency of 1–2 Hz. For 2-PM we developed a custom made motorized brush holder and use the same stimulation protocol as for the manual stimulation. The procedure was repeated three times with two min intervals (**Figure 1A**).

CO_2 Challenge

To evoke hypercapnic hyperemia, mice were ventilated with 10% CO_2 and 30% O_2 in room air for five min (**Figure 2A**). End-tidal CO_2 was measured in % with a capnograph (**Figure 2A**, right) and recorded using a digital data acquisition system (PowerLab, AD Instruments, Australia).

Measurement and Analysis of Local Cerebral Blood Flow by Laser Speckle Imaging

A laser speckle contrast imager (LSCI, Perimed, Järfälla, Sweden) was positioned 10.4 cm above the chronic cranial window and a 0.5 x 0.5 mm field of the cortex was imaged at 4.4 Hz. The data was recorded using the software supplied with the device (Pimsoft, Perimed, Järfälla, Sweden) and analyzed using a custom Matlab script (MATLAB, R2016b, The MathWorks, Natick, MA). First, a spherical region around the rim of the cranial window containing the exposed cortex (ROI), was drawn manually. For each pixel within the ROI, the perfusion signal was filtered with a cut-off frequency of 0.004 Hz to remove any signal drift and allows re-alignment of the acquired frames. This process is important while the brain and cerebral vessels move slightly due to heart beat and breathing. Hence, when using high resolution imaging, e.g., LSCI or 2-PM, images acquired at different time points shift slightly. Therefore, re-alignment is necessary to correctly allocate measurements obtained over time to exactly the same pixel. This filter was implemented using the MATLAB functions cheby1 and filtfilt to design a Chebyshev Type I filter of order 2 and to perform zero-phase digital filtering. Then a threshold was defined using Otsu's method, to detect stimulation periods automatically. The correct detection of stimulation periods was verified visually. To account for a potentially ramp-like increase of the perfusion signal at the beginning of the stimulation, the perfusion signal was averaged within 10 and 30 s after the automatically detected stimulation onset and normalized to the baseline perfusion signal, defined individually for each stimulation period as the average signal within 40 to 10 s before the automatically detected stimulation onset. The hereby resulting, normalized response of the perfusion signal to the stimulation was then averaged across stimulation periods. First individually for each animal and then across animals within each experimental group. To allow averaging across animals, the images, cropped around the spherical ROI, were resized to an image matrix of 120 x 120 pixels. For a better understanding of the individual responses, heat maps were also acquired for individual animals (**Figure 1B**).

Measurement and Analysis of Vessel Diameter by *in vivo* Two-Photon Microscopy

Two-photon microscopy (2-PM) was performed the day after the LSCI imaging using the same anesthesia protocol as described above. For visualizing the cerebral vasculature 0.1 ml of fluorescein isothiocyanate (2,000 kDa) was injected through the tail vein using a mouse tail illuminator (Braintree Scientific, USA). Then mice were transferred under the 2-PM. Pial and parenchymal vessels in the region of the barrel cortex were visualized as time series videos (2 s per frame) at a depth of 50–100 µm with a 10x Zeiss EC Plan—NeoFluar objective using a Li: Ti laser tuned to 800 nm. The whisker stimulation protocol was followed by 5 min 10% CO_2 challenge. A custom-made automated brush holder was used for whisker stimulation while imaging with 2-PM (**Figure 3A**). For this device, a small brush and a voltage controller for frequency adjustments were mounted to a 300 rpm (6 V) battery-powered motor (Walfront, China). A gooseneck holder was used to fix the motor on the imaging platform, which allowed fine-tuning the angle of the brush.

Vessel diameter analysis was performed using a custom-made Matlab routine (MathWorks version R2020a, Natick, Massachusetts, USA; www.mathworks.com) based on imshow3D developed by Maysam Shahedi (https://www.mathworks.com/matlabcentral/fileexchange/41334-imshow3d) and on a Zeiss LSM file reader developed by Cy Y (Zeiss Laser Scanning Confocal Microscope LSM file reader; https://github.com/joe-of-all-trades/lsmread). First, all images have been inspected and the ones containing artifacts (heavy motion between frames, low signal-to-noise ratio) were removed. Then, time series videos were binarized, and diameter and percent change graphs were displayed. Then, line segments were drawn by the user between the vessel walls. Every time a line was drawn, the diameter of the vessel in µm along time frames were calculated by counting the number of voxels with a value of 1 ("1" corresponds to a vessel, while "0" to the background) intersecting with the drawn line and multiplied by the voxel size. Of note, some erythrocytes passing through the vessel are reducing the intensities of specific voxels, which could lead to underestimation of vessel diameter. To minimize this effect, the thickness of the line was defined to 4 voxels and the computation of vessel diameter was thus adapted by averaging the lines around the drawn line. Based on the computation of vessel diameters along time, output graphs are displayed and updated for each new line and depicted with the same color as the line drawn on the image (**Figure 3A**, lower left). Moreover, automatic detection of percentage peak change was provided thanks to the Matlab routine. This peak detection was based on three parameters defined in the graphical interface. Briefly, the algorithm first computed the baseline diameter by averaging a predefined number of initial frames (no stimulation).

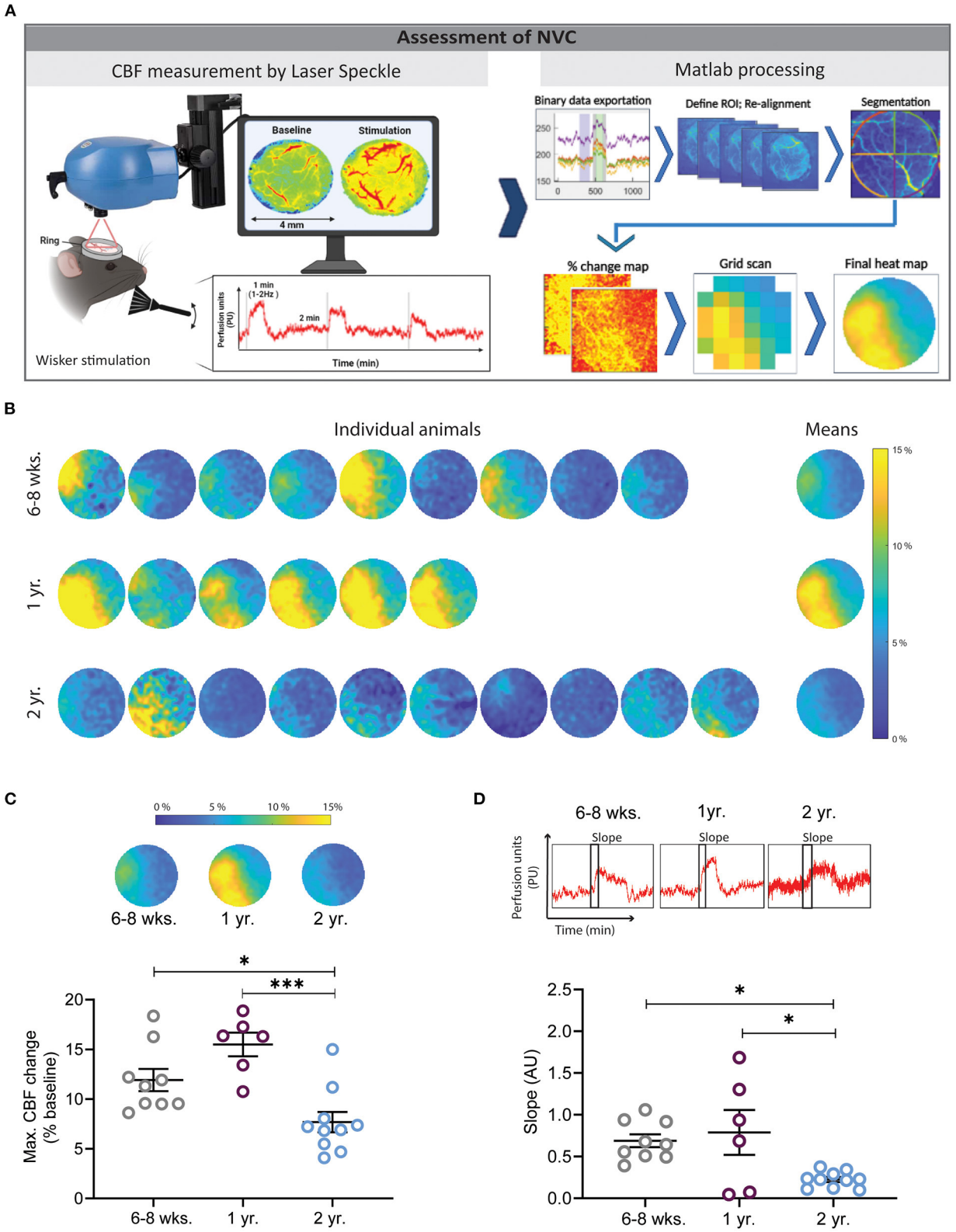

FIGURE 1 | Assessment of neurovascular coupling (NVC) using laser speckle contrast imaging (LSCI) and a Matlab-based analysis pipeline. **(A)** Experimental setup for whisker stimulation and data analysis. Data visualization with LSCI shows a flow map and a perfusion trace (left), data processing steps show binary data exportation,

(Continued)

FIGURE 1 | ROI alignment, segmentation, % change map, grid preparation for quantification, and final averaged heat map (right). **(B)** Heat maps of cerebral perfusion (CBF) in individual mice of different ages following whisker stimulation. Each perfusion map was created by averaging LSCI values from three whisker stimulations. Mean depicts the average of all animals in one group. The dark blue color indicates no or small changes in cortical perfusion, while the yellow color indicates increases of cortical perfusion of up to 15%. **(C)** Quantification of maximal CBF changes. Young and 1-year-old mice had significantly higher NVC responses in comparison to 2 years old mice (*$P < 0.05$: 6–8 weeks vs. 2 years old, ***$P < 0.001$: 1 year vs. 2 year, One-way ANOVA). **(D)** Quantification of the velocity of CBF increase after whisker stimulation by slope analysis. Two year old mice had a significantly slower CBF increase in comparison to young and 1 year old mice (*$P < 0.05$: 6–8 weeks vs. 2 year and 1 year vs. 2 year) (n = 6–10 mice/group, mean ± SEM, One-way ANOVA).

For the peak detection, the difference between the subsequent frames (with stimulation), and the baseline was calculated. After the end of a peak, a new baseline was computed, and the peak detection continued in the subsequent frames. The detected peaks were then displayed in the first graph, in the same color as the line drawn on the image (see screenshots, **Figure 3A**, lower right). The slope of dilation between the maximal vessel diameter of a detected peak and related baseline was also calculated automatically using the following formula:

$$\text{Slope} = \frac{diameter_{max} - diameter_{baseline}}{time_{max} - time_{baseline}}$$

with $diameter_{\max}$, $time_{\max}$, the diameter of the maximal value in the peak and the peak time, and $diameter_{baseline}$, $time_{baseline}$, baseline diameter and the time on when this baseline was calculated (last timepoint before the detection of the peak). This slope was then normalized by the baseline vessel diameter. Finally, the percent of change was calculated by the Matlab routine as the difference between the maximal vessel diameter of a detected peak and related baseline as:

$$\text{Percent change} = \frac{diameter_{max} - diameter_{baseline}}{diameter_{baseline}} \times 100$$

and displayed. For each drawn segment, all vessel diameters along time and information on peaks (start, end, slope, percentage of change) have also been exported in a table for subsequent statistical analyses.

Data Availability

Scripts will be shared upon request.

Statistics

Statistical analyses were performed with GraphPad Prism 7.0 software (GraphPad Software, San Diego, California USA). First, data were tested for normal distribution. Student t-test was used to compare two sets of normally distributed data. Multiple groups were compared with one-way ANOVA or one-way ANOVA on ranks depending on the presence or absence of normal distribution or two-way ANOVA for repetitive measurements. Differences with $P < 0.05$ were considered statistically significant.

RESULTS

In this study, we developed a fast, reliable, and unbiased data processing tool for the analysis of neurovascular reactivity (NVC and CO_2 inhalation) assessed by LSCI and 2-PM. While LSCI provides information about CBF changes in the superficial layers of the cerebral cortex, *in vivo* 2-PM imaging directly visualizes diameter changes of individual cerebral vessels. For the validation of our newly developed analysis tools, we used aging as a model.

Decreased Neurovascular Coupling in Aged Mice

Mice were given three subsequent whisker stimulations (**Figure 1A**). All LSCI data were first acquired with Pimsoft software®. After the acquisition, data were extracted in binary format (.dat) and processed with a custom-made Matlab tool. The results were exported to a spreadsheet file and further analyzed and plotted. Furthermore, the Matlab tool generated an averaged image of all three stimulations, created CBF heat maps of individual mice, and allowed to average CBF values of all investigated mice in one single heat map (**Figure 1B**). The heat maps show an increased CBF in the area of the somatosensory cortex whereas CBF remained unchanged in the unstimulated surrounding cortex. CBF values from the heat maps could be extracted as numerical data and plotted. Two year-old mice had a 46 and 59% lower CBF response as compared to young and 1-year-old mice, respectively (**Figure 1C**, *$P < 0.05$: young vs. 2 year old, ***$P < 0.001$: 1 year vs. 2 year). No significant difference was found between young and 1-year-old mice. Moreover, 1-year-old mice had a moderately higher NVC response in comparison to young mice (**Figure 1C**). The slope of the CBF peak after the NVC stimulation was analyzed and a reduced slope was found in 2-years-old mice in comparison to young and 1-year-old mice, respectively (**Figure 1D**, *$P <$ 0.05: young vs. 2 year and 1 year vs. 2 years), indicating a slower response in this age group. No difference was found between young and 1-year-old mice (**Figure 2D**).

Decreased and Sluggish CO_2 Reactivity in Aged Mice

Following whisker stimulation, animals received 10% CO_2 by inhalation to induce hypercapnia and subsequent cerebral hyperemia. End tidal pCO_2 was assessed by microcapnometry and CBF was measured by LSCI (**Figure 2A**). A typical CBF response consists of an increase in CBF within one min after CO_2 inhalation followed by a plateau phase and a gradual recovery phase after termination of CO_2 inhalation (**Figure 2B**). Two-year-old mice showed a slower and lower CO_2 response curve in comparison to young and 1-year-old mice [$F_{(280,\ 2380)} = 2.329$, ***$P < 0.0001$, 2-way ANOVA]. The peak response in 2-year-old mice was reduced by 31 and 25% in comparison to young and 1-year-old mice, respectively (**Figure 2C**, *$P < 0.05$: young vs. 2 year). Not only the degree, but also the velocity of the

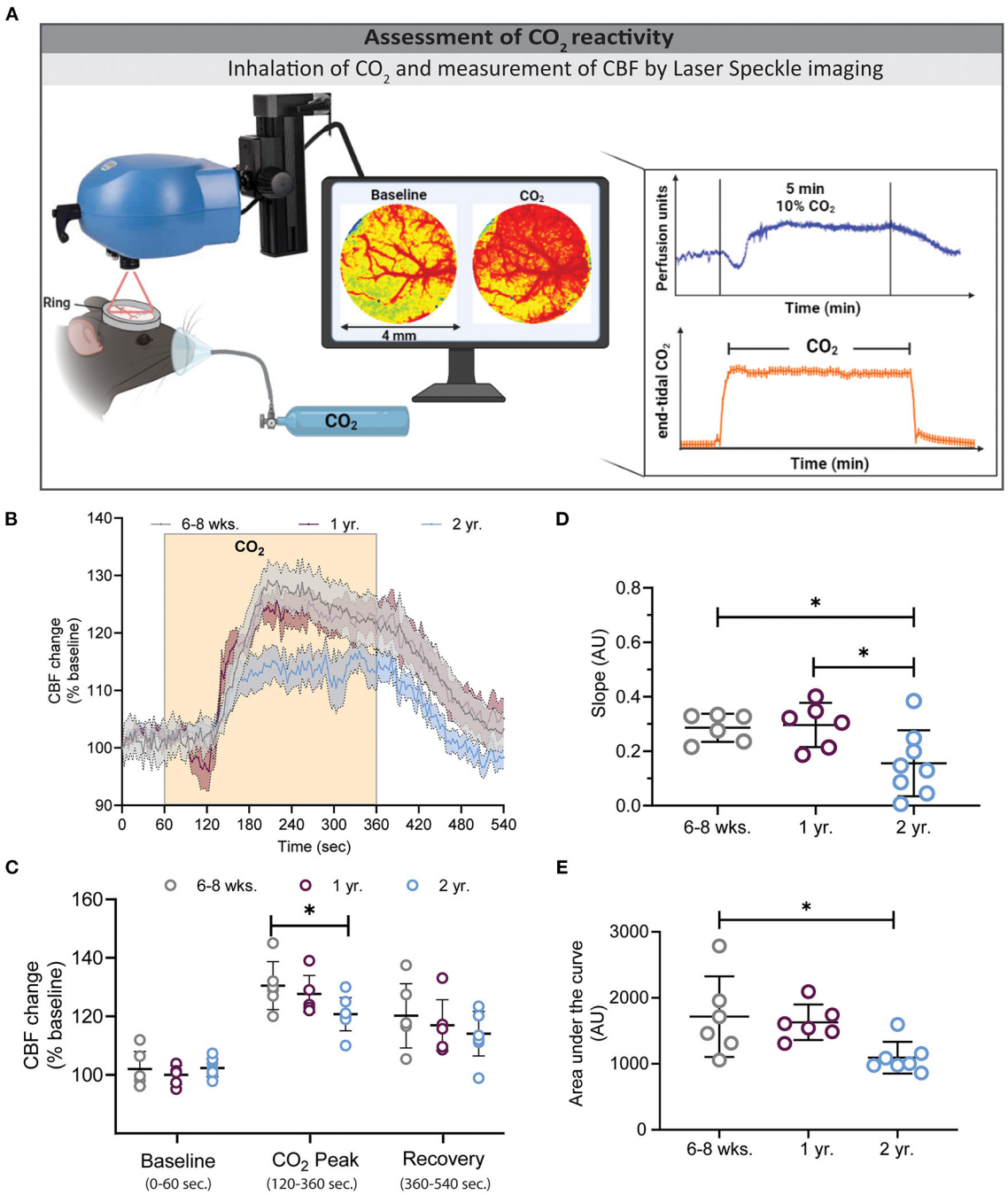

FIGURE 2 | Assessment of CO_2 reactivity using laser speckle contrast imaging (LSCI). **(A)** Experimental setup of the CO_2 challenge (left) and exemplary traces for LSCI perfusion (top right) and end-tidal CO_2 (bottom right). **(B)** CBF changes before, during, and after hypercapnia in the three investigated age groups. Two-year-old mice showed a low **(C)** and slow **(D)** CBF increase during hypercapnia, whereas young and 1-year-old mice had higher peak values (*$P < 0.05$: 6–8 weeks vs. 2 year), and faster slope changes (*$P < 0.05$: 6–8 weeks vs. 2 year and 1 year vs. 2 year). **(E)** Quantification of the area under the curve (AUC) of graph B depicts smaller AUC in 2 year old mice in comparison to 6–8 weeks and 1 year old mice (*$P < 0.05$) (mean ± SEM, $n = 6$–8 mice/group, One-way ANOVA).

CBF response was reduced in 2-year-old mice as indicated by a reduced slope of the CBF increase (**Figure 2D**, *$P < 0.05$: young vs. 2 year and 1 year vs. 2 year). As an integrative measure of the whole CBF response after hypercapnia we calculated the area under the curve (AUC). As expected from the previous measurements, also this value was significantly reduced in 2-year-old mice (**Figure 2E**, *$P < 0.05$: young vs. 2 year and 1 year vs. 2 year).

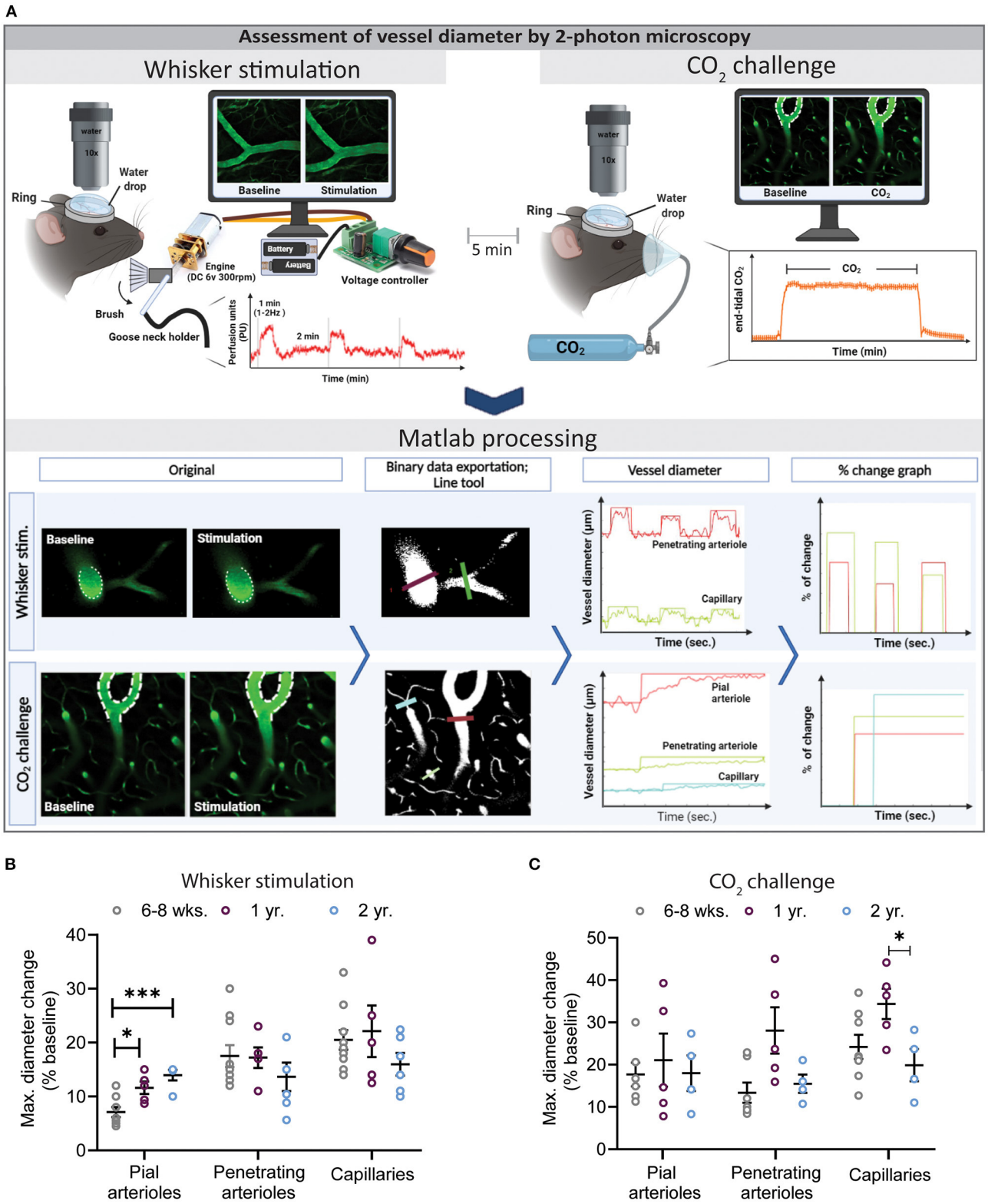

FIGURE 3 | Assessment of vessel diameter by 2-photon microscopy. **(A)** Experimental setup for whisker stimulation (top left) and hypercapnia during (top right) and a schematic drawing of the data analysis work flow by the newly developed Matlab script. **(B)** Quantification of maximal diameter changes in different vessel segments at different ages following whisker stimulation. Pial vessel reactivity increased with age (*$P < 0.05$: 6–8 weeks vs. 1 year and ***$P < 0.001$: 6–8 week vs. 2 year) while over all the capillary response was reduced in 2-year-old mice in comparison to young and 1-year-old mice. **(C)** Quantification of maximal diameter changes in different vessel segments at different ages following hypercapnia. Neurovascular reactivity of cerebral capillaries was impaired in 2-year-old mice as compared to 6–8 weeks and 1-year-old mice (*$P < 0.05$: 1 year vs. 2 year) (mean ± SEM, $n = 4$–10 mice/group, One-way ANOVA).

Reduced Vasodilation During NVC and Hypercapnia in Aged Mice

To directly visualize vascular reactivity in young, adult, and aged mice, animals received the plasma label FITC dextran and cerebral microvessels we imaged by *in vivo* 2-PM. Time series were recorded with the Zen® software (Zeiss, Oberkochen, Germany). Afterwards, original files were processed with our novel, investigator-independent vessel diameter measurement script and diameter changes of different vessel segments (pial arterioles, penetrating arterioles, and capillaries) were analyzed. A straight line crossing the investigated vessel at an angle of 90° was drawn and the inner diameter of the vessel was assessed based on the fluorescence of the injected plasma marker. Absolute changes of vessel diameter following whisker stimulation or hypercapnia were calculated by the script and expressed as % baseline (**Figure 3A**). A total of three whisker stimulations and one CO_2 challenge were performed and analyzed.

The most pronounced vasodilation was observed in capillaries independent of the age of the animals or the stimulation paradigm (**Figures 3B,C**). Two-year-old mice showed a reduced response in penetrating arterioles and in capillaries, specifically after hypercapnia (**Figure 3C**, $^{*}P < 0.05$: 1 year vs. 2 year), suggesting a spatially distinct effect of age on cerebrovascular reactivity.

DISCUSSION

In the current study, we developed two Matlab-based software tools, the "NVC-ToolBox," to analyze neurovascular reactivity by *in vivo* LSCI and 2-PM imaging following whisker stimulation and hypercapnia. The NVC-ToolBox allowed us to analyze neurovascular reactivity in a fully blinded, automatized, fast, and user-friendly manner. Moreover, we used aging as a paradigm to validate the NVC-ToolBox, since aging is well-known to reduce neurovascular reactivity. Our results demonstrate that the NVC-ToolBox is an easy to use and reliable tool for the assessment of neurovascular reactivity. Statistically significant changes in neurovascular reactivity between groups could be identified with a group size of six animals and a reasonable variability. Further, the time needed to analyze the data could be shortened by over 90% and investigator bias was completely eliminated from the analysis process. In the manual analysis procedure, first, frames of 2-PM time series must be exported as separate images which is between 250 and 280 frames. Then these images are binarized, skeletonized and diameters were measured by another plugin using ImageJ software. This procedure takes for the manual analyzer approximately 5 min for each image. However, with the automated tool it takes only 1–2 s to analyze all frames. Therefore the differences between the manual and automated analysis in sense of time and quality is massive. In terms of the effect of age on neurovascular reactivity, our data suggest a differential response during aging. Further, 2-PM imaging revealed a distinct involvement of different vessel segments following NVC and hypercapnia, i.e., the most pronounced vasodilation was found primarily at the capillary level and aging reduced vascular reactivity mainly in this vascular bed; to our surprise pial arteriole reactivity following whisker stimulation was even increased during the aging.

NVC ensures rapid CBF regulation in response to neuronal activity. *In vivo* imaging techniques with a high spatiotemporal resolution are crucial for understanding changes in NVC, a process critical in many pathologies such as aging or dementia. Moreover, reliable assessment of NVC is only possible with proper surgical window preparations, stable animal physiology, reliable and reproducible stimulation modalities, precise data acquisition, and objective image analysis algorithms (38). One of the gold standard techniques for NVC measurements is LSCI which is a simple, non-invasive *in vivo* imaging technique for the measurement of tissue perfusion (39–43). When moving objects are illuminated by dispersed laser light, the scattered light will form an interference ("speckle") pattern, which is proportional to tissue perfusion (44, 45). This technique is well-established and frequently used for dynamic imaging of CBF thanks to its high temporal resolution (11). When NVC is induced by forepaw, hind paw, or whisker stimulation, cerebral arterioles in the respective cortical area dilate to redistribute blood flow to the activated area. The subsequent increase in CBF can be visualized by 2-D heat maps using LSCI. Commercially available LSCI devices display, store and allow analyzing heat maps of individual animals, however, lack modalities to analyze data from cohorts of animals, specifically longitudinally. Since CBF responses can be spatially distinct and vary in intensity, changes often became only apparent when individual values of a group of animals are averaged or superimposed. This approach termed "co-registration" is not completely novel, since it has already been successfully used for the analysis of large cohorts of human and animal MRI, BOLD, or PET data (46, 47), however, it has, to the best of our knowledge, never been employed for the analysis of LSCI data sets. Using the NVC-ToolBox, multiple stimulations from the same subject and multiple subjects from the same experimental group can be averaged and high-resolution images displaying the mean response are created in a fully blinded and automated manner. Using this novel analysis tool, we observed that following whisker stimulation, young mice show a focal CBF response in the middle of the whisker area, while, 1-year-old mice showed a higher response covering almost the whole somatosensory cortex. In 2-year-old mice the response was focused again, but weak (**Figure 1B**). The observed changes in the spatial distribution of the laser speckle recordings could be linked to different factors. We can speculate that either the vascularization or the vascular function (or both) change with age. Many laboratories reported a reduction of capillary number and density in the aged brain (48–51). Others reported a substantial age-related decrease in brain arteriolar density in 24 vs. 13 months old rats (52–54). Some studies suggest that age-related changes can be multiphasic in the sense that capillary density increases during late adulthood and then declines at advanced ages in humans and rats (55, 56). Li et al. suggested a reduced capillary density together with a higher capillary flow velocity and heterogeneous capillary flow pattern in older vs. younger mice by using optical coherence tomography angiography (57). Therefore, oxygen delivery may be reduced during aging (58). Despite these data on vessel density and vessel

function, quite little is known about cerebrovascular plasticity during the aging process. Our data suggest that aging is also associated with significant changes in the spatial CBF response, i.e., that aging induces plastic changes of the neuronal network, which is then followed, by a consecutive vascular change. Further experiments using longitudinal imaging in individual animals may answer this important issue.

Two-photon laser scanning microscopy is a state-of-the-art technique used for observing, and measuring vascular changes *in vivo* with high spatial and temporal resolution with deep tissue penetration (59). In the current study, we used 2-PM to visualize changes of the vascular diameter of different vessel segments upon whisker stimulation or hypercapnia. After acquiring 3-D image stacks from the cerebral cortex, the diameter of vessels needed to be measured in a reliable and efficient manner, since manual analysis of 2-PM data is a tedious, time-consuming, and quite subjective process. To overcome these shortcomings, we developed scripts to measure vessel diameter changes of all vessels present in the 3D stack quickly and reliably. The scripts used for the analysis of LSCI data, as well as the analysis of 2-PM data resulted in statistically significant changes in neurovascular reactivity between groups with a group size of six animals and reasonable variability. In addition, the time needed to analyze the data could be shortened significantly and investigator bias was abolished from the analysis process.

Another advantage of the currently used experimental approach is the use of two different imaging modalities investigating two different aspects of neurovascular reactivity. Two-photon microscopy allows the assessment of vessel reactivity with high spatial and temporal resolution, however, only in a very limited area of the cortex (e.g., 200 x 200 μm), while LSCI has a limited spatial resolution and depth penetration, but is able to assess CBF responses in much larger cortical areas (e.g., 4 x 4 mm or more). Hence, using these two techniques consecutively on the same animal has complementary advantages and will allow a more in depth understanding of neurovascular reactivity in the healthy and diseased brain.

Aging has multiple effects at the systemic, molecular, and cellular level and impairs, among others, cerebrovascular reactivity (8, 26, 27). In the current study, we performed whisker stimulation in three different age groups, namely young (6–8 weeks), 1-year, and 2-year-old mice. Our LSCI analysis tool successfully produced superimposed stimulation responses from individual mice and created high-resolution mean heat maps by averaging the data from a whole group of mice. After the creation of the maps, the visual data was processed with our tool to create numerical values. Thus, we observed a trend toward more pronounced neurovascular reactivity during the first year of age and significantly lower and slower responses in 2-year-old mice. These results are similar to those published by other laboratories, e.g., Park and colleagues also found a significant reduction of NVC in 2-year-old mice (27). Moeini et al. showed no significant tissue pO_2 changes to whisker stimulation at the age of 15–16 months but a significant reduction at the age of 26–28 months (60). On the other hand Tucsek et al. (61) found a decreased NVC response at the age of 7 months by using laser doppler. Soleimanzad et al. also revealed a decreased response to odor stimulation at the age of 10 months by using multiexposure speckle imaging (36). Various results can be related to measurement techniques and response of specific cortex regions to specific stimuli can be differently affected during aging (60). Thus, the NVC-ToolBox generated data in line with the current literature.

Besides whisker response, 2-year-old mice had a reduced and slow vessel dilatation following hypercapnia, while 1-year-old mice showed no pathological response (**Figure 2B**). This data suggests that at the age of 1 year maximal dilation potential of the vessels maintain their ability to fully dilate while this function is significantly impaired by aging. Munting et al. showed no significant differences between young and 1-year-old mice to a 7.5% CO_2 challenge by arterial spin labeling (62). In the current study we recorded a ∼30% CBF increase following hypercapnia in young mice. Other studies, using different imaging techniques and anesthesia protocols, recorded values from 20 to 60% (8, 62, 63). These differences between laboratories emphasize the necessity for standardized and reproducible protocols for the assessment of neurovascular functions.

The analysis of vessel diameters at a depth of up to 100 μm within the cerebral cortex by 2-PM showed an increase in vascular reactivity toward smaller vessels, i.e., the highest response at the level of cortical capillaries. This observation was most pronounced in 1-year-old mature mice and almost eliminated in aged mice. Overall, neurovascular reactivity was reduced in 2-year-old mice in almost all vascular beds, except in pial vessels. This data suggest that different vessel segments react differently to sensory stimuli and that functional deterioration of the capillary bed might be the primary reason for reduced neurovascular reactivity and loss of vascular integrity during aging process (54). In fact, it has been reported that the tortuosity of the whole neurovascular tree (middle, anterior and posterior cerebral arterioles, penetrating arterioles, and capillaries) increases with age in mice and humans (64–67). Hence, such anatomical changes may well be part of the explanation why the functionality of the neurovascular network decreases with age. Moreover, distinct structural and functional characteristics of different vessel segments may explain why aging may have a differential effect on specific vascular beds. While pial arteries have a thick layer of smooth muscle cell lining and elastic lamina, penetrating arterioles have a thin smooth muscle layer, which gets completely lost while they dive deeper into the parenchyma. At the cerebral capillary level, endothelial cells are surrounded by a basement membrane, pericytes, and astrocytic end-feet (2, 68). Hence, these structures may be differentially affected by aging and may thus cause the observed spatially distinct neurovascular dysfunction.

Next to the degree and speed of neurovascular reactivity in different vascular beds, our data also shed some light on the signal transduction occurring along the vascular tree during NVC. A recent study from Rungta et al. showed that following neuronal stimulation blood velocity increases first in the surrounding capillary bed and only somewhat later in penetrating and pial arterioles (69), suggesting that capillaries trigger signals which are transferred to upstream arterioles and recruit them to the coupling response. Consequently, if the capillary response to

neuronal activation is disturbed, also the upstream response should be reduced or interrupted. Interestingly, we did not observe this behavior in our current experiments. On the contrary, aging reduced the reactivity of cortical capillaries, but caused a hyperactive pial response, suggesting that aging may reduce the interaction between the brain parenchyma and cerebral vessels, but that upstream signaling along the vascular tree may remain intact. Hence, reduced capillary dilatation and subsequent lack of tissue perfusion would elicit increased upstream signaling and a hyperactive pial response. Investigating the mechanisms responsible for these changes, such as paravascular nerve fibers, perivascular astrocytes, adenosine, or neuronal nitric oxide (NO) (70–72), may help to reduce age related neurovascular dysfunction. Perivascular astrocytes, for example, which connect NO producing neurons with pial arterioles, are heavily activated in the aged brain (71, 73, 74). Thus, it may be speculated that activated astrocytes trigger dilation of pial arterioles in the presence of an impaired capillary response. On the other hand, pial arterioles are richly innervated by extrinsic perivascular sympathetic and parasympathetic postganglionic neurons (20, 75). Thus, it is possible that in the aged brain loss of cholinergic innervation or noradrenergic signaling could also reveal distinct pial arteriole responses in the aged brain (54, 76). Further experiments using the current developed setup may help to answer this and similar questions in the future.

Another question is of course which cellular or molecular mechanisms are responsible for the observed impairments of neurovascular reactivity during aging. Sufficient supply of the brain parenchyma with blood depends on an intact communication between the cells in the NVU, i.e. endothelial cells, astrocytes, and pericytes. It is well-known that during aging, elements of the NVU start to deteriorate resulting in dysfunction of the blood-brain barrier and capillary dilation (77–82). Reasons for these functional impairments maybe a decline in microvascular remodeling, i.e., the missing replacement of aged cells of the neurovascular unit (83), such as pericytes (80) due to the increased production of reactive oxidative species (ROS) in the aging brain (26, 84, 85) as suggested by Fan and colleagues who found significantly increased ROS production in 2-year-old mice and human brain tissue accompanied by reduced capillary density and cognitive decline (86).

In summary, we measured the effect of aging on neurovascular reactivity using two different imaging modalities and a custom-made, investigator-independent analysis tool. We show increased neurovascular reactivity during brain maturation and reduced neurovascular reactivity during aging. Furthermore, we showed that aging does not affect all cortical vessel segments equally, but has a distinct effect on capillaries. Thus, the NVC-ToolBox turned out to be a reliable, robust, and investigator-independent tool to analyze neurovascular reactivity in the healthy and aged mouse brain.

DATA AVAILABILITY STATEMENT

The raw data supporting the conclusions of this article will be made available by the authors, without undue reservation.

ETHICS STATEMENT

The animal study was reviewed and approved by Government of Upper Bavaria (animal protocol number: Vet_2-15-196).

AUTHOR CONTRIBUTIONS

FS: manuscript preparation, data analysis, figure preparation, and supervised the findings of this work. ZF: carried out the experiments and data analysis. BG: LSCI image processing script writing. MG: 2-PM vessel analysis script writing. RS: figure preparation and proofreading. NP: designed the study, supervised the findings of this work, manuscript writing, and proofreading. All authors contributed to the article and approved the submitted version.

ACKNOWLEDGMENTS

This manuscript contains data from the MD thesis of ZF. Figures were created with BioRender.com.

REFERENCES

1. Hillman EM. Coupling mechanism and significance of the BOLD signal: a status report. *Annu Rev Neurosci.* (2014) 37:161–81. doi: 10.1146/annurev-neuro-071013-014111
2. Iadecola C. The neurovascular unit coming of age: a journey through neurovascular coupling in health and disease. *Neuron.* (2017) 96:17–42. doi: 10.1016/j.neuron.2017.07.030
3. Hu X, De Silva TM, Chen J, Faraci FM. Cerebral vascular disease and neurovascular injury in ischemic stroke. *Circ Res.* (2017) 120:449–71. doi: 10.1161/CIRCRESAHA.116.308427
4. Nicolakakis N, Hamel E. Neurovascular function in Alzheimer's disease patients and experimental models. *J Cereb Blood Flow Metab.* (2011) 31:1354–70. doi: 10.1038/jcbfm.2011.43
5. Hinzman JM, Andaluz N, Shutter LA, Okonkwo DO, Pahl C, Strong AJ, et al. Inverse neurovascular coupling to cortical spreading depolarizations in severe brain trauma. *Brain.* (2014) 137:2960–72. doi: 10.1093/brain/awu241
6. Tiret P, Chaigneau E, Lecoq J, Charpak S. Two-photon imaging of capillary blood flow in olfactory bulb glomeruli. *Methods Mol Biol (Clifton, NJ).* (2009) 489:81–91. doi: 10.1007/978-1-59745-543-5_4
7. van Veluw SJ, Hou SS, Calvo-Rodriguez M, Arbel-Ornath M, Snyder AC, Frosch MP, et al. Vasomotion as a driving force for paravascular clearance in the awake mouse brain. *Neuron.* (2020) 105:549–561.e545. doi: 10.1016/j.neuron.2019.10.033
8. Balbi M, Ghosh M, Longden TA, Jativa Vega M, Gesierich B, Hellal F, et al. Dysfunction of mouse cerebral arteries during early aging. *J Cereb Blood Flow Metab.* (2015) 35:1445–53. doi: 10.1038/jcbfm.2015.107
9. Hayashi A, Yoshida T, Ohki K. Cell type specific representation of vibro-tactile stimuli in the mouse primary somatosensory cortex. *Front Neural Circuits.* (2018) 12:109. doi: 10.3389/fncir.2018.00109
10. Wang Z, Hughes S, Dayasundara S, Menon RS. Theoretical and experimental optimization of laser speckle contrast imaging for high specificity to brain microcirculation. *J Cereb Blood Flow Metab.* (2007) 27:258–69. doi: 10.1038/sj.jcbfm.9600357

11. Dunn AK, Bolay H, Moskowitz MA, Boas DA. Dynamic imaging of cerebral blood flow using laser speckle. *J Cereb Blood Flow Metab.* (2001) 21:195–201. doi: 10.1097/00004647-200103000-00002
12. Bolay H, Reuter U, Dunn AK, Huang Z, Boas DA. Moskowitz MA. Intrinsic brain activity triggers trigeminal meningeal afferents in a migraine model. *Nat Med.* (2002) 8:136–42. doi: 10.1038/nm0202-136
13. Lind BL, Jessen SB, Lønstrup M, Joséphine C, Bonvento G, Lauritzen M. Fast Ca(2+) responses in astrocyte end-feet and neurovascular coupling in mice. *Glia*. (2018) 66:348–58. doi: 10.1002/glia.23246
14. Shih AY, Driscoll JD, Drew PJ, Nishimura N, Schaffer CB, Kleinfeld D. Two-photon microscopy as a tool to study blood flow and neurovascular coupling in the rodent brain. *J Cereb Blood Flow Metab.* (2012) 32:1277–309. doi: 10.1038/jcbfm.2011.196
15. Chow BW, Nuñez V, Kaplan L, Granger AJ, Bistrong K, Zucker HL, et al. Caveolae in CNS arterioles mediate neurovascular coupling. *Nature*. (2020) 579:106–10. doi: 10.1038/s41586-020-2026-1
16. Csipo T, Mukli P, Lipecz A, Tarantini S, Bahadli D, Abdulhussein O, et al. Assessment of age-related decline of neurovascular coupling responses by functional near-infrared spectroscopy (fNIRS) in humans. *GeroScience.* (2019) 41:495–509. doi: 10.1007/s11357-019-00122-x
17. Svennerholm L, Bostrom K. Jungbjer, B. Changes in weight and compositions of major membrane components of human brain during the span of adult human life of Swedes. *Acta Neuropathol.* (1997) 94:345–52. doi: 10.1007/s004010050717
18. Petralia RS, Mattson MP, Yao PJ. Communication breakdown: the impact of ageing on synapse structure. *Ageing Res Rev.* (2014) 14:31–42. doi: 10.1016/j.arr.2014.01.003
19. Gorelick PB, Scuteri A, Black SE, Decarli C, Greenberg SM, Iadecola C, et al. Vascular contributions to cognitive impairment and dementia: a statement for healthcare professionals from the american heart association/american stroke association. *Stroke.* (2011) 42:2672–713. doi: 10.1161/STR.0b013e3182299496
20. Phillips AA, Chan FH, Zheng MM, Krassioukov AV, Ainslie PN. Neurovascular coupling in humans: physiology, methodological advances and clinical implications. *J Cereb Blood Flow Metab*. (2016) 36:647–64. doi: 10.1177/0271678X15617954
21. Tarantini S, Csiszar A, Ungvari Z. Midlife obesity impairs neurovascular coupling responses. *Obesity (Silver Spring).* (2021) 29:17. doi: 10.1002/oby.23072
22. Cooper LL, Woodard T, Sigurdsson S, van Buchem MA, Torjesen AA, Inker LA, et al. Cerebrovascular damage mediates relations between aortic stiffness and memory. *Hypertension.* (2016) 67:176–82. doi: 10.1161/HYPERTENSIONAHA.115.06398
23. Zaletel M, Strucl M, Pretnar-Oblak J, Zvan B. Age-related changes in the relationship between visual evoked potentials and visually evoked cerebral blood flow velocity response. *Funct Neurol.* (2005) 20:115–20.
24. Topcuoglu MA, Aydin H, Saka E. Occipital cortex activation studied with simultaneous recordings of functional transcranial Doppler ultrasound (fTCD) and visual evoked potential (VEP) in cognitively normal human subjects: effect of healthy aging. *Neurosci Lett.* (2009) 452:17–22. doi: 10.1016/j.neulet.2009.01.030
25. Stefanova I, Stephan T, Becker-Bense S, Dera T, Brandt T, Dieterich M. Age-related changes of blood-oxygen-level-dependent signal dynamics during optokinetic stimulation. *Neurobiol Aging.* (2013) 34:2277–86. doi: 10.1016/j.neurobiolaging.2013.03.031
26. Toth P, Tarantini S, Tucsek Z, Ashpole NM, Sosnowska D, Gautam T, et al. Resveratrol treatment rescues neurovascular coupling in aged mice: role of improved cerebromicrovascular endothelial function and downregulation of NADPH oxidase. *Am J Physiol Heart Circ Physiol.* (2014) 306:H299–308. doi: 10.1152/ajpheart.00744.2013
27. Park L, Anrather J, Girouard H, Zhou P, Iadecola C. Nox2-derived reactive oxygen species mediate neurovascular dysregulation in the aging mouse brain. *J Cereb Blood Flow Metab.* (2007) 27:1908–918. doi: 10.1038/sj.jcbfm.9600491
28. Tarumi T, Zhang R. Cerebral blood flow in normal aging adults: cardiovascular determinants, clinical implications, and aerobic fitness. *J Neurochem*. (2018) 144:595–608. doi: 10.1111/jnc.14234
29. Ighodaro ET, Abner EL, Fardo DW, Lin AL, Katsumata Y, Schmitt FA, et al. Risk factors and global cognitive status related to brain arteriolosclerosis in elderly individuals. *J Cereb Blood Flow Metab*. (2017) 37:201–16. doi: 10.1177/0271678X15621574
30. Mayhan WG, Faraci FM, Baumbach GL, Heistad DD. Effects of aging on responses of cerebral arterioles. *Am J Physiol.* (1990) 258:H1138–43. doi: 10.1152/ajpheart.1990.258.4.H1138
31. Villeneuve S, Reed BR, Madison CM, Wirth M, Marchant NL, Kriger S, et al. Vascular risk and Abeta interact to reduce cortical thickness in AD vulnerable brain regions. *Neurology*. (2014) 83:40–7. doi: 10.1212/WNL.0000000000000550
32. de la Torre JC. Is Alzheimer's disease a neurodegenerative or a vascular disorder? Data, dogma, and dialectics. *Lancet Neurol.* (2004) 3:184–90. doi: 10.1016/S1474-4422(04)00683-0
33. Viswanathan A, Rocca WA. Tzourio, C. Vascular risk factors and dementia: how to move forward? *Neurology.* (2009) 72:368–74. doi: 10.1212/01.wnl.0000341271.90478.8e
34. Zlokovic BV. Neurovascular pathways to neurodegeneration in Alzheimer's disease and other disorders. *Nat Rev Neurosci.* (2011) 12:723–38. doi: 10.1038/nrn3114
35. Lipecz A, Csipo T, Tarantini S, Hand RA, Ngo BN, Conley S, et al. Age-related impairment of neurovascular coupling responses: a dynamic vessel analysis (DVA)-based approach to measure decreased flicker light stimulus-induced retinal arteriolar dilation in healthy older adults. *GeroScience.* (2019) 41:341–9. doi: 10.1007/s11357-019-00078-y
36. Soleimanzad H, Montaner M, Ternier G, Lemitre M, Silvestre JS, Kassis N, et al. Obesity in midlife hampers resting and sensory-evoked cerebral blood flow in mice. *Obesity (Silver Spring).* (2021) 29:150–8. doi: 10.1002/oby.23051
37. Bailey-Downs LC, Tucsek Z, Toth P, Sosnowska D, Gautam T, Sonntag WE, et al. Aging exacerbates obesity-induced oxidative stress and inflammation in perivascular adipose tissue in mice: a paracrine mechanism contributing to vascular redox dysregulation and inflammation. *J Gerontol A Biol Sci Med Sci.* (2013) 68:780–92. doi: 10.1093/gerona/gls238
38. Yoon JH, Jeong, Y. *In vivo* imaging for neurovascular disease research. *Arch Pharm Res*. (2019) 42:263–73. doi: 10.1007/s12272-019-01128-x
39. Tarantini S, Fulop GA, Kiss T, Farkas E, Zölei-Szénási D, Galvan V, et al. Demonstration of impaired neurovascular coupling responses in TG2576 mouse model of Alzheimer's disease using functional laser speckle contrast imaging. *GeroScience.* (2017) 39:465–73. doi: 10.1007/s11357-017-9980-z
40. Winship IR. Laser speckle contrast imaging to measure changes in cerebral blood flow. *Methods Mol Biol (Clifton, NJ).* (2014) 1135:223–35. doi: 10.1007/978-1-4939-0320-7_19
41. Ma J, Ma Y, Shuaib A, Winship IR. Impaired collateral flow in pial arterioles of aged rats during ischemic stroke *Transl Stroke Res.* (2020) 11:243–53. doi: 10.1007/s12975-019-00710-1
42. Xie Y, Chen S, Anenberg E, Murphy TH. Resistance of optogenetically evoked motor function to global ischemia and reperfusion in mouse in vivo. *J Cereb Blood Flow Metab.* (2013) 33:1148–52. doi: 10.1038/jcbfm.2013.89
43. Mastantuono T, Starita N, Battiloro L, Di Maro M, Chiurazzi M, Nasti G, et al. Laser speckle imaging of rat pial microvasculature during hypoperfusion-reperfusion damage. *Front Cell Neurosci 11:298.* (2017). doi: 10.3389/fncel.2017.00298
44. Kazmi SM, Richards LM, Schrandt CJ, Davis MA, Dunn AK. Expanding applications, accuracy, and interpretation of laser speckle contrast imaging of cerebral blood flow. *J Cereb Blood Flow Metab.* (2015) 35:1076–84. doi: 10.1038/jcbfm.2015.84
45. Yuan S, Devor A, Boas DA, Dunn AK. Determination of optimal exposure time for imaging of blood flow changes with laser speckle contrast imaging. *Appl Opt.* (2005) 44:1823–30. doi: 10.1364/AO.44.001823
46. Aanerud J, Borghammer P, Chakravarty MM, Vang K, Rodell AB, Jonsdottir KY, et al. Brain energy metabolism and blood flow differences in healthy aging. *J Cereb Blood Flow Metab.* (2012) 32:1177–87. doi: 10.1038/jcbfm.2012.18
47. Chao TH, Chen JH, Yen, CT. Plasticity changes in forebrain activity and functional connectivity during neuropathic pain development in rats with sciatic spared nerve injury *Mol Brain.* (2018) 11:55. doi: 10.1186/s13041-018-0398-z
48. Amenta F, Cavallotti D, Del Valle M, Mancini M, Naves FJ, Vega JA. et al. Age-related changes in brain microanatomy: sensitivity to treatment with the

dihydropyridine calcium channel blocker darodipine (PY 108-068). *Brain Res Bull.* (1995) 36:453–60. doi: 10.1016/0361-9230(94)00210-R
49. Casey MA, Feldman ML. Aging in the rat medial nucleus of the trapezoid body III Alterations in capillaries. *Neurobiol Aging.* (1985) 6:39–46. doi: 10.1016/0197-4580(85)90070-3
50. Jucker M, Bättig K, Meier-Ruge W. Effects of aging and vincamine derivatives on pericapillary microenvironment: stereological characterization of the cerebral capillary network. *Neurobiol Aging.* (1990) 11:39–46. doi: 10.1016/0197-4580(90)90060-D
51. Brown WR, Moody DM, Thore CR, Challa VR, Anstrom, J*A*. Vascular dementia in leukoaraiosis may be a consequence of capillary loss not only in the lesions, but in normal-appearing white matter and cortex as well. *J Neurol Sci.* (2007) 257:62–6. doi: 10.1016/j.jns.2007.01.015
52. Hutchins PM, Lynch CD, Cooney PT, Curseen KA. The microcirculation in experimental hypertension and aging. *Cardiovasc Res.* (1996) 32:772–80. doi: 10.1016/S0008-6363(96)00136-8
53. Sonntag WE, Lynch CD, Cooney PT, Hutchins PM. Decreases in cerebral microvasculature with age are associated with the decline in growth hormone and insulin-like growth factor 1. *Endocrinology.* (1997) 138:3515–20. doi: 10.1210/endo.138.8.5330
54. Farkas E, Luiten PG. Cerebral microvascular pathology in aging and Alzheimer's disease. *Progress Neurobiol.* (2001) 64:575–611. doi: 10.1016/S0301-0082(00)00068-X
55. Hunziker O, Abdel'Al S, Schulz U. The aging human cerebral cortex: a stereological characterization of changes in the capillary net. *J Gerontol.* (1979) 34:345–50. doi: 10.1093/geronj/34.3.345
56. Wilkinson JH, Hopewell JW, Reinhold HS. A quantitative study of age-related changes in the vascular architecture of the rat cerebral cortex. *Neuropathol Appl Neurobiol.* (1981). 7:451–62. doi: 10.1111/j.1365-2990.1981.tb00245.x
57. Li Y, Choi WJ, Wei W, Song S, Zhang Q, Liu J, et al. Aging-associated changes in cerebral vasculature and blood flow as determined by quantitative optical coherence tomography angiography. *Neurobiol Aging.* (2018) 70:148–59. doi: 10.1016/j.neurobiolaging.2018.06.017
58. Østergaard L, Jespersen SN, Engedahl T, Gutiérrez Jiménez E, Ashkanian M, Hansen MB, et al. Capillary dysfunction: its detection and causative role in dementias and stroke. *Curr Neurol Neurosci Rep.* (2015) 15:37. doi: 10.1007/s11910-015-0557-x
59. Kleinfeld D, Mitra PP, Helmchen F, Denk W. Fluctuations and stimulus-induced changes in blood flow observed in individual capillaries in layers 2 through 4 of rat neocortex. *Proc Natll Acad Sci U S A.* (1998) 95:15741–6. doi: 10.1073/pnas.95.26.15741
60. Moeini M, Lu X, Bélanger S, Picard F, Boas D, Kakkar A, et al. Cerebral tissue pO(2) response to stimulation is preserved with age in awake mice. *Neurosci Lett.* (2019) 699:160–66. doi: 10.1016/j.neulet.2019.02.007
61. Tucsek Z. TothP, Tarantini S, Sosnowska D, Gautam T, Warrington JP, et al. Aging exacerbates obesity-induced cerebromicrovascular rarefaction, neurovascular uncoupling, and cognitive decline in mice. *J Gerontol A Biol Sci Med Sci.* (2014) 69:1339–52. doi: 10.1093/gerona/glu080
62. Munting LP, Derieppe MPP, Suidgeest E, Denis de Senneville B, Wells JA, van der Weerd L. Influence of different isoflurane anesthesia protocols on murine cerebral hemodynamics measured with pseudo-continuous arterial spin labeling. *NMR Biomed.* (2019) 32:e4105. doi: 10.1002/nbm.4105
63. Wenzel J, Hansen CE, Bettoni C, Vogt MA, Lembrich B, Natsagdorj R, et al. Impaired endothelium-mediated cerebrovascular reactivity promotes anxiety and respiration disorders in mice. *Proc Natl Acad Sci U S A.* (2020) 117:1753–61. doi: 10.1073/pnas.1907467117
64. Faber JE, Zhang H, Lassance-Soares RM, Prabhakar P, Najafi AH, Burnett MS, et al. Aging causes collateral rarefaction and increased severity of ischemic injury in multiple tissues. *Arteriosclerosis Thrombosis Vasc Biol.* (2011) 31:1748–56. doi: 10.1161/ATVBAHA.111.227314
65. Kang HM, Sohn I, Jung J, Jeong JW, Park, C. Age-related changes in pial arterial structure and blood flow in mice. *Neurobiol Aging.* (2016) 37:161–70. doi: 10.1016/j.neurobiolaging.2015.09.008
66. Bullitt E, Zeng D, Mortamet B, Ghosh A, Aylward SR, Lin W, et al. The effects of healthy aging on intracerebral blood vessels visualized by magnetic resonance angiography. *Neurobiol Aging.* (2010) 31:290–300. doi: 10.1016/j.neurobiolaging.2008.03.022
67. Thore CR, Anstrom JA, Moody DM, Challa VR, Marion MC, Brown, W*R*. Morphometric analysis of arteriolar tortuosity in human cerebral white matter of preterm, young, and aged subjects. *J Neuropathol Exp Neurol.* (2007) 66:337–45. doi: 10.1097/nen.0b013e3180537147
68. Sweeney MD, Ayyadurai S, Zlokovic B*V*. Pericytes of the neurovascular unit: key functions and signaling pathways. *Nat Neurosci.* (2016) 19:771–83. doi: 10.1038/nn.4288
69. Rungta RL, Zuend M, Aydin AK, Martineau É, Boido D, Weber B, et al. Diversity of neurovascular coupling dynamics along vascular arbors in layer II/III somatosensory cortex. *Commun Biol.* (2021) 4:855. doi: 10.1038/s42003-021-02382-w
70. Petzold GC, Murthy, VN. Role of astrocytes in neurovascular coupling. *Neuron.* (2011) 71:782–97. doi: 10.1016/j.neuron.2011.08.009
71. Koehler RC, Gebremedhin D, Harder DR. Role of astrocytes in cerebrovascular regulation. *J Appl Physiol (Bethesda, Md: 1985).* (2006) 100:307–17. doi: 10.1152/japplphysiol.00938.2005
72. Xu HL, Mao L, Ye S, Paisansathan C, Vetri F, Pelligrino DA. Astrocytes are a key conduit for upstream signaling of vasodilation during cerebral cortical neuronal activation *in vivo*. *Am J Physiol Heart Circ Physiol.* (2008) 294:H622–32. doi: 10.1152/ajpheart.00530.2007
73. Wang H, Hitron IM, Iadecola C, Pickel VM. Synaptic and vascular associations of neurons containing cyclooxygenase-2 and nitric oxide synthase in rat somatosensory cortex. *Cerebr Cortex (New York, NY: 1991).* (2005) 15:1250–60. doi: 10.1093/cercor/bhi008
74. Pan J, Ma N, Yu B, Zhang W, Wan, J. Transcriptomic profiling of microglia and astrocytes throughout aging. *J Neuroinflamm.* (2020) 17:97. doi: 10.1186/s12974-020-01774-9
75. Hamel E. Perivascular nerves and the regulation of cerebrovascular tone. *J Appl Physiol (Bethesda, Md: 1985).* (2006) 100:1059–64. doi: 10.1152/japplphysiol.00954.2005
76. Lecrux C, Hamel E. Neuronal networks and mediators of cortical neurovascular coupling responses in normal and altered brain states. *Philos Trans R Soc Lond B Biol Sci.* (2016) 371:20150350. doi: 10.1098/rstb.2015.0350
77. Duncombe J, Lennen RJ, Jansen MA, Marshall I, Wardlaw JM, Horsburgh, K. Ageing causes prominent neurovascular dysfunction associated with loss of astrocytic contacts and gliosis. *Neuropathol Appl Neurobiol.* (2017) 43:477–91. doi: 10.1111/nan.12375
78. Clarke LE, Liddelow SA, Chakraborty C. MunchAE, Heiman M, Barres BA. Normal aging induces A1-like astrocyte reactivity. *Proc Natl Acad Sci U S A.* (2018) 115:E1896–905. doi: 10.1073/pnas.1800165115
79. Tarantini S, Tran CHT, Gordon GR, Ungvari Z, Csiszar A. Impaired neurovascular coupling in aging and Alzheimer's disease: contribution of astrocyte dysfunction and endothelial impairment to cognitive decline. *Exp Gerontol.* (2017) 94:52–58. doi: 10.1016/j.exger.2016.11.004
80. Bell RD, Winkler EA, Sagare AP, Singh I, LaRue B, Deane R, et al. Pericytes control key neurovascular functions and neuronal phenotype in the adult brain and during brain aging. *Neuron.* (2010) 68:409–427. doi: 10.1016/j.neuron.2010.09.043
81. Yang AC, Stevens MY, Chen MB, Lee DP, Stahli D, Gate D, et al. Physiological blood-brain transport is impaired with age by a shift in transcytosis. *Nature.* (2020) 583:425–430. doi: 10.1038/s41586-020-2453-z
82. Kiss T, Nyul-Toth A, Balasubramanian P, Tarantini S, Ahire C, DelFavero J, et al. Single-cell RNA sequencing identifies senescent cerebromicrovascular endothelial cells in the aged mouse brain. *GeroScience.* (2020) 42:429–444. doi: 10.1007/s11357-020-00177-1
83. Harb R, Whiteus C, Freitas C, Grutzendler J. *In vivo* imaging of cerebral microvascular plasticity from birth to death. *J Cereb Blood Flow Metab.* (2013) 33:146–56. doi: 10.1038/jcbfm.2012.152
84. Lourenço CF, Ledo A, Caetano M, Barbosa RM, Laranjinha J. Age-dependent impairment of neurovascular and neurometabolic coupling in the hippocampus. *Front Physiol.* (2018) 9:913. doi: 10.3389/fphys.2018.00913

85. Tarantini S, Valcarcel-Ares MN, Toth P, Yabluchanskiy A, Tucsek Z, Kiss T, et al. Nicotinamide mononucleotide (NMN) supplementation rescues cerebromicrovascular endothelial function and neurovascular coupling responses and improves cognitive function in aged mice. *Redox Biol.* (2019) 24:101192. doi: 10.1016/j.redox.2019.101192
86. Fan LM, Geng L, Cahill-Smith S, Liu F, Douglas G, McKenzie CA, et al. Nox2 contributes to age-related oxidative damage to neurons and the cerebral vasculature. *J Clin Invest.* (2019) 129:3374–86. doi: 10.1172/JCI 125173

Conflict of Interest: The authors declare that the research was conducted in the absence of any commercial or financial relationships that could be construed as a potential conflict of interest.

Publisher's Note: All claims expressed in this article are solely those of the authors and do not necessarily represent those of their affiliated organizations, or those of the publisher, the editors and the reviewers. Any product that may be evaluated in this article, or claim that may be made by its manufacturer, is not guaranteed or endorsed by the publisher.

frontiers in Neurology

ORIGINAL RESEARCH
published: 16 November 2021
doi: 10.3389/fneur.2021.745987

Noninvasive Optical Measurements of Dynamic Cerebral Autoregulation by Inducing Oscillatory Cerebral Hemodynamics

Thao Pham[1†], Cristianne Fernandez[1†], Giles Blaney[1], Kristen Tgavalekos[1], Angelo Sassaroli[1], Xuemei Cai[2], Steve Bibu[2], Joshua Kornbluth[2] and Sergio Fantini[1]*

[1] Department of Biomedical Engineering, Tufts University, Medford, MA, United States, [2] Department of Neurology, Tufts University School of Medicine, Boston, MA, United States

OPEN ACCESS

Edited by:
Xiuyun Liu,
Johns Hopkins University,
United States

Reviewed by:
Zengyong Li,
National Research Center for Rehabilitation Technical Aids, China
David Simpson,
University of Southampton,
United Kingdom

****Correspondence:***
Sergio Fantini
sergio.fantini@tufts.edu

[†] These authors have contributed equally to this work and share first authorship

Specialty section:
This article was submitted to Applied Neuroimaging, a section of the journal Frontiers in Neurology

Received: *23 July 2021*
Accepted: *13 October 2021*
Published: *16 November 2021*

Citation:
Pham T, Fernandez C, Blaney G, Tgavalekos K, Sassaroli A, Cai X, Bibu S, Kornbluth J and Fantini S (2021) Noninvasive Optical Measurements of Dynamic Cerebral Autoregulation by Inducing Oscillatory Cerebral Hemodynamics. Front. Neurol. 12:745987. doi: 10.3389/fneur.2021.745987

Objective: Cerebral autoregulation limits the variability of cerebral blood flow (CBF) in the presence of systemic arterial blood pressure (ABP) changes. Monitoring cerebral autoregulation is important in the Neurocritical Care Unit (NCCU) to assess cerebral health. Here, our goal is to identify optimal frequency-domain near-infrared spectroscopy (FD-NIRS) parameters and apply a hemodynamic model of coherent hemodynamics spectroscopy (CHS) to assess cerebral autoregulation in healthy adult subjects and NCCU patients.

Methods: In five healthy subjects and three NCCU patients, ABP oscillations at a frequency around 0.065 Hz were induced by cyclic inflation-deflation of pneumatic thigh cuffs. Transfer function analysis based on wavelet transform was performed to measure dynamic relationships between ABP and oscillations in oxy- (*O*), deoxy- (*D*), and total- (*T*) hemoglobin concentrations measured with different FD-NIRS methods. In healthy subjects, we also obtained the dynamic CBF-ABP relationship by using FD-NIRS measurements and the CHS model. In healthy subjects, an interval of hypercapnia was performed to induce cerebral autoregulation impairment. In NCCU patients, the optical measurements of autoregulation were linked to individual clinical diagnoses.

Results: In healthy subjects, hypercapnia leads to a more negative phase difference of both *O* and *D* oscillations vs. ABP oscillations, which are consistent across different FD-NIRS methods and are highly correlated with a more negative phase difference CBF vs. ABP. In the NCCU, a less negative phase difference of *D* vs. ABP was observed in one patient as compared to two others, indicating a better autoregulation in that patient.

Conclusions: Non-invasive optical measurements of induced phase difference between *D* and ABP show the strongest sensitivity to cerebral autoregulation. The results from healthy subjects also show that the CHS model, in combination with FD-NIRS, can be applied to measure the CBF-ABP dynamics for a better direct measurement of cerebral autoregulation.

Keywords: cerebral autoregulation, cerebral blood flow, near-infrared spectroscopy, frequency-domain, coherent hemodynamics, neurocritical care, brain, oscillations

1. INTRODUCTION

Cerebral autoregulation is a homeostatic feedback mechanism that maintains stable cerebral blood flow (CBF) despite moderate changes in arterial blood pressure (ABP). This mechanism utilizes the arteries and arterioles of the brain that can dilate and constrict to regulate CBF and limit its variability. In the Neurocritical Care Unit (NCCU), measurements of cerebral autoregulation in patients with traumatic brain injury can help the diagnosis and monitoring of pathological conditions to improve patient care and to prevent further injury to the brain (1). In fact, impaired cerebral autoregulation is linked to poor clinical outcomes in a variety of conditions such as subarachnoid hemorrhage, stroke, traumatic brain injury, etc. (2–4).

Early studies refer to cerebral autoregulation as a static phenomenon described by a non-linear curve with a characteristic CBF plateau in a range of ABP in which cerebral autoregulation is active (5). With the use of transcranial Doppler ultrasound (TCD) for non-invasive and rapid measurements of CBF, dynamic cerebral autoregulation was introduced by investigating CBF transients in response to dynamic ABP changes (6, 7). One common protocol to assess dynamic autoregulation involves targeting ABP oscillations at low frequencies (<0.2 Hz). Such oscillations can occur spontaneously (8) or can be induced by using various protocols including periodic thigh-cuff inflation (9) and paced breathing (10–12). A transfer function analysis is performed to quantify the relationship between ABP (input, as monitored simultaneously by finger plethysmography) and CBF (output, as monitored by TCD). A more positive phase shift between CBF vs. ABP (i.e., a faster recovery of CBF in response to ABP changes) is often associated with an effective cerebral autoregulation (8, 10, 11, 13). This technique has been applied in the clinical setting to assess cerebral autoregulation in patients with intracranial hypertension (14), traumatic brain injury (15), acute ischemic stroke (16, 17), carotid artery occlusive disease (10), intracranial hemorrhage (4), etc. It was shown that a higher correlation coefficient (15) and a smaller phase difference (16) between CBF and ABP implies worsening autoregulation in those patients. Although TCD together with ABP measurements have been widely used for autoregulation assessment in various population, TCD has its limitations as it cannot measure microvascular and localized changes in CBF.

Oscillations in blood flow and blood volume have individual effects on the oscillations of hemoglobin concentrations that can be sensed by near-infrared spectroscopy (NIRS). Specifically, NIRS is an optical technique that can measure cerebral changes in oxy-, deoxy-, and total hemoglobin concentrations [$O(t)$, $D(t)$, and $T(t)$, respectively]. As compared to TCD, NIRS is sensitive to more local changes in hemodynamics in different compartments of the microvasculature. NIRS can provide measurements with a spatial resolution of less than 4 cm spatially and less than 2 cm in depth (18), thus realizing a better self-contained and spatially congruent technology for local CBF and autoregulation assessment (11). Spontaneous and induced oscillations in hemoglobin concentrations measured by NIRS have been shown to be sensitive to cerebral autoregulation in literature. For instance, studies have reported dynamic cerebral autoregulation measured indirectly through the dynamic relationship between D and O (10, 19, 20), between O and ABP (11, 21–24), between D and ABP (10), between T and ABP (25), and between cerebral tissue saturation (the ratio of O to T) and ABP (26, 27). However, there is no clear evidence of which relative dynamic relationship between hemoglobin concentrations and blood pressure is the most sensitive to cerebral autoregulation. This could possibly be due to the issue of NIRS measurements as they are not solely sensitive to CBF but in fact a combination and interplay of CBF, cerebral blood volume (CBV), and cerebral metabolic rate of oxygen ($CMRO_2$). As a result, it is highly relevant to translate NIRS measurements into underlying physiological processes, especially to more correct and direct measurements of CBF dynamics. This can be achieved by using a hemodynamic model for coherent hemodynamics spectroscopy (CHS) (28) that converts frequency-domain (FD) NIRS measurements into a relative CBF changes [$\mathrm{cbf}(t)$]. This model takes into account the effects of CBV changes and blood transit times in the capillary and venous compartments in the measurements of hemoglobin concentrations (29, 30).

One well-known issue with non-invasive cerebral NIRS using continuous-wave (CW) instruments is the contribution to the optical signal from extra cerebral hemodynamics in superficial tissue (scalp) and in the skull. The most common setup for this kind of measurement is using intensity data in a single-distance (SD) configuration, which consists of one source and one detector separated by a set distance. Single-slope (SS) methods, based on either a single source and multiple detectors or a single detector and multiple sources have been introduced to improve the quality of optical measurements of tissue saturation and to reduce sensitivity to superficial tissue (31, 32). Another approach based on a special configuration of two sources and two detectors was proposed in frequency-domain (FD) spectroscopy for self-calibrating absolute measurements of optical properties in diffuse media (33). This method was implemented in commercial CW-NIRS tissue oximeters (34, 35). More recently, this special arrangement was revisited for enhanced depth discrimination on the basis of separate intensity or phase measurements in FD-NIRS (and named dual-slope (DS) method in this context) (18, 36), or the moments of the photon time of flight distribution in time-domain (TD) NIRS (37). Here, we consider separate intensity (I) and phase (ϕ) measurements obtained with FD-NIRS in SD, SS, and DS configurations. Based on previous studies (18, 38), slope measurements (SS, DS) were shown to be more sensitive to cerebral hemodynamics than SD data, and ϕ data were shown to be more sensitive to the brain than I data. Furthermore, from a practical viewpoint, the DS method also provides a benefit of being largely insensitive to instrumental drifts and optical coupling effects (36). We have demonstrated the potential of NIRS-CHS to measure cerebral autoregulation in healthy subjects in a protocol of rapid step changes in ABP (39). While in our previous study only CW measurements were used (39), here we further explore the potentiality of FD measurements for assessment of dynamic cerebral autoregulation in healthy controls and in the clinical settings.

The scope of this work is to first validate our protocol of induced cerebral hemodynamic oscillations to measure cerebral autoregulation in controlled healthy subjects and in NCCU patients. In the sample of healthy subjects, we first targeted the blood-pressure-induced hemoglobin oscillations (i.e., *O*, *D*, and *T* oscillations) at about 0.065 Hz that are most sensitive to cerebral autoregulation impairment by hypercapnia in healthy subjects. Hypercapnia, a state of elevated arterial CO_2 concentration above normal levels (normocapnia), causes vasodilation of arterioles and, thus, an increase in CBF (40) and a decrease in cerebral autoregulation capacity (6, 41, 42). In the sample of NCCU patients, the results from healthy subjects were used to guide the clinical interpretation of three patients. We aim to demonstrate the feasibility of using these optical measurements with a protocol of blood-pressure-induced hemodynamic oscillations to monitor cerebral autoregulation efficiency in patients with brain injuries. The second goal of this study is to propose the applicability of the CHS model to provide optical measurements of CBF-ABP dynamics, which is more directly related to the cerebral autoregulation efficiency than NIRS measurements of *O*, *D*, and *T*, without any model. Finally, we aimed at investigating these results with different kinds of FD-NIRS methods (SD, SS, DS with either I or ϕ data) that may feature different relative sensitivities to cerebral vs. extracerebral hemodynamics, thus helping to address the issue of extracerebral tissue contamination in NIRS signals.

2. MATERIALS AND METHODS

2.1. Human Subjects

Eight subjects participated in the two studies: five healthy subjects (subjects 1–5; one female, four males, age range: 23–33 yr) and three NCCU patients (patients 1–3; one female, two males, age range: 17–67 yr). The NCCU patients were recruited from Tufts Medical Center, and a summary of patient demographic information can be found in **Table 1**. Both studies were approved by the Tufts University Institutional Review Board and all participants signed an informed consent prior to the experiment. For the NCCU patients, patient 1 participated on 3 days, patient 2 on 2 days, and patient 3 on 1 day. Each day, the measurement session was repeated three times. We report the results for a single day and measurement session, selected on the basis of low motion artifacts, high signal-to-noise ratio of the optical data, and maximum extent of induced oscillations in ABP and cerebral hemodynamics.

2.2. Data Acquisition and Experimental Protocol

Figure 1 shows the setups for the experiments on healthy subjects (**Figures 1A,B**) and on NCCU patients (**Figures 1C,D**). In the healthy subjects, the FD-NIRS measurements were performed using a commercial FD-NIRS instrument (Imagent, ISS Inc., Champaign, IL; wavelengths: 690 and 830 nm; modulation frequency: 140.625 MHz) operating at a data acquisition rate of 9.93 Hz. An optical probe was placed on the right side of the subject's forehead. This probe consisted of a linear array of two source fiber pairs and two detector fiber bundles that are symmetrical about the midline between the two sources. This configuration allows for two SD measurements at 35 mm source-detector distances, two SS measurements at source-detector distances of 25 and 35 mm, and one DS measurement with two sets of 25 and 35 mm source-detector distances (**Figure 1A**). In the NCCU, FD-NIRS measurements were done using a second commercial system (OxiplexTs, ISS Inc., Champaign, IL; wavelengths: 690 and 830 nm; modulation frequency: 110 MHz) operating at a data acquisition rate of 12.5 Hz. The optical probe was also placed on the right side of the patient's forehead. The probe consisted of one detector fiber bundle and four separate source fiber pairs, with source-detector distances of 20, 25, 30, and 35 mm (**Figure 1C**). The optical system was calibrated using a phantom of known optical properties, allowing for absolute measurements of tissue optical properties.

In both experiments on healthy subjects and in the NCCU, two pneumatic thigh cuffs were wrapped around the subject's thighs and were connected to an automatic cuff inflation system (E-20 Rapid Cuff Inflation System, D.E. Hokanson, Inc., Bellevue, WA). The air pressure in the thigh cuffs was monitored by a digital manometer (Series 626 Pressure Transmitter, Dwyer Instruments, Inc., Michigan City, IN). The maximum pressure was set to be above systolic blood pressure, specifically to 200 mmHg for healthy subjects, and between 150 and 180 mmHg (reported in **Table 1**) for the NCCU patients. This value was dependent on individual blood pressure and physician's recommendation. Inflation of the pneumatic thigh cuffs was done smoothly to maximum pressure and took approximately 1 s for healthy subjects and approximately 4 s for NCCU subjects. Previous work (not reported) has shown no effect on results due to inflation times.

In the experiment on healthy subjects, the subject breathed through a facemask (AFT25, BIOPAC Systems, Inc., Goleta, CA) medical air (21% O_2, 79% N_2) for 7 min (normocapnic baseline), 5% CO_2 mixed with 21% O_2 and balanced N_2 (5% CO_2, 21% O_2, 74% N_2) for 3 min (hypercapnic interval), and then medical air for 5 min of recovery. The setup for the normocapnia-hypercapnia experiment on healthy subjects was described elsewhere in detail (43). An end-tidal carbon dioxide pressure ($P_{ET}CO_2$) signal was collected by using an infrared-based CO_2 monitor module (CO2100C, BIOPAC Systems, Inc., Goleta, CA) connected to the facemask. The thigh cuff oscillations were performed at a frequency of 0.066 Hz for 1.5 min during the normocapnic baseline and during the second half of the hypercapnia interval. The experimental setup for healthy subjects is shown in **Figure 1B**. In the NCCU, the experimental protocol consisted of 5 min of baseline, 2 min of thigh cuff oscillations at a frequency of 0.063 Hz, and 5 min of recovery (44). The patients were assumed to be in a normocapnic state as they were either independently breathing room air (patient 2) or on ventilator support (patients 1 and 3). The experimental setup for NCCU patients is shown in **Figure 1D**.

In all the experiments, continuous ABP was monitored with a finger plethysmography system (NIBP100D, BIOPAC Systems, Goleta, CA). Analog outputs of the ABP monitor, the pneumatic thigh cuff manometer, and the $P_{ET}CO_2$ monitor (in the case of

TABLE 1 | Summary of patient information from neurocritical care unit.

Patient	Age	Sex	Cuff Pressure (mmHg)	ICP (mmHg)	MAP (mmHg)	CPP (mmHg)	Clinical diagnosis
1	61	M	180	12 [11,14]	82 [80, 84]	69 [66,73]	Left basal ganglia hemorrhage extending out to subcortical and parietal area, cerebral edema, ventricular effacement
2	67	M	150	0 [−1,1]	81 [79,85]	81 [78,85]	Isolated IVH of unclear etiology with no apparent brain tissue injury, Hydrocephalus
3	17	F	170	10 [10,11]	73 [68,77]	63 [58,67]	Left occipital AVM with IVH, AVM involves posterior circulation

Values are reported as median [25%, 75% quartiles] over the entire experimental time trace.
M, Male; F, Female; ICP, Intracranial pressure; MAP, Mean arterial pressure; CPP, Cerebral perfusion pressure; IVH, Intraventricular Hemorrhage; AVM, Arteriovenous Malformation.

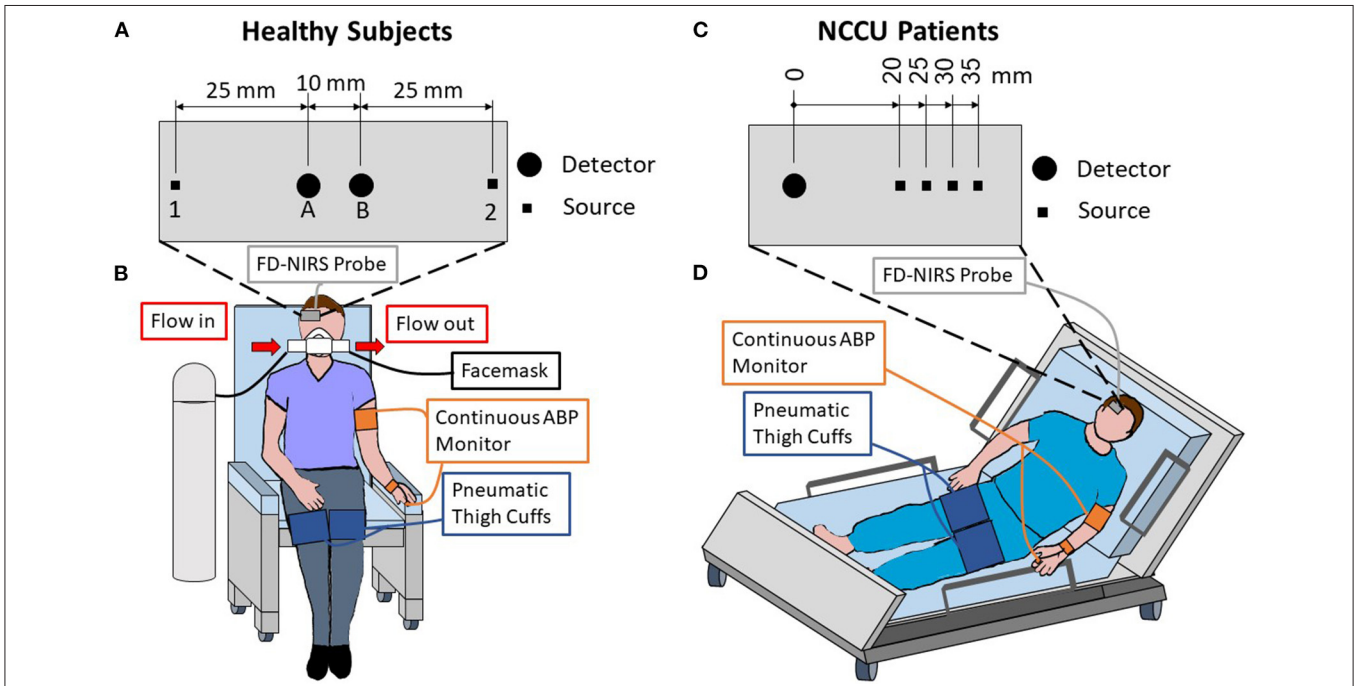

FIGURE 1 | Experimental setup and schematic diagrams of the optical probes used for healthy subjects **(A,B)** and patients in the neurocritical care unit (NCCU; **C,D**). For the healthy subjects, the optical probe was placed on the right side of the forehead and included two sources [1 & 2] and two detectors [A & B] that are symmetrical about the midline of the two sources **(A)**. The probe featured two single-distance (SD) measurements at 35 mm source-detector distances [1B & 2A], two single-slope (SS) measurements with 25 and 35 mm distances [1AB & 2BA], and one dual-slope (DS) measurement with two 25 mm and two 35 mm distances [1AB2]. For the NCCU patients, the optical probe was placed on the right side of the forehead, it featured four source-detector distances of 20, 25, 30, and 35 mm **(C)** in a multi-distance configuration. Both setups included an optical probe, finger plethysmograph to monitor arterial blood pressure (ABP), and pneumatic thigh cuffs wrapped around both thighs **(B,D)**. During the healthy subject experiment **(B)**, a facemask was worn to breath either medical air or 5% CO_2 mixed with 21% O_2 and balanced N_2.

healthy subject experiments) were fed to auxiliary inputs of the FD-NIRS instrument for concurrent recordings with the optical data at the same acquisition rate. In the NCCU, intracranial pressure (ICP) from an invasive ICP probe was recorded continuously during each experiment via an Philips Intellivue monitor (Philips Medical Systems, Eindhoven, the Netherlands) and synced to the optical data. The mean arterial pressure (MAP) was calculated from the non-invasive ABP measurements as a weighted average of systolic and diastolic ABP as MAP = [systolic blood pressure+(2 × diastolic blood pressure)]/3. These two metrics were used to calculate cerebral perfusion pressure (CPP), which is computed as CPP = MAP − ICP for every time

point. **Table 1** reports the median value over the experiment with their respective 25% and 75% quartiles for ICP, MAP, and CPP.

2.3. Data Processing

2.3.1. Measurements of Absolute and Relative Hemoglobin Concentrations

During the initial baseline periods, average absolute oxy-, deoxy-, and total-hemoglobin concentrations (O_0, D_0, and $T_0 = O_0 + D_0$, respectively, with subscript "0" indicating average baseline values) were computed. Specifically, these absolute hemoglobin concentration values were obtained from average baseline absorption coefficients ($\mu_{a,0}$) at two wavelengths (690 and 830 nm) by using known extinction coefficients (45) and an assumed water content of 70% by volume (46). Tissue optical properties at baseline, namely $\mu_{a,0}$ and the reduced scattering coefficient ($\mu'_{s,0}$), were obtained at the two wavelengths using either the self-calibrating method (33) on data from healthy subjects or the calibrated multi-distance method (31) on data from the NCCU patients. Both methods were applied with an iterative approach on the NIRS intensity I and phase ϕ data collected at baseline. A full description of this iterative technique can be found in (47).

Relative changes in hemoglobin concentrations with respect to baseline [$\Delta O(t)$, $\Delta D(t)$, $\Delta T(t) = \Delta O(t) + \Delta D(t)$] were obtained from relative changes in absorption, $\Delta\mu_a(t)$, at two wavelengths. Here, we calculated $\Delta\mu_a(t)$ by using three different configurations (SD, SS, and DS) and two data types (I and ϕ data). SDI and SDϕ measurements refer to the I and ϕ data, respectively, collected by a single source-detector pair. SSI and SSϕ refer to the linear dependence of an I-based function ($\ln[\frac{\rho^2 I}{\sqrt{3\mu_a\mu'_s}+1/\rho}]$) and ϕ on source-detector distance ρ, respectively (43). $\Delta\mu_a$ from SDI and SDϕ were found by using the differential pathlength factors (DPF: DPF_I for I and DPF_ϕ for ϕ), and from SSI and SSϕ by using the differential slope factors (DSF: DSF_I for I and DSF_ϕ for ϕ). The expressions of DPF and DSF were described in detail elsewhere (18), and require the measurements of optical properties at baseline $\mu_{a,0}$ and $\mu'_{s,0}$. DS measurements for I or ϕ can be obtained by taking the average of the two symmetrical SS measurements. With the probe configuration used in the two experiments (**Figure 1**), we reported measurements from two SDI and two SDϕ at 35 mm source-detector distances, two SSI at 25 and 35 mm source-detector distances, one DSI, and one DSϕ for healthy subjects; and measurements from one SDI, one SDϕ at 35 mm, and one SSI measurement at 25 and 35 mm source-detector distances for NCCU patients. SSϕ measurements were not reported in this study due to a poor signal-to-noise ratio (18).

Figure 2 shows typical experimental time traces for a representative healthy subject (subject 1) and a representative NCCU patient (patient 2). The signals include: the recorded pneumatic thigh cuff pressure (P_{CUFF}), $P_{ET}CO_2$ (for the healthy subject), ABP, and time traces of ΔO and ΔD obtained with different data analysis methods.

2.3.2. Wavelet Analysis of Phasor Ratios

We performed transfer function analysis using Wavelet coherence and phasor analysis to determine the phase differences and amplitude ratios of the coherent hemodynamic oscillations (i.e., oscillations in O, D, T) vs. ABP oscillations within the interval of the thigh cuff inflation-deflation oscillations. The processing steps were the same for both healthy subjects and NCCU patients. These analyses were described in references (20, 38) and are summarized here.

Briefly, a continuous wavelet transform with complex Morlet mother wavelet was used to get two-dimensional phasor maps of $\mathbf{D}(t,\omega)$, $\mathbf{O}(t,\omega)$, $\mathbf{T}(t,\omega)$, and $\mathbf{ABP}(t,\omega)$, as functions of time (t) and frequency (ω). Note that we use bold-face notations to indicate phasor values. From these phasor maps, we computed the phasor ratio maps of $\frac{\mathbf{D}(t,\omega)}{\mathbf{ABP}(t,\omega)}$, $\frac{\mathbf{O}(t,\omega)}{\mathbf{ABP}(t,\omega)}$, and $\frac{\mathbf{T}(t,\omega)}{\mathbf{ABP}(t,\omega)}$. The phasor ratio maps refer to the dynamic relationship between oscillations of hemoglobin concentrations and ABP(t) at time t and angular frequency ω. Along with the phasor ratio maps, two-dimensional wavelet coherence maps between two signals (O vs. ABP, D vs. ABP, and T vs. ABP) were also computed. A measure of coherence defines coupling between one signal (ABP) and another [$O(t)$, $D(t)$, or $T(t)$]. A high coherence value (closer to 1) can be used to ensure the validity of phase and amplitude estimations of the phasor ratios (8, 13). We applied a map of coherence threshold values on each corresponding coherence map, and only considered the corresponding time-frequency pixels in the phasor ratio maps with coherence that passed the threshold (significantly high coherence) for further analysis. The coherence threshold map was generated from random surrogate data (48, 49) at a significance level of $\alpha = 0.05$. For the phasor ratio $\frac{\mathbf{D}(t,\omega)}{\mathbf{O}(t,\omega)}$, we used the regions in the time-frequency space with significantly high coherence for both O vs. ABP and D vs. ABP.

After applying the coherence threshold, we only considered the average phasor ratios **D/ABP**, **O/ABP**, **T/ABP**, and **D/O** with significantly high coherence within the time intervals of the thigh cuff oscillation and a frequency band centered at the central frequency of the induced oscillation. The central frequency was 0.066 Hz for the healthy subject data and 0.063 Hz for the NCCU patient data. The bandwidth of the frequency band was determined by the half power bandwidth of a simulated test sinusoidal signal, which resulted in six frequency bands in the range of 0.059–0.079 Hz for the healthy subject data, and five frequency bands in the range of 0.055–0.074 Hz for the NCCU patient data. Further criteria required to include an individual phasor sample in the average were that the region of interest consisted of continuous coherence longer than one period of the oscillation at the central frequency and at least two continuous frequency bands (where one is the central frequency). The argument of the phasor ratio represents the phase difference between the two phasors, and the magnitude represents the amplitude ratio of the two phasors. We used standard statistics and circular statistics (50) for the calculation of the mean and standard deviation of amplitudes and phase angles, respectively, within the induced oscillation interval with significantly high coherence. Standard errors of the measurements were calculated by dividing

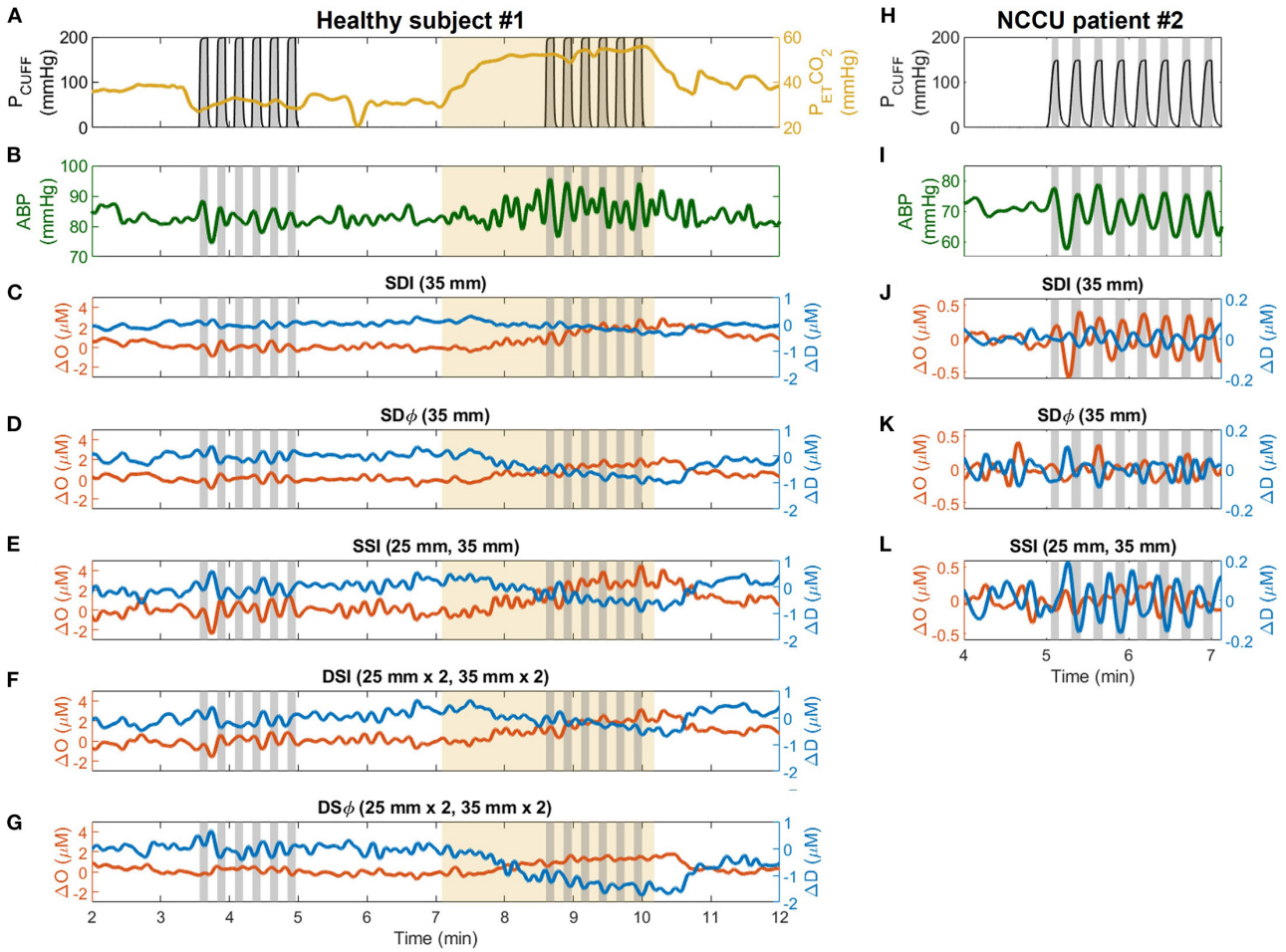

FIGURE 2 | Representative time traces collected during the experiment on healthy subjects (subject 1, *left* column) and patients in the neurocritical care unit (NCCU) (patient 2, *right* column). For the healthy subject, signals are shown for pneumatic thigh cuff pressure (P_{CUFF}, *black*, **A**), end-tidal carbon dioxide pressure ($P_{ET}CO_2$, *yellow*, **A**), arterial blood pressure (ABP, *green*, **B**), and changes in oxyhemoglobin (ΔO, *red*) and deoxyhemoglobin (ΔD, *blue*) measured with single-distance intensity (SDI 2A, 35 mm, **C**), single-distance phase (SDϕ 2A, 35 mm, **D**), single-slope intensity (SSI 1AB, 25 and 35 mm, **E**), dual-slope intensity (DSI 1AB2, 25 and 35 mm, **F**), and dual-slope phase (DSϕ 1AB2, 25 and 35 mm, **G**). For the NCCU patient, signals are shown for P_{CUFF} **(H)**, ABP **(I)**, and for ΔO and ΔD measured with SDI (35 mm, **J**), SDϕ (35 mm, **K**), and SSI (25 and 35 mm, **L**). Gray shaded areas indicate the cuff inflation periods (from start of inflation to start of deflation). Thigh cuffs were inflated and deflated at a frequency of 0.066 Hz for healthy subjects and at 0.063 Hz for NCCU patients. Yellow shaded areas indicate hypercapnic interval. ABP and optical signal traces are lowpass filtered to 0.1 Hz.

the standard deviations by the square root of number of independent observations, which was taken as the number of periods at the induced oscillation that passed the coherence threshold. This amplitude and phase analysis was applied to data collected with all the different analysis methods: SDI, SDϕ, SSI, DSI, and DSϕ for healthy subjects; SDI, SDϕ, and SSI for NCCU patients.

2.3.3. Hemodynamic Model to Determine the Relative Cerebral Blood Flow and Arterial Blood Pressure Dynamics

In the sample of healthy subjects, we applied the dynamic hemodynamic model of CHS introduced by Fantini (28) to calculate dynamic relationship between CBF and ABP. Specifically, the two-dimensional map of the phasor ratio $\frac{\mathbf{cbf}(t,\omega)}{\mathbf{abp}(t,\omega)}$ were obtained from the phasor ratio maps of $\frac{\mathbf{D}(t,\omega)}{\mathbf{ABP}(t,\omega)}$, $\frac{\mathbf{O}(t,\omega)}{\mathbf{ABP}(t,\omega)}$, and $\frac{\mathbf{T}(t,\omega)}{\mathbf{ABP}(t,\omega)}$ with significantly high coherence. Here, cbf and abp refer to normalized changes in CBF (in units of $mL_{blood}/100\ g_{tissue}/min$) and ABP, respectively, with respect to baseline values. The computation of the phasor ratio $\frac{\mathbf{cbf}(t,\omega)}{\mathbf{abp}(t,\omega)}$ by using the frequency-domain CHS model is described in detailed in the **Supplementary Material**. Briefly, the CHS model provides an analytical way to describe how NIRS measurements of hemoglobin concentrations O, D, and T are related to the effects of changes in blood volume in three microvascular compartments (arterial, capillary, venous) and the effects of changes in blood flow and metabolic rate of oxygen in the capillary and venous compartments. Under the

assumption of negligible changes in $CMRO_2$ during the dynamic oscillations, the CHS model can provide measurements of cbf from NIRS measurements of $O(t)$ and $D(t)$. Additional assumptions include negligible changes in capillary (c) blood volume $\mathrm{cbv}^{(c)}(t) = 0$ and equal arterial (a)-to-venous (v) dynamic CBV ratio $\frac{\mathbf{cbv}^{(a)}}{\mathbf{cbv}^{(v)}} = 1$. We assumed values for CHS model parameters such as capillary baseline CBV fraction $\frac{\mathcal{F}^{(c)}\mathrm{CBV}_0^{(c)}}{\mathrm{CBV}_0} = 0.4$, baseline arterial and venous CBV ratios as $\frac{\mathrm{CBV}_0^{(a)}}{\mathrm{CBV}_0} = \frac{\mathrm{CBV}_0^{(v)}}{\mathrm{CBV}_0} = 0.3$, capillary blood transit time $t^{(c)} = 1$ s, venous blood transit time $t^{(v)} = 5$ s, and rate constant of oxygen diffusion $\alpha = 0.8\ s^{-1}$ based on values from healthy human subjects (30). The calculation also requires the input of absolute baseline total-hemoglobin concentration T_0. Using the same method and criteria as described in section 2.3.2, we computed the average phasor ratio **cbf/abp** within the time interval of the thigh cuff oscillation and a frequency band centered at the central frequency of the induced oscillation.

2.4. Statistical Analysis

Statistical tests were used to assess the differences between normocapnia and hypercapnia for phase differences and amplitude ratios of **D** vs. **ABP**, **O** vs. **ABP**, **T** vs. **ABP**, **cbf** vs. **abp**, and **D** vs. **O**. Specifically, the one-sample test for angular mean (50) was applied to test if the mean paired phase difference values during hypercapnia and normocapnia (hypercapnia − normocapnia) is significantly less than 0° (one-tailed test). A paired t-test on a linear scale was applied on the amplitude ratios to test if the mean paired difference between the amplitude ratio values during normocapnia and hypercapnia is significantly different from 0 (two-tailed test). These statistical tests assume that the phase values follow a von Mises distribution (50), and the amplitude ratio values follow a normal distribution. A value of $p < 0.05$ was considered as significant.

3. RESULTS

3.1. Phase and Amplitude Relations in Healthy Controls: Normocapnia vs. Hypercapnia

From five healthy subjects, hypercapnia caused a significant increase in $P_{ET}CO_2$ from 37 ± 2 mmHg to 54 ± 1 mmHg (mean ± standard error, paired t-test $p = 0.001$). **Figure 3** displays box plots showing phase and amplitude measurements of **D/ABP**, **O/ABP**, **T/ABP**, **cbf/abp**, and **D/O** obtained from five healthy subjects during normocapnia and hypercapnia for different FD-NIRS methods (SDI, SDϕ, SSI, DSI, and DSϕ). The median values and the respective [25%, 75%] quartiles of the phase values for normocapnia and hypercapnia are reported in **Table 2**. Note that for every subject from this data set, two measurements of SD and two measurements of SS were reported.

In general, the results presented by **Figure 3** and **Table 2** show that the relative phase of **D** vs. **ABP** (**Figure 3A**), **O** vs. **ABP** (**Figure 3B**), and **cbf** vs. **abp** (**Figure 3D**) are sensitive to autoregulation efficiency in healthy subjects across all measurement methods. The amplitude ratios are generally insensitive to autoregulation in all measurement methods and parameters. For the phase relationships, we observe a sensitivity to cerebral dynamic autoregulation for the relative phase of **D** vs. **ABP** ($p < 0.02$), **O** vs. **ABP** ($p < 0.03$), and **cbf** vs. **abp** ($p < 0.01$). Specifically, from normocapnia to hypercapnia, the phase of **D** vs. **ABP** is reduced by ∼40° across all the methods, the phase of **O** vs. **ABP** is reduced by ∼30°, and the phase of **cbf** vs. **abp** is reduced by ∼25°. On the other hand, the relative phase of **T** vs. **ABP** shows significance for only two methods (SDϕ and DSI, $p = 0.02$ and 0.04, respectively) with the others showing no significant phase difference (remaining measurement methods, $p > 0.09$) to a hypercapnia-induced change in cerebral autoregulation.

While both ∠**D/ABP** and ∠**O/ABP** indicate a significant change in response to a change in cerebral autoregulation efficiency in healthy subjects, **D/ABP** displayed a larger average change in phase in three of the five methods compared to **O/ABP** (**Table 2**). Statistically, the phase change in ∠**D/ABP** between normocapnia and hypercapnia is significantly greater than the phase change in ∠**O/ABP** ($p = 0.02$). This suggests that D oscillations could be a stronger indicator of dynamic cerebral autoregulation compared to O oscillations. Oscillations of D and O during normocapnia and hypercapnia had a mean phase difference of approximately −180° to −250°, indicating a counterphase relationship. For **D/O**, only measurements from I showed a significant reduction in phase from normocapnia to hypercapnia (SDI, SSI, and DSI; $p < 0.03$), while ϕ measurements showed no significant change to a change in cerebral autoregulation efficiency (SDϕ, $p = 0.4$; DSϕ, $p = 0.5$).

Finally, all the measurement methods (SDI, SDϕ, SSI, DSI, DSϕ) are sensitive to cerebral autoregulation changes as measured by ∠**O/ABP**, ∠**D/ABP**, and ∠**cbf/abp**, with $p \leq 0.03$ for all methods and parameters as shown in **Table 2**. Statistical tests show no significant difference between DSI and DSϕ in the phase change from normocapnia to hypercapnia for ∠**O/ABP**, ∠**D/ABP**, and ∠**cbf/abp** ($p > 0.1$). Between SDI and SDϕ, only ∠**O/ABP** shows a significant difference in the normocapnia-hypercapnia phase changes ($p = 0.009$), while other parameters show no significant difference ($p > 0.05$).

3.2. Phase Relations in NCCU Patients

Figure 4 reports the relative phase of **D** vs. **ABP** (**Figure 4A**) and **O** vs. **ABP** (**Figure 4B**) for the three NCCU patients. Results are shown for SDI 35 mm, SDϕ 35 mm, and SSI 25 and 35 mm. The reason for reporting the relative phases of **D** vs. **ABP** and **O** vs. **ABP** for NCCU patients (**Figure 4**) is that the results on healthy subjects (**Figure 3**) showed them to be most sensitive to autoregulation changes, more so than the relative phases of **T** vs. **ABP** and **D** vs. **O**, and any amplitude ratios. We also opted to not report the phase of **cbf** vs. **abp** in NCCU patients because of the need to assume values of hemodynamic parameters (capillary and venous blood transit times, partial blood volume in the arterial, capillary, and venous compartments, etc.) that are expected to be more variable in NCCU patients than in healthy subjects.

It should be noted that the results of **Figure 4** allow for a patient by patient comparison, but the number of patients (three)

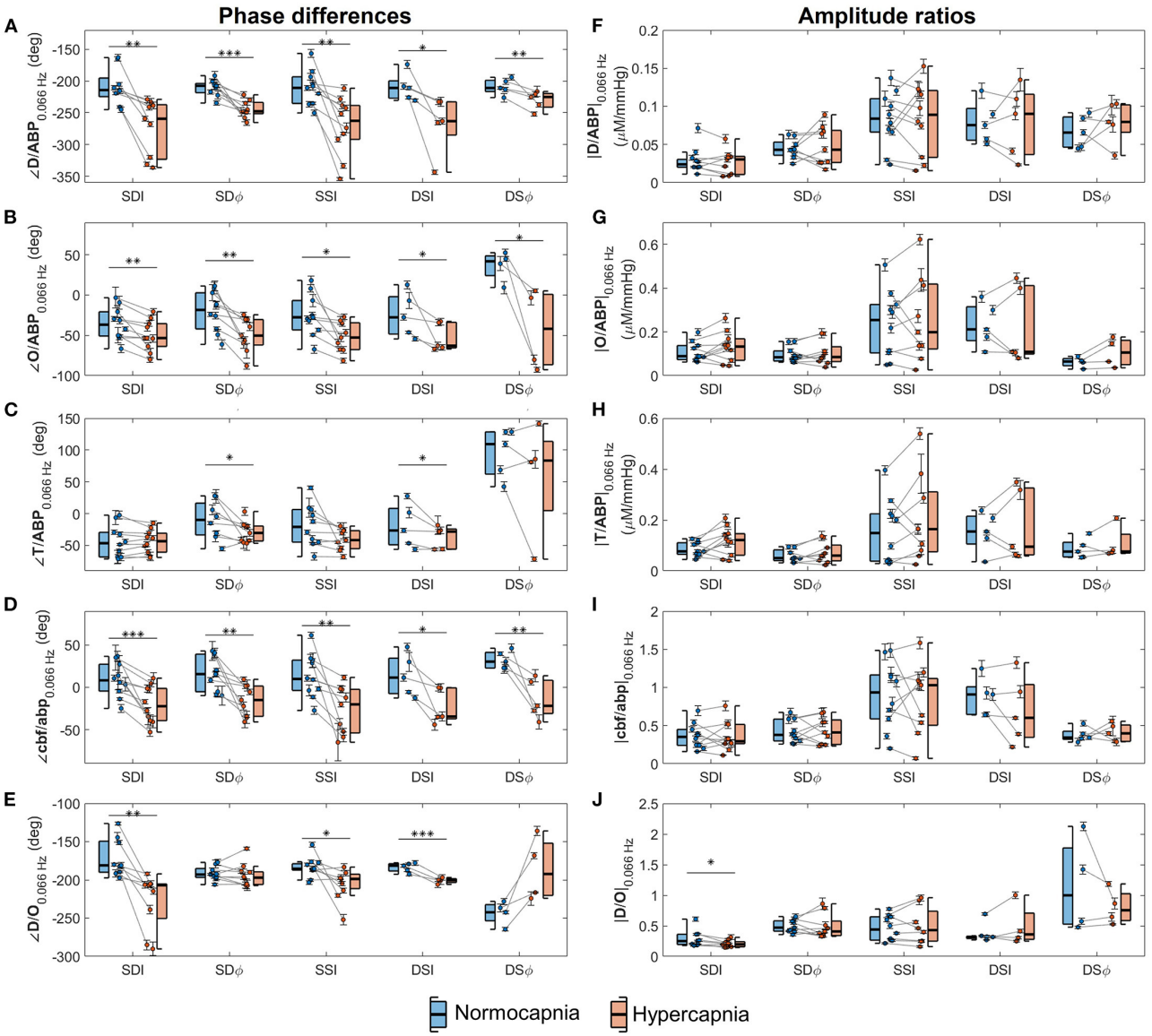

FIGURE 3 | Box plots depicting average phase differences (*left* column) and amplitude ratios (*right* column) of phasors of deoxyhemoglobin (**D**) vs. phasors of arterial blood pressure (**ABP**) (panels **A,F**), oxyhemoglobin (**O**) vs. **ABP** (panels **B,G**), total hemoglobin (**T**) vs. **ABP** (panels **C,H**), normalized cerebral blood flow (**cbf**) vs. normalized arterial blood pressure (**abp**) (panels **D,I**), and **D** vs. **O** (panels **E,J**) at 0.066 Hz. Boxes are shown for normocapnia (*blue*) and hypercapnia (*red*). On each box, the central line is the median, the edges are the 25 and 75% quartiles, and the whiskers indicate the most extreme data points excluding outliers. Circles indicate individual measurements, and error bars represent the standard errors of the measurements. Each *gray* line connects normocapnic and hypercapnic data points from the same measurement session. Horizontal lines (*black*) indicate comparison between normocapnia and hypercapnia by means of statistical tests and corresponding *p*-values are denoted (*$p < 0.05$; **$p < 0.01$; ***$p < 0.001$).

is too small to draw general conclusions. Additionally, we are lacking an independent measurement of cerebral autoregulation in each subject, and cannot make a definite statement on reproducibility among trials in individual patients due to lack of clean data for all three patients. Patients 1 and 3 had high quality data for only 1 day and trial, whereas patient 2 had multiple trials with acceptable data quality in a given day. The inter-trial variability of the relative phase of **D** vs. **ABP** in patient 2 was smaller than the inter-patient differences reported in **Figure 4A**. However, more work needs to be done to better characterize intra-patient and inter-patient variability in these non-invasive optical measurements of cerebral hemodynamics. Nevertheless, these results allow us to report the technical feasibility of NIRS measurements of cerebral oscillatory hemodynamics that are coherent with ABP. Furthermore, the measurements on healthy subjects during normocapnia and hypercapnia provide a key reference to read and interpret the results observed in the NCCU patients in relation to different levels of cerebral autoregulation.

TABLE 2 | Values of the phase differences of phasors of deoxyhemoglobin (**D**) vs. arterial blood pressure (**ABP**), oxyhemoglobin (**O**) vs. **ABP**, total hemoglobin (**T**) vs. **ABP**, normalized cerebral blood flow (**cbf**) vs. normalized arterial blood pressure (**abp**), and **D** vs. **O** during normocapnia and hypercapnia.

		Phase difference (°)						
		Normocapnia (NC)		Hypercapnia (HC)		HC − NC	*p*-values	
∠**D**/**ABP**	SDI	−214	[−225, −195]	−259	[−323, −237]	−50 ± 33	0.003**	($n = 8$)
	SDϕ	−208	[−219, −204]	−248	[−252, −234]	−34 ± 19	0.0003***	($n = 9$)
	SSI	−211	[−235, −193]	−263	[−292, −239]	−59 ± 41	0.001**	($n = 10$)
	DSI	−211	[−227, −200]	−263	[−285, −233]	−56 ± 38	0.02*	($n = 5$)
	DSϕ	−211	[−217, −199]	−225	[−241, −220]	−21 ± 12	0.005**	($n = 5$)
∠**O**/**ABP**	SDI	−37	[−51, −21]	−53	[−64, −36]	−14 ± 12	0.001**	($n = 10$)
	SDϕ	−18	[−42, 3]	−50	[−62, −30]	−33 ± 23	0.002**	($n = 9$)
	SSI	−28	[−43, −7]	−53	[−68, −34]	−26 ± 26	0.02*	($n = 9$)
	DSI	−28	[−48, −2]	−63	[−66, −34]	−27 ± 24	0.03*	($n = 5$)
	DSϕ	42	[24, 49]	−42	[−87, 1]	−78 ± 38	0.01*	($n = 4$)
∠**T**/**ABP**	SDI	−47	[−68, −30]	−43	[−61, −31]	−1 ± 8	0.4	($n = 10$)
	SDϕ	−10	[−34, 17]	−30	[−43, −19]	−22 ± 26	0.02*	($n = 8$)
	SSI	−21	[−45, 7]	−42	[−55, −27]	−17 ± 27	0.09	($n = 9$)
	DSI	−27	[−49, 8]	−28	[−56, −24]	−17 ± 17	0.04*	($n = 5$)
	DSϕ	109	[62, 129]	83	[5, 114]	−20 ± 49	0.2	($n = 5$)
∠**cbf**/**abp**	SDI	8	[−4, 27]	−22	[−39, 1]	−29 ± 19	0.0006***	($n = 10$)
	SDϕ	16	[−5, 39]	−15	[−34, 2]	−34 ± 26	0.006**	($n = 9$)
	SSI	10	[−4, 32]	−20	[−54, −2]	−40 ± 34	0.006**	($n = 9$)
	DSI	12	[−7, 34]	−34	[−37, −1]	−36 ± 24	0.01*	($n = 5$)
	DSϕ	30	[23, 41]	−22	[−31, 8]	−46 ± 24	0.006**	($n = 5$)
∠**D**/**O**	SDI	−181	[−190, −149]	−207	[−250, −205]	−44 ± 30	0.004**	($n = 8$)
	SDϕ	−193	[−197, −185]	−197	[−206, −189]	−1 ± 9	0.4	($n = 9$)
	SSI	−186	[−187, −179]	−199	[−212, −193]	−26 ± 26	0.03*	($n = 8$)
	DSI	−181	[−189, −179]	−201	[−203, −199]	−16 ± 5	0.0007***	($n = 4$)
	DSϕ	−242	[−254, −232]	−192	[−220, −152]	56 ± 31	0.5	($n = 4$)

*Values are reported as median [25%, 75% quartiles] for phase measurements at normocapnia and hypercapnia. The differences in the phase values between hypercapnia and normocapnia are shown as means ± standard deviations. p-values from statistical test on angular means are shown and indicated in red color for significant values; * for $p < 0.05$; ** for $p < 0.01$; and *** for $p < 0.001$.*

Results on healthy subjects (**Figure 3A**) show that an impairment of cerebral autoregulation (during hypercapnia) results in a more negative relative phase of **D** vs. **ABP** as compared to normocapnia. In the NCCU patients (**Figure 4A**), we observe a less negative phase of **D** vs. **ABP** (with all measurements: SDI, SDϕ, SSI) in patient 2 compared to patients 1 and 3, suggesting a better autoregulation in patient 2. The phase between **O** and **ABP** also became more negative with impaired autoregulation in healthy subjects (as shown in **Figure 3B**). The results for the relative phase of **O** vs. **ABP** in the NCCU (**Figure 4B**) were not as clear as those for the relative phase of **D** vs. **ABP**, because of lack of some data (low coherence) for SDϕ patient 3 and SSI patient 2, and opposite results for SDI (more negative phase for patient 2) and SDϕ (less negative phase for patient 2). This result is in line with the smaller impact of autoregulation changes in the phase of **O** vs. **ABP** than **D** vs. **ABP** in the data from healthy subjects. This may be a consequence of incoherent hemodynamics contributions from the arterial compartment in scalp tissue.

4. DISCUSSION

This study showed that: (1) relative dynamics of cerebral *O* and *D* vs. ABP dynamics are sensitive to dynamic cerebral autoregulation changes between normocapnia and hypercapnia in healthy subjects, with the relative phase of **D** vs. **ABP** being the most sensitive indicator of cerebral autoregulation efficiency; (2) the relative phase of **D** vs. **ABP** measured in the oscillation protocol can be used in the NCCU to assess the degree of cerebral autoregulation in patients with brain injuries; (3) it is feasible to measure CBF-ABP dynamics by applying the CHS model on the blood-pressure-induced oscillations in cerebral *O* and *D* measured by FD-NIRS in healthy adult subjects; and (4) all the measurement methods (SDI, SDϕ, SSI, DSI, DSϕ) were found to have similar sensitivity to cerebral autoregulation changes for this specific protocol of hemodynamic oscillations.

The results from healthy subjects showed that both blood-pressure-induced *O* and *D* dynamics are sensitive to dynamic cerebral autoregulation, but the phase difference of **D** vs. **ABP** showed stronger sensitivity to the cerebral autoregulation

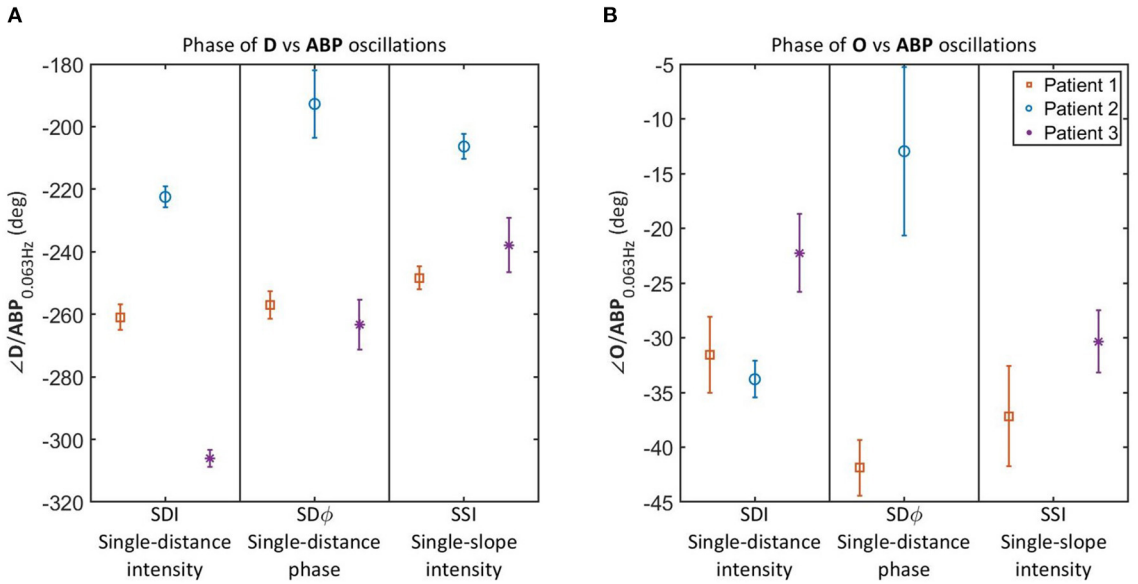

FIGURE 4 | Relative phase of **D** vs. **ABP (A)** and **O** vs. **ABP (B)** for oscillations at 0.063 Hz in 3 NCCU patients measured with single-distance intensity (SDI), single-distance phase (SDϕ), and single-slope intensity (SSI). Color and marker style are consistent for each subject. Error bars represent the standard errors of the measurements. Data for SDϕ in patient 3 and SSI in patient 2 are missing due to a coherence level below the threshold.

changes between normocapnia and hypercapnia than **O** vs. **ABP**. We have shown that these results were consistent across different measurements within five healthy subjects. These results are somewhat in line with the NCCU patients results that suggest *D* oscillations as more robust than *O* oscillations for the assessment of cerebral autoregulation in the NCCU. Many studies in the literature have used *O* oscillations or the **O**-**ABP** phase difference to assess dynamic cerebral autoregulation, mostly because *O* changes are sensitive to all vascular compartments while *D* changes are more sensitive to the venous compartment (23). On the other hand, the results from NCCU patients in our study are consistent with the results from (10), who reported a significant change in the phase difference of **D** vs. **ABP** and no significant change in the phase difference of **O** vs. **ABP** between healthy controls (i.e., intact cerebral autoregulation) and the affected hemisphere of patients with unicarotid stenosis (i.e., impaired cerebral autoregulation). This observation may result from the fact that *O* and *D* are impacted to a similar extent by blood flow changes, whereas *O* is impacted to a greater extent by blood volume changes than *D*. Specifically, *O* is affected by blood volume changes in all vascular compartments, while *D* is mostly affected by blood volume changes in the capillaries and venous compartment. Our results on healthy subjects have shown that the phase of CBF oscillations is sensitive to cerebral autoregulation efficiency, while CBV (or *T*) oscillations do not exhibit significant changes between normocapnia and hypercapnia. This could explain the observation that *D* oscillations are more sensitive to cerebral autoregulation changes than *O* oscillations. Furthermore, it has been observed that NIRS measurements of task-evoked *O* changes measured non-invasively with NIRS correlate more closely than *D* changes with extracerebral functional magnetic resonance imaging (fMRI) signals (51–53), and that scalp tissue has poorer cerebral autoregulation efficiency than in the brain (54).

The pilot clinical study on NCCU patients demonstrated the proof of concept and technical feasibility of applying a protocol involving induced oscillations in ABP and associated coherent cerebral hemodynamics oscillations in a clinical settings. The non-invasive measurement of these coherent cerebral hemodynamics with FD-NIRS techniques, in conjunction with well-defined criteria for the required levels of coherence with ABP, allows for the measurement of quantities that are sensitive to the degree of dynamic cerebral autoregulation. The representative results reported here on three NCCU patients suggest better cerebral autoregulation conditions for patient 2 compared to patients 1 and 3 based on the relative phase of **D** vs. **ABP**. The values of the relative phase of **D** vs. **ABP** for patient 2 are also within the range observed in healthy subjects (-222° to -192° across methods for patient 2, and -214° to -208° for healthy subjects). This is bolstered by the fact that patient 2 recorded the lowest ICP value and highest CPP value over the time of the trial compared to the other two patients, as reported in **Table 1**. A higher ICP value is associated with decreased intracranial compliance, which can lead to lower CPP (55). Clinically, this could be a manifestation of poor cerebral autoregulation (4) resulting in reduced CBF (56). Higher ICP values in patients with a traumatic brain injury have previously been shown to be associated with poorer dynamic autoregulation (14), which alludes to the potential for

patient 2 to have better autoregulation compared to the other two patients. The clinical diagnosis between patients (**Table 1**) indicates that patient 2 had no apparent brain injury and had an intraventricular hemorrhage that caused an obstruction of cerebral spinal fluid (CSF) flow. On the other hand, patient 1 had a large hemorrhage in the left frontal and parietal lobes, and patient 3 had a left occipital hemorrhage, both of these causing a larger brain injury than in patient 2. This larger brain damage in patients 1 and 3 as compared to patient 2 can potentially explain the results seen.

Oscillations in cerebral *O* and *D* as measured by FD-NIRS are the result of oscillations in blood flow and blood volume in the investigated tissue. One significant result of this study on healthy subjects is that we were able to show the feasibility of measuring CBF dynamics from *O* and *D* measurements by using the CHS model, and that the results have demonstrated the sensitivity of the **cbf**-**abp** dynamic relationship on cerebral autoregulation differences during normocapnia and hypercapnia in all of the measurement methods with FD-NIRS. We have also shown that the changes in cerebral *T* represent changes in local blood volume that are insensitive to cerebral autoregulation. This is consistent with (10). In this study, we did not report **cbf** vs. **abp** for NCCU patients since the absolute phase values depend on the assumption of parameter values for the CHS model. We also notice that the reported range of normocapnic phase difference of **cbf** vs. **abp** from healthy subjects (about 8° to 30°) is lower than the expected value of 40° (interquartile range of 30°) as measured by TCD for a frequency range of 0.02–0.07 Hz (8). The phase difference of **cbf** vs. **abp** depends on the assumption of model parameters. For instance, an increase in $t^{(c)}$ from 0.4 to 1 s can cause an increase in the relative phase of **cbf** vs. **abp** by about 10°, and an increase in $t^{(v)}$ from 3 to 7 s can increase the relative phase by up to 20°. However, we note that the relative phase difference between normocapnia and hypercapnia of **cbf** vs. **abp** is less affected by the parameter values assumptions. For example, this relative phase difference only changes by less than 5° and 1° with an increase in $t^{(c)}$ from 0.4 to 1 s and $t^{(v)}$ from 3 to 7 s, respectively. Future studies may include adding induced ABP oscillations at various frequencies (44, 57) or adding a transient change in ABP (30) to find individual values of CHS model parameters. In fact, we have previously demonstrated that the fitting procedure of CHS model at various frequencies to calculate CHS parameters are feasible for applications in the NCCU (44).

The relationship between cerebral **D** and **O** during normocapnia and during impaired autoregulation induced by hypercapnia was also investigated. Many previous studies have considered the phase difference between *D* and *O* oscillations measured by SDI as an indication of cerebral autoregulation (10, 19, 20). In this study, we have shown that different behaviors were observed for **D**/**O** measurements with SDI, SDϕ and DSϕ. Thus, using the dynamic phase relationship between **D** and **O** to interpret cerebral autoregulation may be misleading since the results depend on the measurement method. One possible explanation, at least for the protocol of hypercapnia and normocapnia on healthy subjects considered here, is that **D**/**O** results from the interplay of **O** and **D**, which may feature different sensitivities to hypercapnic-induced vascular hemodynamics in extracerebral and cerebral tissue.

Finally, all the measurement methods (SDI, SDϕ, SSI, DSI, DSϕ) were found to be sensitive to cerebral autoregulation changes as measured by **D**/**ABP** and **cbf**/**abp**. This result may suggest a similar performance of different FD-NIRS measurement methods for sensing autoregulation efficiency in the brain. However, systemic ABP oscillations can induce changes both in blood flow and blood volume of both cerebral and extracerebral tissue. This makes it difficult to interpret the measured quantity without fully understanding the blood volume dynamics in the scalp and the brain. One may notice that the DSϕ measurement of the phase difference of **T** vs. **ABP** at normocapnia is different from other measurement methods, having a positive phase. This may tell us that this measurement is sensitive to different dynamics of blood volume compared to other methods. Finally, a greater sensitivity to deeper tissue (compared to superficial tissue) has been demonstrated for the slope measurements, especially for DSϕ, in a homogeneous tissue setting (18, 38), but the situation can be more complicated in the presence of tissue heterogeneity and different scalp/skull anatomy of the subjects (43). We also stress that the SSϕ data was not reported in both healthy subjects and NCCU patients due to poor signal-to-noise ratio of the phase measurements, particularly in the SS configuration. The application of DSϕ holds promise as it is less affected by noise than SSϕ and largely insensitive to optical couplings and motion artifacts (18).

The results reported in this study are limited by the small sample size of NCCU patients. Due to this, we could not draw any statistical conclusions from the NCCU study but use this data set to show that the collection and processing techniques applied on healthy subjects is applicable outside of the laboratory setting. The major limitation of this approach is that it relies on the need to induce oscillations in blood pressure that have significant coherence with hemodynamic signals. In the NCCU, the thigh cuff occlusions may cause discomfort, and may not be applicable in obese patients. An alternative approach is to use spontaneous oscillations, but the high coherence between hemoglobin concentrations and blood pressure are not usually guaranteed. The second limitation is the requirement of CHS model parameters to calculate **cbf**(ω). In this study, we assumed values for the CHS parameters for healthy controls based on reported range (30). However, for NCCU patients whose physiological conditions are significantly different from healthy subjects, correct values for the model parameters are needed. This usually requires a complicated fitting procedure of CHS model to measurements obtained at multiple induced oscillation frequencies or with a transient change in ABP (30, 44, 57). Finally, subject's position and posture were different between the NCCU patients (lying down) vs. healthy subjects (sitting), which may have affected the variations in CBF dynamics (58, 59). Future studies will focus on the effects of the subject's position and different head of bed angle manipulation on our measurements of

cerebral autoregulation. We will also improve our experimental design by keeping consistent position between healthy controls and patients.

Given the vital role of cerebral blood flow and the importance of its regulation in response to changes in cerebral perfusion pressure, a safe, non-invasive, and reliable technique for the assessment of cerebral autoregulation would play an important role in clinical settings, and especially on patients with acute brain injuries (traumatic brain injury, aneurysmal subarachnoid hemorrhage, ischemic stroke, etc.). Changes in autoregulation and cerebrovascular reactivity is a known marker of injury severity and has the potential to guide therapeutics and patient care (60). The proposed technique, which is based on local optical measurement of cerebral hemodynamics that are driven by systemic variations in ABP, can be extended to spatial mapping of autoregulation. This is potentially important in the assessment of localized brain injuries associated with focal ischemic or hemorrhagic events. Even in cases where cerebral autoregulation is impaired in the entire brain, multiple local measurements may help reduce errors contributed by each individual measurement, thus enhancing reliability and minimizing inter-examiner variability. Future studies will aim to characterize the intra-subject variability of autoregulation measurements, which will serve as a basis for clinical studies on a larger patient population to assess the ability of this technique in determining the level of cerebral autoregulation in different pathological conditions.

5. CONCLUSION

In this study, we have shown that blood-pressure-induced oscillations in the cerebral concentrations of O and D measured by various FD-NIRS methods can be sensitive to cerebral autoregulation efficiency. These O and D measurements were translated into CBF dynamics by using the CHS model on healthy subjects, which is directly related to the measurements of dynamic cerebral autoregulation; we found these CBF dynamics to distinguish autoregulation efficiency between normocapnia and hypercapnia. Further investigations suggested that oscillations of O, and especially D, appeared to be more sensitive to the CBF dynamics than CBV dynamics. We have demonstrated the feasibility of measuring coherent D and ABP oscillations to assess autoregulation in the NCCU. Future studies will target a more complete characterization of the depth sensitivity of various data types of FD-NIRS measurements in heterogeneous tissue, especially in this protocol of systemic blood pressure oscillations, and applications to clinical scenarios with a larger sample size.

DATA AVAILABILITY STATEMENT

The raw data supporting the conclusions of this article will be made available by the authors, without undue reservation.

ETHICS STATEMENT

The studies involving human participants were reviewed and approved by Tufts University Institutional Review Board. Written informed consent to participate in this study was provided by the participant or the participants' legal guardian/next of kin.

AUTHOR CONTRIBUTIONS

TP: study design, data collection on healthy subjects, analysis, and interpretation of healthy subject data. CF: analysis and interpretation of neurocritical care unit data. TP and CF: writing the original draft of the manuscript. KT: study design and data collection in the neurocritical care unit. SF: overall conceptualization, funding acquisition, and project supervision. GB, AS, and SF: data interpretation and critical review of the manuscript. JK and SB: clinical feedback and critical review of the manuscript. JK and XC: clinical study design and patient recruitment. All authors contributed to the article and approved the submitted version.

FUNDING

This research was supported by the National Institutes of Health, Grant No. R01-NS095334. We also acknowledge support from the National Institutes of Health, Grant No. R21-EB020347, for the collection of data from patients in the neurological critical care unit. This study also received partial funding from the Neuroscience and Pain Research Unit at Pfizer, Inc. The funder was not involved in the study design, collection, analysis, interpretation of data, the writing of this article or the decision to submit it for publication.

ACKNOWLEDGMENTS

Some of the reported results in this paper for healthy subjects have appeared in a Ph.D. thesis (61).

SUPPLEMENTARY MATERIAL

The Supplementary Material for this article can be found online at: https://www.frontiersin.org/articles/10.3389/fneur.2021.745987/full#supplementary-material

REFERENCES

1. Rangel-Castilla L, Gasco J, Nauta HJ, Okonkwo DO, Robertson CS. Cerebral pressure autoregulation in traumatic brain injury. *Neurosurg Focus*. (2008) 25:E7. doi: 10.3171/FOC.2008.25.10.E7
2. Donnelly J, Budohoski KP, Smielewski P, Czosnyka M. Regulation of the cerebral circulation: bedside assessment and clinical implications. *Crit Care*. (2016) 20:1–17. doi: 10.1186/s13054-016-1293-6
3. Budohoski KP, Czosnyka M, Smielewski P, Kasprowicz M, Helmy A, Bulters D, et al. Impairment of cerebral autoregulation predicts delayed cerebral

ischemia after subarachnoid hemorrhage: a prospective observational study. *Stroke*. (2012) 43:3230–7. doi: 10.1161/STROKEAHA.112.669788
4. Nakagawa K, Serrador JM, LaRose SL, Sorond FA. Dynamic cerebral autoregulation after intracerebral hemorrhage: a case-control study. *BMC Neurol*. (2011) 11:108. doi: 10.1186/1471-2377-11-108
5. Lassen NA. Cerebral blood flow and oxygen consumption in man. *Physiol Rev*. (1959). 39:183–238. doi: 10.1152/physrev.1959.39.2.183
6. Aaslid R, Lindegaard KF, Sorteberg W, Nornes H. Cerebral autoregulation dynamics in humans. *Stroke*. (1989) 20:45–52. doi: 10.1161/01.STR.20.1.45
7. Panerai RB. Transcranial Doppler for evaluation of cerebral autoregulation. *Clin Auton Res*. (2009) 19:197–211. doi: 10.1007/s10286-009-0011-8
8. Placek MM, Wachel P, Iskander DR, Smielewski P, Uryga A, Mielczarek A, et al. Applying time-frequency analysis to assess cerebral autoregulation during hypercapnia. *PLoS ONE*. (2017) 12:e0181851. doi: 10.1371/journal.pone.0181851
9. Aaslid R, Blaha M, Sviri G, Douville CM, Newell DW. Asymmetric dynamic cerebral autoregulatory response to cyclic stimuli. *Stroke*. (2007) 38:1465–69. doi: 10.1161/STROKEAHA.106.473462
10. Reinhard M, Wehrle-Wieland E, Grabiak D, Roth M, Guschlbauer B, Timmer J, et al. Oscillatory cerebral hemodynamics - the macro- vs. microvascular level. *J Neurol Sci*. (2007) 250:103–9. doi: 10.1016/j.jns.2006.07.011
11. Reinhard M, Schumacher FK, Rutsch S, Oeinck M, Timmer J, Mader I, et al. Spatial mapping of dynamic cerebral autoregulation by multichannel near-infrared spectroscopy in high-grade carotid artery disease. *J Biomed Opt*. (2014) 19:1–9. doi: 10.1117/1.JBO.19.9.097005
12. Diehl RR, Linden D, Lucke D, Berlit P. Phase relationship between cerebral blood flow velocity and blood pressure. *Stroke*. (1995) 26:1801–4. doi: 10.1161/01.STR.26.10.1801
13. Claassen JAHR, Levine BD, Zhang R. Dynamic cerebral autoregulation during repeated squat-stand maneuvers. *J Appl Physiol*. (2009) 106:153–60. doi: 10.1152/japplphysiol.90822.2008
14. Panerai R, Hudson V, Fan L, Mahony P, Yeoman P, Hope T, et al. Assessment of dynamic cerebral autoregulation based on spontaneous fluctuations in arterial blood pressure and intracranial pressure. *Physiol Meas*. (2001) 23:59. doi: 10.1088/0967-3334/23/1/306
15. Sorrentino E, Budohoski KP, Kasprowicz M, Smielewski P, Matta B, Pickard JD, et al. Critical thresholds for transcranial Doppler indices of cerebral autoregulation in traumatic brain injury. *Neurocrit Care*. (2011) 14:188–93. doi: 10.1007/s12028-010-9492-5
16. Reinhard M, Roth M, Guschlbauer B, Harloff A, Timmer J, Czosnyka M, et al. Dynamic cerebral autoregulation in acute ischemic stroke assessed from spontaneous blood pressure fluctuations. *Stroke*. (2005) 36:1684–9. doi: 10.1161/01.STR.0000173183.36331.ee
17. Immink RV, Van Montfrans GA, Stam J, Karemaker JM, Diamant M, van Lieshout JJ. Dynamic cerebral autoregulation in acute lacunar and middle cerebral artery territory ischemic stroke. *Stroke*. (2005) 36:2595–600. doi: 10.1161/01.STR.0000189624.06836.03
18. Blaney G, Sassaroli A, Pham T, Fernandez C, Fantini S. Phase dual-slopes in frequency-domain near-infrared spectroscopy for enhanced sensitivity to brain tissue: First applications to human subjects. *J Biophotonics*. (2020) 13:e201960018. doi: 10.1002/jbio.201960018
19. Watanabe H, Shitara Y, Aoki Y, Inoue T, Tsuchida S, Takahashi N, et al. Hemoglobin phase of oxygenation and deoxygenation in early brain development measured using fNIRS. *Proc Natl Acad Sci USA*. (2017) 114:E1737–44. doi: 10.1073/pnas.1616866114
20. Khaksari K, Blaney G, Sassaroli A, Krishnamurthy N, Pham T, Fantini S. Depth dependence of coherent hemodynamics in the human head. *J Biomed Opt*. (2018) 23:1–9. doi: 10.1117/1.JBO.23.12.121615
21. Papademetriou MD, Tachtsidis I, Elwell CE, Elliot MJ, Hoskote A. Multichannel near infrared spectroscopy indicates regional variations in cerebral autoregulation in infants supported on extracorporeal membrane oxygenation. *J Biomed Opt*. (2012) 17:1–10. doi: 10.1117/1.JBO.17.6.067008
22. Rowley AB, Payne SJ, Tachtsidis I, Ebden MJ, Whiteley JP, Gavaghan DJ, et al. Synchronization between arterial blood pressure and cerebral oxyhaemoglobin concentration investigated by wavelet cross-correlation. *Physiol Meas*. (2007) 28:161–73. doi: 10.1088/0967-3334/28/2/005
23. Andersen A, Simonsen S, Schytz H, Iversen H. Assessing low-frequency oscillations in cerebrovascular diseases and related conditions with near-infrared spectroscopy: a plausible method for evaluating cerebral autoregulation? *Neurophotonics*. (2018) 5:1. doi: 10.1117/1.NPh.5.3.030901
24. Phillip D, Schytz H, Iversen H, Selb J, Boas D, Ashina M. Spontaneous low frequency oscillations in acute ischemic stroke–A near infrared spectroscopy (NIRS) study. *J Neurol Neurophysiol*. (2014) 5:1–5. doi: 10.4172/2155-9562.1000241
25. Tgavalekos K, Pham T, Krishnamurthy N, Sassaroli A, Fantini S. Frequency-resolved analysis of coherent oscillations of local cerebral blood volume, measured with near-infrared spectroscopy, and systemic arterial pressure in healthy human subjects. *PLoS ONE*. (2019) 14:e0211710. doi: 10.1371/journal.pone.0211710
26. Selb J, Wu KC, Sutin J, Farzam P, Bechek S, Shenoy A, et al. Prolonged monitoring of cerebral blood flow and autoregulation with diffuse correlation spectroscopy in neurocritical care patients. *Neurophotonics*. (2018) 5:045005. doi: 10.1117/1.NPh.5.4.045005
27. Zweifel C, Dias C, Smielewski P, Czosnyka M. Continuous time-domain monitoring of cerebral autoregulation in neurocritical care. *Med Eng Phys*. (2014) 36:638–45. doi: 10.1016/j.medengphy.2014.03.002
28. Fantini S. Dynamic model for the tissue concentration and oxygen saturation of hemoglobin in relation to blood volume, flow velocity, and oxygen consumption: Implications for functional neuroimaging and coherent hemodynamics spectroscopy (CHS). *Neuroimage*. (2014) 85:202–21. doi: 10.1016/j.neuroimage.2013.03.065
29. Kainerstorfer JM, Sassaroli A, Hallacoglu B, Pierro ML, Fantini S. Practical steps for applying a new dynamic model to near-infrared spectroscopy measurements of hemodynamic oscillations and transient changes: implications for cerebrovascular and functional brain studies. *Acad Radiol*. (2014) 21:185–96. doi: 10.1016/j.acra.2013.10.012
30. Pham T, Tgavalekos K, Sassaroli A, Blaney G, Fantini S. Quantitative measurements of cerebral blood flow with near-infrared spectroscopy. *Biomed Opt Express*. (2019) 10:2117–34. doi: 10.1364/BOE.10.002117
31. Fantini S, Franceschini MA, Fishkin JB, Barbieri B, Gratton E. Quantitative determination of the absorption spectra of chromophores in strongly scattering media: a light-emitting-diode based technique. *Appl Opt*. (1994). 33:5204–13. doi: 10.1364/AO.33.005204
32. Suzuki S, Takasaki S, Ozaki T, Kobayashi Y. Tissue oxygenation monitor using NIR spatially resolved spectroscopy. In: *Optical Tomography Spectroscopy of Tissue III*. San Jose, CA: International Society for Optics and Photonics (1999). p. 582–92. doi: 10.1117/12.356862
33. Hueber DM, Fantini S, Cerussi AE, Barbieri BB. New optical probe designs for absolute (self-calibrating) NIR tissue hemoglobin measurements. In: Chance B, Alfano RR, Tromberg BJ, editors. *Optical Tomography Spectroscopy of Tissue III*. San Jose, CA: International Society for Optics and Photonics (1999). p. 618–31. doi: 10.1117/12.356784
34. MacLeod DB, Ikeda K, Vacchiano C, Lobbestael A, Wahr JA, Shaw AD. Development and validation of a cerebral oximeter capable of absolute accuracy. *J Cardiothorac Vasc Anesth*. (2012) 26:1007–14. doi: 10.1053/j.jvca.2012.06.010
35. Kleiser S, Ostojic D, Nasseri N, Isler H, Bucher HU, Bassler D, et al. In vivo precision assessment of a near-infrared spectroscopy-based tissue oximeter (OxyPrem v1. 3) in neonates considering systemic hemodynamic fluctuations. *J Biomed Optics*. (2018). 23:067003. doi: 10.1117/1.JBO.23.6.067003
36. Sassaroli A, Blaney G, Fantini S. Dual-slope method for enhanced depth sensitivity in diffuse optical spectroscopy. *J Opt Soc Am A*. (2019) 36:1743–61. doi: 10.1364/JOSAA.36.001743
37. Sawosz P, Liebert A. Method to improve the depth sensitivity of diffuse reflectance measurements to absorption changes in optically turbid medium. *Biomed Opt Express*. (2019) 10:5031–41. doi: 10.1364/BOE.10.005031
38. Blaney G, Sassaroli A, Pham T, Krishnamurthy N, Fantini S. Multi-distance frequency-domain optical measurements of coherent cerebral hemodynamics. *Photonics*. (2019) 6:83. doi: 10.3390/photonics6030083
39. Kainerstorfer JM, Sassaroli A, Tgavalekos KT, Fantini S. Cerebral autoregulation in the microvasculature measured with near-infrared spectroscopy. *J Cereb Blood Flow Metab*. (2015) 35:959–66. doi: 10.1038/jcbfm.2015.5

40. Liu P, De Vis JB, Lu H. Cerebrovascular reactivity (CVR) MRI with CO_2 challenge: a technical review. *Neuroimage*. (2019) 187:104–15. doi: 10.1016/j.neuroimage.2018.03.047
41. Willie C, Tzeng YC, Fisher J, Ainslie P. Integrative regulation of human brain blood flow. *J Physiol*. (2014) 592:841–59. doi: 10.1113/jphysiol.2013.268953
42. Panerai R, Deverson S, Mahony P, Hayes P, Evans D. Effects of CO2 on dynamic cerebral autoregulation measurement. *Physiol Meas*. (1999) 20 3:265–75. doi: 10.1088/0967-3334/20/3/304
43. Pham T, Blaney G, Sassaroli A, Fernandez C, Fantini S. Sensitivity of frequency-domain optical measurements to brain hemodynamics: simulations and human study of cerebral blood flow during hypercapnia. *Biomed Opt Express*. (2021) 12:766–89. doi: 10.1364/BOE.412766
44. Tgavalekos KT, Sassaroli A, Cai X, Kornbluth J, Fantini S. Coherent hemodynamics spectroscopy: initial applications in the neurocritical care unit. In: *Optical Tomography Spectroscopy of Tissue XII*. San Francisco, CA: International Society for Optics Photonics (2017). p. 100591F. doi: 10.1117/12.2251021
45. Bigio I, Fantini S. *Quantitative Biomedical Optics: Theory, Methods, and Applications*. Cambridge, UK: Cambridge University Press (2016). doi: 10.1017/CBO9781139029797
46. Hallacoglu B, Sassaroli A, Wysocki M, Guerrero-Berroa E, Schnaider Beeri M, Haroutunian V, et al. Absolute measurement of cerebral optical coefficients, hemoglobin concentration and oxygen saturation in old and young adults with near-infrared spectroscopy. *J Biomed Opt*. (2012) 17:81406–1. doi: 10.1117/1.JBO.17.8.081406
47. Blaney G, Donaldson R, Mushtak S, Nguyen H, Vignale L, Fernandez C, et al. Dual-slope diffuse reflectance instrument for calibration-free broadband spectroscopy. *Appl Sci*. (2021) 11:1757. doi: 10.3390/app11041757
48. Sassaroli A, Tgavalekos K, Fantini S. The meaning of "coherent" and its quantification in coherent hemodynamics spectroscopy. *J Innov Opt Health Sci*. (2018) 12:1850036. doi: 10.1142/S1793545818500360
49. Blaney G, Sassaroli A, Fantini S. Algorithm for determination of thresholds of significant coherence in time-frequency analysis. *Biomed Signal Process*. (2020). 56:101704. doi: 10.1016/j.bspc.2019.101704
50. Philipp B. CircStat: a MATLAB toolbox for circular statistics. *J Stat Softw*. (2009) 31:1–21. doi: 10.18637/jss.v031.i10
51. Milej D, Shahid M, Abdalmalak A, Rajaram A, Diop M, Lawrence KS. Characterizing dynamic cerebral vascular reactivity using a hybrid system combining time-resolved near-infrared and diffuse correlation spectroscopy. *Biomed Opt Express*. (2020) 11:4571–85. doi: 10.1364/BOE.392113
52. Milej D, Abdalmalak A, Rajaram A, Lawrence KS. Direct assessment of extracerebral signal contamination on optical measurements of cerebral blood flow, oxygenation, and metabolism. *Neurophotonics*. (2020) 7:1–17. doi: 10.1117/1.NPh.7.4.045002
53. Kirilina E, Jelzow A, Heine A, Niessing M, Wabnitz H, Brohl R, et al. The physiological origin of task-evoked systemic artefacts in functional near infrared spectroscopy. *Neuroimage*. (2012) 61:70–81. doi: 10.1016/j.neuroimage.2012.02.074
54. Parthasarathy AB, Gannon KP, Baker WB, Favilla CG, Balu R, Kasner SE, et al. Dynamic autoregulation of cerebral blood flow measured non-invasively with fast diffuse correlation spectroscopy. *J Cereb Blood Flow Metab*. (2018) 38:230–40. doi: 10.1177/0271678X17747833
55. Andrews PJ, Citerio G. Intracranial pressure. *Intensive Care Med*. (2004) 30:1730–3. doi: 10.1007/s00134-004-2376-4
56. Armstead WM. Cerebral blood flow autoregulation and dysautoregulation. *Anesthesiol Clin*. (2016) 34:465–77. doi: 10.1016/j.anclin.2016.04.002
57. Pierro M, Kainerstorfer J, Civiletto A, Sassaroli A, Hallacoglu B, Fantini S. Reduced speed of microvascular blood flow in hemodialysis patients versus healthy controls: a coherent hemodynamics spectroscopy study. *J Biomed Opt*. (2014) 19:26005. doi: 10.1117/1.JBO.19.2.026005
58. Schwarz S, Georgiadis D, Aschoff A, Schwab S. Effects of body position on intracranial pressure and cerebral perfusion in patients with large hemispheric stroke. *Stroke*. (2002) 33:497–501. doi: 10.1161/hs0202.102376
59. Wojner-Alexander AW, Garami Z, Chernyshev OY, Alexandrov AV. Heads down. *Neurology*. (2005) 64:1354–7. doi: 10.1212/01.WNL.0000158284.41705.A5
60. Zeiler FA, Ercole A, Czosnyka M, Smielewski P, Hawryluk G, Hutchinson PJA, et al. Continuous cerebrovascular reactivity monitoring in moderate/severe traumatic brain injury: a narrative review of advances in neurocritical care. *Br J Anaesth*. (2020) 124:440–53. doi: 10.1016/j.bja.2019.11.031
61. Pham TT. *Non-invasive Dynamic Measurements of Cerebral Perfusion with Frequency-Domain Near-Infrared Spectroscopy*. Tufts University (2021).

Conflict of Interest: The authors declare that the research was conducted in the absence of any commercial or financial relationships that could be construed as a potential conflict of interest.

Publisher's Note: All claims expressed in this article are solely those of the authors and do not necessarily represent those of their affiliated organizations, or those of the publisher, the editors and the reviewers. Any product that may be evaluated in this article, or claim that may be made by its manufacturer, is not guaranteed or endorsed by the publisher.

frontiers in Neurology

SYSTEMATIC REVIEW
published: 16 November 2021
doi: 10.3389/fneur.2021.732176

Cerebral Autoregulation in Non-Brain Injured Patients: A Systematic Review

Yaroslava Longhitano[1†], Francesca Iannuzzi[2†], Giulia Bonatti[3], Christian Zanza[4], Antonio Messina[5,6], Daniel Godoy[7], Wojciech Dabrowski[8], Li Xiuyun[9], Marek Czosnyka[10], Paolo Pelosi[2,11], Rafael Badenes[12‡] and Chiara Robba[2,11‡]*

[1] Department of Anesthesiology and Critical Care, AO St. Antonio, Biagio and Cesare Arrigo, Alessandria, Italy, [2] Department of Surgical Sciences and Integrated Diagnostics (DISC), University of Genoa, Genoa, Italy, [3] Anesthesia and Intensive Care, Gaslini Hospital, Genova, Italy, [4] Foundation of "Nuovo Ospedale Alba-Bra" and Department of Emergency Medicine, Anesthesia and Critical Care Division, Michele and Pietro Ferrero Hospital, Verduno, Italy, [5] Humanitas Clinical and Research Center – IRCCS, Milan, Italy, [6] Department of Biomedical Sciences, Humanitas University, Milan, Italy, [7] Neurointensive Care Unit, Sanatorio Pasteur, 2 Intensive Care Unit, Hospital Carlos Malbran, Catamarca, Argentina, [8] Anesthesia and Intensive Care, University of Lublin, Lublin, Poland, [9] Department of Anesthesiology & Critical Care Medicine, John Hopkins University, Baltimore, MD, United States, [10] Brain Physics Laboratory, Department of Clinical Neurosciences, University of Cambridge, Cambridge, United Kingdom, [11] Anesthesia and Critical Care, San Martino Policlinico Hospital, IRCCS for Oncology and Neuroscience, Genoa, Italy, [12] Department of Anesthesiology and Surgical-Trauma Intensive Care, Hospital Clinic Universitari de Valencia, Department of Surgery, University of Valencia, Valencia, Spain

OPEN ACCESS

Edited by:
Danilo Cardim, University of Texas Southwestern Medical Center, United States

Reviewed by:
Shraddha Mainali, The Ohio State University, United States
RajaNandini Muralidharan, Winthrop University Hospital, United States

***Correspondence:**
Yaroslava Longhitano
lon.yaro@gmail.com

[†]These authors share first authorship

[‡]These authors share last authorship

Specialty section:
This article was submitted to Neurocritical and Neurohospitalist Care, a section of the journal Frontiers in Neurology

Received: *28 June 2021*
Accepted: *11 October 2021*
Published: *16 November 2021*

Citation:
Longhitano Y, Iannuzzi F, Bonatti G, Zanza C, Messina A, Godoy D, Dabrowski W, Xiuyun L, Czosnyka M, Pelosi P, Badenes R and Robba C (2021) Cerebral Autoregulation in Non-Brain Injured Patients: A Systematic Review. Front. Neurol. 12:732176. doi: 10.3389/fneur.2021.732176

Introduction: Cerebral autoregulation (CA) plays a fundamental role in the maintenance of adequate cerebral blood flow (CBF). CA monitoring, through direct and indirect techniques, may guide an appropriate therapeutic approach aimed at improving CBF and reducing neurological complications; so far, the role of CA has been investigated mainly in brain-injured patients. The aim of this study is to investigate the role of CA in non-brain injured patients.

Methods: A systematic consultation of literature was carried out. Search terms included: "CA and sepsis," "CA and surgery," and "CA and non-brain injury."

Results: Our research individualized 294 studies and after screening, 22 studies were analyzed in this study. Studies were divided in three groups: CA in sepsis and septic shock, CA during surgery, and CA in the pediatric population. Studies in sepsis and intraoperative setting highlighted a relationship between the incidence of sepsis-associated delirium and impaired CA. The most investigated setting in the pediatric population is cardiac surgery, but the role and measurement of CA need to be further elucidated.

Conclusion: In non-brain injured patients, impaired CA may result in cognitive dysfunction, neurological damage, worst outcome, and increased mortality. Monitoring CA might be a useful tool for the bedside optimization and individualization of the clinical management in this group of patients.

Keywords: cerebral autoregulation, non-brain injury, neurologic outcome, sepsis, perioperative care, pediatric surgery

INTRODUCTION

Cerebral autoregulation (CA) is a complex mechanism of brain protection against changes in cerebral perfusion pressure (CPP) in order to maintain an adequate cerebral blood flow (CBF) (1). CA works by balancing vasoconstriction and vasodilation of the cerebral vessels regulating CBF with the aim to maintain a constant CBF (1). The concept of CA was introduced approximately half a century ago and afterward it was progressively used as a parameter to help in the management of mean arterial blood pressure in relationship with CBF in the neuro-intensive care unit (neuro-ICU) settings. Indeed, monitoring CA has shown to be particularly useful in the context of acute subarachnoid hemorrhage, traumatic brain injury (TBI), and acute stroke (2–5). Although no randomized controlled trials (RCTs) assessing the effect of autoregulation on outcome are available at present, it is accepted among experts that impairment of CA can lead to secondary cerebral insult and poor outcomes also in patients without primary brain injury (6–10).

The latest guidelines from the Brain Trauma Foundation suggest to maintain a CPP of 60–70 mm Hg in patients with TBI (11); however, the concept of "one-size-fits-all" may not be appropriate, as it does not represent the physiological needs of an individual and changes of CA; more recently, experts suggest a personalized management of CA based on the intrinsic autoregulatory state and function of single patients (12). In this context, several methods aimed to individualize the assessment of CA status have been proposed (13). The gold standard for CA measurement is represented by the neuroimaging studies, which allow to obtain a direct visualization of CBF such as PET, single-photon emission CT (SPECT), and CT perfusion. However, these methods are expensive, time-consuming, and have a very limited role in the clinical context. Therefore, a number of indirect techniques aimed at CA monitoring by the bedside have been proposed and evaluated including invasive methods (based on intracranial pressure and invasive cerebral oxygenation monitoring) and non-invasive methods [based on transcranial Doppler (TCD) and near-IR spectroscopy (NIRS)]; both of them are widely adopted in the neuro-ICU population.

The aim of this study is to systematically review the role of CA in non-brain injured patients, in different clinical settings, such as surgery, sepsis, and septic shock and in the pediatric population.

METHODS

Data Sources and Search Strategy

In this study, we adhered to the *Preferred Reporting Items for Systematic Review and Meta-Analysis Protocols* (PRISMA-P) guidelines (14). A systematic literature search was performed by using the following databases to identify relevant studies in indexed scientific journals: the PubMed, the Medical Literature Analysis and Retrieval System Online (MEDLINE) (*via* Ovid), the Excerpta Medica dataBASE (EMBASE) (*via* Ovid), and the Cochrane Central Register of Controlled Trials by using the terms: cerebral autoregulation and sepsis, cerebral autoregulation and surgery and/or perioperative, and cerebral autoregulation and non-brain injured patients with filters for humans, language (English), and time of publication (January 1, 2010 to February 28, 2021). Inclusion criteria were studies describing the measurement of CA in non-brain injured patients and its effect on outcome of patients (evaluated as mortality and/or neurological outcome). This study was limited to clinical trials, meta-analysis, RCTs, review, and systematic review. Search criteria included "CA and surgery," "CA and sepsis and/or metabolic coma," "CA and general intensive care," and "CA and non-brain injured patients." A specific literature search was then conducted for the pediatric population, with the same search strategy, but including patients <18 years. We excluded literature concerning brain injury population and not concerning CA specifically or not mentioning the effect of CA measurement on outcome. We also excluded editorials, commentaries, letters to the editor, opinion articles, reviews, meeting abstracts, and original articles lacking abstract.

Study Selection and Data Collection

Two authors (FI and GB) selected the articles independently screening titles, abstracts, and full texts. The standardized data extraction form included aim and study design. The articles were then subdivided into three subgroups: "included" and "excluded" (if the two examiners agreed with the selection) or "uncertain" (in case of disagreement). In the case of "uncertain" classification, discrepancies were resolved by further examination performed by the two expert authors (CR and YL). We used a standardized electronic spreadsheet (Microsoft Excel, version 14.4.1; Microsoft, Redmond, Washington, USA) to extract the data from all the included studies and recording trial characteristics.

Endpoints

The primary outcome of this study is to investigate the CA in patients without brain injury. Secondary outcome is to assess whether alteration in CA in different settings such as surgery, sepsis, and septic shock and in the pediatric population can have an effect on morbidity and mortality.

Risk of Bias Assessment in the Included Studies

Two examiners (FI and YL) independently assessed the internal validity of the included studies and discrepancies were resolved by a third senior author (AM or CR) by using the version 2 of the Cochrane risk-of-bias tool for randomized trials (RoB 2). The RoB 2 considers five bias domains: (1) the randomization process, (2) the deviations from intended interventions, (3) missing outcome data, (4) measurement of the outcome, and (5) selection of the reported results. Finally, the overall risk of bias was calculated and, accordingly, studies were included in either high-risk/unclear risk/low-risk groups.

RESULTS

After general screening, initial results from this search lead to a number of 40 studies (**Figure 1**, Flowchart). Among them, 22 studies were further selected, which were divided in three sections (CA in sepsis and septic shock, CA in surgery, and CA in the

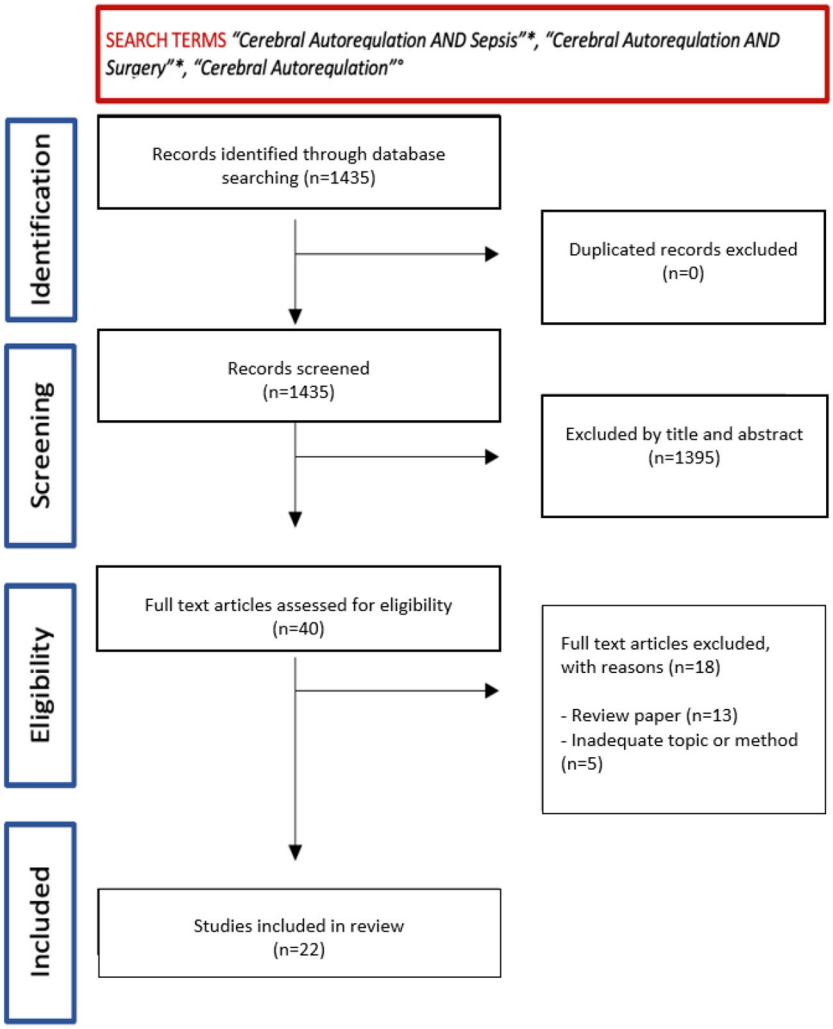

FIGURE 1 | Flowchart.

pediatric population) (**Tables 1**, **2**). Specific reasons for exclusion of the studies are presented in **Table 3**. The risk of bias assessment reported: "low risk" for 13 papers (59%), "unclear risk" for 9 articles (41%), and none of them reported high risk of bias. The bias was mostly related to the randomization process selection of the reported results (**Table 4**).

Cerebral Autoregulation in Sepsis and Septic Shock

A total of six studies were screened for septic shock and sepsis (**Table 1**). A disruption of CA prolonged over time can lead to cerebral hypoperfusion and consequently neuronal ischemia. In a prospective, observational study, 100 adult patients with sepsis were evaluated with the hypothesis that impaired CA may lead to brain hypoperfusion and neuronal damage (17). Crippa et al. registered impaired CA in 50 patients (50%) and this represented one of the independent predictors of sepsis-associated brain dysfunction (SABD), which was diagnosed in 57 patients (57%). SABD was defined as the Glasgow Coma Scale (GCS) score < 15 or when disorientation, altered thinking, or agitation was reported. In case of continuous sedation ($n = 6$), patients were considered as having SABD. The CA was evaluated by using the mean flow index (Mxa) assessed by TCD (17). The authors concluded that in SABD, brain hypoperfusion and neuronal damage were probably caused by impaired CA and this could lead to a higher morbidity and mortality in these patients. The findings of this prospective observational study support the concept that cerebral hypoxia could contribute to the development of SABD, despite its multifactorial pathophysiology. Schramm et al. also found a relationship between impaired CA and sepsis-associated delirium (SAD). Indeed, in the majority of septic patients, CA is impaired, in particular the first 2 days, suggesting an important contribution of CA in the development of SAD (15). In this study (15), 30 patients were evaluated with the average Acute Physiologic Assessment and Chronic Health Evaluation (APACHE) score of 32 ± 6. The CA was estimated by

TABLE 1 | Summary of the included studies about CA in sepsis and pediatric population: primary findings, type of method to assess autoregulation, number of patients evaluated.

First author	Year	Journal	N of patients	Type autoregulation	Design of study	Findings
CEREBRAL AUTOREGULATION IN SEPSIS AND SEPTIC SHOCK						
Schramm et al. (15)	2012	Critical Care	30	TCD	Prospective study	AR is impaired in the great majority of patients with severe sepsis during the first two days. Impaired AR is associated with SAD, suggesting that dysfunction of CA is one of the trigger mechanisms contributing to the development of SAD.
Berg et al. (8)	2016	Scand J Clin Lab	9	TCD	Prospective study	Dynamic CA is enhanced during the very early stages of sepsis, they remain inconclusive with regard to more advanced stages of disease, because thigh-cuff deflation failed to induce sufficient MAP reductions in patients.
Bindra et al. (16)	2016	Critic Care Resusc	28	NIRS	Prospective, observational	CA is impaired early in septic shock and is independently associated with mortality at 3-month follow-up. Information based on bedside monitoring of CA in the ICU could form a valuable adjunct to guide haemodynamic optimization in patients with septic shock.
Crippa et al. (17)	2018	Crit Care	100	TCD	Prospective, observational	CA was altered in half of the patients with sepsis and was associated with the development of SABD. These findings support the concept that cerebral hypoxia could contribute to the development of SABD.
Rosenblatt et al. (18)	2020	J Intensive Care Medicine	6	NIRS / COx	Case series	In this high-fidelity group of patients with SAE, continuous, NIRS-based monitoring can identify blood pressure ranges that improve autoregulation. This is important given the association between cerebral autoregulatory function and severity of encephalopathy. Individualizing blood pressure goals using bedside autoregulation monitoring may better preserve cerebral perfusion in SAE than current practice
Berg et al. (8)	2016	Scand J Clin Lab	7	TCD	Prospective study	Cerebral CO_2 vasoreactivity was found to be preserved in septic patients; nevertheless, and in contrast to our working hypothesis, short-term mechanical hyperventilation did not enhance dCA.
CEREBRAL AUTOREGULATION IN PEDIATRIC CRITICALLY ILL PATIENTS						
Easley et al. (10)	2018	Cardiol Young	57	NIRS	multicenter observational pilot study	Individual, dynamic non-invasive cerebrovascular reactivity monitoring demonstrated transient periods of impairment related to possible silent brain injury. The association between an impaired autoregulation burden and elevation in the serum brain biomarker may identify brain perfusion risk that could result in injury.
Brady et al. (19)	2010	Crit Care Medicine	54	NIRS	prospective, observational pilot study	This pilot study of COx monitoring in pediatric patients demonstrates an association between hypotension during CPB and impairment of autoregulation. The COx may be useful to identify arterial blood pressure-dependent limits of during CPB. Larger trials with neurological outcomes are indicated.
Thewissen et al. (20)	2018	Pediatr Res	22	NIRS	Prospective, observational study	Drug-related hypotension and decreased cerebral activity after intubation with low propofol doses in preterm neonates were observed, without evidence of cerebral ischemic hypoxia. CA remained intact during drug-related hypotension in 95.5% of patients. Cerebral monitoring including CA clarifies the cerebral impact of MAP fluctuations.
Joram et al. (21)	2020	Neurocritical Care	29	NIRS	Prospective observational study	CA assessment is feasible in pediatric ECMO. The first 24 h following ECMO represents the most critical period regarding CA. Impaired autoregulation is significantly more severe among patients who experience acute neurological event.

TDC, Transcranial Doppler; AR, Autoregulation; SAD, Sepsis-associated Delirium; MAP, Mean Arterial Pressure; NIRS, Near InfraRed Spectroscopy; CVAR: Cerebrovascular Autoregulation; ICU: Intensive Care Unit; SABD, Sepsis-associated brain dysfunction; COx, cerebral oxygen index; SAE, Sepsis-associated Encephalopathy; CA, cerebral autoregulation; CPB, cardio-pulmonary by-pass.

TABLE 2 | Summary of the included studies about CA in surgery: primary findings, type of method to assess autoregulation, number of patients evaluated.

First author	Year	Journal	N of patients	Type autoregulation	Design of study	Finding
CEREBRAL AUTOREGULATION DURING SURGERY						
Caldas et al. (22)	2019	Clin Neurophysiol	67	TCD	Sistematic review	Dynamic CA was impaired after CABG surgery with CPB and was a significant independent risk factor of PD.
Ono et al. (23)	2013	Crit Care Med	410	NIRS	Prospective observational study.	Excursions of MAP below the limit of autoregulation and not absolute MAP are independently associated with for AKI. Monitoring Cox may provide a novel method for precisely guiding MAP targets during CPB.
Hori et al. (24)	2014	J Cardiothorac Vasc Anesth	110	NIRS	Prospective randomized clinical trial	The presence of delirium was not associated with perioperative blood pressure excursions, but the secondary analysis showed the association between excursion above the optimal mean arterial pressure and the severity of delirium in early PO period.
Hori et al. (25)	2014	Br J Anaesth J	491	NIRS	Prospective observational study	Excursions of MAP above the upper limit of CA during CPB are associated with risk for delirium. Optimizing MAP during CPB to remain within the CA range might reduce risk of delirium.
Hori et al. (24)	2016	Interact CardioVasc Thorac Surg	110	UT-NIRS	Prospective observational study	Excursion below optimal blood pressure during perioperative period is associated with CSA-AKI.
Sperna Weiland et al. (26)	2017	Br J Anaesth	14	TCD	Prospective study	During surgery, CA indices were similar to values determined before surgery. This indicates that CA can be quantified reliably and non-invasively using this novel method and confirms earlier evidence that CA is unaffected by sevoflurane anaesthesia.
Chuan et al. (27)	2018	Acta Anaesthesiol Scand	140	NIRS	prospective observational single centre study	In older and higher risk patients having major noncardiac surgery, impaired CA was associated with failure of cognitive recovery in the early postoperative period and with 1-month mortality and morbidity.
Goettel et al. (28)	2016	J Clin Monit Comput	133	TCD	prospective observational cohort study	The autoregulatory plateau is shortened in both young and older patients under Sevoflurane anesthesia with approximately 1 MAC. Lower and upper limits of CBF autoregulation, as well as the autoregulatory range, are not influenced by the age of anesthetized patients.
Zheng et al. (29)	2012	Neurocrit Care	9	TCD, NIRS	Prospective observational study	These results suggest that autoregulation is impaired in patients undergoing liver transplantation, even in the absence of acute, fulminant liver failure. Identification of patients at risk for neurologic complications after surgery may allow for prompt neuroprotective interventions, including directed pressure management
Nomura et al. (9)	2018	Anesthesia Analgesia	346	TCD, MRI	retrospective cohort analysis	Impaired CBF autoregulation is prevalent during CPB predisposing affected patients to brain hypoperfusion or hyperperfusion with low or high blood pressure, respectively. Small vessel, but not large vessel, cerebral vascular disease, male sex, and higher average body temperature during CPB appear to be associated with impaired CA.
Goettel et al. (28)	2017	Geriatric Anesthesia	82	TCD, NIRS	prospective observational cohort study	Impairment of intraoperative CBF autoregulation is not predictive of early POCD in elderly patients, although secondary analyses indicate that an association probably exists.
Hogue et al. (30)	2020	Semin Thorac Cardiovasc Surg	460	TCD	Prospective randomized clinical trial	Basing MAP during CPB on cerebral autoregulation monitoring did not reduce the frequency of the primary neurological outcome in high-risk patients compared with usual care but it was associated with a reduction in the frequency of delirium and better performance on tests of memory 4-6 weeks after surgery

TDC, Transcranial Doppler; MAP, Mean Arterial Pressure; NIRS, Near InfraRed Spectroscopy; CA, Cerebral Autoregulation; ICU, Intensive Care Unit; SABD, Sepsis-associated brain dysfunction; SAE, Sepsis-associated Encephalopathy; AKI, Acute Kidney Injury; CPB, Cardiac Pulmonary Bypass; PO, postoperative; CABG, Coronary Artery Bypass Graft; PD, Post-operative Delirium; CBF, Cerebral Blood Flow.

TABLE 3 | Summary of excluded studies and reasons for exclusion.

Excluded studies	Reason for exclusion
Taccone et al., Current Vascular Pharmacology 2013	Narrative Review
Tauber et al., Expert Review of Anti-Infective Therapy 2016	Narrative Review
Donnelly et al., Critical Care 2016	Narrative Review
Goodson et al., JICM 2018	Narrative Review
Danielski et al., Molecular Neurobiology 2018	Narrative Review
Masse et al., Critical Care Medicine 2018	Not about cerebral autoregulation specifically, but about cerebral perfusion in septic patients
Gu et al., Neurotoxicity Research 2020	Narrative Review
Semenyutin et al., Frontiers in Physiology 2017	Deal with indications to surgery in patients with compromised dynamic cerebral autoregulation
Vranken et al., The Journal of Extra-Corporeal Technology 2017	Narrative Review
Lewis et al., Journal of Cardiothoracic and Vascular Anesthesia 2018	Narrative Review
Saxena et al., Presse Medicale 2018	Narrative Review
Bonow et al., Neurosurgical Focus 2019	Narrative Review
Kooi et al., Expert Review of Neurotherapeutics 2018	Narrative Review
Rhee et al., Pediatric Research 2018	Narrative Review
Jildenstål et al., Pediatric Anaesthesia 2019	Evaluate the agreement between frontal and occipital recordings of $rScO_2$%
Montgomery et al., Anesthesia and Analgesia 2020	The aim is to determine the performance of the co-trending method by comparing CA metrics to data derived from TCD methods.
Kooi et al., Clinics in Perinatology 2020	Narrative Review
Govindan et al., Journal of Perinatology 2020;	Determine whether ventilator-related fluctuations in CBV

rScO2%, regional cerebral oxygen saturation; CA, cerebral autoregulation; TDC, transcranial doppler; CBV, cerebral blood volume.

using TCD and the Confusion Assessment Method for the ICU (CAM-ICU) was assessed at day 4 when sedative medications were temporarily reduced to reach the Richmond Agitation and Sedation Scale (RASS) score greater than−2. SAD was detected in 76% of patients. This study concluded that impaired CA at day 1 was associated with the incidence of SAD at day 4 ($p = 0.035$) (15).

Cerebral autoregulation can be also evaluated to guide optimal blood pressure. Indeed, in a study including six patients (18), pharmacological sedation free with extracranial sepsis and cerebral oximetry was measured with NIRS to identify blood pressure range, demonstrating feasibility to optimize autoregulation maintaining adequate blood pressure range. In this case series, Rosenblatt et al. found an association between cerebral autoregulatory function and the development and severity of encephalopathy defined as GCS < 15 but ≥ 13 (mild encephalopathy), whereas values < 13 were defined as moderate or severe impairment (18). The authors concluded that individualizing blood pressure goals by using bedside autoregulation monitoring may preserve cerebral perfusion by individualizing blood pressure range in Sepsis-associated encephalopathy (SAE) (18). In another prospective observational study, Bindra et al. investigated 28 patients with early septic shock in the ICU to understand if impaired CA was associated with neurological outcome and mortality (16). This study concluded that the mortality at 3-month follow-up was independently associated with impaired CA in early septic shock. Thus, bedside monitoring of CA could adjunct important information for hemodynamic optimization of patients with septic shock. Other two studies discussed the management of CA in the early stages of septic shock (8, 31). Both were based on small groups of patients (seven and nine patients, respectively). The first study analyzed seven critically ill patients, who underwent hyperventilation (8) and the second one described healthy volunteers, who underwent lipopolysaccharide (LPS) infusion to reproduce early sepsis (31). The CA was evaluated by TCD and the authors concluded that dynamic CA (dCA) to spontaneous fluctuations in blood pressure was enhanced and cerebral carbon dioxide vasoreactivity was preserved in the early phases of sepsis, but this regulation disappeared in the late stages (8, 31).

Cerebral Autoregulation During Surgery

A total of 12 studies were selected in the literature about CA in surgery (**Table 2**). A high number of articles about CA during surgery were performed in cardiac surgery, where a possible association between impaired CA and postoperative delirium (PD) was evaluated. Caldas et al. in his single-center observational and prospective study analyzed 67 patients undergoing cardiopulmonary bypass. All the enrolled subjects underwent TCD and the CAM-ICU assessment preoperatively at 24 h and 7 days after the procedure to evaluate CA and PD, respectively. Impaired CA was found in 55% of patients 24 h postoperatively and in 20% after 7 days. In addition, the authors concluded that impaired CA during coronary artery bypass graft (CABG) surgery is a significant independent risk factor for PD ($p = 0.003$) (22). Another study analyzed the use of CA with NIRS. In the prospective observational study, 110 patients who underwent cardiac surgery were analyzed (24). They were monitored with NIRS during surgery and in the first 3 h postoperatively and their CAM-ICU score was calculated on postoperative (PO) days 1 and 3. A total of 42.7% of patients presented delirium. Hori et al. observed no association

TABLE 4 | Risk of bias evaluation.

	Randomization process	Deviation from intended interventions	Missing outcome data	Measurement of the outcome	Selection of the reported result	Overall
Schramm et al. (15)	+	+	+	+	+	+
Berg et al. (8)	!	+	!	+	+	!
Bindra et al. (16)	+	+	!	+	+	+
Crippa et al. (17)	+	+	+	!	+	+
Rosenblatt et al. (18)	!	+	!	+	+	!
Berg et al. (8)	!	+	+	!	+	!
Easley et al. (10)	+	!	+	+	!	!
Brady et al. (19)	!	+	+	+	+	+
Thewissen et al. (20)	!	!	!	+	+	!
Caldas et al. (22)	+	+	+	!	+	+
Ono et al. (23)	+	+	+	!	+	+
Hori et al. (24)	+	+	+	+	!	+
Hori et al. (25)	+	+	+	+	!	+
Hori et al. (24)	+	+	+	+	+	+
Sperna Weiland et al. (26)	!	+	+	+	+	+
Chuan et al. (27)	+	+	!	+	+	+
Goettel et al. (28)	+	!	!	+	!	!
Zheng et al. (29)	!	+	+	+	+	!
Nomura et al. (9)	!	!	+	+	+	!
Goettel et al. (28)	!	!	+	+	+	!
Hogue et al. (30)	+	+	+	+	+	+
Joram et al. (21)	!	+	+	+	+	+

+ *low risk of bias;* ! *unclear risk of bias;* ! *high risk of bias.*

between the perioperative blood pressure excursion and PD, but a secondary analysis showed higher blood pressure excursions above the optimal medial arterial pressure in the group who developed delirium postoperatively ($r = 0.27$, $p = 0.011$) (24). These data were also confirmed by a large prospective study, which analyzed 491 patients who were monitored with NIRS during surgery and the PD was assessed by the CAM-ICU. In this case, delirium was diagnosed in 9.2% of cases and the excursion of mean arterial pressure (MAP) above the upper limit of CA during cardiopulmonary bypass was independently associated with PO delirium [odds ratio (OR), 1.09; 95% CI, 1.03–1.15] (25).

In addition to a possible neuronal damage, an acute kidney injury (AKI) related to CA was investigated. Ono et al. in a large (410 patients) prospective study monitored CBF intraoperatively by using NIRS and evaluated the incidence of AKI by using the Risk, Injury, Failure, Loss of kidney function, and End-stage kidney disease (RIFLE) criteria during the first 7 days postoperatively. The results showed that MAP excursions below the lower limit of CBF autoregulation during cardiopulmonary bypass were independently associated with AKI [relative risk (RR), 1.02; 95% CI, 1.01 to 1.03; $p < 0.0001$] (23). These results were confirmed by another prospective study, which included 110 patients who underwent cardiopulmonary bypass.

The CBF was monitored by NIRS during the surgery and the monitoring of AKI was performed for 2 days after surgery. A total of 27.3% of subjects developed AKI and the excursion below optimal blood pressure values during the perioperative period was associated with the development of AKI postoperatively ($p = 0.008$) (32). Other studies aimed to evaluate the principal risk factors associated to CA alteration. In a large prospective randomized clinical trial, 346 patients which underwent cardiac surgery and performed standardized general anesthesia were evaluated with preoperative TCD and cerebral MRI performed between days 3 and 5 after surgery to assess the preoperative factors, which can be associated with impaired CA in cardiac surgery. The presence of small vessel cerebral vascular disease was strongly associated with impaired CBF autoregulation (OR, 3.25; 95% CI, 1.21–8.71; $p = 0.019$). Other risk factors were male sex, high body temperature during surgery, elderly, and large vessel disease (10). Based on these evidences, it is possible to affirm that changes in CA during cardiac surgery influence clinical outcomes as rated by Caldas et al. in a recently published study (33). Also, Hogue et al. investigated the neurological impairment related to CA during cardiac surgery. A total of 460 patients were analyzed by TCD to correlate CA impairment with ischemic injury, PD, and performance on memory test 4–6 weeks after surgery. The presence of ischemic injuries was not related to intraoperative CA impairment ($p = 0.752$), instead both the delirium and memory test performance were strongly related to CA ($p = 0.035$ and $p = 0.019$, respectively) (30). However, further studies are needed to develop the therapeutic approaches in order to better understand the prognostic implications of this evidence.

In non-cardiac surgery, the role of CA was less frequently investigated and the results are discordant. Two large studies are available in scientific literature. The first one (27) is prospective and it is focused on PD and CA in major non-cardiac surgery. A total of 110 patients were included, who were intraoperatively monitored by NIRS and PO cognitive disorders were recorded. Chuan et al. concluded that impaired CA in these patients was associated with failure of cognitive recovery in the early PO period ($p = 0.02$) with 1-month mortality and morbidity ($p = 0.04$) (27). The second one (28) also investigated an association between impaired CA and PO cognitive dysfunction (POCD). Indeed, Goettel et al. recruited 86 patients who underwent non-cardiac surgery and standardized anesthesia and were intraoperatively evaluated with both the TCD and NIRS. In addition, C-reactive protein (CRP) and two biomarkers of neuronal injury neuron-specific enolase (NSE) and S100β protein were dosed on PO days 2 and 7. The study participants completed a battery of neuropsychological tests at baseline and 1 week after surgery and 3 months postoperatively. Authors concluded that dysregulation of CBF was not predictive of cognitive dysfunction after surgery, but there may be an association not yet fully explained (28). The risk factors associated with impaired CA in non-cardiac surgery were also evaluated in a study including 133 patients who underwent sevoflurane anesthesia during non-cardiac major surgery and subsequently they were divided in two groups depending on age. CBF thresholds were not influenced by the age of patients ($p = 0.075$) and autoregulatory plateau was shortened in both the groups during anesthesia with sevoflurane (34). In contrast, Sperna et al. evaluated CA in general anesthesia with TCD before surgery during 3 min of paced breathing at 6, 10, and 15 beats per min (bpm) and during surgery. The authors concluded that sevoflurane did not affect CA because preoperative and intraoperative values were superimposable (26). Finally, one study investigated the role of CA in liver transplant surgery. In this study, six patients were retrospectively analyzed with TCD to evaluate CA and its changes in perioperative period. Authors revealed marked alterations of CBF and they concluded that direct pressure management and others neuroprotective measures may reduce the risk for neurological complications in this group of patients (29).

Cerebral Autoregulation in the Pediatric Critically Ill Population

With respect to CA in the pediatric population, four studies were included (**Table 1**). Even in the pediatric population, the most studied field for CA use is the cardiac surgery. In the first study included (19), the lower limit of autoregulation during cardiac surgery was measured; hypotensive events were associated with increased values of the cerebral oximetry index (Cox) ($p < 0.0001$) and the mean lower limits of pressure autoregulation were 42 ± 7 mm Hg. Authors concluded that despite larger studies must confirm these findings, COx can be useful to determine the arterial blood pressure-dependent limits of autoregulation in the pediatric population (19). Another study (10) conducted in cardiac surgery aimed to detect brain hypoperfusion injuries by elevation in serum glial fibrillary acidic protein levels due to impaired cerebrovascular reactivity. A total of 57 children were analyzed and transient period of compromised CA was detected with dynamic noninvasive cerebrovascular reactivity monitoring that showed transient periods of impairment related to possible silent brain injury (10). Out of cardiac surgery settings, CA after propofol infusion in the pediatric population was investigated. During general anesthesia, hypotension due to low dose of propofol infusion before endotracheal intubation did not lead to cerebral hypoxia and with stable levels of regional cerebral oxygen saturation. Unharmed CA drug-related hypotension was detected, underlining its importance during MAP fluctuations (20).

Another study evaluated CA during Extracorporeal Membrane Oxygenation (ECMO) treatment. This prospective observational study analyzed 29 children, who required ECMO support; in particular, the CA was evaluated with NIRS (21). In this study, 34.5% experienced acute neurological events; it concluded that the first 24 h following ECMO is the most critical period regarding CA and altered CA is associated with acute neurological events ($p = 0.04$) (21).

DISCUSSION

In this study, we set out to describe how CA can be modified in patients without brain injury in sepsis/septic shock during surgery and in pediatric critically ill patients. Impaired autoregulation in these pathological situations can

result in cognitive dysfunction, neurological damage, increased morbidity, and mortality even in non-brain injured patient (6–9). These pathological situations can alter the autoregulatory mechanisms and values, thus modifying the ability of CA to preserve good CBF and prevent possible secondary neuronal injury (8, 17, 24).

In sepsis and septic shock, the systemic alterations that involve compromise in CA have been studied by several authors for whom the condition of SABD has also been defined (24). Despite this, the timing at which impaired CA begins with respect to the onset of the disease still needs further investigations (33). Furthermore, a correlation was found between impaired CA and outcome and mortality of septic patients independently from baseline septic disease severity (16, 18). The lack of homogeneous outcomes found in the studies included can be explained by the different settings applied and makes difficult to draw any conclusion regarding the possible effects of brain monitoring on outcome. The presence of sedation during neurological evaluation, the use of different scores for neurological impairment, and CA evaluation methods can also impact on the reproducibility of the results; nevertheless, all the studies suggest that measuring CA is safe and feasible and can potentially provide important information regarding intracerebral changes during the ICU stay and possibly improve outcomes (16–18). The analyzed studies confirm the presence of frequently altered CA in sepsis or septic shock, mostly during latest phases of sepsis and altered CA is the important risk factor for cognitive dysfunction (15, 17).

Important consequences of impaired CA were also found in the PO period. The studies included were mainly conducted in the context of cardiac surgery, in particular during cardiopulmonary bypass in which the cause of PD must be sought together with other risk factors (22, 24, 25). In support of this theory, an increased level of neuronal biomarkers was found in the serum of patients with impaired CA in the PO period, but further studies are needed to fully understand the association between POCD and altered brain flow as a consequence of the loss of CA (28). Besides cardiac surgery, in a study conducted in liver transplant surgery, we found that blood pressure management and neuroprotective measures may help in reducing the neurological complications (29). In this pathological setting, the alteration of CA is related to PO neurological and cognitive impairment (22, 27, 34), but it is not the only one comorbidity related to altered CBF. Indeed, also AKI was associated with altered CA (23, 32).

In the pediatric population, CA was evaluated mainly during cardiopulmonary bypass surgery (10, 19). An increase in PO serum neurological biomarkers following impaired CA was also detected in pediatric patients. This has been related to major fluctuations in MAP and intraoperative hypotension (10). Although evidence is limited in this setting, even in this population, the use of CA monitoring seems to be beneficial to early detect the intracerebral complications (10).

The CBF was evaluated mostly by NIRS and TCD. In case of TCD, the correlation between systemic MAP and mean flow velocity (FVm) in the middle cerebral artery was used to evaluate CA (Mx index) (15, 22, 33). Instead, in case of NIRS, the CA can be monitored by the Pearson's correlation coefficient between MAP and NIRS signals to generate the variable COx. When MAP is within the limits of CBF autoregulation, Mx and Cox approach zero or are negative, but when MAP is outside the limits of autoregulation, Mx and Cox have positive values, indicating that CBF is blood pressure passive (16, 25). Sperna et al. evaluated CA with an innovative method by using paced breathing. Indeed, the blood pressure and CBF velocity fluctuate spontaneously around the two predominant frequencies. The low frequency is due to baroreflex-mediated sympathetic nervous system activity and the high frequency is due to respiration. By using "frequency domain" analysis, the power of these fluctuations can determine the efficacy of CA (26).

This study has some limitations. First, this study summarizes the available evidence. There are still inadequate data describing the impact of CA on outcome and its clinical use in both the adult and pediatric population without brain injury. Second, the studies described in our review included a small number of patients and are extremely heterogeneous with often important methodological limitations. This makes difficult to draw any conclusion and makes a meta-analysis of the available evidence unviable.

CONCLUSION

Impaired autoregulation in different pathological conditions can result in cognitive dysfunction, neurological damage, worse outcome, and increased mortality, even in non-brain injured patients. The analyzed studies show an association between alteration in CA and outcome; however, the heterogeneity of the studies and the low level of quality in the study design and methods further suggest that more in-depth investigations are needed, especially considering the different subgroups.

DATA AVAILABILITY STATEMENT

The raw data supporting the conclusions of this article will be made available by the authors, without undue reservation.

AUTHOR CONTRIBUTIONS

FI, YL, GB, and CZ contributed to the analysis of scientific literature and writing of manuscript. AM, DG, WD, LX, MC, PP, and CR contributed to the revision of manuscript and fundamental conceptual contribution. RB reviewed the manuscript and added fundamental contribution. All authors contributed to the article and approved the submitted version.

SUPPLEMENTARY MATERIAL

The Supplementary Material for this article can be found online at: https://www.frontiersin.org/articles/10.3389/fneur.2021.732176/full#supplementary-material

REFERENCES

1. Armstead WM. Cerebral blood flow autoregulation and dysautoregulation. *Anesthesiol Clin.* (2016) 34:465–77. doi: 10.1016/j.anclin.2016.04.002
2. Robba C, Citerio G. How I manage intracranial hypertension. *Crit Care.* (2019) 23:243. doi: 10.1186/s13054-019-2529-z
3. Robba C, Bonatti G, Battaglini D, Rocco PRM, Pelosi P. Mechanical ventilation in patients with acute ischaemic stroke: from pathophysiology to clinical practice. *Crit Care.* (2019) 23:388. doi: 10.1186/s13054-019-2662-8
4. Rivera-Lara L, Zorrilla-Vaca A, Geocadin RG, Healy RJ, Ziai W, Mirski MA. Cerebral autoregulation-oriented therapy at the bedside: a comprehensive review. *Anesthesiology.* (2017) 126:1187–99. doi: 10.1097/ALN.0000000000001625
5. Klein SP, Depreitere B, Meyfroidt G. How I monitor cerebral autoregulation. *Crit Care.* (2019) 23:160. doi: 10.1186/s13054-019-2454-1
6. Depreitere B, Citerio G, Smith M, Adelson PD, Aries MJ, Bleck TP, et al. Cerebrovascular autoregulation monitoring in the management of adult severe traumatic brain injury: a delphi consensus of clinicians. *Neurocrit Care.* (2021) 34:731–8. doi: 10.1007/s12028-020-01185-x
7. de Azevedo DS, Salinet ASM, de Lima Oliveira M, Teixeira MJ, Bor-Seng-Shu E, de Carvalho Nogueira R. Cerebral hemodynamics in sepsis assessed by transcranial Doppler: a systematic review and meta-analysis. *J Clin MonitComput.* (2017) 31:1123–32. doi: 10.1007/s10877-016-9945-2
8. Berg RM, Plovsing RR. Effects of short-term mechanical hyperventilation on cerebral blood flow and dynamic cerebral autoregulation in critically ill patients with sepsis. *Scand J Clin Lab Invest.* (2016) 76:226–33. doi: 10.3109/00365513.2015.1137350
9. Nomura Y, Faegle R, Hori D, Al-Qamari A, Nemeth AJ, Gottesman R, et al. Cerebral small vessel, but not large vessel disease, is associated with impaired cerebral autoregulation during cardiopulmonary bypass: a retrospective cohort study. *Anesth Analg.* (2018) 127:1314–22. doi: 10.1213/ANE.0000000000003384
10. Easley RB, Marino BS, Jennings J, Cassedy AE, Kibler KK, Brady KM, et al. Impaired cerebral autoregulation and elevation in plasma glial fibrillary acidic protein level during cardiopulmonary bypass surgery for CHD. *Cardiol Young.* (2018) 28:55–65. doi: 10.1017/S1047951117001573
11. Hutchinson PJ, Kolias AG, Tajsic T, Adeleye A, Aklilu AT, Apriawan T, et al. Consensus statement from the International Consensus Meeting on the Role of Decompressive Craniectomy in the Management of Traumatic Brain Injury: Consensus statement. *Acta Neurochir (Wien).* (2019) 161:1261–74. doi: 10.1007/s00701-019-03936-y
12. Czosnyka M. In a Search of Pressure Which Optimizes Autoregulation of Cerebral Blood Flow. *Crit Care Med.* (2019) 47:1472–3. doi: 10.1097/CCM.0000000000003947
13. Donnelly J, Aries MJ, Czosnyka M. Further understanding of cerebral autoregulation at the bedside: possible implications for future therapy. *Expert Rev Neurother.* (2015) 15:169–85. doi: 10.1586/14737175.2015.996552
14. Shamseer L, Moher D, Clarke M, Ghersi D, Liberati A, Petticrew M, et al. Preferred reporting items for systematic review and meta-analysis protocols (PRISMA-P) 2015: elaboration and explanation. *BMJ.* (2015) 350:g7647. doi: 10.1136/bmj.g7647
15. Schramm P, Klein KU, Falkenberg L, Berres M, Closhen D, Werhahn KJ, et al. Impaired cerebrovascular autoregulation in patients with severe sepsis and sepsis-associated delirium. *Crit Care.* (2012) 16:R181. doi: 10.1186/cc11665
16. Bindra J, Pham P, Chuan A, Jaeger M, Aneman A. Is impaired cerebrovascular autoregulation associated with outcome in patients admitted to the ICU with early septic shock? *Crit Care Resusc.* (2016) 18:95–101.
17. Crippa IA, Subirà C, Vincent JL, Fernandez RF, Hernandez SC, Cavicchi FZ, et al. Impaired cerebral autoregulation is associated with brain dysfunction in patients with sepsis. *Crit Care.* (2018) 22:327. doi: 10.1186/s13054-018-2258-8
18. Rosenblatt K, Walker KA, Goodson C, Olson E, Maher D, Brown CH. Cerebral autoregulation-guided optimal blood pressure in sepsis-associated encephalopathy: a case series. *J Intensive Care Med.* (2020) 35:1453–64. doi: 10.1177/0885066619828293
19. Brady KM, Mytar JO, Lee JK, Cameron DE, Vricella LA, Thompson WR, et al. Monitoring cerebral blood flow pressure autoregulation in pediatric patients during cardiac surgery. *Stroke.* (2010) 41:1957–62. doi: 10.1161/STROKEAHA.109.575167
20. Thewissen L, Caicedo A, Dereymaeker A, Van Huffel S, Naulaers G, Allegaert K, et al. Cerebral autoregulation and activity after propofol for endotracheal intubation in preterm neonates. *Pediatr Res.* (2018) 84:719–25. doi: 10.1038/s41390-018-0160-3
21. Joram N, Beqiri E, Pezzato S, Andrea M, Robba C, Liet JM, et al. Continuous monitoring of cerebral autoregulation in children supported by extracorporeal membrane oxygenation: a pilot study. *Neurocrit Care.* (2021) 34:935–45. doi: 10.1007/s12028-020-01111-1
22. Caldas JR, Panerai RB, Bor-Seng-Shu E, Ferreira GSR, Camara L, Passos RH, et al. Dynamic cerebral autoregulation: A marker of post-operative delirium? *Clin Neurophysiol.* (2019) 130:101–8. doi: 10.1016/j.clinph.2018.11.008
23. Ono M, Arnaoutakis GJ, Fine DM, Brady K, Easley RB, Zheng Y, et al. Blood pressure excursions below the cerebral autoregulation threshold during cardiac surgery are associated with acute kidney injury. *Crit Care Med.* (2013) 41:464–71. doi: 10.1097/CCM.0b013e31826ab3a1
24. Hori D, Max L, Laflam A, Brown C, Neufeld KJ, Adachi H, et al. Blood pressure deviations from optimal mean arterial pressure during cardiac surgery measured with a novel monitor of cerebral blood flow and risk for perioperative delirium: a pilot study. *J CardiothoracVascAnesth.* (2016) 30:606–12. doi: 10.1053/j.jvca.2016.01.012
25. Hori D, Brown C, Ono M, Rappold T, Sieber F, Gottschalk A, et al. Arterial pressure above the upper cerebral autoregulation limit during cardiopulmonary bypass is associated with postoperative delirium. *Br J Anaesth.* (2014) 113:1009–17. doi: 10.1093/bja/aeu319
26. Sperna Weiland NH, Hermanides J, Hollmann MW, Preckel B, Stok WJ, van Lieshout JJ, et al. Novel method for intraoperative assessment of cerebral autoregulation by paced breathing. *Br J Anaesth.* (2017) 119:1141–9. doi: 10.1093/bja/aex333
27. Chuan A, Short TG, Peng AZY, Wen SYB, Sun AX, Ting TH, et al. Is cerebrovascular autoregulation associated with outcomes after major noncardiac surgery? A prospective observational pilot study. *Acta Anaesthesiol Scand.* (2019) 63:8–17. doi: 10.1111/aas.13223
28. Goettel N, Burkhart CS, Rossi A, Cabella BC, Berres M, Monsch AU, et al. Associations between impaired cerebral blood flow autoregulation, cerebral oxygenation, and biomarkers of brain injury and postoperative cognitive dysfunction in elderly patients after major noncardiac surgery. *Anesth Analg.* (2017) 124:934–42. doi: 10.1213/ANE.0000000000001803
29. Zheng Y, Villamayor AJ, Merritt W, Pustavoitau A, Latif A, Bhambhani R, et al. Continuous cerebral blood flow autoregulation monitoring in patients undergoing liver transplantation. *Neurocrit Care.* (2012) 17:77–84. doi: 10.1007/s12028-012-9721-1
30. Hogue CW, Brown CH, Hori D, Ono M, Nomura Y, Balmert LC, et al. Personalized blood pressure management during cardiac surgery with cerebral autoregulation monitoring: a randomized trial. *Semin Thorac Cardiovasc Surg.* (2021) 33:429–38. doi: 10.1053/j.semtcvs.2020.09.032
31. Berg RM, Plovsing RR, Bailey DM, Holstein-Rathlou NH, Møller K. Dynamic cerebral autoregulation to induced blood pressure changes in human experimental and clinical sepsis. *Clin PhysiolFunct Imaging.* (2016) 36:490–6. doi: 10.1111/cpf.12256
32. Hori D, Hogue C, Adachi H, Max L, Price J, Sciortino C, et al. Perioperative optimal blood pressure as determined by ultrasound tagged near infrared spectroscopy and its association with postoperative acute kidney injury in cardiac surgery patients. *Interact Cardiovasc Thorac Surg.* (2016) 22:445–51. doi: 10.1093/icvts/ivv371
33. Caldas JR, Haunton VJ, Panerai RB, Hajjar LA, Robinson TG. Cerebral autoregulation in cardiopulmonary bypass surgery: a systematic review. *Interact Cardiovasc Thorac Surg.* (2018) 26:494–503. doi: 10.1093/icvts/ivx357
34. Goettel N, Patet C, Rossi A, Burkhart CS, Czosnyka M, Strebel SP, et al. Monitoring of cerebral blood flow autoregulation in adults undergoing

sevoflurane anesthesia: a prospective cohort study of two age groups. *J Clin Monit Comput.* (2016) 30:255–64. doi: 10.1007/s10877-015-9754-z

Conflict of Interest: The authors declare that the research was conducted in the absence of any commercial or financial relationships that could be construed as a potential conflict of interest.

Publisher's Note: All claims expressed in this article are solely those of the authors and do not necessarily represent those of their affiliated organizations, or those of the publisher, the editors and the reviewers. Any product that may be evaluated in this article, or claim that may be made by its manufacturer, is not guaranteed or endorsed by the publisher.

frontiers in Neurology

MINI REVIEW
published: 17 November 2021
doi: 10.3389/fneur.2021.765333

Cerebrovascular Disease in the Setting of Posterior Reversible Encephalopathy Syndrome

XiaoQing Cheng[1†], *JianRui Li*[1†], *Ying Lan*[2], *Jia Liu*[1], *Sui Chen*[1] *and GuangMing Lu*[1*]

[1] *Department of Medical Imaging, Jinling Hospital, Nanjing University School of Medicine, Nanjing, China,* [2] *Special Medical Service, Lushan Rehabilitation and Recuperation Center of People's Liberation Army (PLA), Jiujiang, China*

Overlap between the pathogenesis of posterior reversible encephalopathy syndrome and that of cerebrovascular disease can confound their clinical and radiological presentations, posing a diagnostic challenge. This article presents a literature review and discussion of the clinical manifestations, pathological mechanisms, and imaging manifestations of subarachnoid hemorrhage and vasculitis leading to posterior reversible encephalopathy syndrome, coexistence of posterior reversible encephalopathy syndrome with reversible cerebral vasoconstriction syndrome, and hemorrhage and infarction secondary to posterior reversible encephalopathy syndrome. The findings show that posterior reversible encephalopathy syndrome shares some overlapping pathophysiological mechanisms with cerebrovascular disease. Importantly, neuroimaging plays an important role in identifying this entity in a timely manner and differentiating it from other diseases.

Keywords: posterior reversible encephalopathy syndrome, reversible cerebral vasoconstriction syndrome, magnetic resonance imaging, blood brain barrier, angiography, diffusion-weighted imaging

OPEN ACCESS

Edited by:
Dong Ming,
Tianjin University, China

Reviewed by:
Bo Gao,
Affiliated Hospital of Guizhou Medical University, China
Fabio Pilato,
Policlinico Universitario Campus Bio-Medico, Italy
Hongliang Zhang,
National Natural Science Foundation of China, China

***Correspondence:**
GuangMing Lu
cjr.luguangming@vip.163.com

[†] *These authors have contributed equally to this work*

Specialty section:
This article was submitted to Applied Neuroimaging, a section of the journal Frontiers in Neurology

Received: *26 August 2021*
Accepted: *25 October 2021*
Published: *17 November 2021*

Citation:
Cheng X, Li J, Lan Y, Liu J, Chen S and Lu G (2021) Cerebrovascular Disease in the Setting of Posterior Reversible Encephalopathy Syndrome. Front. Neurol. 12:765333. doi: 10.3389/fneur.2021.765333

INTRODUCTION

Posterior reversible encephalopathy syndrome (PRES) is a reversible acute neurological disorder characterized by varied neurological symptoms, including seizure, headache, focal neurological deficit, visual disturbance, and altered consciousness (1–3). Case series have shown that hypertension, eclampsia, renal failure, systemic lupus erythematosus, and use of some immunosuppressive agents are common causes of PRES (1–4). Brain MRI, particularly fluid-attenuated inversion recovery is the most sensitive sequence for detecting PRES, and usually reveals characteristic vasogenic edema predominantly affecting subcortical white matter of the parietal and occipital lobes (5, 6).

Among the various theories that have been proposed for the pathogenesis of PRES, hypertension and endothelial injury are often cited as the underlying mechanisms (1). Rapidly developing hypertension exceeds the upper limit of cerebral blood flow autoregulation and causes hyperperfusion, which leads to breakdown of the blood–brain–barrier and subsequent vasogenic brain edema (7, 8). Thus, multiple interactions exist between PRES and cerebrovascular diseases, such as subarachnoid hemorrhage (SAH) and vasculitis (9, 10), reversible cerebral vasoconstriction syndrome (RCVS) (11–13), and cerebral hemorrhage and infarction secondary to PRES (5, 14–16).

Overlap between PRES and cerebrovascular disease in terms of their clinical and pathological mechanisms and imaging manifestations can easily lead to misdiagnosis, differences in treatment modalities, and a poor prognosis when secondary hemorrhage and infarction are indicated. Therefore, it is important to understand and identify PRES associated with cerebrovascular

disease (**Table 1**). In this review, we discuss PRES and multiple cerebrovascular diseases in terms of their clinical features, pathological mechanisms, and imaging manifestations.

PRES SECONDARY TO SAH AND VASCULITIS

Clinical Features

SAH is most commonly caused by rupture of an intracranial aneurysm (17). After SAH, delayed cerebral ischemia (DCI) may occur when cerebral perfusion falls below the level required to meet metabolic demands, and this could lead to the development of cerebral infarction. Induced hypertension therapy raises blood pressure to above normal levels and results in an increase in cerebral blood flow; it remains the mainstay of treatment for DCI (18). However, in patients treated with induced hypertension therapy, an elevation in arterial blood pressure may exceed the threshold for autoregulatory function of the brain and may lead to spontaneous angioedema (19).

To date, PRES has been reported in 20 cases as a consequence of induced hypertension therapy, and 80% of the patients were female (19). Allen et al. (18) reported induced hypertension therapy in 68 patients with SAH, of which 5 patients (7%) were diagnosed with PRES, which most often occurred when mean arterial pressure was raised well above baseline to levels that exceed traditional autoregulatory thresholds. According to the latest data reported by Angermann et al. (9) showing that the incidence of PRES among patients with SAH after induced hypertension therapy is 1.7%, the authors noted that no safe upper limit of mean arterial pressure has been established during the treatment of vasospasm with induced hypertension therapy.

Takayasu's arteritis (TA) is a rare chronic inflammatory disease that primarily affects the aorta, aortic branches, and the pulmonary artery (10). PRES secondary to TA has been reported in 13 patients, according to a PubMed search (10, 20). In addition to TA secondary to PRES, in isolated cases, PRES has also been reported to occur secondary to rare vasculitis, such as cerebral amyloid angiopathy-related inflammation (21), and antineutrophil cytoplasmic antibody-associated vasculitis (22).

Pathological Mechanisms

According to the literature, the pathophysiological mechanism of PRES caused by induced hypertension therapy for SAH is unclear, and it is speculated that multiple factors may be responsible. On the one hand, acute hypertension caused by catecholamine surge during aneurysm rupture stimulates the sympathetic nerves, leading to a sudden increase in blood pressure, which may induce autonomic vasoconstriction and lead to ischemia and vasogenic edema in the affected area (23). Another hypothesis is that induced hypertension therapy may increase intravascular hydrostatic pressure over the damaged blood–brain barrier and cause the rupture of vascular endothelial junctions, leading to the development of acute PRES (19, 24). Accordingly, it has been found that the percentage change in blood pressure is significantly greater in patients with PRES than in those without PRES, and that an increase in mean arterial pressure to 50 mm Hg above the patients' physiological levels or to an absolute range of >130–140 mm Hg is a sensitive predictor of PRES (18).

The main pathophysiological change in TA is panarteritis involving all vessel wall layers. In the acute phase, production of inflammatory cytokines and mediators induces continuous endothelial injury, while in the chronic phase, hyperplasia of the vessel wall and fibrosis of the arterial wall cause luminal narrowing and can lead to the development of hypertension (20). Endothelial injury and hypertension in patients with TA make this disease an ideal environment for PRES development. Furthermore, the treatment of TA begins with control of acute arteritis with immunosuppressive drugs; however, their use is also a possible factor that contributes to PRES development (9).

Imaging Manifestations

As PRES is treated differently from vasospasm, and both may occur secondary to SAH, it is crucial to identify the two in a timely manner. Vasospasm usually develops 3–4 days after SAH and continues for 10–14 days (25). Yet, PRES is most often delayed, occurring ∼1 week after induced hypertension therapy. Moreover, PRES is more likely to occur in older patients and in patients with a mean arterial pressure of 50 mmHg above habitual levels (or absolute levels of >130–140 mmHg) (18). CT perfusion imaging helps to identify delayed cerebral ischemia related to vasospasm, which can manifest as decreased cerebral blood flow and a prolonged mean transit time in the blood supply area of affected vessels (26). However, CT and MRI perfusion studies in PRES are contradictory, with two patterns: hyperperfusion and hypoperfusion. Hyperperfusion shows increased cerebral blood flow and cerebral blood volume and decreased time to peak and mean transit time, the mechanism behind which may be severe hypertension exceeding the limits of vascular autoregulation, leading to hyperperfusion (27, 28). Hypoperfusion possibly occurs due to vasoconstriction as a compensatory mechanism for hypertension, leading to decreased cerebral blood flow, near-normal cerebral blood volume, and increased time to peak and mean transit time (29, 30). The conflicting results likely reflect the complex pathophysiology of PRES. Therefore, although perfusion imaging cannot completely distinguish delayed cerebral ischemia from PRES by assessing hyperperfusion and hypoperfusion, assessing whether vasospasm leads to hemodynamic changes can help screen patients for induced hypertension therapy, avoiding blind lowering of blood pressure, which can lead to PRES development.

PRES secondary to TA presents as fluid-attenuated inversion recovery hyperintensities on MRI, while there is usually no diffusion restriction on DWI (10, 20). The onset could be in the bilateral parieto-occipital lobes, bilateral temporoparietal-occipital lobes, and the cerebellum, as reported for PRES caused by other factors (10, 20). In addition, after CTA or MRA, TA should be considered when combined intracranial artery stenosis, intracranial aneurysm, carotid artery occlusion, and other vascular changes are found.

TABLE 1 | PRES and cerebrovascular disease.

	PRES secondary to SAH and vasculitis	PRES coexisting with RCVS	Hemorrhage and infarction secondary to PRES
Incidence	1. Incidence of PRES among patients with SAH after induced hypertension therapy is 1.7–7% 2. PRES secondary to TA has been reported in 13 patients	RCVS is present in ∼8–85% of patients with PRES	1. The incidence of intracranial hemorrhage secondary to PRES was 15.2–64.5% 2. The incidence of cerebral infarction secondary to PRES is 9%
Pathogenesis	1. Ruptured aneurysm causing a sudden increase in blood pressure and BBB breakdown after induced hypertension therapy; 2. Panarteritis involving vessel wall layers	1. Abnormal cerebral autoregulation 2. BBB breakdown 3. Vascular endothelial damage	1. Vessel rupture 2. Reperfusion injury 3. Cytotoxic edema
Imaging	1. Vasospasm and PRES can be differentiated by time of onset, age, blood pressure and perfusion imaging 2. Hemodynamic changes provided by perfusion imaging can help screen patients with SAH for induced hypertension therapy 3. TA combined with intracranial artery stenosis, intracranial aneurysm, carotid artery occlusion and other vascular changes	1. The distribution of edema secondary to RCVS is different from the typical PRES lesions 2. Follow-up CTA or MRA can assess reversible vascular changes in RCVS 3. MR vessel wall imaging may be helpful in distinguishing RCVS from vasculitis 4. Perfusion imaging may be a useful approach in identifying cerebral hypoperfusion secondary to RCVS	1. Intracranial hematoma secondary to PRES occurs within the area of brain parenchyma affected by edema 2. SAH typically secondary to PRES occurs in the cerebral convexities overlying vasogenic edema and is rarely seen in basal cisterns 3. Decreased ADC values represent cytotoxic edema and can help predict infarction and irreversible tissue damage

ADC, apparent diffusion coefficient; BBB, blood-brain barrier; RCVS, reversible cerebral vasoconstriction syndrome; PRES, posterior reversible encephalopathy syndrome; SAH, subarachnoid hemorrhage.

PRES COEXISTING WITH RCVS

Clinical Features

RCVS is a clinical and radiological syndrome characterized by "thundering" headaches, transient, multifocal and segmental cerebral arterial vasoconstriction lasting weeks to months, and focal neurological symptoms that may also complicate ischemic or hemorrhagic stroke (13). Although RCVS is frequently reported in the literature, most studies on RCVS are observational and thus the etiology, and the underlying mechanism remain largely unknown. The occurrence of PRES with coexisting RCVS is not uncommon in clinical practice. Studies report that RCVS is present in ∼8–85% of patients with PRES who undergo MRA or catheter angiography (11–13). The diagnostic criteria for RCVS emphasize acute onset of "thundering" headache with reversible, multisegmental cerebral vasoconstriction on imaging, while excluding other diagnoses such as aneurysmal SAH or central nervous system vasculitis.

Pathological Mechanisms

The main pathophysiological mechanisms for coexistence of PRES and RCVS include blood–brain barrier breakdown and abnormal cerebral autoregulation (3). Considering that RCVS occurs in the postpartum period and after vasoactive drug use, it is presumed that hormonal changes and drug-induced vascular endothelial damage are more directly responsible for RCVS occurrence with PRES. In addition, both vasoconstriction and hypoperfusion improve with increasing maturity of the involved brain region; thus, it has been suggested in the literature that children might be more prone to PRES and its complications (31).

RCVS has high hemorrhagic complications, some researchers attributed the high rate of hemorrhagic complications in RCVS to a reperfusion injury following the episode of severe vasoconstriction (32), and it has also been suggested that subarachnoid hemorrhage actually preceded typical segmental vasoconstriction revealed by DSA (33). However, in clinical observational studies, a causal relationship between subarachnoid hemorrhage and RCVS seems difficult to prove.

Imaging Manifestations

Radiological presentations, taken together with clinical context and symptoms, may help to reach a differential diagnosis. On MRI, the typical lesion distribution in patients with PRES is characterized by bilateral symmetrical parieto-occipital lesions, whereas vasogenic edematous changes secondary to RCVS are mostly distributed in periventricular white matter and lack cortical involvement (**Figure 1**). Of note, it has been reported in the literature that PRES in children exhibits more of a suprafrontal sulcus pattern, while the typical parieto-occipital pattern is less frequent in children compared with adults (4). Furthermore, patients with RCVS do not usually present with seizures or severe cerebral or brainstem edema (34). From the angiographic presentation, digital subtraction angiography is the gold standard for the diagnosis of vascular lesions, while CT angiography and MRA allow for non-invasive assessment of reversible vascular changes and facilitate follow-up review (12) (**Figures 1E,F,H,I**). In addition, MR vessel wall imaging may be helpful in distinguishing RCVS from vasculitis, since RCVS demonstrates arterial wall thickening with absent to minimal enhancement of vessel walls compared with more pronounced enhancement in vasculitis (35). Perfusion imaging

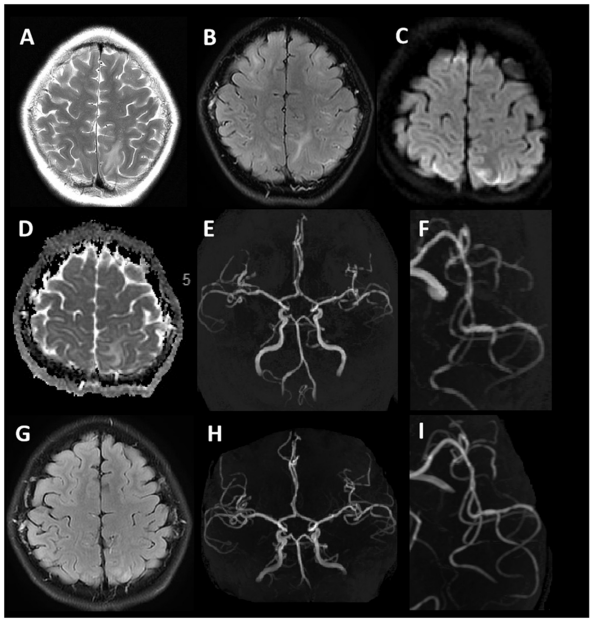

FIGURE 1 | Typical MRI findings in PRES coexisting with RCVS. A 12-year-old female with lupus nephritis. T2WI and T2 -FLAIR imaging **(A,B)** show hyperintense signals involving bilateral subcortical white matter of the frontal, parietal, and temporal lobes. DWI **(C)** shows hyperintense signals in bilateral frontoparietal lobes. The corresponding ADC map **(D)** shows no diffusion restriction. MRA **(E,F)** demonstrates segmental vasoconstriction in the left middle cerebral artery branch. Follow-up MRI after 10 days (T2-FLAIR) **(G)** demonstrates complete resolution of signal abnormalities. MRA **(H,I)** demonstrates normalization of vessel irregularity.

may be a useful approach in identifying cerebral hypoperfusion secondary to RCVS and to assess radiographic improvement after treatment (36).

When PRES and RCVS coexist, given the complicated disease course, the appropriate therapy is often controversial (37). Usual treatment for PRES in the setting of hypertension is to gradually lower blood pressure. However, in the setting of RCVS, an argument could be made to maintain or elevate blood pressure. Chung et al. (38) proposed the use of near-infrared spectroscopy, which is a non-invasive modality to monitor regional cerebral oxygenation and guide subsequent decision making. Therefore, the purpose of imaging is not to completely differentiate between RCVS and PRES, but to exclude other diseases and provide appropriate treatment recommendations and predict prognosis by assessing cerebral hemodynamics and cerebral oxygen saturation.

HEMORRHAGE AND INFARCTION SECONDARY TO PRES

Clinical Features

Intracranial hemorrhage is a common complication of PRES, with an incidence of 15.2–64.5% (14, 15), and is associated with incomplete resolution of PRES (39). Intracranial hemorrhage manifests in three main patterns: intracranial hematoma, subarachnoid hemorrhage, and microhemorrhage, with intracranial hematoma being the most common (14). Susceptibility-weighted imaging (SWI) sequences are more sensitive than conventional T2 gradient-recalled echo imaging in detecting cerebral hemorrhage and microhemorrhage (**Figures 2E–H**), and 58% of patients with PRES combined with microhemorrhage were identified by SWI (15).

Vasogenic edema is a predominant feature of PRES, and the presence of restricted diffusion in some cases may represent the earliest irreversible sign: severe vasogenic edema progresses to cytotoxic edema, which further progresses to cerebral infarction (6). Covarrubias et al. (40) reported a group of 22 patients with PRES, 6 of whom developed diffusion abnormalities and 2 (9%) of whom showed progression to infarction at follow-up. Several studies have evaluated the clinical and radiological findings of patients with PRES and reported incomplete recovery and poor functional outcomes when PRES was associated with hemorrhage and infarction (3, 37, 41). Thus, early MRI features may be warning signs of a poor prognosis.

Pathological Mechanisms

In terms of etiology, hemorrhage in PRES is associated with ongoing therapeutic anticoagulation, intrinsic coagulopathy, bone marrow transplantation, and thrombocytopenia (8). There are multiple underlying pathophysiological mechanisms that can cause hemorrhage in patients with PRES. Pial vessel rupture during severe hypertension, reperfusion injury in the setting of vasoconstriction, and endothelial injury directly caused by use of immunosuppressive agents have all been postulated as mechanisms leading to hemorrhagic PRES (7). In 2020, three patients with coronavirus disease 2019 compatible with hemorrhagic PRES were reported (42, 43). Available data suggest that the severe acute respiratory syndrome coronavirus 2 directly infects endothelial cells, causing damage to their lining, and thus increasing the permeability of the blood–brain barrier. In addition, further secondary hemorrhage can occur due to cytokine release syndrome resulting from liver dysfunction and depletion of coagulation factors (1).

On the basis of vasogenic edema caused by PRES, when further arterial vasospasm and endothelial injury lead to a decrease in local cerebral blood flow and hypoxia in brain tissue, further cytotoxic edema can develop, leading to infarction (40, 41).

Imaging Manifestations

Intracranial hematoma secondary to PRES occurs within the area of the brain parenchyma affected by edema (**Figures 2A–D**). SAH secondary to PRES typically occurs in the cerebral convexities overlying vasogenic edema and is rarely seen in the basal cisterns; this is different from the area of distribution of SAH caused by aneurysm rupture and can help in the differential diagnosis of the two entities (44). In addition, PRES and cerebral venous sinus thrombosis have similar clinical presentations, causative factors, and imaging findings, such as vasogenic edema, diffusion restriction on DWI, and hemorrhage (45). The key to

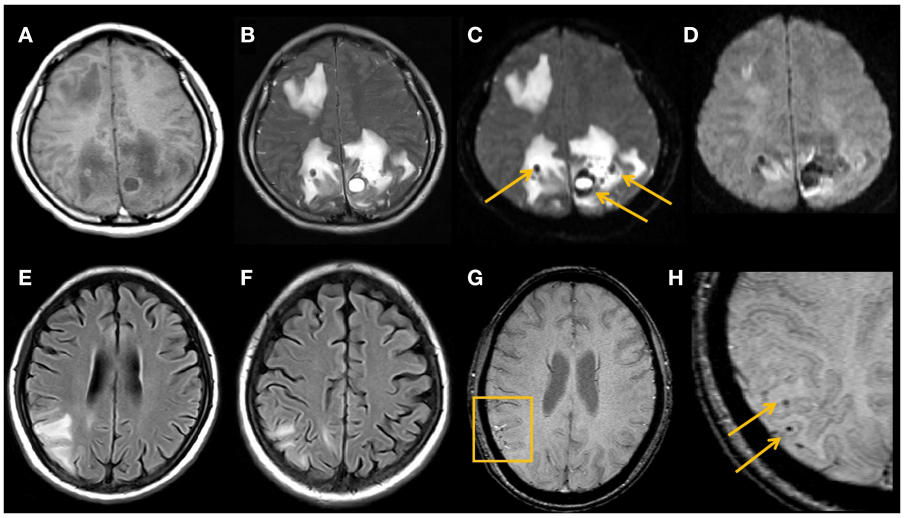

FIGURE 2 | Typical MRI findings in hemorrhage secondary to PRES.Imaging studies in a 29-year-old female with lupus **(A–D)**. MRI shows vasogenic edema in the right frontal lobe and bilateral parieto-occipital lobes, multiple hematomas are seen in the area affected by the edema, with heterogeneous high signal on T1WI **(A)**, low signal on T2WI **(B)**, low signal on DWI b = 0 images (arrows) **(C)**, and magnetically sensitive artifacts of high signal around the hematoma visible on DWI b = 1,000 images **(D)**. An 18-year-old young female with nephrotic syndrome **(E–H)**. PRES-related right parieto-occipital cortical and subcortical edema on MRI FLAIR image **(E,F)**, with multiple small microhemorrhages on SWI (arrows) **(G,H)**.

differentiating between them is the use of CT or MRI venography to exclude venous sinus thrombosis.

From an imaging perspective, DWI can help predict conversion to infarction and irreversible tissue damage (46). The hallmark of PRES lesions is a pattern of vasogenic edema, which is shown as an increased apparent diffusion coefficient (ADC), while decreased ADC values indicate cytotoxic edema that inevitably induces cell death and progression to true infarction. However, when vasogenic edema is combined with cytotoxic edema, it usually presents as small areas or short cortical gyriform foci of restricted diffusion within larger regions of vasogenic edema (7), unlike the territorial infarctions due to arterial occlusion.

CONCLUSION

In conclusion, the occurrence of PRES is associated with various pathological mechanisms, such as abnormalities in brain autoregulation, blood–brain barrier breakdown, and vascular endothelial damage, which are also factors associated with the development of related cerebrovascular diseases. Neuroimaging plays an important role in revealing the pathophysiological mechanisms of PRES, differentiating PRES from other cerebrovascular diseases, guiding treatment, and predicting a poor prognosis.

AUTHOR CONTRIBUTIONS

XC: study design, data analysis, drafting the manuscript, and revising it critically. JLi and SC: acquisition of data, drafting the manuscript, and revising it critically. YL and JLiu: image processing, interpretation of the data, drafting the manuscript, and revising it critically. GL: study concept and design, review of all the images and advise on the findings. All authors have read and approved the manuscript.

FUNDING

This work was supported by the major project of the National Natural Scientific Foundation of China (Grant Number: 81790653).

REFERENCES

1. Fugate JE, Rabinstein AA. Posterior reversible encephalopathy syndrome: clinical and radiological manifestations, pathophysiology, and outstanding questions. *Lancet Neurol.* (2015) 14:914–25. doi: 10.1016/S1474-4422(15)00111-8
2. Bartynski WS. Posterior reversible encephalopathy syndrome, part 1: fundamental imaging and clinical features. *AJNR Am J Neuroradiol.* (2008) 29:1036–42. doi: 10.3174/ajnr.A0928
3. Lee MJ, Cha J, Choi HA, Woo SY, Kim S, Wang SJ, et al. Blood-brain barrier breakdown in reversible cerebral vasoconstriction syndrome: implications for pathophysiology and diagnosis. *Ann Neurol.* (2017) 81:454–66. doi: 10.1002/ana.24891
4. Gavrilovici C, Miron I, Voroneanu L, Bădărau S, Stârcea M. Posterior reversible encephalopathy syndrome in children with kidney disease. *Int Urol Nephrol.* (2017) 49:1793–800. doi: 10.1007/s11255-017-1684-x
5. McKinney AM, Sarikaya B, Gustafson C, Truwit CL. Detection of microhemorrhage in posterior reversible encephalopathy syndrome using

susceptibility-weighted imaging. *AJNR Am J Neuroradiol.* (2012) 33:896–903. doi: 10.3174/ajnr.A2886
6. Schweitzer AD, Parikh NS, Askin G, Nemade A, Lyo J, Karimi S, et al. Imaging characteristics associated with clinical outcomes in posterior reversible encephalopathy syndrome. *Neuroradiology.* (2017) 59:379–86. doi: 10.1007/s00234-017-1815-1
7. Chen Z, Shen GQ, Lerner A, Gao B. Immune system activation in the pathogenesis of posterior reversible encephalopathy syndrome. *Brain Res Bull.* (2017) 131:93–9. doi: 10.1016/j.brainresbull.2017.03.012
8. Lai CC, Chen WS, Chang YS, Wang SH, Huang CJ, Guo WY, et al. Huang DF, clinical features and outcomes of posterior reversible encephalopathy syndrome in patients with systemic lupus erythematosus. *Arthritis Care Res.* (2013) 65:1766–74. doi: 10.1002/acr.22047
9. Angermann M, Jablawi F, Keulers A, Angermann M, Schubert GA, Weiss M, et al. Posterior reversible encephalopathy syndrome after induced hypertension therapy for delayed cerebral ischemia after subarachnoid hemorrhage: a case-control study. *J Neurol Sci.* (2021) 421:117313. doi: 10.1016/j.jns.2021.117313
10. Camara-Lemarroy CR, Lara-Campos JG, Perez-Contreras E, Rodríguez-Gutiérrez R, Galarza-Delgado DA. Takayasu's arteritis and posterior reversible encephalopathy syndrome: a case-based review. *Clin Rheumatol.* (2013) 32:409–15. doi: 10.1007/s10067-012-2151-9
11. Mayama M, Uno K, Tano S, Yoshihara M, Ukai M, Kishigami Y, et al. Incidence of posterior reversible encephalopathy syndrome in eclamptic and patients with preeclampsia with neurologic symptoms. *Am J Obstet Gynecol.* (2016) 215:239.e1–e2395. doi: 10.1016/j.ajog.2016.02.039
12. Bartynski WS, Boardman JF. Catheter angiography, MR angiography, and MR perfusion in posterior reversible encephalopathy syndrome. *AJNR Am J Neuroradiol.* (2008) 29:447–55. doi: 10.3174/ajnr.A0839
13. Li Y, Gor D, Walicki D, Jenny D, Jones D, Barbour P, et al. Spectrum and potential pathogenesis of reversible posterior leukoencephalopathy syndrome. *J Stroke Cerebrovasc Dis.* (2012) 21:873–82. doi: 10.1016/j.jstrokecerebrovasdis.2011.05.010
14. Hefzy HM, Bartynski WS, Boardman JF, Lacomis D. Hemorrhage in posterior reversible encephalopathy syndrome: imaging and clinical features. *AJNR Am J Neuroradiol.* (2009) 30:1371–79. doi: 10.3174/ajnr.A1588
15. Hiremath SB, Anantrao Gautam A, Anil S, Thomas R, Benjamin G. Susceptibility-weighted angiography and diffusion-weighted imaging in posterior reversible encephalopathy syndrome - is there an association between hemorrhage, cytotoxic edema, blood pressure and imaging severity?. *J Neuroradiol.* (2017) 44:319–25. doi: 10.1016/j.neurad.2017.05.002
16. Liang H, Li D, Xu Z, Luo B. Isolated pons variant of posterior reversible encephalopathy syndrome complicated with ischemic stroke in a young patient. *Neurol Sci.* (2013) 34:585–7. doi: 10.1007/s10072-012-1082-1
17. Chen J, Li M, Zhu X, Chen L, Yang S, Zhang C, et al. Atorvastatin reduces cerebral vasospasm and infarction after aneurysmal subarachnoid hemorrhage in elderly Chinese adults. *Aging.* (2020) 12:2939–51. doi: 10.18632/aging.102788
18. Allen ML, Kulik T, Keyrouz SG, Dhar R. Posterior reversible encephalopathy syndrome as a complication of induced hypertension in subarachnoid hemorrhage: a case-control study. *Neurosurgery.* (2019) 85:223–30. doi: 10.1093/neuros/nyy240
19. Muhammad S, Güresir Á, Greschus S, Scorzin J, Vatter H, Güresir E. Posterior reversible encephalopathy syndrome as an overlooked complication of induced hypertension for cerebral vasospasm: systematic review and illustrative case. *Stroke.* (2016) 47:519–22. doi: 10.1161/STROKEAHA.115.011697
20. Dunne RM, Duignan J, Tubridy N, O'Neill L, Kinsella JA, Omer TA, et al. Posterior reversible encephalopathy syndrome with Lilliputian hallucinations secondary to Takayasu's arteritis. *Radiol Case Rep.* (2020) 15:1999–2002. doi: 10.1016/j.radcr.2020.07.080
21. Masrori P, Montagna M, De Smet E, Loos C. Posterior reversible encephalopathy syndrome caused by cerebral amyloid angiopathy-related inflammation. *Acta Neurol Belg.* (2019) 119:505–7. doi: 10.1007/s13760-019-01172-w
22. Sakai R, Sakurai S, Okada T, Takahashi T, Hayakawa S, Koji H, et al. Case report: atypical posterior reversible encephalopathy syndrome (PRES) and thrombotic microangiopathy (TMA) in a hemodialysis patient with ANCA-associated vasculitis: a case report. *Nihon Naika Gakkai Zasshi.* (2016) 105:275–9. doi: 10.2169/naika.105.275
23. Nanba T, Kashimura H, Saura H, Takeda M. Subarachnoid hemorrhage due to ruptured intracranial aneurysm following posterior reversible encephalopathy syndrome. *J Neurosci Rural Pract.* (2016) 7:440–2. doi: 10.4103/0976-3147.182767
24. Elsamadicy AA, Koo AB, Reeves BC, Sujijantarat N, David WB, Malhotra A, et al. Posterior reversible encephalopathy syndrome caused by induced hypertension to treat cerebral vasospasm secondary to aneurysmal subarachnoid hemorrhage. *World Neurosurg.* (2020) 143:e309–3. doi: 10.1016/j.wneu.2020.07.135
25. Borkar SA, Singh M, Kale SS, Suri A, Chandra PS, Kumar R, et al. Spinal cerebrospinal fluid drainage for prevention of vasospasm in aneurysmal subarachnoid hemorrhage: a prospective, randomized controlled study. *Asian J Neurosurg.* (2018) 13:238–46. doi: 10.4103/1793-5482.228512
26. Fragata I, Alves M, Papoila AL, Diogo M, Canhão P, Canto-Moreira N. Temporal evolution of cerebral computed tomography perfusion after acute subarachnoid hemorrhage: a prospective cohort study. *Acta Radiol.* (2020) 61:376–85. doi: 10.1177/0284185119858701
27. Hedna VS, Stead LG, Bidari S, Patel A, Gottipati A, Favilla CG, et al. Posterior reversible encephalopathy syndrome (PRES) and CT perfusion changes. *Int J Emerg Med.* (2012) 5:12. doi: 10.1186/1865-1380-5-12
28. Oehm E, Hetzel A, Els T, Berlis A, Keck C, Will HG, et al. Cerebral hemodynamics and autoregulation in reversible posterior leukoencephalopathy syndrome caused by pre-/eclampsia. *Cerebrovasc Dis.* (2006) 22:204–08. doi: 10.1159/000093810
29. Vanacker P, Matias G, Hagmann P, Michel P. Cerebral hypoperfusion in posterior reversible encephalopathy syndrome is different from transient ischemic attack on CT perfusion. *J Neuroimaging.* (2015) 25:643–46. doi: 10.1111/jon.12158
30. Sarbu N, López-Rueda A, Chirife O, Capurro S. CT-perfusion time-maps likely disclose the earliest imaging signs of posterior reversible encephalopathy syndrome (PRES). *J Neuroradiol.* (2014) 41:147–9. doi: 10.1016/j.neurad.2013.08.003
31. Donmez FY, Guleryuz P, Agildere M. MRI findings in childhood PRES: what is different than the adults? *Clin Neuroradiol.* (2016) 26:209–13. doi: 10.1007/s00062-014-0350-2
32. Ducros A, Fiedler U, Porcher R, Boukobza M, Stapf C, Bousser MG. Hemorrhagic manifestations of reversible cerebral vasoconstriction syndrome: frequency, features, and risk factors. *Stroke.* (2010) 41:2505–11. doi: 10.1161/STROKEAHA.109.572313
33. Noda K, Fukae J, Fujishima K, Mori K, Urabe T, Hattori N, et al. Reversible cerebral vasoconstriction syndrome presenting as subarachnoid hemorrhage, reversible posterior leukoencephalopathy, and cerebral infarction. *Internal Med.* (2011) 50:1227–33. doi: 10.2169/internalmedicine.50.4812
34. Miller TR, Shivashankar R, Mossa-Basha M, Gandhi D. Reversible cerebral vasoconstriction syndrome, part 2: diagnostic work-up, imaging evaluation, and differential diagnosis. *AJNR Am J Neuroradiol.* (2015) 36:1580–88. doi: 10.3174/ajnr.A4215
35. Obusez EC, Hui F, Hajj-Ali RA, Cerejo R, Calabrese LH, Hammad T, et al. High-resolution MRI vessel wall imaging: spatial and temporal patterns of reversible cerebral vasoconstriction syndrome and central nervous system vasculitis. *AJNR Am J Neuroradiol.* (2014) 35:1527–32. doi: 10.3174/ajnr.A3909
36. Komatsu T, Kimura T, Yagishita A, Takahashi K, Koide R. A case of reversible cerebral vasoconstriction syndrome presenting with recurrent neurological deficits: evaluation using noninvasive arterial spin labeling MRI. *Clin Neurol Neurosurg.* (2014) 126:96–8. doi: 10.1016/j.clineuro.2014.08.023
37. Pilato F, Distefano M, Calandrelli R. Posterior reversible encephalopathy syndrome and reversible cerebral vasoconstriction syndrome: clinical and radiological considerations. *Front Neurol.* (2020) 11:34. doi: 10.3389/fneur.2020.00034
38. Chung DY, Claassen J, Agarwal S, Schmidt JM, Mayer SA. Assessment of noninvasive regional brain oximetry in posterior reversible encephalopathy syndrome and reversible cerebral vasoconstriction syndrome. *J Intensive Care Med.* (2016) 31:415–9. doi: 10.1177/0885066615623465

39. Alhilali LM, Reynolds AR, Fakhran S. A multi-disciplinary model of risk factors for fatal outcome in posterior reversible encephalopathy syndrome. *J Neurol Sci.* (2014) 347:59–65. doi: 10.1016/j.jns.2014.09.019
40. Covarrubias DJ, Luetmer PH, Campeau NG. Posterior reversible encephalopathy syndrome: prognostic utility of quantitative diffusion-weighted MR images. *AJNR Am J Neuroradiol.* (2002) 23:1038–48. doi: 10.1055/s-2002-32034
41. Chen Z, Zhang G, Lerner A, Wang AH, Gao B, Liu J. Risk factors for poor outcome in posterior reversible encephalopathy syndrome: systematic review and meta-analysis. *Quan Imaging Med Surg.* (2018) 8:421–32. doi: 10.21037/qims.2018.05.07
42. Franceschi AM, Ahmed O, Giliberto L, Castillo M. Hemorrhagic posterior reversible encephalopathy syndrome as a manifestation of COVID-19 infection. *AJNR Am J Neuroradiol.* (2020) 41:1173–76. doi: 10.3174/ajnr.A6595
43. Princiotta Cariddi L, Tabaee Damavandi P, Carimati F, Banfi P, Clemenzi A, Marelli M, et al. Reversible encephalopathy syndrome (PRES) in a COVID-19 patient. *J Neurol.* (2020) 267:3157–60. doi: 10.1007/s00415-020-10001-7
44. Sharma A, Whitesell RT, Moran KJ. Imaging pattern of intracranial hemorrhage in the setting of posterior reversible encephalopathy syndrome. *Neuroradiology.* (2010) 52:855–63. doi: 10.1007/s00234-009-0632-6
45. Petrovic BD, Nemeth AJ, McComb EN, Walker MT. Posterior reversible encephalopathy syndrome and venous thrombosis. *Radiol Clin North Am.* (2011) 49:63–80. doi: 10.1016/j.rcl.2010.07.016
46. Ay H, Buonanno FS, Schaefer PW, Le DA, Wang B, Gonzalez RG, et al. Posterior leukoencephalopathy without severe hypertension: utility of diffusion-weighted MRI. *Neurology.* (1998) 51:1369e76. doi: 10.1212/WNL.51.5.1369

Conflict of Interest: The authors declare that the research was conducted in the absence of any commercial or financial relationships that could be construed as a potential conflict of interest.

frontiers in Neurology

REVIEW
published: 13 December 2021
doi: 10.3389/fneur.2021.767470

Cerebral Microcirculation, Perivascular Unit, and Glymphatic System: Role of Aquaporin-4 as the Gatekeeper for Water Homeostasis

Jacek Szczygielski[1,2]*, *Marta Kopańska*[3], *Anna Wysocka*[4] and *Joachim Oertel*[2]

[1] Department of Neurosurgery, Institute of Medical Sciences, University of Rzeszów, Rzeszów, Poland, [2] Department of Neurosurgery, Faculty of Medicine and Saarland University Medical Center, Saarland University, Homburg, Germany, [3] Department of Pathophysiology, Institute of Medical Sciences, University of Rzeszów, Rzeszów, Poland, [4] Chair of Internal Medicine and Department of Internal Medicine in Nursing, Faculty of Health Sciences, Medical University of Lublin, Lublin, Poland

OPEN ACCESS

Edited by:
Marek Czosnyka,
University of Cambridge,
United Kingdom

Reviewed by:
Mootaz M. Salman,
University of Oxford, United Kingdom
Yoichiro Abe,
Keio University, Japan

***Correspondence:**
Jacek Szczygielski
jacek.szczygielski@vp.pl

Specialty section:
This article was submitted to Neurocritical and Neurohospitalist Care, a section of the journal Frontiers in Neurology

Received: 30 August 2021
Accepted: 12 November 2021
Published: 13 December 2021

Citation:
Szczygielski J, Kopańska M, Wysocka A and Oertel J (2021) Cerebral Microcirculation, Perivascular Unit, and Glymphatic System: Role of Aquaporin-4 as the Gatekeeper for Water Homeostasis. Front. Neurol. 12:767470. doi: 10.3389/fneur.2021.767470

In the past, water homeostasis of the brain was understood as a certain quantitative equilibrium of water content between intravascular, interstitial, and intracellular spaces governed mostly by hydrostatic effects i.e., strictly by physical laws. The recent achievements in molecular bioscience have led to substantial changes in this regard. Some new concepts elaborate the idea that all compartments involved in cerebral fluid homeostasis create a functional continuum with an active and precise regulation of fluid exchange between them rather than only serving as separate fluid receptacles with mere passive diffusion mechanisms, based on hydrostatic pressure. According to these concepts, aquaporin-4 (AQP4) plays the central role in cerebral fluid homeostasis, acting as a water channel protein. The AQP4 not only enables water permeability through the blood-brain barrier but also regulates water exchange between perivascular spaces and the rest of the glymphatic system, described as pan-cerebral fluid pathway interlacing macroscopic cerebrospinal fluid (CSF) spaces with the interstitial fluid of brain tissue. With regards to this, AQP4 makes water shift strongly dependent on active processes including changes in cerebral microcirculation and autoregulation of brain vessels capacity. In this paper, the role of the AQP4 as the gatekeeper, regulating the water exchange between intracellular space, glymphatic system (including the so-called neurovascular units), and intravascular compartment is reviewed. In addition, the new concepts of brain edema as a misbalance in water homeostasis are critically appraised based on the newly described role of AQP4 for fluid permeation. Finally, the relevance of these hypotheses for clinical conditions (including brain trauma and stroke) and for both new and old therapy concepts are analyzed.

Keywords: aquaporin-4, glymphatic system, brain edema, neruovascular unit, cerebral fluid homeostasis

1. INTRODUCTION

Apart from the exchange of information, one of the most challenging tasks of the mammalian brain is to maintain the internal water and electrolyte homeostasis independent from the caprices of the external environment, in order to provide the neurons with nourishing substances and guarantee them a constancy of electrolyte concentration and osmolarity, required for their proper function (1, 2). As the modern techniques of histopathological and physiological research developed, the various tasks regarding global cerebral function have been attributed to the different cellular and acellular components of the brain tissue. Here, the neurons as the cells generating and propagating electrical impulses (which is considered as the major task of the whole brain), have been accorded the exclusive role of managing the information. Meanwhile, other brain components only play a minor role in maintaining the intracellular and molecular environment in optimal conditions for the appropriate function of the fastidious neural cells (3, 4). For instance, according to the common perception, the extracellular compartment is merely a vast space filled with a quite homogenous fluid, consisting mostly of water, substrate molecules, and the products of both the neuronal and glial metabolism floating together with nourishing vessels (2).

Certainly, this oversimplification is far from even approximating the whole complexity of the structure of brain fluid spaces, not to mention its extremely composed function regarding cerebral water turnover. The multidisciplinary research of recent years has delivered solid evidence that the intracerebral water balance is a highly complex, actively regulated process, involving all types of glia cells as well as the neurons and being highly responsible for the electrolyte and water homeostasis of the latter, thus impacting significantly the proper function of the whole central nervous system as a physiological unit (2, 4–6).

Due to a variable number of (sometimes concurring) theories, it is impossible to outline all neurobiological concepts describing how the brain water homeostasis is maintained in the limited text volume of the journal paper. Thus, the main goal of this narrative review is to provide the Reader with the critical appraisal of some of the latest ideas, which attempt to unify the recent findings in (micro-)anatomy, molecular neurophysiology, and biophysics into the form of a concise model of brain fluid turnover. In particular, the concept of the glymphatic system, conjoining the anatomic spaces filled with cerebrospinal fluid and the ultrastructures of extracellular space needs to be outlined (2, 7–10). The common denominator of all these theories is the function of cellular membrane components, called water channel proteins. Among these, particular attention was paid recently to the structure and function of aquaporins (AQPs), where aquaporine-4 (AQP4) has been acknowledged as the water channel protein of main importance for water turnover in the mammalian brain (11). First, recognized as a passive water channel, due to results of numerous neuromolecular studies, AQP4 has recently been acknowledged as an active and precise water homeostasis regulator, playing a crucial role both in physiological conditions as well as in situations where the exchange of fluids between all cerebral compartments is essential for the course of the disease (12–15). Here, the prime example is the development and subsidence of brain edema, being the major manifestation of the secondary cerebral damage in traumatic brain injury and in cerebral ischemia (16–18). For this reason, the potential of AQP4 as the target point for therapeutic methods will also be discussed.

2. CONCEPTS OF CEREBRAL INTEGRATED WATER SPACE

With the advent of modern neurosurgery, several concepts of cerebral fluid circulation and water turnover have been developed with the classic model of cerebrospinal fluid (CSF) flow also termed "third circulation" published by Cushing, which has since then become universally accepted (2, 19). According to his view, the brain was enveloped by the CSF layer being in constant flow. The CSF is produced in the lateral ventricles/choroid plexi, transported to the third ventricle, passing through the aqueduct and fourth ventricle, flowing to basal cisterns and distributed upon both hemispheres, where a paramedial area (superior sagittal sinus and arachnoid granulations) plays a major role in CSF reabsorption (2, 20). Already an important remark has been made, that the brain, despite its high water content lacks a usual lymphatic apparatus and lymph flow, and the CSF circulation was assumed to fulfill the role of the lymphatic circulation (provision and cleavage of water-soluble metabolites) in the brain (7, 21, 22). This macroscopic and very gross description of CSF turnover has been modified recently. In particular, the view that CSF production and resorption are the main forces behind brain fluid transportation needed to be revised (23–30). Here, the importance of perivascular spaces, called Virchow-Robin spaces (VRS) should be outlined. These fluid-filled areas, surrounding both arteries and veins running in the direct proximity or through the nervous tissue was attributed the role of the intermediate zone, joining the macroscopical subpial space, filled with CSF with the microscopically delineated extracellular area, in which single brain cells, including neurons and glia, were sustained (12, 31). Of note, in several studies, it was demonstrated that the fluid contained in VRS is moved not by simple diffusion or only due to a high pressure gradient, but is rather propelled by the pulsatile activity of arterial vessels (32–36). Such a pump mechanism seems to depend upon the cerebral microcirculation (37, 38) and the condition of disturbed vascular

Abbreviations: AM, acetoxymethyl ester, APRE, acute phase response elements, AQP4, aquaporin-4, AQPs, aquaporins, ar/R, aromatic/arginine, BBB, blood-brain barrier, CaM, calmodulin, CBF, cerebral blood flow, CNS, central nervous system, CCI, controlled cortical impact, cGMP, cyclic guanosine monophosphate, cRNA, complementary ribonucleic acid, CSF, cerebrospinal fluid, Kir4.1, inwardly rectifying potassium channel 4.1, MAPK, mitogen-activated protein kinase, mRNA, messenger ribonucleic acid, NMO, neuromyelitis optica, NO, nitric oxide, NPA, asparagine–proline–arginine (motif), NPY, neuropeptide Y, nsSNPs, non-synonymous single nucleotide polymorphisms, NVU, neurovascular unit, OAPs, orthogonal arrays of particles, PKA, protein kinase A, siRNA, small interfering ribonucleic acid, Snta-1, syntrophin-1-alpha, TBI, traumatic brain injury, TFP, trifluoperazine, TRPV4, transient receptor potential cation channel subfamily V member 4, VIP, vasoactive intestinal peptide, VRS, Virchow-Robin space(s).

autoregulation impairs also the mechanism of bulk flow along the VRS (39–45). On the other hand, the raise of cerebral blood flow on the level of microcirculation can increase the dynamics of perivascular fluid (37). Clearly, cerebral microcirculation in physiological conditions relies on the metabolic demand of the nervous tissues, supplied by both blood and cerebral fluid flow (46–48). In respect to complex interactions between the cerebral vessels (including cerebral vasculature i.e., endothelial cells and pericytes, as well as astrocytes and neurons with their processes), the term neurovascular unit (NVU) has been coined. The concept of an NVU [exhaustively reviewed in (49)] encompasses these varieties of cells and their function, the interactions of which maintain the ionic, metabolic, and molecular homeostasis of the brain. In particular, the neuronal and astrocytic activity is able to provoke a dilation or a contraction of the arterial vessels [executed by smooth muscle cells (50)] or capillaries [provided by pericytes, being an integral part of NVU (51)] via a number of mediator substances, the release of which is strictly dependent on neuronal or astrocytic activity. This list includes not only the nitric oxide (NO), as the prime example of vasoactive substance (52, 53), but also products of cyclooxygenase-2 activity (prostanoids) (54, 55), D-serine of astrocytic origin (56), peptide-based vasoactive mediators including vasopressin (57), somatostatin (58), neuropeptide Y (NPY) (59, 60), and vasoactive intestinal peptide (VIP) (61), all of which the neurons or astrocytes are capable of secreting. This means, that depending on the current activity of the neurons, the autoregulation of the cerebral blood flow (on the level of microcirculation/NVU) would be able to adapt not only the blood supply but also, indirectly the control of CSF and the extracellular fluid extravasal flow (62).

Though the view of arteries and arterioles and their pulsatile action as the main pumping mechanism for cerebral fluid movement is quite straightforward and easy to understand, several physiological observations undermine this simplified concept of brain fluid mechanics (63). Here, the oscillating or even retrograde flow along VRS has been postulated and documented in several *in vivo* experiments (64, 65), drawing a conclusion that additional mechanisms exist (possibly on the molecular level) which contribute to the production, mixing, and flow of the fluid on the level of cerebral extracellular spaces. One of the most important factors is the temporal change in permeability for water and electrolytes or even larger particles of the blood-brain barrier (BBB) (66–69). The BBB, with its key component—tight junctions between endothelial cells lining the interior wall of cerebral microcirculation, used to be perceived as a seal, which prevented larger molecules from passing between the intravascular lumen and extracellular space. In this early concept, water and electrolytes were allowed to pass the BBB depending mostly on physical and chemical laws of osmosis and hydrostatic pressure (70, 71). However, the idea of BBB as the passive membrane exposed to the tides of CSF and blood circulation has been revised recently. Here, the exchange of electrolytes and larger particles (e.g., aminoacids) across the BBB has been described as an active, closely regulated process (72, 73), dependent on the energetic state of neurons, astrocytes, and endothelial cells (74, 75). The key argument, that BBB is not a passive, but an active structure, regulating the circulation of cerebral fluid on the ultramicroscopic level, was the capability of BBB to precisely regulate the amount of water passing across it. Moreover, in relation to water permeability, the BBB demonstrated high dynamics in changes of this property, both temporal and spatial (76–79). Thus, due to the rapid and physiological changes in BBB permeability to water and electrolytes, the brain can create compartments of fluid spaces, slightly but significantly different from the rest of global fluid space (80–83), in order to create a biochemical environment that is optimally adjusted to the current needs of the population of brain cells, both neurons and glia. Certainly, this dynamic function requires the presence of multiple molecular control systems, responsible for rapid changes in the transmission rate across BBB for different compounds (84). Regarding water permeability, the major control system is composed of several membrane proteins, labeled water channel proteins, with the AQP4 being appreciated as the most relevant for cerebral water turnover (85). The physiological function of AQP4 clearly results from its biochemical structure and gene expression as is described in the following chapter.

3. STRUCTURE, GENETICS, AND DISTRIBUTION OF AQP4

The AQP4 protein is a member of the large family of AQPs, the membrane water channels, which are widespread in all investigated organisms from bacteria and plants to vertebrates and responsible for bidirectional water permeability of phospholipid bilayers of cells (86). The AQP4 was first identified as 32-kDa mercurial-insensitive water channel in a rat lung (87) and then described in many different epithelial cells such as renal principal cells of collecting ducts, retina, iris, ciliary body, stomach parietal cells, colon epithelial cells, excretory tubules of lacrimal and salivary glands, organ of Corti, and in skeletal muscles. But it is mostly present in the mammalian brain and spinal cord, where it is localized in astrocytes directly in contact with capillaries and pia and in subpopulations of ependymal cells (88–91).

3.1. AQP4 Protein Structure

The structure of the monomeric subunit of AQP4 is similar for all AQPs and was at first described for AQP1 in human erythrocytes membrane (92). Any single subunit comprises two repeated segments, each built from three domains of the alpha-helix structure. All six domains (in pairs of the three) are arranged in the form of a non-polar bilayer and connected by five loops (A to E). The loops B and E (which connect the second and third domain in each segment) consist of highly conserved located motifs of three amino acids: asparagine—proline—arginine (NPA). According to the hourglass model, they cover the space between the bilayer leaflets and allow the water pore formation (92–94). The hemipore (as are also called B and E loops) is maintained by the van der Waals forces (95). The width of the pore along its lumen is not identical. The narrowest part, localized about 8Å above the center of the

membrane, has a diameter of 2.8Å, similar to a single particle of water. In this site, NPA motifs make contact with each other. The pore diameter increases in the direction of the extra and intracellular layer of the membrane, which creates the hourglass-like shape of the whole structure (96). Several isoforms of AQP4 have been identified. In the rat brain, Jung et al. described two overlapping polypeptides of 323 or 301 amino acids, currently known as classical forms M1 and M23, transcribed from this same gene, but from differently localized initiation sites at the upstream (M1) and downstream (M23) of the gene. Authors have determined a polypeptide structure, similar to earlier identified AQP1, consisting of six membrane bilayer-spanning domains and five connecting loops, including hydrophobic loops B and E and containing, respectively, NPA 97–99 and NPA 213–216 sequences. The cytoplasmic amino terminus comprises both potential initiation sites, the carboxyl terminus, also localized in the cytoplasm consists of approximately 70 amino acids. Opposite to other AQPs, in the AQP4 amino acid chain no cysteine at site G94 nor at site A210, both responsible for mercurial inhibition, was found. In the amino acid sequence also three potential N-glycosylation sites were identified with the first (N153) localized in extracellular loop C. Both protein isoforms were synthesized in the presence of microsomes. When cRNA contained the downstream site, a single polypeptide of 301 amino acids and 30 kDA arose. In the presence of both initiation sites, besides the minor product, also the 323 amino acids polypeptide of 32 kDa were synthesized (93). Together with these first two AQP4 isoforms identified in humans, rats, and mice (87, 93, 97), nine AQP4 isoforms are as yet found (AQPa–f, 4, a ex and c ex) (98–100). When, as a result of the AQP4 rat gene mapping, four additional forms of AQP4 were described, the new terminology was implemented. M1 and M23 isoforms, respectively, have received names AQP4a and AQP4c, and AQP4 isoforms newly identified in rats were named AQPb and e-f (101). AQP4a, AQP4c, and AQP4e, considered classic, have six bilayer-spanning domains (1–6) and five interconnecting loops (A–E). AQP4b, AQP4d, AQP4f isoforms are devoid of helices 4 and 5 as well as connecting loop D. AQP4Δ found in human skeletal muscles is devoid of the terminal part of helix 5 and loop E (94). The recently identified isoforms of AQP4 in humans named a ex and c ex are characterized by C—terminal extension containing 29 amino acids (102). The AQP4 monomers independently of the isoform are organized into more complex structures in the form of tetramers, which additionally aggregate into orthogonal arrays of particles (OAPs) considerably various in respect of the size and shape as well as the isoform content (100, 103). The size of OAPs diameter evaluated by different microscopic methods reaches 100–500 nm (100) and the molecular weight of these higher-order structures is about 1,000 kDa (104). AQP4 a and AQP4 c are both incorporated into OAPs (105) as well as their extended variants AQPa ex and AQP4c ex (102). Additionally, it was reported that AQP4 a is able to attach to OAPs only in the presence of AQP4c, being the component of the OAPs core (106) and AQP4 c ex by the limitation of incorporated tetramers affect the size of OAPs (102). The AQP4e undergoes the incorporation into OAPs, while AQPs b and d do not (although both indirectly modulate the OAPs amount) and AQP4 f was not yet evaluated (100, 101, 103). Similarly, AQP4Δ lacks the ability to be attached to OAPs, but in the endoplasmatic reticulum, it exerts an effect limiting both the abundance and size of OAPs. This dominant-negative modulation is imposed through the interactions between AQP4 isoforms of the plasma membrane (99, 100).

3.2. AQP4 Gene Arrangement

All AQP4 isoforms are coded by a single copy of the gene localized in humans on chromosome 18 at the junction of q11.2 and q 12.1 (97, 98). As with other AQPs, the gene coding AQP4 consists of four exons including, respectively, 127, 55, 27, and 92 amino acids, between which three introns of 0.8, 0.3, and 5.2 kb are located. The unique feature, distinguishing the *AQP4* gene from other *AQPs* genes is an alternative initiation sequence situated 2.7 kb upstream and named exon 0. It allows, after the splicing process, to encode the M1 and next 10 amino acids by exon 0 and subsequent 11 amino acids with M23 by exon 1 (97). In the promoter region, such regulatory elements as TATAAAA (TATA box) at 385 bp upstream from initiation codon, one CAAT box, and AP-1 were identified and additionally SP1, two E-boxes, two AP-2, and acute phase response elements (APRE). It was shown that the transcription initiation site is located at 46 bp downstream from the TATA box. In addition, it was revealed that at 138 bp downstream of the stop codon a sequence AATAAA is situated which is the signal of polyadenylation (107). The mRNA of AQP4 b, d, and f is formed after alternative splicing omitting exon 2 from AQP4 a, c, and e, respectively (101, 107). The AQP4Δ mRNA is alternatively spliced from AQP4 a with a lack of exon 4 (99). The variants AQP4 a and c ex are extended through translational readthrough (102). In the *AQP4* gene, numerous polymorphic sites were reported across the entire gene including coding and non-coding regions, as well as 3' and 5', flanking regions (108), but the gene is considered as highly conservative and non-synonymous single nucleotide polymorphisms (nsSNPs) are rather rare (approximately 1–2% allele frequencies) (109). Several known nsSNPs influence the protein structure and function. The occurrence of variants I128T, D184E, I205L, M224T, and M278T, although all are localized relatively far from the NPA motifs, affect protein stability. The Ile-Thr substitution in position 128 results in the change of hydrophobic to hydrophilic residue in the transmembrane region and Met-Thr substitution exerts a similar effect in a loop if it involves position 224 or the C—terminal domain and position 278. Additionally, the substitution Met—Thr deprives the amino–acid residue of a sulfur atom. The chemical relevance of two other substitutions Asp—Glu and Ile—Leu is less significant. Nevertheless, all five nsSNPs impact the AQP4 function—I128T, D184E, I205L, M224T reducing, and M278T increasing water permeability (109).

3.3. AQP4 Distribution

As it was mentioned AQP4 is found predominantly in the astrocytes, but the AQP4 gene expression is different in various areas of the central nervous system (CNS) with the highest levels detected in astrocytes localized near the subarachnoid space, along ventricles and blood vessels. Also in areas engaged with water balance maintaining and responsible for the osmoregulation such as the supraoptic nucleus or subfornical

organ, the intense AQP4 expression was recorded (90). The distribution of AQP4 isoforms inside astrocytes varies depending on the individual isoform. The most accurately is determined for AQP4a and AQP4c (known also as M1 and M23), being two first described and best-investigated isoforms. Both of them as well as their extended forms (AQP4a ex and AQP4c ex) were found at the plasma membrane aggregated in OAPs with the isoform c in the core of OAP and isoform an attached to c (98, 100, 105, 110). The isoform a may also occur in the plasma membrane in the simpler form of tetramers (111). The isoform e is localized not only at the plasma membrane, but also intracellularly (100, 101). Other isoforms were detected only in the intracellular structures such as Golgi apparatus (isoforms b,d, and f) or endoplasmatic reticulum (Δ4) (99, 100). Additionally, isoforms b and d were found in lysosomes and early endosomes (100, 103).

Several studies underlined the fact, that the regulation of AQP4 activity relies more on the subcellular relocation than on the expression of its gene. Both isoforms of AQP4 can be translated from the same full-length transcript by a "leaky scanning" mechanism (112, 113). Previous evidence shows that both isoforms are relocated equally and that the surface localization of AQP4 increased without changing the level of protein expression. In a study by Salman et al. mild hypothermic treatment increased the surface localization of AQP4 in human astrocytes even in the lack of significant change in total protein expression levels. Here, AQP4 mRNA increased modestly in cultured human primary astrocytes following 4 h mild hypothermia (32°C) compared with control cells grown at 37°C but this increase in transcript did not result in a change in protein level. Nevertheless, the decrease in temperature influenced the surface localization of AQP4, creating a space for the potential use of therapeutic brain hypothermia as an antiedematous treatment (114). Furthermore, analysis of Ciappelloni et al. indicated that the deleterious effect of anti-AQP4 autoantibodies involved in neuromyelitis optica (NMO) is probably based on perturbation of AQP4 surface dynamic and distribution. This impact differed between both isoforms of AQP4. Notably, in this study, the water transporting function of single AQP4 molecules remained intact despite exposition to AQP4 antibodies. This puts the nanoscale distribution of AQP4 in the spotlight as a major pathophysiological mechanism and the target for potential therapeutic strategy (15, 115), see also Chapter 6.

4. AQUAPORIN 4: ITS PHYSIOLOGICAL FUNCTION

The biochemical and molecular properties of AQP4 including its expression, assembly of subunits, and integration into organelle clearly define it as one of the membrane proteins. Indeed, the proper physiological function of AQP4 requires its polarized integration and anchoring into astrocytic cell membranes (116–119) and this process is regulated already at the stage of translation and protein folding (120). In particular, the location of the AQP4 along the parts of astrocytic membranes reflects its crucial function in regulating the water exchange between intra- and extravascular space: the density of AQP4 arrays is about 10 times higher in endfeet areas adjacent to cerebral microvasculature than in other zones (90, 117, 121) and this inhomogeneous localization seems to be crucial for the BBB integrity (122, 123). But even if the majority of AQP4 complexes are located in endfoot areas, the presence of AQP4 has also been demonstrated in astrocytic membrane zones, directly neighboring synaptic areas (124, 125), in particular excitatory synapses (90). This localization of AQP4 defines its main physiological functions: a direct impact on the clearance of water and cellular metabolites, altering extracellular fluid dynamics, and (most probably indirect and less precisely described) regulation of neuronal and synaptic activity including plasticity (thus impacting memory and behavior). Certainly, the role of AQP4 and the whole AQP family in the physiology of the nervous system is not limited to these two domains. Currently, up to 13 different AQPs have been identified. The diversity of their physiological roles comprises physiological solute transport including glycerol, ammonia, urea, carbon dioxide, and hydrogen peroxide (126). The permeability of water channels for different small, polar substrates depends not exclusively on transmembrane proteins, which form a more narrow or wider space but expresses considerably more complex interactions between the features of the solute as well as the pore constriction and polarity. Especially important in the highlighting of these phenomena seems to be recently described relevance between the single amino acid substitutions within the aromatic/arginine (ar/R) motifs known as the selectivity filters of different AQPs and between glycerol and urea permeability. In AQP4 the ar/R- motif is formed by phenylalanine in position 1, histidine, in position 2, and, being a small residue, alanine in position 3. *In vitro*, the mutagenesis of ar/R motifs of AQP4 consisting in substitution of histidine in position 2 and arginine in position 4 creates glycerol or urea permeable channels. The H201A and H206G substitutions, respectively, allow the glycerol and the urea permeable channels to form, while the R216A substitution creates the channel permeable for both substrates. Some authors hypothesized that the H201A mutation along with F77 composes a hydrophobic corner contacting with the alkyl chain of the glycerol due to van der Waals forces, while the loss of the alanine in the H201G mutation causes a disruption of this corner and accessibility of the V197 backbone carbonyl group for binding with water or solutes such as urea due to hydrogen bounds. Oppositely, analogous mutagenesis of AQP1 (R195A and H180/G) did not lead to the formation of urea or glycerol permeable channels (127). AQPs are also responsible for the trafficking of other membrane proteins and are involved in intercellular molecular interactions resulting in cell-cell adhesions. Due to their selectivity in ion transfer across the cell membrane and ability to counteract the osmotic changes, AQP has been attributed the role of cell volume/size regulators. As to the AQP4 itself, its role in cell adhesion (probably by facilitating aggregation or localization of other adhesion molecules) has been previously described (128, 129). For the exhaustive reviews on diversity in AQP family and AQP4 function see also (13, 130, 131), however for the sake of clarity and clinical context of this review we will focus on the AQP4

functions that are the most relevant for the function of the perivascular unit.

4.1. Role of AQP4 in Fluid Management

The information that is crucial for understanding AQP4 function for fluid homeostasis has been mostly (but not exclusively) gained through studies implementing animal lines with the genetic modification of AQP4 function. Accordingly, AQP4 knockout animals demonstrate enlarged interstitial fluid spaces (132, 133), increased brain water content (134, 135), and reduced capability to get rid of extracellular brain water excess (135, 136). These findings are highly suggestive of a regulatory role of AQP4 in water transportation across BBB between extracellular and perivascular space (137). Indeed, multiple attempts to trace the fluid movement demonstrated suppression of glymphatic flow in the absence of AQP4. Of note, this observation has been made not only in regard to exogenous, drug-like substances as mannitol (138) or dextran (137) but also applied to endogenous substances like tau (139–141), beta-amyloid (138, 140, 142, 143) or lipoproteins (144), which are involved in the pathogenesis of degenerative encephalopathies. Of note, the AQP4 role in facilitating the exchange of solute distribution and waste substance clearance is strongly dependent on adequate localization of AQP4 in the perivascular processes (145). Disturbance in the cell-level distribution of AQP4, as provoked by syntrophin-1-alpha *(Snta-1)* gene deletion (146) or seen in brains affected by aging (147), trauma (148), or ischemic damage (149) is related to impaired function of glymphatic clearance. Undoubtedly, it sheds new light on the role of the glymphatic system in the pathophysiology of diseases such as Alzheimer's disease or posttraumatic neurodegeneration.

Notably, based on the results of (150) and (151) a competitive hypothesis has emerged, assuming that an alternative, AQP4 independent system of fluid transportation exists. In both experiments, implementing alternative ways of tracer administration to the extracellular fluid space in experimental animals, the fluid/tracer transportation was not impacted by the AQP4 genetic status and thus by aquaporin function in both wildtype and AQP4-knockout animals.

However, the recent multicenter research effort, provided by five laboratories implementing independently developed transgenic animal models with impaired AQP function, clearly demonstrated, that transport of the tracers, cleared from extracellular space via perivascular fluid compartment is strongly dependent on the proper function of perivascular aquaporins (146).

In conclusion, the main and widely accepted role of AQP4 is the facilitation of fluid exchange between the extracellular space and the perivascular spaces (both being essential parts of the glymphatic system and incorporated in brain fluid circulation) as well as in the cleavage of several cerebral metabolites, crucial in pathophysiology of neurodegeneration. Importantly, even under the physiological condition, transportation of cerebral fluid does not represent a steady-state but is a very dynamic process constantly adapting to the current needs, being related to the energetic state of neurons and thus linked to autoregulation of microvasculature. Let us take a closer look at the previous evidence regarding this area.

4.2. AQP4 as a Potential Regulator of Glymphatic Flow

Soon after describing glymphatic system with the continuous fluid flow as its main function, the evidence about its dynamic adaptation to the current physiological status appeared. Of importance, the increased energetic demand of neurons on the one hand clearly increases cerebral blood flow on the level of microcirculation (152–155) [a phenomenon described as neurovascular coupling, for some recent reviews of molecular background, see also (156–159)], but on the other hand reduction of interstitial flow as the neuronal activity grew has been observed (160). More so, the conditions, that are clearly related to reduced neuronal activity i.e., sleep (161–163) and general anesthesia (164–167)—albeit in a dose-dependent manner (168) [reviewed also recently in (169, 170)]—have been associated with the enhanced glymphatic flow and interstitial fluid circulation.

Is the activity of AQP4 channels somehow responsible for this inversed relationship between neurovascular coupling and glymphatic flow? Indeed, the trend to the physiological flow reduction in regions of neuronal activation was reversed in AQP4 knockouts (171). AQP4 expression and polarization are also strongly dependent on circadian rhythm (162, 172), suggesting that proper AQP4 activity is required for physiological glymphatic stagnancy in periods/areas of neuronal excitation. Also, in clinical conditions, an increased volume of extracellular fluid/PVS spaces [as seen in AQP4 knockout animals (132, 133)] have been observed in subjects affected by neurodegenerative conditions with documented reduced daily cognitive activity (41). The linkage between neuronal excitation, increased blood microcirculation, and reduced glymphatic flow is not completely understood, but the properties of AQP4 allow us to hypothesize several interrelations between these physiological phenomena. One possibility is the direct impact of vasoactive substances on AQP4 function and expression. Indeed, NO was able to modulate AQP4 expression in cultured astrocytes via a cGMP-/MAPK controlled mechanism (173, 174) as well as in the setting of animal experiments (175). Also, vasopressin an activation of its receptors seems to impact the density and function of AQP4 (176, 177) or AQP1 (178) channels. Finally, inflammatory vasoactive substances as thromboxane (179) seem to share AQP4 as the parallel lever of action triggering astrocytic swelling. However, some more direct and swifter response mechanisms of AQP4 response to increased neuronal activity do exist. Here, the participation of AQP4 channels in moderating the K^+ exchange related to increased neuronal activity needs to be discussed [albeit some reports deny the importance of Kir4.1/AQP4 complex for the mechanism of astrocytic swelling (180), being proposed as the mechanism of the reduced glymphatic flow (181)]. The participation of AQP4 channels in potassium homeostasis is well-documented [as reviewed exhaustively in (130) and (182)] and relies mostly on providing the water flux necessary for spatial redistribution of K^+ ions, released during the phase of neuronal activation (183). Importantly,

the key role of AQP4 in managing K^+ excess has been underlined by molecular studies in conditions directly related to neuronal hyperexcitation as spreading depolarization (184, 185) or seizures [both in experimental (186–190) and clinical (191–193) settings]. Since K^+ surplus in extracellular fluid space is linked to the function of cerebral micro perfusion, including neurovascular coupling (194–197), it may be hypothesized, that disturbed AQP4 function underlies the pathophysiology of several conditions related to improper reactivity of small vessels, including migraine and cluster headache (198, 199) via this mechanism. More importantly, the disturbance in potassium homeostasis attributable to AQP4 misfunction seems to result in ischemic exacerbation of secondary brain damage as may be noticed in stroke (200–202), subarachnoid hemorrhage (203–207), spontaneous intracerebral hemorrhage (208, 209) or traumatic brain injury (210–213). With regard to these conditions, even stronger links between secondary injury and AQP4 function do exist, namely the development of brain edema, which is the most direct result of impaired cerebral fluid homeostasis.

5. BRAIN EDEMA AND ROLE OF AQP4 IN ITS PATHOPHYSIOLOGY

Certainly, the role of AQP4 in the development and subsiding of brain edema in different cerebral pathologies is of paramount importance for our understanding of the (patho-) physiology of cerebral fluid circulation. According to the canonical concept, forged by Klatzo and his research group, there are two main forms of cerebral edema existing. Vasogenic edema is characterized by extracellular water accumulation due to BBB dysfunction and increased transcytosis of plasma elements, including water (145). In turn, in cytotoxic edema water excess is gathered inside the cells (both neurons and astrocytes), manifested by beading i.e., swelling of astrocytic cells and neuronal dendrites (214–218). This dichotomy has, later on, been refined by numerous works by Marmarou and associates, describing in detail energetic depletion as the major drive for cytotoxic edema development as well as radiological manifestation of both edema types (219–224). In more recent works, a third kind of brain swelling, namely ionic edema, is distinguished. This type of edema is characterized by an early influx of both water and sodium ions from the perivascular compartment into the brain parenchyma, predominantly into the astrocytic cells. Ionic edema usually precedes the impairment of tight junctions being the first phase of ischemia-related edema formation (217, 225) and is associated with brain swelling of cytotoxic character (145, 217). Until the appearance of AQP4 on the stage, the main role in the molecular performance of both ionic and vasogenic edema remained vacant. Upon discovery and description of AQP4 function in water transportation (both in physiological and pathological conditions), our view on extracellular space and, more recently, the glymphatic system for development of brain edema has evolved dramatically (226).

Initially, the results of the experiments both *in vivo* and *in vitro* seemed to be inconclusive, since AQP4 and its expression demonstrated both surge and depletion of its activity due to developing brain edema. Thus, Ke et al. reported a reduction of AQP4 expression in areas of the traumatically swollen brain (227) and a similar observation has been made by Kiening et al. (228) and Bixt et al. in a rat model of posttraumatic edema (229). On the other hand, Fukuda et al. reported a delayed but significant raise in AQP4 level, following the development of posttraumatic brain edema (230) in juvenile rats, and similar observation has been made in adult animals by Taya et al. (231) and Zhang et al. (232). These observations were hard to reconcile until AQP4 knockout animals were available. Here, consequent analysis of different forms of edema in diverse experimental paradigms revealed that in the models with predominating cytotoxic edema demonstrable in transient or persistent ischemia models, lack of AQP4 function resulted in reduced water accumulation (233–235) and/or improved outcome (236–238). One possible explanation of these findings is, that in the absence of AQP4 channels, water excess, that would be accumulated in the swelling astrocytes due to compensatory mechanism after energetic depletion, remains in extracellular space and is managed by the glymphatic system and transported by perivascular spaces, being less effective (141) although more abundant in AQP4 knockouts (233). In conditions of vasogenic edema, the AQP4 channels seem to play a beneficial role, helping in the transportation of the fluid excess from the interstitial space to the glymphatic system. This hypothesis is sound with the observation, that in animal models of predominantly vasogenic edema, as in hemorrhagic stroke (209, 239–241) brain infection (136, 242–245) or brain tumor/cold lesion model (136, 246) brain edema subsides more efficiently in the presence of properly functioning AQP4. Importantly, not only the crude amount of AQP4 units defines its impact on brain edema or spinal cord edema development. AQP4-related permeability of astrocytic membranes is strongly dependent from subcellular localization of AQP4 water channels (112, 114). Pivotal study of Kitchen et al. demonstrated, that relocation of AQP4 units is modulated mainly by calmodulin (CaM), binding directly with AQP4 domains, while this action is further enhanced by AQP4 phosphorylation, performed by protein kinase A (PKA) (15). Thus, subcellular localization of AQP4 particles seems to be even more important for brain edema formation than expression of *AQP4* genes.

The topic of AQP4 dual impact on brain edema development/resolution is the most clearly seen in neurotrauma research. Here, several traumatic brain injury (TBI) models exist, in which the dominance of cytotoxic or vasogenic edema type relies not only on the mechanism of primary injury but changes dynamically over time as the influence of AQP4 does. Several studies implementing controlled cortical impact paradigm (CCI) (227, 229, 247) (with an initial predominance of cytotoxic edema) demonstrated a decrease in AQP4 activity and expression accompanying edema development (227–229) [although Taya et al. (231) and Fukuda et al. (248) described an AQP4 concentration raise in early stages of CCI]. To the contrary, animal studies using fluid percussion injury (with predominantly vasogenic edema) (249, 250) or weight drop models (148) demonstrated a rise of AQP activity/expression. Notably, in models of more severe brain damage, the molecular

effect of AQP4 activation may be counteracted by loss of the cells being AQP4 carriers, possibly making the interpretation of data even more difficult (251). The same refers to the models with mixed type of posttraumatic edema (232), demonstrable in several head injury studies conducted in AQP4 knockout animals, where the net differences in edema development were not as clear as in experiments, in which conditions of purely cytotoxic or purely vasogenic edema were analyzed (13, 252). Nevertheless, in long-term outcome analysis, it was documented that animals lacking AQP4 demonstrated better recovery regarding neuroinflammatory events and cognitive function (18). On the other hand, AQP4 deficiency was also associated with the lower threshold of posttraumatic seizures (188). Notably, in the animal model of minor head injury, where brain edema is of lesser relevance for the posttraumatic course, lack of AQP4 was demonstrated to be neuroprotective (253) (an effect similar to pathophysiological conditions with cerebral edema of cytotoxic type) (13). As was discussed above, previous studies have shown that AQP4 seems to have different functions and outcomes in different CNS disorders. Hence, the need for accurate and reproducible methods evaluating the activity of AQP4 should be underlined. These needs meet the recently developed calcein fluorescence assay. Shortly, calcein is a dye with fluorescent properties that is provided to plate adherent cells as the membrane-permeable and non-fluorescent acetoxymethyl ester (calcein-AM). Next, the calcein-AM is metabolized by intracellular enzymes to fluorescent calcein. Then, cell shrinkage is induced by using a hypertonic medium and the quenching fluorescence of calcein is continuously measured. The concentration-dependent fluorescence reflects cells volume and enables the evaluation of water transport across the plasma membrane. Obtained curves of the shrinkage of the cell allow quantifying relative and absolute water permeability (254). Of note, calcein fluorescent assay is only one of several *ex vivo* methods to assess AQP4 function. Here, the spectrum of methodology reaches from cell culture-based osmotic swelling tests over stopped-flow spectroscopy tests in e.g., liposome suspensions up to *in silico* computational assays. This variety of research methods should be critically considered, since every single assay carries its advantages and limitations, as outlined in exhaustive reviews of Verkman et al. (255) and Abi-Awan et al. (256).

6. DISCUSSION: AQP4 AS A TARGET FOR THERAPEUTICAL APPROACHES

Due to the ambiguous properties of AQP4 regarding its impact on water homeostasis in different types of edema, the results of experimental studies in which AQP4 function is blocked or enhanced need to be critically analyzed before being translated into clinical practice. Indeed, recently several compounds have been claimed to execute beneficial impact on the course of secondary brain damage, including brain edema via interference with AQP4 function and expression. Here, neuroprotective and antiedematous action of erythropoietin has been linked with the preservation of AQP4 function in trauma (257), hydrocephalus (258), and cerebral ischemia (259). Further, the neuroprotective action of several (food) antioxidants has been explained by the adjustment of AQP4 channel functions (260–264). Notably, the antiedematous effect of well-known osmolar drugs such as hypertonic saline and mannitol has been recently linked to modulation of AQP4-water channel permeability (265, 266). Finally, the idea of repurposing some of these well-known drugs like acetazolamide (267–269) or levetiracetam (270) was based on their presumed or proven effect on AQP4 channels. Even more promising is the therapeutic strategy, in which the AQP4 subcellular relocation as the main driver promoting brain or spinal cord edema is targeted. Here, the pharmacological inhibition of PKA and CaM as main regulators for AQP4 subcellular localization was efficient against spinal cord edema formation, breakdown of blood-spinal cord barrier, and improved functional outcome in a rat model of spinal cord injury (15). Since CaM inhibition was provided by trifluoperazine (TFP), a compound that is already approved as an antipsychotic drug, the perspective of swift clinical implementation of these experimental results emerges. Significantly, TFP has proven its neuroprotective and antiodematous effect also in experimental models of brain ischemia (271, 272). In the most recent study, implementing photothrombic stroke model, TFP has downregulated AQP4 expression, reduced the amount of brain edema, and improved the metabolic function (as demonstrated via increased glycogen level of astrocytes located in ischemic penumbra) (271).

Certainly, analyses of Kitchen et al. (15) and Sylvain et al. (271) clearly document the relationship between AQP4, its subcellular location, and the beneficial role of interfering AQP4 relocalization after an injury as the main mechanism for beneficial action of TFP. Nevertheless, for most of the other studies, the question emerges: are the antiedematous or neuroprotective properties truly mediated via impact on AQP4 activity, or is the shift in AQP4 expression/function only secondary and thus reflects rather an adapting reaction of the whole glymphatic system to the beneficial action of the given drug? This question should not hinder the research community in further search for treatment strategies, in which the pivotal position of AQP4 in cerebral edema management is utilized for the improvement of outcome and neuronal protection. A good example here is the use of decompressive craniectomy. This rapid change in physical properties of the skull and brain, including hydrostatic pressure change has been associated with increased AQP4 activity, at least in areas not affected by the abundant loss of neural and glial cells (250, 251). It is imaginable, that adding AQP4-targeted therapy [like acetazolamide (267, 273) or selective AQP4 channel blocker as TGN-020, being one of the most promising candidate drugs (274–277)] to the surgical decompression would allow reducing the risk of edema surplus, related with loss of hydrostatic resistance in the decompressed brain (267). Importantly, the list of structurally non-related compounds displaying the AQP4-inhibitory properties is long and includes ethoxzolamide, topiramate, lamotrigine, zonisamide, acetylsulfanilamide, phenytoin, bumetanide, furosemide, tetraethylammonium, and IMD0354 (273, 274, 278, 279). Obviously, this list encompasses

several drugs that, similar to acetazolamide, have been already approved or tested for uses other than counteracting brain edema. Hence, the strategy of drug repurposing will open a fast track for the search for efficient AQP4-targeted treatment of brain edema. The importance of this approach is underlined by the fact, that despite several assays of AQP4 water transport function are available and has been abundantly used in basic research studies [for exhaustive review see (255, 256)], no single drug exists, that has yet been approved to successfully target AQP4 water channel function in a clinical setting (256). One of the possible obstacles is the toxicity and reduced selectivity of the compounds (including heavy metal derivates), which attempted to be used according to the traditional pore-blocking approach. It is difficult to circumvent this problem, even if modern pharmacodynamic forms of drug administration (e.g., liposome-encapsulated compounds) are used (256). Unfortunately, the strategy of virtually screening myriads of candidate inhibitors does not solve this problem but rather multiplies the number of putative AQP4 blockers that fail to exert their function *in vivo*. The possible reason here is the characteristic of AQP4 molecule, with the relatively small diameter of its pore and simple structure of its molecule, that, contrary to regular membrane receptors, lacks any complex intrinsic gating and transport mechanism (255). This makes AQP4 channels less prone to be targeted by the small inhibitory molecules, dramatically shortening the list of candidate drugs (255, 256). For this reason, the use of AQP4 targeted immunotherapy or *AQP4*-gene targeted treatment should be considered. Here, in the specific condition of NMO, the anti-AQP4 monoclonal antibody (aquaporumab), competitively binding to AQP4 has proven its efficacy in reducing lesions, at least in preclinical tests (280–283). It is noteworthy to consider an antibody-based approach in conditions where AQP4 function (as cytotoxic edema, ocular neovascularization, and astroglia proliferation including glial scarring and infiltration of glial tumors) is related to exacerbation or propagation of pathologic conditions. Limiting AQP4 expression by use of

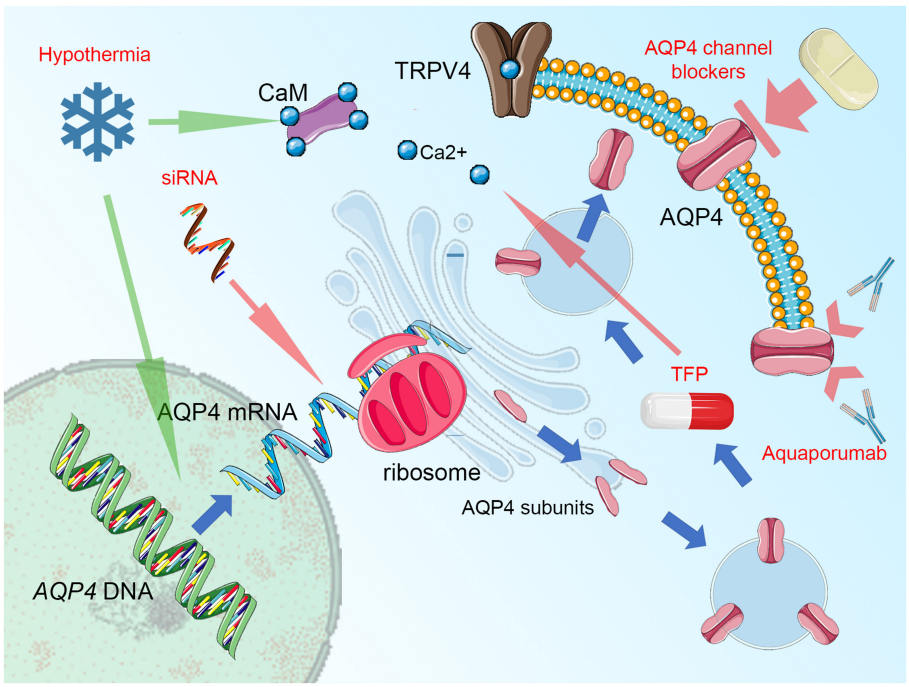

FIGURE 1 | Summary figure, demonstrating aquaporin-4 (AQP4) cellular trafficking as a possible target for treatment. Blue arrows represent the process of AQP4 production and relocation, the groups of potential therapeutics are labeled by red text and their impact is marked by green (enhancing) or red arrows (blocking activity). AQP4 expression (transcription of the *AQP4* gene and translation of AQP4 mRNA with ribosomal production of AQP single subunits may be disturbed by small interfering RNA (siRNA), attaching selectively to AQP4 mRNA domains and preventing the translational readout. The single subunits of AQP4 are organized into orthogonal arrays of particles (OAPs) and as tetramers are transferred by endosomal vesicles to the proximity of cell membrane (predominantly in astrocytic endfoot area). Here, the AQP4 translocation to the cell surface takes place. This process relies on the activity of vanilloid-receptor-related subfamily 4 calcium channel (TRPV4) and calmodulin (CaM), directly binding to the AQP4 particles. Importantly, blocking CaM activity by trifluoperazine (TFP) was efficient against AQP4 relocation and the formation of cytotoxic brain edema. Notably, hypothermia exerts opposite action enhancing AQP4 surface exposition and this effect may be counteracted by TRPV4 inhibitors, Ca^{2+} chelating compounds, or CaM blockers. This effect is more relevant than the impact of hypothermia on AQP4 expression, with increased transcription reported by some, but not all relevant studies. The AQP4 channel, while integrated into astrocytic surface membrane, may be simply blocked by a number of compounds, including acetazolamide, topiramate, lamotrigine, zonisamide, acetylsulfanilamide, phenytoin, bumetanide, furosemide, tetraethylammonium, and IMD0354 as well as by heavy metal derivates or—more selectively—by TGN-020. In conditions of autoimmune response that is driven against AQP4 channels, as seen in neuromyelitis optica (NMO), blocking of antigen epitopes by monoclonal antibodies (aquaporumab), has been demonstrated as an effective NMO treatment, at least in experimental conditions. Figure created with the use of Servier Medical Art images/content of smart.servier.com in compliance with the terms of the Creative Commons Attribution 3.0 Unported Licence.

small interfering RNAs (siRNA) to suppress the translation process is another viable option (256), efficiently reducing the development of posttraumatic brain edema, at least in animal models (284, 285). Finally, the implementation of physical methods interfering with AQP4 function should be mentioned. For instance, global or focal brain hypothermia seems to exert their beneficial action not only by increasing AQP4 expression (286) but also partially via impacting the function of AQP4 channels (251, 287–289). Focusing on this aspect and enhancing the impact of cerebral hypothermia treatment with AQP4-active drugs would potentially allow the second renaissance of the latter treatment mode (currently abandoned due to clinical burden of side effects, including ionic disbalance) (290, 291). The key points of cellular AQP4 trafficking that are relevant for developing new treatment strategies are outlined in **Figure 1**.

7. CONCLUSION

There is growing interest in the structure and function of cerebral extracellular spaces described recently as the glymphatic system. Certainly, the glymphatic flow as well as water metabolismis dependent on numerous physical laws and molecular factors. However, evidence from recent years, regarding the role of cellular water channels in physiological conditions and diverse brain pathologies clearly point out AQP4 as the key component of cerebral fluid homeostasis, acting not only as a passive channel for water and small molecular substances but playing a key role in the proper functioning of blood-brain barrier and perivascular unit. Hereby adapting the glymphatic flow to the phases of neuronal activity with increased blood flow demand in an alternating manner. The knowledge about the role of AQP4 in cerebral fluid homeostasis is vast and continually growing, however, there is still a lot to discover in this field. For this reason, as well as the ambiguity of the impact of AQP4 on the neurological outcome of cerebral edema, attempts to translate somehow the positive results of *in vivo* studies into clinical practice should await more precise and more critical benefit-risk calculations for an inhomogeneous group of conditions, in which brain edema and/or neurovascular uncoupling play a major role.

AUTHOR CONTRIBUTIONS

JS, MK, AW, and JO contributed the conception and design of the review. JS, MK, and AW wrote sections of the manuscript. All authors contributed to manuscript revision, read, and approved the submitted version.

ACKNOWLEDGMENTS

We thank Claude Lionel Ngassam Djeumen MD (Department of Neurosurgery Saarland University) for his comments on the manuscript and its linguistic corrections.

REFERENCES

1. Schrier RW, Chen YC, Cadnapaphornchai MA. From finch to fish to man: role of aquaporins in body fluid and brain water regulation. *Neuroscience.* (2004) 129:897–904. doi: 10.1016/j.neuroscience.2004.06.043
2. Rasmussen MK, Mestre H, Nedergaard M. Fluid transport in the brain. *Physiol Rev.* (2021). doi: 10.1152/physrev.00031.2020 [Epub ahead of print].
3. Olsen ML, Khakh BS, Skatchkov SN, Zhou M, Lee CJ, Rouach N. New insights on astrocyte ion channels: critical for homeostasis and neuron-glia signaling. *J Neurosci.* (2015) 35:13827–35. doi: 10.1523/JNEUROSCI.2603-15.2015
4. Verkhratsky A, Nedergaard M. The homeostatic astroglia emerges from evolutionary specialization of neural cells. *Philos Trans R Soc Lond B Biol Sci.* (2016) 371:20150428. doi: 10.1098/rstb.2015.0428
5. Verkhratsky A, Nedergaard M, Hertz L. Why are astrocytes important? *Neurochem Res.* (2015) 40:389–401. doi: 10.1007/s11064-014-1403-2
6. Verkhratsky A, Nedergaard M. Astroglial cradle in the life of the synapse. *Philos Trans R Soc Lond B Biol Sci.* (2014) 369:20130595. doi: 10.1098/rstb.2013.0595
7. Natale G, Limanaqi F, Busceti CL, Mastroiacovo F, Nicoletti F, Puglisi-Allegra S, et al. Glymphatic system as a gateway to connect neurodegeneration from periphery to CNS. *Front Neurosci.* (2021) 15:639140. doi: 10.3389/fnins.2021.639140
8. Mestre H, Mori Y, Nedergaard M. The brain's glymphatic system: current controversies. *Trends Neurosci.* (2020) 43:458–466. doi: 10.1016/j.tins.2020.04.003
9. Jessen NA, Munk AS, Lundgaard I, Nedergaard M. The glymphatic system: a beginner's guide. *Neurochem Res.* (2015) 40:2583–99. doi: 10.1007/s11064-015-1581-6
10. Zhou X, Li Y, Lenahan C, Ou Y, Wang M, He Y. Glymphatic system in the central nervous system, a novel therapeutic direction against brain edema after stroke. *Front Aging Neurosci.* (2021) 13:698036. doi: 10.3389/fnagi.2021.698036
11. Xu M, Xiao M, Li S, Yang B. Aquaporins in nervous system. *Adv Exp Med Biol.* (2017) 969:81–103. doi: 10.1007/978-94-024-1057-0_5
12. Nakada T, Virchow-Robin space and aquaporin-4: new insights on an old friend. *Croat Med J.* (2014) 55:328–36. doi: 10.3325/cmj.2014.55.328
13. Verkman AS, Binder DK, Bloch O, Auguste K, Papadopoulos MC. Three distinct roles of aquaporin-4 in brain function revealed by knockout mice. *Biochim Biophys Acta.* (2006) 1758:1085–93. doi: 10.1016/j.bbamem.2006.02.018
14. Manley GT, Binder DK, Papadopoulos MC, Verkman AS. New insights into water transport and edema in the central nervous system from phenotype analysis of aquaporin-4 null mice. *Neuroscience.* (2004) 129:983–1. doi: 10.1016/j.neuroscience.2004.06.088
15. Kitchen P, Salman MM, Halsey AM, Clarke-Bland C, MacDonald JA, Ishida H, et al. Targeting aquaporin-4 subcellular localization to treat central nervous system edema. *Cell.* (2020) 181:784–99.e19. doi: 10.1016/j.cell.2020.03.037
16. Amorini AM, Dunbar JG, Marmarou A. Modulation of aquaporin-4 water transport in a model of TBI. *Acta Neurochir Suppl.* (2003) 86:261–3. doi: 10.1007/978-3-7091-0651-8_56
17. Xiong A, Xiong R, Yu J, Liu Y, Liu K, Jin G, et al. Aquaporin-4 is a potential drug target for traumatic brain injury via aggravating the severity of brain edema. *Burns Trauma.* (2021) 9:tkaa050. doi: 10.1093/burnst/tkaa050
18. Liu X, Xie Y, Wan X, Wu J, Fan Z, Yang L. Protective effects of aquaporin-4 deficiency on longer-term neurological outcomes in a mouse model. *Neurochem Res.* (2021) 46:1380–9. doi: 10.1007/s11064-021-03272-7
19. Gardner WJ. The brain's third circulation. *Arch Neurol.* (1977) 34:200. doi: 10.1001/archneur.1977.00500150086021
20. Proulx ST, Cerebrospinal fluid outflow: a review of the historical and contemporary evidence for arachnoid villi, perineural

routes, dural lymphatics. *Cell Mol Life Sci.* (2021) 78:2429–57. doi: 10.1007/s00018-020-03706-5
21. Kumar A, Ghosh SK, Faiq MA, Deshmukh VR, Kumari C, Pareek V. A brief review of recent discoveries in human anatomy. *QJM.* (2019) 112:567–73. doi: 10.1093/qjmed/hcy241
22. Rasmussen MK, Mestre H, Nedergaard M. The glymphatic pathway in neurological disorders. *Lancet Neurol.* (2018) 17:1016–24. doi: 10.1016/S1474-4422(18)30318-1
23. Nakada T, Kwee IL. Fluid dynamics inside the brain barrier: current concept of interstitial flow, glymphatic flow, and cerebrospinal fluid circulation in the brain. *Neuroscientist.* (2019) 25:155–66. doi: 10.1177/1073858418775027
24. Zhang Y, Song J, He XZ, Xiong J, Xue R, Ge JH, et al. Quantitative determination of glymphatic flow using spectrophotofluorometry. *Neurosci Bull.* (2020) 36:1524–37. doi: 10.1007/s12264-020-00548-w
25. Ramos M, Burdon Bechet N, Battistella R, Pavan C, Xavier ALR, Nedergaard M, et al. Cisterna magna injection in rats to study glymphatic function. *Methods Mol Biol.* (2019) 1938:97–104. doi: 10.1007/978-1-4939-9068-9_7
26. Albargothy NJ, Johnston DA, MacGregor-Sharp M, Weller RO, Verma A, Hawkes CA, et al. Convective influx/glymphatic system: tracers injected into the CSF enter and leave the brain along separate periarterial basement membrane pathways. *Acta Neuropathol.* (2018) 136:139–52. doi: 10.1007/s00401-018-1862-7
27. Zhang C, Lin J, Wei F, Song J, Chen W, Shan L, et al. Characterizing the glymphatic influx by utilizing intracisternal infusion of fluorescently conjugated cadaverine. *Life Sci.* (2018) 201:150–60. doi: 10.1016/j.lfs.2018.03.057
28. Yang L, Kress BT, Weber HJ, Thiyagarajan M, Wang B, Deane R, et al. Evaluating glymphatic pathway function utilizing clinically relevant intrathecal infusion of CSF tracer. *J Transl Med.* (2013) 11:107. doi: 10.1186/1479-5876-11-107
29. Taoka T, Naganawa S. Glymphatic imaging using MRI. *J Magn Reson Imaging.* (2020) 51:11–24. doi: 10.1002/jmri.26892
30. Benveniste H, Lee H, Ozturk B, Chen X, Koundal S, Vaska P, et al. Glymphatic cerebrospinal fluid and solute transport quantified by MRI and PET imaging. *Neuroscience.* (2020) 474:63–79. doi: 10.1016/j.neuroscience.2020.11.014
31. Bèchet NB, Shanbhag NC, Lundgaard I. Glymphatic pathways in the gyrencephalic brain. *J Cereb Blood Flow Metab.* (2021) 41:2264–79. doi: 10.1177/0271678X21996175
32. Raghunandan A, Ladron-de-Guevara A, Tithof J, Mestre H, Du T, Nedergaard M, et al. Bulk flow of cerebrospinal fluid observed in periarterial spaces is not an artifact of injection. *eLife.* (2021) 10:65958. doi: 10.7554/eLife.65958
33. Gutierrez J, DiTullio M, YK KC, Alperin N, Bagci A, R LS, et al. Brain arterial dilatation modifies the association between extracranial pulsatile hemodynamics and brain perivascular spaces: the Northern Manhattan Study. *Hypertens Res.* (2019) 42:1019–28. doi: 10.1038/s41440-019-0255-1
34. Mestre H, Tithof J, Du T, Song W, Peng W, Sweeney AM, et al. Flow of cerebrospinal fluid is driven by arterial pulsations and is reduced in hypertension. *Nat Commun.* (2018) 9:4878. doi: 10.1038/s41467-018-07318-3
35. Iliff JJ, Wang M, Zeppenfeld DM, Venkataraman A, Plog BA, Liao Y, et al. Cerebral arterial pulsation drives paravascular CSF-interstitial fluid exchange in the murine brain. *J Neurosci.* (2013) 33:18190–9. doi: 10.1523/JNEUROSCI.1592-13.2013
36. Vinje V, Bakker E, Rognes ME. Brain solute transport is more rapid in periarterial than perivenous spaces. *Sci Rep.* (2021) 11:16085. doi: 10.1038/s41598-021-95306-x
37. Cheng Y, Liu X, Ma X, Garcia R, Belfield K, Haorah J. Alcohol promotes waste clearance in the CNS via brain vascular reactivity. *Free Radic Biol Med.* (2019) 143:115–26. doi: 10.1016/j.freeradbiomed.2019.07.029
38. Venkat P, Chopp M, Chen J. New insights into coupling and uncoupling of cerebral blood flow and metabolism in the brain. *Croat Med J.* (2016) 57:223–8. doi: 10.3325/cmj.2016.57.223
39. Han F, Chen J, Belkin-Rosen A, Gu Y, Luo L, Buxton OM, et al. Reduced coupling between cerebrospinal fluid flow and global brain activity is linked to Alzheimer disease-related pathology. *PLoS Biol.* (2021) 19:e3001233. doi: 10.1371/journal.pbio.3001233
40. Han F, Brown GL, Zhu Y, Belkin-Rosen AE, Lewis MM, Du G, et al. Decoupling of global brain activity and cerebrospinal fluid flow in Parkinson's Disease cognitive decline. *Mov Disord.* (2021) doi: 10.1101/2021.01.08.425953
41. Ramirez J, Holmes MF, Berezuk C, Kwan D, Tan B, Beaton D, et al. MRI-visible perivascular space volumes, sleep duration and daytime dysfunction in adults with cerebrovascular disease. *Sleep Med.* (2021) 83:83–88. doi: 10.1016/j.sleep.2021.03.043
42. Manouchehrian O, Ramos M, Bachiller S, Lundgaard I, Deierborg T. Acute systemic LPS-exposure impairs perivascular CSF distribution in mice. *J Neuroinflammation.* (2021) 18:34. doi: 10.1186/s12974-021-02082-6
43. Mortensen KN, Sanggaard S, Mestre H, Lee H, Kostrikov S, Xavier ALR, et al. Impaired glymphatic transport in spontaneously hypertensive rats. *J Neurosci.* (2019) 39:6365–77. doi: 10.1523/JNEUROSCI.1974-18.2019
44. Chen W, Huang P, Zeng H, Lin J, Shi Z, Yao X. Cocaine-induced structural and functional impairments of the glymphatic pathway in mice. *Brain Behav Immun.* (2020) 88:97–104. doi: 10.1016/j.bbi.2020.04.057
45. Blair GW, Thrippleton MJ, Shi Y, Hamilton I, Stringer M, Chappell F, et al. Intracranial hemodynamic relationships in patients with cerebral small vessel disease. *Neurology.* (2020) 94:e2258–69. doi: 10.1212/WNL.0000000000009483
46. Hudetz AG, Regulation of oxygen supply in the cerebral circulation. *Adv Exp Med Biol.* (1997) 428:513–20. doi: 10.1007/978-1-4615-5399-1_73
47. McCarron RM, Chen Y, Tomori T, Strasser A, Mechoulam R, Shohami E, et al. Endothelial-mediated regulation of cerebral microcirculation. *J Physiol Pharmacol.* (2006) 57(Suppl. 11):133–44. doi: 10.26402/jpp
48. Duchemin S, Boily M, Sadekova N, Girouard H. The complex contribution of NOS interneurons in the physiology of cerebrovascular regulation. *Front Neural Circuits.* (2012) 6:51. doi: 10.3389/fncir.2012.00051
49. McConnell HL, Kersch CN, Woltjer RL, Neuwelt EA. The translational significance of the neurovascular unit. *J Biol Chem.* (2017) 292:762–70. doi: 10.1074/jbc.R116.760215
50. Quelhas P, Baltazar G, Cairrao E. The neurovascular unit: focus on the regulation of arterial smooth muscle cells. *Curr Neurovasc Res.* (2019) 16:502–15. doi: 10.2174/1567202616666191026122642
51. Zheng Z, Chopp M, Chen J. Multifaceted roles of pericytes in central nervous system homeostasis and disease. *J Cereb Blood Flow Metab.* (2020) 40:1381–401. doi: 10.1177/0271678X20911331
52. Gotoh J, Kuang TY, Nakao Y, Cohen DM, Melzer P, Itoh Y, et al. Regional differences in mechanisms of cerebral circulatory response to neuronal activation. *Am J Physiol Heart Circ Physiol.* (2001) 280:H821–9. doi: 10.1152/ajpheart.2001.280.2.H821
53. Dormanns K, Brown RG, David T. The role of nitric oxide in neurovascular coupling. *J Theor Biol.* (2016) 394:1–17. doi: 10.1016/j.jtbi.2016.01.009
54. Niwa K, Araki E, Morham SG, Ross ME, Iadecola C. Cyclooxygenase-2 contributes to functional hyperemia in whisker-barrel cortex. *J Neurosci.* (2000) 20:763–70. doi: 10.1523/JNEUROSCI.20-02-00763.2000
55. Lacroix A, Toussay X, Anenberg E, Lecrux C, Ferreirós N, Karagiannis A, et al. COX-2-derived prostaglandin E2 produced by pyramidal neurons contributes to neurovascular coupling in the rodent cerebral cortex. *J Neurosci.* (2015) 35:11791–810. doi: 10.1523/JNEUROSCI.0651-15.2015
56. Stobart JL, Lu L, Anderson HD, Mori H, Anderson CM. Astrocyte-induced cortical vasodilation is mediated by D-serine and endothelial nitric oxide synthase. *Proc Natl Acad Sci USA.* (2013) 110:3149–54. doi: 10.1073/pnas.1215929110
57. Du W, Stern JE, Filosa JA. Neuronal-derived nitric oxide and somatodendritically released vasopressin regulate neurovascular coupling in the rat hypothalamic supraoptic nucleus. *J Neurosci.* (2015) 35:5330–41. doi: 10.1523/JNEUROSCI.3674-14.2015
58. Cauli B, Tong X-K, Rancillac A, Serluca N, Lambolez B, Rossier J, et al. Cortical GABA interneurons in neurovascular coupling: relays for subcortical vasoactive pathways. *J Neurosci.* (2004) 24:8940–49. doi: 10.1523/JNEUROSCI.3065-04.2004
59. Perrenoud Q, Rossier J, Férézou I, Geoffroy H, Gallopin T, Vitalis T, et al. Activation of cortical 5-HT(3) receptor-expressing interneurons induces NO mediated vasodilatations and NPY mediated vasoconstrictions. *Front Neural Circuits.* (2012) 6:50. doi: 10.3389/fncir.2012.00050

60. Abounader R, Villemure JG, Hamel E. Characterization of neuropeptide Y (NPY) receptors in human cerebral arteries with selective agonists and the new Y1 antagonist BIBP 3226. *Br J Pharmacol.* (1995) 116:2245–50. doi: 10.1111/j.1476-5381.1995.tb15060.x
61. Yaksh TL, Wang JY, Go VL. Cortical vasodilatation produced by vasoactive intestinal polypeptide (VIP) and by physiological stimuli in the cat. *J Cereb Blood Flow Metab.* (1987) 7:315–26. doi: 10.1038/jcbfm.1987.69
62. Nakada T, Kwee IL, Igarashi H, Suzuki Y. Aquaporin-4 functionality and virchow-robin space water dynamics: physiological model for neurovascular coupling and glymphatic flow. *Int J Mol Sci.* (2017) 18:1798. doi: 10.3390/ijms18081798
63. Martinac AD, Fletcher DF, Bilston LE. Phase offset between arterial pulsations and subarachnoid space pressure fluctuations are unlikely to drive periarterial cerebrospinal fluid flow. *Biomech Model Mechanobiol.* (2021) 10:10102. doi: 10.1007/s10237-021-01474-0
64. Kedarasetti RT, Drew PJ, Costanzo F. Arterial pulsations drive oscillatory flow of CSF but not directional pumping. *Sci Rep.* (2020) 10:10102. doi: 10.1038/s41598-020-66887-w
65. Ichimura T, Fraser PA, Cserr HF. Distribution of extracellular tracers in perivascular spaces of the rat brain. *Brain Res.* (1991) 545:103–13. doi: 10.1016/0006-8993(91)91275-6
66. Segarra M, Aburto MR, Acker-Palmer A. Blood-brain barrier dynamics to maintain brain homeostasis. *Trends Neurosci.* (2021) 44:393–405. doi: 10.1016/j.tins.2020.12.002
67. Hamasaki S, Mukuda T, Koyama Y, Nakane H, Kaidoh T. Constitutive accessibility of circulating proteins to hippocampal neurons in physiologically normal rats. *Brain Behav.* (2020) 10:e01544. doi: 10.1002/brb3.1544
68. Nordström CH, Koskinen LO, Olivecrona M. Aspects on the physiological and biochemical foundations of neurocritical care. *Front Neurol.* (2017) 8:274. doi: 10.3389/fneur.2017.00274
69. Dickie BR, Parker GJM, Parkes LM. Measuring water exchange across the blood-brain barrier using MRI. *Prog Nucl Magn Reson Spectrosc.* (2020) 116:19–39. doi: 10.1016/j.pnmrs.2019.09.002
70. Olson JE, Banks M, Dimlich RV, Evers J. Blood-brain barrier water permeability and brain osmolyte content during edema development. *Acad Emerg Med.* (1997) 4:662–73. doi: 10.1111/j.1553-2712.1997.tb03757.x
71. Rapoport SI, Matthews K, Thompson HK, Pettigrew KD. Osmotic opening of the blood-brain barrier in the rhesus monkey without measurable brain edema. *Brain Res.* (1977) 136:23–9. doi: 10.1016/0006-8993(77)90128-7
72. Harik SI, Blood–brain barrier sodium/potassium pump: modulation by central noradrenergic innervation. *Proc Natl Acad Sci USA.* (1986) 83:4067–70. doi: 10.1073/pnas.83.11.4067
73. Komura J, Tamai I, Senmaru M, Terasaki T, Sai Y, Tsuji A. Sodium and chloride ion-dependent transport of beta-alanine across the blood-brain barrier. *J Neurochem.* (1996) 67:330–5. doi: 10.1046/j.1471-4159.1996.67010330.x
74. Zhang Y, Liu GQ. Sodium and chloride-dependent high and low-affinity uptakes of GABA by brain capillary endothelial cells. *Brain Res.* (1998) 808:1–7. doi: 10.1016/S0006-8993(98)00767-7
75. Zaragozá R, Transport of amino acids across the blood-brain barrier. *Front Physiol.* (2020) 11:973. doi: 10.3389/fphys.2020.00973
76. Shao X, Ma SJ, Casey M, D'Orazio L, Ringman JM, Wang DJJ. Mapping water exchange across the blood-brain barrier using 3D diffusion-prepared arterial spin labeled perfusion MRI. *Magn Reson Med.* (2019) 81:3065–079. doi: 10.1002/mrm.27632
77. Shao X, Jann K, Ma SJ, Yan L, Montagne A, Ringman JM, et al. Comparison between blood-brain barrier water exchange rate and permeability to gadolinium-based contrast agent in an elderly cohort. *Front Neurosci.* (2020) 14:571480. doi: 10.3389/fnins.2020.571480
78. Chassidim Y, Veksler R, Lublinsky S, Pell GS, Friedman A, Shelef I. Quantitative imaging assessment of blood-brain barrier permeability in humans. *Fluids Barriers CNS.* (2013) 10:9. doi: 10.1186/2045-8118-10-9
79. Prager O, Chassidim Y, Klein C, Levi H, Shelef I, Friedman A. Dynamic *in vivo* imaging of cerebral blood flow and blood-brain barrier permeability. *Neuroimage.* (2010) 49:337–44. doi: 10.1016/j.neuroimage.2009.08.009
80. Davoodi-Bojd E, Ding G, Zhang L, Li Q, Li L, Chopp M, et al. Modeling glymphatic system of the brain using MRI. *Neuroimage.* (2019) 188:616–27. doi: 10.1016/j.neuroimage.2018.12.039
81. Ringstad G, Valnes LM, Dale AM, Pripp AH, Vatnehol SS, Emblem KE, et al. Brain-wide glymphatic enhancement and clearance in humans assessed with MRI. *JCI Insight.* (2018) 3:121537. doi: 10.1172/jci.insight.121537
82. Lee H, Mortensen K, Sanggaard S, Koch P, Brunner H, Quistorff B, et al. Quantitative Gd-DOTA uptake from cerebrospinal fluid into rat brain using 3D VFA-SPGR at 9.4T. *Magn Reson Med.* (2018) 79:1568–78. doi: 10.1002/mrm.26779
83. Zong X, Lian C, Jimenez J, Yamashita K, Shen D, Lin W. Morphology of perivascular spaces and enclosed blood vessels in young to middle-aged healthy adults at 7T: dependences on age, brain region, breathing gas. *Neuroimage.* (2020) 218:116978. doi: 10.1016/j.neuroimage.2020.116978
84. Osipova ED, Semyachkina-Glushkovskaya OV, Morgun AV, Pisareva NV, Malinovskaya NA, Boitsova EB, et al. Gliotransmitters and cytokines in the control of blood-brain barrier permeability. *Rev Neurosci.* (2018) 29:567–91. doi: 10.1515/revneuro-2017-0092
85. Azad AK, Raihan T, Ahmed J, Hakim A, Emon TH, Chowdhury PA. Human aquaporins: functional diversity and potential roles in infectious and non-infectious diseases. *Front Genet.* (2021) 12:654865. doi: 10.3389/fgene.2021.654865
86. King LS, Kozono D, Agre P. From structure to disease: the evolving tale of aquaporin biology. *Nat Rev Mol Cell Biol.* (2004) 5:687–98. doi: 10.1038/nrm1469
87. Hasegawa H, Ma T, Skach W, Matthay MA, Verkman AS. Molecular cloning of a mercurial-insensitive water channel expressed in selected water-transporting tissues. *J Biol Chem.* (1994) 269:5497–500. doi: 10.1016/S0021-9258(17)37486-0
88. Frigeri A, Gropper MA, Turck CW, Verkman AS. Immunolocalization of the mercurial-insensitive water channel and glycerol intrinsic protein in epithelial cell plasma membranes. *Proc Natl Acad Sci USA.* (1995) 92:4328–31. doi: 10.1073/pnas.92.10.4328
89. Frigeri A, Gropper MA, Umenishi F, Kawashima M, Brown D, Verkman AS. Localization of MIWC and GLIP water channel homologs in neuromuscular, epithelial and glandular tissues. *J Cell Sci.* (1995) 108(Pt 9):2993–3002. doi: 10.1242/jcs.108.9.2993
90. Nielsen S, Nagelhus EA, Amiry-Moghaddam M, Bourque C, Agre P, Ottersen OP. Specialized membrane domains for water transport in glial cells: high-resolution immunogold cytochemistry of aquaporin-4 in rat brain. *J Neurosci.* (1997) 17:171–80. doi: 10.1523/JNEUROSCI.17-01-00171.1997
91. Takumi Y, Nagelhus EA, Eidet J, Matsubara A, Usami S, Shinkawa H, et al. Select types of supporting cell in the inner ear express aquaporin-4 water channel protein. *Eur J Neurosci.* (1998) 10:3584–95. doi: 10.1046/j.1460-9568.1998.00360.x
92. Agre P, Preston GM, Smith BL, Jung JS, Raina S, Moon C, et al. Aquaporin CHIP: the archetypal molecular water channel. *Am J Physiol.* (1993) 265:F463–76. doi: 10.1152/ajprenal.1993.265.4.F463
93. Jung JS, Bhat RV, Preston GM, Guggino WB, Baraban JM, Agre P. Molecular characterization of an aquaporin cDNA from brain: candidate osmoreceptor and regulator of water balance. *Proc Natl Acad Sci USA.* (1994) 91:13052–6. doi: 10.1073/pnas.91.26.13052
94. Fujiyoshi Y, K. Mitsuoka, de Groot BL, Philippsen A, Grubmüller H, Agre P, Engel A. Structure and function of water channels. *Curr Opin Struct Biol.* (2002) 12:509–15. doi: 10.1016/S0959-440X(02)00355-X
95. Murata K, Mitsuoka K, Hirai T, Walz T, Agre P, Heymann JB, et al. Structural determinants of water permeation through aquaporin-1. *Nature.* (2000) 407:599–605. doi: 10.1038/35036519
96. Agre P, Kozono D. Aquaporin water channels: molecular mechanisms for human diseases. *FEBS Lett.* (2003) 555:72–8. doi: 10.1016/S0014-5793(03)01083-4
97. Lu M, Lee MD, Smith BL, Jung JS, Agre P, Verdijk MA, et al. The human AQP4 gene: definition of the locus encoding two water channel polypeptides in brain. *Proc Natl Acad Sci USA.* (1996) 93:10908–12. doi: 10.1073/pnas.93.20.10908
98. Palazzo C, Buccoliero C, Mola MG, Abbrescia P, Nicchia GP, Trojano M, et al. AQP4ex is crucial for the anchoring of AQP4 at the astrocyte end-feet and for

neuromyelitis optica antibody binding. *Acta Neuropathol Commun.* (2019) 7:51. doi: 10.1186/s40478-019-0707-5

99. M. De Bellis, Pisani F, Mola MG, Basco D, Catalano F, Nicchia GP, et al. A novel human aquaporin-4 splice variant exhibits a dominant-negative activity: a new mechanism to regulate water permeability. *Mol Biol Cell.* (2014) 25:470–80. doi: 10.1091/mbc.e13-06-0331
100. Jorgačevski J, Zorec R, Potokar M. Insights into cell surface expression, supramolecular organization, and functions of aquaporin 4 isoforms in astrocytes. *Cells.* (2020) 9:2622. doi: 10.3390/cells9122622
101. Moe SE, Sorbo JG, Sogaard R, Zeuthen T, Petter Ottersen O, Holen T. New isoforms of rat Aquaporin-4. *Genomics.* (2008) 91:367–77. doi: 10.1016/j.ygeno.2007.12.003
102. M. De Bellis, Pisani F, Mola MG, Rosito S, Simone L, Buccoliero C, et al. Translational readthrough generates new astrocyte AQP4 isoforms that modulate supramolecular clustering, glial endfeet localization, water transport. *Glia.* (2017) 65:790–803. doi: 10.1002/glia.23126
103. Lisjak M, Potokar M, Zorec R, Jorgačevski J. Indirect role of AQP4b and AQP4d isoforms in dynamics of astrocyte volume and orthogonal arrays of particles. *Cells.* (2020) 9:735. doi: 10.3390/cells9030735
104. Sorbo JG, Moe SE, Ottersen OP, Holen T. The molecular composition of square arrays. *Biochemistry.* (2008) 47:2631–7. doi: 10.1021/bi702146k
105. Rossi A, Moritz TJ, Ratelade J, Verkman AS. Super-resolution imaging of aquaporin-4 orthogonal arrays of particles in cell membranes. *J Cell Sci.* (2012) 125:4405–12. doi: 10.1242/jcs.109603
106. Jin BJ, Rossi A, Verkman AS. Model of aquaporin-4 supramolecular assembly in orthogonal arrays based on heterotetrameric association of M1-M23 isoforms. *Biophys J.* (2011) 100:2936–45. doi: 10.1016/j.bpj.2011.05.012
107. Yang B, Ma T, Verkman AS. cDNA cloning, gene organization, and chromosomal localization of a human mercurial insensitive water channel. Evidence for distinct transcriptional units. *J Biol Chem.* (1995) 270:22907–13. doi: 10.1074/jbc.270.39.22907
108. National Center for Biotechnology Information. Database of single nucleotide polymorphisms (dbsnp): homo sapiens. *Nucleic Acids Res.* (2021) 28:352–55. Retreived from: https://www.ncbi.nlm.nih.gov/snp/ (accessed August 20, 2021).
109. Sorani MD, Zador Z, Hurowitz E, Yan D, Giacomini KM, Manley GT. Novel variants in human Aquaporin-4 reduce cellular water permeability. *Hum Mol Genet.* (2008) 17:2379–89. doi: 10.1093/hmg/ddn138
110. Crane JM, Van Hoek AN, Skach WR, Verkman AS. Aquaporin-4 dynamics in orthogonal arrays in live cells visualized by quantum dot single particle tracking. *Mol Biol Cell.* (2008) 19:3369–78. doi: 10.1091/mbc.e08-03-0322
111. Furman CS, Gorelick-Feldman DA, Davidson KG, Yasumura T, Neely JD, Agre P, et al. Aquaporin-4 square array assembly: opposing actions of M1 and M23 isoforms. *Proc Natl Acad Sci USA.* (2003) 100:13609–14. doi: 10.1073/pnas.2235843100
112. Kitchen P, Day RE, Taylor LH, Salman MM, Bill RM, Conner MT, et al. Identification and molecular mechanisms of the rapid tonicity-induced relocalization of the aquaporin 4 channel. *J Biol Chem.* (2015) 290:16873–81. doi: 10.1074/jbc.M115.646034
113. Rossi A, Pisani F, Nicchia GP, Svelto M, Frigeri A. Evidences for a leaky scanning mechanism for the synthesis of the shorter M23 protein isoform of aquaporin-4: implication in orthogonal array formation and neuromyelitis optica antibody interaction. *J Biol Chem.* (2010) 285:4562–9. doi: 10.1074/jbc.M109.069245
114. Salman MM, Kitchen P, Woodroofe MN, Brown JE, Bill RM, Conner AC, et al. Hypothermia increases aquaporin 4 (AQP4) plasma membrane abundance in human primary cortical astrocytes via a calcium/transient receptor potential vanilloid 4 (TRPV4)- and calmodulin-mediated mechanism. *Eur J Neurosci.* (2017) 46:2542–7. doi: 10.1111/ejn.13723
115. Ciappelloni S, Bouchet D, Dubourdieu N, Boué-Grabot E, Kellermayer B, Manso C, et al. Aquaporin-4 surface trafficking regulates astrocytic process motility and synaptic activity in health and autoimmune disease. *Cell Rep.* (2019) 27:3860–72.e4. doi: 10.1016/j.celrep.2019.05.097
116. Amiry-Moghaddam M, Frydenlund DS, Ottersen OP. Anchoring of aquaporin-4 in brain: molecular mechanisms and implications for the physiology and pathophysiology of water transport. *Neuroscience.* (2004) 129:999–1010. doi: 10.1016/j.neuroscience.2004.08.049
117. Nagelhus EA, Veruki ML, Torp R, Haug FM, Laake JH, Nielsen S, et al. Aquaporin-4 water channel protein in the rat retina and optic nerve: polarized expression in Müller cells and fibrous astrocytes. *J Neurosci.* (1998) 18:2506–19. doi: 10.1523/JNEUROSCI.18-07-02506.1998
118. Neely JD, Amiry-Moghaddam M, Ottersen OP, Froehner SC, Agre P, Adams ME. Syntrophin-dependent expression and localization of Aquaporin-4 water channel protein. *Proc Natl Acad Sci USA.* (2001) 98:14108–13. doi: 10.1073/pnas.241508198
119. Amiry-Moghaddam M, Otsuka T, Hurn PD, Traystman RJ, Haug FM, Froehner SC, et al. An alpha-syntrophin-dependent pool of AQP4 in astroglial end-feet confers bidirectional water flow between blood and brain. *Proc Natl Acad Sci USA.* (2003) 100:2106–11. doi: 10.1073/pnas.0437946100
120. Pitonzo D, Skach WR. Molecular mechanisms of aquaporin biogenesis by the endoplasmic reticulum Sec61 translocon. *Biochim Biophys Acta.* (2006) 1758:976–88. doi: 10.1016/j.bbamem.2006.04.021
121. Nagelhus EA, Horio Y, Inanobe A, Fujita A, Haug FM, Nielsen S, et al. Immunogold evidence suggests that coupling of K+ siphoning and water transport in rat retinal Müller cells is mediated by a coenrichment of Kir4.1 and AQP4 in specific membrane domains. *Glia.* (1999) 26:47–54. doi: 10.1002/(SICI)1098-1136(199903)26:1<47::AID-GLIA5>3.0.CO;2-5
122. Fallier-Becker P, Sperveslage J, Wolburg H, Noell S. The impact of agrin on the formation of orthogonal arrays of particles in cultured astrocytes from wild-type and agrin-null mice. *Brain Res.* (2011) 1367:2–12. doi: 10.1016/j.brainres.2010.09.092
123. Huang J, Li J, Feng C, Huang X, Wong L, Liu X, et al. Blood-brain barrier damage as the starting point of leukoaraiosis caused by cerebral chronic hypoperfusion and its involved mechanisms: effect of agrin and aquaporin-4. *Biomed Res Int.* (2018) 2018:2321797. doi: 10.1155/2018/2321797
124. Bobik M, Ellisman MH, Rudy B, Martone ME. Potassium channel subunit Kv3.2 and the water channel aquaporin-4 are selectively localized to cerebellar pinceau. *Brain Res.* (2004) 1026:168–78. doi: 10.1016/j.brainres.2004.07.088
125. Ozawa Y, Toda E, Kawashima H, Homma K, Osada H, Nagai N, et al. Aquaporin 4 suppresses neural hyperactivity and synaptic fatigue and fine-tunes neurotransmission to regulate visual function in the mouse retina. *Mol Neurobiol.* (2019) 56:8124–35. doi: 10.1007/s12035-019-01661-2
126. Hara-Chikuma M, Verkman AS. Physiological roles of glycerol-transporting aquaporins: the aquaglyceroporins. *Cell Mol Life Sci.* (2006) 63:1386–92. doi: 10.1007/s00018-006-6028-4
127. Kitchen P, Salman MM, Pickel SU, Jennings J, Törnroth-Horsefield S, Conner MT, et al. Water channel pore size determines exclusion properties but not solute selectivity. *Sci Rep.* (2019) 9:20369. doi: 10.1038/s41598-019-56814-z
128. McCoy E, Sontheimer H. Expression and function of water channels (aquaporins) in migrating malignant astrocytes. *Glia.* (2007) 55:1034–43. doi: 10.1002/glia.20524
129. Smith AJ, Jin BJ, Ratelade J, Verkman AS. Aggregation state determines the localization and function of M1- and M23-aquaporin-4 in astrocytes. *J Cell Biol.* (2014) 204:559–73. doi: 10.1083/jcb.201308118
130. Nagelhus EA, Ottersen OP. Physiological roles of aquaporin-4 in brain. *Physiol Rev.* (2013) 93:1543–62. doi: 10.1152/physrev.00011.2013
131. Kitchen P, Day RE, Salman MM, Conner MT, Bill RM, Conner AC. Beyond water homeostasis: Diverse functional roles of mammalian aquaporins. *Biochim Biophys Acta.* (2015) 1850:2410–21. doi: 10.1016/j.bbagen.2015.08.023
132. Yao X, Hrabetová S, Nicholson C, Manley GT. Aquaporin-4-deficient mice have increased extracellular space without tortuosity change. *J Neurosci.* (2008) 28:5460–4. doi: 10.1523/JNEUROSCI.0257-08.2008
133. Teng Z, Wang A, Wang P, Wang R, Wang W, Han H. The effect of aquaporin-4 knockout on interstitial fluid flow and the structure of the extracellular space in the deep brain. *Aging Dis.* (2018) 9:808–16. doi: 10.14336/AD.2017.1115
134. Haj-Yasein NN, Vindedal GF, Eilert-Olsen M, Gundersen GA, Skare Ø, Laake P, et al. Glial-conditional deletion of aquaporin-4 (Aqp4) reduces blood-brain water uptake and confers barrier function on perivascular astrocyte endfeet. *Proc Natl Acad Sci USA.* (2011) 108:17815–20. doi: 10.1073/pnas.1110655108

135. Bloch O, Auguste KI, Manley GT, Verkman AS. Accelerated progression of kaolin-induced hydrocephalus in aquaporin-4-deficient mice. *J Cereb Blood Flow Metab.* (2006) 26:1527–37. doi: 10.1038/sj.jcbfm.9600306
136. Papadopoulos MC, Manley GT, Krishna S, Verkman AS. Aquaporin-4 facilitates reabsorption of excess fluid in vasogenic brain edema. *FASEB J.* (2004) 18:1291–3. doi: 10.1096/fj.04-1723fje
137. Binder DK, Papadopoulos MC, Haggie PM, Verkman AS. *In vivo* measurement of brain extracellular space diffusion by cortical surface photobleaching. *J Neurosci.* (2004) 24:8049–56. doi: 10.1523/JNEUROSCI.2294-04.2004
138. Iliff JJ, Wang M, Liao Y, Plogg BA, Peng W, Gundersen GA, et al. A paravascular pathway facilitates CSF flow through the brain parenchyma and the clearance of interstitial solutes, including amyloid β. *Sci Transl Med.* (2012) 4:147ra111. doi: 10.1126/scitranslmed.3003748
139. Zhang R, Liu Y, Chen Y, Li Q, Marshall C, Wu T, et al. Aquaporin 4 deletion exacerbates brain impairments in a mouse model of chronic sleep disruption. *CNS Neurosci Ther.* (2020) 26:228–39. doi: 10.1111/cns.13194
140. Cao X, Xu H, Feng W, Su D, Xiao M. Deletion of aquaporin-4 aggravates brain pathology after blocking of the meningeal lymphatic drainage. *Brain Res Bull.* (2018) 143:83–96. doi: 10.1016/j.brainresbull.2018.10.007
141. Iliff JJ, Chen MJ, Plog BA, Zeppenfeld DM, Soltero M, Yang L, et al. Impairment of glymphatic pathway function promotes tau pathology after traumatic brain injury. *J Neurosci.* (2014) 34:16180–93. doi: 10.1523/JNEUROSCI.3020-14.2014
142. Rosu GC, Catalin B, Balseanu TA, Laurentiu M, Claudiu M, Kumar-Singh S, et al. Inhibition of aquaporin 4 decreases amyloid Aβ40 drainage around cerebral vessels. *Mol Neurobiol.* (2020) 57:4720–34. doi: 10.1007/s12035-020-02044-8
143. Xu Z, Xiao N, Chen Y, Huang H, Marshall C, Gao J, et al. Deletion of aquaporin-4 in APP/PS1 mice exacerbates brain Aβ accumulation and memory deficits. *Mol Neurodegener.* (2015) 10:58. doi: 10.1186/s13024-015-0056-1
144. Achariyar TM, Li B, Peng W, Verghese PB, Shi Y, McConnell E, et al. Glymphatic distribution of CSF-derived apoE into brain is isoform specific and suppressed during sleep deprivation. *Mol Neurodegener.* (2016) 11:74. doi: 10.1186/s13024-016-0138-8
145. Salman MM, Kitchen P, Halsey A, Wang MX, Tornroth-Horsefield S, Conner AC, et al. Emerging roles for dynamic aquaporin-4 subcellular relocalization in CNS water homeostasis. *Brain.* (2021). doi: 10.1093/brain/awab311 [Epub ahead of print].
146. Mestre H, Hablitz LM, Xavier AL, Feng W, Zou W, Pu T, et al. Aquaporin-4-dependent glymphatic solute transport in the rodent brain. *eLife.* (2018) 7:40070. doi: 10.7554/eLife.40070
147. Kress BT, Iliff JJ, Xia M, Wang M, Wei HS, Zeppenfeld D, et al. Impairment of paravascular clearance pathways in the aging brain. *Ann Neurol.* (2014) 76:845–61. doi: 10.1002/ana.24271
148. Ren Z, Iliff JJ, Yang L, Yang J, Chen X, Chen MJ, Giese RN, Wang B, Shi X, Nedergaard M. 'Hit & Run' model of closed-skull traumatic brain injury (TBI) reveals complex patterns of post-traumatic AQP4 dysregulation. *J Cereb Blood Flow Metab.* (2013) 33:834–45. doi: 10.1038/jcbfm.2013.30
149. Wang M, Iliff JJ, Liao Y, Chen MJ, Shinseki MS, Venkataraman A, et al. Cognitive deficits and delayed neuronal loss in a mouse model of multiple microinfarcts. *J Neurosci.* (2012) 32:17948–60. doi: 10.1523/JNEUROSCI.1860-12.2012
150. Smith AJ, Yao X, Dix JA, Jin BJ, Verkman AS. Test of the 'glymphatic' hypothesis demonstrates diffusive and aquaporin-4-independent solute transport in rodent brain parenchyma. *eLife.* (2017) 6:27679. doi: 10.7554/eLife.27679
151. Smith AJ, Akdemir G, Wadhwa M, Song D, Verkman AS. Application of fluorescent dextrans to the brain surface under constant pressure reveals AQP4-independent solute uptake. *J Gen Physiol.* (2021) 153:e202112898. doi: 10.1085/jgp.202112898
152. Rungta RL, Zuend M, Aydin AK, Martineau É, Boido D, Weber B, et al. Diversity of neurovascular coupling dynamics along vascular arbors in layer II/III somatosensory cortex. *Commun Biol.* (2021) 4:855. doi: 10.1038/s42003-021-02382-w
153. Csipo T, Lipecz A, Mukli P, Bahadli D, Abdulhussein O, Owens CD, et al. Increased cognitive workload evokes greater neurovascular coupling responses in healthy young adults. *PLoS ONE.* (2021) 16:e0250043. doi: 10.1371/journal.pone.0250043
154. Lecrux C, Hamel E. Neuronal networks and mediators of cortical neurovascular coupling responses in normal and altered brain states. *Philos Trans R Soc Lond B Biol Sci.* (2016) 371:20150350. doi: 10.1098/rstb.2015.0350
155. Uhlirova H, Kiliç K, Tian P, Thunemann M, Desjardins M, Saisan PA, et al. Cell type specificity of neurovascular coupling in cerebral cortex. *eLife.* (2016) 5:14315. doi: 10.7554/eLife.14315
156. Kleinfeld D, Blinder P, Drew PJ, Driscoll JD, Muller A, Tsai PS, et al. A guide to delineate the logic of neurovascular signaling in the brain. *Front Neuroenerget.* (2011) 3:1. doi: 10.3389/fnene.2011.00001
157. Cauli B, Hamel E. Revisiting the role of neurons in neurovascular coupling. *Front Neuroenerget.* (2010) 2:9. doi: 10.3389/fnene.2010.00009
158. Buxton RB, Griffeth VE, Simon AB, Moradi F, Shmuel A. Variability of the coupling of blood flow and oxygen metabolism responses in the brain: a problem for interpreting BOLD studies but potentially a new window on the underlying neural activity. *Front Neurosci.* (2014) 8:139. doi: 10.3389/fnins.2014.00241
159. Kiyatkin EA. Central and peripheral mechanisms underlying physiological and drug-induced fluctuations in brain oxygen in freely-moving rats. *Front Integr Neurosci.* (2018) 12:44. doi: 10.3389/fnint.2018.00044
160. Shi C, Lei Y, Han H, Zuo L, Yan J, He Q, et al. Transportation in the interstitial space of the brain can be regulated by neuronal excitation. *Sci Rep.* (2015) 5:17673. doi: 10.1038/srep17673
161. Tuura RO, Volk C, Callaghan F, Jaramillo V, Huber R. Sleep-related and diurnal effects on brain diffusivity and cerebrospinal fluid flow. *Neuroimage.* (2021) 241:118420. doi: 10.1016/j.neuroimage.2021.118420
162. Hablitz LM, Plá V, Giannetto M, Vinitsky HS, Stæger FF, Metcalfe T, et al. Circadian control of brain glymphatic and lymphatic fluid flow. *Nat Commun.* (2020) 11:4411. doi: 10.1038/s41467-020-18115-2
163. Xie L, Kang H, Xu Q, Chen MJ, Liao Y, Thiyagarajan M, et al. Sleep drives metabolite clearance from the adult brain. *Science.* (2013) 342:373–7. doi: 10.1126/science.1241224
164. Hablitz LM, Vinitsky HS, Sun Q, Stæger FF, Sigurdsson B, Mortensen KN, et al. Increased glymphatic influx is correlated with high EEG delta power and low heart rate in mice under anesthesia. *Sci Adv.* (2019) 5:eaav5447. doi: 10.1126/sciadv.aav5447
165. Benveniste H, Lee H, Ding F, Sun Q, Al-Bizri E, Makaryus R, et al. Anesthesia with dexmedetomidine and low-dose isoflurane increases solute transport via the glymphatic pathway in rat brain when compared with high-dose isoflurane. *Anesthesiology.* (2017) 127:976–88. doi: 10.1097/ALN.0000000000001888
166. Stanton EH, Persson N, Gomolka RS, Lilius T, Sigurð*sson B, Lee H, et al. Mapping of CSF transport using high spatiotemporal resolution dynamic contrast-enhanced MRI in mice: effect of anesthesia. *Magn Reson Med.* (2021) 85:3326–42. doi: 10.1002/mrm.28645
167. Bèchet NB, Kylkilahti TM, Mattsson B, Petrasova M, Shanbhag NC, Lundgaard I. Light sheet fluorescence microscopy of optically cleared brains for studying the glymphatic system. *J Cereb Blood Flow Metab.* (2020) 40:1975–86. doi: 10.1177/0271678X20924954
168. Gakuba C, Gaberel T, Goursaud S, Bourges J, Di Palma C, Quenault A, et al. Martinez de Lizarrondo, Vivien D, Gauberti M. General anesthesia inhibits the activity of the "glymphatic system". *Theranostics.* (2018) 8:710–22. doi: 10.7150/thno.19154
169. Benveniste H, Heerdt PM, Fontes M, Rothman DL, Volkow ND. Glymphatic system function in relation to anesthesia and sleep states. *Anesth Analg.* (2019) 128:747–58. doi: 10.1213/ANE.0000000000004069
170. DiNuzzo M, Nedergaard M. Brain energetics during the sleep-wake cycle. *Curr Opin Neurobiol.* (2017) 47:65–72. doi: 10.1016/j.conb.2017.09.010
171. Li Y, Han H, Shi K, Cui D, Yang J, Alberts IL, et al. The mechanism of downregulated interstitial fluid drainage following neuronal excitation. *Aging Dis.* (2020) 11:1407–22. doi: 10.14336/AD.2020.0224
172. Liu DX, He X, Wu D, Zhang Q, Yang C, Liang FY, et al. Continuous theta burst stimulation facilitates the clearance efficiency of the glymphatic

pathway in a mouse model of sleep deprivation. *Neurosci Lett.* (2017) 653:189–94. doi: 10.1016/j.neulet.2017.05.064
173. Oku H, Morishita S, Horie T, Kida T, Mimura M, Fukumoto M, et al. Nitric oxide increases the expression of aquaporin-4 protein in rat optic nerve astrocytes through the cyclic guanosine monophosphate/protein kinase G pathway. *Ophthalmic Res.* (2015) 54:212–21. doi: 10.1159/000440846
174. Rao KV, Jayakumar AR, Reddy PV, Tong X, Curtis KM, Norenberg MD. Aquaporin-4 in manganese-treated cultured astrocytes. *Glia.* (2010) 58:1490–9. doi: 10.1002/glia.21023
175. Mohammadi MT, Dehghani GA. Nitric oxide as a regulatory factor for aquaporin-1 and 4 gene expression following brain ischemia/reperfusion injury in rat. *Pathol Res Pract.* (2015) 211:43–9. doi: 10.1016/j.prp.2014.07.014
176. Lykke K, Assentoft M, Fenton RA, Rosenkilde MM, MacAulay N. Vasopressin receptors V1a and V2 are not osmosensors. *Physiol Rep.* (2015) 3:12519. doi: 10.14814/phy2.12519
177. Nakayama S, Amiry-Moghaddam M, Ottersen OP, Bhardwaj A. Conivaptan, a selective arginine vasopressin V1a and V2 receptor antagonist attenuates global cerebral edema following experimental cardiac arrest via perivascular pool of aquaporin-4. *Neurocrit Care.* (2016) 24:273–82. doi: 10.1007/s12028-015-0236-4
178. Rauen K, Pop V, Trabold R, Badaut J, Plesnila N. Vasopressin V(1a) receptors regulate cerebral aquaporin 1 after traumatic brain injury. *J Neurotrauma.* (2020) 37:665–74. doi: 10.1089/neu.2019.6653
179. Saito M, Tanaka H, Sasaki M, Kurose H, Nakahata N. Involvement of aquaporin in thromboxane A2 receptor-mediated, G 12/13/RhoA/NHE-sensitive cell swelling in 1321N1 human astrocytoma cells. *Cell Signal.* (2010) 22:41–6. doi: 10.1016/j.cellsig.2009.09.006
180. Larsen BR, MacAulay N. Activity-dependent astrocyte swelling is mediated by pH-regulating mechanisms. *Glia.* (2017) 65:1668–81. doi: 10.1002/glia.23187
181. Rosic B, Dukefoss DB, Åbjørsbråten KS, Tang W, Jensen V, Ottersen OP, Enger R, et al. Aquaporin-4-independent volume dynamics of astroglial endfeet during cortical spreading depression. *Glia.* (2019) 67:1113–21. doi: 10.1002/glia.23604
182. MacAulay N. Molecular mechanisms of K(+) clearance extracellular space shrinkage-Glia cells as the stars. *Glia.* (2020) 68:2192–211. doi: 10.1002/glia.23824
183. Amiry-Moghaddam M, Williamson A, Palomba M, Eid T, de Lanerolle NC, Nagelhus EA, et al. Delayed K+ clearance associated with aquaporin-4 mislocalization: phenotypic defects in brains of alpha-syntrophin-null mice. *Proc Natl Acad Sci USA.* (2003) 100:13615–20. doi: 10.1073/pnas.2336064100
184. Yao X, Smith AJ, Jin BJ, Zador Z, Manley GT, Verkman AS. Aquaporin-4 regulates the velocity and frequency of cortical spreading depression in mice. *Glia.* (2015) 63:1860–9. doi: 10.1002/glia.22853
185. Enger R, Dukefoss DB, Tang W, Pettersen KH, Bjørnstad DM, Helm PJ, et al. Deletion of aquaporin-4 curtails extracellular glutamate elevation in cortical spreading depression in awake mice. *Cereb Cortex.* (2017) 27:24–33. doi: 10.1093/cercor/bhw359
186. Binder DK, Yao X, Zador Z, Sick TJ, Verkman AS, Manley GT. Increased seizure duration and slowed potassium kinetics in mice lacking aquaporin-4 water channels. *Glia.* (2006) 53:631–6. doi: 10.1002/glia.20318
187. Binder DK, Oshio K, Ma T, Verkman AS, Manley GT. Increased seizure threshold in mice lacking aquaporin-4 water channels. *Neuroreport.* (2004) 15:259–62. doi: 10.1097/00001756-200402090-00009
188. Szu JI, Patel DD, Chaturvedi S, Lovelace JW, Binder DK. Modulation of posttraumatic epileptogenesis in aquaporin-4 knockout mice. *Epilepsia.* (2020) 61:1503–14. doi: 10.1111/epi.16551
189. Lei S, He Y, Zhu Z, Liu Z, Lin Y, He Y, et al. Inhibition of NMDA receptors downregulates astrocytic AQP4 to suppress seizures. *Cell Mol Neurobiol.* (2020) 40:1283–95. doi: 10.1007/s10571-020-00813-6
190. Szu JI, Chaturvedi S, Patel DD, Binder DK. Aquaporin-4 dysregulation in a controlled cortical impact injury model of posttraumatic epilepsy. *Neuroscience.* (2020) 428:140–53. doi: 10.1016/j.neuroscience.2019.12.006
191. Eid T, Lee TS, Thomas MJ, Amiry-Moghaddam M, Bjørnsen LP, Spencer DD, et al.C. de Lanerolle, Loss of perivascular aquaporin 4 may underlie deficient water and K+ homeostasis in the human epileptogenic hippocampus. *Proc Natl Acad Sci USA.* (2005) 102:1193–8. doi: 10.1073/pnas.0409308102
192. Lee TS, Eid T, Mane S, Kim JH, Spencer DD, Ottersen OP, et al.C. de Lanerolle, Aquaporin-4 is increased in the sclerotic hippocampus in human temporal lobe epilepsy. *Acta Neuropathol.* (2004) 108:493–502. doi: 10.1007/s00401-004-0910-7
193. Mhatre R, Anita M, Phillip M, Saini J, Arimappamagan A, Bharath RD, et al. Altered vascular permeability but not angiogenesis may play a role in the epileptogenesis of human hippocampal sclerosis. *Epileptic Disord.* (2021) 23:490–9. doi: 10.1684/epd.2021.1290
194. Chang JC, Shook LL, Biag J, Nguyen EN, Toga AW, Charles AC, et al. Biphasic direct current shift, haemoglobin desaturation and neurovascular uncoupling in cortical spreading depression. *Brain.* (2010) 133:996–1012. doi: 10.1093/brain/awp338
195. Oka F, Sadeghian H, Yaseen MA, Fu B, Kura S, Qin T, et al. Intracranial pressure spikes trigger spreading depolarizations. *Brain.* (2021). doi: 10.1093/brain/awab256 [Epub ahead of print].
196. Moshkforoush A, Ashenagar B, Harraz OF, Dabertrand F, Longden TA, Nelson MT, et al. The capillary Kir channel as sensor and amplifier of neuronal signals: modeling insights on K(+)-mediated neurovascular communication. *Proc Natl Acad Sci USA.* (2020) 117:16626–37. doi: 10.1073/pnas.2000151117
197. Koide M, Moshkforoush A, Tsoukias NM, Hill-Eubanks DC, Wellman GC, Nelson MT, et al. The yin and yang of K(V) channels in cerebral small vessel pathologies. *Microcirculation.* (2018) 25:12436. doi: 10.1111/micc.12436
198. Staehr C, Rajanathan R, Matchkov VV. Involvement of the Na(+),K(+) -ATPase isoforms in control of cerebral perfusion. *Exp Physiol.* (2019) 104:1023–8. doi: 10.1113/EP087519
199. Staehr C, Rajanathan R, Postnov DD, Hangaard L, Bouzinova EV, Lykke-Hartmann K, et al. Abnormal neurovascular coupling as a cause of excess cerebral vasodilation in familial migraine. *Cardiovasc Res.* (2020) 116:2009–20. doi: 10.1093/cvr/cvz306
200. Migliati ER, Amiry-Moghaddam M, Froehner SC, Adams ME, Ottersen OP, Bhardwaj A. Na(+)-K (+)-2Cl (-) cotransport inhibitor attenuates cerebral edema following experimental stroke via the perivascular pool of aquaporin-4. *Neurocrit Care.* (2010) 13:123–31. doi: 10.1007/s12028-010-9376-8
201. Monai H, Wang X, Yahagi K, Lou N, Mestre H, Xu Q, et al. Adrenergic receptor antagonism induces neuroprotection and facilitates recovery from acute ischemic stroke. *Proc Natl Acad Sci USA.* (2019) 116:11010–11019. doi: 10.1073/pnas.1817347116
202. Steiner E, Enzmann GU, Lin S, Ghavampour S, Hannocks MJ, Zuber B, et al. Loss of astrocyte polarization upon transient focal brain ischemia as a possible mechanism to counteract early edema formation. *Glia.* (2012) 60:1646–59. doi: 10.1002/glia.22383
203. Yan JH, Khatibi NH, Han HB, Hu Q, Chen CH, Li L, et al. p53-induced uncoupling expression of aquaporin-4 and inwardly rectifying K+ 4.1 channels in cytotoxic edema after subarachnoid hemorrhage. *CNS Neurosci Ther.* (2012) 18:334–42. doi: 10.1111/j.1755-5949.2012.00299.x
204. Anzabi M, Ardalan M, Iversen NK, Rafati AH, Hansen B, Østergaard L. Hippocampal atrophy following subarachnoid hemorrhage correlates with disruption of astrocyte morphology and capillary coverage by AQP4. *Front Cell Neurosci.* (2018) 12:19. doi: 10.3389/fncel.2018.00019
205. Rickels E, Zumkeller M. Vasospasm after experimentally induced subarachnoid haemorrhage and treatment with nimodipine. *Neurochirurgia.* (1992) 35:99–102. doi: 10.1055/s-2008-1052257
206. Young HA, Kolbeck RC, Schmidek H, Evans JN. Reactivity of rabbit basilar artery to alterations in extracellular potassium and calcium after subarachnoid hemorrhage. *Neurosurgery.* (1986) 19:346–9. doi: 10.1227/00006123-198609000-00002
207. Pu T, Zou W, Feng W, Zhang Y, Wang L, Wang H, et al. Persistent malfunction of glymphatic and meningeal lymphatic drainage in a mouse model of subarachnoid hemorrhage. *Exp Neurobiol.* (2019) 28:104–18. doi: 10.5607/en.2019.28.1.104
208. Bao H, Yang X, Huang Y, Qiu H, Huang G, Xiao H, et al. The neuroprotective effect of apelin-13 in a mouse model of intracerebral hemorrhage. *Neurosci Lett.* (2016) 628:219–24. doi: 10.1016/j.neulet.2016.06.046
209. Chu H, Tang Y, Dong Q. Protection of vascular endothelial growth factor to brain edema following intracerebral hemorrhage and its involved mechanisms: effect of aquaporin-4. *PLoS ONE.* (2013) 8:e66051. doi: 10.1371/journal.pone.0066051

210. Taya K, Gulsen S, Okuno K, Prieto R, Marmarou CR, Marmarou A. Modulation of AQP4 expression by the selective V1a receptor antagonist, SR49059, decreases trauma-induced brain edema. *Acta Neurochir Suppl.* (2008) 102:425–9. doi: 10.1007/978-3-211-85578-2_83
211. Reinert M, Khaldi A, Zauner A, Doppenberg E, Choi S, Bullock R. High extracellular potassium and its correlates after severe head injury: relationship to high intracranial pressure. *Neurosurg Focus.* (2000) 8:e10. doi: 10.3171/foc.2000.8.1.2027
212. Reeves TM, Kao CQ, Phillips LL, Bullock MR, Povlishock JT. Presynaptic excitability changes following traumatic brain injury in the rat. *J Neurosci Res.* (2000) 60:370–9. doi: 10.1002/(SICI)1097-4547(20000501)60:3<370::AID-JNR12>3.0.CO;2-B
213. Darbin O, Carre E, Naritoku D, Risso JJ, Lonjon M, Patrylo PR. Glucose metabolites in the striatum of freely behaving rats following infusion of elevated potassium. *Brain Res.* (2006) 1116:127–31. doi: 10.1016/j.brainres.2006.06.095
214. Klatzo I. Pathophysiological aspects of brain edema. *Acta Neuropathol.* (1987) 72:236–9. doi: 10.1007/BF00691095
215. Klatzo I. Blood-brain barrier and ischaemic brain oedema. *Z Kardiol.* (1987) 76(Suppl 4):67–9.
216. Kimelberg HK, Current concepts of brain edema. review of laboratory investigations. *J Neurosurg.* (1995) 83:1051–9. doi: 10.3171/jns.1995.83.6.1051
217. Simard JM, Kent TA, Chen M, Tarasov KV, Gerzanich V. Brain oedema in focal ischaemia: molecular pathophysiology and theoretical implications. *Lancet Neurol.* (2007) 6:258–68. doi: 10.1016/S1474-4422(07)70055-8
218. Badaut J, Ashwal S, Obenaus A. Aquaporins in cerebrovascular disease: a target for treatment of brain edema? *Cerebrovasc Dis.* (2011) 31:521–31. doi: 10.1159/000324328
219. Stiefel MF, Tomita Y, Marmarou A. Secondary ischemia impairing the restoration of ion homeostasis following traumatic brain injury. *J Neurosurg.* (2005) 103:707–14. doi: 10.3171/jns.2005.103.4.0707
220. Barzó P, Marmarou A, Fatouros P, Hayasaki K, Corwin F. Contribution of vasogenic and cellular edema to traumatic brain swelling measured by diffusion-weighted imaging. *J Neurosurg.* (1997) 87:900–7. doi: 10.3171/jns.1997.87.6.0900
221. Marmarou A, Portella G, Barzo P, Signoretti S, Fatouros P, Beaumont A, et al. Distinguishing between cellular and vasogenic edema in head injured patients with focal lesions using magnetic resonance imaging. *Acta Neurochir Suppl.* (2000) 76:349–51. doi: 10.1007/978-3-7091-6346-7_72
222. Beaumont A, Marmarou A, Fatouros P, Corwin F. Secondary insults worsen blood brain barrier dysfunction assessed by MRI in cerebral contusion. *Acta Neurochir Suppl.* (2002) 81:217–9. doi: 10.1007/978-3-7091-6738-0_56
223. Marmarou A, Signoretti S, Aygok G, Fatouros P, Portella G. Traumatic brain edema in diffuse and focal injury: cellular or vasogenic? *Acta Neurochir Suppl.* (2006) 96:24–9. doi: 10.1007/3-211-30714-1_6
224. Marmarou A, Signoretti S, Fatouros PP, Portella G, Aygok GA, Bullock MR. Predominance of cellular edema in traumatic brain swelling in patients with severe head injuries. *J Neurosurg.* (2006) 104:720–30. doi: 10.3171/jns.2006.104.5.720
225. Young W, Rappaport ZH, Chalif DJ, Flamm ES. Regional brain sodium, potassium, and water changes in the rat middle cerebral artery occlusion model of ischemia. *Stroke.* (1987) 18:751–9. doi: 10.1161/01.STR.18.4.751
226. Marmarou A, A review of progress in understanding the pathophysiology and treatment of brain edema. *Neurosurg Focus.* (2007) 22:E1. doi: 10.3171/foc.2007.22.5.2
227. Ke C, Poon WS, Ng HK, Pang JC, Chan Y. Heterogeneous responses of aquaporin-4 in oedema formation in a replicated severe traumatic brain injury model in rats. *Neurosci Lett.* (2001) 301:21–4. doi: 10.1016/S0304-3940(01)01589-0
228. Kiening KL, van Landeghem FK, Schreiber S, Thomale UW, von Deimling A, Unterberg AW, et al. Decreased hemispheric Aquaporin-4 is linked to evolving brain edema following controlled cortical impact injury in rats. *Neurosci Lett.* (2002) 324:105–8. doi: 10.1016/S0304-3940(02)00180-5
229. Blixt J, Svensson M, Gunnarson E, Wanecek M. Aquaporins and blood-brain barrier permeability in early edema development after traumatic brain injury. *Brain Res.* (2015) 1611:18–28. doi: 10.1016/j.brainres.2015.03.004
230. Fukuda AM, Pop V, Spagnoli D, Ashwal S, Obenaus A, Badaut J. Delayed increase of astrocytic aquaporin 4 after juvenile traumatic brain injury: possible role in edema resolution? *Neuroscience.* (2012) 222:366–78. doi: 10.1016/j.neuroscience.2012.06.033
231. Taya K, Marmarou CR, Okuno K, Prieto R, Marmarou A. Effect of secondary insults upon aquaporin-4 water channels following experimental cortical contusion in rats. *J Neurotrauma.* (2010) 27:229–39. doi: 10.1089/neu.2009.0933
232. Zhang C, Chen J, Lu H. Expression of aquaporin-4 and pathological characteristics of brain injury in a rat model of traumatic brain injury. *Mol Med Rep.* (2015) 12:7351–7. doi: 10.3892/mmr.2015.4372
233. Chmelova M, Sucha P, Bochin M, Vorisek I, Pivonkova H, Hermanova Z, et al. The role of aquaporin-4 and transient receptor potential vaniloid isoform 4 channels in the development of cytotoxic edema and associated extracellular diffusion parameter changes. *Eur J Neurosci.* (2019) 50:1685–99. doi: 10.1111/ejn.14338
234. Yao X, Derugin N, Manley GT, Verkman AS. Reduced brain edema and infarct volume in aquaporin-4 deficient mice after transient focal cerebral ischemia. *Neurosci Lett.* (2015) 584:368–72. doi: 10.1016/j.neulet.2014.10.040
235. Liu X, Zhang W, Alkayed NJ, Froehner SC, Adams ME, Amiry-Moghaddam M, et al. Lack of sex-linked differences in cerebral edema and aquaporin-4 expression after experimental stroke. *J Cereb Blood Flow Metab.* (2008) 28:1898–906. doi: 10.1038/jcbfm.2008.83
236. Hirt L, Fukuda AM, Ambadipudi K, Rashid F, Binder D, Verkman A, et al. Improved long-term outcome after transient cerebral ischemia in aquaporin-4 knockout mice. *J Cereb Blood Flow Metab.* (2017) 37:277–90. doi: 10.1177/0271678X15623290
237. Akdemir G, Ratelade J, Asavapanumas N, Verkman AS. Neuroprotective effect of aquaporin-4 deficiency in a mouse model of severe global cerebral ischemia produced by transient 4-vessel occlusion. *Neurosci Lett.* (2014) 574:70–5. doi: 10.1016/j.neulet.2014.03.073
238. Katada R, Akdemir G, Asavapanumas N, Ratelade J, Zhang H, Verkman AS. Greatly improved survival and neuroprotection in aquaporin-4-knockout mice following global cerebral ischemia. *FASEB J.* (2014) 28:705–14. doi: 10.1096/fj.13-231274
239. Tang Y, Wu P, Su J, Xiang J, Cai D, Dong Q. Effects of Aquaporin-4 on edema formation following intracerebral hemorrhage. *Exp Neurol.* (2010) 223:485–95. doi: 10.1016/j.expneurol.2010.01.015
240. Chiu CD, Chen CC, Shen CC, Chin LT, Ma HI, Chuang HY, et al. Hyperglycemia exacerbates intracerebral hemorrhage via the downregulation of aquaporin-4: temporal assessment with magnetic resonance imaging. *Stroke.* (2013) 44:1682–9. doi: 10.1161/STROKEAHA.113.675983
241. Qiu GP, Xu J, Zhuo F, Sun SQ, Liu H, Yang M, et al. Loss of AQP4 polarized localization with loss of β-dystroglycan immunoreactivity may induce brain edema following intracerebral hemorrhage. *Neurosci Lett.* (2015) 588:42–8. doi: 10.1016/j.neulet.2014.12.053
242. Bloch O, Papadopoulos MC, Manley GT, Verkman AS. Aquaporin-4 gene deletion in mice increases focal edema associated with staphylococcal brain abscess. *J Neurochem.* (2005) 95:254–62. doi: 10.1111/j.1471-4159.2005.03362.x
243. Papadopoulos MC, Verkman AS. Aquaporin-4 gene disruption in mice reduces brain swelling and mortality in pneumococcal meningitis. *J Biol Chem.* (2005) 280:13906–12. doi: 10.1074/jbc.M413627200
244. Gao M, Lu W, Shu Y, Yang Z, Sun S, Xu J, et al. Poldip2 mediates blood-brain barrier disruption and cerebral edema by inducing AQP4 polarity loss in mouse bacterial meningitis model. *CNS Neurosci Ther.* (2020) 26:1288–302. doi: 10.1111/cns.13446
245. Huang J, Lu WT, Sun SQ, Yang ZB, Huang SQ, Gan SW, et al. Upregulation and lysosomal degradation of AQP4 in rat brains with bacterial meningitis. *Neurosci Lett.* (2014) 566:156–61. doi: 10.1016/j.neulet.2014.02.054
246. McCoy ES, Haas BR, Sontheimer H. Water permeability through aquaporin-4 is regulated by protein kinase C and becomes rate-limiting for glioma invasion. *Neuroscience.* (2010) 168:971–81. doi: 10.1016/j.neuroscience.2009.09.020
247. Osier ND, Dixon CE. The controlled cortical impact model: applications, considerations for researchers, future directions. *Front Neurol.* (2016) 7:134. doi: 10.3389/fneur.2016.00134

248. Fukuda AM, Adami A, Pop V, Bellone JA, Coats JS, Hartman RE, et al. Posttraumatic reduction of edema with aquaporin-4 RNA interference improves acute and chronic functional recovery. *J Cereb Blood Flow Metab.* (2013) 33:1621–32. doi: 10.1038/jcbfm.2013.118
249. Quintard H, Lorivel T, Gandin C, Lazdunski M, Heurteaux C. MLC901, a Traditional Chinese Medicine induces neuroprotective and neuroregenerative benefits after traumatic brain injury in rats. *Neuroscience.* (2014) 277:72–86. doi: 10.1016/j.neuroscience.2014.06.047
250. Tomura S, Nawashiro H, Otani N, Uozumi Y, Toyooka T, Ohsumi A, et al. Effect of decompressive craniectomy on aquaporin-4 expression after lateral fluid percussion injury in rats. *J Neurotrauma.* (2011) 28:237–43. doi: 10.1089/neu.2010.1443
251. Szczygielski J, Glameanu C, Müller A, Klotz M, Sippl C, Hubertus V, et al. Changes in posttraumatic brain edema in craniectomy-selective brain hypothermia model are associated with modulation of aquaporin-4 level. *Front Neurol.* (2018) 9:799. doi: 10.3389/fneur.2018.00799
252. Yao X, Uchida K, Papadopoulos MC, Zador Z, Manley GT, Verkman AS. Mildly reduced brain swelling and improved neurological outcome in aquaporin-4 knockout mice following controlled cortical impact brain injury. *J Neurotrauma.* (2015) 32:1458–64. doi: 10.1089/neu.2014.3675
253. Liang F, Luo C, Xu G, Su F, He X, Long S, et al. Deletion of aquaporin-4 is neuroprotective during the acute stage of micro traumatic brain injury in mice. *Neurosci Lett.* (2015) 598:29–35. doi: 10.1016/j.neulet.2015.05.006
254. Kitchen P, Salman MM, Abir-Awan M, Al-Jubair T, Törnroth-Horsefield S, Conner AC, et al. Calcein fluorescence quenching to measure plasma membrane water flux in live mammalian cells. *STAR Protoc.* (2020) 1:100157. doi: 10.1016/j.xpro.2020.100157
255. Verkman AS, Anderson MO, Papadopoulos MC. Aquaporins: important but elusive drug targets. *Nat Rev Drug Discov.* (2014) 13:259–77. doi: 10.1038/nrd4226
256. Abir-Awan M, Kitchen P, Salman MM, Conner MT, Conner AC, Bill RM. Inhibitors of mammalian aquaporin water channels. *Int J Mol Sci.* (2019) 20: doi: 10.3390/ijms20071589
257. Blixt J, Gunnarson E, Wanecek M. Erythropoietin attenuates the brain edema response after experimental traumatic brain injury. *J Neurotrauma.* (2018) 35:671–80. doi: 10.1089/neu.2017.5015
258. M. Rizwan Siddiqui, Attar F, Mohanty V, Kim KS, Shekhar Mayanil C, Tomita T. Erythropoietin-mediated activation of aquaporin-4 channel for the treatment of experimental hydrocephalus. *Childs Nerv Syst.* (2018) 34:2195–2202. doi: 10.1007/s00381-018-3865-z
259. Wang R, Wu X, Zhao H, Min L, Tao Z, Ji X, et al. Effects of erythropoietin combined with tissue plasminogen activator on the rats following cerebral ischemia and reperfusion. *Brain Circ.* (2016) 2:54–60. doi: 10.4103/2394-8108.178552
260. Zhang M, Cui Z, Cui H, Cao Y, Zhong C, Wang Y. Astaxanthin alleviates cerebral edema by modulating NKCC1 and AQP4 expression after traumatic brain injury in mice. *BMC Neurosci.* (2016) 17:60. doi: 10.1186/s12868-016-0295-2
261. Liu L, Kelly MG, Wierzbicki EL, Escober-Nario IC, Vollmer MK, Doré S. Nrf2 plays an essential role in long-term brain damage and neuroprotection of korean red ginseng in a permanent cerebral ischemia model. *Antioxidants.* (2019) 8:8080273. doi: 10.3390/antiox8080273
262. Liu YL, Xu ZM, Yang GY, Yang DX, Ding J, Chen H, et al. Sesamin alleviates blood-brain barrier disruption in mice with experimental traumatic brain injury. *Acta Pharmacol Sin.* (2017) 38:1445–55. doi: 10.1038/aps.2017.103
263. Wang X, An F, Wang S, An Z, Wang S. Orientin attenuates cerebral ischemia/reperfusion injury in rat model through the AQP-4 and TLR4/NF-κB/TNF-α signaling pathway. *J Stroke Cerebrovasc Dis.* (2017) 26:2199–2214. doi: 10.1016/j.jstrokecerebrovasdis.2017.05.002
264. Xu LX, Lv Y, Li YH, Ding X, Wang Y, Han X, et al. Melatonin alleviates brain and peripheral tissue edema in a neonatal rat model of hypoxic-ischemic brain damage: the involvement of edema related proteins. *BMC Pediatr.* (2017) 17:90. doi: 10.1186/s12887-017-0824-x
265. Arima H, Yamamoto N, Sobue K, Umenishi F, Tada T, Katsuya H, et al. Hyperosmolar mannitol simulates expression of aquaporins 4 and 9 through a p38 mitogen-activated protein kinase-dependent pathway in rat astrocytes. *J Biol Chem.* (2003) 278:44525–34. doi: 10.1074/jbc.M304368200
266. Jiang W, Cao WJ, Zhang YK, Wei XY, Kuang F. Bolus injection of hypertonic solutions for cerebral edema in rats: challenge of homeostasis of healthy brain. *Neurosci Lett.* (2012) 509:44–9. doi: 10.1016/j.neulet.2011.12.045
267. Szczygielski J, Hubertus V, Kruchten E, Müller A, Albrecht LF, Mautes AE, et al. Brain edema formation and functional outcome after surgical decompression in murine closed head injury are modulated by acetazolamide administration. *Front Neurol.* (2019) 10:273. doi: 10.3389/fneur.2019.00273
268. Hao JQ, He XY, Yang X, Xiao YC, Duan SQ, Wang H, et al. Acetazolamide alleviate cerebral edema induced by ischemic stroke through inhibiting the expression of AQP4 mRNA. *Neurocrit Care.* (2021) doi: 10.1007/s12028-021-01261-w
269. Glober NK, Sprague S, Ahmad S, Mayfield KG, Fletcher LM, Digicaylioglu MH, et al. Acetazolamide treatment prevents redistribution of astrocyte aquaporin 4 after murine traumatic brain injury. *Neurosci J.* (2019) 2019:2831501. doi: 10.1155/2019/2831501
270. Jin H, Li W, Dong C, Ma L, Wu J, Zhao W. Effects of different doses of levetiracetam on aquaporin 4 expression in rats with brain edema following fluid percussion injury. *Med Sci Monit.* (2016) 22:678–86. doi: 10.12659/MSM.897201
271. Sylvain NJ, Salman MM, Pushie MJ, Hou H, Meher V, Herlo R, et al. The effects of trifluoperazine on brain edema, aquaporin-4 expression and metabolic markers during the acute phase of stroke using photothrombotic mouse model. *Biochim Biophys Acta Biomembr.* (2021) 1863:183573. doi: 10.1016/j.bbamem.2021.183573
272. Kuroda S, Nakai A, Kristían T, Siesjö BK. The calmodulin antagonist trifluoperazine in transient focal brain ischemia in rats. Anti-ischemic effect and therapeutic window. *Stroke.* (1997) 28:2539–44. doi: 10.1161/01.STR.28.12.2539
273. Huber VJ, Tsujita M, Yamazaki M, Sakimura K, Nakada T. Identification of arylsulfonamides as Aquaporin 4 inhibitors. *Bioorg Med Chem Lett.* (2007) 17:1270–3. doi: 10.1016/j.bmcl.2006.12.010
274. Salman MM, Kitchen P, Iliff JJ, Bill RM. Aquaporin 4 and glymphatic flow have central roles in brain fluid homeostasis. *Nat Rev Neurosci.* (2021) 22:650–1. doi: 10.1038/s41583-021-00514-z
275. MacAulay N, Reply to 'Aquaporin 4 and glymphatic flow have central roles in brain fluid homeostasis'. *Nat Rev Neurosci.* (2021) 22:651–2. doi: 10.1038/s41583-021-00515-y
276. Igarashi H, Huber VJ, Tsujita M, Nakada T. Pretreatment with a novel aquaporin 4 inhibitor, TGN-020, significantly reduces ischemic cerebral edema. *Neurol Sci.* (2011) 32:113–6. doi: 10.1007/s10072-010-0431-1
277. Toft-Bertelsen TL, Larsen BR, Christensen SK, Khandelia H, Waagepetersen HS, MacAulay N. Clearance of activity-evoked K(+) transients and associated glia cell swelling occur independently of AQP4: a study with an isoform-selective AQP4 inhibitor. *Glia.* (2021) 69:28–41. doi: 10.1002/glia.23851
278. Nakhoul NL, Davis BA, Romero MF, Boron WF. Effect of expressing the water channel aquaporin-1 on the CO2 permeability of Xenopus oocytes. *Am J Physiol.* (1998) 274:C543–8. doi: 10.1152/ajpcell.1998.274.2.C543
279. Huber VJ, Tsujita M, Kwee IL, Nakada T. Inhibition of aquaporin 4 by antiepileptic drugs. *Bioorg Med Chem.* (2009) 17:418–24. doi: 10.1016/j.bmc.2007.12.038
280. Jha RM, Kochanek PM, Simard JM. Pathophysiology and treatment of cerebral edema in traumatic brain injury. *Neuropharmacology.* (2019) 145:230–46. doi: 10.1016/j.neuropharm.2018.08.004
281. Papadopoulos MC, Bennett JL, Verkman AS. Treatment of neuromyelitis optica: state-of-the-art and emerging therapies. *Nat Rev Neurol.* (2014) 10:493–506. doi: 10.1038/nrneurol.2014.141
282. Tradtrantip L, Zhang H, Saadoun S, Phuan P-W, Lam C, Papadopoulos MC, et al. Anti-Aquaporin-4 monoclonal antibody blocker therapy for neuromyelitis optica. *Ann Neurol.* (2012) 71:314–22. doi: 10.1002/ana.22657
283. Huang P, Takai Y, Kusano-Arai O, Ramadhanti J, Iwanari H, Miyauchi T, et al. The binding property of a monoclonal antibody against the extracellular domains of aquaporin-4 directs aquaporin-4 toward endocytosis. *Biochem Biophys Rep.* (2016) 7:77–83. doi: 10.1016/j.bbrep.2016.05.017
284. Guan Y, Li L, Chen J, Lu H. Effect of AQP4-RNAi in treating traumatic brain edema: Multi-modal MRI and histopathological changes of early stage edema in a rat model. *Exp Ther Med.* (2020) 19:2029–36. doi: 10.3892/etm.2020.8456

285. Lu H, Zhan Y, Ai L, Chen H, Chen J. AQP4-siRNA alleviates traumatic brain edema by altering post-traumatic AQP4 polarity reversal in TBI rats. *J Clin Neurosci.* (2020) 81:113–9. doi: 10.1016/j.jocn.2020.09.015
286. Fujita Y, Yamamoto N, Sobue K, Inagaki M, Ito H, Arima H, et al. Effect of mild hypothermia on the expression of aquaporin family in cultured rat astrocytes under hypoxic condition. *Neurosci Res.* (2003) 47:437–44. doi: 10.1016/j.neures.2003.08.006
287. Kurisu K, Abumiya T, Nakamura H, Shimbo D, Shichinohe H, Nakayama N, et al. Transarterial regional brain hypothermia inhibits acute aquaporin-4 surge and sequential microvascular events in ischemia/reperfusion injury. *Neurosurgery.* (2016) 79:125–34. doi: 10.1227/NEU.0000000000001088
288. Gao D, Ding F, Lei G, Luan G, Zhang S, Li K, et al. Effects of focal mild hypothermia on thrombin-induced brain edema formation and the expression of protease activated receptor-1, matrix metalloproteinase-9 and aquaporin 4 in rats. *Mol Med Rep.* (2015) 11:3009–14. doi: 10.3892/mmr.2014.3111
289. Duan Y, Wu D, Huber M, Shi J, An H, Wei W, et al. New endovascular approach for hypothermia with intrajugular cooling and neuroprotective effect in ischemic stroke. *Stroke.* (2020) 51:628–36. doi: 10.1161/STROKEAHA.119.026523
290. Dietrich WD, Bramlett HM. Therapeutic hypothermia and targeted temperature management for traumatic brain injury: experimental and clinical experience. *Brain Circ.* (2017) 3:186–98. doi: 10.4103/bc.bc_28_17
291. Hirst TC, Klasen MG, Rhodes JK, Macleod MR, Andrews PJD. A systematic review and meta-analysis of hypothermia in experimental traumatic brain injury: why have promising animal studies not been replicated in pragmatic clinical trials? *J Neurotrauma.* (2020) 37:2057–68. doi: 10.1089/neu.2019.6923

Conflict of Interest: JO is a consultant to the Karl Storz Company and receives grants from the Erbe Company. These companies were not involved in the design and workflow during the preparation of the present review.

The remaining authors declare that the research was conducted in the absence of any commercial or financial relationships that could be construed as a potential conflict of interest.

Publisher's Note: All claims expressed in this article are solely those of the authors and do not necessarily represent those of their affiliated organizations, or those of the publisher, the editors and the reviewers. Any product that may be evaluated in this article, or claim that may be made by its manufacturer, is not guaranteed or endorsed by the publisher.

frontiers in Neurology

ORIGINAL RESEARCH
published: 20 December 2021
doi: 10.3389/fneur.2021.735469

The Use of Different Components of Brain Oxygenation for the Assessment of Cerebral Haemodynamics: A Prospective Observational Study on COVID-19 Patients

Chiara Robba[1,2], Danilo Cardim[3], Lorenzo Ball[1,2], Denise Battaglini[2,4], Wojciech Dabrowski[5], Matteo Bassetti[6,7], Daniele Roberto Giacobbe[6,7], Marek Czosnyka[8], Rafael Badenes[9], Paolo Pelosi[1,2], Basil Matta[10] and the GeCovid group*

[1] Department of Surgical Sciences and Integrated Diagnostics (DISC), University of Genoa, Genoa, Italy, [2] San Martino Policlinico Hospital, IRCCS for Oncology and Neuroscience, Genoa, Italy, [3] Department of Neurology, University of Texas Southwestern Medical Center, Dallas, TX, United States, [4] Department of Medicine, University of Barcelona, Barcelona, Spain, [5] Department of Anesthesiology and Intensive Care, Medical University of Lublin, Lublin, Poland, [6] Department of Health Sciences (DISSAL), University of Genoa, Genoa, Italy, [7] Infectious Diseases Unit, Ospedale Policlinico San Martino, IRCCS for Oncology and Neuroscience, Genoa, Italy, [8] Brain Physics Laboratory, Department of Clinical Neurosciences, Neurosurgery Unit, Addenbrooke's Hospital, Cambridge, United Kingdom, [9] Department of Anesthesia and Intensive Care, Hospital Clinic Universitari, INCLIVA Research Health Institute, University of Valencia, Valencia, Spain, [10] Neurocritical Care Unit, Addenbrooke's Hospital, Cambridge, United Kingdom

Introduction: The role of near-infrared spectroscopy (NIRS) for the evaluation of cerebral haemodynamics is gaining increasing popularity because of its noninvasive nature. The aim of this study was to evaluate the role of the integral components of regional cerebral oxygenation (rSO_2) measured by NIRS [i.e., arterial-oxyhemoglobin (O_2Hbi) and venous-deoxyhemoglobin (HHbi)-components], as indirect surrogates of cerebral blood flow (CBF) in a cohort of critically ill patients with coronavirus disease 2019 (COVID-19). We compared these findings to the gold standard technique for noninvasive CBF assessment, Transcranial Doppler (TCD).

Methods: Mechanically ventilated patients with COVID-19 admitted to the Intensive Care Unit (ICU) of Policlinico San Martino Hospital, Genova, Italy, who underwent multimodal neuromonitoring (including NIRS and TCD), were included. rSO_2 and its components [relative changes in O_2Hbi, HHbi, and total haemoglobin (cHbi)] were compared with TCD (cerebral blood flow velocity, CBFV). Changes (Δ) in CBFV and rSO_2, ΔO_2Hbi, ΔHHbi, and ΔcHbi after systemic arterial blood pressure (MAP) modifications induced by different manoeuvres (e.g., rescue therapies and haemodynamic manipulation) were assessed using mixed-effect linear regression analysis and repeated measures correlation coefficients. All values were normalised as percentage changes from the baseline (Δ%).

Results: One hundred and four measurements from 25 patients were included. Significant effects of Δ%MAP on Δ%CBF were observed after rescue manoeuvres for

OPEN ACCESS

Edited by:
Vijay Sharma, National University of Singapore, Singapore

Reviewed by:
Shinji Nakamura, Kagawa University, Japan
Yu Shang, North University of China, China
Anirban Dutta, University at Buffalo, United States
Ajay Rajaram, Boston Children's Hospital and Harvard Medical School, United States

***Correspondence:**
Rafael Badenes
rafaelbadenes@gmail.com

Specialty section:
This article was submitted to Neurocritical and Neurohospitalist Care, a section of the journal Frontiers in Neurology

Received: *02 July 2021*
Accepted: *29 October 2021*
Published: *20 December 2021*

Citation:
Robba C, Cardim D, Ball L, Battaglini D, Dabrowski W, Bassetti M, Giacobbe DR, Czosnyka M, Badenes R, Pelosi P, Matta B and the GeCovid group (2021) The Use of Different Components of Brain Oxygenation for the Assessment of Cerebral Haemodynamics: A Prospective Observational Study on COVID-19 Patients. Front. Neurol. 12:735469. doi: 10.3389/fneur.2021.735469

CBFV, ΔcHbi, and ΔO_2Hbi. The highest correlation was found between ΔCBFV and $\Delta\Delta O_2$Hbi ($R = 0.88$, $p < 0.0001$), and the poorest between ΔCBFV and ΔΔHHbi ($R = 0.34$, $p = 0.002$).

Conclusions: ΔO_2Hbi had the highest accuracy to assess CBF changes, reflecting its role as the main component for vasomotor response after changes in MAP. The use of indexes derived from the different components of rSO_2 can be useful for the bedside evaluation of cerebral haemodynamics in mechanically ventilated patients with COVID-19.

Keywords: cerebral oxygenation, brain injury, autoregulation dysfunction, intensive care, NIRS (near infrared reflectance spectroscopy)

INTRODUCTION

Several neuromonitoring tools have been adopted as surrogate or indirect measures of cerebral blood flow (CBF) (1–3). Among these, transcranial Doppler (TCD)-derived cerebral blood flow velocity (CBFV) has been largely applied, being currently the most used technique for the evaluation of bedside cerebral haemodynamics (4), and is considered as the gold standard for noninvasive assessments of static cerebral autoregulation (CA) (3).

Near-infrared spectroscopy (NIRS) represents a promising but not highly utilised technique in critical care. NIRS measures the relative proportion of oxy (O_2Hbi)- and -deoxy(HHbi) haemoglobin based on the transmission and absorption of near-infrared light as it passes through biological tissues (5, 6). For instance, NIRS enables the continuous non-invasive evaluation of cerebral oxygenation (6), which could potentially be used as a surrogate of CBF. A major concern of NIRS is the undesired contamination of extracranial blood and the intracranial venous blood (7, 8). However, recent improvement in technology has led to the availability of tools, which can measure not only the total rSO_2 but also discriminate its different components, e.g., the arterial and venous compartments of cerebral circulation. This could potentially lead to a more detailed evaluation of CBF with NIRS, focusing on the role of different intracerebral components in the vasomotor response, and to assess the effect of mean arterial blood pressure (MAP) changes, specifically considering the arterial component of rSO_2, thus minimising any confounding factors from the venous compartment. Such assessments can be relevant in acute critical care patients, especially those in risk of developing neurological complications due to non-traumatic brain injuries. In the temporal context of the present work, the severe acute respiratory syndrome coronavirus 2 (SARS-CoV-2) pandemic has led to insurmountable clinical challenges regarding the assessment of such potential, unknown neurological complications that could become another major burden to coronavirus disease 2019 (COVID-19) survivors.

Therefore, the aim of this study was to assess the role of rSO_2 and its different components as surrogates of CBF in a cohort of mechanically ventilated critically ill patients with COVID-19 undergoing different rescue therapies and haemodynamic manipulations yielding MAP changes. The primary objective was to assess the correlation of the different components of rSO_2 with the gold standard CBFV. The secondary aim was to investigate which component of rSO_2 is the best predictor of CBF in response to haemodynamic changes. We hypothesised that the arterial component of rSO_2 is better correlated with CBFV and should better reflect MAP changes than its venous component, or total rSO_2, after systemic blood pressure changes.

METHODS

We adhered to the "Strengthening the Reporting of Observational Studies in Epidemiology (STROBE)" statement guidelines for observational cohort studies (**Supplementary Material 1**) (9).

This single centre prospective, observational study was performed at Policlinico San Martino Hospital, IRCCS for Oncology and Neuroscience, Genoa, Italy, from October 1, to December 15, 2020, and the protocol was approved by the local ethical review board (Comitato Etico Regione Liguria, protocol n. CER Liguria: 23/2020). Written consent was obtained from the next of kin, as the patients were unconscious at the time of inclusion.

Adult mechanically ventilated patients admitted to ICU [previously included in two studies (10, 11) from our group]; with a confirmed SARS-CoV-2 polymerase chain reaction test using nasopharyngeal swab or bronchoalveolar lavage; requiring any type of manoeuvre clinically indicated to optimise respiratory and haemodynamic functions with an effect on ABP; and who contemporarily underwent multimodal neuromonitoring (NIRS and TCD) were included.

These manoeuvres comprised ventilatory rescue therapies (such as recruitment manoeuvres, prone positioning, etc.) or haemodynamic strategies (such as passive leg raising test, fluid challenges, and norepinephrine administration) as previously described (10, 11). Despite different indications and types of manoeuvres, they all had in common to produce an effect on systemic haemodynamics and MAP, which could affect cerebral hemodynamics.

Exclusion criteria were patients negative for SARS-CoV-2 infection; patients who did not undergo any intervention with a haemodynamic effect, or who did not receive multimodal neuromonitoring (TCD and NIRS) or with known neurological

conditions before or during ICU admission, which might have impaired cerebral haemodynamics *a priori* (stroke, trauma, intracerebral masses, etc.).

Patient Management and Data Collection

A combination of propofol, midazolam, and fentanyl was used to maintain sedation. The patients were mechanically ventilated using pressure-controlled ventilation, using a tidal volume (V_T) of 4–8 ml/kg of predicted body weight, aiming to achieve plateau pressure (Pplat) < 28 cmH_20; inspired fraction of oxygen (FiO_2) and positive end expiratory pressure (PEEP) were titrated to achieve peripheral saturation of oxygen (SpO_2) = 88–92%, and the respiratory rate was set to maintain arterial partial pressure of carbon dioxide ($PaCO_2$) = 35–45 mmHg. Indications and methods for each one of the strategies considered for the analyses have been previously presented in detail (10).

Data were reviewed and collected by physicians trained in critical care (10). Data collection included baseline characteristics, demographics, clinical data at ICU admission, laboratory and ventilatory parameters (i.e., V_T, FiO_2, PEEP), as well as haemodynamic and neuromonitoring data before (T0) and after (T1) the application of any type of manoeuvre. In brief, T1 measurements were taken after 5 min after recruitment manoeuvres and prone positioning, 5 min after the beginning of norepinephrine administration and fluid challenges administration, and immediately after passive leg raising test (10, 11). These procedures are standardised in our institution and, therefore, were expected to obtain a similar haemodynamic effect.

The decision to start any type of manoeuvre was related to the assessment and judgement of the clinician. Details on the different manoeuvres have been previously described (10, 11).

Neuromonitoring

Cerebral Oxygenation

We used the Masimo Root monitor® (Irvine, CA, USA) for the measurement of rSO_2, applying bilateral sensors to the frontotemporal area of the patients. Final values of rSO_2 and its components at T0 and T1 were calculated as the mean between single instant measurements obtained from the right and left frontotemporal sensors.

The parameters obtained included:

- rSO_2, which represents the total regional cerebral oxygen saturation;
- ΔO_2Hbi, which represents the change in the oxyhemoglobin component of the rSO_2 calculation, i.e., changes in the cerebral arterial compartment;
- ΔHHbi, which represents the change in the deoxyhemoglobin component of the rSO_2 calculation, i.e., changes in the cerebral venous compartment;
- ΔcHbi, the sum of the values of ΔO_2Hbi e ΔHHbi.

Transcranial Doppler

A low frequency (2 MHz) echographic micro convex probe was employed to investigate intracranial vessels. The temporal window was privileged for the passage of Doppler signals for middle cerebral artery (MCA) insonation. Single instant measurements of mean cerebral blood flow velocities (CBFV) were obtained bilaterally from the MCA at T0 and T1. Cerebrovascular resistance (CVRi - pressure gradient/flow) and conductance (CVCi - flow/pressure gradient) indices of vasoconstriction and vasodilation were also calculated at each time point.

Statistical Analysis

The Shapiro–Wilk test was used to test the normality of the distribution of the results. Data are reported as the median and interquartile range [IQR = 25th−75th percentiles]. Comparisons between different variables at T0 and T1 were performed by the Wilcoxon-signed rank test.

Dependent variables were expressed as a change from the baseline (T0) in both absolute (Δ change) and relative terms (Δ% change). Changes in CBFV, NIRS parameters, CVCi, and CVRi (both derived from the ratio of mean CBFV/NIRS parameters and MAP) from the baseline were used to show changes for these dependent variables across the range of MAP in response to the rescue manoeuvres.

The correlations coefficients [95% confidence interval (CI)] between CBFV and the different NIRS variables were verified using the Bland and Altman method for repeated measurements (12, 13).

To provide prediction models for the relationship between CBFV and NIRS parameters with the observed changes in MAP, the relationships between Δ% CBFV and the Δ% NIRS parameters (rSO_2, ΔO_2Hbi, ΔHHbi, and ΔcHbi) with Δ% MAP were expressed as linear mixed effects models [*R* Software's package *lme4* (14)]. As fixed effects, we entered Δ% CBFV or Δ% NIRS parameters and Δ% MAP into each respective model. As random effects, we had intercepts and slopes for the repeated measurement points for each patient ($N = 104$ measurements).

All statistical analyses were performed using RStudio software (version 4.0.3). A $p < 0.05$ was considered statistically significant.

RESULTS

One hundred and four measurements from 25 patients were analyzed. The patients had a range of three to six manoeuvres performed (mean ± SD: 4.16 ± 0.88). The characteristics of the patients are presented in **Supplementary Table S1**. The median age was 62 [57–69], and 80% were male. Fifteen patients (60%) died in ICU, and five (20%) patients were diagnosed with delirium. Non-survivors had smaller changes in CBFV and O_2Hbi compared to survivors (−5 vs. 2 cm/s, $p < 0.001$, and −1.5 vs. 0.25-μM cm, $p = 0.02$, respectively).

Main variables at T0 and T1 are described in **Table 1**. At T1, compared to T0, MAP significantly increased by 6.0 (−1.25–8.25) mmHg ($p < 0.0001$); CBFV significantly decreased by −4.0 [−7–(−2)] cm/s ($p = 0.03$); ΔO_2Hbi decreased by −1.3 (−1.9-0.3) (μM.cm) ($p < 0.001$); ΔHHbi significantly increased by 0.9 (0.1–1.3) (μM.cm) ($p < 0.0001$). $PaCO_2$ decreased by −1.0 [−5.25–3.0] mmHg, although not statistically significant

TABLE 1 | Systemic and brain haemodynamics haemodynamics and oxygenation at baseline (T0) and post-event (T1). Data are presented as median (IQR).

	MAP (mmHg)	CBFV (cm/sec)	rSO_2 (%)	ΔcHbi	ΔO_2Hbi	ΔHHbi	$PaCO_2$ (mmHg)	SpO_2 (%)
T0	65.0 (61.0–71.0)	56.0 (50.0–59.2)	53.0 (51.7–58.0)	4.7 (3.2–6.3)	3.5 (2.8–4.4)	1.1 (0.4–1.9)	51.0 (46.0–66.2)	86.5 (61.0–89.0)
T1	69.5 (66.0–73.2)	53.0 (46.0–58.2)	57.0 (53.0–59.0)	4.8 (3.3–7.0)	2.7 (1.6–4.2)	1.9 (1.3–2.8)	48.0 (45.0–56.0)	91.0 (89.0–92.0)
Δ changes	**6.0 (−1.2–8.2)**	**−4.0 (−7–(−2))**	2.0 (−3.2–5.2)	−0.2 (−1.7–1.3)	**−1.3 (−1.9–0.3)**	**0.9 (0.1–1.3)**	−1.0 (−5.2–3.0)	**6.0 (0.0–29.2)**

CBFV, cerebral blood flow velocity (cm/s); ΔcHbi, sum of ΔO_2Hbi and ΔHHbi components of the regional tissue oxygen saturation (μM.cm); ΔO_2Hbi, index representing the change in the oxyhemoglobin of the regional tissue oxygen saturation (μM.cm); ΔHHbi, index representing the change in the deoxyhemoglobin of the regional tissue oxygen saturation (μM.cm); rSO_2, regional tissue oxygen saturation (%); MAP, mean arterial blood pressure (mm Hg); $PaCO_2$, partial pressure of CO_2 (mm Hg); SpO_2, systemic oxygen saturation (%). Bold values indicate statistical significance ($p < 0.05$).

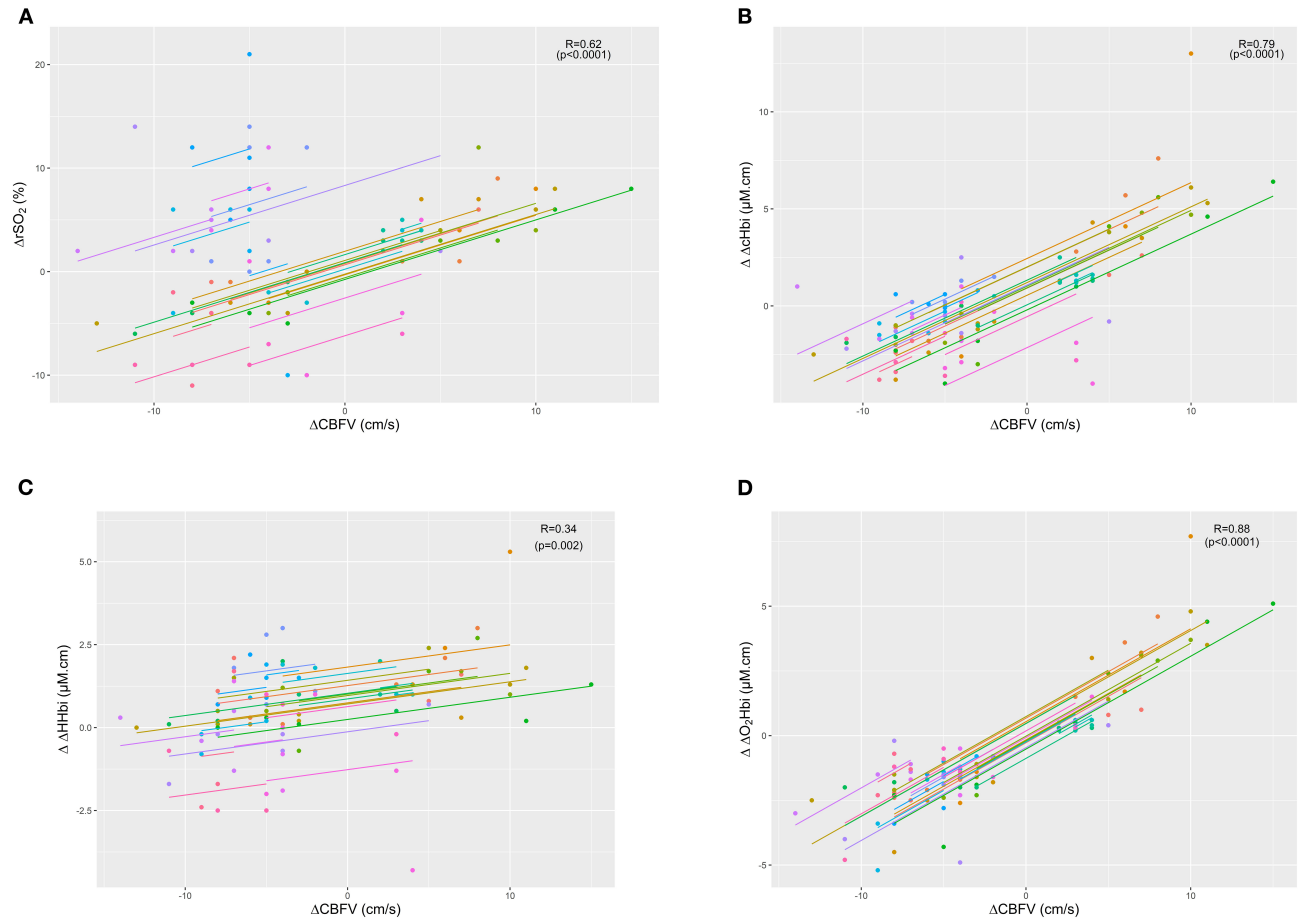

FIGURE 1 | Scatter plots showing the linear association and correlation (R) between changes in cerebral blood flow velocity (ΔCBFV) vs. total cerebral oxygenation (ΔrSO_2 - plot A) **(A)**, sum of arterial and venous components of cerebral oxygenation (Δ ΔcHbi - plot B) **(B)**, venous component (ΔΔHHbi - plot C) **(C)**, and arterial component (Δ ΔO_2Hbi - plot D) **(D)**. Repeated measurements for each patient are plotted in the same colour pattern. Linear regression lines are correspondent to repeated measurements within patients.

($p = 0.06$). SpO_2 significantly increased by 6.0 (−0.0–29.2) % ($p < 0.0001$).

ΔCBFV, the gold standard for CBF assessment, showed the highest correlation with the arterial component of cerebral oxygenation (ΔO_2Hbi; R = 0.88 (0.81–0.92), $p < 0.0001$), followed by ΔcHbi and ΔrSO_2 values (R = 0.79 (0.68–0.86), $p < 0.0001$ and R = 0.62 (0.46–0.74), $p < 0.0001$) (**Figure 1**). The lowest correlation was found for ΔHHbi [R = 0.34 (0.13–0.52), $p = 0.002$]. **Table 2** shows the correlation coefficients of cerebrovascular resistance index (CVRi) and cerebrovascular conductance index (CVCi) for CBFV and NIRS parameters. Consistently, NIRS parameters of CVCi, not CVRi, were better correlated with CBFV.

Individual data of CBF responses to changes in MAP from T0 to T1 and linear mixed-effects models marginal mean values of CBF are presented in **Figure 2**. Model parameters

TABLE 2 | Correlation of cerebrovascular resistance index (CVRi) and cerebrovascular conductance index (CVCi) for cerebral blood flow velocity (CBFV) and NIRS parameters.

	$\Delta CVRi_{CBFV}$	*p*–value		$\Delta CVCi_{CBFV}$	*p*–value
$\Delta CVRi_{rSO2}$	0.99 (0.99–0.99)	**<0.0001**	**$\Delta CVCi_{rSO2}$**	0.8 (0.71–0.81)	**<0.0001**
$\Delta CVRi_{\Delta}$cHbi	0.17 (−0.05–0.38)	0.12	**$\Delta CVCi_{\Delta}$cHbi**	0.62 (0.47–0.74)	**<0.0001**
$\Delta CVRi_{\Delta}$O2Hbi	0.28 (0.06–0.47)	**0.01**	**$\Delta CVCi_{\Delta}$O2Hbi**	0.71 (0.58–0.80)	**<0.0001**
$\Delta CVRi_{\Delta}$HHbi	0.01 (−0.22–0.23)	0.95	**$\Delta CVCi_{\Delta}$HHbi**	0.32 (0.11–0.51)	**0.004**

CBFV, cerebral blood flow velocity; CI, confidence interval; ΔcHbi, sum of ΔO_2Hbi and ΔHHbi components of the regional tissue oxygen saturation; ΔO_2Hbi, index representing the change in the oxyhemoglobin of the regional tissue oxygen saturation; ΔHHbi, index representing the change in the deoxyhemoglobin of the regional tissue oxygen saturation; rSO_2, regional cerebal oxygenation.

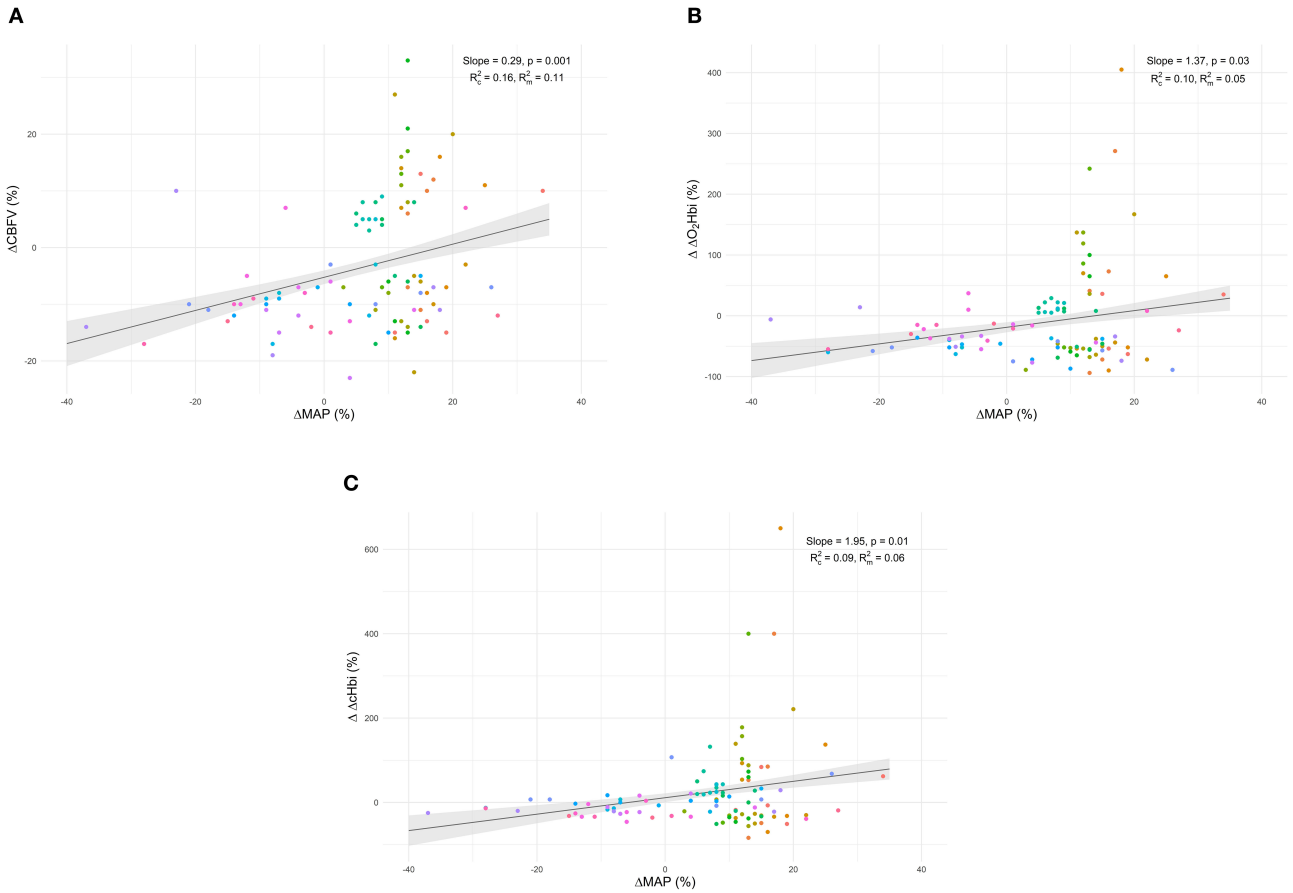

FIGURE 2 | Individual data of cerebral blood flow relative response changes to MAP from T0 to T1 and linear mixed-effects models marginal mean values of CBF for cerebral blood flow velocity (ΔCBFV–plot A) **(A)**, the arterial component of cerebral oxygenation (ΔO_2Hbi–plot B) **(B)**, and arterial plus venous components (ΔcHbi–plot C) **(C)**.

for the fixed effects of the Δ% CBF to Δ% MAP models are presented in **Table 3**. Significant effects of Δ% MAP on Δ% CBF from T0 to T1 were observed for CBFV (p = 0.001) and for ΔcHbi and ΔO_2Hbi (p = 0.01 and 0.03, respectively) (**Figures 2A–C**, **Table 3**), but not for ΔHHbi and rSO_2. Inclusion of $PaCO_2$ as a covariate did not improve any of the models fits. Boxplot panels showing the delta difference (T1-T0) for each patient concerning the different parameters analysed are shown in ESM **Supplementary Figure S1**. A representative patient, showing the individual trajectories of the different parameters across the measurement points, is shown in ESM **Supplementary Figure S2**.

DISCUSSION

In a cohort of mechanically ventilated patients with COVID-19 undergoing different rescue therapies and haemodynamic manipulations, we found that: (1) ΔO_2Hbi was better correlated

TABLE 3 | Linear mixed–model estimates of fixed effects of CBF responses to changes in MAP.

	Models	Parameter	Estimate	Std. Error	p value	95% Confidence Interval	
						Lower bound	Upper bound
Δ% CBFV	Model 1	β_0 *Intercept*	−5.24	1.19	**<0.001**	−7.76	−2.68
		β_1 Δ% *MAP*	0.29	0.08	**0.001**	0.11	0.50
	AIC	800.2					
	R^2_m	0.11					
	R^2_c	0.16					
Δ% ΔcHbi	Model 2	β_0 *Intercept*	0.11	0.10	0.28	−0.10	0.32
		β_1 Δ% *MAP*	1.95	0.77	**0.01**	0.42	3.58
	AIC	296.8					
	R^2_m	0.06					
	R^2_c	0.09					
Δ% ΔO_2Hbi	Model 3	β_0 *Intercept*	−0.19	0.08	**0.02**	−0.36	−0.02
		β_1 Δ% *MAP*	1.37	0.62	**0.03**	0.12	2.80
	AIC	247.3					
	R^2_m	0.05					
	R^2_c	0.10					

AIC, Akaike information criterion; CBFV, cerebral blood flow velocity; ΔcHbi, sum of ΔO_2Hbi and ΔHHbi components of the regional tissue oxygen saturation; ΔO_2Hbi, index representing the change in the oxyhemoglobin of the regional tissue oxygen saturation. R^2_m: marginal coefficient of determination of the model, describing the proportion of variance explained by the fixed effects. R^2_c: conditional coefficient of determination of the model, describing the proportion of variance explained by both the fixed and random effects.

with ΔCBFV than ΔHHbi and other components of cerebral oxygenation. ΔHHbi showed the poorest correlation with ΔCBFV; (2) CVCi indices derived from NIRS parameters, especially rSO_2, correlated consistently better with CBFV than CVRi; (3) changes in MAP led to cerebral vasoreactive responses, which could be detected using the arterial component of rSO_2, but not total rSO_2 or its venous component. Our data suggest that, as the arterial compartment is responsible for the major changes in cerebrovascular tone following arterial blood pressure changes, the ΔO_2Hbi component of NIRS can more specifically describe these variations.

To our knowledge, this is the first study evaluating the role of NIRS in response to secondary changes in systemic haemodynamics in mechanically ventilated patients with COVID-19. Compared to our previous work (11), where CA was measured with TCD, we aimed to use for the first time NIRS and its components for the assessment of CBF changes, comparing it with TCD, the gold standard for noninvasive cerebral haemodynamics assessment. The novelty of this study relies on the use and comparison of the different components of rSO_2 to assess CBF, which is allowed by the Masimo® device. We believe that this is important, as there is a knowledge gap concerning the comparison of specific components of the NIRS signal with CBFV.

Although NIRS has been previously used as surrogate of cerebral blood flow in the dynamic measurement of autoregulation (15, 16), its use is importantly limited by the fact that it takes into account both arterial and venous cerebral compartments, which do not take part in the same way for CBF regulation. Moreover, it has been mainly used in the paediatric population (15, 16), and data on patients with COVID-19 are lacking.

Although this is just a preliminary study, our results suggest that using only the arterial component of rSO_2 could improve the accuracy in estimating CBF changes, eliminating the venous contamination (17). Furthermore, NIRS can provide reliable, practical, and quick assessments of cerebral haemodynamics in the challenging setting of critical care in the patients with COVID-19 with acute respiratory syndrome, in whom the development of neurological complications are common (18).

Several studies have highlighted the importance of the evaluation of cerebral haemodynamics and CA in the management of patients who are brain injured and patients who are non-brain injured (3–5). At present, no randomised controlled trials exploring the effect on the outcome of a therapeutic approach based on CA are available (19, 20); however, experts agree that the maintenance of the homeostasis of autoregulatory status of patients should be kept in consideration when managing patients who are brain injured, as impaired CBF dynamics can lead to secondary cerebral insult (6, 19).

The Brain Trauma Foundation Guidelines only suggest to maintain a cerebral perfusion pressure (CPP) of 60–70 mmHg in patients who are traumatically brain injured (21). However, the use of one single target of CPP for all the patients may not represent the individual physiological needs and CA changes over time (22, 23). An individualised management of CBF, based on the intrinsic autoregulatory state of the single patients and its changes over time, may better represent the physiological changes occurring in the vasomotor response of patients with brain injury (3, 24–26).

Amongst the methods proposed as possible surrogates of CBF (24), neuroimaging techniques, such as Positron Emission Tomography (PET) and Single-Photon Emission Computed Tomography (SPECT), are very accurate, but these are expensive,

time-consuming, not available at bedsides of patients, and have a limited role in the clinical context (24).

A number of indirect techniques have been proposed based on invasive surrogates of CBF (intracranial pressure, invasive cerebral oxygenation monitoring) and non-invasive methods (TCD, NIRS) (24). Optical techniques, which can directly measure flow (i.e., diffuse correlation spectroscopy), and dynamic contrast enhanced NIRS have been used to measure CBF and validated against PET for regional cerebral blood flow measurement (25), but there is a paucity of studies in the literature regarding their use to assess cerebral haemodynamic responses (26).

CBF and CA can be evaluated by measuring relative blood flow changes in response to a steady-state change in the blood pressure (static methods) or during the response to spontaneous changes in blood pressure (dynamic methods) (23). Although dynamic methods do not require MAP manipulations (which can be dangerous in patients who are critically ill) and better reflect the changes of CA over time, they require the use of software, which is not always available at bedsides of patients (24). After MAP increase, a contemporary augmentation of CBFV, for instance, indicates a loss of CA, whereas, if CBFV decreases or remains constant, it indicates a functioning vasomotor response and preserved CA (27).

Outside the assessment of CA using TCD-based indices obtained *via* neuromonitoring software platforms (limited to few centres with technical resources and relevant clinical expertise), the simple assessment of CVRi/CVCi in response to systemic stimuli can be performed. Although routine assessment of these metrics is not always feasible, they present wide clinical applications, from the determination of stroke risk in individuals with severe asymptomatic carotid or intracranial steno-occlusive disease to concussions and patients with neurodegenerative conditions, such as Alzheimer's disease. In fact, previous works have described that changes in conductance (CVCi) better reflect the response in pressure regulation than do changes in resistance (CVRi) (28). This hypothesis is confirmed by the present data showing that CVCi measured by rSO_2 correlated consistently better with CBFV when compared to CVRi in response to rescue therapies and haemodynamic changes.

In this context, rSO_2 could potentially be applied as surrogate of CBF, as NIRS- similarly to TCD- is a low cost, easy available, and safe neuromonitoring tool (27). For example, NIRS has been previously used for the dynamic assessment of CA, with promising results, but several concerns have been raised regarding its routine use (7, 8, 29, 30). In particular, as NIR light penetrates skin, subcutaneous fat, skull, and underlying muscles and brain tissue, the absorption of light from chromophores depends on both the changes in oxygenated and deoxygenated haemoglobin, and, therefore, from both the arteriolar and venular beds. As a consequence, it has been shown that the absolute number of rSO_2, as well as its changes, might not be always reliable in practise since venous contamination can lead to misinterpretation of the data (29, 31).

The use of a device capable of effectively discriminating the changes of the arterial and venous compartments can, therefore, improve the accuracy of NIRS in different clinical contexts, especially in the assessment of CBF. As CBF is mainly regulated by the vasomotor response, which is a mechanism that primarily affects the arterial compartment, we have demonstrated that, by eliminating the effect of the venular bed, the estimation of CBF is more accurate than using the total rSO_2 values. Therefore, we believe that our results could pave the way for the application of a new technique for a quick and bedside assessment of CBF, with the adoption of tools, which are currently easily available and can provide important bedside information for cerebral haemodynamics assessment and management.

There are several limitations in this study that need to be mentioned. Firstly, although TCD is considered the gold standard for evaluation of cerebral haemodynamics, it only represents an indirect surrogate of CBF. A linear relationship has been demonstrated between CBFV and CBF (3), but with the assumption that the diameter of the insonated artery remains constant over time. Secondly, although in this study we included all rescue manoeuvres with a potential effect on MAP, these included a heterogeneous number of interventions (including fluids and norepinephrine administration, prone positioning, recruitment manoeuvres etc.); therefore, the increase in MAP was not standardised in the measurements. Typically, static cerebral autoregulation is assessed when MAP is increased by continuous infusion of a vasopressor (such as phenylephrine) to slowly increase MAP by ∼20 mm Hg. In our study, MAP increased only by 6 mm Hg. As this was an observational study, we could not target to a specific MAP to guide our treatment; we just observed the effect of a treatment on different patients. This is an important limitation as, in our cohort, we were able to assess mainly the changes of CBF rather than static CA. In fact, as previously reported, the accuracy of estimating the autoregulatory curve, or its different segments, from only two points is considered unreliable (32).

In addition, TCD evaluates major arteries, while NIRS measures the cerebral oxygenation at the microvasculature level (i.e., tissue oxygenation). This could lead to a decoupling between large and micro vessels. However, both methods are currently considered as surrogate of CBF (24, 33). Finally, we did not have measurements of the arteriovenous oxygen content difference concomitantly with the TCD/NIRS assessments to determine the cerebral metabolic rate of oxygen.

CONCLUSIONS

The arterial component of rSO_2 had the highest accuracy in assessing CBF changes, reflecting its role as the main component for vasomotor response after changes in MAP. These findings indicate that CBF assessed with NIRS, specifically through ΔO_2Hbi, is comparable to TCD in this patient population. The use of indices derived from the different components of rSO_2 can be useful for the bedside evaluation of cerebral haemodynamics in patients who are critically ill in order to optimise haemodynamics of patients and potentially improve their outcome. Further studies are warranted to better define the role of this technique in the clinical practise, especially the continuous assessment of cerebral autoregulation

in mechanically ventilated patients with COVID-19, with acute respiratory syndrome.

THE GECOVID GROUP

Ospedale Policlinico San Martino, IRCCS for Oncology and Neuroscience, Genoa, Italy: Iole Brunetti, Maurizio Loconte, Fabio Tarantino, Marco Sottano, Francesco Marramao, Angelo Gratarola, Paolo Frisoni. Department of Surgical Sciences and Integrated Diagnostics (DISC), University of Genoa, Italy: Elena Ciaravolo. Infectious Diseases Unit, Ospedale Policlinico San Martino, Genoa, Italy: Chiara Dentone, Lucia Taramasso, Laura Magnasco, Antonio Vena. Department of Neurosurgery, Ospedale Policlinico San Martino, Genoa, Italy: Gianluigi Zona. Department of Neurosurgery, Ospedale Policlinico San Martino, Genoa, Italy: Pietro Fiaschi.

DATA AVAILABILITY STATEMENT

The raw data supporting the conclusions of this article will be made available by the authors, without undue reservation.

ETHICS STATEMENT

The studies involving human participants were reviewed and approved by Comitato Etico Regione Liguria, protocol n. CER Liguria: 23/2020. The patients/participants provided their written informed consent to participate in this study.

AUTHOR CONTRIBUTIONS

CR writing of the manuscript, paper revision, fundamental conceptual contribution, and data analysis. LB, DB, DG, WD, MB, MC, RB, PP, and BM paper revision and fundamental conceptual contribution. DC, paper revision, fundamental conceptual contribution, and data analysis. All authors contributed to the article and approved the submitted version.

SUPPLEMENTARY MATERIAL

The Supplementary Material for this article can be found online at: https://www.frontiersin.org/articles/10.3389/fneur.2021.735469/full#supplementary-material

REFERENCES

1. Tisdall MM, Taylor C, Tachtsidis I, Leung TS, Elwell CE, Smith M. The effect on cerebral tissue oxygenation index of changes in the concentrations of inspired oxygen and end-tidal carbon dioxide in healthy adult volunteers. *Anesth Analg.* (2009) 109:906. doi: 10.1213/ane.0b013e3181aedcdc
2. Sekhon MS, Smielewski P, Bhate TD, Brasher PM, Foster D, Menon DK, et al. Using the relationship between brain tissue regional saturation of oxygen and mean arterial pressure to determine the optimal mean arterial pressure in patients following cardiac arrest: A pilot proof-of-concept study. *Resuscitation.* (2016) 106:120–5. doi: 10.1016/j.resuscitation.2016.05.019
3. Robba C, Cardim D, Sekhon M, Budohoski K, Czosnyka M. Transcranial Doppler: a stethoscope for the brain-neurocritical care use. *J Neurosci Res.* (2018) 96:720–30. doi: 10.1002/jnr.24148
4. Brady KM, Lee JK, Kibler KK, Easley RB, Koehler RC, Shaffner DH. Continuous measurement of autoregulation by spontaneous fluctuations in cerebral perfusion pressure: comparison of 3 methods. *Stroke.* (2008) 39:2531–7. doi: 10.1161/STROKEAHA.108.514877
5. Smielewski P, Czosnyka M, Zweifel C, Brady K, Hogue C, Steiner L, et al. Multicentre experience of using ICM+ for investigations of cerebrovascular dynamics with near-infrared spectroscopy. *Crit Care.* (2010) 14:1. doi: 10.1186/cc8580
6. Ghosh A, Elwell C, Smith M. Cerebral near-infrared spectroscopy in adults: A work in progress. *Anesth Analg.* (2012) 115:1373–83. doi: 10.1213/ANE.0b013e31826dd6a6
7. Caccioppola A, Carbonara M, Macrì M, Longhi L, Magnoni S, Ortolano F, et al. Ultrasound-tagged near-infrared spectroscopy does not disclose absent cerebral circulation in brain-dead adults. *Br J Anaesth.* (2018) 121:588–94. doi: 10.1016/j.bja.2018.04.038
8. Cardim D, Griesdale DE. Near-infrared spectroscopy: unfulfilled promises. *Br J Anaesth.* (2018) 121:523–6. doi: 10.1016/j.bja.2018.05.058
9. von Elm E, Altman DG, Egger M, Pocock SJ, Gøtzsche PC, Vandenbroucke JP. The strengthening the reporting of observational studies in epidemiology (STROBE) statement: Guidelines for reporting observational studies. *Int J Surg.* (2014) 85:867–72. doi: 10.2471/BLT.07.045120
10. Robba C, Ball L, Battaglini D, Cardim D, Moncalvo E, Brunetti I, et al. Early effects of ventilatory rescue therapies on systemic and cerebral oxygenation in mechanically ventilated COVID-19 patients with acute respiratory distress syndrome: a prospective observational study. *Crit Care.* (2021) 25:1–3. doi: 10.1186/s13054-021-03537-1
11. Robba C, Messina A, Battaglini D, Ball L, Brunetti I, Bassetti M, et al. Early effects of passive leg-raising test, fluid challenge, and norepinephrine on cerebral autoregulation and oxygenation in COVID-19 critically ill patients. *Front Neurol.* (2021) 12:829. doi: 10.3389/fneur.2021.674466
12. Bland JM, Altman DG. Statistics notes: calculating correlation coefficients with repeated observations: Part 2–correlation between subjects. *BMJ.* (1995) 310:633–633. doi: 10.1136/bmj.310.6980.633
13. Bakdash JZ, Marusich LR. Repeated measures correlation. *Front Psychol.* (2017) 8:456. doi: 10.3389/fpsyg.2017.00456
14. Bates D, Maechler M, Bolker B, Walker S. Package lme4. *J Stat Softw.* (2015) 67:1–91. doi: 10.18637/jss.v067.i01
15. Traub TM, Grabowski R, Rais-Bahrami K. Pilot study of cerebral and somatic autoregulation using NIRS in preterm neonates. *J Neonatal Perinatal Med.* (2021) 12:1–8. doi: 10.3233/NPM-200601
16. Joram N, Beqiri E, Pezzato S, Andrea M, Robba C, Liet JM, et al. Continuous monitoring of cerebral autoregulation in children supported by extracorporeal membrane oxygenation: a pilot study. *Neurocrit Care.* (2021) 34:935–45. doi: 10.1007/s12028-020-01111-1
17. Klein SP, Depreitere B, Meyfroidt G. How I monitor cerebral autoregulation. *Crit Care*. (2019) 23:160. doi: 10.1186/s13054-019-2454-1
18. Battaglini D, Santori G, Chandraptham K, Iannuzzi F, Bastianello M, Tarantino F, et al. Neurological complications and noninvasive multimodal neuromonitoring in critically ill mechanically ventilated COVID-19 patients. *Front Neurol.* (2020) 11:602114. doi: 10.3389/fneur.2020.602114
19. Depreitere B, Citerio G, Smith M, Adelson PD, Aries MJ, Bleck TP, et al. Cerebrovascular autoregulation monitoring in the management of adult severe traumatic brain injury: a delphi consensus of clinicians. *Neurocrit Care.* (2021) 34:731–8. doi: 10.1007/s12028-020-01185-x
20. Beqiri E, Smielewski P, Robba C, Czosnyka M, Cabeleira MT, Tas J, et al. Feasibility of individualised severe traumatic brain injury management using an automated assessment of optimal cerebral perfusion pressure: the COGiTATE phase II study protocol. *BMJ Open.* (2019) 9:e030727. doi: 10.1136/bmjopen-2019-030727
21. Carney N, Totten AM, O'Reilly C, Ullman JS, Hawryluk GWJ, Bell MJ, et al. Guidelines for the management of severe traumatic brain injury, fourth edition. *Neurosurgery.* (2016) 19:1. doi: 10.1227/NEU.0000000000001432

22. Donnelly J, Czosnyka M, Adams H, Robba C, Steiner LA, Cardim D, et al. Individualising individualising thresholds of cerebral perfusion pressure using estimated limits of autoregulation. *Crit Care Med.* (2017) 45:1464. doi: 10.1097/CCM.0000000000002575
23. Liu X, Donnelly J, Czosnyka M, Aries MJH, Brady K, Cardim D, et al. Cerebrovascular pressure reactivity monitoring using wavelet analysis in traumatic brain injury patients: a retrospective study. *PLoS Med.* (2017) 14:e1002348. doi: 10.1371/journal.pmed.1002348
24. Donnelly J, Aries MJ, Czosnyka M. Further understanding of cerebral autoregulation at the bedside: possible implications for future therapy. *Expert Rev Neurother.* (2015) 15:169–85. doi: 10.1586/14737175.2015.996552
25. Giovannella M, Andresen B, Andersen JB, El-Mahdaoui S, Contini D, Spinelli L, et al. Validation of diffuse correlation spectroscopy against (15)O-water PET for regional cerebral blood flow measurement in neonatal piglets. *J Cereb Blood Flow Metab.* (2020) 40:2055–65. doi: 10.1177/0271678X19883751
26. Selb J, Boas DA, Suk-Tak Chan ST, Evans KC. BuckleyE, Carp SA. Sensitivity of near-infrared spectroscopy and diffuse correlation spectroscopy to brain hemodynamics: simulations and experimental findings during hypercapnia. *Neurophotonics.* (2014) 1:015005. doi: 10.1117/1.NPh.1.1.015005
27. Sekhon MS, Griesdale DE, Czosnyka M, Donnelly J, Liu X, Aries MJ, et al. The effect of red blood cell transfusion on cerebral autoregulation in patients with severe traumatic brain injury. *Neurocrit Care.* (2015) 23:210–6. doi: 10.1007/s12028-015-0141-x
28. O'Leary DS. Regional vascular resistance vs. conductance: which index for baroreflex responses? *Am J Physiol.* (1991) 260:H632–7. doi: 10.1152/ajpheart.1991.260.2.H632
29. Ajayan N, Thakkar K, Lionel KR, Hrishi AP. Limitations of near infrared spectroscopy (NIRS) in neurosurgical setting: our case experience. *J Clin Monit Comput.* (2019) 33:743–6. doi: 10.1007/s10877-018-0209-1
30. Joram N, Beqiri E, Pezzato S, Andrea M, Robba C, Liet JM, et al. Smielewski. Impact of arterial carbon dioxide and oxygen content on cerebral autoregulation monitoring among children supported by ECMO. *Neurocrit Care.* (2021) 35:480–90. doi: 10.1007/s12028-021-01201-8
31. Diedler J, Zweifel C, Budohoski KP, Kasprowicz M, Sorrentino E, Haubrich C, et al. The limitations of near-infrared spectroscopy to assess cerebrovascular reactivity: the role of slow frequency oscillations. *Anesth Analg.* (2011) 113:849–57. doi: 10.1213/ANE.0b013e3182285dc0
32. Panerai RB. Assessment of cerebral pressure autoregulation in humans–a review of measurement methods. *Physiol Meas.* (1998) 19:305–38. doi: 10.1088/0967-3334/19/3/001
33. Brauer P, Kochs E, Werner C, Bloom M, S Pentheny PS, Yonas H, et al. Correlation of transcranial Doppler sonography mean flow velocity with cerebral blood flow in patients with intracranial pathology. *J Neurosurg Anesthesiol.* (1998) 10:80–5. doi: 10.1097/00008506-199804000-00003

Conflict of Interest: BM is the senior medical director of Masimo. CR, PP, and RB report personal fees from Masimo. MB reports personal fees and others from Angelini, personal fees and others from AstraZeneca, others from Bayer, personal fees and others from Cubist, personal fees and others from Pfizer, personal fees and others from Menarini, personal fees and others from MSD, others from Nabriva, others from Paratek, others from Roche, others from Shionogi, others from Tetraphase, others from the Medicine Company, personal fees and others from AstellasPharma Inc., personal fees from Gilead Sciences, personal fees from Teva, personal fees from Novartis, grants from Ranbaxy, personal fees from Correvio, personal fees from Molteni, personal fees from Thermo Fisher, outside the submitted work. Dr Herrmann is a cofounder and shareholder in OscillaVent, Inc, and a consultant for ZOLL Medical Corporation, both outside the submitted work. MC is recipient of part of the licensing fee for ICM+ software (Cambridge Enterprise Ltd., UK) outside the submitted work. DG reports personal fees from Stepstone Pharma GmbH, personal fees from MSD Italia and personal fees from Correvio Italia, outside the submitted work.

The remaining authors declare that the research was conducted in the absence of any commercial or financial relationships that could be construed as a potential conflict of interest.

Publisher's Note: All claims expressed in this article are solely those of the authors and do not necessarily represent those of their affiliated organizations, or those of the publisher, the editors and the reviewers. Any product that may be evaluated in this article, or claim that may be made by its manufacturer, is not guaranteed or endorsed by the publisher.

frontiers in Neurology

ORIGINAL RESEARCH
published: 12 January 2022
doi: 10.3389/fneur.2021.740338

Relationship Between Baroreflex and Cerebral Autoregulation in Patients With Cerebral Vasospasm After Aneurysmal Subarachnoid Hemorrhage

Agnieszka Uryga[1†], Nathalie Nasr[2,3†], Magdalena Kasprowicz[1], Karol Budohoski[4], Marek Sykora[5,6], Peter Smielewski[4], Małgorzata Burzyńska[7†] and Marek Czosnyka[4,8†]*

[1] Department of Biomedical Engineering, Faculty of Fundamental Problems of Technology, Wroclaw University of Science and Technology, Wrocław, Poland, [2] INSERM UMR 1297, Institute of Cardiovascular and Metabolic Diseases (I2MC), Toulouse, France, [3] Department of Neurology, Toulouse University Hospital, Toulouse, France, [4] Brain Physics Laboratory, Division of Neurosurgery, Department of Clinical Neurosciences, University of Cambridge, Cambridge, United Kingdom, [5] Department of Neurology, St. John's Hospital, Vienna, Austria, [6] Medical Faculty, Sigmund Freud University, Vienna, Austria, [7] Department of Anaesthesiology and Intensive Care, Wroclaw Medical University, Wrocław, Poland, [8] Institute of Electronic Systems, Faculty of Electronics and Information Technology, Warsaw University of Technology, Warsaw, Poland

OPEN ACCESS

Edited by:
Christian Senft,
University Hospital Jena, Germany

Reviewed by:
Sepide Kashefiolasl,
University Hospital Frankfurt, Germany
Verena Rass,
Medizinische Universität Innsbruck, Austria

***Correspondence:**
Agnieszka Uryga
agnieszka.uryga@pwr.edu.pl

[†] These authors have contributed equally to this work

Specialty section:
This article was submitted to Neurocritical and Neurohospitalist Care, a section of the journal Frontiers in Neurology

Received: 12 July 2021
Accepted: 02 December 2021
Published: 12 January 2022

Citation:
Uryga A, Nasr N, Kasprowicz M, Budohoski K, Sykora M, Smielewski P, Burzyńska M and Czosnyka M (2022) Relationship Between Baroreflex and Cerebral Autoregulation in Patients With Cerebral Vasospasm After Aneurysmal Subarachnoid Hemorrhage. Front. Neurol. 12:740338. doi: 10.3389/fneur.2021.740338

Introduction: Common consequences following aneurysmal subarachnoid hemorrhage (aSAH) are cerebral vasospasm (CV), impaired cerebral autoregulation (CA), and disturbance in the autonomic nervous system, as indicated by lower baroreflex sensitivity (BRS). The compensatory interaction between BRS and CA has been shown in healthy volunteers and stable pathological conditions such as carotid atherosclerosis. The aim of this study was to investigate whether the inverse correlation between BRS and CA would be lost in patients after aSAH during vasospasm. A secondary objective was to analyze the time-trend of BRS after aSAH.

Materials and Methods: Retrospective analysis of prospectively collected data was performed at the Neuro-Critical Care Unit of Addenbrooke's Hospital (Cambridge, UK) between June 2010 and January 2012. The cerebral blood flow velocity (CBFV) was measured in the middle cerebral artery using transcranial Doppler ultrasonography (TCD). The arterial blood pressure (ABP) was monitored invasively through an arterial line. CA was quantified by the correlation coefficient (Mxa) between slow oscillations in ABP and CBFV. BRS was calculated using the sequential cross-correlation method using the ABP signal.

Results: A total of 73 patients with aSAH were included. The age [median (lower-upper quartile)] was 58 (50–67). WFNS scale was 2 (1–4) and the modified Fisher scale was 3 (1–3). In the total group, 31 patients (42%) had a CV and 42 (58%) had no CV. ABP and CBFV were higher in patients with CV during vasospasm compared to patients without CV ($p = 0.001$ and $p < 0.001$). There was no significant correlation between Mxa and BRS in patients with CV, neither during nor before vasospasm. In patients without CV, a

significant, although moderate correlation was found between BRS and Mxa ($r_S = 0.31$; $p = 0.040$), with higher BRS being associated with worse CA. Multiple linear regression analysis showed a significant worsening of BRS after aSAH in patients with CV ($R_p = -0.42$; $p < 0.001$).

Conclusions: Inverse compensatory correlation between BRS and CA was lost in patients who developed CV after aSAH, both before and during vasospasm. The impact of these findings on the prognosis of aSAH should be investigated in larger studies.

Keywords: autonomic nervous system, subarachnoid hemorrhage, cerebral vasospasm, baroreflex, cerebral autoregulation, cerebrovascular regulation

INTRODUCTION

Subarachnoid hemorrhage caused by the rupture of an aneurysm (aSAH), can lead to the neurological disability or death. The aSAH can cause molecular alterations (oxidative stress, inflammatory reaction) and loss of vascular integrity, leading to brain edema or delayed cerebral ischemia (1).

One of the most common complications following aSAH is cerebral vasospasm (CV), which occurs on average 4–7 days after ictus. Despite intensive research effort, CV following aSAH remains incompletely understood from a pathogenic perspective and does not solely explain the occurrence of delayed ischemic deficit (2). Several factors are potentially pathogenic: decreased nitric oxide (NO) availability, calcium-dependent vasoconstriction, free radicals, inflammation, dysfunctional endothelial neuronal apoptosis, or neurogenic factors (3). Impaired cerebral autoregulation (CA) might play an important role in the occurrence of delayed ischemic deficit in patients who developed CV after aSAH (4). Impairment of the cardiovascular autonomic nervous system in the acute phase of aSAH, as reflected by the low-baroreflex sensitivity (BRS), also appears to impact prognosis as it has been associated with adverse outcomes 3 months post aSAH (5). Furthermore, it has been shown that BRS was lower in non-survivors than in survivors. Moreover, patients with disturbed BRS had more extensive hemorrhage (6). Finally, both the impaired BRS and impaired CA have been associated with unfavorable prognoses. These two homeostatic mechanisms are inversely correlated in both the healthy volunteers and patients suffering from stable chronic diseases, such as carotid stenosis or occlusion (7). However, the way they interact in acute neurological diseases such as aSAH is not known. Short-term time trends of BRS in acute pathological events and more specifically in aSAH are not well-documented, in contrast to changes in BRS during medium- and long-term physiological conditions (8–10).

In this study, our primary objective was to assess CA and BRS in relation to the occurrence of CV. We hypothesized that the inverse correlation between BRS and CA previously found in physiology and in stable pathological disease could be lost in patients with aSAH and more specifically in patients with CV. A secondary objective of this study was to investigate the changes of BRS in the days following aSAH.

MATERIALS AND METHODS

Study Design and Patient Management

The study was a retrospective analysis of data prospectively collected at the neuro- critical care unit of Addenbrooke's Hospital (Cambridge, UK) between June 2010 and January 2012. A total of 97 patients suffering from aSAH were screened for compatibility with the study inclusion criteria: ≥18 years of age; admission to the hospital <5 days after aSAH with an intracerebral aneurysm likely to be the source of bleeding [as determined by computed tomography angiography or digital subtraction angiography (DSA)]; continuous multimodal monitoring. Patients were not enrolled in the study if they had autoregulation monitoring only during CV or if the quality of the signals was poor. The study was approved by the Research Ethics Committee of Addenbrooke's Hospital (Protocol 29 LREC: 97/291). All patients or their next-of-kin were required to sign written consent before inclusion. Seventy-three patients were enrolled for the study (flow chart depicted in **Figure 1**).

All patients were treated according to the guidelines applicable at the time of admission (11). Decisions concerning surgical clipping or endovascular embolization were made by the neurosurgical and interventional neuroradiology team. Conservative treatment was applied in a few patients with very severe and poor-grade aSAH. On admission, patients were assessed using the Glasgow Coma Scale (GCS). Neurologic state on admission was evaluated with the World Federation of Neurosurgical Societies (WFNS) grading system. The extent of hemorrhage was assessed using a modified Fisher (mFisher) scale and patients who had clinical or radiological signs of hydrocephalus were treated with external ventricular drainage (EVD), lumbar drainage, or serial lumbar punctures until the permanent diversion of cerebrospinal fluid was required. The treatment protocol included euvolemia, nimodipine, and cardiopulmonary support. Although "Triple-H" therapy was recommended at the time of admission, only induced hypertension was used. Delayed cerebral ischemia (DCI) was defined as focal neurological impairment (a two-point decrease in GCS) lasting for at least 1 h or cerebral infarction, which was not apparent immediately after aneurysm occlusion and was attributable to ischemia and not to other causes (12). Patients with diagnosed DCI underwent hemodynamic therapy with intravenous crystalloids administration to achieve central venous pressure between 8 and 12 mm Hg, as well as blood pressure

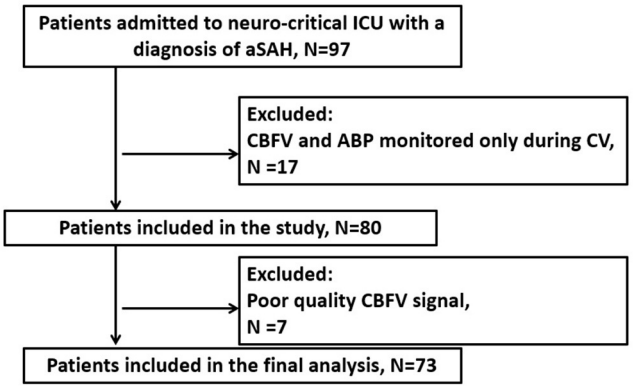

FIGURE 1 | Flow diagram of the study. ABP, arterial blood pressure; CBFV, cerebral blood flow velocity; CV, cerebral vasospasm; aSAH, aneurysmal subarachnoid hemorrhage.

support using individually titrated doses of vasopressors. The outcome was evaluated at discharge from the hospital and then after 3 months using the Modified Rankin Scale for Neurologic Disability (mRS). Scores of 0 to 2 on mRS were classified as good and scores of 3–6 on mRS were classified as poor outcomes.

Signal Monitoring

Arterial blood pressure (ABP) was measured invasively in the radial artery using a pressure transducer and a pressure monitoring kit (Baxter Healthcare, Deerfield, IL, USA). Bilateral cerebral blood flow velocity (CBFV) in the middle cerebral artery (MCA) was monitored with transcranial Doppler ultrasonography (TCD) (DopplerBox; DWL Compumedics, Singen, Germany) using a head positioning device (Lam Rack, DWL Compumedics) through the temporal acoustic window. Data were acquired at a frequency of 200 Hz using an Intensive Care Monitor System (ICM+; Cambridge Enterprise Ltd, Cambridge, UK), and digitized using an analog-to-digital converter. All artifacts were identified manually or by custom-written algorithms. ABP and CBFV were measured in all patients.

Multimodal signal monitoring was started during the first days after admission. All patients had TCD performed every 1–2 days by a single investigator (BK). CBFV was monitored for about one hour; the minimum time was a half-hour and the maximum of one and a half hour. The median ± interquartile range (IQR) of the time of the start of the TCD recordings was 3 ± 3 days. The median ± IQR of the recordings per patient was 4 ± 3 (min-max: 1–11). There was one recording per day. The medians and IQRs of the observation time were: 11 days ± 5 days (min-max: 6–26 days) in the CV group and 7 days ± 5 days (min-max: 1–15 days) in the non-CV group, respectively. Illustrative time trends of the monitored signals are presented in **Figure 2**.

Cerebral Vasospasm

Cerebral vasospasm was defined using TCD as mean CBFV in the MCA above 120 cm/s with a concomitant Lindegaard ratio (LR) above 3.0, where LR = $CBFV_{MCA}/CBFV_{ICA}$. When DSA was performed CV was defined as 25% narrowing of cerebral arteries on DSA irrespective of TCD findings. Routine postoperative CT and DSA were not performed. The side on which CV was diagnosed at the time of monitoring was labeled as the ipsilateral side. In patients in whom bilateral vasospasm was diagnosed, an average of parameters on both sides was used and labeled as the ipsilateral side. In patients in whom no vasospasm was diagnosed, the aneurysm side was used as the ipsilateral side. In patients with midline aneurysms but without diagnosed vasospasm, an average of parameters on both sides was used as the ipsilateral side. CBFV and CA were assessed on the ipsilateral side.

Cerebral Autoregulation

CA was assessed from slow-wave oscillations of ABP and CBFV. The mean velocity index (Mxa) was calculated as the Pearson linear correlation coefficient between these signals (averaged over 10-s intervals) in a 5-min moving average window updated every 10 s. Values of Mxa >0.3 reflect impaired CA (13).

Baroreflex Sensitivity

The BRS was calculated using the sequential cross-correlation method (also called x-BRS), published by Westerhof (14), which was embedded in ICM+. ABP systolic peaks were used to obtain RR interval time series. BRS was estimated as the slope of the regression line between the segments of systolic ABP (the input signal) and the RR interval (the output signal). BRS calculations were performed using a moving 10-s window along with mean values of the other vital signs variables included in the analysis. The BRS algorithm required the systolic ABP and RR time series to be incrementally shifted with respect to each other in search of the highest value of cross-correlation. Thus, the total window length used in each BRS calculation was extended to 17 s (7). BRS was returned when the *p*-value of the correlation coefficient was <0.01 and no ectopic beats were detected (15).

Statistics

The normality distribution of the data was assessed using the Kruskal–Wallis test with the Lilliefors correction. Non–parametric tests were applied because the normality condition was not met for most of the analyzed parameters. The differences in median values were tested using the Mann–Whitney *U*-test. For non-numeric data, the Pearson CHI^2 test (Fisher exact test/The Fisher-Freeman-Halton test) was used. McNemar's test was used to assess the increase in subjects with impaired CA during CV in comparison with the period before CV. Differences in median values before and during CV were compared using the Wilcoxon signed-rank test. Median values of CA and BRS were calculated using the entire time period in patients without CV, and using separately the time periods before and during vasospasm in patients with CV. Correlation analysis was performed using Spearman's rank test. The relationships between elapsed time (days) and physiological parameters were calculated using multiple linear regression analyses, with subjects treated as categorical factors using dummy variables (with respect to the inter– subject variability) and a partial coefficient (R_p) between analyzed variables as recommended by Bland and Altman (16, 17). Results are presented as medians ± interquartile ranges or median (25–75th percentile) if not otherwise specified. The

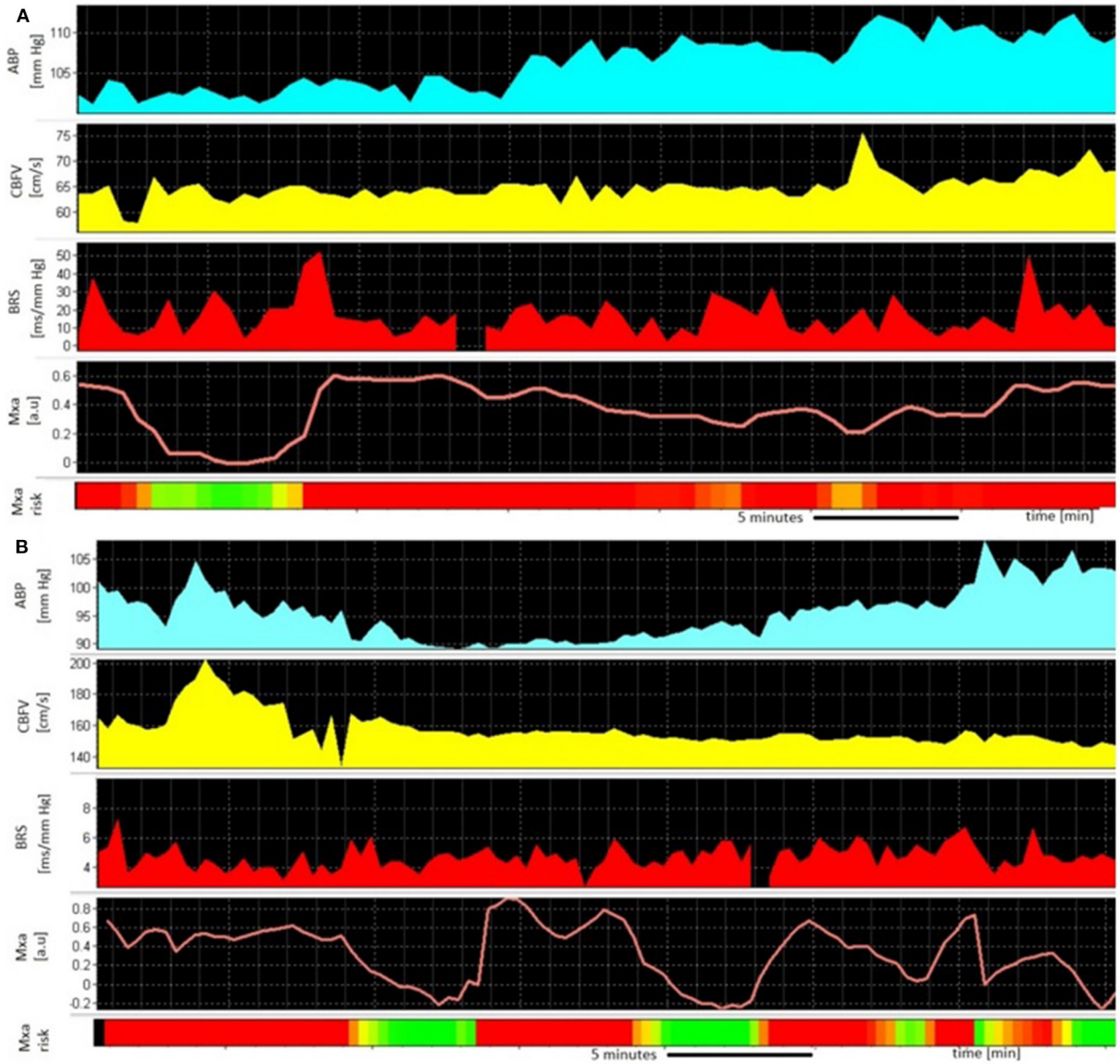

FIGURE 2 | An example of the monitoring of **(A)** 45-year old man without cerebral vasospasm (CV) 12 days after aneurysmal subarachnoid hemorrhage (aSAH) from a ruptured aneurysm in the posterior cerebral artery (PCA). The high values of Mxa [worse cerebral autoregulation (CA), red panel] are counterbalanced with efficient, high-cardiac baroreflex sensitivity (BRS); **(B)** 67-year old woman during CV 8 days after aSAH from a ruptured aneurysm in the anterior communicating artery (ACom). The high values of Mxa (worse CA, red panel) occur in parallel with disrupted, low BRS; ABP, arterial blood pressure; CBFV, cerebral blood flow velocity; BRS, baroreflex sensitivity; Mxa, mean velocity index; the Mxa above 0.3 is interpreted as pathological.

level of significance was set at 0.05. Statistical analysis was performed using STATISTICA version 13 (Tibco, Palo Alto, CA, USA).

RESULTS

Baseline Characteristics

The group consisted of 24 (33%) men and 49 (67%) women, with a median age of 58 (50–67) years. Clinical data for the total group are presented in **Table 1**. Twenty-six patients (36%) underwent coiling and 51 (70%) underwent surgical clipping. In 5 patients (7%) conservative treatment was applied due to their severe condition. In this group, 3 patients died (60%), and these deaths were 50% of all deaths in this aSAH group. The 2 remaining patients were discharged from the hospital with good outcomes according to the evaluation of the mRS scale. Median WFNS scale was 2 (1–4) and median mFisher scale was 3 (1–3). CV was observed in 31 patients (42%) and occurred on day 8 ± 3. Mechanical ventilation was applied in 24 (33%) patients: 12 (39%) in the CV group and 12 (28%) in the non-CV group.

TABLE 1 | Patient characteristics.

	All patients $n = 73$	CV $n = 31$	Non–CV $n = 42$	p
Female, *n* (%)	49 (67%)	21 (64%)	28 (67%)	0.922[b]
Age (years), median (IQR)	58 (50–67)	55 (48–63)	62 (53–71)	**0.009**[a]
GCS, median (IQR)	14 (11-15)	12 (11-15)	14 (13-15)	0.372[a]
mFisher, median (IQR)	3 (1-3)	3 (3)	3 (1-3)	0.415[a]
1, *n* (%)	19 (26%)	4 (13%)	15 (36%)	**0.030**[b]
2, *n* (%)	4 (6%)	2 (6%)	2 (4%)	
3, *n* (%)	36 (49%)	21 (68%)	15 (36%)	
4, *n* (%)	14 (19%)	4 (13%)	10 (24%)	
WFNS, median (IQR)	2 (1-4)	2 (1-4)	2 (1-3)	0.499[a]
1, *n* (%)	26 (36%)	10 (32%)	16 (38%)	0.772[b]
2, *n* (%)	26 (32%)	10 (32%)	14 (33%)	
3, *n* (%)	4 (6%)	1 (3%)	3 (7%)	
4, *n* (%)	16 (22%)	9 (30%)	7 (17%)	
5, *n* (%)	3 (4%)	1 (3%)	2 (4%)	
Treatments[#]				
Endovascular coiling, *n* (%)	26 (36%)	8 (26%)	18 (43%)	0.133[b]
Surgical clipping, *n* (%)	51 (70%)	25 (81%)	26 (62%)	0.085[b]
Conservative treatment, *n* (%)	5 (7%)	0 (0%)	5 (12%)	0.068[b]
Mechanical ventilation, *n* (%)	24 (33%)	12 (39%)	12 (28%)	0.327[b]
Vasopressor agents, *n* (%)	26 (36%)	18 (58%)	8 (19%)	**0.006**[b]
Complications				
Hydrocephalus, *n* (%)	37 (51%)	18 (58%)	19 (45%)	0.279[b]
EVD, *n* (%)	24 (33%)	13 (42%)	11 (26%)	0.157[b]
DCI, *n* (%)	22 (30%)	19 (61%)	3 (7%)	**<0.001**[b]
Rebleeding, *n* (%)	6 (8%)	1 (3%)	5 (12%)	0.227[b]
Outcome				
Deaths, *n* (%)	6 (8%)	2 (6%)	4 (10%)	0.491[b]
mRS at discharge, median (IQR)	2 (1-3)	2 (1-3)	2 (1-4)	0.648[a]
0–2, *n* (%)	46 (63%)	17 (55%)	29 (69%)	0.214[b]
3–6, *n* (%)	27 (37%)	14 (45%)	13 (31%)	
3 months mRS, median (IQR)	1 (0–2)	1 (0–2)	1 (0–2)	0.799[a]
0–2, *n* (%)	60 (82%)	35 (83%)	25 (81%)	0.767[b]
3–6, *n* (%)	13 (18%)	7 (17%)	6 (19%)	

p-values marked with bold indicate statistically significant differences between the groups. CV, cerebral vasospasm; EVD, external ventricular drain; DCI, delayed cerebral ischemia; mRS, modified rankin scale; a–U mann-whitney test, b–Chi-squared test, #-More than one procedure per patient allowed.

Vasopressor agents were used in 26 (36%) patients: 18 (58%) in the CV group and 8 (19%) in the non-CV group.

Clinical Data in the CV and Non-CV Groups

A comparison of clinical data for the CV group and the non-CV group is presented in **Table 1**. There were no significant differences between the CV and the non-CV group for the following parameters: sex, WFNS, and GCS scales. There were no significant differences between the CV and the non-CV group concerning treatment: the proportion of patients with mechanical ventilation, coiling, or clipping did not differ significantly between the two groups. DCI occurred more frequently in patients with CV than without CV: 61% vs. 7%, $p < 0.001$. Patients with CV had more extended hemorrhage (mFisher 4–5): 81% in the CV group vs. 61% in the non-CV group, $p = 0.030$. Patients with CV were significantly younger compared to patients without CV: 55 (43–63) vs. 62 (53–71), $p = 0.009$. There were no significant differences in the outcome at discharge or after 3 months, nor in the death rate between the CV and the non-CV group.

Physiological Metrics in the CV and Non-CV Groups

The results of the comparison of ABP, HR, and CBFV between the CV and non-CV groups are presented in **Table 2**. There was no significant difference in the physiological metrics between patients with CV in the period before vasospasm and averaged values of these parameters in patients without CV, except for a higher value of CBFV ($p = 0.005$, **Table 2**). In the CV group during vasospasm patients had significantly higher ABP ($p = 0.001$) and CBFV ($p < 0.001$) than averaged values of these parameters in patients without CV (**Table 2**). In the CV group during vasospasm, we observed a substantial increase

in the following parameters compared with the period before vasospasm: ABP ($p = 0.025$), HR ($p = 0.001$), and CBFV ($p < 0.001$, **Table 2**).

Baroreflex Sensitivity and Cerebral Autoregulation in the CV and Non-CV Groups

There was no significant difference in BRS between patients without CV and patients with CV, neither in the period before vasospasm nor during vasospasm (**Table 2**). In the patients with CV, BRS decreased substantially during vasospasm compared with the period before vasospasm: 9.53 (5.95–12.20) (ms/mm Hg) vs. 13.73 (8.41–20.50) (ms/mm Hg), $p < 0.001$.

The CA was impaired in 74% of patients without CV. In the CV group CA was significantly worse during vasospasm than before vasospasm [Mxa: 0.43 (0.36–0.52) vs. 0.37 (0.28–0.42), $p = 0.002$]. Moreover, in the CV group the proportion of patients with impaired CA increased from 68% before vasospasm to almost 90% during vasospasm. According to McNemar's test, CV was significantly associated with worse CA ($p = 0.001$).

Relationship Between Cerebral Autoregulation and Baroreflex Sensitivity in the CV and Non-CV Groups

There was a significant and moderate correlation between Mxa and BRS in patients without CV: $r_s = 0.31$, $p = 0.040$ (higher—better BRS associated with higher—worse CA), **Figure 3A**. There was no significant correlation between Mxa and BRS in the CV group, neither before vasospasm ($r_s = 0.24$, $p = 0.187$, **Figure 3B**) nor during vasospasm ($r_s = -0.04$, $p = 0.799$, **Figure 3C**). There was no relationship between impairment of CA, BRS, and DCI.

The Potential Impact of Treatment With Vasopressors

There were 26 (36%) patients who received vasopressors: 8 (19%) without CV, and 18 (58%) with CV. There was no significant difference for BRS between patients with vasopressors ($n = 26$) and patients without vasopressors ($n = 47$): $Z = -0.81$; $p = 0.420$. Moreover, in the CV group, BRS was significantly lower during CV compared with the period before CV both in patients with vasopressors ($Z = 2.85$; $p = 0.004$) as in patients without vasopressors ($Z = 2.97$; $p = 0.003$). Loss of inverse correlation between BRS and Mxa before and during CV was found in the CV group, regardless of treatment with vasopressors. In the non-CV group, the inverse correlation between Mxa and BRS was not found when patients treated with vasopressors were excluded. However, the analysis of the impact of vasopressors on the relationship between BRS and CA could be biased by the limited number of observations in this subgroup.

Time Trends of Physiological Metrics, Baroreflex Sensitivity and Cerebral Autoregulation in the CV and Non-CV Groups

In patients with CV, multiple linear regression analysis showed a significant increase in ABP, HR, and CBFV in the days that followed aSAH—ABP: $R_p = 0.31$, $p < 0.001$; HR: $R_p = 0.46$, $p < 0.001$; CBFV: $R_p = 0.29$, $p < 0.001$. Furthermore, a moderate decrease in BRS was found in the days that followed aSAH in patients with CV: $R_p = -0.42$; $p < 0.001$ (**Figure 4**), but not in patients without CV.

DISCUSSION

Inverse correlation between BRS and CA was found to be lost in aSAH in patients with vasospasm both during vasospasm and during the period that preceded vasospasm. BRS decreased substantially in these patients during vasospasm as compared to the period before vasospasm. In patients without CV, a significant moderate correlation was found between BRS and CA, with worse BRS being associated with better CA, a finding previously termed as "inverse correlation" (7). Multiple linear regression analysis showed a significant relationship between the decrease in BRS, and the days elapsed from aSAH in the CV group.

Cerebral autoregulation regulates cerebral blood flow (CBF) in the distal arteries and stabilizes CBF in the face of changes in ABP mainly through myogenic and neurogenic mechanisms (18). CA is frequently impaired after aSAH (19, 20), even without any evidence of changes in flow velocity in the major arteries (21). It was found in this study that CA was getting worse during the CV. This observation is consistent with previous studies in patients with SAH, where Mxa was higher in patients with vasospasm compared to baseline (22, 23). It was shown that autoregulation is impaired in most patients with vasospasm of large cerebral arteries due to low-perfusion pressure distal to large arteries, and responsive maximal dilation of downstream vessels (23, 24).

Inverse correlation between CA and BRS was preserved in patients without CV. From a dynamic systems theory, the interaction between BRS and CA provides stable perfusion of the brain. The failure of both systems has previously been reported before syncope (25). The compensatory interaction between blood pressure regulation and cerebral perfusion pressure mechanisms was found in a previous study in the healthy young humans (7, 26). These studies have shown that impaired CA was counterbalanced with better BRS and *vice-versa*. The same observation has been found in patients with atherosclerotic stenosis or occlusion (7) and also in a cohort of patients with aSAH (6). Regulation of CBF is maintained through both arterial baroreflex control of blood pressure and CA operating through changes of cerebrovascular resistance. However, the relation between these two homeostatic mechanisms is still not clear. Rather than interpretation in a finalistic view, a mechanistic approach has been favored to explain the inverse correlation, linking better CA to enhanced cerebral vasomotor tone due to the increased sympathetic activity associated with diminished BRS (7). A finalist view, however, cannot be excluded and can be based on the theory of the physiological system complexity states that the structure is optimally configured to support its functions (27).

In this study, we found that inverse correlation between CA and BRS is lost in patients with aSAH, who developed CV. This finding could be the result of mechanical alterations caused

TABLE 2 | Physiological metrics and cerebral autoregulation in patients with and without cerebral vasospasm (CV).

Parameter	No-CV $n = 42$	CV Before $n = 31$	CV During $n = 31$	p^*	$p^{\#}$	$p^{\dagger}$
ABP (mm Hg)	89.49 (90.51–80.87)	93.74 (82.91–106.44)	106.50 (89.70–116.65)	0.145	**0.001**	**0.025**
HR (bpm)	71.99 (64,03–76.19)	66.41 (61.12–81.15)	75. 12 (63.76–86.92)	0.425	0.281	**0.001**
CBFV (cm/s)	65.33 (48.63–76.33)	76.65 (63.31–96.89)	143.20 (122.99–154.71)	**0.005**	**<0.001**	**<0.001**
Mxa ipsilateral (a.u.)	0.37 (0.30–0.46)	0.37 (0.28–0.42)	0.43 (0.36–0.52)	0.691	**0.039**	**0.002**
Mxa ipsilateral >0.3 [*n* (%)]	31 (74%)	21 (68%)	28 (90%)	0.571	0.068	**0.001**
BRS (ms/mm Hg)	10.92 (7.53–15.93)	13.73 (8.41–20.50)	9.53 (5.95–12.20)	0.130	0.244	**<0.001**

Data are presented as median (lower quartile–upper quartile). p-values marked with bold indicate statistically significant differences between the groups. Following comparisons are presented for patients: non-CV vs. before CV (U Mann-Whitney test), non-CV vs. during CV# (U Mann-Whitney test), before CV vs. during CV† (Wilcoxon signed rank test); ABP, arterial blood pressure; HR, heart rate; CBFV, cerebral blood flow velocity; Mxa, mean velocity index of cerebral autoregulation; BRS, baroreflex sensitivity.*

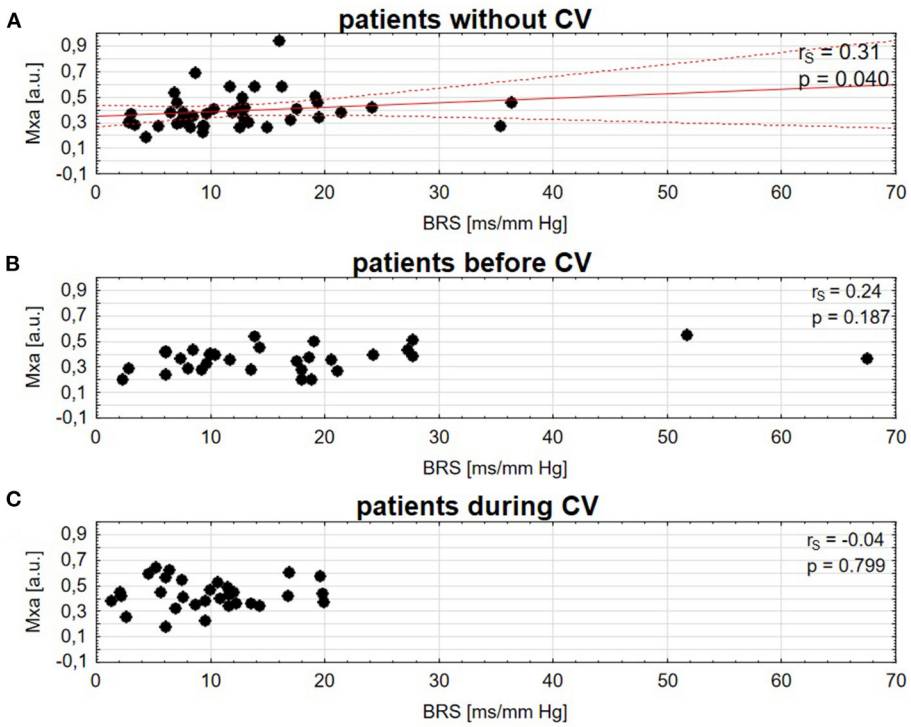

FIGURE 3 | Spearman correlation of cerebral autoregulation (Mxa) and baroreflex sensitivity (BRS) in patients **(A)**, without cerebral vasospasm (CV), **(B)** before CV, **(C)** during CV. A solid red line is a linear regression and dashed lines represent 95% CI.

by the local modifications in the cerebral vasomotor tone as a consequence of the degradation of hemoglobin after aSAH (28) that can potentially override the systemic input of the cardiovascular autonomic nervous system on CA. The potential consequences of the observed loss of inverse correlation between BRS and CA are not known. It might play a role in the occurrence of delayed ischemic deficit in a proportion of patients who develop CV after aSAH. However, we found that impaired BRS and CA occurred both in patients with DCI and non-DCI. Potentially improving both of these metrics should be targeted in post-SAH clinical management.

The findings on the relationship between the BRS–CA relationship and age are currently inconclusive. The correlation between pressure index reactivity (PRx) and BRS has been shown to be reciprocal in the elderly patients (>60 years) with traumatic brain injury (15). On the other hand, a study in the healthy volunteers (20–80 years) has shown that in older subjects BRS and CA were not correlated (29). Previous studies have shown that spontaneous BRS decreases significantly with age and that the loss of arterial distensibility with age would be the main mechanism responsible for the reduction in BRS in the older subjects. However, in our study, patients with CV were younger than patients without CV, so the decrease in BRS in that group of patients is not biased by age (30).

Another result from this study pertains to the behavior of BRS as a time-trend parameter, decreasing during the days that followed aSAH. BRS decreased significantly after aSAH and

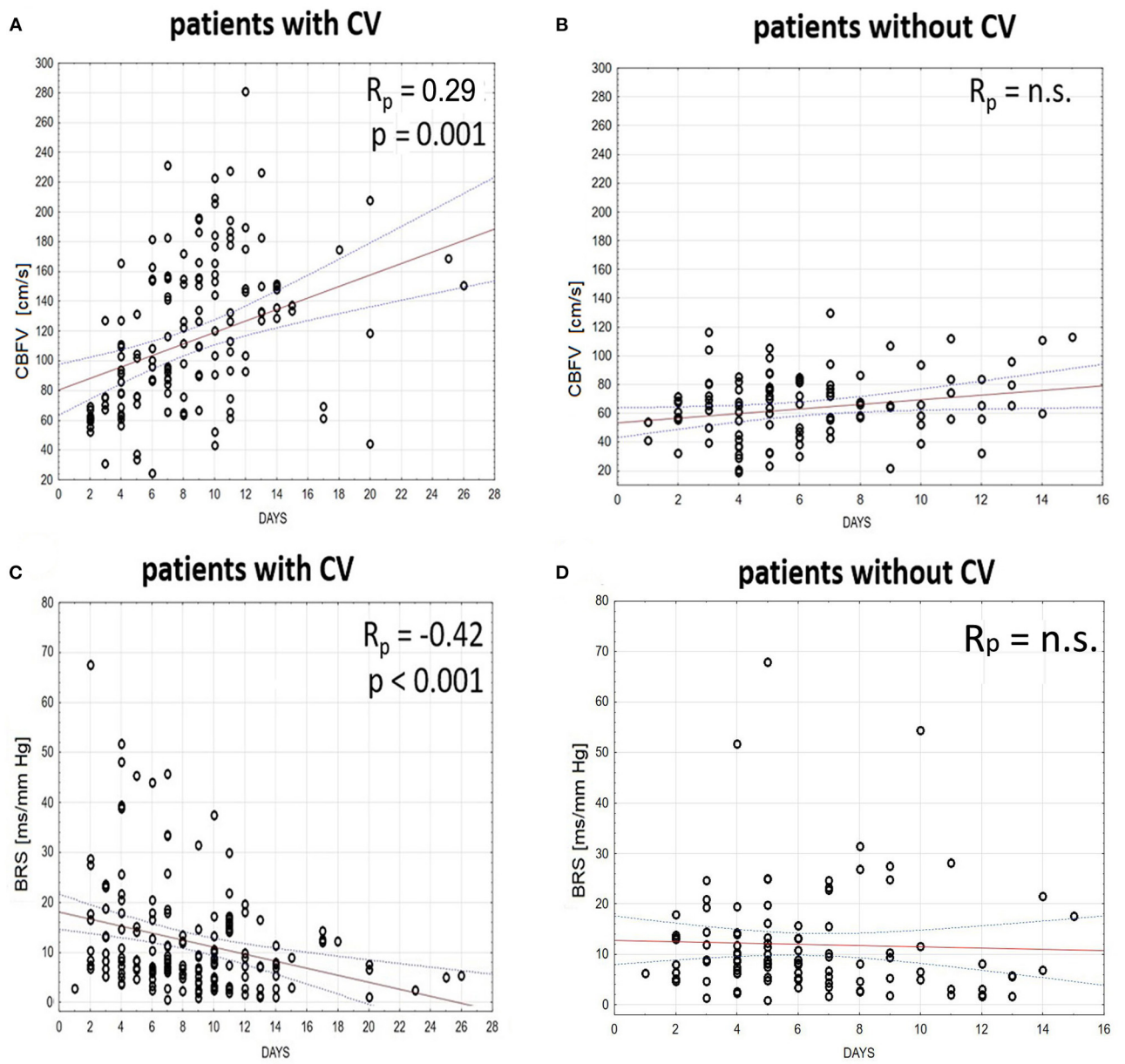

FIGURE 4 | Time trends (solid red line) and the 95% CI (dashed line) of **(A,B)** cerebral blood flow velocity (CBFV) and **(C,D)** baroreflex sensitivity (BRS) in patients **(A,C)** with and **(B,D)** without cerebral vasospasm (CV) analyzed in the days that follow aneurysmal subarachnoid hemorrhage (aSAH). The relationship between days and physiological parameters was calculated using multiple linear regression analyses with subjects treated as categorical factors using dummy variables (with respect to the intersubject variability) and a partial coefficient (R_p) between analyzed variables.

"stunned" values of BRS were observed in patients with CV almost three weeks after onset. In the non-CV group, a non-significant trend to a moderate decrease in BRS was also observed in the days following aSAH.

Baroreflex is central to the cardiovascular homeostasis maintained by the autonomic nervous system. An increase in sympathetic activity is associated with lower BRS (31). Autonomic nervous system impairment is common in patients with acute brain insult (32, 33). It can also occur in the subacute neurological diseases, such as Guillain–Barre syndrome (34). Thus, BRS impairment reflects a non-specific systemic impairment of the cardiovascular autonomic nervous system in the context of acute brain injury. Our study was not designed to assess the clinical significance of the loss of inverse correlation between CA and BRS during the CV. However, in case future studies confirm the loss of inverse correlation between BRS and CA in patients at risk of clinical deterioration after aSAH a comprehensive continuous real-time assessment of BRS along with CA could provide valuable information in patients with aSAH as both BRS and CA have been shown to be associated with

outcome at 3 months (4, 5). In less acute pathological situations, medical therapy combined with baroreflex activation therapy (BAT) has been successful, such as in resistant hypertension (35) and heart failure with reduced ejection fraction (36). It is yet to demonstrate that BRS is a potential therapeutic target after an acute brain injury such as aSAH.

The cohort of patients utilized in our study has already been analyzed for assessment of prognosis in relation to BRS (5), and cerebral hemodynamic parameters (4, 37, 38). In this study, we aimed to assess integrative pathophysiology evaluating the interaction between the two main cardiovascular and cerebral homeostatic mechanisms that have been associated with prognosis after aSAH, e.g., BRS (5) and CA (4). The signal recordings analyzed in this study were routinely sampled at 200 Hz frequency and were appropriate for the calculation of xBRS in addition to CA assessment. The fact that signals have been recorded a few years ago have probably not affected the conclusions of this study. Concerning aSAH treatment, it has slightly changed from the guidelines applicable at the time of admission with the most significant change concerning the recommendation for systemic and cardiovascular monitoring to be applied (39).

Limitations

This study has several limitations. First, a relatively limited number of patients were included. In addition, patients were not stratified according to the previous comorbidities. DSA, which is assumed to be the gold standard for detecting the cause of SAH and for the preoperative evaluation of aSAH, was not available in all the included cases. Therefore, in those patients, aSAH had been diagnosed by CT angiography. A small proportion of patients had conservative treatment because of the poor grade SAH. A potentially confounding factor was the younger age of the patients with CV compared to the patients without CV in our study. This could be due to a bias related to the fact that in our study we used the same threshold for velocities to define vasospasm both in the young and old patients, although there is evidence that in older patients, CV is associated with lower velocities (40). However, there are no recommendations to diagnose CV in older patients based on different thresholds. As a consequence of the classic choice we made for similar thresholds for velocities to diagnose CV in younger and older patients, CV could have been underdiagnosed in the older patients. Another potentially confounding factor was a higher ABP in the CV group, which is the expected result of the applied therapeutics. However, it is unlikely that this result has biased the BRS assessment. Indeed, although resetting BRS to adapt to higher ABP values is known to occur in chronically hypertensive patients (41), there is no evidence that a short-term increase in ABP modifies BRS. Our study included mechanically ventilated patients, which could be another potential confounding factor. A previous study has shown that mechanical ventilation can attenuate respiratory arrhythmia and alter BRS (42). However, in this study, there was no significant difference in BRS between mechanically ventilated ($n = 24$) and non-mechanically ventilated patients ($n = 49$). Also, we found that BRS was significantly lower during CV compared to before CV both in patients with CV and mechanical ventilation ($p = 0.016$) and in patients with CV and without mechanical ventilation ($p = 0.001$). Furthermore, the loss of inverse correlation between Mxa and BRS was observed before vasospasm and during vasospasm in patients with CV regardless of mechanical ventilation. Thus, it seems unlikely that the correlation between BRS and CA was biased by mechanical ventilation. This study included sedated and mechanically ventilated patients in whom the main sedation drugs used were propofol and fentanyl. Propofol administration has been reported to reduce sympathetic autonomic outflow and decrease ABP due to its vasodilator effect (43, 44). However, propofol was shown to not significantly change the average HR, based on which BRS is measured (45, 46). As for fentanyl, it was reported that its effect on the autonomic nervous system is highly dose dependent. Our study population was homogeneous in terms of medical procedures and the use of drugs. However, patients have received individually titrated doses of vasopressors, which may alter BRS. Although in our study there was no significant difference in BRS between patients with vasopressors and patients without vasopressors, more studies are needed to assess the impact of vasopressors on the relationship between BRS and CA in patients with aSAH.

CONCLUSION

Inverse correlation between BRS and CA was lost in patients with CV following aSAH. Furthermore, BRS significantly decreased during the days that followed aSAH in patients who developed CV. These findings may have an impact on the prognosis of these patients and need to be investigated in larger multicentric studies.

DATA AVAILABILITY STATEMENT

The raw data supporting the conclusions of this article will be made available by the authors, without undue reservation.

ETHICS STATEMENT

The studies involving human participants were reviewed and approved by research Ethics Committee at Addenbrooke's Hospital (Protocol 29 LREC: 97/291). The patients/participants or their next-of-kin provided written informed consent to participate in this study.

AUTHOR CONTRIBUTIONS

Study concept and design, drafting of the manuscript, and literature search was done by AU, NN, MK, and MB. Figure acquisition was perfomed by AU and NN. Critical revisions were done by AU, NN, MK, PS, MC, KB, MS, and MB. MC, PS, MS, and MB supervised the article. All authors contributed to the article and approved the submitted version.

FUNDING

This work was supported by (National Science Centre, Poland, under the MINIATURA 5 grant, Nr DEC-2021/05/X/ST7/00454 and Foundation for Polish Science FNP) to AU, (Polish National Agency for Academic Exchange under the International Academic Partnerships program) to MK, and (NIHR, Biomedical Research Centre Cambridge, United Kingdom) to MC.

ACKNOWLEDGMENTS

The authors would thank Mr. Adam Pelah for proofreading the article.

REFERENCES

1. Fujii M, Yan J, Rolland WB, Soejima Y, Caner B, Zhang JH. Early brain injury, an evolving frontier in subarachnoid hemorrhage research. *Transl Stroke Res.* (2013) 4:432–46. doi: 10.1007/s12975-013-0257-2
2. Lin CL, Dumont AS, Zhang JH, Zuccarello M, Muroi C. Cerebral vasospasm after aneurysmal subarachnoid hemorrhage: mechanism and therapies. *Biomed Res Int.* (2014) 2014:679014. doi: 10.1155/2014/679014
3. Kolias AG, Sen J, Belli A. Pathogenesis of cerebral vasospasm following aneurysmal subarachnoid hemorrhage: putative mechanisms and novel approaches. *J Neurosci Res.* (2009) 87:1–11. doi: 10.1002/jnr.21823
4. Budohoski KP, Czosnyka M, Smielewski P, Kasprowicz M, Helmy A, Bulters D, et al. Impairment of cerebral autoregulation predicts delayed cerebral ischemia after subarachnoid hemorrhage: a prospective observational study. *Stroke.* (2012) 43:3230–7. doi: 10.1161/STROKEAHA.112.669788
5. Nasr N, Gaio R, Czosnyka M, Budohoski K, Liu X, Donnelly J, et al. Baroreflex impairment after subarachnoid hemorrhage is associated with unfavorable outcome. *Stroke.* (2018) 49:1632–38. doi: 10.1161/STROKEAHA.118.020729
6. Uryga A, Burzyńska M, Tabakow P, Kasprowicz M, Budohoski KP, Kazimierska A, et al. Baroreflex sensitivity and heart rate variability are predictors of mortality in patients with aneurysmal subarachnoid haemorrhage. *J. Neurol. Sci.* (2018) 394:112–9. doi: 10.1016/j.jns.2018.09.014
7. Nasr N, Czosnyka M, Pavy-Le Traon A, Custaud M-A, Liu X, Varsos GV, et al. Baroreflex and cerebral autoregulation are inversely correlated. *Circ J.* (2014) 78:2460–7. doi: 10.1253/circj.CJ-14-0445
8. Fu Q, Okazaki K, Shibata S, Shook RP, Vangunday TB, Galbreath MM, et al. Menstrual cycle effects on sympathetic neural responses to upright tilt. *J Physiol.* (2009) 587:2019–31. doi: 10.1113/jphysiol.2008.168468
9. Moertl MG, Ulrich D, Pickel KI, Klaritsch P, Schaffer M, Flotzinger D, et al. Changes in haemodynamic and autonomous nervous system parameters measured non-invasively throughout normal pregnancy. *Eur J Obstet Gynecol Reprod Biol.* (2009) 144:S179–83. doi: 10.1016/j.ejogrb.2009.02.037
10. Gallo C, Ridolfi L, Scarsoglio S. Cardiovascular deconditioning during long-term spaceflight through multiscale modeling. *Npj Microg.* (2020) 6:1–14. doi: 10.1038/s41526-020-00117-5
11. Bederson JB, Connolly ES, Batjer HH, Dacey RG, Dion JE, Diringer MN, et al. Guidelines for the management of aneurysmal subarachnoid hemorrhage: a statement for healthcare professionals from a special writing group of the stroke council, American heart association. *Stroke.* (2009) 40:994–1025. doi: 10.1161/STROKEAHA.108.191395
12. Francoeur CL, Mayer SA. Management of delayed cerebral ischemia after subarachnoid hemorrhage. *Crit Care.* (2016) 20:277. doi: 10.1186/s13054-016-1447-6
13. Lang EW, Mehdorn HM, Dorsch NWC, Czosnyka M. Continuous monitoring of cerebrovascular autoregulation: a validation study. *J Neurol Neurosurg Psychiatry.* (2002) 72:583–586. doi: 10.1136/jnnp.72.5.583
14. Westerhof BE, Gisolf J, Stok WJ, Wesseling KH, Karemaker JM. Time-domain cross-correlation baroreflex sensitivity: performance on the EUROBAVAR data set. *J Hypertens.* (2004) 22:1–101. doi: 10.1097/01.hjh.0000125439.28861.ed
15. Sykora M, Czosnyka M, Liu X, Donnelly J, Nasr N, Diedler J, et al. Autonomic impairment in severe traumatic brain injury: a multimodal neuromonitoring study. *Crit Care Med.* (2016) 44:1173–81. doi: 10.1097/CCM.0000000000001624
16. Bland M, Altman DG. Statistics notes: calculating correlation coefficients with repeated observations: Part 1–correlation within subjects. *BMJ.* (1995) 310:446. doi: 10.1136/bmj.310.6977.446
17. Bland M, Altman DG. Calculating correlation coefficients with repeated observations: Part 2–correlation between subjects. *BMJ.* (1995) 310:633. doi: 10.1136/bmj.310.6980.633
18. Zhang R, Zuckerman JH, Iwasaki K, Wilson TE, Crandall CG, Levine BD. Autonomic neural control of dynamic cerebral autoregulation in humans. *Circulation.* (2002) 106:1814–20. doi: 10.1161/01.CIR.0000031798.07790.FE
19. Olsen MH, Riberholt CG, Mehlsen J, Berg RMG, Møller K. Reliability validity of the mean flow index (Mx) for assessing cerebral autoregulation in humans: a systematic review of the methodology. *J Cereb Blood Flow Metab.* (2021). doi: 10.1177/0271678X211052588. [Epub ahead of print].
20. Calviere L, Nasr N, Arnaud C, Czosnyka M, Viguier A, Tissot B, et al. Prediction of delayed cerebral ischemia after subarachnoid hemorrhage using cerebral blood flow velocities and cerebral autoregulation assessment. *Neurocrit Care.* (2015) 23:253–8. doi: 10.1007/s12028-015-0125-x
21. Jaeger M, Soehle M, Schuhmann MU, Meixensberger J. Clinical significance of impaired cerebrovascular autoregulation after severe aneurysmal subarachnoid hemorrhage. *Stroke.* (2012) 43:2097–101. doi: 10.1161/STROKEAHA.112.659888
22. Czosnyka M, Smielewski P, Czosnyka Z, Piechnik S, Steiner LA, Schmidt E, et al. Continuous assessment of cerebral autoregulation: clinical and laboratory experience. *Acta Neurochir Suppl.* (2003) 86:581–5. doi: 10.1007/978-3-7091-0651-8_118
23. Soehle M, Czosnyka M, Pickard JD, Kirkpatrick PJ. Continuous assessment of cerebral autoregulation in subarachnoid hemorrhage. *Anesth Analg.* (2004) 98:1133–9. doi: 10.1213/01.ANE.0000111101.41190.99
24. Yundt KD, Grubb RL, Diringer MN, Powers WJ. Autoregulatory vasodilation of parenchymal vessels is impaired during cerebral vasospasm. *J Cereb Blood Flow Metab.* (1998) 18:419–24. doi: 10.1097/00004647-199804000-00010
25. Faes L, Porta A, Rossato G, Adami A, Tonon D, Corica A, et al. Investigating the mechanisms of cardiovascular and cerebrovascular regulation in orthostatic syncope through an information decomposition strategy. *Auton Neurosci Basic Clin.* (2013) 178:76–82. doi: 10.1016/j.autneu.2013.02.013
26. Tzeng Y-C, Lucas SJE, Atkinson G, Willie CK, Ainslie PN. Fundamental relationships between arterial baroreflex sensitivity and dynamic cerebral autoregulation in humans. *J Appl Physiol.* (2010) 108:1162–8. doi: 10.1152/japplphysiol.01390.2009
27. Witter T, Tzeng YC, O'Donnell T, Kusel J, Walker B, Berry M, et al. Inter-individual relationships between sympathetic arterial baroreflex function and cerebral perfusion control in healthy males. *Front Neurosci.* (2017) 11:457. doi: 10.3389/fnins.2017.00457
28. Allhorn M, Bülow M, Hansson L, Ley S, Olsson DL, Schmidtchen ML, et al. Pathological conditions involving extracellular hemoglobin: molecular mechanisms, clinical significance, and novel therapeutic opportunities for alpha(1)-Microglobulin. *Antioxid Redox Signal.* (2012) 17:813. doi: 10.1089/ars.2011.4282
29. Teixeira SC, Madureira JB, Azevedo EI, Castro PM. Ageing affects the balance between central and peripheral mechanisms of cerebrovascular regulation with increasing influence of systolic blood pressure levels. *Eur J Appl Physiol.* (2019) 119:519–29. doi: 10.1007/s00421-018-4036-3
30. Kardos A, Watterich G, Menezes R, de, Csanády M, Casadei B, et al. Determinants of spontaneous baroreflex sensitivity in a healthy working population. *Hypertension.* (2001) 37:911–6. doi: 10.1161/01.HYP.37.3.911
31. Tafil-Klawe M, Klawe J, Majcherczyk S, Trzebski A. Sympatho-inhibitory baroreflex in conscious rabbits: simultaneous recordings of sympathetic and aortic nerve activity. *J Auton Nerv Syst.* (1989) 28:227–32. doi: 10.1016/0165-1838(89)90150-1

32. Schmidt HB, Werdan K, Müller-Werdan U. Autonomic dysfunction in the ICU patient. *Curr Opin Crit Care.* (2001) 7:314–22. doi: 10.1097/00075198-200110000-00002
33. Hilz MJ, Liu M, Roy S, Wang R. Autonomic dysfunction in the neurological intensive care unit. *Clin Auton Res.* (2019) 29:301–11. doi: 10.1007/s10286-018-0545-8
34. Benghanem S, Mazeraud A, Azabou E, Chhor V, Shinotsuka CR, Claassen J, et al. Brainstem dysfunction in critically ill patients. *Crit Care.* (2020) 24:1–14. doi: 10.1186/s13054-019-2718-9
35. Bisognano JD, Bakris G, Nadim MK, Sanchez L, Kroon AA, Schafer J, et al. Baroreflex activation therapy lowers blood pressure in patients with resistant hypertension results from the double-blind, randomized, placebo-controlled rheos pivotal trial. *J Am Coll Cardiol.* (2011) 58:765–73. doi: 10.1016/j.jacc.2011.06.008
36. Wachter R, Abraham WT, Lindenfeld J, Weaver FA, Zannad F, Wilks S, et al. Positive effects of baroreflex activation therapy in heart failure with reduced ejection fraction are independent of baseline blood pressure. *Eur Heart J.* (2017) 38:ehx502.P1475. doi: 10.1093/eurheartj/ehx502.P1475
37. Varsos GV, Budohoski KP, Czosnyka M, Kolias AG, Nasr N, Donnelly J, et al. Cerebral vasospasm affects arterial critical closing pressure. *J Cereb Blood Flow Metab.* (2015) 35:285–91. doi: 10.1038/jcbfm.2014.198
38. Papaioannou VE, Budohoski KP, Placek MM, Czosnyka Z, Smielewski P, Czosnyka M. Association of transcranial doppler blood flow velocity slow waves with delayed cerebral ischemia in patients suffering from subarachnoid hemorrhage: a retrospective study. *Intensive Care Med Exp.* (2021) 9:1–17. doi: 10.1186/s40635-021-00378-8
39. Diringer MN, Bleck TP, Hemphill JC, Menon D, Shutter L, Vespa P, et al. Critical care management of patients following aneurysmal subarachnoid hemorrhage: recommendations from the neurocritical care society's multidisciplinary consensus conference. *Neurocrit Care.* (2011) 15:211–40. doi: 10.1007/s12028-011-9605-9
40. Torbey MT, Hauser TK, Bhardwaj A, Williams MA, Ulatowski JA, Mirski MA, et al. Effect of age on cerebral blood flow velocity and incidence of vasospasm after aneurysmal subarachnoid hemorrhage. *Stroke.* (2001) 32:2005–11. doi: 10.1161/hs0901.094622
41. Mussalo H, Vanninen E, Ikäheimo R, Laitinen T, Laakso M, Länsimies E, et al. Baroreflex sensitivity in essential and secondary hypertension. *Clin Auton Res.* (2002) 12:465–71. doi: 10.1007/s10286-002-0069-z
42. Van De Louw A, Médigue C, Papelier Y, Cottin F. Breathing cardiovascular variability and baroreflex in mechanically ventilated patients. *Am J Physiol Regul Integr Comp Physiol.* (2008) 295:R1934–40. doi: 10.1152/ajpregu.90475.2008
43. Cullen PM, Turtle M, Prys-Roberts C, Way WL, Dye J. Effect of propofol anesthesia on baroreflex activity in humans. *Anesth Analg.* (1987) 66:1115–20. doi: 10.1213/00000539-198711000-00008
44. Chen Z, Purdon PL, Harrell G, Pierce ET, Walsh J, Brown EN, et al. Dynamic assessment of baroreflex control of heart rate during induction of propofol anesthesia using a point process method. *Ann Biomed Eng.* (2011) 39:260–76. doi: 10.1007/s10439-010-0179-z
45. Ebert TJ. Sympathetic and hemodynamic effects of moderate and deep sedation with propofol in humans. *Anesthesiology.* (2005) 103:20–4. doi: 10.1097/00000542-200507000-00007
46. Dorantes Mendez G, Aletti F, Toschi N, Canichella A, Dauri M, Coniglione F, et al. Baroreflex sensitivity variations in response to propofol anesthesia: comparison between normotensive and hypertensive patients. *J Clin Monit Comput.* (2013) 27:417–26. doi: 10.1007/s10877-012-9426-1

Conflict of Interest: MC and PS are authors of ICM+ software. They have a financial interest in a part of the licensing fee for ICM + distributed by Cambridge Enterprise Ltd., UK.

The remaining authors declare that the research was conducted in the absence of any commercial or financial relationships that could be construed as a potential conflict of interest.

Publisher's Note: All claims expressed in this article are solely those of the authors and do not necessarily represent those of their affiliated organizations, or those of the publisher, the editors and the reviewers. Any product that may be evaluated in this article, or claim that may be made by its manufacturer, is not guaranteed or endorsed by the publisher.

frontiers in Neurology

ORIGINAL RESEARCH
published: 13 January 2022
doi: 10.3389/fneur.2021.757050

Vascular Reactivity to Hypercapnia Is Impaired in the Cerebral and Retinal Vasculature in the Acute Phase After Experimental Subarachnoid Hemorrhage

*Laura Warner[1], Annika Bach-Hagemann[1], Walid Albanna[2], Hans Clusmann[2], Gerrit A. Schubert[2,3], Ute Lindauer[1,2] and Catharina Conzen-Dilger[2]**

[1] Translational Neurosurgery and Neurobiology, Department of Neurosurgery, Medical Faculty, RWTH Aachen University, Aachen, Germany, [2] Department of Neurosurgery, Medical Faculty, RWTH Aachen University, Aachen, Germany, [3] Department of Neurosurgery, Kantonsspital Aarau, Aarau, Switzerland

OPEN ACCESS

Edited by:
Xiuyun Liu,
Johns Hopkins University,
United States

Reviewed by:
Patrick Schuss,
Unfallkrankenhaus Berlin, Germany
Ayhan Kanat,
Recep Tayyip Erdoğan University, Turkey

***Correspondence:**
Catharina Conzen-Dilger
cconzen@ukaachen.de

Specialty section:
This article was submitted to Stroke, a section of the journal Frontiers in Neurology

Received: *11 August 2021*
Accepted: *22 November 2021*
Published: *13 January 2022*

Citation:
Warner L, Bach-Hagemann A, Albanna W, Clusmann H, Schubert GA, Lindauer U and Conzen-Dilger C (2022) Vascular Reactivity to Hypercapnia Is Impaired in the Cerebral and Retinal Vasculature in the Acute Phase After Experimental Subarachnoid Hemorrhage. Front. Neurol. 12:757050. doi: 10.3389/fneur.2021.757050

Objective: Impaired cerebral blood flow (CBF) regulation, such as reduced reactivity to hypercapnia, contributes to the pathophysiology after aneurysmal subarachnoid hemorrhage (SAH), but temporal dynamics in the acute phase are unknown. Featuring comparable molecular regulation mechanisms, the retinal vessels participate in chronic and subacute stroke- and SAH-associated vessel alterations in patients and can be studied non-invasively. This study is aimed to characterize the temporal course of the cerebral and retinal vascular reactivity to hypercapnia in the acute phase after experimental SAH and compare the potential degree of impairment.

Methods: Subarachnoid hemorrhage was induced by injecting 0.5 ml of heparinized autologous blood into the cisterna magna of male Wistar rats using two anesthesia protocols [isoflurane/fentanyl $n = 25$ (Sham + SAH): Iso—Group, ketamine/xylazine $n = 32$ (Sham + SAH): K/X—Group]. CBF (laser speckle contrast analysis) and physiological parameters were measured continuously for 6 h. At six predefined time points, hypercapnia was induced by hypoventilation controlled *via* blood gas analysis, and retinal vessel diameter (RVD) was determined non-invasively.

Results: Cerebral reactivity and retinal reactivity in Sham groups were stable with only a slight attenuation after 2 h in RVD of the K/X—Group. In the SAH Iso—Group, cerebral and retinal CO_2 reactivity compared to baseline was immediately impaired starting at 30 min after SAH (CBF $p = 0.0090$, RVD $p = 0.0135$) and lasting up to 4 h ($p = 0.0136$, resp. $p = 0.0263$). Similarly, in the K/X—Group, cerebral CO_2 reactivity was disturbed early after SAH (30 min, $p = 0.003$) albeit showing a recovery to baseline after 2 h while retinal CO_2 reactivity was impaired over the whole observation period (360 min, $p = 0.0001$) in the K/X—Group. After normalization to baseline, both vascular beds showed a parallel behavior regarding the temporal course and extent of impairment.

Conclusion: This study provides a detailed temporal analysis of impaired cerebral vascular CO_2 reactivity starting immediately after SAH and lasting up to 6 h. Importantly, the retinal vessels participate in these acute changes underscoring the promising role of the retina as a potential non-invasive screening tool after SAH. Further studies will be required to determine the correlation with functional outcomes.

Keywords: aneurysmal subarachnoid hemorrhage, acute phase, autoregulation, microvascular function, hypercapnia, retinal vessel analysis

INTRODUCTION

Aneurysmal subarachnoid hemorrhage (SAH) frequently leads to poor neurological outcomes with a high case fatality rate (1). Pathophysiological processes are complex, start early, and evolve with time, frequently causing neurological deterioration (delayed cerebral ischemia, DCI) and/or cerebral infarction with a typical delay time of 2 week after bleeding. The latest research identifies—among other factors, such as early brain injury, inflammation, microthrombosis, cortical spreading depolarization, and vasospasm—microcirculatory dysfunction with disturbance of cerebral blood flow (CBF) regulation as one of the driving mechanisms (2–5). The maintenance of a stable CBF is crucial for physiological brain function. To date, there are three key mechanisms specified: cerebral autoregulation (blood pressure-dependent cerebral vessel reaction), neurovascular coupling (local CBF regulation due to neuronal activity), and cerebrovascular reactivity to carbon dioxide (CO_2) partial pressure [maintaining central pH and respiratory drive (6, 7)]. CO_2 elevation (hypercapnia) in particular leads to strong vasodilatation in healthy brain tissue causing a "wash out" effect (6). For all three CBF regulation mechanisms, growing experimental (8–12) and clinical evidence of profound changes exist early and late after SAH, which are associated with the development of DCI and poor neurological outcome (2, 13). However, experimental data for the acute phase after SAH, where the complex pathophysiologic cascades accelerate, are scarce. Balbi et al. demonstrated a complete loss of CO_2 reactivity 3 and 24 h after SAH in mice (8, 9) and similarly, Friedrich et al. demonstrated that cerebral arterioles were non-reactive to CO_2 elevation at the same time points in rats after SAH (11). However, a detailed temporal profile of the CO_2 reactivity as a key regulator early after SAH is still missing.

Assessment of CBF regulation after SAH in patients is still a diagnostic challenge that requires invasive and time-consuming diagnostic tools and algorithms (14) precluding this promising approach for most clinicians. As an embryologically original part of the central nervous system, the retina shares important features with the brain in morphology, vascular function, and pathophysiology (15). Furthermore, the retina and the brain both feature the three blood flow regulation mechanisms autoregulation, neurovascular coupling, and reactivity to CO_2 elevation (16). In contrast to the brain, a considerable advantage is the comparatively easy diagnostic assessment of retinal vasculature and reactivity; new techniques, such as retinal vessel analysis, provide non-invasive and bedside direct insights on the retinal microcirculation and vasculature. Several studies report a link between retinal pathologies and neurodegenerative or cerebrovascular diseases raising expectations for a "window to the brain" (17). It has been shown that the retina participates in chronic cerebrovascular changes observed in patients with different types of dementia [for review (15)] and patients with suspected cerebral small vessel disease causing acute lacunar strokes (18). Subacute retinal changes up to 1 week following ischemic stroke (19) have also been reported. Furthermore, we recently presented the first clinical evidence of retinal vasculature changes after aneurysmal SAH. Days after SAH, retinal arteries were constricted, and neurovascular coupling was impaired compared to healthy controls. These changes were reversible in parts 3 mo after SAH indicating a time-dependent process of the observed alterations (20–22).

However, it is unclear whether these changes occur directly after SAH in the acute phase, which is substantially important to the further course of the disease. Also, it remains to be determined whether there is a correlation between the extent of pathophysiologic changes of cerebral vasculature and retinal vasculature, an indispensable requirement for the usability of retinal vascular assessment as a surrogate for cerebral circulation. As a diagnostic assessment in the acute prehospital phase is not feasible in patients and further a simultaneous assessment of retinal and cerebrovascular changes would acquire an immense and invasive effort, these questions were transferred from bed to bench side in a translational approach.

Therefore, the aim of this study was first to characterize the time course of vascular reactivity to hypercapnia in the important acute phase after experimental SAH. Second, cerebral vasculature and retinal vasculature were simultaneously assessed to investigate the comparability of the retinal alterations in the acute alterations. Finally, the extension of disturbance of the cerebral and retinal reactivity was compared.

METHODS

Animals

All experiments were performed in compliance with the German Animal Welfare Act and the EU Directive 2010/63. The study was approved by the national state authorities (LANUV, Recklinghausen, Germany, file reference: 84-02.04.2015.A412).

Fifty-seven male Wistar rats weighing between 314 ± 19 g (Janvier Labs, Le Genest-Saint-Isle, France) were used. The animals were kept in the animal facility of the Institute of Laboratory Animal Science of the University Hospital Aachen

(quality management certified according to ISO9001:2015) in 2000P type cages with water and food available ad libitum (V1534-300, Ssniff, Soest, Germany). The light-dark cycle was set at 12 h (07:00–19:00). Room temperature was kept constant at 22 ± 2°C and humidity at 55 ± 5%. Health monitoring of animals was carried out according to the Federation of European Laboratory Animal Science Associations (FELASA) recommendations (23).

To allow the animals to sufficiently acclimate to the new environment, they underwent a 7-day adaptation period. The care and health control during the adaptation phase was performed by the animal caretakers of the Institute of Laboratory Animal Science of the University Hospital of RWTH Aachen.

Animal Preparation and Monitoring

Surgical preparation and monitoring were conducted by the same surgeon and performed as previously described (10, 24).

Surgery started at around 8 a.m. Briefly, anesthesia was induced by isoflurane, and the animal was placed in a supine position on a heating plate to maintain a constant body temperature (BT) of 37 ± 0.5°C. Ropivacaine (Ropivacaine hydrochloride, 2 mg/ml, Fresenius Kabi, Bad Homburg, Germany) as local anesthesia was used before each skin incision. After tracheotomy for artificial ventilation, femoral artery and vein were cannulated on one side for continuously measuring arterial blood pressure (ABP) and applying intravenous (i.v.) medication, respectively. Heart rate and oxygen saturation were monitored by pulse oximetry, and blood gas analyses were performed regularly. For CBF measurement, a closed cranial window was created by thinning out the bone with a drill under constant cooling over the right parietal cortex (12 × 5 mm, the center of the window ∼8 mm caudal and 2.5 mm lateral of bregma). Afterward, anesthesia was changed to ketamine/xylazine (ketamine, K: 20 mg/kg/h, xylazine, X: 2 mg/kg/h) *via* continuous i.v. infusion for the K/X—Group. For the isoflurane/fentanyl group (Iso—Group), anesthesia with isoflurane and fentanyl (0.02 mg/kg/h) was continued. Additionally, both groups received a muscle relaxant to prevent involuntary eye movements (K/X—Group: Vecuronium i.v. 7.8 mg/kg/h, Iso—Group: Pancuronium bromide i.p. 1.5 mg/kg every 2 h). Two small craniotomies were performed for EEG measurement and cisterna magna blood injection. Continuous intracranial pressure (ICP) measurement was implemented *via* a needle inserted in the cisterna magna through the atlanto-occipital membrane.

For SAH induction, 0.5 ml of heparinized autologous blood, withdrawn from the femoral artery catheter, was injected over 1 min into cisterna magna as previously described (10). Sham animals underwent the same procedure as SAH animals except for the blood injection. ABP, EEG, and ICP were measured and recorded continuously during the whole observation period (starting 30 min pre-SAH for baseline record and continued until 6 h after SAH). At the end of the observation period after 6 h, the animals were sacrificed in deep anesthesia by i.v. injection of potassium chloride (2.5 M). Brains were removed, inspected, and documented for successful SAH induction.

Experimental Design

Anesthetic Protocols and Group Design

As isoflurane is a potent vasodilator by itself and has been reported to increase the retinal blood flow by 29% (25), the experiments were performed following two established anesthetic protocols: isoflurane/fentanyl (Iso—Group) and ketamine/xylazine (K/X—Group) summing up in 4 groups: Iso—Group Sham, Iso—Group SAH, K/X—Group Sham, and K/X—Group SAH (**Figure 2**). With this approach, we were able to analyze cerebral and retinal blood flow reactions to hypercapnia starting from two different base levels in health and disease. Sample size calculation was performed by *a priori* power analysis (G*Power 3.1.7) with alpha = 0.05 and power (1-beta) = 0.80, based on previous experience with comparable study design. Twenty-five animals were included in the Iso—Group (Sham $n = 9$; SAH $n = 16$). In the K/X—Group, 32 animals were included (Sham $n = 16$, SAH $n = 16$; **Figure 2**). Experiments of the Iso—Group were performed first, followed by K/X—Group with randomization between Sham and SAH in this group only.

CBF—Recording

Cerebral blood flow was measured, recorded, and evaluated as previously described (10). Briefly, animals were placed in a prone position under a prototype superficial tissue imaging system (STIS, Biomedical Optics Laboratory, RheinAhrCampus, Remagen, Germany). Data processing was performed offline. CBF was calculated from raw images of laser speckle contrast within a region of interest positioned over the somatosensory cortex at an area of microcirculation devoid of larger pial vessels (**Figure 1**). For CBF analysis, an initial baseline was recorded for 5 min with the further course of CBF normalized to this baseline. The increase during the triggered hypercapnia was calculated as the percentage change from the respective actual baseline immediately before the hypercapnic phase.

Retinal Vessel Diameter (RVD)—Recording

To measure the RVD at selected time points, the camera system RCrodent from Imedos (IMEDOS Systems UG, Jena, Germany) was used for dynamic vessel analysis. To dilate the pupil, a mydriatic (Pharma Stulln GmbH, Stulln, Germany) was applied to the left eye, and a lens (Ocular Instruments, Bellevue, WA, USA) was positioned in front of the eye using a micromanipulator. The eye was regularly moistened with a transparent protective gel to avoid dehydration of the cornea. Illumination (530 nm) was set to a maximum of 30 lux. Videos of the retinae were recorded over a 9-min period (1 min baseline, 5 min hypercapnia, and 3 min regression phase). Vessel dilations were calculated offline. From each video sequence, four to eight arterial vessels were selected with a mean distance from the optic nerve head (ONH) of 2.5 × ONH plexus diameters, and diameter analysis (expressed in arbitrary units) was automatically performed by the commercial RCrodent Imedos-software (**Figure 1**). In each animal, the artery with the best reactivity at baseline was selected for subsequent analysis at later time points in Sham or after SAH. Due to variations in the quality of the fundus recordings between the subsequent hypercapnia periods, it was not always possible to

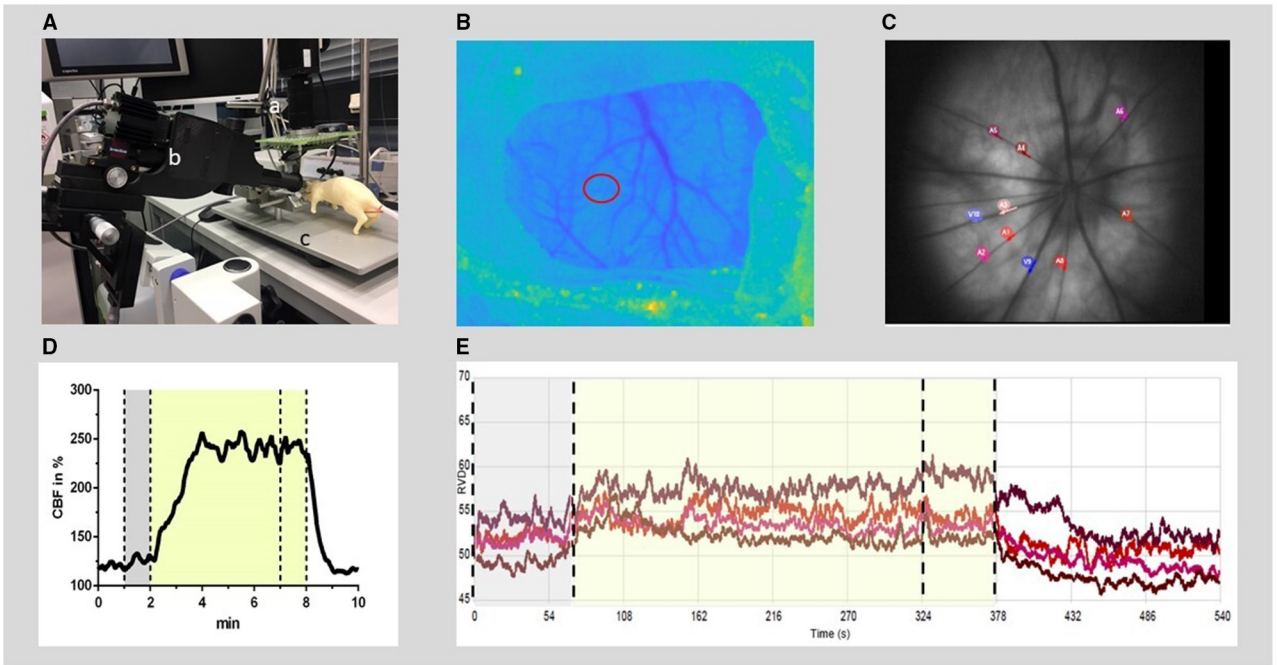

FIGURE 1 | Experimental setup for RVD and CBF recording and offline analysis. **(A)** Experimental setup: the rat (dummy rat used for illustration) was positioned in a stereotactic frame (c) under a superficial tissue imaging system (a) and CBF was calculated from continuously recorded raw images of laser speckle contrast. A retinal vessel analyzer (b) was positioned in front of the left eye. RVDs were recorded intermittently during hypercapnia challenges induced by hypoventilation. **(B)** Anatomical image at the cranial window (thinned bone) with the region of interest for CBF time course calculation (red circle). **(C)** Example of a fundus image: 4–8 arteries were selected (red and purple circles) for offline analysis of RVD from each video sequence. **(D)** Typical time course of CBF during the hypercapnic period at baseline. **(E)** Example of diameter analysis of retinal vessels at baseline, performed by the commercial RCrodent Imedos- software. **(D,E)** The time period of hypercapnia is marked by the transparent yellow area, dotted lines indicate the recording period used for baseline (gray) and hypercapnic response calculation, respectively. RVD, retinal vessel diameter; CBF, cerebral blood flow.

record from identical vessel segments within each experiment over time. Reactivity to hypercapnia was expressed as percentage change from the individual baseline preceding each period of hypercapnia.

Hypercapnia

To evaluate the reactivity of cerebral and retinal vasculature to CO_2 elevation, hypercapnia challenges were performed at several predefined time points: at baseline before SAH, and 30, 60, 120, 240, and 360 min after SAH, respectively, after the start of the 360 min recording period in Sham animals. Cerebral vasoreactivity and retinal vasoreactivity to hypercapnia were measured simultaneously in each animal. Measurements of RVD were exclusively performed at these time points, while measurement of CBF, EEG, ICP, and ABP was continuously recorded. Before each hypercapnia challenge, an arterial blood gas analysis was performed to document pCO_2 and pO_2. Each hypercapnia period lasted 9 min, after 1 min of measuring under physiological conditions, hypoventilation was started by reducing the respiratory rate by 20 breaths/min to induce hypercapnia. To prevent hypoxia, the O_2 supply was simultaneously increased. After 4 min, blood gas analysis was performed again to verify the CO_2 elevation. One minute later, the respiratory rate was increased back to normoventilation, followed by another 3 min of recording of the recovery phase of the vessels.

Statistical Analysis

For statistical analysis and graph design, GraphPad Prism (versions 9.1.1 and 9.1.2) was used. Data were tested for normal distribution *via* the Shapiro-Wilk test or Kolmogorov-Smirnov test. Statistical comparisons within each group against baseline were performed by 2-Way-ANOVA or mixed-model-ANOVA, if data points were missing, with time as the dependent factor and treatment (Iso—Group Sand SAH, K/X—Group Sham and SAH) as the independent factor, followed by Dunnett's multiple comparisons test and by Sidak's test for comparison of CBF with RVD reactivity, respectively. For comparison of vascular reactivity to CO_2 elevation between retinal and cerebral vasculature in each group, reactivity was normalized to baseline for each group and vascular bed, respectively. In rare cases of comparably small reactivity at baseline, the normalization procedure may result in a disproportional and thus erroneously high percentage change even when only small changes of the original data occurred. Therefore, after normalization, Grubbs test with $p < 0.01$ was performed to identify outliers: Nine outliers out of 234 data points were removed as suggested by the test (0 of 36 in Iso-CBF, 3 of 36 in Iso-RVD, 2 of 78 in K/X-CBF,

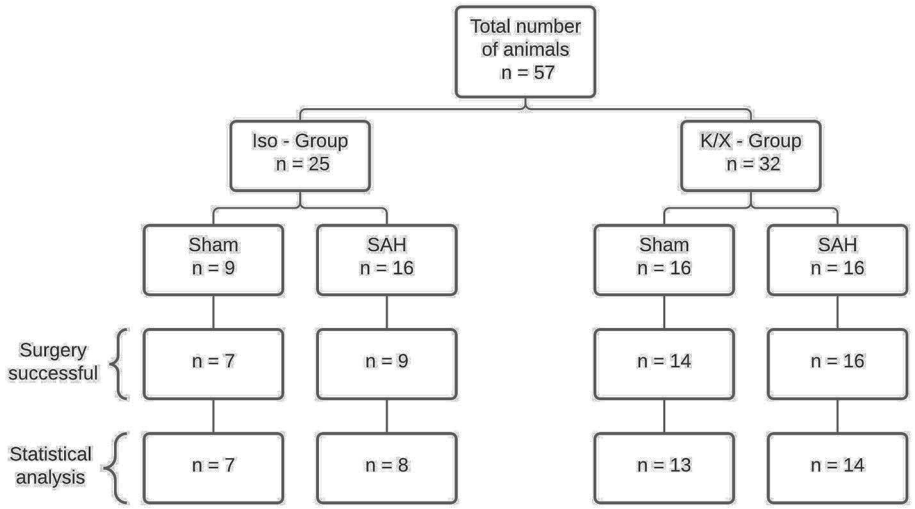

FIGURE 2 | Diagram of sample size distribution. A total of $n = 57$ animals were allocated to two different anesthesia groups. Within the group, a distinction was made between Sham and SAH. A total of 42 animals were included for statistical analysis. Reasons for exclusion were death during surgery ($n = 11$), failed SAH induction ($n = 3$), and uncontrollable bleeding from the surgery wound at the cranial window with distortion of CBF measurement ($n = 1$); SAH, subarachnoid hemorrhage; Iso, isoflurane; K/X, ketamine/xylazine.

and 4 of 84 in K/X-RVD). The same test to identify outliers performed on the original (not-normalized) data set did not suggest excluding any data. Data written in the text are presented as median [first quartile to the third quartile]. In the figures, data are presented as boxplots with median and 25 and 75% percentile as boxes and data range as whiskers (**Figures 3**, **4**) or as median as symbol and 25 and 75% percentile as whiskers (**Figure 5**). A $p < 0.05$ was considered as significantly different.

RESULTS

Animals and ICP and CBF Courses in SAH Groups

A total of 57 rats were randomly assigned to two different anesthetic groups. For data analysis, the following criteria had to be fulfilled to ensure successful SAH induction: increase in ICP and/or drop in CBF, and assessment of brains after SAH. A total of $n = 15$ animals were excluded for death during surgery ($n = 11$), failed SAH induction ($n = 3$), and uncontrollable bleeding from the surgery wound at the cranial window with distortion of CBF measurement ($n = 1$; **Figure 2**). The ICP showed the typical course known from other studies of the group (10, 24), presenting a high peak at the end of the 1 min blood-injection period, followed by a moderate, yet still significantly elevated plateau phase throughout the observation period (except for ICP in Iso—Group at 360 min), with no significant difference between both anesthesia protocols (**Supplementary Figure 1A**). With CBF starting from the baseline of 100%, after a transient severe drop to ischemic values at the time of the ICP peak (Iso—Group SAH: 6.1% [5.5–14.6], $p < 0.0001$; K/X—Group SAH: 9.3% [7.2–21.8], $p < 0.0001$; no significant difference between groups), CBF reached normal values again within 15 min in the K/X—Group and within 60 min in the Iso—Group, respectively. Further-on, a slight albeit significant hyperemia was detectable at 240 min (129.2% [116.6–137.6], $p = 0.0198$) and 360 min [136.3% [124.0–146.9], $p = 0.0310$) in K/X—Group, whereas a mild decrease in CBF occurred at the end of the measurement under Iso-anesthesia (70.8 [62.2–83.4], $p = 0.0101$). Significant differences occurred between both anesthesia protocols at 30 min ($p = 0.0464$) and 360 min ($p = 0.0016$; **Supplementary Figure 1B**).

Physiological Parameters

Arterial blood gas analyses (BGA; pO_2, pCO_2, pH), mean ABP, heart rate (HR), O_2 saturation (SpO_2), and BT remained within physiological ranges throughout the measurement (except for blood gases during hypercapnia; **Table 1**). While comparing the data at baseline with the data at the end of the measurement for each parameter, a slight but significant reduction in ABP occurred in the Iso-SAH-group ($p = 0.047$) and the K/X-Sham-group ($p = 0.0242$). The reduced values are still well above the lower limit of pressure autoregulation, therefore an impact on vascular reactivity to hypercapnia can be ruled out.

Verification of Hypercapnia

During hypoventilation, there was a significant increase of pCO_2 compared to baseline values in both SAH and Sham groups (K/X—Group: Sham 41.3 mmHg [20.2–44.4] vs. 57.1 mmHg [30.3–57.1], $p < 0.0001$, SAH 40.3 mmHg [34.5–44.6] vs. 60.3 mmHg [49.4–68.2], $p < 0.0001$, Iso—Group: Sham 39.7 mmHg [36.2–43.8] vs. 56.4 mmHg [50.8–65.6], $p < 0.0001$, SAH 36.0 mmHg [30.9–39.3] vs. 53.5 mmHg [48.0–61.9], $p < 0.0001$), with no difference in CO_2 elevation between groups. In the Iso—Group, the pO_2 remained stable (Sham 131.7 mmHg [108.0–150.8] vs. 128.3 mmHg [109.7–152.6], SAH 119.8 mmHg [103.4–140.9] vs. 132.2 mmHg [104.2–150.0]), whereas it was increased

TABLE 1 | Physiological parameters at baseline and after 6 h.

	Iso—Group, baseline		K/X—Group, baseline	
	Sham	**SAH**	**Sham**	**SAH**
pO_2 (mmHg):	151 [130–166]	140 [125–141]	107 [103–130]	129 [109–157]
pCO_2 (mmHg)	38.6 [28.2–40.4]	35.4 [32.3–42.8]	40.5 [36.8–46.3]	39.1 [33.8–46.3]
pH:	7.38 [7.37–7.40]	7.39 [7.37–7.40]	7.37 [7.33–7.39]	7.38 [7.36–7.42]
ABP (mmHg):	74 [63–83]	90 [70–104]*	89 [78–97]$^{+}$	83 [76–93]
BT (°C):	37.3 [37.0–37.5]	37.4 [36.9–37.4]$^{\#}$	37.8 [37.3–37.9]$^{\#}$	37.4 [37.0–37.6]
HR (bpm):	337 [311–359]	379 [346–420]	344 [305–405]	354 [305–429]
SpO_2 (%):	99 [99–99]	99 [99–99]	99 [99–99]	99 [99–99]
	Iso—Group, 6 h		**K/X—Group, 6 h**	
	Sham	**SAH**	**Sham**	**SAH**
pO_2 (mmHg):	145 [116–161]	145 [106–186]	132 [114–142]	124 [114–146]
pCO_2 (mmHg)	35.4 [31.7–39.4]	37.2 [34.0–38.3]	41.9 [39.4–44.5]	41.3 [37.1–45.6]
pH:	7.36 [7.33–7.38]	7.38 [7.37–7.39]	7.36 [7.34–7.37]	7.36 [7.35–7.39]
ABP (mmHg):	74 [69–78]	76 [70–81]*	82 [70–85]$^{+}$	77 [73–83]
BT (°C):	37.5 [37.3–37.5]	37.2 [37.0–37.6]	37.3 [37.1–37.7]	37.5 [37.2–37.7]
HR (bpm):	347 [331–363]	349 [306–369]	367 [332–419]	319 [295–347]
SpO_2 (%):	99 [99–99]	99 [99–99]	99 [99–99]	99 [99–99]

*All parameters remained within physiological ranges during the measuring period. ABP, mean arterial blood pressure; BT, body temperature; HR, heart rate in beats per minute; SpO_2, systemic oxygen saturation; *,$^{+}$ $p < 0.05$ for bl vs. 6 h in the respective group; $^{\#}p < 0.05$ between respective groups at baseline.*

significantly in the K/X—Group (Sham 120.9 mmHg [106.8–140.39] vs. 155.8 mmHg [133.4–180.1], $p < 0.0001$, SAH 117.2 mmHg [103.6–139.3] vs. 147.8 mmHg [133.1–167.2], $p < 0.0001$; **Figure 3**).

Cerebral Vascular Reactivity to Hypercapnia

In both anesthetic protocols, cerebral CO_2 reactivity in Sham-operated animals was stable over the observation period (**Supplementary Figure 2**).

In the Iso—Group SAH, cerebral CO_2 reactivity was immediately impaired compared to baseline starting at 30 min after blood injection (baseline 55.2% [50.2–84.7] vs. 30 min 1.8% [−5.8–10.5], $p = 0.0090$) and lasting up to 240 min (240 min 7.3 % [−1.8–30.9], $p = 0.0136$). In the K/X—Group SAH, impairment of cerebral CO_2 reactivity was comparable, however, with a faster recovery compared to Iso anesthesia. CO_2 response was significantly impaired up to 120 min compared to baseline (baseline 38.5% [19.9–55.4] vs. 30 min 1.1% [−11.8–10.1], $p = 0.0003$; 120 min 14.0% [7.1–21.0], $p = 0.0469$; **Figure 4**).

Retinal Vascular Reactivity to Hypercapnia and Analysis of Resting Diameters

Retinal CO_2 reactivity in Sham-operated animals was stable over the observation period with a slight albeit significant increase of CO_2 reaction in the K/X—Group after 120 min.

Following SAH, similar to the cerebral vasculature, an impaired vascular reactivity to CO_2 of the retinal vasculature was observed in both anesthesia groups. Under isoflurane, retinal vasculature showed disturbed CO_2 reactivity during hypercapnia, even with a tendency toward vasoconstriction immediately after SAH (baseline 15.5% [9.6–19.9] vs. 30 min −0.4% [−1.4–1.1], $p = 0.0135$), and a reduced response lasting up to 240 min compared to baseline (240 min 3.9% [−1.9–8.6], $p = 0.0263$). In the K/X—Group SAH, retinal CO_2 reactivity was significantly impaired over the whole observation period compared to baseline (baseline 13.43% [9.0–20.7] vs. 30 min 3.8% [0.1–6.4], $p < 0.0001$, vs. 360 min 4.5% [2.0–7.2], $p = 0.0001$; **Figure 4**).

For the cerebral circulation, it is known from this and our previous studies (10, 24) that with isoflurane anesthesia strong hypoperfusion occurs up to 2 h after SAH induction in this model. We, therefore, compared the resting diameters of the retinal vessels (in arbitrary units), taken directly before the hypercapnic challenges, at baseline with each time point thereafter in Sham or SAH. The diameters remained stable over the observation period in Sham and, in contrast to the known changes in CBF, we did not detect a significant change after SAH either (**Supplementary Figure 3**).

Comparison of Vascular Reactivity to CO_2 Elevation Between Retinal and Cerebral Vasculature

Retinal and cerebral reactivity to hypercapnia was compared to assess whether they are comparably affected (**Figure 5**). For this purpose, reactivity was normalized to baseline for each group and vascular bed, respectively. In the Iso—Group, reactivity to hypercapnia in both cerebral and retinal vasculature was comparably and strongly disturbed up to 360 min after SAH induction, with a transient recovery of the retinal but not of the cerebral vasculature at 120 min. Under K/X anesthesia, the reactivity to hypercapnia in both the cerebral and retinal vasculature was again at least transiently disturbed up to 120 min after SAH induction. Retinal hypercapnia response remained persistently impaired, whereas reactivity in the cerebral circulation transiently recovered at 60 min ($p = 0.1894$), was impaired again at 120 min ($p = 0.0064$), and permanently recovered thereafter until the end of the measurement phase. While comparing retinal with cerebral reactivity at each time point in each group, no statistically significant difference was observed.

DISCUSSION

Our experimental study on vascular reactivity to hypercapnia in the acute phase of SAH documents an immediate and pronounced disturbance of this key component of blood flow regulation both in the cerebral and the retinal vasculature. After

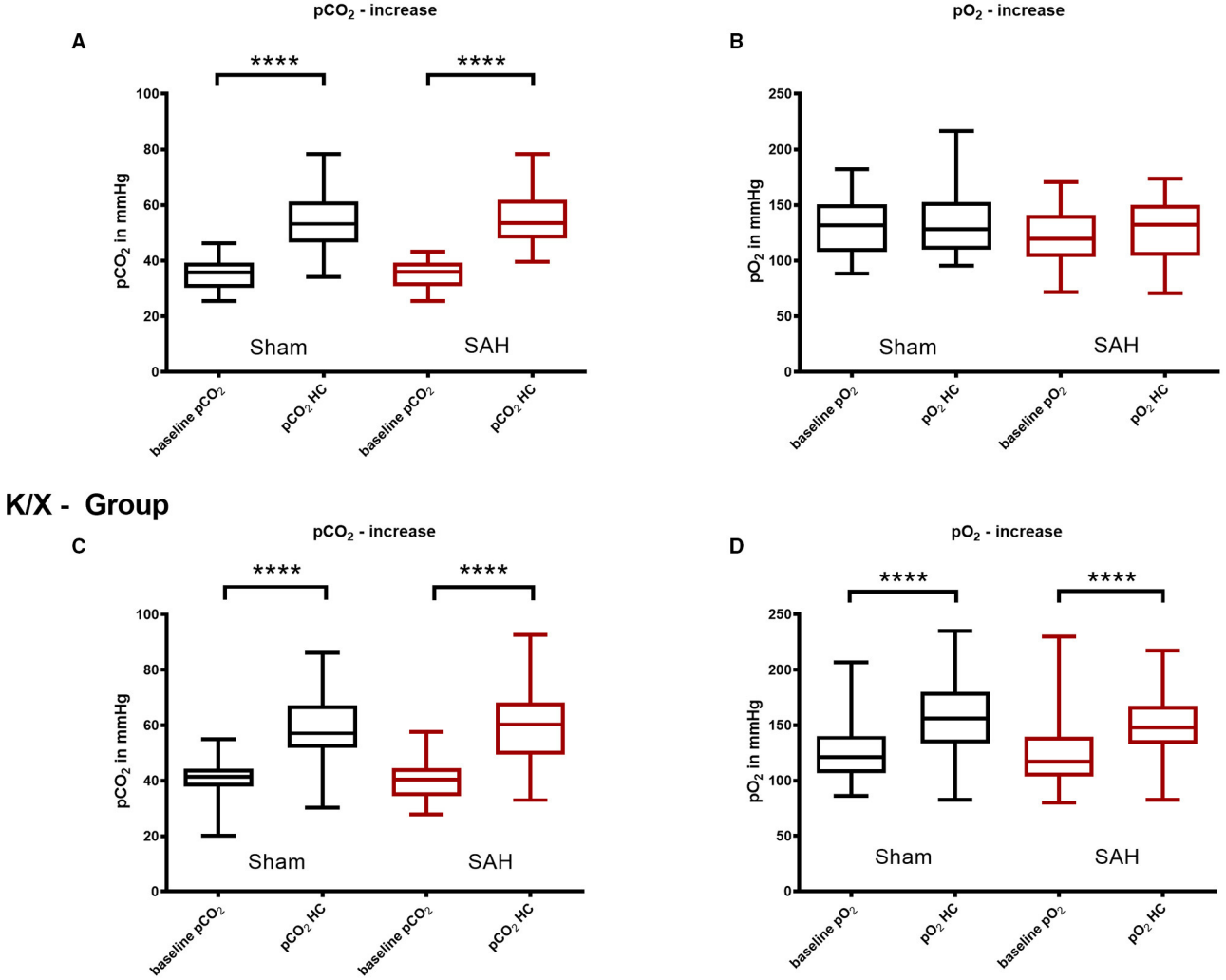

FIGURE 3 | Arterial pCO_2 and pO_2 analysis in hypercapnia periods. Blood gas analysis was performed before and during hypercapnia. In the Iso—Group there was a significant pCO_2 increase during hypercapnia **(A)**, while pO_2 did not change significantly **(B)**; during hypercapnia, both pCO_2 **(C)** and pO_2 **(D)** increased significantly in the K/X—Group; SAH, subarachnoid hemorrhage; Iso, isoflurane; K/X, ketamine/xylazine; HC, hypercapnia; boxes show median and 25 and 75% percentile and whiskers show data range; ****$p < 0.0001$.

SAH, the disturbance was observed as early as 30 min after induction and lasted for several hours in both compartments indicating the participation of the retinal vasculature in acute pathophysiologic alterations primarily affecting the brain. Notably, after normalization to baseline, not only a simultaneous and parallel behavior of both vascular beds but also a comparable extent of impairment could be observed. Additionally, we found that the two different anesthetic protocols neither influence the extent of impaired hypercapnia reactivity nor the temporal pattern except for a faster recovery of CBF in the K/X group.

Previous studies on the hypercapnia reactivity in the acute phase after experimental SAH also reported a significant impairment, albeit with a larger extent of disturbance: Friedrich et al. found that after SAH, the pial and cortical tissue microcirculation were non-reactive to CO_2 after 3 and 24 h in mice and rats (11). Similarly, in additional studies from the same group, Balbi et al. also described a complete loss of CO_2 reactivity after 3 and 24 h after SAH in mice (8, 9). In our study, we detected a significant reduction of the cerebrovascular reactivity, with a complete loss observed in some animals especially at the earliest time points. Depending on the anesthesia protocol, the CO_2 reactivity in our study in rats was significantly reduced up to 2 or 4 h, respectively, with a recovery toward the end of the observation time of 6 h. Of note, there are inherent differences between the studies regarding the anesthesia protocol [combination of medetomidine/midazolam/fentanyl in mice (8, 9, 11), chloral hydrate in rats (11) vs. isoflurane/fentanyl or ketamine/xylazine in our study], the rat strain [Sprague Dawley

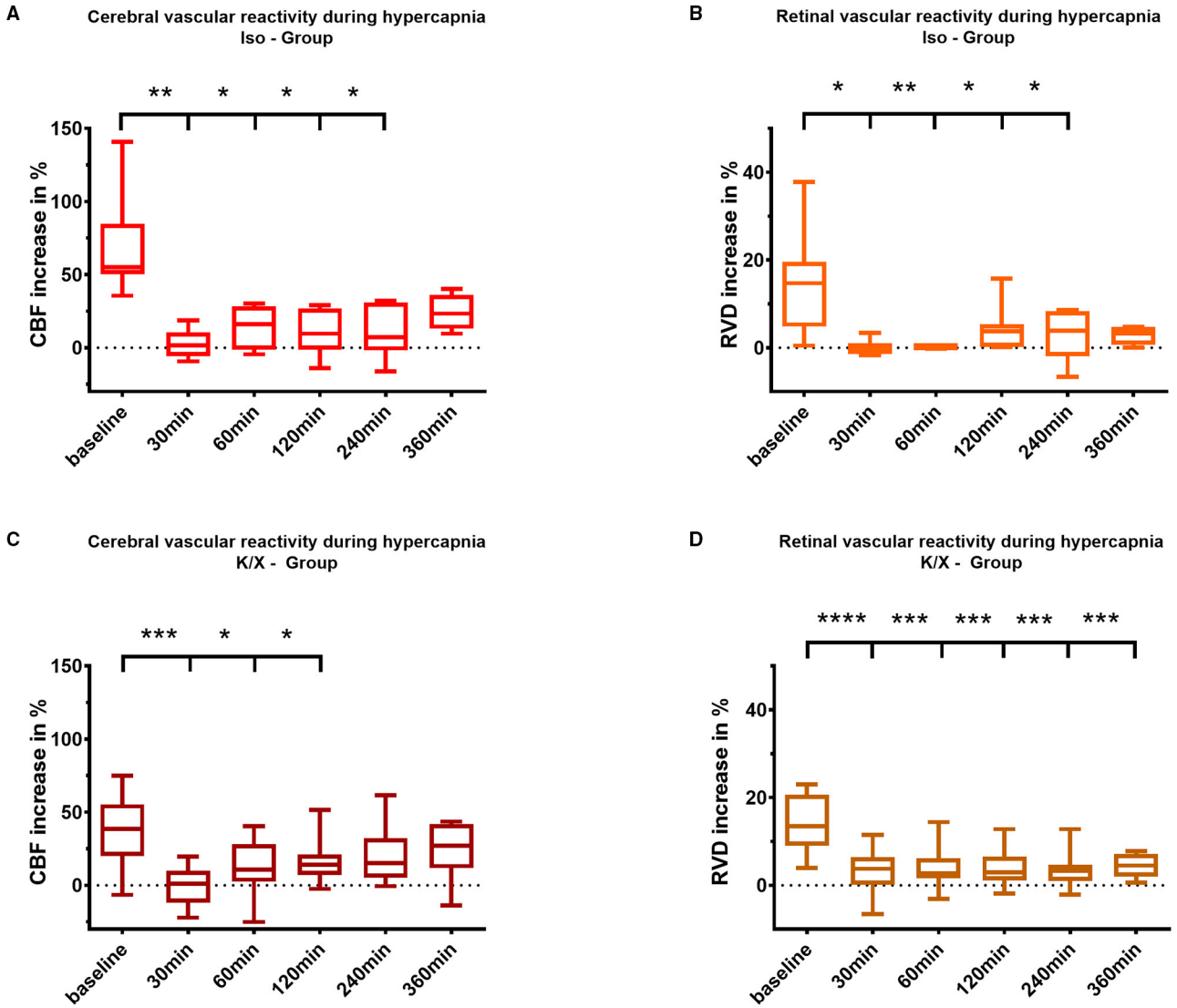

FIGURE 4 | Cerebral and retinal vascular reactivity to hypercapnia after SAH. Iso—Group: Cerebral vascular reactivity **(A)** as well as retinal vascular reactivity **(B)** to hypercapnia were impaired up to 240 min after SAH; K/X—Group: Cerebral CO_2 reactivity was disturbed up to 120 min after SAH **(C)**, whereas impairment of retinal vessels persisted throughout the whole measurement period of 360 min **(D)**. SAH, subarachnoid hemorrhage; Iso, Isoflurane; K/X, Ketamine/Xylazine; CBF, cerebral blood flow; RVD, retinal vessel diameter; boxes show median and 25% and 75% percentile and whiskers show data range; $^{*}p < 0.05$, $^{**}p < 0.01$, $^{***}p < 0.001$, $^{****}p < 0.0001$.

(11) vs. Wistar in our study], and the SAH model [filament perforation model (8, 9, 11) vs. blood injection model in our study]. Thus, albeit a direct comparison to our data is impeded, the occurrence of significantly disturbed hypercapnia reactivity under variable experimental conditions points toward a universal pathophysiological alteration of the cerebral vasculature early after SAH.

Until now, experimental data about impaired hypercapnia reactivity during the hyperacute phase (within the first hour) and at more prolonged time points (up to 6 h) after SAH and data about retinal reactivity to CO_2 after SAH, in general, are lacking. Our study is, therefore, the first to report a distinct temporal pattern of vascular CO_2 reactivity in the acute phase after SAH both within the cerebral and the retinal vascular bed, with immediate impairment lasting over several hours.

There are several issues from our findings worthy of discussion: vascular dysfunction starts immediately after bleeding. This short time period possibly indicates the importance of the ictus itself with a massive ICP peak within the first minutes after bleeding, followed by a moderate plateau, with no significant difference between both anesthesia protocols. However, it seems unlikely that the elevated ICP during the plateau phase contributes to the reduced vascular responses to hypercapnia. After a transient severe drop to ischemic values

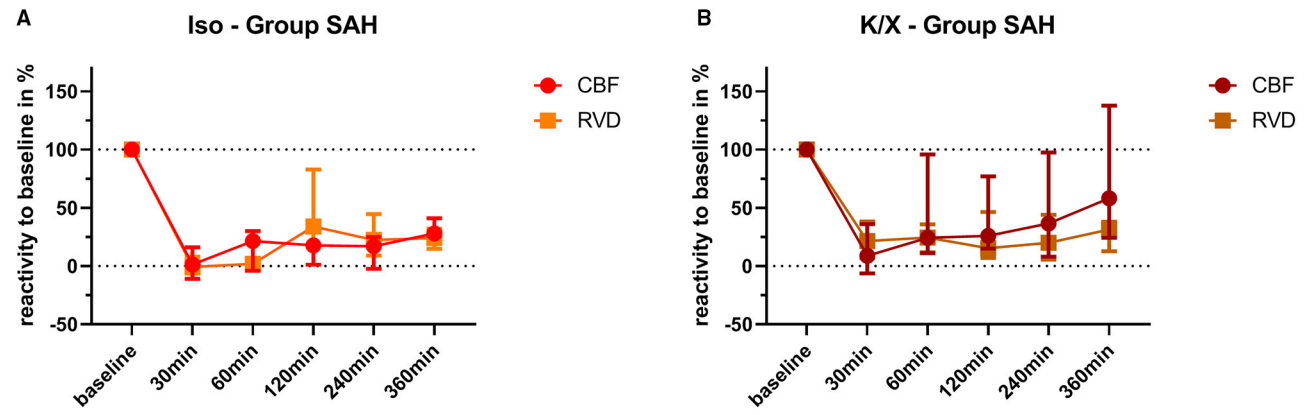

FIGURE 5 | Comparison of vascular reactivity to hypercapnia between retinal and cerebral vasculature. Reactivity at baseline was normalized to 100% for each vascular bed in each animal, and the changes in percentage were calculated over time after SAH. Averaged data of both vascular beds of each group are depicted for comparison. No significant differences were found in the Iso—Group **(A)** and in the K/X—Group **(B)** for all time points of hypercapnia challenge. SAH, subarachnoid hemorrhage; Iso, isoflurane; K/X, ketamine/xylazine; CBF, cerebral blood flow; RVD, retinal vessel diameter; symbols show median and whiskers show 25 and 75% percentile.

at the time of the ICP peak, the CBF reached normal values again within 15 min in the K/X-Group and within 60 min in the Iso-Group, respectively. In addition, it has been shown that CBF and blood volume responses to functional activation remained preserved during moderately elevated ICP (26). We, therefore, assume that a primarily pressure induced impact on the blood supply to the brain and on cerebrovascular reactivity can be ruled out. A metabolic response evoked by blood degradation products in the subarachnoid space also seems more improbable in view of the immediate reaction. Based on our knowledge of the dependence of the cerebral vasculature on a basal nitric oxide (NO) availability for physiological neurovascular coupling and CO_2 reactivity (27–29), functional impairment of vascular reactivity by scavenging of perivascular NO by—at this early time point still intact—erythrocytes seems reasonable (30). Wang et al. observed a decrease of CO_2 reactivity after regional SAH caused by the punctuation of a single pial arteriole after 3 h (31). This makes an additional impact on the subarachnoid blood itself possible. Besides the blood-cell-induced reduction of perivascular NO, cortical spreading depolarization waves have to be considered as a further possible mechanism, as the hypercapnic response has been shown to be severely reduced for hours after a single CSD wave in healthy animals (32). The frequent occurrence of CSDs has recently been shown in the acute phase after SAH in mice (33) and has to be further evaluated in our SAH model in rats.

An ultra-early and at least sub-acutely protracted inability of the cerebral vasculature to properly react to hypercapnia might be of interest in translational research. A conceivable therapeutic potential of the vascular reactivity to CO_2 after SAH will only be of success when the cerebral vasculature is physiologically reacting to changes of arterial pCO_2. Results from experimental studies in mice show that CO_2 reactivity recovers in the chronic phase 1 mo after SAH (34). In a clinical phase 1 study, CO_2 as a potent vasodilator was used aiming at increasing CBF therapeutically on days 4–14 after SAH (35). A recently published follow-up study investigating the optimum duration of the hypercapnic challenge for CBF elevation again suggested hypercapnia as a promising approach for perfusion enhancement in the critical phase of DCI (36). Whether this potentially improves outcome remains to be determined. Importantly, spontaneous hyperventilation and consecutive cerebral hypoperfusion are associated with DCI and poorer neurological outcomes (37), underlining the crucial role of profound knowledge on the ability or disability of the cerebral vasculature to react to CO_2 after SAH.

Therefore, an easily applicable bedside method for the assessment of cerebrovascular reactivity would be highly desirable. In the present experimental study, we demonstrate for the first time that the retinal vascular bed participates in the acute dysfunction of the cerebral vasculature after SAH not only in temporality but also in the degree of the observed disturbance. Only while using K/X as an anesthesia regime, there was a discrepancy between the retinal and the cerebral reactivity toward the end of the observation period, with persistent impairment of the retinal hypercapnic response throughout the measurement period while the CBF reactivity already recovered within 240 min. The reason for this difference is not known so far, however, specific mechanisms of the anesthetic drugs may be involved. Ketamine has been shown to be neuroprotective (38) and to reduce the occurrence of cerebral spreading depolarization in the acute phase after SAH (33) which may both specifically protect the neurovascular unit in the brain. Another explanation of the prolonged RVD reduction in the K/X-Group may be that isoflurane and ketamine/xylazine differently affect the intraocular pressure and associated functions, such as the scotopic threshold responses (39). However, due to methodological reasons, we did not additionally measure the intraocular pressure in our study. In summary, we think more data are needed to determine whether there is a truly prolonged

impairment in the retinal vessels at time point 360 min or whether it is rather a narcotic effect.

Our findings of an overall parallel impairment of the hypercapnic reactivity of the retinal and cerebral vasculature extend the previous knowledge about the retina as a window to the brain in chronic neurodegenerative diseases, such as Alzheimer's and inaugurate, a potential new monitoring method as a non-invasive diagnostic tool for acute neurological diseases. From an embryological point of view, the retina is part of the central nervous system, more precisely of the diencephalon. The vascular supply of the retina is provided by the ophthalmic artery, thus sharing important autoregulatory mechanisms, such as CO_2 reactivity or neurovascular coupling with strictly intracranial vessels. The optic nerve and the ophthalmic artery within its sheath directly connect the retina with the brain: Of note, in SAH, between 12 and 23% of the patients develop a vitreous/ and or subhyaloid hemorrhage (Terson's Syndrome). The pathophysiology is mostly but not exclusively linked to the raised ICP in the moment of bleeding (40). Furthermore, the latest research indicates a glymphatic system not only in the brain but in the retina (41) assuming perivascular pathways through which vasoactive agents of the subarachnoid space may also directly reach the retinal microvasculature. In summary, acute changes of retinal vascular reactivity in SAH seem reasonable. Our findings underscore the latest clinical research, where altered RVD and impairment of neurovascular coupling days after SAH were observed in patients. Importantly, changes were in parts reversible at the time of follow up implying an acute but transient effect of SAH on the retinal vasculature (20–22). However, information about the degree of parallel CBF impairment in these patients is lacking precluded by the invasive and extensive character of the necessary diagnostic procedures. Our experimental data show that in simultaneous measurement of CBF and RVD, both vessel beds behave in a parallel way in rats in the early phase after SAH. This supports the assumption that retinal vessel analysis may hold the key for a possible new, non-invasive, and bedside diagnostic tool enabling live vascular assessment in SAH. However, the clinical relevance in terms of DCI and neurological outcome of these findings still needs to be proven. In addition, further studies are needed to evaluate possible common mechanisms of impairment in both vascular beds for example by the spread of blood degradation products within the glymphatic space (41) or by autonomous nervous system dysfunction (42) in the acute and a chronic course of the disease.

Limitations

Our complex experimental setup with extensive surgical preparation on the one hand and the delicate and easily vulnerable brain and retinal tissue requiring careful preparation and maintenance on the other hand entailed a comparatively high drop-out rate of 26%. The drop-out rate was accentuated in the Iso—Group SAH causing comparatively few data points especially at the end of the observation period. This may have led to a sample size bias with a higher probability of effect inflation (43).

For the experiments, two different anesthesia protocols were used with the Iso—Group performed first, using our well-established regime (10, 24), resulting in significant increases to hypercapnia in the retinal and the cerebral vasculature, albeit with some variability between the animals. It is well-known that isoflurane itself dilates systemic and cerebral vasculature, probably being partly responsible for the variability. In addition, the isoflurane-induced dilation has been shown to be even larger in the retinal vasculature compared with the cerebral vasculature (44). To rule out that our finding is influenced by the type of anesthesia, we repeated the study while using a common protocol of ketamine/xylazine combination, which has been shown to significantly reduce the retinal blood flow at unstimulated conditions (45). Due to this sequential procedure, we were not able to randomize between the two anesthesia protocols, which may have introduced a possibly existing, albeit probably only small, bias.

Similar to every animal model, the single injection model used in this study has some important limitations itself. Especially the missing vessel perforation mimicking the human SAH in having an injured vessel with direct hemorrhagic brain lesions is an important drawback. The double hemorrhage model mimics best the cerebral vasospasm and delayed ischemic lesions and, therefore, seems to be more suitable to study the delayed effects of SAH (46, 47). However, we choose the single hemorrhage model instead of the perforation model because of better control of the subarachnoid blood amount resulting in a more comparable acute brain injury (SAH severity) and lower mortality rates.

Hypercapnia was achieved by controlled hypoventilation for a predefined time period in all animals. Simultaneously, the O_2 supply was slightly increased to prevent hypoxia. This procedure was verified *via* blood gas analysis for every single measure period. In both KX—Groups, there was a slight but significant increase of arterial pO_2 during hypercapnia. However, this moderate hyperoxia is not expected to influence functional vascular reactivity at all (48, 49).

CONCLUSION

This study demonstrates fundamental changes of one important CBF regulation mechanism in the acute phase after SAH in two vascular beds: the cerebral and the retinal vascular reactivity to hypercapnia is deeply impaired. Pathologic alterations start immediately after SAH and last up to several hours. Importantly, the retinal vasculature not only participates in these acute changes of altered cerebral vascular reactivity to hypercapnia but behaves in a parallel way regarding the degree of vascular impairment and the temporal course.

With this bedside to bench approach in form of a simultaneous assessment of CBF and retinal vessel reactivity after SAH, our results support and extend first data in patients with human SAH, which showed retinal vessel alterations several days after SAH. This underscores the potential role of the retina as a non-invasive, bedside screening tool even for highly

acute neurological diseases. Further studies will be required to determine the long-time changes after experimental SAH and correlation with functional outcome.

DATA AVAILABILITY STATEMENT

The raw data supporting the conclusions of this article will be made available by the authors, without undue reservation.

ETHICS STATEMENT

The animal study was reviewed and approved by Landesamt für Natur, Umwelt und Verbraucherschutz (LANUV) Nordrhein—Westfalen, Recklinghausen, Germany (file reference: 84-02.04.2015.A412) in line with the EU Directive 2010/63/EU on the protection of animals used for scientific purposes, and was performed in accordance with the ARRIVE Guidelines.

AUTHOR CONTRIBUTIONS

CC-D, GS, and UL: conceived and designed the experiments and the study protocol. LW, AB-H, WA, UL, and CC-D: constructed experimental set up. LW: performed the experiments. LW, CC-D, and UL: analyzed the data, interpretation of the data, and illustrations. CC-D and LW: first drafting of the manuscript. AB-H, HC, GS, WA, UL, and CC-D: critical review of the manuscript. All authorship requirements have been met and the final manuscript was critically revised and approved by all authors.

FUNDING

This work was supported by the grants from the START – Program of the Faculty of Medicine RWTH Aachen University for CC, German Research Foundation (Deutsche Forschungsgemeinschaft DFG, grant number LI 588/5-1, LI 588/5-2) as part of the research unit "Severity assessment in animal based research" FOR2591 for UL, and 50% financial support for the RCrodent from Imedos (IMEDOS Systems UG, Jena, Germany) by the Faculty of Medicine RWTH Aachen University for UL.

ACKNOWLEDGMENTS

The authors cordially thank Dr. med. vet. Sarah Pinkernell for supporting the experimental setup and performing the first feasibility tests of the retinal vessel analyses device. Special thanks go to Dr. med. Tobias Philip Schmidt, MD and Dr. med. Guangshan Hao, MD for their support in the surgical training period.

SUPPLEMENTARY MATERIAL

The Supplementary Material for this article can be found online at: https://www.frontiersin.org/articles/10.3389/fneur.2021.757050/full#supplementary-material

REFERENCES

1. Macdonald RL, Schweizer TA. Spontaneous subarachnoid haemorrhage. *Lancet.* (2017) 389:655–66. doi: 10.1016/S0140-6736(16)30668-7
2. Budohoski KP, Czosnyka M, Smielewski P, Kasprowicz M, Helmy A, Bulters D, et al. Impairment of cerebral autoregulation predicts delayed cerebral ischemia after subarachnoid hemorrhage: a prospective observational study. *Stroke.* (2012) 43:3230–7. doi: 10.1161/STROKEAHA.112.669788
3. Foreman B. The pathophysiology of delayed cerebral ischemia. *J Clin Neurophysiol.* (2016) 33:174–82. doi: 10.1097/WNP.0000000000000273
4. Francoeur CL, Mayer SA. Management of delayed cerebral ischemia after subarachnoid hemorrhage. *Crit Care.* (2016) 20:277. doi: 10.1186/s13054-016-1447-6
5. Sehba FA, Hou J, Pluta RM, Zhang JH. The importance of early brain injury after subarachnoid hemorrhage. *Prog Neurobiol.* (2012) 97:14–37. doi: 10.1016/j.pneurobio.2012.02.003
6. Ainslie PN, Duffin J. Integration of cerebrovascular CO2 reactivity and chemoreflex control of breathing: mechanisms of regulation, measurement, and interpretation. *Am J Physiol Regul Integr Comp Physiol.* (2009) 296:R1473–95. doi: 10.1152/ajpregu.91008.2008
7. Glodzik L, Randall C, Rusinek H, de Leon MJ. Cerebrovascular reactivity to carbon dioxide in Alzheimer's disease. *J Alzheimers Dis.* (2013) 35:427–40. doi: 10.3233/JAD-122011
8. Balbi M, Koide M, Schwarzmaier SM, Wellman GC, Plesnila N. Acute changes in neurovascular reactivity after subarachnoid hemorrhage in vivo. *J Cereb Blood Flow Metab.* (2017) 37:178–87. doi: 10.1177/0271678X15621253
9. Balbi M, Koide M, Wellman GC, Plesnila N. Inversion of neurovascular coupling after subarachnoid hemorrhage in vivo. *J Cereb Blood Flow Metab.* (2017) 37:3625–34. doi: 10.1177/0271678X16686595
10. Conzen C, Becker K, Albanna W, Weiss M, Bach A, Lushina N, et al. The acute phase of experimental subarachnoid hemorrhage: intracranial pressure dynamics and their effect on cerebral blood flow and autoregulation. *Transl Stroke Res.* (2019) 10:566–82. doi: 10.1007/s12975-018-0674-3
11. Friedrich B, Michalik R, Oniszczuk A, Abubaker K, Kozniewska E, Plesnila N. CO2 has no therapeutic effect on early microvasospasm after experimental subarachnoid hemorrhage. *J Cereb Blood Flow Metab.* (2014) 34:e1–6. doi: 10.1038/jcbfm.2014.96
12. Pappas AC, Koide M, Wellman GC. Astrocyte Ca2+ signaling drives inversion of neurovascular coupling after subarachnoid hemorrhage. *J Neurosci.* (2015) 35:13375–84. doi: 10.1523/JNEUROSCI.1551-15.2015
13. Santos GA, Petersen N, Zamani AA, Du R, LaRose S, Monk A, et al. Pathophysiologic differences in cerebral autoregulation after subarachnoid hemorrhage. *Neurology.* (2016) 86:1950–6. doi: 10.1212/WNL.0000000000002696
14. Donnelly J, Budohoski KP, Smielewski P, Czosnyka M. Regulation of the cerebral circulation: bedside assessment and clinical implications. *Crit Care.* (2016) 20:129. doi: 10.1186/s13054-016-1293-6
15. Cabrera DeBuc D, Somfai GM, Koller A. Retinal microvascular network alterations: potential biomarkers of cerebrovascular and neural diseases. *Am J Physiol Heart Circ Physiol.* (2017) 312:H201–12. doi: 10.1152/ajpheart.00201.2016
16. Kur J, Newman EA, Chan-Ling T. Cellular and physiological mechanisms underlying blood flow regulation in the retina and choroid in health and disease. *Prog Retin Eye Res.* (2012) 31:377–406. doi: 10.1016/j.preteyeres.2012.04.004
17. London A, Benhar I, Schwartz M. The retina as a window to the brain-from eye research to CNS disorders. *Nat Rev Neurol.* (2013) 9:44–53. doi: 10.1038/nrneurol.2012.227

18. Lindley RI, Wang JJ, Wong MC, Mitchell P, Liew G, Hand P, et al. Retinal microvasculature in acute lacunar stroke: a cross-sectional study. *Lancet Neurol.* (2009) 8:628–34. doi: 10.1016/S1474-4422(09)70131-0
19. De Silva DA, Manzano JJ, Liu EY, Woon FP, Wong WX, Chang HM, et al. Retinal microvascular changes and subsequent vascular events after ischemic stroke. *Neurology.* (2011) 77:896–903. doi: 10.1212/WNL.0b013e31822c623b
20. Albanna W, Conzen C, Weiss M, Clusmann H, Fuest M, Mueller M, et al. Retinal Vessel Analysis (RVA) in the context of subarachnoid hemorrhage - a proof of concept study. *PLoS One.* (2016) 11:e0158781. doi: 10.1371/journal.pone.0158781
21. Albanna W, Conzen C, Weiss M, Seyfried K, Kotliar K, Schmidt TP, et al. Non-invasive assessment of neurovascular coupling after aneurysmal subarachnoid hemorrhage: a prospective observational trial using retinal vessel analysis. *Front Neurol.* (2021) 12:690183. doi: 10.3389/fneur.2021.690183
22. Conzen C, Albanna W, Weiss M, Kurten D, Vilser W, Kotliar K, et al. Vasoconstriction and impairment of neurovascular coupling after subarachnoid hemorrhage: a descriptive analysis of retinal changes. *Transl Stroke Res.* (2018) 9:284–93. doi: 10.1007/s12975-017-0585-8
23. Mahler Convenor M, Berard M, Feinstein R, Gallagher A, Illgen-Wilcke B, Pritchett-Corning K, et al. FELASA recommendations for the health monitoring of mouse, rat, hamster, guinea pig and rabbit colonies in breeding and experimental units. *Lab Anim.* (2014) 48:178–92. doi: 10.1177/0023677213516312
24. Bach A, Conzen C, Schubert GA, Bleilevens C, Lindauer U. Acute changes of pro-inflammatory markers and corticosterone in experimental subarachnoid haemorrhage: a prerequisite for severity assessment. *PLoS One.* (2019) 14:e0220467. doi: 10.1371/journal.pone.0220467
25. Muir ER, Duong TQ. MRI of retinal and choroidal blood flow with laminar resolution. *NMR Biomed.* (2011) 24:216–23. doi: 10.1002/nbm.1576
26. Fuchtemeier M, Leithner C, Offenhauser N, Foddis M, Kohl-Bareis M, Dirnagl U, et al. Elevating intracranial pressure reverses the decrease in deoxygenated hemoglobin and abolishes the post-stimulus overshoot upon somatosensory activation in rats. *Neuroimage.* (2010) 52:445–54. doi: 10.1016/j.neuroimage.2010.04.237
27. Iadecola C, Zhang F, Xu X. SIN-1 reverses attenuation of hypercapnic cerebrovasodilation by nitric oxide synthase inhibitors. *Am J Physiol.* (1994) 267:R228–35. doi: 10.1152/ajpregu.1994.267.1.R228
28. Lindauer U, Kunz A, Schuh-Hofer S, Vogt J, Dreier JP, Dirnagl U. Nitric oxide from perivascular nerves modulates cerebral arterial pH reactivity. *Am J Physiol Heart Circ Physiol.* (2001) 281:H1353–63. doi: 10.1152/ajpheart.2001.281.3.H1353
29. Lindauer U, Megow D, Matsuda H, Dirnagl U. Nitric oxide: a modulator, but not a mediator, of neurovascular coupling in rat somatosensory cortex. *Am J Physiol.* (1999) 277:H799–811. doi: 10.1152/ajpheart.1999.277.2.H799
30. Helms CC, Gladwin MT, Kim-Shapiro DB. Erythrocytes and vascular function: oxygen and nitric oxide. *Front Physiol.* (2018) 9:125. doi: 10.3389/fphys.2018.00125
31. Wang CX, Lin YX, Xie GB, Shi JX, Zhou ML. Constriction and dysfunction of pial arterioles after regional hemorrhage in the subarachnoid space. *Brain Res.* (2015) 1601:85–91. doi: 10.1016/j.brainres.2015.01.012
32. Scheckenbach KE, Dreier JP, Dirnagl U, Lindauer U. Impaired cerebrovascular reactivity after cortical spreading depression in rats: restoration by nitric oxide or cGMP. *Exp Neurol.* (2006) 202:449–55. doi: 10.1016/j.expneurol.2006.07.007
33. Zheng Z, Schoell M, Sanchez-Porras R, Diehl C, Unterberg A, Sakowitz OW. Spreading depolarization during the acute stage of experimental subarachnoid hemorrhage in mice. *Acta Neurochir Suppl.* (2020) 127:97–103. doi: 10.1007/978-3-030-04615-6_16
34. Balbi M, Vega MJ, Lourbopoulos A, Terpolilli NA, Plesnila N. Long-term impairment of neurovascular coupling following experimental subarachnoid hemorrhage. *J Cereb Blood Flow Metab.* (2020) 40:1193–202. doi: 10.1177/0271678X19863021
35. Westermaier T, Stetter C, Kunze E, Willner N, Holzmeier J, Weiland J, et al. Controlled hypercapnia enhances cerebral blood flow and brain tissue oxygenation after aneurysmal subarachnoid hemorrhage: results of a phase 1 study. *Neurocrit Care.* (2016) 25:205–14. doi: 10.1007/s12028-016-0246-x
36. Stetter C, Weidner F, Lilla N, Weiland J, Kunze E, Ernestus RI, et al. Therapeutic hypercapnia for prevention of secondary ischemia after severe subarachnoid hemorrhage: physiological responses to continuous hypercapnia. *Sci Rep.* (2021) 11:11715. doi: 10.1038/s41598-021-91007-7
37. Williamson CA, Sheehan KM, Tipirneni R, Roark CD, Pandey AS, Thompson BG, et al. The association between spontaneous hyperventilation, delayed cerebral ischemia, and poor neurological outcome in patients with subarachnoid hemorrhage. *Neurocrit Care.* (2015) 23:330–8. doi: 10.1007/s12028-015-0138-5
38. Bell JD. In vogue: ketamine for neuroprotection in acute neurologic injury. *Anesth Analg.* (2017) 124:1237–43. doi: 10.1213/ANE.0000000000001856
39. Choh V, Gurdita A, Tan B, Feng Y, Bizheva K, McCulloch DL, et al. Isoflurane and ketamine:xylazine differentially affect intraocular pressure-associated scotopic threshold responses in Sprague-Dawley rats. *Doc Ophthalmol.* (2017) 135:121–32. doi: 10.1007/s10633-017-9597-7
40. Czorlich P, Skevas C, Knospe V, Vettorazzi E, Westphal M, Regelsberger J. Terson's syndrome - pathophysiologic considerations of an underestimated concomitant disease in aneurysmal subarachnoid hemorrhage. *J Clin Neurosci.* (2016) 33:182–6. doi: 10.1016/j.jocn.2016.04.015
41. Wostyn P, De Groot V, Van Dam D, Audenaert K, De Deyn PP, Killer HE. The glymphatic system: a new player in ocular diseases? *Invest Ophthalmol Vis Sci.* (2016) 57:5426–7. doi: 10.1167/iovs.16-20262
42. Findik H, Kanat A, Aydin MD, Cakir M, Ozmen SA, Okutucu M, et al. Describing a new mechanism of retinal detachment secondary to ophthalmic artery vasospasm following subarachnoid hemorrhage: an experimental study. *J Neurol Surg A Cent Eur Neurosurg.* (2019) 80:430–40. doi: 10.1055/s-0039-1685186
43. Button KS, Ioannidis JP, Mokrysz C, Nosek BA, Flint J, Robinson ES, et al. Power failure: why small sample size undermines the reliability of neuroscience. *Nat Rev Neurosci.* (2013) 14:365–76. doi: 10.1038/nrn3475
44. Li Y, Cheng H, Duong TQ. Blood-flow magnetic resonance imaging of the retina. *Neuroimage.* (2008) 39:1744–51. doi: 10.1016/j.neuroimage.2007.10.030
45. Moult EM, Choi W, Boas DA, Baumann B, Clermont AC, Feener EP, et al. Evaluating anesthetic protocols for functional blood flow imaging in the rat eye. *J Biomed Opt.* (2017) 22:16005. doi: 10.1117/1.JBO.22.1.016005
46. Guresir E, Schuss P, Borger V, Vatter H. Experimental subarachnoid hemorrhage: double cisterna magna injection rat model–assessment of delayed pathological effects of cerebral vasospasm. *Transl Stroke Res.* (2015) 6:242–51. doi: 10.1007/s12975-015-0392-z
47. Lee JY, Sagher O, Keep R, Hua Y, Xi G. Comparison of experimental rat models of early brain injury after subarachnoid hemorrhage. *Neurosurgery.* (2009) 65:331–43; discussion 43. doi: 10.1227/01.NEU.0000345649.78556.26
48. Lindauer U, Leithner C, Kaasch H, Rohrer B, Foddis M, Fuchtemeier M, et al. Neurovascular coupling in rat brain operates independent of hemoglobin deoxygenation. *J Cereb Blood Flow Metab.* (2010) 30:757–68. doi: 10.1038/jcbfm.2009.259
49. Wolf T, Lindauer U, Villringer A, Dirnagl U. Excessive oxygen or glucose supply does not alter the blood flow response to somatosensory stimulation or spreading depression in rats. *Brain Res.* (1997) 761:290–9. doi: 10.1016/S0006-8993(97)00354-5

Conflict of Interest: The authors declare that the research was conducted in the absence of any commercial or financial relationships that could be construed as a potential conflict of interest.

frontiers in Neurology

ORIGINAL RESEARCH
published: 07 March 2022
doi: 10.3389/fneur.2022.760293

Cerebral Autoregulation Indices Are Not Interchangeable in Patients With Sepsis

Juliana Caldas[1,2,3†], Armin Alvaro Quispe-Cornejo[4†], Ilaria Alice Crippa[4], Carles Subira[5], Jacques Creteur[4], Ronney Panerai[6,7] and Fabio Silvio Taccone[4]*

[1] Escola Bahiana de Medicina e Saúde Pública, Salvador, Brazil, [2] Universidade de Salvador, Universidade y Faculdade Salvador (UNIFACS), Salvador, Brazil, [3] Instituto D'Or de Pesquisa e Ensino (IDOR), Salvador, Brazil, [4] Department of Intensive Care Unit, Erasme Hospital, Université Libre de Bruxelles, Brussels, Belgium, [5] Department of Intensive Care Medicine, Alhaia Xarxa Assistencial Universitaria de Manresa, Barcelona, Spain, [6] Department of Cardiovascular Sciences, University of Leicester, Leicester, United Kingdom, [7] National Institute for Health Research (NIHR) Leicester Biomedical Research Centre, Leicester, United Kingdom

OPEN ACCESS

Edited by:
Xiuyun Liu,
Johns Hopkins University,
United States

Reviewed by:
Li Xiong,
The Chinese University of Hong Kong, China
Markus Harboe Olsen,
Rigshospitalet, Denmark
Pedro Castro,
University of Porto, Portugal

***Correspondence:**
Armin Alvaro Quispe-Cornejo
arminquispe@gmail.com

†These authors have contributed equally to this work and share first authorship

Specialty section:
This article was submitted to Neurocritical and Neurohospitalist Care, a section of the journal Frontiers in Neurology

Received: *17 August 2021*
Accepted: *26 January 2022*
Published: *07 March 2022*

Citation:
Caldas J, Quispe-Cornejo AA, Crippa IA, Subira C, Creteur J, Panerai R and Taccone FS (2022) Cerebral Autoregulation Indices Are Not Interchangeable in Patients With Sepsis. Front. Neurol. 13:760293. doi: 10.3389/fneur.2022.760293

Introduction: Dynamic cerebral autoregulation (dCA) is frequently altered in patients with sepsis and may be associated with sepsis-associated brain dysfunction. However, the optimal index to quantify dCA in patients with sepsis is currently unknown.

Objective: To assess the agreement between two validated dCA indices in patients with sepsis.

Methods: Retrospective analysis of prospectively collected data in patients with sepsis; those with acute or chronic intracranial disease, arrhythmias, mechanical cardiac support, or history of supra-aortic vascular disease were excluded. Transcranial Doppler was performed on the right or left middle cerebral artery (MCA) with a 2-MHz probe, and MCA blood flow velocity (FV) and arterial pressure (BP) signals were simultaneously recorded. We calculated two indices of dCA: the mean flow index (Mxa), which is the Pearson correlation coefficient between BP and FV (MATLAB, MathWorks), and the autoregulation index (ARI), which is the transfer function analysis of spontaneous fluctuations in BP and FV (custom-written FORTRAN code). Impaired dCA was defined as Mxa >0.3 or ARI ≤ 4. The agreement between the two indices was assessed by Cohen's kappa coefficient.

Results: We included 95 patients (age 64 $\pm$ 13 years old; male 74%); ARI was 4.38 [2.83–6.04] and Mxa was 0.32 [0.14–0.59], respectively. There was no correlation between ARI and Mxa ($r = -0.08$; $p = 0.39$). dCA was altered in 40 (42%) patients according to ARI and in 50 (53%) patients according to Mxa. ARI and Mxa were concordant in classifying 23 (24%) patients as having impaired dCA and 28 (29%) patients as having intact dCA. Cohen's kappa coefficient was 0.08, suggesting poor agreement. ARI was altered more frequently in patients on mechanical ventilation than others (27/52, 52% vs. 13/43, 30%, $p = 0.04$), whereas Mxa did not differ between those two groups. On the contrary, Mxa was altered more frequently in patients receiving sedatives than others (23/34, 68% vs. 27/61, 44%, $p = 0.03$), whereas ARI did not differ between these two groups.

Conclusions: Agreement between ARI and Mxa in assessing dCA in patients with sepsis was poor. The identification of specific factors influencing the dCA analysis might lead to a better selection of the adequate cerebral autoregulation (CAR) index in critically ill patients with sepsis.

Keywords: correlation, autoregulation index, Mxa, cerebral autoregulation, sepsis

INTRODUCTION

Sepsis is a common cause of admission to the intensive care unit (ICU), with a great impact on mortality (1). Sepsis-associated brain dysfunction (SABD), ranging from delirium to coma, is common during sepsis and can be associated to poor outcomes (2). The pathophysiology of encephalopathy occurring during sepsis remains unclear, but likely involves alterations in neurotransmission, microglial activation, and blood–brain barrier dysfunction (3). Cerebral hypoperfusion may also play a role, indeed, cerebral blood flow (CBF) may be inadequate secondary to microcirculatory dysfunction (4, 5). Cerebral autoregulation (CAR) is the intrinsic cerebrovascular mechanism that maintains CBF constant within different ranges of cerebral perfusion pressure (CPP); indeed, cerebral arterioles can constrict or dilate in response to the elevation or reduction in CPP, the so-called pressure autoregulation, thus keeping CBF within stable values. As CPP is determined by the interaction between intracranial pressure and mean arterial pressure (MAP), the latter can be used as a valid surrogate of CPP in those patients in whom intracranial pressure is not expected to be elevated (6). Mechanisms of autoregulation are efficient for a range of MAP, which varies between subject, but is considered to be around 50–150 mmHg; as a consequence, alterations in CAR may result in brain hypoperfusion at MAP levels, which are considered to be adequate in routine practice (5). During sepsis, an impaired CAR has been reported in several studies (5, 7–10); such disturbances have been associated with increased serum concentrations of brain injury biomarkers (11) and with the occurrence of brain dysfunction (5).

Several studies investigating alterations of CAR in patients with sepsis and non-sepsis have been published. However, they differed in timing of autoregulation assessment, technique of assessment, and alteration measurements and definition. The autoregulation index (ARI) (12) and the mean flow index (Mxa) (13) have been validated in patients with critical illness. Both are based on spontaneous fluctuation in MAP and its correlation with intracranial artery blood flow velocity (FV) as measured by transcranial Doppler (TCD) (14). As no specific index is currently considered to be the "gold standard" in patients with critical illness, the classification of CAR based on different indices may result in divergent results when applied to the same study cohort. However, no study has previously compared ARI and Mxa in patients with sepsis.

The aim of this study was to compare the assessment of CAR using ARI and Mxa in a large cohort of patients with sepsis.

METHODS

Study Population and Data Collection

Retrospective analysis of prospectively collected data including adult (>18 years) patients who were diagnosed with sepsis either on admission or during ICU stay at Erasme University Hospital (from October 2018 to December 2020; Université Libre de Bruxelles, Belgium) and Althaia Foundation Hospital (from June 2012 to June 2015; University of Manresa, Barcelona, Spain), and who had a TCD performed within 72 h from diagnosis (**Table 1**). Exclusion criteria were chronic or acute cerebrovascular disease (i.e., ischemic or hemorrhagic stroke), history of supra-aortic vascular stenosis, cardiac arrhythmias, mechanical cardiac support (i.e., veno-arterial extracorporeal membrane oxygenation, left ventricular assist device, intra-aortic balloon pump counter-pulsation), severe hypotension (MAP < 50 mmHg), severe hypercapnia (i.e., $PaCO_2$ > 65 mmHg), pregnancy, moribund patient or withdrawal of life-sustaining therapy, absence of transtemporal bone window for TCD examination, and absence of invasive arterial BP monitoring. We collected demographic data, Acute Physiology and Chronic Health Evaluation II (APACHE II) score, site of infection, the pathogen(s) involved, and the outcome at ICU discharge. Use of sedation and/or neuromuscular blocking agents (NMBAs), vasopressors, and mechanical ventilation at the moment of CAR assessment was also recorded. The study protocol was approved by local ethics committees; due to the retrospective and anonymous nature of the study, the need for an informed consent was waived.

Cerebral Autoregulation Assessment

Transcranial Doppler was performed on the right or the left middle cerebral artery (MCA) using a 2-MHz, 100 Hz sampling TCD monitoring probe (Compumedics DWL, Germany), which was kept in place using a special helmet to ensure a constant angle of insonation for 8 min length recording at the bedside. FV and invasive arterial BP signals were downloaded on a personal computer. Patients were maintained in steady-state conditions throughout the examination. Modifications in respiratory settings and/or pharmacological or fluidic therapy were avoided either before or during TCD examination. Samples were automatically (by a custom-written script) and visually expected for artifacts (e.g., due to tracheal suctioning, arterial line flushing, or transducer malfunction); in case of artifacts, the entire cardiac cycle was discarded; in case of artifacts >10% of the total recording, the entire recording was discarded.

The Mxa is the Pearson correlation coefficient between BP and FV and was calculated as previously reported (5, 13), i.e., both signals were averaged on 10-s consecutive windows with

TABLE 1 | Characteristics of the study population ($n = 95$). Data are presented as count (%), mean (±SD), or median [25th−75th percentiles].

Age, years	64 (13)
Male gender, *n* (%)	70 (74)
APACHE II score on admission	23 [15–32]
ICU length of stay, days	6 [3–14]
ICU mortality, *n* (%)	75 (79)
Car indices	
ARI	4.38 [2.83–6.04]
Mxa	0.32 [0.14–0.59]
At time of car assessment	
Sedation, *n* (%)	34 (36)
NMBA, *n* (%)	13 (14)
Mechanical ventilation, *n* (%)	52 (55)
Vasopressors, *n* (%)	69 (73)
Infection source	
Abdominal, *n* (%)	42 (44)
Respiratory, *n* (%)	26 (27)
Urinary tract, *n* (%)	7 (7)
Others, *n* (%)	20 (21)
Pathogen	
Bacterial, *n* (%)	66 (70)
Fungus, *n* (%)	9 (10)
Virus, *n* (%)	3 (3)
Unknown, *n* (%)	17 (18)

APACHE II, Acute Physiology Age Chronic Health Evaluation II; ICU, intensive care unit; LOS, length of stay; Mxa, mean flow index; dCA, dynamic cerebral autoregulation; NMBA, neuromuscular blocking agent; CAR, cerebral autoregulation.

50% overlap for the entire length of the recording; therefore, the correlation coefficient was calculated using MATLAB (MathWorks, Natick, MA, USA). The Pearson correlation coefficient (r) represents the strength and direction of a relationship between two variables. It has a value between +1 and −1, where +1 represents a total positive correlation, 0 represents no correlation, and −1 represents total negative correlation. The correlation is considered to be moderately positive when $r > 0.3$. Given that changes in FV mirrors changes in CBF, Mxa > 0.3 means that CBF is dependent on BP changes and dynamic cerebral autoregulation (dCA) is impaired; when BP and FV have a weak or a negative correlation (Mxa $\leq$ 0.3), dCA is considered intact.

Autoregulation index was calculated as follows: all signals were low-pass filtered using an eighth-order Butterworth with a cutoff frequency of 20 Hz. Beat-to-beat parameters were interpolated with a third-order polynomial and resampled at 5 Hz to generate signals with a uniform time base. The Welch method was adopted for smoothing spectral estimates obtained with the fast Fourier transform (102.4 s segments, 50% superposition) (15). An interpolation procedure was adopted to obtain ARI values (ARI = 0 indicates absent dCA, whereas ARI = 9 corresponds to the most efficient dCA) that can be observed by fitting a second-order polynomial to the integer values of ARI neighboring the region of minimum error (15). Objective criteria were adopted for the acceptance of estimates of ARI, using the normalized mean square error for fitting the Tiecks model (15) to the FV step response and the 95% CI for the mean coherence function in the frequency interval 0.15–0.25 Hz (16). ARI $\leq$ 4 or Mxa < 0.3 defined "impaired" dCA (14, 16).

Statistical Analysis

Data were tested for normality using the Kolmogorov–Smirnov test. Categorical variables were compared using the Fisher exact test or chi-square test, as appropriate, and the Student t-test or the Mann–Whitney U-test was used to compare continuous variables, as appropriate. The correlation between ARI and Mxa was assessed using Pearson's coefficient. Cohen's kappa (κ) coefficient (17) defined agreement between ARI and Mxa classification of dCA as either altered or intact: agreement was defined poor if $\kappa < 0.2$; fair if $0.21 < \kappa < 0.4$; moderate if $0.41 < \kappa < 0.6$; substantial if $0.61 < \kappa < 0.8$; almost perfect if $\kappa > 0.8$. If ARI and Mxa were concordant, patients were categorized as having "impaired" dCA or "intact" dCA, accordingly; a third group, named "divergent" dCA included those patients for whom the classification was not concordant between the two indices. dCA according to ARI and Mxa was assessed in different subgroups of patients according to: (a) mechanical ventilation; (b) administration of sedatives; (c) administration of NMBAs; (d) use of vasopressors at the time of TCD assessment; and (e) ICU outcome. Statistical analysis was performed using SPSS (IBM SPSS Statistics 25.0 for Macintosh). For all statistical tests, the significance was set at $p < 0.05$. Data are presented as median (25th−75th percentiles) or mean ± SD, as appropriate. Categorical variables are presented as counts (%).

RESULTS

A total of 95 patients (mean age 64 years old; male 74%) were eligible over the study period; APACHE II score on admission was 23 [15–32], and the ICU length of stay was 6 [3–14] days. Most infections were due to bacteria ($n = 66$, 70%), and mostly affected the abdomen ($n = 42$, 44%) and the lungs ($n = 26$, 28%). ICU mortality was observed in 20 (21%) patients.

At the dCA assessment, sedatives, neuromuscular blocking agents, mechanical ventilation, and vasopressors were used in 34 (36%), 13 (14%), 52 (55%), and 69 (73%) patients, respectively. Median ARI and Mxa values were 4.38 [2.83–6.04] and 0.32 [0.14–0.59], respectively; there was no significant correlation between ARI and Mxa ($r = -0.08$; $p = 0.39$; **Figure 1**). Impaired dCA according to the ARI threshold was observed in 40 (42%) patients; impaired dCA according to Mxa threshold was observed in 50 (53%) patients. In particular, ARI and Mxa were concordant in classifying 23 (24%) patients with impaired dCA and 28 (29%) patients with intact dCA (**Table 2**); a poor agreement between the two indices to categorize dCA was therefore obtained (Cohen's kappa coefficient = 0.08).

There were no differences in clinical variables according to different ARI and Mxa combinations (**Table 3**). ARI was altered more frequently in patients on mechanical ventilation than others (27/52, 52% vs. 13/43, 30%, $p = 0.04$), whereas Mxa did not differ between these two groups. On the contrary, Mxa was altered more frequently in patients receiving sedatives than

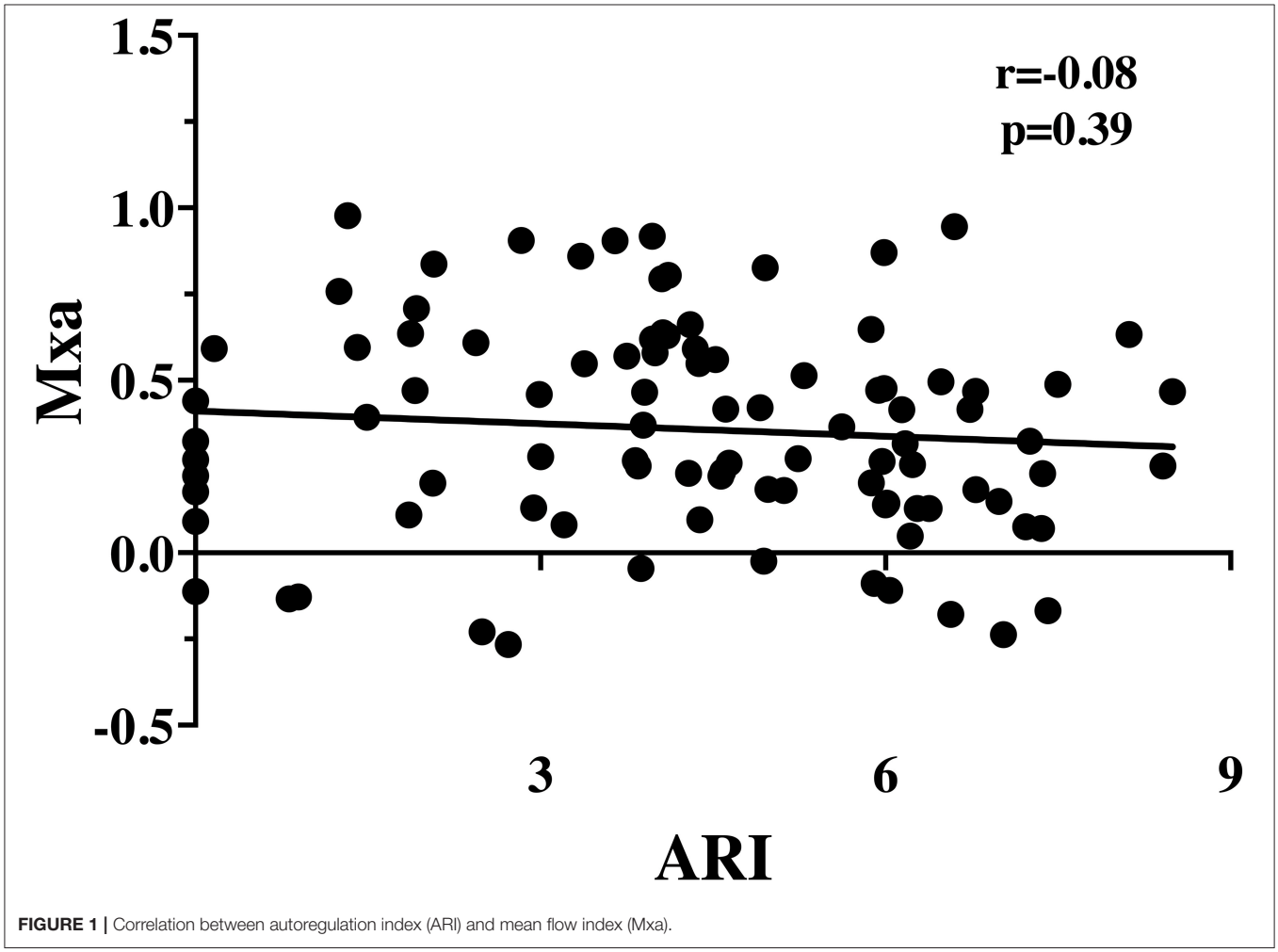

FIGURE 1 | Correlation between autoregulation index (ARI) and mean flow index (Mxa).

TABLE 2 | Comparison of altered and intact cerebral autoregulation using autoregulation index (ARI) and mean flow index (Mxa) thresholds.

		Mxa		
		Altered	**Preserved**	**Total**
ARI	Altered	23	17	40
	Preserved	27	28	55
	Total	50	45	95

others (23/34, 68% vs. 27/61, 44%, $p = 0.03$), whereas ARI did not differ between these two groups. No other differences were found between subgroups (**Table 4**).

DISCUSSION

In this study, we have shown that ARI and Mxa, two validated indices to assess dCA using invasive BP signal and cerebral FVs, are not inter-changeable in a large cohort of critically ill patients with sepsis. These data underline the need for further comparison between various indices of dCA in clinical practice in order to better standardize the approach to analyze this important physiological phenomenon.

Given the limited understanding of the pathophysiological processes of brain dysfunction in sepsis and the complexity of the mechanisms underlying CAR, identifying the "gold standard" index that would be suitable to quantify dCA at the bedside in these patients remains a difficult task. Over the last years, different studies have introduced new indices of dCA (i.e., based on oxygen saturation, COx; or on brain oxygen pressure, ORx), which have been "validated" not using direct measurements of CBF and their relationship to BP variations, but through the comparison with other available dCA indices (as an example, one based on intracranial pressure monitoring, PRx) (18). Although this approach has been repeatedly used in the literature, it has some important caveats: (a) a significant correlation between two indices does not imply that they have the same accuracy to define impaired dCA; (b) the presence of an acute brain injury in the studied population may affect the generalizability of one specific dCA index into a non-brain injured patients' population, as the pathophysiological mechanisms resulting in impaired dCA might differ between these two groups; and (c) the methodological

TABLE 3 | Differences between patients according to the combination of mean flow index (Mxa) and autoregulation index (ARI) values (see "Methods" Section).

	All patients ($n = 95$)	Altered CAR ($n = 23$)	Divergent CAR ($n = 44$)	Intact CAR ($n = 28$)	*p*-value
Age, years	64 (13)	65 (14)	64 (14)	63 (12)	0.86
Male gender, *n* (%)	70 (74)	17 (74)	32 (73)	21 (75)	0.99
APACHE II score on admission	23 (11)	26 (11)	23 (11)	22 (9)	0.38
ICU length of stay, days	6 [3–14]	8 [4–18]	5 [3–14]	5 [3–12]	0.29
ICU mortality, *n* (%)	20 (21)	6 (26)	12 (27)	2 (7)	0.09
At time of dCA assessment					
Sedation, *n* (%)	34 (36)	11 (48)	19 (43)	4 (14)	0.14
NMBA, *n* (%)	13 (14)	3 (13)	9 (21)	1 (4)	0.11
Mechanical ventilation, *n* (%)	52 (55)	17 (74)	24 (55)	11 (39)	0.05
Vasopressors, *n* (%)	69 (73)	20 (87)	29 (66)	20 (71)	0.19
Infection source, *n* (%)					
Abdominal	42 (44)	8 (35)	21 (48)	13 (46)	0.62
Respiratory	26 (27)	5 (22)	15 (34)	6 (21)	0.44
Urinary tract	7 (7)	3 (13)	1 (2)	3 (11)	0.18
Others	20 (21)	7 (30)	7 (16)	6 (21)	0.34
Pathogen, *n* (%)					
Bacterial	66 (70)	14 (61)	35 (80)	17 (61)	0.14
Fungus	9 (10)	5 (22)	3 (7)	1 (4)	0.09
Virus	3 (3)	0 (0)	2 (5)	1 (4)	0.80
Unknown bug	17 (18)	4 (17)	4 (9)	9 (32)	0.29

Data are presented as count (%), mean (SD), or median [(25^{th}–75^{th}) percentiles].
APACHE II, Acute Physiology Age Chronic Health Evaluation II; ICU, intensive care unit; LOS, length of stay; NMBA, neuromuscular blocking agent; dCA, dynamic cerebral autoregulation; CAR, cerebral autoregulation.

TABLE 4 | Differences between impaired cerebral autoregulation according to Mxa and ARI in different subgroups of patients.

	Altered ARI ($n = 40$)	Altered Mxa ($n = 50$)	*p*-value
MV *(n = 52)*	27	31	0.54
NON MV *(n = 43)*	13	19	0.26
p-value	0.04	0.15	
Sedatives *(n = 34)*	18	23	0.36
No-sedatives *(n = 61)*	22	27	0.42
p-value	0.13	0.03	
NMBA *(n = 13)*	8	7	0.99
No-NMBA *(n = 82)*	32	43	0.09
p-value	0.14	0.99	
Vasopressors *(n = 69)*	33	36	0.71
No vasopressors *(n = 26)*	7	14	0.12
p-value	0.10	0.99	
Survivors *(n = 75)*	29	37	0.22
Non-survivors *(n = 20)*	11	13	0.77
p-value	0.21	0.31	

MV, mechanical ventilation; NMBA, neuromuscular blocking agent; Mxa, mean flow index; ARI, autoregulation index.

characteristics to obtain some of these indices (i.e., for PRx, how long the recording should be, how many seconds the window of assessment should last, and which is the percentage of overlap between windows) are not entirely standardized and may vary across studies (19); reliability, reproducibility, and diagnostic and prognostic values are not always similar.

In our study focusing on patients with sepsis, ARI and Mxa showed a non-significant correlation, had a poor agreement to categorize the dCA impairment and even the proportion of patients identified as "impaired dCA" was different according to the used index. In the subgroup analysis, the presence of mechanical ventilation and sedation had a different impact on the determination of CAR function between the different indices. Unfortunately, we do not have a clear explanation for these findings, and some hypotheses include the use of different analytic constructs to obtain ARI and Mxa, the presence of "noise" or an inappropriate assumption, i.e., the analysis if performed at a "steady state," whereas this is not the case in reality.

If we consider the analytic constructs underlying Mxa and ARI, both indices investigate dCA by measuring fluctuations of the MCA blood FV and arterial BP; however, Mxa is computed using a linear regression analysis, it is a non-parametric value and is not based on a predefined model (18). Moreover, Mxa describes the stability of CBF to changes in BP and quantifies how the variation of pressure would be significantly associated with variations in flow. As this approach is purely based on a time-domain measurement of dCA, Mxa has a "quasi-static" approach, since in most cases no information can be obtained about the speed of the response (20). On the contrary, ARI is based on a model in which the response of flow to a hypothetical impulse

change in BP is estimated and therefore compared with the theoretical impulse response; as such, ARI explains how rapidly flow recovers after any change in pressure and is theoretically more sensitive to physiological changes than Mxa. ARI reflects both the temporal and amplitude relationship between CPP and CBF, which characterizes the dynamic dCA assessment (14, 19, 21). However, the validity of such model in different categories of patients remains unknown.

Another potential explanation is the presence of known or unknown "noise," which can be present during recordings in different categories of patients. These factors could be minimal changes in $PaCO_2$, which is a potent modulator of vascular reactivity, PaO_2, which can also modify CBF in case of extreme oxygen values, or intracranial pressure (6). As not all patients in our cohort were on mechanical ventilation, $PaCO_2$ might present significant fluctuations, therefore impacting on BF recordings. In one study, the addition of different intensity of "noise" to artificial BF and BP recordings resulted in a flattening of the relationship between ARI and Mx (22).

In one study conducted in patients with traumatic brain injury (TBI), ARI was significantly related to Mx (i.e., an index derived from CPP and FVs, which has a similar construct than Mxa), although the relationship was not linear (23). However, the authors also pointed out that both indices lost sensitivity for extreme values (i.e., close to −1 or +1 for Mx and ARI of <2). In another study from the same group focusing again on TBI, ARI, and Mx showed a significant linear relationship and correlated with outcome (18). These differences with our findings might be related to the different patients' populations (i.e., TBI vs. sepsis), the presence of brain injury and/or elevated intracranial pressure, which is extremely rare in sepsis, and different therapeutic strategies, which could result in different baseline BP values (i.e., higher in TBI than in sepsis) and lower BP variability (i.e., autonomous nervous system dysfunction during sepsis) (24) between groups. Other studies have also compared different indices among them, reporting conflicting results (18, 25–27). Only one of these studies compared different indices in patients with sepsis (28), used near-infrared spectroscopy and transfer Fourier analysis, concluding that these metrics are not interchangeable either. Future research should focus more frequently on comparison between different dCA indices in various diseases and quantify CAR through multiple analytical approaches, paying attention to their respective limitations and the caveats that must be considered.

A number of limitations of this study need to be mentioned. Our study was limited to only two of the many indices that are commonly used for the assessment of dCA. Including other indices could have identified better agreements. The application of Mxa and ARI to spontaneous BP recordings is also a limitation; it has been reported that increased variability of BP leads to more robust estimates of autoregulation (29, 30), accepting that different protocols, such as sit-to-stand or sudden release of compressed thigh-cuffs (31) can lead to different values of metrics. Nevertheless, protocols that induce significant changes in BP are not feasible in a critical care environment. Third, we routinely recorded $PaCO_2$ values; $PaCO_2$ is one of the strongest determinants of dCA performance (5), and it could have affected the ARI and Mxa in different ways. However, not all patients were on the controlled mechanical ventilation, and this might have resulted in variable $PaCO_2$ values over the recording period for those on spontaneous breathing. Fourth, dCA was dichotomized as intact or impaired using specific thresholds proposed in previous studies; however, at least for Mxa, a threshold of 0.45 has also been suggested to better identify impaired dCA (32, 33), and healthy volunteers have also been found with Mxa values above 0.3 (33). However, the lack of correlation between absolute Mxa and ARI values would not significantly change the conclusions of our study if a different Mxa threshold would have been used to define impaired dCA. Fifth, we did not specifically assess the relationship of ARI or Mxa with the occurrence of brain complications, brain imaging, or mortality, and these analyses were beyond the scope of this investigation. Finally, Mxa could be highly dependent on the analytic approach (i.e., blocks, correlation periods, and overlaps of FV and BP), with a moderate repeatability (34); a recognized "gold standard" approach has not been identified yet.

CONCLUSIONS

In this cohort of patients with sepsis, two of the most common indices used for the assessment of dCA, the ARI, and the Mxa, had a weak correlation and a poor agreement to classify dCA. These findings underline the limitations in comparing results on dCA from different studies, which used different analytic approaches to characterize dCA. A standardization for the dCA assessment is definitely warranted.

DATA AVAILABILITY STATEMENT

The raw data supporting the conclusions of this article will be made available by the authors, without undue reservation.

ETHICS STATEMENT

The studies involving human participants were reviewed and approved by Comité d'Ethique Erasme-ULB. Written informed consent for participation was not required for this study in accordance with the national legislation and the institutional requirements.

AUTHOR CONTRIBUTIONS

AQ-C, JC, and FT conceived the study and wrote the draft of the paper. AQ-C, IC, and CS selected the population and performed the TCD. AQ-C, JC, IC, and CS collected the data. AQ-C and FT conducted the statistical analysis. FT and RP revised the text for intellectual content. The authors read and approved the final manuscript.

REFERENCES

1. Perner A, Gordon AC, De Backer D, Dimopoulos G, Russell JA, Lipman J, et al. Sepsis: frontiers in diagnosis, resuscitation and antibiotic therapy. *Intensive Care Med.* (2016) 42:1958–69. doi: 10.1007/s00134-016-4577-z
2. Fleischmann C, Scherag A, Adhikari NKJ, Hartog CS, Tsaganos T, Schlattmann P, et al. Assessment of global incidence and mortality of hospital-treated sepsis. Current estimates and limitations. *Am J Respir Crit Care Med.* (2016) 193:259–72. doi: 10.1164/rccm.201504-0781OC
3. Mazeraud A, Righy C, Bouchereau E, Benghanem S, Bozza FA, Sharshar T. Septic-associated encephalopathy: a comprehensive review. *Neurother J Am Soc Exp Neurother.* (2020) 17:392–403. doi: 10.1007/s13311-020-00862-1
4. Taccone FS, Su F, De Deyne C, Abdellhai A, Pierrakos C, He X, et al. Sepsis is associated with altered cerebral microcirculation and tissue hypoxia in experimental peritonitis. *Crit Care Med.* (2014) 42:e114–22. doi: 10.1097/CCM.0b013e3182a641b8
5. Crippa IA, Subirà C, Vincent J-L, Fernandez RF, Hernandez SC, Cavicchi FZ, et al. Impaired cerebral autoregulation is associated with brain dysfunction in patients with sepsis. *Crit Care Lond Engl.* (2018) 22:327. doi: 10.1186/s13054-018-2258-8
6. Paulson OB, Strandgaard S, Edvinsson L. Cerebral autoregulation. *Cerebrovasc Brain Metab Rev.* (1990) 2:161–92.
7. Rosenblatt K, Walker KA, Goodson C, Olson E, Maher D, Brown CH, et al. Cerebral autoregulation-guided optimal blood pressure in sepsis-associated encephalopathy: a case series. *J Intensive Care Med.* (2020) 35:1453–64. doi: 10.1177/0885066619828293
8. Berg RMG, Plovsing RR, Bailey DM, Holstein-Rathlou N-H, Møller K. Dynamic cerebral autoregulation to induced blood pressure changes in human experimental and clinical sepsis. *Clin Physiol Funct Imaging.* (2016) 36:490–6. doi: 10.1111/cpf.12256
9. Ferlini L, Su F, Creteur J, Taccone FS, Gaspard N. Cerebral autoregulation and neurovascular coupling are progressively impaired during septic shock: an experimental study. *Intensive Care Med Exp.* (2020) 8:44. doi: 10.1186/s40635-020-00332-0
10. Berg RMG, Plovsing RR. Effects of short-term mechanical hyperventilation on cerebral blood flow and dynamic cerebral autoregulation in critically ill patients with sepsis. *Scand. J Clin Lab Invest.* (2016) 76:226–33. doi: 10.3109/00365513.2015.1137350
11. Ebersoldt M, Sharshar T, Annane D. Sepsis-associated delirium. *Intensive Care Med.* (2007) 33:941–50. doi: 10.1007/s00134-007-0622-2
12. Tiecks FP, Lam AM, Aaslid R, Newell DW. Comparison of static and dynamic cerebral autoregulation measurements. *Stroke J Cereb Circ.* (1995) 26:1014–9. doi: 10.1161/01.STR.26.6.1014
13. Czosnyka M, Smielewski P, Kirkpatrick P, Menon DK, Pickard JD. Monitoring of cerebral autoregulation in head-injured patients. *Stroke.* (1996) 27:1829–34. doi: 10.1161/01.STR.27.10.1829
14. Panerai RB. Transcranial Doppler for evaluation of cerebral autoregulation. *Clin Auton Res Off J Clin Auton Res Soc.* (2009) 19:197–211. doi: 10.1007/s10286-009-0011-8
15. Caldas JR, Passos RH, Ramos JGR, Ramalho C, Sancho LS, Salinet AM, et al. Dynamic autoregulation is impaired in circulatory shock. *Shock Augusta Ga.* (2020) 54:183–9. doi: 10.1097/SHK.0000000000001488
16. Czosnyka M, Miller C, Participants in the international multidisciplinary consensus conference on multimodality monitoring. Monitoring of cerebral autoregulation. *Neurocrit Care.* (2014) 21(Suppl. 2):S95–102. doi: 10.1007/s12028-014-0046-0
17. Cohen J. A coefficient of agreement for nominal scales. *Educ Psychol Meas.* (1960) 20:37–46. doi: 10.1177/001316446002000104
18. Czosnyka M, Smielewski P, Lavinio A, Pickard JD, Panerai R. An assessment of dynamic autoregulation from spontaneous fluctuations of cerebral blood flow velocity: a comparison of two models, index of autoregulation and mean flow index. *Anesth Analg.* (2008) 106:234–9. doi: 10.1213/01.ane.0000295802.89962.13
19. Panerai RB, White RP, Markus HS, Evans DH. Grading of cerebral dynamic autoregulation from spontaneous fluctuations in arterial blood pressure. *Stroke J Cereb Circ.* (1998) 29:2341–6. doi: 10.1161/01.STR.29.11.2341
20. Simpson DM, Payne SJ, Panerai RB. The INfoMATAS project: methods for assessing cerebral autoregulation in stroke. *J Cereb Blood Flow Metab Off J Int Soc Cereb Blood Flow Metab.* (2021) 42:411–29. doi: 10.1177/0271678X211029049
21. Panerai RB, Haunton VJ, Hanby MF, Salinet AS, Robinson TG. Statistical criteria for estimation of the cerebral autoregulation index (ARI) at rest. *Physiol Meas.* (2016) 37:661–72. doi: 10.1088/0967-3334/37/5/661
22. Liu X, Czosnyka M, Donnelly J, Cardim D, Cabeleira M, Lalou DA, et al. Assessment of cerebral autoregulation indices – a modelling perspective. *Sci Rep.* (2020) 10:9600. doi: 10.1038/s41598-020-66346-6
23. Liu X, Czosnyka M, Donnelly J, Budohoski KP, Varsos GV, Nasr N, et al. Comparison of frequency and time domain methods of assessment of cerebral autoregulation in traumatic brain injury. *J Cereb Blood Flow Metab.* (2014) 35:248–56. doi: 10.1038/jcbfm.2014.192
24. Carrara M, Bollen Pinto B, Baselli G, Bendjelid K, Ferrario M. Baroreflex sensitivity and blood pressure variability can help in understanding the different response to therapy during acute phase of septic shock. *Shock.* (2018) 50:78–86. doi: 10.1097/SHK.0000000000001046
25. Eriksen VR, Hahn GH, Greisen G. Cerebral autoregulation in the preterm newborn using near-infrared spectroscopy: a comparison of time-domain and frequency-domain analyses. *J Biomed Opt.* (2015) 20:037009. doi: 10.1117/1.JBO.20.3.037009
26. Zhang Y, Liu X, Steiner L, Smielewski P, Feen E, Pickard JD, et al. Correlation between cerebral autoregulation and carbon dioxide reactivity in patients with traumatic brain injury. *Acta Neurochir.* (2016) 122:205–9. doi: 10.1007/978-3-319-22533-3_41
27. Tzeng YC, Ainslie PN, Cooke WH, Peebles KC, Willie CK, MacRae BA, et al. Assessment of cerebral autoregulation: the quandary of quantification. *Am J Physiol Circ Physiol.* (2012) 303:658. doi: 10.1152/ajpheart.00328.2012
28. Berg RMG, Plovsing RR. Near-infrared spectroscopy versus transcranial Doppler ultrasound for assessing dynamic cerebral autoregulation by transfer function analysis in sepsis. *Scand J Clin Lab Invest.* (2016) 76:88–91. doi: 10.3109/00365513.2015.1091495
29. Simpson DM, Panerai RB, Ramos EG, Lopes JMA, Marinatto MNV, Nadal J, et al. Assessing blood flow control through a bootstrap method. *IEEE Trans Biomed Eng.* (2004) 51:1284–6. doi: 10.1109/TBME.2004.827947
30. Liu J, Simpson DM, Allen R. High spontaneous fluctuation in arterial blood pressure improves the assessment of cerebral autoregulation. *Physiol Meas.* (2005) 26:725–41. doi: 10.1088/0967-3334/26/5/012
31. Mahdi A, Nikolic D, Birch AA, Olufsen MS, Panerai RB, Simpson DM, et al. Increased blood pressure variability upon standing up improves reproducibility of cerebral autoregulation indices. *Med Eng Phys.* (2017) 47:151–8. doi: 10.1016/j.medengphy.2017.06.006
32. Schmidt EA, Piechnik SK, Smielewski P, Raabe A, Matta BF, Czosnyka M. Symmetry of cerebral hemodynamic indices derived from bilateral transcranial Doppler. *J Neuroimaging.* (2003) 13:248–54. doi: 10.1111/j.1552-6569.2003.tb00186.x
33. Olsen MH, Riberholt CG, Mehlsen J, Berg RM, Møller K. Reliability and validity of the mean flow index (Mx) for assessing cerebral autoregulation in humans: a systematic review of the methodology. *J Cereb Blood Flow Metab.* (2021) 42:27–38. doi: 10.1177/0271678X211052588
34. Olsen MH, Riberholt CG, Plovsing RR, Møller K, Berg RMG. Reliability of the mean flow index (Mx) for assessing cerebral autoregulation in healthy volunteers. *Physiol Rep.* (2021) 9:e14923. doi: 10.14814/phy2.14923

Conflict of Interest: The authors declare that the research was conducted in the absence of any commercial or financial relationships that could be construed as a potential conflict of interest.

frontiers in Neurology

ORIGINAL RESEARCH
published: 08 March 2022
doi: 10.3389/fneur.2022.823494

Effects of Early-Stage Blood Pressure Variability on the Functional Outcome in Acute Ischemic Stroke Patients With Symptomatic Intracranial Artery Stenosis or Occlusion Receiving Intravenous Thrombolysis

Mian-Xuan Yao, Dong-Hai Qiu, Wei-Cheng Zheng, Jiang-Hao Zhao, Han-Peng Yin, Yong-Lin Liu and Yang-Kun Chen**

Department of Neurology, Affiliated Dongguan People's Hospital, Southern Medical University, Dongguan, China

OPEN ACCESS

Edited by:
Xiuyun Liu,
Johns Hopkins University,
United States

Reviewed by:
Zhen-Ni Guo,
First Affiliated Hospital of Jilin University, China
Peter Ringleb,
Heidelberg University, Germany
Chih-Hao Chen,
National Taiwan University Hospital, Taiwan

***Correspondence:**
Yong-Lin Liu
ly_twins@126.com
Yang-Kun Chen
cykun78@163.com

Specialty section:
This article was submitted to Stroke, a section of the journal Frontiers in Neurology

Received: *27 November 2021*
Accepted: *08 February 2022*
Published: *08 March 2022*

Citation:
Yao M-X, Qiu D-H, Zheng W-C, Zhao J-H, Yin H-P, Liu Y-L and Chen Y-K (2022) Effects of Early-Stage Blood Pressure Variability on the Functional Outcome in Acute Ischemic Stroke Patients With Symptomatic Intracranial Artery Stenosis or Occlusion Receiving Intravenous Thrombolysis. Front. Neurol. 13:823494. doi: 10.3389/fneur.2022.823494

Background: Studies exploring the relationship between blood pressure (BP) fluctuations and outcome in acute ischemic stroke (AIS) patients treated with intravenous thrombolysis (IVT) are limited. We aimed to investigate the influence of blood pressure variability (BPV) during the first 24 h after IVT on early neurological deterioration (END) and 3-month outcome after IVT in terms of different stroke subtypes.

Methods: Clinical data from consecutive AIS patients who received IVT were retrospectively analyzed. The hourly systolic BP of all patients were recorded during the first 24 h following IVT. We calculated three systolic BPV parameters, including coefficient of variability (CV), standard deviation of mean BP (SD) and successive variation (SV), within the first 6, 12, and 24 h after IVT. END was defined as neurological deterioration with an increase in the National Institutes of Health Stroke Scale (NIHSS) score $\geq$ 4 points within the first 72 h after admission. Follow-up was performed at 90 days after onset, and favorable and poor outcomes were defined as a modified Rankin Scale scores (mRS) of $\leq$1 or $\geq$2, respectively.

Results: A total of 339 patients, which were divided into those with (intracranial artery stenosis or occlusion group, SIASO group) and without (non-SIASO group) SIASO, were included. Among them, 110 patients (32.4%) were with SIASO. Patients in SIASO group had higher NIHSS on admission and difference in term of mRS at 90 days compared with non-SIASO group ($P < 0.001$). In SIASO group, patients in favorable outcome group were younger and had lower NIHSS on admission, lower SV-24 h (14.5 $\pm$ 4.3 vs. 11.8 $\pm$ 3.2, respectively) and lower SD-24 h (12.7 $\pm$ 3.8 vs. 10.9 $\pm$ 3.3, respectively), compared with patients with poor outcome (all $P < 0.05$). In the multivariable logistic regression analysis, compared with the lowest SV (SV < 25% quartile), $SV_{50-75\%}$ [odds ratio (OR) = 4.449, 95% confidence interval (CI) = 1.231–16.075, $P = 0.023$] and $SV_{>75\%}$ (OR = 8.676, 95% CI = 1.892–39.775, $P = 0.005$) were significantly associated with poor

outcome at 3 months in patients with SIASO, adjusted for age, NIHSS on admission and atrial fibrillation. No BPV parameters were associated with END in SIASO group. In non-SIASO group, there were no significant association between BPV patterns and END or 90-day outcome.

Conclusions: SV-24 h had a negative relationship with 3-month outcome in AIS patients with SIASO treated with IVT, indicating that BPV may affect the outcome of AIS.

Keywords: blood pressure variability, symptomatic intracranial artery stenosis or occlusion, intravenous thrombolysis, acute ischemic stroke, prognosis

BACKGROUND

Globally, stroke is the second most common cause of death and the third most common disabling disease (1, 2). Intravenous thrombolysis therapy (IVT) can significantly improve functional outcomes. However, previous studies have reported that IVT outcomes are associated with various factors (3–5), including age (6), Trial of Org 10172 in Acute Stroke Treatment (TOAST) classification (7–10), National Institutes of Health Stroke Scale (NIHSS) score on admission, and systolic blood pressure (SBP) on admission (11).

Previous studies have confirmed that racial difference in intracranial atherosclerosis stenosis (ICAS), and non-Caucasian population are at higher risk of ICAS (12–16). The incidence of ICAS is up to 46.6% in Chinese with ischemic (17). ICAS is an important risk factor for poor prognosis after acute ischemic stroke (AIS) (18, 19).

Blood pressure variability (BPV) is the fluctuation of blood pressure (BP) over a certain period. BP fluctuations are a process of constant adjustment in response to various environmental factors, both inside and outside the body, to better adapt to the needs of the body. Fluctuations of BP are related to a range of factors, such as mood, temperature, and circadian rhythms. These factors ultimately influence BP by affecting nerve and humoral regulation (20). Recently, higher BPV within 24 h after stroke was reported to be associated with poor outcome after IVT (11, 19, 21–23). However, ICAS, which is identified to be associated with poor outcome after AIS as we mentioned before, was not analyzed in these previous studies. Hemodynamic change is one of the possible mechanisms for cerebral infarction caused by ICAS. The hemodynamic status in the ICAS territory can be easily altered by BP fluctuation (24, 25). Under normal condition, cerebral autoregulation occurs to maintain the cerebral blood flow against the effect of hypoperfusion or hyperperfusion (26). However, cerebral autoregulation is impaired after ischemic stroke, especially for patients with ICAS (24). The fluctuation of peripheral blood pressure can significantly affect cerebral perfusion pressure in these patients. A rapid drop of BP may easily lead to a rapidly decreasing perfusion, especially in patients with ICAS, while a rapid rise of BP may potentially lead to intracranial hemorrhage, which might result in early neurological deterioration (END) and poorer outcome (24, 25). Nevertheless, studies focusing on the relationship between BPV and outcome of AIS patients with symptomatic ICAS are still limited. In the present study, we aimed to explore the influence of BPV during the first 24 h after IVT on END and 3-month outcome in patients who had intracranial artery stenosis or occlusion (SIASO) and received IVT.

METHODS

Patient Selection

Patients with AIS who were treated with recombinant tissue plasminogen activator (r-tPA) IVT and admitted to Dongguan People's Hospital between 1 January 2017 and 31 December 2019 were consecutively recruited. The inclusion criteria were as follows: (1) aged >18 years; (2) AIS was confirmed by magnetic resonance imaging (MRI) during hospitalization; (3) onset of ischemic stroke symptoms was within 4.5 h of treatment with r-tPA; (4) clinical features and BP were recorded at baseline and then hourly for 24 h after IVT; (5) prestroke modified Rankin Scale (mRS) score ≤1; and (6) follow-up by face-to-face consultation or by phone at 3 months, with complete documentation. The exclusion criteria were as follows: (1) additional endovascular therapy after IVT; (2) incomplete clinical data or lost to follow-up. This study was approved by the ethics committee of Dongguan People's Hospital (approval number: KYKT2018-002). The study was considered exempt from requiring informed consent from patients because of its retrospective nature.

Definition of SIASO

SIASO was defined as no <50% stenosis of the intracranial artery that was responsible for the AIS (27). Symptomatic intracranial artery occlusion (SIAO) was defined as signal loss of distal blood flow ipsilateral to the infarction (27). Patients who didn't meet the criteria of SIAO were those with symptomatic intracranial artery stenosis (SIAS) in SIASO group. The degree of stenosis was measured using three-dimensional time-of-flight magnetic resonance angiography [the MRI parameters are detailed in our previous article (28)] by comparing the vessel diameter at the site of stenosis with the normal vessel diameter distal to the stenosis (29).

Data Collection

Demographic data including age, sex, and a history of hypertension, diabetes mellitus, smoking, atrial fibrillation (AF), and previous stroke were collected. Stroke subtypes were classified according to the TOAST criteria (30), and the NIHSS

on admission, onset-to-treatment time, SBP on admission, and hourly SBP for 24 h after IVT were also collected.

Definition of BPV

The hourly SBPs of all patients were recorded during the first 24 h after IVT using a cuff-type BP monitor. According to the guidelines (31), intravenous urapidil was administered to reduce BP levels to <185/110 mmHg just before r-tPA administration, and to maintain BP levels at <180/105 mmHg during the first 24 h after IVT. The BPV was calculated using the following equation (19):

(1) Standard deviation of mean BP (SD): $\sqrt{1/(n-1)\sum_{i=1}^{(n-1)}(BP_i - BP_{mean})}$,
(2) Coefficient of variability (CV [%]): $SD/BP_{mean} \times 100$,
(3) Successive variation (SV): $\sqrt{1/(n-1)\sum_{i=1}^{(n-1)}(BP_{i+1} - BP_i)^2}$ (19).

Definition of END

In our study, the definition of END referred to neurological deterioration, with an increase in NIHSS score ≥4 points in the first 72 h after admission (32).

Clinical Outcome

We followed up these patients and assessed their mRS scores at 90 days after onset. Favorable and poor outcomes were defined as mRS ≤1 and ≥2, respectively. Incidents of stroke recurrence and death within the follow-up period were also recorded.

Analysis of BPV

BPVs within 6 h (SV-6 h, SD-6 h, CV-6 h), 12 h (SV-12 h, SD-12 h, CV-12 h), and 24 h (SV-24 h, SD-24 h, CV-24 h) after IVT was calculated.SV was a continuous variable and SV-24 h was divided into four grades based on the quartiles. We assessed the relationship between SV and END, so did the relationship between SV and the 3-month outcome. We also assessed the relationship between each interval of SV-24 h and END, as well as the relationship between each interval of SV-24 h and the 3-month outcome.

Statistical Analysis

Statistical analyses were conducted using SPSS for Windows (v.20.0; IBM Corp., Armonk, NY, USA). Continuous variables with a normal distribution were reported as the mean ± SD and non-normally distributed variables as the median and interquartile range. Univariate analyses were performed using the *t*-test/Mann–Whitney *U*-test (for two groups) or one-way analysis of variance/Kruskal–Wallis *H*-test (for three or more groups) for continuous variables, and the χ^2 test for categorical variables. Variables with $P < 0.05$ in the univariate analysis were included in further binary multivariate logistic regressions. Statistical significance was defined as $P < 0.05$ (two-sided). Statistical graphs were drawn using GraphPad Prism (v.9.0; GraphPad Software, San Diego, CA, USA).

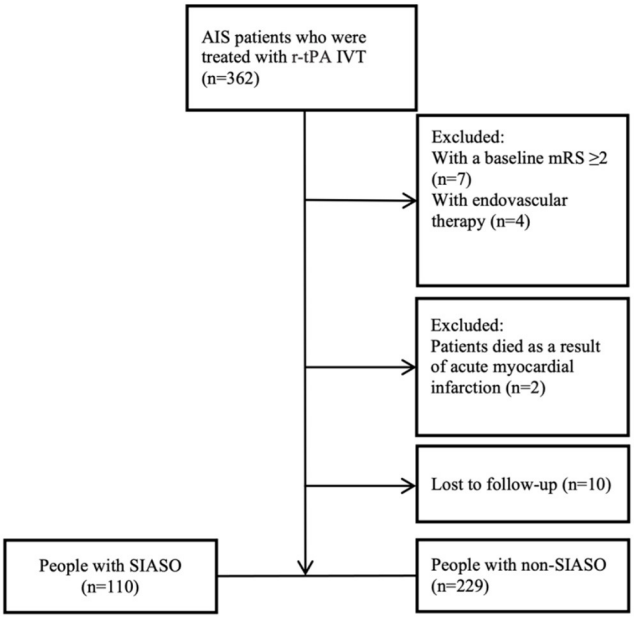

FIGURE 1 | Flowchart of the selection process. AIS, acute ischemic stroke; IVT, intravenous thrombolysis; mRS, modified rankin scale; SIASO, symptomatic intracranial artery stenosis or occlusion.

RESULTS

Patients' Characteristics

Three hundred and sixty-two AIS patients who were treated with r-tPA IVT in our stroke unit were collected consecutively. Among these 362 patients, 23 patients were excluded for the following reasons: baseline mRS ≥ 2 ($n = 7$), underwent additional endovascular therapy ($n = 4$), died as a result of acute myocardial infarction ($n = 2$), and lost to follow-up ($n = 10$). Therefore, 339 patients were enrolled in this study and among them, 110 patients were with SIASO (**Figure 1**).

These 339 patients had a mean age of 61.9 ± 12.1 years. Among them, 248 patients (73.2%) were male, and urapidil was used to lower BP in 34 patients (10.0%) before IVT. Forty-two patients (12.4%) had END and 195 patients (57.5%) had a poor outcome at the 3-month follow-up (**Table 1**).

We divided these 339 patients into two groups (SIASO group and non-SIASO group) based on whether they were with SIASO. There is no difference between these two groups in terms of age (62.0 ± 12.5 vs. 61.8 ± 12.0 years, $P = 0.864$), male (78.2 vs. 70.7%, $P = 0.148$), hypertension (66.4 vs. 72.5%, $P = 0.247$), diabetes mellitus (26.4 vs. 27.1%, $P = 0.890$), smokers/ex-smokers (43.6 vs. 34.1%, $P = 0.088$), AF (20.9 vs. 21.8%, $P = 0.846$), previous stroke (20.9 vs. 14.4%, $P = 0.131$), onset to treatment time (OTT, 194.2 ± 54.8 vs. 195.7 ± 56.6 min, $P = 0.823$) or symptomatic hemorrhagic transformation (sHT, 5.5 vs. 2.2%, $P = 0.112$). Patients in the SIASO group had a higher NIHSS on admission [9.0 (5.8–14.0) vs. 6.0 (4.0–9.0), respectively], a higher mRS at 90 days and a higher rate

TABLE 1 | Characteristics of the study sample.

Characteristics	Total sample ($n = 339$)	SIASO group ($n = 110$)	Non-SIASO group ($n = 229$)	*P*-value
Age[a] (years)	61.9 (12.1)	62.0 (12.5)	61.8 (12.0)	0.864
Men[b], *n* (%)	248 (73.2%)	86 (78.2%)	162 (70.7%)	0.148
Hypertension[b], *n* (%)	239 (70.5%)	73 (66.4%)	166 (72.5%)	0.247
Use antihypertensive therapy before IVT[b], *n* (%)	34 (10.0%)	9 (8.2%)	25 (10.9%)	0.330
Diabetes mellitus[b], *n* (%)	91 (26.8%)	29 (26.4%)	62 (27.1%)	0.890
History of hypercholesterolemia[b], *n* (%)	132 (38.9%)	41 (37.3%)	91 (39.7%)	0.806
Smokers/ex-smokers[b], *n* (%)	126 (37.2%)	48 (43.6%)	78 (34.1%)	0.088
AF[b], *n* (%)	73 (21.5%)	23 (20.9%)	50 (21.8%)	0.846
History of coronary heart disease[b], *n* (%)	18 (5.3%)	9 (8.2%)	19 (8.3%)	0.971
Previous stroke[b], *n* (%)	56 (16.5%)	23 (20.9%)	33 (14.4%)	0.131
Systolic blood pressure on admission[a]	156.5 (24.7)	153.7 (24.0)	158.3 (25.0)	0.141
OTT[a] (minutes)	195.2 (55.9)	194.2 (54.8)	195.7 (56.6)	0.823
NIHSS on admission[c] (IQR, 25–75)	7.0 (4.0–10.0)	9.0 (5.8–14.0)	6.0 (4.0–9.0)	**<0.001**
SIAS[b], *n* (%)	84 (24.8%)	84 (76.4%)	–	–
SIAO[b], *n* (%)	26 (7.7%)	26 (23.6%)	–	–
END[b], *n* (%)	42 (12.4%)	20 (18.2%)	22 (9.6%)	0.019
HT[b], *n* (%)	74 (21.8%)	33 (30.0%)	41 (17.9%)	**0.012**
sHT[b], *n* (%)	10 (2.9%)	6 (5.5%)	5 (2.2%)	0.112
mRS at 90 days[b], *n* (%)				**<0.001**
0	121 (35.7%)	20 (18.2%)	101 (44.1%)	
1	74 (21.8%)	17 (15.5%)	57 (24.9%)	
2	49 (14.5%)	21 (19.1%)	28 (12.2%)	
3	41 (12.1%)	17 (15.5%)	24 (10.5%)	
4	31 (9.1%)	19 (17.3%)	12 (5.2%)	
5	10 (2.9%)	6 (5.5%)	4 (1.7%)	
6	13 (3.8%)	10 (9.1%)	3 (1.3%)	

[a]*Mean (SD), t-test.*
[b]*n (%), chi-square test.*
[c]*Mann–Whiteny U-test.*
NIHSS, national institutes of health stroke scale; OTT, onset to treatment time; AF, atrial fibrillation; mRS, modified rankin scale; END, early neurological deterioration; IVT, intravenous thrombolysis; SIASO, symptomatic intracranial artery stenosis or occlusion; SIAS, symptomatic intracranial arterial stenosis; SIAO, symptomatic intracranial arterial occlusion; HT, hemorrhagic transformation; sHT, symptomatic hemorrhagic transformation. The bold values mean P < 0.05.

of hemorrhagic transformation (HT) compared with the non-SIASO group ($P < 0.05$, respectively). In the SIASO group, there were 26 patients (23.6%) with SIAS and 84 patients (76.4%) with SIAO. The respective characteristics of patients are shown in **Table 1**.

In SIASO group, there were significant differences among these four groups of SV quartiles in terms of age, hypertension, use of antihypertensive therapy before IVT, AF, and mRS score at 90 days. In the non-SIASO group, there were significant differences among the quartiles of SV in terms of hypertension, smokers/ex-smokers, systolic blood pressure on admission, OTT and NIHSS on admission (**Table 2**). In the univariable analysis of risk factors for END, there were no differences in age, AF, SBP on admission, OTT, NIHSS on admission, or medical history between the SIASO and non-SIASO groups (**Table 3**; **Supplementary Table 1**).

In SIASO group, compared with those with favorable outcome, patients with poor outcome were older, with higher NIHSS scores on admission and were more likely to have AF (**Table 3**). In non-SIASO group, those with favorable outcome were older, with higher NIHSS scores on admission as well as longer OTT and were more likely to have AF compared with people in poor outcome group (**Supplementary Table 1**).

Association Between BPV Parameters and Outcomes

Relationship Between BPV Parameters and 3-Month Outcome

Compared with patients in the favorable outcome group, SV-24 h and SD-24 h were significantly higher in the poor outcome group (all $P < 0.05$) in SIASO group, while CV-24 h did not differ between the two groups (**Table 3**). However, SV-24 h, SD-24 h, and CV-24 h were not related with 3-month poor outcome in non-SIASO group (**Supplementary Table 1**).

Independent variables in SIASO group that were significantly different between the favorable and poor outcome groups in the univariable analysis ($p < 0.05$) were then entered into the subsequent logistic regression models (**Table 4**). We set two

TABLE 2 | Successive blood pressure variability of the study sample.

Characteristics	SIASO group ($n = 110$)					Non-SIASO ($n = 229$)				
	$SV_{<25\%}$ < 10.84 ($n = 27$)	**$SV_{25–50\%}$ = 10.84–13.25 ($n = 28$)**	**$SV_{50–75\%}$ = 13.26–16.00 ($n = 27$)**	**$SV_{>75\%}$ > 16.00 ($n = 28$)**	***P*-value**	**$SV_{<25\%}$ < 10.08 ($n = 57$)**	**$SV_{25–50\%}$ = 10.08–12.93 ($n = 57$)**	**$SV_{50–75\%}$ = 12.94–15.32 ($n = 58$)**	**$SV_{>75\%}$ > 15.32 ($n = 57$)**	***P*-value**
Age[a] (years)	55.4 (13.4)	60.2 (14.1)	67.7 (8.7)	64.7 (9.8)	**0.004**	61.4 (12.3)	60.9 (11.6)	61.7 (12.0)	63.2 (12.2)	0.645
Men[b], *n* (%)	21 (77.8%)	23 (82.1%)	22 (81.5%)	20 (71.4%)	0.475	43 (75.4%)	40 (70.2%)	37 (63.8%)	42 (73.7%)	0.464
Hypertension[b], *n* (%)	16 (59.3%)	16 (57.1%)	17 (63.0%)	24 (85.7%)	**0.026**	41 (71.9%)	38 (66.7%)	38 (65.5%)	49 (86.0%)	**0.050**
Use antihypertensive therapy before IVT[b], *n* (%)	1 (3.7%)	1 (3.6%)	0	7 (25.0%)	**0.002**	4 (7.0%)	5 (8.8%)	12 (20.7%)	4 (7.0%)	0.089
Diabetes mellitus[b], *n* (%)	4 (14.8%)	6 (21.4%)	9 (33.3%)	10 (35.7%)	0.472	12 (21.1%)	16 (28.1%)	17 (29.3%)	17 (29.8%)	0.822
History of hypercholesterolemia[b], *n* (%)	7 (25.9%)	11 (39.3%)	11 (40.7%)	12 (42.9%)	0.787	19 (33.3%)	23 (40.4%)	22 (37.9%)	27 (47.4%)	0.408
Smokers/ex-smokers[b], *n* (%)	11 (40.7%)	13 (46.4%)	9 (33.3%)	15 (53.6%)	0.082	24 (42.1%)	11 (19.3%)	21 (36.2%)	22 (38.6%)	**0.042**
AF[b], *n* (%)	3 (11.1%)	5 (17.9%)	6 (22.2%)	9 (32.1%)	**0.006**	15 (26.3%)	10 (17.5%)	14 (24.1%)	11 (19.3%)	0.575
History of coronary heart disease[b], *n* (%)	1 (3.7%)	1 (3.6%)	5 (18.5%)	2 (7.1%)	0.705	7 (12.3%)	4 (7.0%)	3 (5.2%)	5 (8.8%)	0.591
Previous stroke[b], *n* (%)	3 (11.1%)	4 (14.3%)	4 (14.8%)	12 (42.9%)	0.137	9 (15.8%)	7 (12.3%)	10 (17.2%)	7 (12.3%)	0.818
Systolic blood pressure on admission[a]	148.1 (23.8)	150.8 (27.8)	147.1 (21.8)	168.9 (16.1)	0.353	149.3 (23.5)	154.7 (24.7)	167.1 (25.7)	162.1 (22.4)	**0.001**
OTT[a] (minutes)	183.0 (55.2)	181.1 (52.7)	215.9 (47.8)	197.3 (58.4)	0.067	219.5 (47.9)	185.6 (59.0)	184.0 (59.6)	193.9 (53.1)	**0.011**
NIHSS on admission[c] (IQR, 25–75)	8.0 (4.0–14.0)	9.5 (6.0–14.0)	7.0 (4.0–15.0)	9.0 (6.3–13.8)	0.091	6.0 (4.0–10.0)	7.0 (4.0–11.0)	5.5 (4.0–8.0)	5.0 (3.0–7.0)	**0.021**
END[b], *n* (%)	2 (7.4%)	5 (17.9%)	4 (14.8%)	9 (32.1%)	0.320	5 (8.8%)	8 (14.0%)	6 (10.3%)	3 (5.3%)	0.449
mRS at 90 days[b], *n* (%)					**0.007**					0.232
0	7 (25.9%)	4 (14.3%)	4 (14.8%)	5 (17.9%)		26 (45.6%)	18 (31.6%)	28 (48.3%)	29 (50.9%)	
1	6 (22.2%)	7 (25.0%)	2 (7.4%)	2 (7.1%)		14 (24.6%)	15 (26.3%)	12 (20.7%)	16 (28.1%)	
2	6 (22.2%)	1 (3.6%)	7 (25.9%)	7 (25.0%)		9 (15.8%)	7 (12.3%)	8 (13.8%)	4 (7.0%)	
3	3 (11.1%)	6 (21.4%)	4 (14.8%)	4 (14.3%)		2 (3.5%)	12 (21.1%)	5 (8.6%)	5 (8.8%)	
4	5 (18.5%)	6 (21.4%)	7 (25.9%)	1 (3.6%)		3 (5.3%)	5 (8.0%)	2 (3.4%)	2 (3.5%)	
5	0	2 (7.1%)	2 (7.4%)	2 (7.1%)		2 (3.5%)	0	2 (3.4%)	0	
6	0	2 (7.1%)	1 (3.7%)	7 (25.0%)		1 (1.8%)	0	1 (1.7%)	1 (1.8%)	

[a]*One-way ANOVA.*

[b]x^2 *test.*

[c]*Kruskal-Wallis H test.*

SV, successive variability of systolic blood pressure; NIHSS, national institutes of health stroke scale; OTT, onset to treatment time; AF, atrial fibrillation; mRS, modified rankin scale; END, early neurological deterioration; IVT, intravenous thrombolysis; SIASO, symptomatic intracranial artery stenosis or occlusion. The bold values mean P < 0.05.

TABLE 3 | Risk factors of the 3-month poor outcome and END in univariable analysis of SIASO group.

	Poor outcome (mRS = 2–6) (*n* = 73)	Favorable outcome (mRS = 0–1) (*n* = 37)	$t/X^2/z$ value	*P*-value	With END (*n* = 20)	Without END (*n* = 90)	$t/X^2/z$ Value	*P*-value
Age[a] (years)	64.8 (10.9)	56.7 (13.8)	−3.129	**0.003**	64.8 (10.3)	61.43 (12.9)	−1.077	0.284
Men[b], *n* (%)	12 (16.4%)	12 (32.4%)	3.682	0.055	17 (85.0%)	69 (76.7%)	0.666	0.556
Hypertension[b], *n* (%)	51 (69.9%)	22 (59.5%)	1.191	0.275	17 (85.0%)	56 (62.2%)	3.803	0.067
Use antihypertensive therapy before IVT[b], *n* (%)	7 (9.6%)	2 (5.4%)	0.572	0.715	4 (20.0%)	5 (5.6%)	4.545	0.055
Diabetes mellitus[b], *n* (%)	21 (28.8%)	8 (21.6%)	0.646	0.422	6 (30.0%)	23 (25.6%)	0.167	0.683
History of hypercholesterolemia[b], *n* (%)	25 (34.7%)	16 (43.2%)	0.756	0.385	6 (68.4%)	35 (61.1%)	0.357	0.550
Smokers/ex-smokers[b], *n* (%)	31 (42.5%)	17 (45.9%)	0.121	0.728	11 (55.0%)	37 (41.1%)	1.283	0.257
AF[b], *n* (%)	20 (27.4%)	3 (8.1%)	5.525	**0.024**	6 (30.0%)	17 (18.9%)	1.222	0.269
History of coronary heart disease[b], *n* (%)	8 (11.0%)	1 (2.7%)	2.228	0.268	2 (10.0%)	7 (7.8%)	0.108	0.666
Previous stroke[b], *n* (%)	19 (26.1%)	4 (10.8%)	3.438	0.083	6 (30.0%)	17 (18.9%)	1.222	0.269
Systolic blood pressure on admission[a]	153.7 (24.4)	153.2 (24.2)	−0.108	0.914	161.2 (25.6)	151.9 (23.7)	−1.488	0.140
OTT[a] (minutes)	201 (49.8)	180.9 (62.0)	−1.842	0.068	193.0 (56.8)	194.5 (54.6)	0.115	0.909
NIHSS on admission[c] (IQR, 25–75)	11.0 (7.0–16.0)	6.0 (3.5–9.0)	−4.377	**<0.001**	10 (5.3–16.3)	9 (5.8–14.0)	−0.641	0.522
SV-24 h[a]	14.5 (4.3)	11.8 (3.2)	−3.650	**<0.001**	15.2 (4.3)	13.2 (4.0)	−1.972	0.051
SD-24 h[a]	12.7 (3.8)	10.9 (3.3)	−2.569	**0.012**	13.7 (4.8)	11.7 (3.4)	−1.751	0.093
CV-24 h[a]	8.9 (2.6)	8.0 (2.4)	−3.650	0.092	9.2 (3.2)	8.5 (2.4)	−1.165	0.247

[a]*Mean (SD), t-test.*
[b]*n (%), chi-square test.*
[c]*Mann–Whiteny U-test.*
SV-24 h, successive variability of systolic blood pressure within the first 24 hours after IVT; SD-24 h, standard deviation of systolic blood pressure within the first 24 hours after IVT; CV-24 h, coefficient of systolic blood pressure variation within the first 24 hours after IVT; NIHSS, national institutes of health stroke scale; OTT, onset to treatment time; IVT, intravenous thrombolysis; AF, atrial fibrillation; mRS, modified rankin scale; END, early neurological deterioration; SIASO, symptomatic intracranial artery stenosis or occlusion. The bold values mean P < 0.05.

models for logistic regression. In Model 1, age, NIHSS score on admission, AF, SD-24 h, and overall SV-24 h were entered using a backward Wald method. NIHSS score on admission [odds ratio (OR) = 1.206, 95% confidence interval (CI) = 1.084–1.342, $P = 0.001$] and overall SV (OR = 1.182, 95% CI = 1.035–1.348, $P = 0.013$) were significantly associated with poor outcome at 3 months. In Model 2, patients were divided into four groups based on systolic SV value quartiles ($SV_{<25\%} < 10.84$, $SV_{25-50\%} = 10.84$–13.25, $SV_{50-75\%} = 13.26$–16.00 and $SV_{>75\%} > 16.00$), and these were entered into the model along with the other variables used in Model 1. NIHSS score on admission (OR = 1.227, 95% CI = 1.099–1.369, $P < 0.001$), $SV_{50-75\%}$ ($SV_{<25\%}$ as reference; OR = 4.449, 95% CI = 1.231–16.075, $P = 0.023$), and $SV_{>75\%}$ ($SV_{<25\%}$ as reference; OR = 8.676, 95% CI = 1.892–39.775, $P = 0.005$) were significant predictors of poor outcome at 3 months (**Table 4**). The univariable analysis and logistic regression for non-SIASO patients were shown in **Supplementary Table 2**. The mRS score distribution in SIASO group according to SV quartiles is shown in **Figure 2**.

Interaction Analysis

The interaction analysis of age, AF, hypertension and SV-24 h showed only age and SV-24 h (OR = 1.161, 95% CI = 1.031–1.308, $P = 0.014$) were significantly associated with poor outcome at 3 months in SIASO group, while SV-24 h by age (OR = 0.996, 95% CI = 0.986–1.006, $P = 0.389$), SV-24 h by AF (OR = 1.059, 95% CI = 0.959–1.168, $P = 0.257$) or SV-24 h by hypertension (OR = 1.011, 95% CI = 0.941–1.087, $P = 0.760$) was not significantly associated with poor outcome at 3 months in SIASO group (**Supplementary Table 3**). Interaction analysis of BPV and SIASO on the 3-month poor outcome in all patients with IVT showed NIHSS on admission and SV-24 h by SIASO (interaction variable between SV-24 h and SIASO) (OR = 1.104, 95% CI = 1.060–1.149, $P = <0.001$), rather than SV-24 h (OR = 0.992, 95% CI = 0.937–1.050, $P = <0.774$) or SIASO (OR = 0.388, 95% CI = 0.067–2.247, $P = 0.291$), were significantly associated with poor outcome at 3 months (**Supplementary Table 4**).

Relationship Between BPV Parameters Within the First 6, 12 h After IVT and 3-Month Outcome

In the univariate analysis, compared with patients in the favorable outcome group, SV-6 h, SV-12 h, and SD-12 h were significantly higher in the poor outcome group (all $P < 0.05$) in SIASO group, while SD-6 h, CV-6 h, and CV-12 h did not differ between the two groups (**Supplementary Table 5**). Age,

TABLE 4 | Multivariate logistic regression of risk factors for 3-month poor outcome in SAISO group.

Variable	3-month		
	β	OR (95% CI)	*P*-value
Model[a]			
Age	0.038	1.038 (0.998–1.081)	0.064
NIHSS on admission	0.187	1.206 (1.084–1.342)	**0.001**
AF	0.204	1.227 (0.278–5.403)	0.787
SV-24 h	0.167	1.182 (1.035–1.348)	**0.013**
SD-24 h	−0.048	0.954 (0.780–1.166)	0.643
Model[b]			
Age	0.033	1.033 (0.992–1.076)	0.114
NIHSS on admission	0.204	1.227 (1.099–1.369)	**<0.001**
AF	−0.007	0.993 (0.218–4.520)	0.993
SD-24 h	0.005	1.005 (0.855–1.181)	0.951
SV ($SV_{<25\%}$ as reference)			**0.013**
$SV_{25-50\%}$	0.766	2.152 (0.650–7.128)	0.210
$SV_{50-75\%}$	1.493	4.449 (1.231–16.075)	**0.023**
$SV_{>75\%}$	2.161	8.676 (1.892–39.775)	**0.005**

[a]*With overall SV entered.*
[b]*With categorized SV entered.*
SV-24 h, successive variability of systolic blood pressure within the first 24 hours after IVT; SD-24 h, standard deviation of systolic blood pressure within the first 24 hours after IVT; SIASO, symptomatic intracranial artery stenosis or occlusion; AF, atrial fibrillation. The bold values mean P < 0.05.

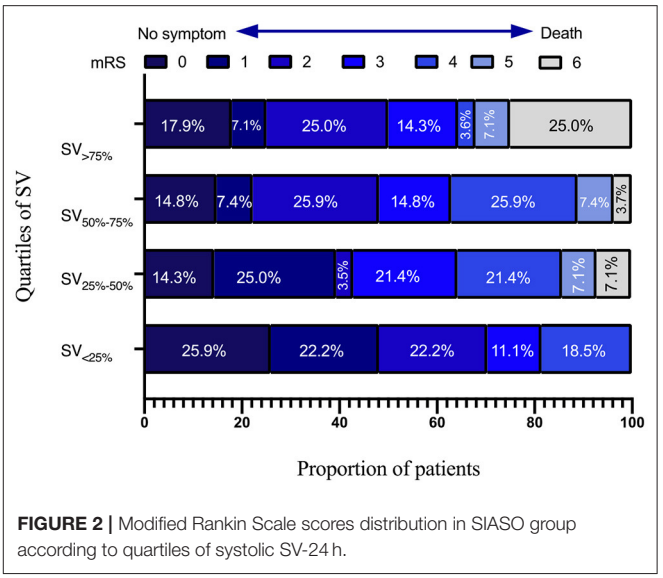

FIGURE 2 | Modified Rankin Scale scores distribution in SIASO group according to quartiles of systolic SV-24 h.

NIHSS score on admission, AF, SV-6 h, SD-12 h, and SV-12 h were entered into the subsequent logistic regression models (**Supplementary Table 6**). SV-6 h ($P = 0.130$), SD-12 h ($P = 0.960$), and SV-12 h ($P = 0.066$) were not significantly associated with poor outcome at 3 months (**Supplementary Table 6**).

Relationship Between BPV Parameters and END

In SIASO group, although SV-24 h, SD-24 h, and CV-24 h all appeared to be higher in END group than in without-END group, there were no significant differences between the two groups (**Table 3**). In non-SIASO group, SV-24 h, SD-24 h, and CV-24 h were also not significantly different between END and without-END groups (**Supplementary Table 1**).

Relationship Between BPV Parameters and HT or sHT

No relationship was found between the 3 BPV patterns (SV-24 h, SD-24 h, and CV-24 h) and all HT or sHT neither in SIASO group or in non-SIASO group, (**Supplementary Tables 7**, **8**).

DISCUSSION

In the present study, higher systolic SV-24 was associated with poorer 3-month outcome in patients with SIASO who were treated with IVT. An increase in systolic SV-24 h may thus predict a higher risk of poor outcome at 3 months. However, there was no clear relationship between any pattern of BPV and 3-month outcome in patients without SIASO. There was not relationship between BPV and END in neither of the two groups. Our findings may help physicians to identify patients with a relatively high risk of poor outcome at 3 months.

SV is an important index of BPV, and in our study SV-24 h was associated with 3-month outcome in AIS patients after IVT in patients with SIASO, while it was not associated with 3-month outcome in patients without SIASO. A study by Yong and Kaste (33) in the European Cooperative Acute Stroke Study II trial revealed that high SBP variability is associated with poor outcome. Furthermore, an analysis from the Third International Stroke Trial (IST-3) reported an association between higher BPV and adverse events, the occurrence of symptomatic intracranial hemorrhage, and poor 6-month outcome (34). However, patients with and without SIASO were not assessed separately in those studies. In the IST-3 study, BP was measured only at three timepoints after IVT (34), while we measured BP hourly for at least 24 h after IVT. Thus, the BPV in our study was likely more accurate than in other studies that measured BP less frequently. Additionally, we studied the effect of BPV within different times after IVT on 3 months poor outcome and we found that SV-24 h, rather than BPV patterns within the first 6 or 12 h after IVT, was associated with poor outcomes at 3 months, which was rarely reported in previous studies. Therefore, it is important to avoid excessive fluctuations in BP within 24 h after IVT in patients with SIASO. We also analyzed the 3-month poor outcome of all IVT patients by the interaction of SV-24 h and SIASO, and it showed that the interaction did have a significant effect on 3 months poor outcome, which also confirms the finding that SV-24 h affect the 3-month outcome only in patients with SIASO.

Our study indicated that higher SV-24 h was associated with worse outcome at 3 months after IVT in patients with SIASO rather than in those without SIASO. Although there were some studies on the relationship between BPV and prognosis of AIS after IVT, they did not focus on the patients with SIASO. As ischemic stroke is a clinical syndrome with various pathogenesis,

including large artery atherosclerosis, small arterial occlusion, and cardiogenic embolism, and BP fluctuations have different effects on ischemic stroke caused by different mechanisms (35), our research will be more targeted. In addition, 33–55% of ischemic stroke in Chinese is caused by intracranial arterial stenosis or occlusion (IASO) (35). Therefore, IASO should be taken into consideration when studying the relationship between BPV and ischemic stroke outcome. In our study, we evaluated intracranial arteries by 3D-TOF-MRA. Due to the limitations of MRA for assessing the degree of stenosis of cerebral arteries, it was difficult to distinguish SIAO from SIAS accurately. Therefore, it would be reasonable to combine SIAO and SIAS into the category of SIASO.

Recent studies have reported that many patients have autonomic dysfunction after ischemic stroke (36–38). BP fluctuation is a manifestation of autonomic dysfunction. During the early stage of ischemic stroke, a rapid increase in BP may cause intracranial pressure to rise and edema or bleeding to occur at the infarction site, which can lead to death or poor functional outcome (25). However, a large decrease in BP may lead to low perfusion in the infarct area; this effect might be much clearer in AIS patients with large-artery stenosis because patients with SIASO are very sensitive to BP fluctuations, especially in the first few hours after AIS (25, 26).

Cerebral autoregulation (CA) is the ability of the brain to regulate its own blood supply, which maintains an adequate and stable cerebral blood flow despite changes in cerebral perfusion pressure. However, CA is impaired after ischemic stroke, and this autoregulation is damaged in patients with SIASO; furthermore, patients with more severe stenosis tend to have more severe dysautoregulation (35). One study reported that CA impairment ipsilateral to the AIS is associated with a larger infarction and poorer clinical outcome compared with patients with unimpaired CA ipsilateral to the AIS (35, 39). With CA impairment, BP fluctuations have an important effect on cerebral blood flow. Moreover, when BPV increases to levels beyond the regulation of CA, it can lead to hypoperfusion or hyperperfusion in the infarction area (35, 39).

In the present study, high SV-24 h after IVT among patients with SIASO increased the risk of poor outcome at 3 months. This finding may help physicians to screen the most high-risk patients with poor prognosis from other high-risk patients at the early stage of AIS, and thus provide more appropriate interventions. Theoretically, since BP fluctuation in early stage of ischemic stroke may lead to hypoperfusion or intracerebral hemorrhage (24), BPV should be associated with END. However, we did not find any correlation between BPV and END. One possible reason is that in our study, there were only 20 patients (18.2%) with END in SIASO group which may not be powerful to detect the difference of BPV between with END and without END groups. Nevertheless, we found a tendency of association between high BPV and the occurrence of END. Besides, previous studies by other researchers have also failed to find a link between short-term outcome (2-week outcome and in-hospital outcome) and BPV during the acute phase of ischemic stroke (11, 39, 40).

The accuracy of BP measurement for patients with AF might be controversial. In theory, irregular ventricular rate in patients with AF may lead to more pronounced fluctuation in BP than in patients with sinus heart rate. However, we didn't exclude patients with AF in our study. Olson et al. analyzed 42 patients with AF in the condition of AF and sinus rhythm, and the result showed they had similar BPV in these two conditions (41). Maria et al. studied 13,827 patients and found no significant difference in BPV between patients with AF and patients with sinus rhythm (42). Besides, Guideline from American Heart Association in 2009 also specified that oscillographic blood pressure monitors were reliable in patients with AF (43).

Commonly-used BPV parameters consist of SV, SD, and CV. In our study, we found that a high SV-24 h, rather than SD-24 h or CV-24 h, may predict 3-month poor outcome in SIASO group. SD represents the dispersion of values around the mean but does not reflect the effect of the measuring sequence of BP. Since CV is calculated from SD, it does not reflect the aforementioned effect, either. SV estimates the variation in successive measurements and thus takes the sequence into account (44). Therefore, SV is more commonly used in studies because it better reflects the time-series variability of BP. In contrast, SD and CV couldn't reflect the temporal changes in the data, which can result in the same SD or CV in individuals with different clinical characteristics (45).

In our study, SV-24 h was higher in patients who were older and more likely to have hypertension or AF. However, an interaction term analysis was performed (**Supplementary Table 7**) and it demonstrated that SV-24 h was a risk factor of poor outcome independent of age and hypertension, which was similar to a previous review (46).

There were several strengths to our study. First, BPV was calculated by recording hourly BP within 24 h after thrombolysis, which was far more frequently than in other studies and led to more accurate BPV results [11, 14]. Second, to the best of our knowledge, ours was one of the few studies to have focused on AIS patients after IVT and consider the effects of SIASO on prognosis. However, there were also several limitations in our study. First, the sample size was relatively small. Second, our study was a retrospective study. Third, magnetic resonance angiography was used to evaluate arterial stenosis in this study; however, this method is not as accurate as digital subtraction angiography for evaluating arterial stenosis and might overestimate SIASO. Forth, only four stroke patients received EVT during our research from 2017 to 2019 as we were still developing emergent endovascular therapy in our hospital, thus the finding of our study may be limited. Lastly, intermittent cuff measurement was used to monitor BP in the present study, while continuous cuff monitoring or invasive arterial BP are more accurate.

CONCLUSION

Systolic SV had a negative relationship with 3-month outcome in AIS patients with SIASO who were treated with IVT, which indicates that BPV may affect the outcome of AIS. Further multi-center prospective studies with larger sample sizes are warranted.

DATA AVAILABILITY STATEMENT

The raw data supporting the conclusions of this article will be made available by the authors, without undue reservation.

ETHICS STATEMENT

The studies involving human participants were reviewed and approved by the Ethics Committee of Dongguan People's Hospital (approval number: KYKT2018-002). Written informed consent for participation was not required for this study in accordance with the national legislation and the institutional requirements.

AUTHOR CONTRIBUTIONS

Y-KC and Y-LL designed the work and analyzed the data. M-XY, W-CZ, D-HQ, W-CZ, and H-PY collected the clinical data. M-XY and Y-LL wrote the manuscript. M-XY and J-HZ wrote the diagrams. All authors read and approved the final manuscript, contributed toward data analysis, drafted and revised the paper, and agreed to be accountable for all aspects of the work.

FUNDING

This study was funded by the Guangdong Sci-Tech Commissioner Project, Grant/Award (Number: 20201800500572). The funding body had no role in the design of the study, collection, analysis, and interpretation of the data, and in writing of the manuscript.

SUPPLEMENTARY MATERIAL

The Supplementary Material for this article can be found online at: https://www.frontiersin.org/articles/10.3389/fneur.2022.823494/full#supplementary-material

REFERENCES

1. Lozano R, Naghavi M, Foreman K, Lim S, Shibuya K, Aboyans V, et al. Global and regional mortality from 235 causes of death for 20 age groups in 1990 and 2010: a systematic analysis for the global burden of disease study 2010. *Lancet*. (2016) 380:2095–128. doi: 10.1016/S0140-6736(12)61728-0
2. Murray CJ, Vos T, Lozano R, Naghavi M, Flaxman AD, Michaud C, et al. Disability-adjusted life years (DALYs) for 291 diseases and injuries in 21 regions, 1990–2010: a systematic analysis for the global burden of disease study 2010. *Lancet*. (2012) 380:2197–223. doi: 10.1016/S0140-6736(12)61689-4
3. Liu YL, Xiao WM, Lu JK, Wang YZ, Lu ZH, Zhong HH, et al. Asymmetrical cortical vessel sign predicts prognosis after acute ischemic stroke. *Brain Behav*. (2020) 10:e01657. doi: 10.1002/brb3.1657
4. Marler JR, Tilley BC, Lu M, Brott TG, Lyden PC, Grotta JC, et al. Early stroke treatment associated with better outcome: The NINDS rt-PA stroke study. *Neurology*. (2000) 55:1649–55. doi: 10.1212/WNL.55.11.1649
5. Lees KR, Bluhmki E, von Kummer R, Brott TG, Toni D, Grotta JC, et al. Time to treatment with intravenous alteplase and outcome in stroke: an updated pooled analysis of ECASS, ATLANTIS, NINDS, and EPITHET trials. *Lancet*. (2010) 375:1695–703. doi: 10.1016/S0140-6736(10)60491-6
6. Broderick JP, Phillips SJ, O'Fallon WM, Frye RL, Whisnant JP. Relationship of cardiac disease to stroke occurrence, recurrence, and mortality. *Stroke*. (1992) 23:1250–6. doi: 10.1161/01.STR.23.9.1250
7. Thanvi B, Treadwell S, Robinson T. Early neurological deterioration in acute ischaemic stroke: predictors, mechanisms and management. *Postgrad Med J*. (2008) 84:412–7. doi: 10.1136/pgmj.2007.066118
8. Simonsen CZ, Schmitz ML, Madsen MH, Mikkelsen IK, Chandra RV, Leslie-Mazwi T, et al. Early neurological deterioration after thrombolysis: clinical and imaging predictors. *Int J Stroke*. (2016) 11:776–82. doi: 10.1177/1747493016650454
9. Kim JM, Moon J, Ahn SW, Shin HW, Park KY. The etiologies of early neurological deterioration after thrombolysis and risk factors of ischemia progression. *J Stroke Cerebrovasc Dis*. (2016) 25:383–8. doi: 10.1016/j.jstrokecerebrovasdis.2015.10.010
10. Ray BK, Hazra A, Ghosal M, Banerjee T, Chaudhuri A, Singh V, et al. Early and delayed fatality of stroke in Kolkata, India: Results from a 7-year longitudinal population-based study. *J Stroke Cerebrovasc Dis*. (2013) 22:281–9. doi: 10.1016/j.jstrokecerebrovasdis.2011.09.002
11. Kellert L, Hametner C, Ahmed N, Rauch G, MacLeod MJ, Perini F, et al. Reciprocal interaction of 24-hour blood pressure variability and systolic blood pressure on outcome in stroke thrombolysis. *Stroke*. (2017) 48:1827–34. doi: 10.1161/STROKEAHA.117.016876
12. Caplan LR, Gorelick PB, Hier DB. Race, sex and occlusive cerebrovascular disease: a review. *Stroke*. (1986) 17:648–55. doi: 10.1161/01.STR.17.4.648
13. Wong K, Li H, Chan Y, Ahuja A, Lam W, Wong A, et al. Use of transcranial Doppler ultrasound to predict outcome in patients with intracranial large-artery occlusive disease. *Stroke*. (2000) 31:2641–7. doi: 10.1161/01.STR.31.11.2641
14. Cruz-Flores S, Mazighi M, Ducrocq X, Bracard S, Houdart E, Woimant F. Prospective study of symptomatic atherothrombotic intracranial stenoses: the GESICA study. *Neurology*. (2006) 66:1187–91. doi: 10.1212/01.wnl.0000208404.94585.b2
15. Huang YN, Gao S, Li SW, Huang Y, Li JF, Wong KS, et al. Vascular lesions in Chinese patients with transient ischemic attacks. *Neurology*. (1997) 48:524–5. doi: 10.1212/WNL.48.2.524
16. Lee SJ, Cho S-J, Moon H-S, Shon YM, Chung CS. Combined extracranial and intracranial atherosclerosis in Korean patients. *Arch Neurol*. (2003) 60:1561–4. doi: 10.1001/archneur.60.11.1561
17. Wang Y, Zhao X, Liu L, Soo Y, Pu Y, Pan Y, et al. Prevalence and outcomes of symptomatic intracranial large artery stenoses and occlusions in China: the Chinese Intracranial Atherosclerosis (CICAS) Study. *Stroke*. (2014) 45:663–9. doi: 10.1161/STROKEAHA.113.003508
18. Famakin BM, Chimowitz MI, Lynn MJ, Stern BJ, George MG. Causes and severity of ischemic stroke in patients with symptomatic intracranial arterial stenosis. *Stroke*. (2009) 40:1999–2003. doi: 10.1161/STROKEAHA.108.546150
19. Barnett HJ, Gunton RW, Eliasziw M, Fleming L, Sharpe B, Gates P, et al. Causes and severity of ischemic stroke in patients with internal carotid artery stenosis. *JAMA*. (2000) 283:1429–36. doi: 10.1001/jama.283.11.1429
20. Sayk F, Teckentrup C, Becker C, Heutling D, Wellhöner P, Lehnert H, et al. Effects of selective slow-wave sleep deprivation on nocturnal blood pressure dipping and daytime blood pressure regulation. *Am J Physiol Regul*. (2010) 67:R191–7. doi: 10.1152/ajpregu.00368.2009
21. Endo K, Kario K, Koga M, Nakagawara J, Shiokawa Y, Yamagami H, et al. Impact of early blood pressure variability on stroke outcomes after thrombolysis the SAMURAI rt-PA registry. *Stroke*. (2013) 44:816–8. doi: 10.1161/STROKEAHA.112.681007
22. Kellert L, Sykora M, Gumbinger C, Herrmann O, Ringleb PA. Blood pressure variability after intravenous thrombolysis in acute stroke does not predict intracerebral hemorrhage but poor outcome. *Cerebrovasc Dis*. (2021) 33:135–40. doi: 10.1159/000334186
23. Castillo J, Leira R, García MM, Serena J, Blanco M, Dávalos A. Blood pressure decrease during the acute phase of ischemic stroke is associated

with brain injury and poor stroke outcome. *Stroke.* (2004) 35:520–6. doi: 10.1161/01.STR.0000109769.22917.B0
24. Ko Y, Park JH, Yang MH, Ko SB, Han MK, Oh CW, et al. The significance of blood pressure variability for the development of hemorrhagic transformation in acute ischemic stroke. *Stroke.* (2010) 41:2512–8. doi: 10.1161/STROKEAHA.110.595561
25. Powers WJ. Acute hypertension after stroke: the scientific basis for treatment decisions. *Neurology*. (1993) 43:461–7. doi: 10.1212/WNL.43.3_Part_1.461
26. Markus H, Cullinane M. Severely impaired cerebrovascular reactivity predicts stroke and TIA risk in patients with carotid artery stenosis and occlusion. *Brain*. (2001) 124(Pt 3):457–67. doi: 10.1093/brain/124.3.457
27. Chimowitz MI, Strong J, Brown MB, Perkins A, Fayad PB. Prognosis of patients with symptomatic vertebral or basilar artery stenosis. *Stroke.* (1998) 29:1389–92. doi: 10.1161/01.STR.29.7.1389
28. Yin HP, Qiu DH, Qu JF, Lu ZH, Wang F, Liang MQ. Multiple hypointense vessels on susceptibility-weighted imaging predict early neurological deterioration in acute ischaemic stroke patients with severe intracranial large artery stenosis or occlusion receiving intravenous thrombolysis. *Stroke Vasc Neurol.* (2020) 5:361–7. doi: 10.1136/svn-2020-000343
29. Buchan AM. North American Symptomatic Carotid Endarterectomy Trial Collaborators. Beneficial effect of carotid endarterectomy in symptomatic patients with high grade carotid stenosis. *N Engl J Med.* (1991) 325:445–53. doi: 10.1056/NEJM199108153250701
30. Adams Jr HP, Bendixen BH, Kappelle LJ, Biller J, Love BB, Gordon DL, et al. Classification of subtype of acute ischemic stroke. Definitions for use in a multicenter clinical trial. TOAST. Trial of Org 10172 in Acute Stroke Treatment. *Stroke*. (1993) 24:35–41. doi: 10.1161/01.STR.24.1.35
31. Shinohara Y, Yanagihara T, Abe K, Yoshimine T, Fujinaka T, Chuma T, et al. II. Cerebral infarction/transient ischemic attack (TIA). *J Stroke Cerebrovasc Dis.* (2011) 20:S31–73. doi: 10.1016/j.jstrokecerebrovasdis.2011.05.004
32. Siegler JE, Schild SM. Early Neurological seterioration (END) after stroke: the END depends on the definition. *Int J Stroke.* (2011) 6:211–2. doi: 10.1111/j.1747-4949.2011.00596.x
33. Yong M, Kaste M. Association of characteristics of blood pressure profiles and stroke outcomes in the ECASS-II trial. *Stroke.* (2008) 39:366–72. doi: 10.1161/STROKEAHA.107.492330
34. Berge E, Cohen G, Lindley RI, Sandercock P, Wardlaw JM, Sandset EC, et al. Effects of blood pressure and blood pressure-lowering treatment during the first 24 hours among patients in the Third International Stroke Trial of Thrombolytic treatment for acute ischemic stroke. *Stroke.* (2015) 46:3362–9. doi: 10.1161/STROKEAHA.115.010319
35. Chen J, Liu J, Xu WH, Xu R, Hou B, Cui LY, et al. Impaired dynamic cerebral autoregulation and cerebrovascular reactivity in middle cerebral artery stenosis. *PLoS ONE.* (2014) 9:e88232. doi: 10.1371/journal.pone.0088232
36. Tang S, Xiong L, Fan Y, Mok V, Leung TW. Stroke outcome prediction by blood pressure variability, heart rate variability, and baroreflex sensitivity. *Stroke.* (2020) 51:1317–20. doi: 10.1161/STROKEAHA.119.027981
37. Dütsch M, Burger M, Dörfler C, Schwab S, Hilz MJ. Cardiovascular autonomic function in poststroke patients. *Neurology.* (2007) 69:2249–55. doi: 10.1212/01.wnl.0000286946.06639.a7
38. Li X, Ge T, Leung H, Soo Y, Leung T. Autonomic dysfunction predicts clinical outcomes after acute ischemic stroke: a prospective observational study. *Stroke.* (2018) 49:215–8. doi: 10.1161/STROKEAHA.117.019312
39. Tziomalos K, Giampatzis V, Bouziana SD, Spanou M, Kostaki S, Papadopoulou M, et al. No association observed between blood pressure variability during the acute phase of ischemic stroke and in-hospital outcomes. *Am J Hypertens.* (2016) 29:841–6. doi: 10.1093/ajh/hpv191
40. Manning LS, Mistri AK, Potter J, Rothwell PM, Robinson TG. Short-term blood pressure variability in acute stroke: post hoc analysis of the controlling hypertension and hypotension immediately post stroke and continue or stop post-stroke antihypertensives collaborative study trials. *Stroke.* (2015) 46:1518–24. doi: 10.1161/STROKEAHA.115.009078
41. Olsen R, Amlie A, Omvik P. Twenty-four-hour ambulatory blood pressure monitoring in atrial fibrillation. *Blood Press Monit.* (2002) 7:149–56. doi: 10.1097/00126097-200206000-00002
42. Mehlum MH, Liestøl K, Wyller TB, Hua TA, Rostrup M, Berge E. Blood pressure variability in hypertensive patients with atrial fibrillation in the VALUE trial. *Blood Press.* (2019) 28:1–7. doi: 10.1080/08037051.2018.1524707
43. Muntner P, Shimbo D, Carey RM, Charleston JB. Measurement of blood pressure in humans: a scientific statement from the American Heart Association. *Hypertension.* (2019) 73:e35–66. doi: 10.1161/HYP.0000000000000087
44. Divani AA, Liu X, Napoli MD, Lattanzi S, Ziai Z, James MJA, et al. Blood pressure variability predicts poor in-hospital outcome in spontaneous intracerebral hemorrhage. *Stroke.* (2019) 50:2023–9. doi: 10.1161/STROKEAHA.119.025514
45. Xu B, Ji Q, Zhang Y, Shen L, Cao M, Cai K. Postoperative blood pressure variability exerts an influence on clinical outcome after coil embolization of ruptured intracranial aneurysms. *Neurol Res.* (2017) 39:813–8. doi: 10.1080/01616412.2017.1348653
46. Appiah KOB, Patel M, Panerai RB, Robinson TG, Haunton VJ. Increased blood pressure variability following acute stroke is associated with poor long-term outcomes: a systematic review. *Blood Press Monit.* (2019) 24:67–73. doi: 10.1097/MBP.0000000000000366

Conflict of Interest: The authors declare that the research was conducted in the absence of any commercial or financial relationships that could be construed as a potential conflict of interest.

Publisher's Note: All claims expressed in this article are solely those of the authors and do not necessarily represent those of their affiliated organizations, or those of the publisher, the editors and the reviewers. Any product that may be evaluated in this article, or claim that may be made by its manufacturer, is not guaranteed or endorsed by the publisher.

frontiers in Neurology

ORIGINAL RESEARCH
published: 22 March 2022
doi: 10.3389/fneur.2022.780896

Alterations in Functional Network Topology Within Normal Hemispheres Contralateral to Anterior Circulation Steno-Occlusive Disease: A Resting-State BOLD Study

Junjie Wu[1], *Fadi Nahab*[2,3], *Jason W. Allen*[1,2,4], *Ranliang Hu*[1], *Seena Dehkharghani*[5,6] *and Deqiang Qiu*[1,4*]

[1] Department of Radiology and Imaging Sciences, Emory University School of Medicine, Atlanta, GA, United States, [2] Department of Neurology, Emory University School of Medicine, Atlanta, GA, United States, [3] Department of Pediatrics, Emory University School of Medicine, Atlanta, GA, United States, [4] Joint Department of Biomedical Engineering, Emory University and Georgia Institute of Technology, Atlanta, GA, United States, [5] Department of Radiology, New York University Langone Medical Center, New York, NY, United States, [6] Department of Neurology, New York University Langone Medical Center, New York, NY, United States

OPEN ACCESS

Edited by:
Xiuyun Liu,
Johns Hopkins University,
United States

Reviewed by:
Liming Hsu,
University of North Carolina at Chapel Hill, United States
Ali Golestani,
University of Toronto, Canada

***Correspondence:**
Deqiang Qiu
deqiang.qiu@emory.edu

Specialty section:
This article was submitted to Applied Neuroimaging, a section of the journal Frontiers in Neurology

Received: 21 September 2021
Accepted: 21 February 2022
Published: 22 March 2022

Citation:
Wu J, Nahab F, Allen JW, Hu R, Dehkharghani S and Qiu D (2022) Alterations in Functional Network Topology Within Normal Hemispheres Contralateral to Anterior Circulation Steno-Occlusive Disease: A Resting-State BOLD Study. Front. Neurol. 13:780896. doi: 10.3389/fneur.2022.780896

The purpose of this study was to assess spatially remote effects of hemodynamic impairment on functional network topology contralateral to unilateral anterior circulation steno-occlusive disease (SOD) using resting-state blood oxygen level-dependent (BOLD) imaging, and to investigate the relationships between network connectivity and cerebrovascular reactivity (CVR), a measure of hemodynamic stress. Twenty patients with unilateral, chronic anterior circulation SOD and 20 age-matched healthy controls underwent resting-state BOLD imaging. Five-minute standardized baseline BOLD acquisition was followed by acetazolamide infusion to measure CVR. The BOLD baseline was used to analyze network connectivity contralateral to the diseased hemispheres of SOD patients. Compared to healthy controls, reduced network degree (z-score $= -1.158 \pm 1.217$, $P < 0.001$, false discovery rate (FDR) corrected), local efficiency (z-score $= -1.213 \pm 1.120$, $P < 0.001$, FDR corrected), global efficiency (z-score $= -1.346 \pm 1.119$, $P < 0.001$, FDR corrected), and enhanced modularity (z-score $= 1.000 \pm 1.205$, $P = 0.002$, FDR corrected) were observed in the contralateral, normal hemispheres of SOD patients. Network degree ($P = 0.089$, FDR corrected; $P = 0.027$, uncorrected) and nodal efficiency ($P = 0.089$, FDR corrected; $P = 0.045$, uncorrected) showed a trend toward a positive association with CVR. The results indicate remote abnormalities in functional connectivity contralateral to the diseased hemispheres in patients with unilateral SOD, despite the absence of macrovascular disease or demonstrable hemodynamic impairment. The clinical impact of remote functional disruptions requires dedicated investigation but may portend far reaching consequence for even putatively unilateral cerebrovascular disease.

Keywords: cerebrovascular reserve, functional magnetic resonance imaging, graph theory, functional connectivity, cerebrovascular disease

INTRODUCTION

Patients with chronic steno-occlusive disease (SOD) of the cerebrovascular system are at risk of ischemic stroke (1, 2). Cerebral hypoperfusion and impaired hemodynamics, which can be evaluated by cerebrovascular reactivity (CVR), lead to ischemic or potentially selective neuronal damage among these patients (3). Previous resting-state fMRI studies in stroke and cerebrovascular disease have detected blood oxygen level-dependent (BOLD) connectivity disruptions within several brain networks, including motor, attention, frontoparietal and default mode networks (4–8), and may include long range changes distant or even contralateral to areas of injury, such as in motor networks or interhemispheric functional connectivity (9, 10).

Observations of remote and widespread network dysfunction (11) have compelled investigation into its relation to hemodynamic failure and autoregulation. Graph theory provides an effective tool for capturing the topological principles that govern brain networks (12, 13). Under this framework, numerous lines of evidence support that brain organization is shaped by an optimal balance between functional segregation and integration (14, 15), as well as a trade-off between wiring costs, principles of minimum work, and efficiency of parallel information transfer (16). This configuration can be influenced by brain maturation (17), cognitive states (18–20), and brain diseases (21, 22). While disrupted organization of functional networks has been found in stroke and cerebrovascular disease (23–26), little is known about whether network topology in normal-appearing brain areas contralateral to lesions is similarly vulnerable.

A challenge to such paradigms, however, rests in the nature of BOLD functional network connectivity, which is influenced both by changes in neurovascular coupling and true neural connections (27, 28). In cerebrovascular disease, neurovascular coupling is likely impaired, particularly in the diseased hemispheres, which can undermine attempts to recover BOLD changes and thus faithful representations of connectivity (29, 30). Importantly, however, as even normal-appearing brain parenchyma contralateral to SOD may be affected by sub-clinical hemodynamic compromise and increased stroke risk (31, 32), we anticipated that remote, occult alterations in the hemodynamic response function could accompany or even drive changes in BOLD functional connectivity within the putatively normal hemispheres of such patients. Examining BOLD networks in the contralateral hemispheres and their associations with CVR may deepen our understanding of functional brain networks in cerebrovascular disease and potentially illuminate well-recognized, non-ischemic consequence of SOD such as cognitive and other functional impairments (33).

In the present study, we aimed to investigate remote effects of hemodynamic compromise on BOLD functional connectivity of the contralateral hemispheres in unilateral, chronic cerebral SOD, hypothesizing the presence of measurable disturbances in functional connectivity remote and even contralateral to SOD in patients with unilateral macrovascular disease on cross-sectional or catheter angiographic cerebrovascular imaging. Graph-theory metrics of functional networks were estimated using resting-state BOLD, addressing two questions: (i) As compared to healthy controls, do observable network alterations exist within the contralateral, normal hemispheres in SOD patients? (ii) Does network connectivity correlate with cerebral hemodynamics as measured by CVR in the normal-appearing hemispheres of the patients?

MATERIALS AND METHODS

Participants

Twenty patients with unilateral chronic SOD of the anterior circulation were studied (age, 49.00 ± 11.38 years; range, 29–70 years; seven males, 13 females; seven patients with right-sided disease), including eight patients with occlusion or high-grade (>75%) stenosis of the cervical internal carotid artery (ICA), 6 patients with occlusion or high-grade (>75%) stenosis of the intracranial ICA, 1 patient with occlusion of the middle cerebral artery, and five patients with idiopathic intracranial SOD. For each patient, the diseased hemisphere was determined on 3D time-of-flight MR angiography ($N = 20$), as well as on CT angiography ($N = 7$) or digital subtraction angiography ($N = 13$) when available. All imaging was assessed by a vascular neurologist (F.N.) and one of neuroradiologists (J.W.A. and S.D.), each with >10 years of experience.

Twenty age-matched healthy controls (age, 40.75 ± 16.21 years; range, 20-68 years; 12 males, 8 females) were enrolled for comparison. This study was approved by the Institutional Review Board at Emory University School of Medicine. Informed consent was obtained from healthy controls and retrospective review of patient data was performed.

Data Acquisition and Preprocessing

MR imaging was performed on a Siemens Tim Trio 3-Tesla scanner (Siemens Healthcare, Erlangen, Germany) equipped with a 32-channel head array coil in all patients with SOD. Twenty-minute (600 volumes) continuous BOLD data were collected using a gradient-echo echo-planar imaging (EPI) sequence (TR/TE = 2,000/30 ms, FA = 78°, FOV = 220 × 220 mm^2, matrix = 64 × 64, slice thickness = 4 mm, 30 slices). After 5 min of baseline BOLD acquisition, acetazolamide (ACZ) (1 gram dissolved in 10 mL normal saline) was slowly infused intravenously over 3–5 min, followed by normal saline flush. The healthy controls underwent resting-state BOLD imaging without ACZ enhanced BOLD measurement for 13.33 min (400 volumes) using the same scan protocol with the same MRI scanner and coil models (Siemens Tim Trio with 32-channel head array coil). To avoid bias, the same duration of BOLD measurement from both patients and healthy controls was used for network analysis, as detailed below. In both patient and control groups, a high-resolution 3D anatomical image was also acquired using an axial T_1-weighted magnetization-prepared rapid acquisition with gradient echo (MPRAGE) sequence (TR/TE = 1,900/3.52 ms, FA = 9°, FOV = 216 × 256 mm^2, matrix = 216 × 256, slice thickness = 1 mm, 176 slices).

Images were processed using SPM8 (Wellcome Trust Center for Neuroimaging, University College London, London, UK) and MATLAB (MathWorks, Natick, Massachusetts, USA).

Anatomical MPRAGE image was co-registered to BOLD images, and segmented to create gray matter, white matter (WM) and cerebrospinal fluid (CSF) masks. BOLD data preprocessing comprised removal of the first 10 volumes (20 s), slice-timing correction, motion correction, normalization to Montreal Neurological Institute space, and spatial smoothing with a 6-mm Gaussian kernel. For network analysis, the first 5 min of data were used, and underwent linear detrending, regression of nuisance signals and temporal band-pass filtering (0.01–0.1 Hz). The nuisance signals included head-motion profiles as well as WM and CSF signals. WM and CSF signals were extracted from contralateral hemispheres in the patients to eliminate contamination from lesions (8), and from both left and right hemispheres in the healthy controls.

CVR Calculation

CVR was measured by estimating the cerebrovascular response to ACZ. Although breath holding or inhalation of gas with increased CO_2 concentration could be also used for CVR measurement, both approaches have their disadvantages. Breath-holding approach requires good subject cooperation and is difficult to control CO_2 concentration in the lungs. While inhalation of gas with increased CO_2 concentration is used in studies and has its advantages, complex gas delivery and sampling apparatus are required, limiting its translation to clinical settings. In contrast, ACZ is a safe and highly tolerated agent, and its intravenous administration is a relatively easy and accepted medical procedure in most patients (34).

In the patients, the mean BOLD images before ($BOLD_{pre-ACZ}$) and after ($BOLD_{post-ACZ}$) ACZ administration were generated by averaging the first and the last 30 volumes (1 min, not including previously discarded volumes) of BOLD data, respectively. CVR maps were then determined as $CVR = (BOLD_{post-ACZ} - BOLD_{pre-ACZ}) / BOLD_{pre-ACZ} \times 100\%$ (34).

Network Construction and Analysis

A network (i.e., graph) comprising *nodes* and *edges* that connect the nodes was established separately for each hemisphere for the purposes of hemispheric analysis. For the patients, the normal-appearing hemispheres contralateral to SOD were analyzed. For the healthy controls, individual hemispheres were analyzed separately to produce hemispheric, reference standard connectivity profiles for comparison and normalization. Nodes were defined by regions of interest (ROIs) in Anatomical Automatic Labeling atlas (35) that divides each hemisphere into 45 regions, and edges represented interregional functional connectivity, measured by Pearson correlation coefficients. Symmetric correlation matrices were built after computing the Pearson correlation coefficients of the average temporal signals between all pairs of ROIs. To convert the correlation matrices to sparse networks, a sparsity threshold, defined as the ratio of the number of actual edges to the maximum possible number of edges in a network, was used. The sparsity-based thresholding method ensures the same number of edges in the resultant networks by applying a network-specific correlation threshold. Currently, there is no definitive way to accurately determine thresholds, therefore the sparsity thresholds in this study were set to 20, 30, and 40%, which are within typical sparsity ranges of human neuron networks (36, 37).

Graph theory was applied to quantify the topological properties of weighted undirected networks using Brain Connectivity Toolbox (38) (http://www.brain-connectivity-toolbox.net). We calculated node-based network metrics including node degree, nodal efficiency E_{nodal}, local efficiency E_{local} and betweenness centrality, and global network metrics including global efficiency E_{global}, modularity and assortativity coefficient. Degree is the sum of all edge weights connected to a node. Nodal efficiency E_{nodal} is defined as the reciprocal of the harmonic mean of shortest path lengths between a given node and all other nodes. The average E_{nodal} across all nodes can be used to evaluate global efficiency E_{global} of parallel information processing in a network. Local efficiency E_{local} is the global efficiency calculated in node neighborhoods. E_{local} is an indicator of fault tolerance, measuring how well the information is transferred between the immediate neighbors of a given node when it is eliminated. Betweenness centrality is determined as the fraction of all shortest paths in the network that pass through a given node, thereby used to detect important nodes for information transfer. Modularity is defined as the ability of a network to be decomposed into subnetworks that are more linked within modules than between modules. Given that the optimal modular structure may be slightly different from run to run owing to heuristics in the algorithm (39), the modularity analysis was repeated 500 times and the averaged modularity was calculated. Assortativity coefficient is a correlation coefficient for the degrees of neighboring nodes, which measures how often nodes with a certain degree are connected to nodes with a similar degree. As an indicator of resilience, assortativity coefficient reflects network vulnerability to insult.

Statistical Analysis

In the healthy controls, the mean and standard deviation (SD) of network measures were calculated for both left and right hemispheres separately as a reference standard for the patients. To evaluate abnormalities in the hemispheres contralateral to SOD in the patient population, network parameters were scored in terms of z-values relative to the mean and SD of the respective hemispheres across all the healthy controls calculated above (**Figure 1**). Specifically, if a patient had right-sided disease, z-scores of network parameters in the left hemisphere were calculated relative to the mean and SD of the left hemispheres across all controls. One-sample t-test was performed to test if the z-scores had a mean of zero. The correlations between network parameters and ROI-specific CVR were evaluated using a linear mixed-effects model, with subject-specific slopes and intercepts modeled as random effects to assess the linear relationships between test variables. The false discovery rate (FDR; $Q < 0.05$) method was employed to correct for multiple comparisons.

RESULTS

Figure 2 shows the averaged maps of degree, local efficiency E_{local}, nodal efficiency E_{nodal}, and betweenness centrality in both hemispheres of the healthy controls and in the contralateral

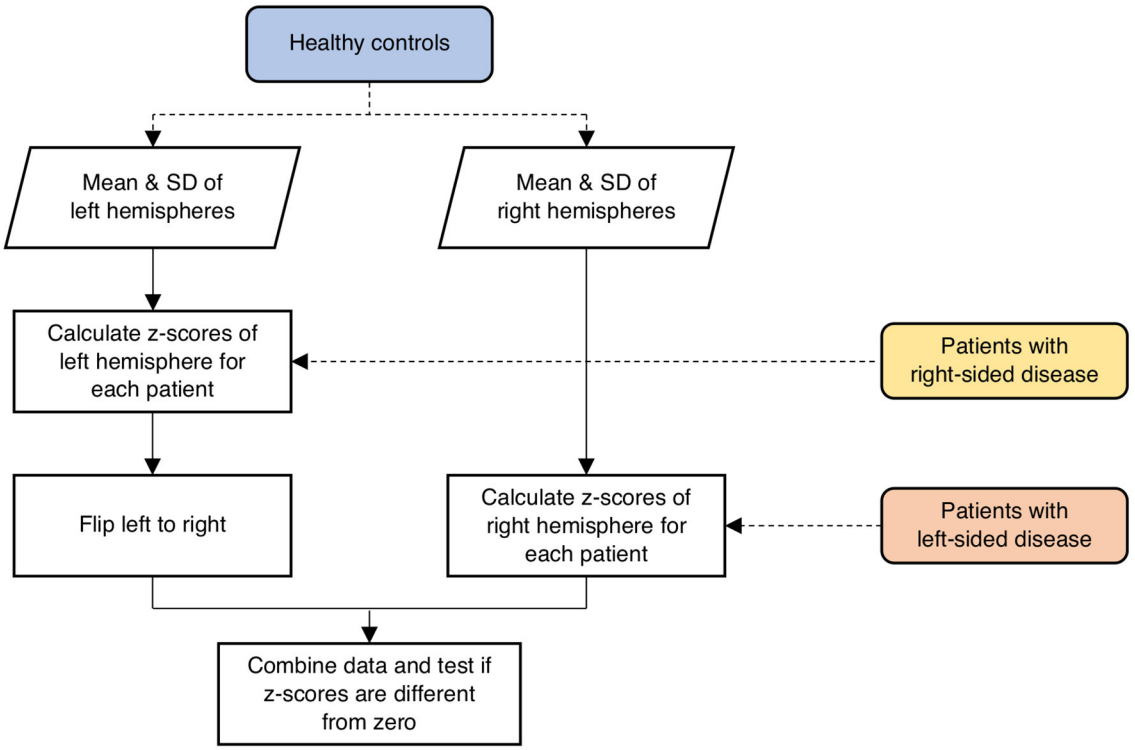

FIGURE 1 | Schematic illustration of the procedure involved in calculating *z*-scores of network parameters in the contralateral hemispheres of the patients relative to the respective hemispheres of the healthy controls. SD, standard deviation.

hemispheres of the patients. In general, degree, E_{local} and E_{nodal} were lower in the patients as compared to the healthy controls. These observations were confirmed by *z*-scores of network parameters in the contralateral hemispheres of the patients relative to the respective hemispheres of the controls (**Figure 3**). One-sample *t*-test showed that at connectivity sparsity = 40%, the z-scores of degree ($P < 0.001$, FDR corrected), E_{local} ($P < 0.001$, FDR corrected), and E_{gobal} ($P < 0.001$, FDR corrected) were lower than zero, suggesting compromised network strength and efficiency in the patient cohort. The z-score of modularity was higher than zero ($P = 0.002$, FDR corrected), which suggests that the brain networks are subdivided into more clearly delineated groups in the patients. Similar results were obtained at connectivity sparsity = 20 and 30% (**Table 1**).

Figure 4 shows the z-maps of degree, E_{local}, E_{nodal}, and betweenness centrality in the contralateral hemispheres averaged over all patients. One-sample *t*-test with FDR correction showed that negative *z*-scores of degree were primarily observed in the supplementary motor, fusiform and temporal cortices. The *z*-scores of network efficiency were lower than zero across the brain. The *z*-scores of betweenness centrality were negative in the Rolandic operculum and inferior temporal gyrus (see **Supplementary Table 1** for more details).

Figure 5 shows maps of CVR and network parameters in the contralateral hemispheres of two representative patients. Visual inspection suggested relationships between degree and CVR, as well as between E_{nodal} and CVR. Mixed-effects model showed a trend toward significant correlations between degree and CVR ($P = 0.089$, FDR corrected; $P = 0.027$, uncorrected), and between E_{nodal} and CVR ($P = 0.089$, FDR corrected; $P = 0.045$, uncorrected), while significance was not observed between E_{local} and CVR ($P = 0.115$, FDR corrected; $P = 0.086$, uncorrected), and between betweenness centrality and CVR ($P = 0.472$, FDR corrected; $P = 0.472$, uncorrected) (**Figure 6**). For the correlations of degree, E_{local} and E_{nodal} with CVR, one patient exhibited a trend deviating from the remainder of the cohort (arrows in **Figure 6**). To estimate the influences of the potential outlier, the same analyses were repeated after excluding this participant. After the outlier exclusion, the associations between degree and CVR ($P = 0.023$, FDR corrected), and between E_{nodal} and CVR ($P = 0.023$, FDR corrected) became significant.

DISCUSSION

This study reveals altered organization of BOLD functional brain networks contralateral to unilateral anterior circulation steno-occlusive disease. Reduced degree and efficiency, and enhanced modularity of functional networks were observed in normal-appearing hemispheres contralateral to SOD in patients as compared to healthy controls, indicating potentially long-range consequence to hemodynamic impairment manifesting in network disruptions or reorganization even remote from

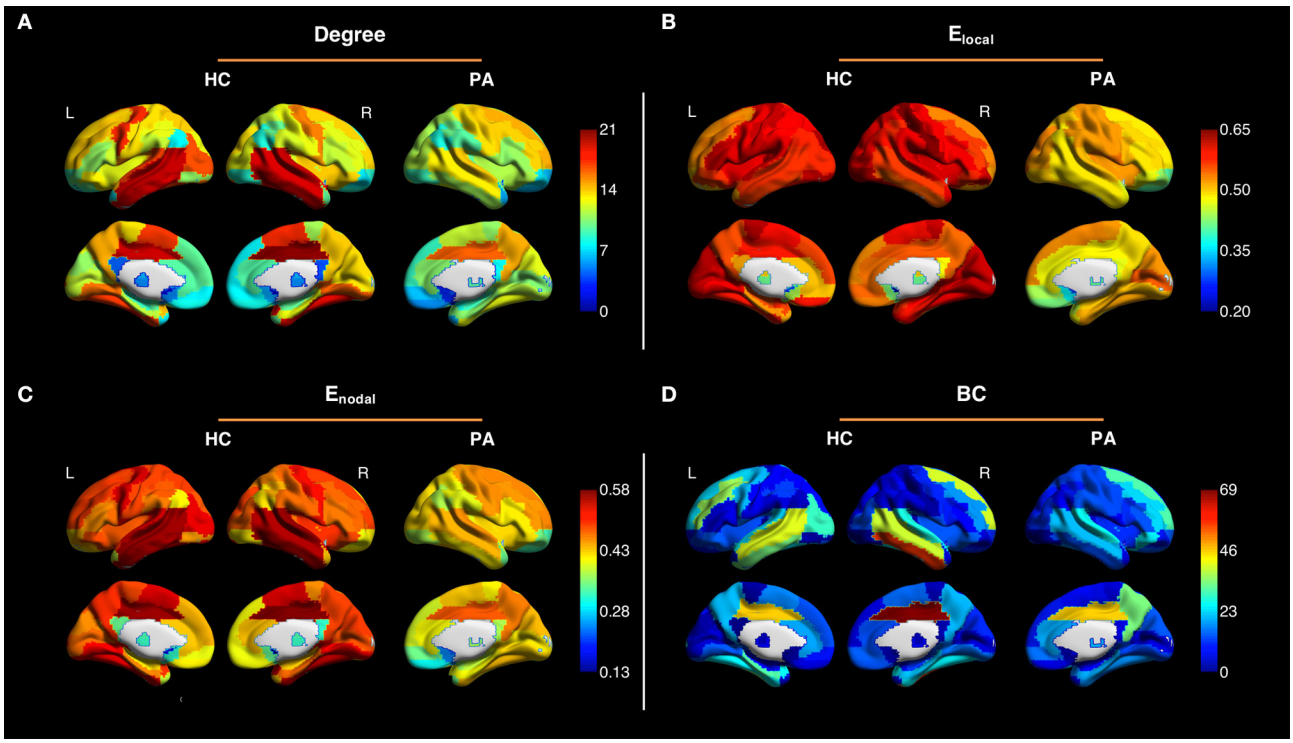

FIGURE 2 | Averaged maps of degree **(A)**, local efficiency E_{local} **(B)**, nodal efficiency E_{nodal} **(C)**, and betweenness centrality (BC) **(D)** in the left and right hemispheres of the healthy controls (HC) and in the contralateral hemispheres of the patients (PA) (connectivity sparsity = 40%). The maps of the patients with right-sided disease were left-right flipped to create the averaged maps. Overall, degree, E_{local} and E_{nodal} were lower in the patients as compared to the healthy controls.

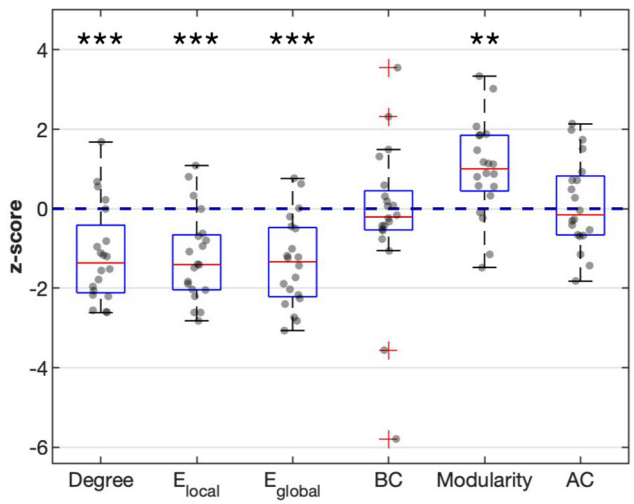

FIGURE 3 | Z-scores of degree, local efficiency E_{local}, global efficiency E_{global}, betweenness centrality (BC), modularity, and assortativity coefficient (AC) in the contralateral hemispheres of the patients relative to the respective hemispheres of the healthy controls (connectivity sparsity = 40%). The z-scores of degree, E_{local}, and E_{nodal} were significantly lower than zero, while the *z*-score of modularity was significantly higher than zero. Asterisks indicate statistical significance determined by one-sample *t*-test (**$P < 0.005$, ***$P < 0.001$; false discovery rate corrected).

areas of apparent disease. The network degree and nodal efficiency furthermore showed a close relationship with CVR, suggesting that cerebral hemodynamics may be predictive of BOLD network metrics.

fMRI has been widely utilized to explore brain function (40) including in cerebrovascular disease and stroke (41–43). Compared to task-related fMRI, resting-state fMRI does not involve explicit or intentional task performance. Flexible *post-hoc* analyses for estimating intrinsic functional connectivity can be applied on resting-state data to explore multiple functional networks, thus resting-state imaging is potentially well-suited to clinical settings, including patients unable to perform complex tasks.

While most fMRI studies have interpreted BOLD signal as a measure of neural activity, based in the assumption that neurovascular coupling is relatively consistent (27), neurovascular coupling may be disrupted in patients with cerebrovascular disease, especially in affected hemispheres (29, 30). Moreover, based on comparisons with healthy controls, previous studies (31, 32) have reported compromised CVR even in putatively normal contralateral hemispheres, suggesting that a BOLD hemodynamic response function could be altered even contralateral to regions of macrovascular disease and without demonstrable vascular pathology on cross-sectional or catheter angiographic imaging.

TABLE 1 | Mean *z*-scores of network parameters in the contralateral hemispheres.

	Connectivity sparsity = 20%		Connectivity sparsity = 30%		Connectivity sparsity = 40%	
	***z*-score (mean ± SD)**	***P*-value[a]**	***z*-score (mean ± SD)**	***P*-value[a]**	***z*-score (mean ± SD)**	***P*-value[a]**
Degree	−1.108 ± 1.131	0.002	−1.146 ± 1.186	<0.001	−1.158 ± 1.217	<0.001
E_{local}	−0.868 ± 1.191	0.006	−1.409 ± 1.272	<0.001	−1.213 ± 1.120	<0.001
E_{global}	−0.835 ± 1.022	0.005	−1.306 ± 1.056	<0.001	−1.346 ± 1.119	<0.001
Betweenness Centrality	0.284 ± 0.933	0.226	−0.038 ± 1.453	0.907	−0.195 ± 1.931	0.656
Modularity	0.721 ± 0.920	0.005	0.786 ± 1.115	0.008	1.000 ± 1.205	0.002
Assortativity Coefficient	−0.111 ± 1.091	0.654	0.065 ± 1.163	0.907	0.127 ± 1.130	0.656

[a]*P-value of one-sample t-test with false discovery rate correction to assess for zero mean z-scores.*
SD, standard deviation; E_{local}, local efficiency; E_{global}, global efficiency.

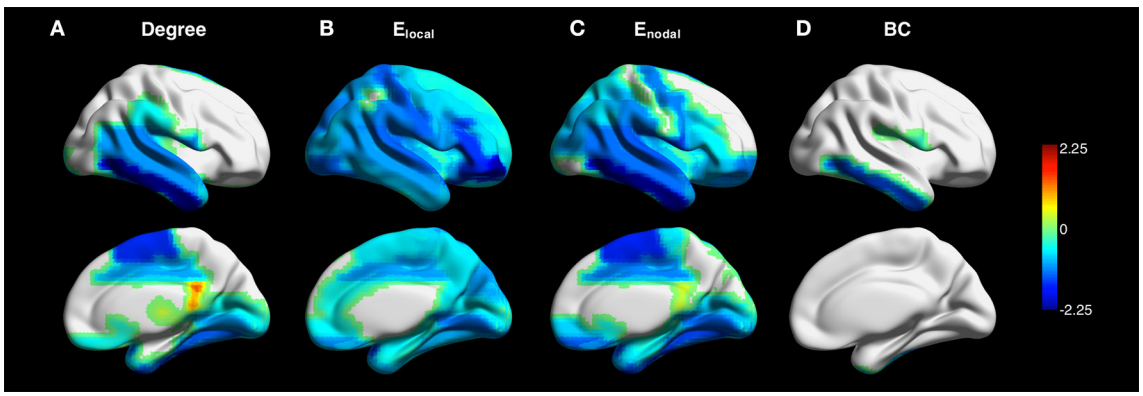

FIGURE 4 | *Z*-maps of degree **(A)**, local efficiency E_{local} **(B)**, nodal efficiency E_{nodal} **(C)**, and betweenness centrality (BC) **(D)** in the contralateral hemispheres averaged across all patients (connectivity sparsity = 40%). The maps of the patients with right-sided disease were left-right flipped to create the averaged maps. One-sample *t*-test with false discovery rate correction showed that negative *z*-scores of degree were primarily observed in the supplementary motor, fusiform and temporal cortices. Negative z-scores were found across the brain for E_{local} and E_{nodal}. The *z*-scores of betweenness centrality were negative in the Rolandic operculum and inferior temporal gyrus.

BOLD functional networks likely reflect underlying physiology. Recent fMRI studies in healthy participants have reported relationships between network efficiency and cerebral blood flow (CBF) (44), and between functional connectivity and CVR (45). In this work, we further explored the physiological basis of functional connectivity among a patient group with cerebrovascular disease. Our results showed a trend toward significant correlations between either network degree or nodal efficiency and vascular reserve as quantified by CVR, implying that cerebral hemodynamics may at least partially account for the observed changes in functional networks. Importantly, the direction of influence between CVR and functional connectivity was not studied directly, and the findings do not specifically implicate the presence of intrinsic vascular pathology in the contralateral hemisphere, wherein a remote functional influence upon local vasoreactivity could alternatively modulate augmentation profiles. This potential impact of neurovascular uncoupling and perhaps anatomic variables including the extent of vascular connectivity (for instance across the anterior communicating artery) also cannot be easily disambiguated from our results; nevertheless, the correlations suggest that caution is merited when assessing BOLD functional connectivity among patients with cerebrovascular compromise, and that corrections for CVR effects should be contemplated when studying even remote BOLD connectivity in cerebrovascular disease.

Cerebrovascular disease may produce not only territorial, lacunar, and borderzone ischemia, but also demonstrable silent infarctions or even subclinical damage below the resolution of conventional imaging. It should be noted that neurophysiological changes occur even in anatomically intact areas (46). Remote alterations have been observed in neuronal activity, cortical metabolism and CBF (9). To further investigate remote manifestations, we examined the organization of apparent functional networks contralateral to cerebrovascular compromise. The results showed that network strength and efficiency were impaired in normal-appearing hemispheres, while the brain networks were subdivided into more clearly delineated groups. The most compromised brain regions were observed in the temporal lobe. Our findings corroborate the notion that apparent network dysfunction extends into the structurally intact regions (9, 25). However, as noted above it remains unclear to what extent such alterations in the contralateral hemispheres result from true differences in neuronal functional connectivity versus changes in

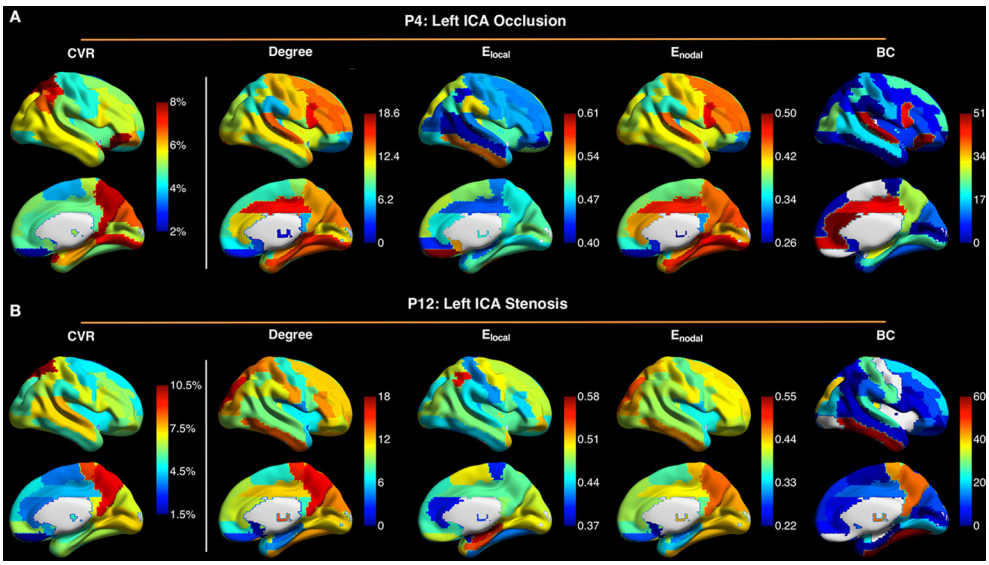

FIGURE 5 | Maps of cerebrovascular reactivity (CVR), degree, local efficiency E_{local}, nodal efficiency E_{nodal}, and betweenness centrality (BC) in the contralateral hemispheres in a patient with occlusion of left internal carotid artery (ICA) (P4) **(A)**, and in a patient with stenosis of the left ICA (P12) **(B)**. The CVR maps are similar to the maps of degree and E_{nodal}. Connectivity sparsity was set to 40%.

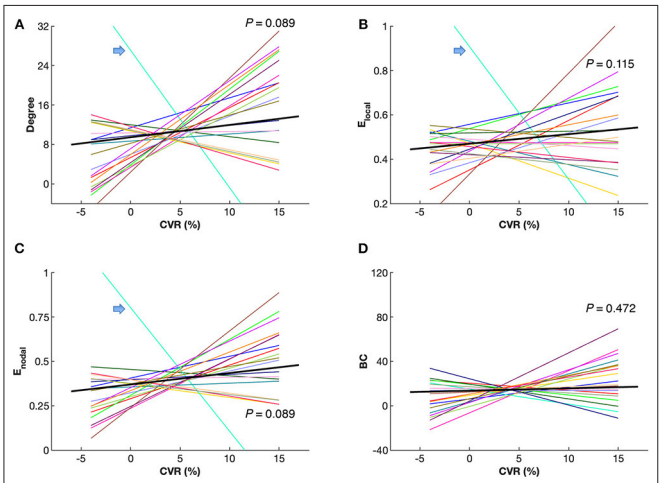

FIGURE 6 | Correlations between cerebrovascular reactivity (CVR) and network parameters, including degree **(A)**, local efficiency E_{local} **(B)**, nodal efficiency E_{nodal} **(C)** and betweenness centrality (BC) **(D)** in the contralateral hemispheres of the patients. Mixed-effects model showed a trend toward significant correlations between CVR and degree, as well as between CVR and E_{nodal} ($P < 0.10$, false discovery rate corrected). Each colored line represents an individual patient. The black bold lines indicate overall trends across patients. Arrows indicate a single patient (P9) with a trend deviating from the others. Connectivity sparsity was set to 40%.

neurovascular coupling. Systematic investigations are necessary to evaluate neurovascular coupling further within areas free of macrovascular disease.

Several issues remain to be addressed. First, the information of handedness and education was not collected in the participants. A balance between these factors is needed in the future. Second, a trend toward significant correlations of network degree and nodal efficiency with CVR was observed after FDR correction, perhaps due to the limited statistical power associated with the relatively small sample size in the present study. Future studies with larger sample size are needed to confirm this finding. Third, we investigated network parameters in the network level, where network analysis was performed for each hemisphere. For the analysis in module level, the statistical power is limited owing to the relatively small sample size in this study. Further studies with larger sample size are needed for the analysis in module level. Fourth, relatively large ROIs were selected to construct networks in the current study. Assessing functional connectivity strength to investigate voxel-wise changes in the patients is a focus of future study in our group. Fifth, single-band single-echo EPI with relatively low temporal (TR = 2 s) and spatial (voxel size = 3.4 × 3.4 × 4 mm^3) resolution was employed for BOLD imaging in this study. A recently developed multi-band multi-echo EPI (47) can be used to increase temporal and/or spatial resolution (48, 49) and functional contrast-to-noise (50), thereby improving measurement accuracy. Finally, with an assumption of temporal stationarity, functional connectivity was calculated across the whole scan duration, and the future study of resting-state functional networks in terms of temporal fluctuations among patients with stroke and cerebrovascular disease may offer further mechanistic insights into the nature of remote functional connectivity in such patients.

In conclusion, our study provides evidence for altered BOLD functional connectivity contralateral to the diseased hemispheres in patients with unilateral SOD. The close relationship between network connectivity

and CVR further suggests that caution should be taken when evaluating BOLD brain networks in cerebrovascular disease, even in regions with putatively normal macrovasculature.

DATA AVAILABILITY STATEMENT

The raw data supporting the conclusions of this article will be made available by the authors, without undue reservation.

ETHICS STATEMENT

The studies involving human participants were reviewed and approved by Institutional Review Board at Emory University School of Medicine. The patients/participants provided their written informed consent to participate in this study.

AUTHOR CONTRIBUTIONS

JW, FN, SD, and DQ contributed to study concept and design. JW, FN, JA, RH, SD, and DQ contributed to data acquisition and analysis and contributed to drafting the manuscript and figures. All authors contributed to the article and approved the submitted version.

FUNDING

This research was supported by internal fund of Emory University and National Institutes of Health (R01AG072603).

SUPPLEMENTARY MATERIAL

The Supplementary Material for this article can be found online at: https://www.frontiersin.org/articles/10.3389/fneur.2022.780896/full#supplementary-material

REFERENCES

1. Hankey GJ, Warlow CP. The role of imaging in the management of cerebral and ocular ischaemia. *Neuroradiology.* (1991) 33:381–90. doi: 10.1007/BF00598608
2. Adams HP, Bendixen BH, Kappelle LJ, Biller J, Love BB, Gordon DL, et al. Classification of subtype of acute ischemic stroke. Definitions for use in a multicenter clinical trial. TOAST. Trial of Org 10172 in Acute Stroke Treatment. *Stroke.* (1993) 24:35–41. doi: 10.1161/01.STR.24.1.35
3. Baron J-C, Yamauchi H, Fujioka M, Endres M. Selective neuronal loss in ischemic stroke and cerebrovascular disease. *J Cerebr Blood Flow Metab.* (2014) 34:2–18. doi: 10.1038/jcbfm.2013.188
4. Carter AR, Astafiev SV, Lang CE, Connor LT, Rengachary J, Strube MJ, et al. Resting interhemispheric functional magnetic resonance imaging connectivity predicts performance after stroke. *Ann Neurol.* (2010) 67:365–75. doi: 10.1002/ana.21905
5. Park, C.-H., Chang WH, Ohn SH, Kim ST, Bang OY, et al. Longitudinal changes of resting-state functional connectivity during motor recovery after stroke. *Stroke.* (2011) 42:1357–62. doi: 10.1161/STROKEAHA.110.596155
6. Cheng HL, Lin CJ, Soong BW, Wang PN, Chang FC, Wu YT, et al. Impairments in cognitive function and brain connectivity in severe asymptomatic carotid stenosis. *Stroke.* (2012) 43:2567–73. doi: 10.1161/STROKEAHA.111.645614
7. Avirame K, Lesemann A, List J, Witte AV, Schreiber SJ, Flöel A. Cerebral autoregulation and brain networks in occlusive processes of the internal carotid artery. *J Cerebr Blood Flow Metab.* (2015) 35:240–7. doi: 10.1038/jcbfm.2014.190
8. Wu J, Dehkharghani S, Nahab F, Allen J, Qiu D. The effects of acetazolamide on the evaluation of cerebral hemodynamics and functional connectivity using blood oxygen level–dependent MR imaging in patients with chronic steno-occlusive disease of the anterior circulation. *Am J Neuroradiol.* (2017) 38:139–45. doi: 10.3174/ajnr.A4973
9. Carrera E, Tononi G. Diaschisis: past, present, future. *Brain.* (2014) 137:2408–22. doi: 10.1093/brain/awu101
10. Siegel JS, Ramsey LE, Snyder AZ, Metcalf NV, Chacko RV, Weinberger K, et al. Disruptions of network connectivity predict impairment in multiple behavioral domains after stroke. *Proc Natl Acad Sci USA.* (2016) 113:E4367–76. doi: 10.1073/pnas.1521083113
11. Fornito A, Zalesky A, Breakspear M. The connectomics of brain disorders. *Nat Rev Neurosci.* (2015) 16:159–72. doi: 10.1038/nrn3901
12. Bullmore E, Sporns O. Complex brain networks: graph theoretical analysis of structural and functional systems. *Nat Rev Neurosci.* (2009) 10:186–98. doi: 10.1038/nrn2575
13. Kaiser M. A tutorial in connectome analysis: topological and spatial features of brain networks. *NeuroImage.* (2011) 57:892–907. doi: 10.1016/j.neuroimage.2011.05.025
14. Stam CJ, Reijneveld JC. Graph theoretical analysis of complex networks in the brain. *Nonlinear Biomed Phys.* (2007) 1:3. doi: 10.1186/1753-4631-1-3
15. He Y, Evans A. Graph theoretical modeling of brain connectivity. *Curr Opin Neurol.* (2010) 23:341–50. doi: 10.1097/WCO.0b013e32833aa567
16. Bullmore E, Sporns O. The economy of brain network organization. *Nat Rev Neurosci.* (2012) 13:336–49. doi: 10.1038/nrn3214
17. Boersma M, Smit DJA, De Bie HMA, Van Baal GCM, Boomsma DI, De Geus EJC, et al. Network analysis of resting state EEG in the developing young brain: structure comes with maturation. *Hum Brain Mapp.* (2011) 32:413–25. doi: 10.1002/hbm.21030
18. Bassett DS, Wymbs NF, Porter MA, Mucha PJ, Carlson JM, Grafton ST. Dynamic reconfiguration of human brain networks during learning. *Proc Natl Acad Sci USA.* (2011) 108:7641–6. doi: 10.1073/pnas.1018985108
19. Wu J, Zhang J, Liu C, Liu D, Ding X, Zhou C. Graph theoretical analysis of EEG functional connectivity during music perception. *Brain Res.* (2012) 1483:71–81. doi: 10.1016/j.brainres.2012.09.014
20. Wu J, Zhang J, Ding X, Li R, Zhou C. The effects of music on brain functional networks: a network analysis. *Neuroscience.* (2013) 250:49–59. doi: 10.1016/j.neuroscience.2013.06.021
21. Stam CJ, De Haan W, Daffertshofer A, Jones BF, Manshanden I, Van Cappellen Van Walsum AM, et al. Graph theoretical analysis of magnetoencephalographic functional connectivity in Alzheimer's disease. *Brain.* (2009) 132:213–24. doi: 10.1093/brain/awn262
22. Baggio HC, Sala-Llonch R, Segura B, Marti MJ, Valldeoriola F, Compta Y, et al. Functional brain networks and cognitive deficits in Parkinson's disease. *Hum Brain Mapp.* (2014) 35:4620–34. doi: 10.1002/hbm.22499
23. De Vico Fallani F, Astolfi L, Cincotti F, Mattia D, La Rocca D, Maksuti E, et al. Evaluation of the brain network organization from EEG signals: a preliminary evidence in stroke patient. *Anat Rec.* (2009) 292:2023–31. doi: 10.1002/ar.20965
24. Wang L, Yu C, Chen H, Qin W, He Y, Fan F, et al. Dynamic functional reorganization of the motor execution network after stroke. *Brain.* (2010) 133:1224–38. doi: 10.1093/brain/awq043
25. Gratton C, Nomura EM, Pérez F, D'esposito M. Focal brain lesions to critical locations cause widespread disruption of the modular organization of the brain. *J Cogn Neurosci.* (2012) 24:1275–85. doi: 10.1162/jocn_a_00222
26. Chang TY, Huang KL, Ho MY, Ho PS, Chang CH, Liu CH, et al. Graph theoretical analysis of functional networks and its relationship to cognitive decline in patients with carotid stenosis. *J Cerebr Blood Flow Metab.* (2016) 36:808–18. doi: 10.1177/0271678X15608390

27. Liu TT. Neurovascular factors in resting-state functional MRI. *NeuroImage.* (2013) 80:339–48. doi: 10.1016/j.neuroimage.2013.04.071
28. Archila-Meléndez ME, Sorg C, Preibisch C. Modeling the impact of neurovascular coupling impairments on BOLD-based functional connectivity at rest. *NeuroImage.* (2020) 218:116871. doi: 10.1016/j.neuroimage.2020.116871
29. Veldsman M, Cumming T, Brodtmann A. Beyond BOLD: optimizing functional imaging in stroke populations. *Hum Brain Mapp.* (2015) 36:1620–36. doi: 10.1002/hbm.22711
30. Siegel JS, Shulman GL, Corbetta M. Measuring functional connectivity in stroke: approaches and considerations. *J Cerebr Blood Flow Metab.* (2017) 37:2665–78. doi: 10.1177/0271678X17709198
31. Derdeyn CP, Videen TO, Yundt KD, Fritsch SM, Carpenter DA, Grubb RL, et al. Variability of cerebral blood volume and oxygen extraction: stages of cerebral haemodynamic impairment revisited. *Brain.* (2002) 125:595–607. doi: 10.1093/brain/awf047
32. Sam K, Small E, Poublanc J, Han JS, Mandell DM, Fisher JA, et al. Reduced contralateral cerebrovascular reserve in patients with unilateral steno-occlusive disease. *Cerebrovasc Dis.* (2014) 38:94–100. doi: 10.1159/000362084
33. Marshall RS, Festa JR, Cheung YK, Chen R, Pavol MA, Derdeyn CP, et al. Cerebral hemodynamics and cognitive impairment: baseline data from the RECON trial. *Neurology.* (2012) 78:250–5. doi: 10.1212/WNL.0b013e31824365d3
34. Wu J, Dehkharghani S, Nahab F, Qiu D. Acetazolamide-augmented dynamic BOLD (aczBOLD) imaging for assessing cerebrovascular reactivity in chronic steno-occlusive disease of the anterior circulation: an initial experience. *NeuroImage.* (2017) 13:116–22. doi: 10.1016/j.nicl.2016.11.018
35. Tzourio-Mazoyer N, Landeau B, Papathanassiou D, Crivello F, Etard O, Delcroix N, et al. Automated anatomical labeling of activations in SPM using a macroscopic anatomical parcellation of the MNI MRI single-subject brain. *NeuroImage.* (2002) 15:273–89. doi: 10.1006/nimg.2001.0978
36. Achard S, Bullmore E. Efficiency and cost of economical brain functional networks. *PLOS Comp Biol.* (2007) 3:e17. doi: 10.1371/journal.pcbi.0030017
37. Braun U, Plichta MM, Esslinger C, Sauer C, Haddad L, Grimm O, et al. Test–retest reliability of resting-state connectivity network characteristics using fMRI and graph theoretical measures. *NeuroImage.* (2012) 59:1404–12. doi: 10.1016/j.neuroimage.2011.08.044
38. Rubinov M, Sporns O. Complex network measures of brain connectivity: uses and interpretations. *NeuroImage.* (2010) 52:1059–69. doi: 10.1016/j.neuroimage.2009.10.003
39. Newman MEJ. Modularity and community structure in networks. *Proc Natl Acad Sci USA.* (2006) 103:8577–82. doi: 10.1073/pnas.0601602103
40. Logothetis NK, Pauls J, Augath M, Trinath T, Oeltermann A. Neurophysiological investigation of the basis of the fMRI signal. *Nature.* (2001) 412:150–7. doi: 10.1038/35084005
41. Grefkes C, Fink GR. Connectivity-based approaches in stroke and recovery of function. *Lancet Neurol.* (2014) 13:206–16. doi: 10.1016/S1474-4422(13)70264-3
42. Ovadia-Caro S, Margulies DS, Villringer A. The value of resting-state functional magnetic resonance imaging in stroke. *Stroke.* (2014) 45:2818–24. doi: 10.1161/STROKEAHA.114.003689
43. Baldassarre A, Ramsey LE, Siegel JS, Shulman GL, Corbetta M. Brain connectivity and neurological disorders after stroke. *Curr Opin Neurol.* (2016) 29:706–13. doi: 10.1097/WCO.0000000000000396
44. Liang X, Zou Q, He Y, Yang Y. Coupling of functional connectivity and regional cerebral blood flow reveals a physiological basis for network hubs of the human brain. *Proc Natl Acad Sci USA.* (2013) 110:1929–34. doi: 10.1073/pnas.1214900110
45. Golestani AM, Kwinta JB, Strother SC, Khatamian YB, Chen JJ. The association between cerebrovascular reactivity and resting-state fMRI functional connectivity in healthy adults: the influence of basal carbon dioxide. *NeuroImage.* (2016) 132:301–13. doi: 10.1016/j.neuroimage.2016.02.051
46. Feeney DM, Baron, J.-C. Diaschisis. *Stroke.* (1986) 17:817–30. doi: 10.1161/01.STR.17.5.817
47. Wu J, Saindane AM, Zhong X, Qiu D. Simultaneous perfusion and permeability assessments using multiband multi-echo EPI (M2-EPI) in brain tumors. *Magn Reson Med.* (2019) 81:1755–68. doi: 10.1002/mrm.27532
48. Feinberg DA, Setsompop K. Ultra-fast MRI of the human brain with simultaneous multi-slice imaging. *J Magn Reson.* (2013) 229:90–100. doi: 10.1016/j.jmr.2013.02.002
49. Boubela R, Kalcher K, Nasel C, Moser E. Scanning fast and slow: current limitations of 3 Tesla functional MRI and future potential. *Front Phys.* (2014) 2:00001. doi: 10.3389/fphy.2014.00001
50. Kundu P, Inati SJ, Evans JW, Luh W-M, Bandettini PA. Differentiating BOLD and non-BOLD signals in fMRI time series using multi-echo EPI. *NeuroImage.* (2012) 60:1759–70. doi: 10.1016/j.neuroimage.2011.12.028

Conflict of Interest: SD — UNRELATED: Unpaid scientific consultation and collaboration with Ischemaview; Past travel support from Ischemaview as an individual; Scientific consulting with Regeneron as an individual; Domestic and international patent filed by institution for inventor's disclosure in the development of device to measure brain electrical properties; Grant funding paid to institution from undisclosed donor for study on the development of remote stroke detection devices.

The remaining authors declare that the research was conducted in the absence of any commercial or financial relationships that could be construed as a potential conflict of interest.

Publisher's Note: All claims expressed in this article are solely those of the authors and do not necessarily represent those of their affiliated organizations, or those of the publisher, the editors and the reviewers. Any product that may be evaluated in this article, or claim that may be made by its manufacturer, is not guaranteed or endorsed by the publisher.

frontiers | Frontiers in Neurology

ORIGINAL RESEARCH
published: 03 May 2022
doi: 10.3389/fneur.2022.784836

Cerebral Augmentation Effect Induced by External Counterpulsation Is Not Related to Impaired Dynamic Cerebral Autoregulation in Ischemic Stroke

Li Xiong[1,2]*, *Xiangyan Chen*[3]*, *Jia Liu*[4], *Lawrence Ka Sing Wong*[2] and *Thomas W. Leung*[2]

[1] Clinical Trials Centre, The Eighth Affiliated Hospital of Sun Yat-sen University, Shenzhen, China, [2] Department of Medicine & Therapeutics, The Chinese University of Hong Kong, Shatin, Hong Kong SAR, China, [3] Department of Health Technology and Informatics, The Hong Kong Polytechnic University, Shatin, Hong Kong SAR, China, [4] Shenzhen Institute of Advanced Technology, Chinese Academy of Sciences, Shenzhen, China

OPEN ACCESS

Edited by:
Xiuyun Liu,
Johns Hopkins University,
United States

Reviewed by:
Edwin M. Nemoto,
University of New Mexico,
United States
Andrew Donald Robertson,
University of Waterloo, Canada

***Correspondence:**
Li Xiong
li790730@163.com
Xiangyan Chen
fiona.chen@polyu.edu.hk

Specialty section:
This article was submitted to Stroke, a section of the journal Frontiers in Neurology

Received: 28 September 2021
Accepted: 28 March 2022
Published: 03 May 2022

Citation:
Xiong L, Chen X, Liu J, Wong LKS and Leung TW (2022) Cerebral Augmentation Effect Induced by External Counterpulsation Is Not Related to Impaired Dynamic Cerebral Autoregulation in Ischemic Stroke. Front. Neurol. 13:784836. doi: 10.3389/fneur.2022.784836

Background and Purpose: Dynamic cerebral autoregulation is impaired after ischemic stroke. External counterpulsation (ECP) augments the cerebral blood flow of patients with ischemic stroke by elevation of blood pressure (BP). We aimed to investigate if cerebral augmentation effects during ECP were associated with impaired dynamic cerebral autoregulation in patients after acute ischemic stroke.

Methods: Forty patients with unilateral ischemic stroke and large artery atherosclerosis in the anterior circulation territory within 7 days from symptom onset and eighteen healthy controls were recruited. We monitored changes in mean flow velocity over both middle cerebral arteries (MCA) by transcranial Doppler (TCD) before, during, and immediately after ECP. Cerebral augmentation index was MCA mean flow velocity increase in percentage during ECP compared with baseline to evaluate the augmentation effects of ECP. Spontaneous arterial BP and cerebral blood flow velocity in both bilateral MCAs were recorded using a servo-controlled plethysmograph and TCD, respectively. Transfer function analysis was used to derive the autoregulatory parameters, including phase difference (PD), and gain.

Results: The cerebral augmentation index in patients with stroke was significantly higher on both the ipsilateral and contralateral sides than that in controls, while the PD in patients with stroke was significantly lower on both sides than those in controls (all $P < 0.05$). The cerebral augmentation index did not correlate with PD and gain on either the ipsilateral or contralateral side of patients with stroke or in controls (all $P > 0.05$). The cerebral augmentation index of patients with stroke was significantly related to mean BP change on the ipsilateral side ($R^2 = 0.108$, $P = 0.038$).

Conclusion: The degree of ECP-induced cerebral augmentation effects as measured by the cerebral augmentation index did not correlate with the magnitude of impaired dynamic cerebral autoregulation.

Keywords: cerebral blood flow, external counterpulsation, dynamic cerebral autoregulation, transfer function analysis, ischemic stroke

INTRODUCTION

In the traditional view, cerebral autoregulation ensures the constancy of cerebral blood flow to the brain as the systemic blood pressure (BP), and hence, cerebral perfusion pressure changes over a wide range. However, considering the compelling evidence currently available, cerebral blood flow regulation is far more pressure-passive in nature than traditionally believed. Indeed, cerebral blood flow will not necessarily remain stable in some physiological/clinical conditions (1). Cerebral autoregulation is impaired after ischemic stroke (2, 3). The brain becomes more vulnerable to ischemic damage caused by changes in systemic BP or intracranial pressure. Although the management of BP following acute ischemic stroke remains controversial, the available clinical data suggest that the use of BP augmentation may improve perfusion to ischemic tissue, which can result in at least short-term neurological improvement (4, 5).

External counterpulsation (ECP) is a noninvasive and well-established method for ischemic heart disease (6–8). ECP operates by applying electrocardiography-triggered diastolic pressure to the lower extremities through air-filled cuffs. The diastolic augmentation of the blood flow and the simultaneously decreasing systolic afterload increases the blood flow of vital organs such as the heart, brain, and kidneys (9, 10). Our pilot study showed that ECP is feasible for patients with ischemic stroke with large artery disease by improving neurological deficits (11). ECP may improve cerebral perfusion and collateral blood supply in ischemic stroke by augmenting BP and cerebral blood flow velocity (CBFV) (12). Without cerebral autoregulation, CBFV would passively follow BP. The cerebral augmentation effects induced by ECP possibly worked *via* impaired cerebral autoregulation. Furthermore, we first proposed the cerebral augmentation index to evaluate the degree of cerebral augmentation effects induced by ECP. Recently, we found that the higher cerebral augmentation index on the side ipsilateral to the infarct was independently correlated with an unfavorable functional outcome after acute ischemic stroke (13).

Without too much cooperation from patients, transfer function analysis (TFA) is a frequently used method to assess dynamic cerebral autoregulation using spontaneous oscillations in BP and CBFV despite the controversies and variations in its interpretation from different research groups (14, 15). TFA quantifies cerebral autoregulation in the parameters phase difference (PD), gain, and coherence with the assumption that cerebral autoregulation is a linear control system. It is based on the concept that cerebral autoregulation minimizes the effect of dynamic BP fluctuations on CBFV, which is reflected by reduced low-frequency gain and phase-lead of CBFV over BP (16, 17). Without cerebral autoregulation, CBFV would passively follow BP, and TFA would show constant gain and zero phases across the low-frequency band. In acute ischemic stroke, recent meta-analyses of TFA parameters, obtained from spontaneous fluctuations of BP at rest, have demonstrated that PD and the autoregulation index can show highly significant differences in comparison with healthy controls, while less clear-cut results were obtained for gain (18).

Therefore, in this study, we aimed to investigate whether the degree of cerebral blood flow augmentation effects induced by ECP was related to the magnitude of impaired dynamic cerebral autoregulation in patients with ischemic stroke, assessed by cerebral augmentation index and PD and gain, respectively.

METHODS

Subjects

Patients with unilateral ischemic stroke in the anterior circulation territory and large artery occlusive disease with a good acoustic window within 7 days of stroke onset in Prince of Wales Hospital in Hong Kong between November 2011 and December 2013 were recruited. Diagnosis of stroke was made based on the definition of the WHO, and ischemia was confirmed by computerized tomography or MRI. All patients were examined by TCD, duplex ultrasound, or magnetic resonance angiography to verify with intracranial or extracranial large artery stenosis (moderate stenosis or $>$ 50% diameter reduction). Based on our previous study, (19). we excluded patients with evidence of cardioembolic strokes such as atrial fibrillation and rheumatic heart disease, evidence of hemorrhage on brain computerized tomography, evidence of arteriovenous malformation, arteriovenous fistula or aneurysm, a history of intracerebral hemorrhage, brain tumor or malignancy, sustained hypertension (systolic $>$ 180 mmHg or diastolic $>$ 100 mmHg), severe symptomatic peripheral vascular disease, evidence of co-existing systemic diseases such as renal failure (creatinine $>$ 300 μmol/L, if known), cirrhosis, thrombocytopenia [platelet count $<$ 1,00,000/mm (3)] and severe dementia of psychosis as well as pregnant women. Patients with tissue plasminogen activator (tPA) and thrombectomy intervention were excluded due to their effects on dynamic cerebral autoregulation (20, 21). Healthy volunteers without a history of cerebrovascular events and risk factors were recruited as control subjects. Each healthy subject underwent TCD and carotid duplex to rule out large artery occlusive disease. Written informed consent was obtained from all participants prior to enrolment. This study was approved by the local medical ethics committee (Joint CUHK-NTEC Clinical Research Ethics Committee).

ECP TCD Monitoring

All the participants were asked to lie in the supine position for 15 mins prior to the beginning of data acquisition. ECP was performed using the Enhanced External Counterpulsation system, model number MC2 (Vamed Medical Instrument Company, Foshan, China). The treatment pressure of ECP was 150 mm Hg. TCD monitoring was performed using the ST3 TCD system (Spencer Technologies, Seattle, WA). The patients lay on the ECP treatment bed and their legs were wrapped with 3 pairs of air cuffs. Two 2-MHz probes were mounted on a head frame, which was fitted individually and worn on the head of patients. M1 segments of bilateral MCAs were insonated at the depth of highest mean flow velocity between 50 and 60 mm. We recorded bilateral CBFV of bilateral MCAs and continuous beat-to-beat arterial BP using a finger plethysmograph using the Task Force Monitor system (CNSystems Medizintechnik AG, Graz, Austria)

before and during ECP, respectively, for 3 mins. The cerebral augmentation index was used to assess the augmentation effect of ECP, which was calculated by the increase in the percentage of mean flow velocity during ECP compared with baseline (12).

Dynamic Cerebral Autoregulation Measurement and Data Analysis

Continuous CBFV of bilateral MCAs *via* TCD and continuous beat-to-beat arterial BP were recorded simultaneously from each subject in the supine position for 10 mins. The recorded data were then used to evaluate dynamic cerebral autoregulation by the method of TFA (15, 22). The data were post-processed using MATLAB (MathWorks, Inc, Natick, MA). A cross-correlation function between arterial BP and CBFV was used to align the raw data in order to eliminate the possible time lags. The signals were then down-sampled to 1 Hz after the application of an anti-alias filter with a cutoff frequency of 0.5 Hz. The dynamic relationship between arterial BP and CBFV was assessed by TFA with an algorithm used in previous studies (23). PD, gain, and coherence within a low-frequency range, 0.06 to 0.12 Hz, were then derived from TFA to evaluate dynamic cerebral autoregulation. The autoregulatory parameters were accepted for further statistical analysis only when coherence was higher than 0.4 within 0.06 to 0.12 Hz.

Statistical Analysis

The mean flow velocity of MCA was automatically recorded by the TCD system, which was the mean value of the area under the envelope curve in a cardiac cycle. Data of patients with stroke were analyzed based on the side ipsilateral or contralateral to the infarct. Mean CBFV, cerebral augmentation index, PD, and gain on the right and left sides in the control group were averaged and used. Continuous data were analyzed by independent-sample Student *t*-tests when there was a normal distribution and by the Mann–Whitney test, if there was a skewed distribution between both sides of stroke and control groups. Category data were analyzed by the Pearson χ^2 test or Fisher's exact test. The paired *t*-test was used to compare the difference in CBFV between baseline and during ECP in each group. Pearson correlation analysis was performed between cerebral augmentation index and PD or gain in the two groups as well as between cerebral augmentation index and BP changes in the stroke group by SPSS V.24.0 (SPSS, Inc, Chicago, IL). Differences with $P < 0.05$ were considered significant.

TABLE 1 | Baseline characteristics.

Parameters	Stroke patients ($n = 40$)	Healthy controls ($n = 18$)	*P*
Gender (male/female)	36/4	9/9	0.002*
Age (mean ± SD), years	65.0 ± 10.6	61.1 ± 4.5	0.051
Day from symptom onset to recruitment (mean ± SD, d)	5.2 ± 3.0	NA	
Admission NIHSS (median, range)	5 (4–9)	NA	
Hypertension, *n* (%)	35 (87.5)	NA	
Diabetes, *n* (%)	18 (45.0)	NA	
Ischemic heart disease, *n* (%)	4 (10.0)	NA	
Hyperlipidemia, *n* (%)	20 (50.0)	NA	
Previous stroke, *n* (%)	11 (27.5)	NA	
Smoker, *n* (%)	21 (52.5)	NA	
Drinker, *n* (%)	7 (17.5)	NA	
Intracranial large artery disease, *n* (%)	34 (85.0)	NA	
Extracranial large artery disease, *n* (%)	2 (5.0)	NA	
Intra- and extracranial large artery disease, *n* (%)	4 (10.0)	NA	
Left side infarct, *n* (%)	24 (60.0)	NA	
Right side infarct, *n* (%)	16 (40.0)	NA	

NIHSS, National Institutes of Health stroke scale.
**Pearson χ^2 test.*

TABLE 2 | Cerebral augmentation effects of ECP and dynamic cerebral autoregulation.

Parameters	Stroke ipsilateral ($n = 40$)	Stroke contralateral ($n = 40$)	Healthy controls ($n = 18$)
ECP-induced hemodynamics changes			
Mean CBFV at baseline (cm/s)	57.5 ± 22.2	56.3 ± 21.5	57.5 ± 11.9
Mean CBFV during ECP (cm/s)	59.9 ± 22.7	59.4 ± 23.5	56.9 ± 11.3
P (baseline vs ECP)	< 0.001	< 0.001	0.297
CAI (%)	4.4± 5.6*	5.3 ± 5.1*	−0.7 ± 3.6
Dynamic cerebral autoregulation			
Phase difference (degree)	32.7 ± 39.1*	28.6 ± 369*	52.6 ± 13.9
Gain (cm/s/mmHg)	1.2 ± 0.9	1.0 ± 0.6	0.9 ± 0.5
Correlation *P* value (CAI vs. phase)	0.326	0.791	0.050
Correlation P value (CAI vs. gain)	0.821	0.389	0.840

ECP, external counterpulsation; CBFV, cerebral blood flow velocity; CAI, cerebral augmentation index.
**P < 0.05 in comparison with healthy controls.*

RESULTS

Forty ischemic stroke patients with large artery disease and eighteen healthy controls were recruited. There were more men in patients with stroke (36 men [90%]) compared with controls (9 men [50%]) ($P = 0.002$). The mean interval from stroke onset to examination was about 5 days, and the median admission National Institutes of Health Stroke Scale score in the patient group was 5 (**Table 1**). Among the forty stroke patients with large artery disease, 85% (34 cases) had intracranial large artery disease (MCA involved in 21 cases, intracranial internal carotid artery in 9 cases, and anterior cerebral artery in 4 cases) and two patients had extracranial large artery disease. A total of 4 patients had both intracranial and extracranial large artery disease.

Baseline mean CBFV of patients with stroke on both sides showed no significant difference in comparison with healthy controls ($P = 0.854$ on the ipsilateral side; $P = 0.162$ on the contralateral side). There were no differences in all parameters between the ipsilateral and contralateral sides in the stroke group (all $P > 0.05$). The mean CBFV of patients with stroke significantly increased during ECP as shown in **Table 2**. In the control group, mean CBFV did not change significantly during

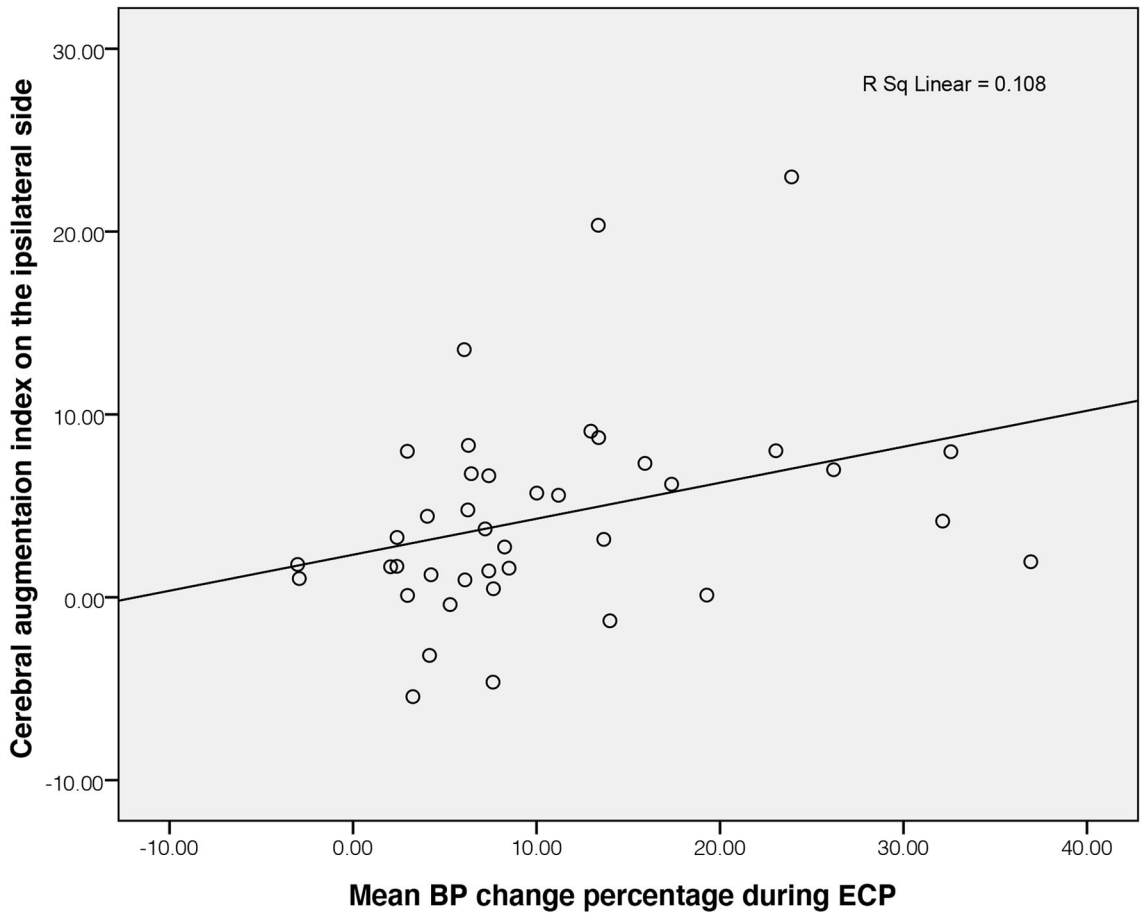

FIGURE 1 | Correlation of BP change and ipsilateral cerebral augmentation index in patients with stroke. BP, blood pressure; ECP, external counterpulsation.

ECP from baseline. The cerebral augmentation index of stroke patients was much higher than that of controls. In the patient with stroke group, PD was significantly lower on the ipsilateral side (32.71 ± 39.13 degrees) as well as the contralateral side (28.59 ± 36.87 degrees) than that in the control group (52.64 ± 13.94 degrees, all $P < 0.05$), but there was no significant difference in gain on both sides between the two groups. The cerebral augmentation index did not correlate with PD or gain for either the ipsilateral or contralateral side in the stroke group (all $P > 0.05$). The correlation between cerebral augmentation index and PD was borderline significant in the control group ($P = 0.05$). During ECP, the cerebral augmentation index of patients with stroke was related to the mean BP change on the ipsilateral side ($R^2 = 0.108$, $P = 0.038$, **Figure 1**). There was no significant correlation between cerebral augmentation index and BP change in controls ($R^2 = 0.349$, $P = 0.131$) as well as on the contralateral side in patients with stroke ($R^2 = 0.041$, $P = 0.801$).

DISCUSSION

The present study was a continuation of our previous research work (12, 13, 19, 23). We further correlated the cerebral blood flow augmentation degree induced by ECP as measured by cerebral augmentation index with the impaired dynamic cerebral autoregulation using TFA analysis. We speculate ECP augmented cerebral blood flow of ischemic stroke *via* impaired dynamic cerebral autoregulation, while the degree of ECP-induced cerebral augmentation effects was not related to the magnitude of impaired dynamic cerebral autoregulation.

External counterpulsation increased the mean MCA flow velocities on both ipsilateral and contralateral sides in patients with unilateral ischemic stroke and large artery atherosclerosis. However, it did not change the flow velocities in healthy controls, although mean BP was elevated as well, which was consistent with our previous study (12). Differently, in the same patient cohorts, we investigated their status of dynamic cerebral autoregulation to study the possible hemodynamic mechanisms of augmentation effects following ECP treatment. TFA examines the transfer of the BP oscillations to CBFV as a measure of autoregulation. The autoregulation is supposed to attenuate the influence of ABP on CBFV by preventing a direct transfer of the waveform at a low-frequency range (normally < 0.2 Hz). Previous studies of dynamic cerebral autoregulation suggested that autoregulatory parameters in a low-frequency band (0.06–0.12 Hz), used in our

study, are more meaningful than in the other frequency bands (24, 25). A coherence threshold of > 0.4 was chosen to define a lower limit of the linearity between arterial BP and CBFV to apply the TFA (15). In the transfer function between BP and CBFV, the gain represents the damping effect of cerebral autoregulation on the magnitude of the BP oscillations. A low gain indicates efficient autoregulation, whereas an increase in gain represents a diminished efficiency of the dynamic process of cerebral autoregulation. PD can be considered a surrogate measure for the time delay of the autoregulatory response. A low PD indicates that CBFV follows the changes in mean BP passively, whereas a higher value of PD suggests that CBFV is actively regulated against the fluctuations of mean BP which represents the better status of autoregulation (26). The PD values on both cerebral sides of patients were significantly lower than that of controls. It indicated that dynamic cerebral autoregulation was bilaterally impaired on the ipsilateral side and contralateral side in the ischemic stroke patients with large artery atherosclerosis, which was comparable with a series of studies on the pattern of dynamic cerebral autoregulation in acute ischemic stroke patients with different subtypes (23, 27).

However, the interesting finding was that the cerebral augmentation index did not correlate with PD and gain on either the ipsilateral or contralateral side of patients with stroke or in controls. It meant the degree of ECP-induced cerebral augmentation effects was not related to the magnitude of impaired dynamic cerebral autoregulation. To the best of our knowledge, two approaches have been introduced to quantify cerebral autoregulation: the static cerebral autoregulation, which reflects the steady-state outcome of cerebral blood flow following a persistent change in BP using thigh cuff inflation, (28, 29) and the dynamic cerebral autoregulation, which investigates the transient relationship between BP and cerebral blood flow based on spontaneous fluctuations of BP (17, 28). To date, little evidence exists concerning the relationship between dynamic and static cerebral autoregulation. Dawson et al. investigated 61 patients with ischemic stroke within 96 h of ictus, and 54 age- and sex-matched controls and found dynamic but not static cerebral autoregulation was globally impaired in acute ischemic stroke (29). One recent study also found no linear correlations between dynamic and static cerebral autoregulation indices in healthy older adults (30). The response of flow velocities following the persistent change in BP induced by ECP may be comparable with the concept of static cerebral autoregulation, which is likely to elucidate a lack of linear correlations between cerebral augmentation effects of ECP and dynamic cerebral autoregulation, quantified by gain and PD in the current study.

The hidden mechanisms are largely unknown. Experimental studies found that ECP reduces endothelial damage, arrests vascular smooth muscle cell proliferation and migration, decreases the proliferating cell nuclear antigen proliferative index, suppresses extracellular matrix formation, and eventually inhibits intimal hyperplasia and the development of atherosclerosis by increasing the arterial wall shear stress, which in turn activates the endothelial-derived nitric oxide (NO) synthase/NO pathway and probably suppresses extracellular signal-regulated kinase 1/2 overactivation (31). In clinical studies on chronic angina (32, 33), a significant increase in plasma NO levels, which is a vasodilator, a decrease in endothelial endothelin-1 (ET-1) levels, which is a vasoconstrictor, and an increase in plasma vascular endothelial growth factor (VEGF), which plays a key role in angiogenesis, were reported after a course of ECP or after the completion of 35 1 h sessions of ECP. Such release of these biomarkers and augmented BP may help open the collateral channels and, thus, augments the collateral perfusion. Although all evidence of biomarker changes now comes from patients with the ischemic disease, we believe the cerebral augmentation effects induced by ECP in patients with stroke should be derived through the same mechanisms. However, there was uncertainty whether 3 min of a single ECP event instead of a series of ECP treatment sessions may produce these beneficial effects. We need to further test the biomarkers released by short-term ECP intervention in patients with acute ischemic stroke. Various neurohumoral, metabolic, and endothelial mechanisms participate in the stability and adjustment of cerebral blood flow (34). Some biomarkers released such as NO and increased activities of the sympathetic control by neurohumoral activation may affect the dynamic cerebral autoregulation, (35). which contributed to the final cerebral augmentation effect degree of ECP.

The limitations of this study included, first, the sample size was relatively small. We failed to subdivide patients with stroke into those with intracranial disease and with the additional extracranial disease, although it may influence cerebral augmentation effects of ECP. Second, age and gender were not comparable between patients with stroke and controls, although they were not the major reason influencing their distinct hemodynamic responses to ECP (36). Third, we independently quantified dynamic cerebral autoregulation using TFA and gain analysis between BP and CBFV fluctuations without ECP intervention, instead of measuring them during ECP. ECP does not compromise the dynamic cerebral autoregulation in healthy persons and patients with atherosclerotic, as revealed by stable values of PD and gain between BP and CBFV oscillations (37). However, the effects of ECP as a treatment on dynamic cerebral autoregulation remain unclear. There is an ongoing randomized controlled trial to investigate the effects of 35 h of daily 1-h ECP treatment sessions on impaired dynamic cerebral autoregulation in patients with ischemic stroke in our center (registration No. ChiCTR-TRC-07000706). The results from that study will be more convincing on whether ECP as a treatment is beneficial for impaired dynamic cerebral autoregulation or not.

In conclusion, the degree of ECP-induced cerebral augmentation effects as measured by the cerebral augmentation index did not correlate with the magnitude of impaired dynamic cerebral autoregulation.

DATA AVAILABILITY STATEMENT

The raw data supporting the conclusions of this article will be made available by the authors, without undue reservation.

ETHICS STATEMENT

The studies involving human participants were reviewed and approved by Joint CUHK-NTEC Clinical Research Ethics Committee. The patients/participants provided their written informed consent to participate in this study.

AUTHOR CONTRIBUTIONS

LX conceived and designed the project and drafted the manuscript. XC helped acquisition of data and interpretation of data. JL helped guide TFA method. LW helped design the project. TL helped recruit participants. All authors had full access to the data, contributed to the study, approved the final version for publication, and take responsibility for its accuracy and integrity.

FUNDING

This study was supported by grants from the National Natural Science Foundation of China (No. 82171291), the National Key R&D Program of China (2016YFC1301605), and the Research Grants Council, Hong Kong (CUHK 14100215).

REFERENCES

1. Brassard P, Labrecque L, Smirl JD, Tymko MM, Caldwell HG, Hoiland RL, et al. Losing the dogmatic view of cerebral autoregulation. *Physiol Rep.* (2021) 9:e14982. doi: 10.14814/phy2.14982
2. Eames PJ, Blake MJ, Dawson SL, Panerai RB, Potter JF. Dynamic cerebral autoregulation and beat to beat blood pressure control are impaired in acute ischaemic stroke. *J Neurol Neurosurg Psychiatry.* (2002) 72:467–72. doi: 10.1136/jnnp.72.4.467
3. Dawson SL, Panerai RB, Potter JF. Serial changes in static and dynamic cerebral autoregulation after acute ischaemic stroke. *Cerebrovasc Dis.* (2003) 16:69–75. doi: 10.1159/000070118
4. Schwarz S, Georgiadis D, Aschoff A, Schwab S. Effects of induced hypertension on intracranial pressure and flow velocities of the middle cerebral arteries in patients with large hemispheric stroke. *Stroke.* (2002) 33:998–1004. doi: 10.1161/01.STR.0000014584.17714.2E
5. Wityk RJ. Blood pressure augmentation in acute ischemic stroke. *J Neurol Sci.* (2007) 261:63–73. doi: 10.1016/j.jns.2007.04.033
6. Bonetti PO, Barsness GW, Keelan PC, Schnell TI, Pumper GM, Kuvin JT, et al. Enhanced external counterpulsation improves endothelial function in patients with symptomatic coronary artery disease. *J Am Coll Cardiol.* (2003) 41:1761–8. doi: 10.1016/S0735-1097(03)00329-2
7. Lawson WE. Current use of enhanced external counterpulsation and patient selection. *Clin Cardiol.* (2002) 25:II16–21. doi: 10.1002/clc.4960251406
8. Linnemeier G. Enhanced external counterpulsation–a therapeutic option for patients with chronic cardiovascular problems. *J Cardiovasc Manag.* (2002) 13:20–5.
9. Bonetti PO, Holmes DR. Jr., Lerman A, Barsness GW. *Enhanced external counterpulsation for ischemic heart disease: What's behind the curtain? J Am Coll Cardiol.* (2003) 41:1918–25. doi: 10.1016/S0735-1097(03)00428-5
10. Zheng ZS Yu LQ, Cai SR, Kambic H, Li TM, Ma H, et al. New sequential external counterpulsation for the treatment of acute myocardial infarction. *Artif Organs.* (1984) 8:470–7. doi: 10.1111/j.1525-1594.1984.tb04323.x
11. Han JH, Leung TW, Lam WW, Soo YO, Alexandrov AW, Mok V, et al. Preliminary findings of external counterpulsation for ischemic stroke patient with large artery occlusive disease. *Stroke.* (2008) 39:1340–3. doi: 10.1161/STROKEAHA.107.500132
12. Lin W, Xiong L, Han J, Leung TW, Soo YO, Chen X, et al. External counterpulsation augments blood pressure and cerebral flow velocities in ischemic stroke patients with cerebral intracranial large artery occlusive disease. *Stroke.* (2012) 43:3007–11. doi: 10.1161/STROKEAHA.112.659144
13. Xiong L, Lin W, Han J, Chen X, Leung TW, Soo YO, et al. A retrospective pilot study of correlation of cerebral augmentation effects of external counterpulsation with functional outcome after acute ischaemic stroke. *BMJ Open.* (2015) 5:e009233. doi: 10.1136/bmjopen-2015-009233
14. Panerai RB. Assessment of cerebral pressure autoregulation in humans—-a review of measurement methods. *Physiol Meas.* (1998) 19:305–38. doi: 10.1088/0967-3334/19/3/001
15. Zhang R, Zuckerman JH, Giller CA, Levine BD. Transfer function analysis of dynamic cerebral autoregulation in humans. *Am J Physiol.* (1998) 274:H233–241. doi: 10.1152/ajpheart.1998.274.1.H233
16. Meel–van den Abeelen AS, Simpson DM, Wang LJ, Slump CH, Zhang R, Tarumi T, et al. Between–centre variability in transfer function analysis, a widely used method for linear quantification of the dynamic pressure–flow relation: the carnet study. *Med Eng Phys.* (2014). 36:620–627. doi: 10.1016/j.medengphy.2014.02.002
17. Claassen JA. Meel–van den Abeelen AS, Simpson DM, Panerai RB. Transfer function analysis of dynamic cerebral autoregulation: A white paper from the international cerebral autoregulation research network. *J Cereb Blood Flow Metab.* (2016) 36:665–80. doi: 10.1177/0271678X15626425
18. Intharakham K, Beishon L, Panerai RB, Haunton VJ, Robinson TG. Assessment of cerebral autoregulation in stroke: a systematic review and meta–analysis of studies at rest. *J Cereb Blood Flow Metab.* (2019) 39:2105–16. doi: 10.1177/0271678X19871013
19. Lin W, Xiong L, Han J, Leung T, Leung H, Chen X, et al. Hemodynamic effect of external counterpulsation is a different measure of impaired cerebral autoregulation from vasoreactivity to breath–holding. *Eur J Neurol.* (2014) 21:326–31. doi: 10.1111/ene.12314
20. Reinhard M, Wihler C, Roth M, Harloff A, Niesen WD, Timmer J, et al. Cerebral autoregulation dynamics in acute ischemic stroke after rtpa thrombolysis. *Cerebrovasc Dis.* (2008) 26:147–55. doi: 10.1159/000139662
21. Sheriff F, Castro P, Kozberg M, LaRose S, Monk A, Azevedo E, et al. Dynamic cerebral autoregulation post endovascular thrombectomy in acute ischemic stroke. *Brain Sci.* (2020) 10:9. doi: 10.3390/brainsci10090641
22. Liu J, Simpson DM, Allen R. High spontaneous fluctuation in arterial blood pressure improves the assessment of cerebral autoregulation. *Physiol Meas.* (2005) 26:725–41. doi: 10.1088/0967-3334/26/5/012
23. Xiong L, Tian G, Lin W, Wang W, Wang L, Leung T, et al. Is dynamic cerebral autoregulation bilaterally impaired after unilateral acute ischemic stroke? *J Stroke Cerebrovasc Dis.* (2017) 26:1081–7. doi: 10.1016/j.jstrokecerebrovasdis.2016.12.024
24. Reinhard M, Muller T, Guschlbauer B, Timmer J, Hetzel A. Transfer function analysis for clinical evaluation of dynamic cerebral autoregulation—-a comparison between spontaneous and respiratory–induced oscillations. *Physiol Meas.* (2003) 24:27–43. doi: 10.1088/0967-3334/24/1/303
25. Reinhard M, Roth M, Muller T, Guschlbauer B, Timmer J, Czosnyka M, et al. Effect of carotid endarterectomy or stenting on impairment of dynamic cerebral autoregulation. *Stroke.* (2004) 35:1381–7. doi: 10.1161/01.STR.0000127533.46914.31
26. van Beek AH, Claassen JA, Rikkert MG, Jansen RW. Cerebral autoregulation: An overview of current concepts and methodology with special focus on the elderly. *J Cereb Blood Flow Metab.* (2008) 28:1071–85. doi: 10.1038/jcbfm.2008.13
27. Petersen NH. Ortega–Gutierrez S, Reccius A, Masurkar A, Huang A, Marshall RS. Dynamic cerebral autoregulation is transiently impaired for 1 week after large–vessel acute ischemic stroke. *Cerebrovasc Dis.* (2015) 39:144–50. doi: 10.1159/000368595
28. Aaslid R, Lindegaard KF, Sorteberg W, Nornes H. Cerebral autoregulation dynamics in humans. *Stroke.* (1989) 20:45–52. doi: 10.1161/01.STR.20.1.45
29. Dawson SL, Blake MJ, Panerai RB, Potter JF. Dynamic but not static cerebral autoregulation is impaired in acute ischaemic stroke. *Cerebrovasc Dis.* (2000) 10:126–32. doi: 10.1159/000016041

30. de Jong DLK, Tarumi T, Liu J, Zhang R, Claassen J. Lack of linear correlation between dynamic and steady–state cerebral autoregulation. *J Physiol.* (2017) 595:5623–36. doi: 10.1113/JP274304
31. Zhang Y, He X, Chen X, Ma H, Liu D, Luo J, et al. Enhanced external counterpulsation inhibits intimal hyperplasia by modifying shear stress responsive gene expression in hypercholesterolemic pigs. *Circulation.* (2007) 116:526–34. doi: 10.1161/CIRCULATIONAHA.106.647248
32. Barsness GW. Enhanced external counterpulsation in unrevascularizable patients. *Curr Interv Cardiol Rep.* (2001) 3:37–43.
33. Masuda D, Nohara R, Hirai T, Kataoka K, Chen LG, Hosokawa R, et al. Enhanced external counterpulsation improved myocardial perfusion and coronary flow reserve in patients with chronic stable angina; evaluation by(13)n–ammonia positron emission tomography. *Eur Heart J.* (2001) 22:1451–8. doi: 10.1053/euhj.2000.2545
34. Hilz MJ, Stemper B, Heckmann JG, Neundorfer B [mechanisms of cerebral autoregulation, assessment and interpretation by means of transcranial doppler sonography]. *Fortschr Neurol Psychiatr.* (2000) 68:398–412. doi: 10.1055/s-2000-11798
35. Guo ZN, Shao A, Tong LS, Sun W, Liu J, Yang Y. The role of nitric oxide and sympathetic control in cerebral autoregulation in the setting of subarachnoid hemorrhage and traumatic brain injury. *Mol Neurobiol.* (2016) 53:3606–15. doi: 10.1007/s12035-015-9308-x
36. Xiong L, Lin W, Han J, Chen X, Leung T, Soo Y, et al. Enhancing cerebral perfusion with external counterpulsation after ischaemic stroke: How long does it last? *J Neurol Neurosurg Psychiatry.* (2016) 87:531–6. doi: 10.1136/jnnp-2014-309842
37. Marthol H, Werner D, Brown CM, Hecht M, Daniel WG, Hilz MJ. Enhanced external counterpulsation does not compromise cerebral autoregulation. *Acta Neurol Scand.* (2005) 111:34–41. doi: 10.1111/j.1600-0404.2004.00352.x

Conflict of Interest: The authors declare that the research was conducted in the absence of any commercial or financial relationships that could be construed as a potential conflict of interest.

Advantages of publishing in Frontiers

OPEN ACCESS
Articles are free to read for greatest visibility and readership

FAST PUBLICATION
Around 90 days from submission to decision

HIGH QUALITY PEER-REVIEW
Rigorous, collaborative, and constructive peer-review

TRANSPARENT PEER-REVIEW
Editors and reviewers acknowledged by name on published articles

Frontiers
Avenue du Tribunal-Fédéral 34
1005 Lausanne | Switzerland

Visit us: www.frontiersin.org
Contact us: frontiersin.org/about/contact

REPRODUCIBILITY OF RESEARCH
Support open data and methods to enhance research reproducibility

DIGITAL PUBLISHING
Articles designed for optimal readership across devices

FOLLOW US
@frontiersin

IMPACT METRICS
Advanced article metrics track visibility across digital media

EXTENSIVE PROMOTION
Marketing and promotion of impactful research

LOOP RESEARCH NETWORK
Our network increases your article's readership